Thioureas as Organocatalysts for Asymmetric Isocyanide-based Multicomponent Reactions

Zur Erlangung des akademischen Grades eines

DOKTORS DER NATURWISSENSCHAFTEN

(Dr. rer. nat.)

von der KIT-Fakultät für Chemie und Biowissenschaften

des Karlsruher Instituts für Technologie (KIT)

genehmigte

DISSERTATION

von

M. Sc. Andreas Ganzbuhl

aus Karlsruhe

1. Referent: Prof. Dr. Michael A. R. Meier
2. Referent: Prof. Dr. Stefan Bräse

Tag der mündlichen Prüfung: 11.02.2025

Declaration of Authorship

Die vorliegende Arbeit wurde von Oktober 2021 bis Januar 2025 unter Anleitung von Prof. Dr. Michael A. R. Meier am Institut für Organische Chemie (IOC) des Karlsruher Instituts für Technologie (KIT) durchgeführt.

Erklärung

Hiermit versichere ich, dass ich die Arbeit selbstständig angefertigt, nur die angegebenen Quellen und Hilfsmittel benutzt und mich keiner unzulässigen Hilfe Dritter bedient habe. Insbesondere habe ich wörtlich oder sinngemäß aus anderen Werken übernommene Inhalte als solche kenntlich gemacht. Die Satzung des Karlsruher Instituts für Technologie (KIT) zur Sicherung wissenschaftlicher Praxis habe ich beachtet. Des Weiteren erkläre ich, dass ich mich derzeit in keinem laufenden Promotionsverfahren befinde, und auch keine vorausgegangenen Promotionsversuche unternommen habe. Die elektronische Version der Arbeit stimmt mit der schriftlichen Version überein und die Primärdaten sind gemäß Abs. A(6) der Regeln zur Sicherung guter wissenschaftlicher Praxis des KIT beim Institut abgegeben und archiviert.

Karlsruhe, 07.01.2025

Andreas Ganzbuhl

I Acknowledgement

An dieser Stelle möchte ich all denjenigen meinen herzlichsten Dank aussprechen, die mich auf dem Weg zur Promotion unterstützt und motiviert haben. Ohne diese Menschen wäre es kaum möglich gewesen, diese Thesis zu erstellen.

Mein besonderer Dank gilt dir, Mike. Seit meiner Bachelorzeit bist du eine entscheidende Stütze in meiner wissenschaftlichen Laufbahn. Du hast mich in deine Arbeitsgruppe aufgenommen und mir nicht nur diese Thesis, sondern auch meine Bachelor- und Masterarbeiten ermöglicht. Ich danke dir herzlich für das Vertrauen, die Ermutigung und die stets unterstützende Begleitung, insbesondere in Momenten, in denen ich durch enttäuschende Ergebnisse entmutigt war. Du hast immer mit Rat und Tat zur Seite gestanden und ein einzigartiges Arbeitsklima geschaffen, in dem man sich wohl und geschätzt fühlt.

Meinen herzlichen Dank richte ich an den gesamten Arbeitskreis sowie alle ehemaligen Mitglieder: Dr. Hatice Mutlu, Dr. Marc von Czapiewski, Dr. Andreas Boukis, Dr. Patrick Dannecker, Dr. Rebekka Schneider, Dr. Benjamin Bitterer, Dr. Yasmin Raupp, Dr. Katharina Wetzel, Dr. Eren Esen, Dr. Maximiliane Frölich, Dr. Pia Löser, Dr. Philipp Bohn, Dr. Kevin Waibel, Dr. Julian Windbiel, Dr. Daniel Hahn, Dr. Luca Filippi, Dr. Dennis Barther, Dr. Anja Kirchberg, Dr. Jiangling Liu, Dr. Roman Nickisch, Dr. Federico Ferrari, Dr. Michael Rhein, Dr. Clara Scheelje, Dr. Jonas Wolfs, Dr. Dafni Moatsou, Ann-Kathrin Werther, Pinar Sancar, Stefano Sechi, Jonas Wenzel, Rebecca Seim, Rieke Schulte, Svenja Gröbel, Elena Foitzik, Lisa Wanner, Michelle Karsten, Luis Santos Correa, Francesca Destaso, Qianyu Cai, Peter Conen, Nichollas Jaques, Hendrik Kirchhoff, Celeste Libretti, Federico Mundo, Luca Narducci, Timo Sehn, Sandra Wegelin, Laura Seidling, Simon Werling, Till Paha, Leonie Grutke, Florian Dobreff, Benjamin Felker und Leon Bartlewski. Dank euch wurde der Arbeitsalltag zu einer bereichernden und angenehmen Erfahrung. Unsere gemeinsamen Grillabende und Ausflüge werden mir immer in bester Erinnerung bleiben.

Ein besonderer Dank gilt Herrn Prof. Dr. Bräse und Herrn Prof. Dr. Wenzel, die mich während meiner Zeit in der BIF-IGS Graduiertenschule mit wertvollen Ratschlägen und Ideen unterstützt haben. Besonders danke ich für die daraus entstandene Kooperation zwischen der Wenzel-Gruppe und der Meier-Gruppe, die ein spannendes Projekt ins Leben gerufen hat.

Furthermore, I would like to thank Jeneesh and Sonia from the Wenzel Group for their support and their effort in carrying out the DFT calculations.

Ein großes Dankeschön geht an die BIG-IGS Graduiertenschule für die Aufnahme in das Programm und die Bereitstellung eines vielfältigen Kursangebots.

Ebenso danke ich der analytischen Abteilung des Organischen Instituts am KIT, insbesondere Pia Lang, Tanja Ohmer, Despina Savvidou, Angelika Mösle und Sina Zimmermann, sowie Christoph Götz von der Chemikalienausgabe. Ein großes Dankeschön auch an Andreas Rapp, ohne den das NMR sicher schon den Geist aufgegeben hätte. Ein besonderer Dank gilt auch Lara Hirsch danke ich besonders für ihren Einsatz und ihre Geduld beim Messen meiner zahllosen Proben.

Vielen Dank an meine fleißigen Korrekturleser Qianyu, Peter, Luis, Tina, Clara, Bohni, Henni, Celeste, Leon, Sandra und Simon,

Ebenso möchte ich allen danken, die mich synthetisch unterstützt haben: Lars, Jonathan, Patrick, Paul, Max, Leander, Marnie, Phillip, Tabea, Hannah, Johannes, Sarah, Michelle, Trung, Milada, Samuel und Christina. Simon und Felix danke ich dafür, dass ich eure Abschlussarbeiten betreuen durfte – ich hoffe, ich konnte euch etwas mit auf den Weg geben. Florian Dicks und Aaron Seider, euch gilt mein besonderer Dank für eure Hilfe in den letzten Wochen im Labor. Aaron, deine unerschütterliche Motivation und gute Laune waren ein echter Lichtblick.

Den Mitgliedern des Labors 103B danke ich für die gute Zeit, die einzigartige musikalische Untermalung und den Zusammenhalt: Roman, Federico F., Federico M., Michi, Dennis, Peter, Luis, Timo, Francesca und Luca – dank euch wurde die Arbeit zu einem Erlebnis.

Ein besonderes Dankeschön gilt Roman. Roman, ich möchte dir von Herzen für deine immense Unterstützung zu Beginn meiner Masterarbeit danken. Da meine Thesis auf der Grundlage deiner Hilfe entstanden ist, hast du sozusagen den Grundstein für dieses gesamte Projekt gelegt. Deine Hilfsbereitschaft ist wirklich bemerkenswert, und deine Fähigkeit, für jedes Problem eine Lösung zu finden, hat mich tief beeindruckt.

Michi, dir möchte ich für deine Geduld und deine lehrreichen Versuche, mir das Rage-Cage-Spiel beizubringen, danken – auch wenn der große Erfolg bei mir ausgeblieben ist. Außerdem danke ich dir für die Einladung zu deiner legendären Feier in deiner Heimat – ein unvergessliches Erlebnis.

Anja und Celeste, vielen Dank für die schönen Pausen draußen auf den Steinen. Ihr beide seid mindestens genauso süchtig nach Sonnenschein wie ich und habt es nicht gescheut bereits im Februar in dicker Jacke die ersten Sonnenstrahlen des Jahres mittags zu genießen.

Pete, dir gebührt mein Dank für unsere spannenden Schachpartien. Auch wenn ich es nur selten geschafft habe, dich ins Schwitzen zu bringen, habe ich viel von dir gelernt. Du bist einer der engagiertesten und hilfsbereitesten Menschen, die ich kenne – bleib genauso, wie du bist!

Timo, ich hätte nie gedacht, dass ich mich einmal für Pferderennen begeistern könnte. Doch dank dir und deinem kleinen Wettbüro hat sich mein Blickwinkel erweitert – vielen Dank dafür! Luis, deine einzigartigen Playlists und humorvollen Beiträge, egal ob zu Laborthemen oder darüber hinaus, haben mir oft ein Lächeln ins Gesicht gezaubert. Danke für die musikalische und menschliche Bereicherung!

Clara, ich danke dir herzlich für deine Thioureas und für deine tatkräftige Unterstützung während des Antragsschreibens. Du bist eine der hilfsbereitesten Personen, die ich kenne, und dein offenes Ohr bedeutet mir viel. Bohni, deine unermüdliche Motivation und gute Laune waren ansteckend, und ich danke dir, dass du mir die Möglichkeit gegeben hast, an der Twincore-Kooperation mitzuwirken.

Qianyu, dir danke ich aufrichtig dafür, dass du mir die Welt der DFT-Berechnungen nähergebracht hast. Ohne dich wäre ich da wohl nie durchgestiegen.

France and Luca, both I would like to thank for many conversations and good times together. Luca, I especially want to thank you for sharing the heater in freezing cold hours.

Leon und Henni, euch möchte ich für die ganzen Fußball Diskussionen danken und ich hoffe, dass wir uns bald wieder im Stadion wiedersehen werden.

Max, Danny, Torben, Julian, Jonathan und Tobias — ihr wart immer eine große Motivation und ein fester Rückhalt für mich. Auf euch konnte ich immer zählen, und dafür bin ich euch unendlich dankbar.

Mein tiefster Dank gilt meiner Familie. Ohne euch wäre ich heute nicht der Mensch, der ich bin. Eure Liebe und euer Glaube an mich haben mich immer getragen. Vielen Dank, dass ihr stets für mich da seid.

Zuletzt, aber ganz besonders, möchte ich Alejandra danken. Du warst in den vergangenen Jahren meine größte Unterstützung und hast mir in schwierigen Momenten immer wieder geholfen, die Motivation nicht zu verlieren. Dein unerschütterlicher Beistand und deine Liebe bedeuten mir mehr, als Worte ausdrücken können. Danke, dass du immer an meiner Seite bist.

II Abstract

Multicomponent reactions (MCRs) have emerged as powerful tools in organic synthesis, valued for their efficiency, atom economy, and ability to rapidly construct structurally diverse molecules. Among these, the Ugi and Passerini reactions stand out as prominent examples of isocyanide-based multicomponent reactions (IMCRs). However, achieving enantioselectivity in such reactions remains a significant challenge.

This study explores the applicability of thioureas as organocatalysts for both the Ugi and Passerini reactions. Thioureas, a class of organocatalysts, facilitate catalysis through non-covalent interactions, specifically hydrogen bonding. A diverse library of thiourea organocatalysts was synthesised, if applicable guided by the principles of green chemistry outlined by Anastas *et al*. A multicomponent reaction was employed as part of their synthesis, and it was discovered that this approach could be extended to produce thiohydantoins — a class of compounds widely utilised in medicinal chemistry.

A systematic catalyst design study for the enantioselective catalysis of the Passerini reaction was conducted, followed by a screening for optimal reaction conditions and an investigation into the scope of reactants. The results demonstrated that thioureas are highly effective at catalysing the Passerini reaction, yielding significant improvements in product formation and reactant conversion. Additionally, an enantiomeric excess (*ee*) of up to 19% was achieved, even with sterically less demanding reactants such as acetic acid and octanal. Mechanistic studies provided further insights into the thiourea-catalysed reaction pathway.

Preliminary experiments also revealed the potential of thioureas to catalyse the Ugi reaction enantioselectively. In an initial study, an *ee* of over 11% was achieved. Remarkably, product formation was observed even under conditions that would otherwise hinder the Ugi reaction, emphasising the catalytic capability of thioureas.

In conclusion, this work lays the foundation for further research into the use of thioureas as alternative catalysts in asymmetric isocyanide-based multicomponent reactions. The promising results presented here aim to inspire continued exploration in this field, broadening the scope of thioureas as versatile organocatalysts.

III Zusammenfassung

Multikomponentenreaktionen (MCRs) haben sich als leistungsstarke Werkzeuge in der organischen Synthese etabliert, die für ihre Effizienz, Atomökonomie und die Möglichkeit, schnell und einfach strukturell diverse Moleküle zu synthetisieren, geschätzt werden. Bekannte Beispiele unter diesen sind die Ugi- und die Passerini Reaktion, die zu den Isocyanid-basierten Multikomponentenreaktionen (IMCRs) zählen. Die enantioselektive Katalyse solcher Reaktionen ist jedoch immer noch eine große Herausforderung.

In dieser Arbeit wird die Anwendbarkeit von Thioharnstoffen als Organokatalysatoren für die Ugi- und Passerini-Reaktion untersucht. Thioharnstoffe sind eine Klasse von Organokatalysatoren, deren Effektivität auf nicht-kovalente Wechselwirkungen, insbesondere Wasserstoffbrücken-bindungen basiert. Zu diesem Zweck wurde eine Vielzahl von verschiedenen Thioharnstoffen synthetisiert, wobei soweit möglich die Prinzipien der „Grünen Chemie“ von Anastas *et al*. berücksichtig wurden. Deren Synthese beinhaltete teilweise eine weitere MCR, wobei sich zeigte, dass diese Methode auf die Herstellung von Thiohydantoinen erweitert werden kann – eine Molekülklasse, die häufig in der medizinischen Chemie Anwendung findet.

Es wurde eine systematische Studie zum Katalysatordesign für die enantioselektive Katalyse der Passerini-Reaktion durchgeführt, gefolgt von einem Screening optimaler Reaktionsbedingungen. Zusätzlich wurde das Spektrum möglicher Reaktanten untersucht, um eine breite Anwendbarkeit zu gewährleisten. Die Ergebnisse zeigten, dass Thioharnstoffe wirksame Katalysatoren für die Passerini Reaktion sein können und zu höheren Umsätzen der Reaktanten und auch zu höheren Produktausbeuten führen können. Darüber hinaus konnte ein Enantiomerenüberschuss (*ee*) von bis zu 19 % erzielt werden, selbst bei sterisch weniger anspruchsvollen Reaktanten wie Essigsäure und Octanal. Mechanistische Studien lieferten zusätzlich erste Einblicke in den Thioharnstoff-katalysierten Reaktionsweg.

Erste Untersuchungen zeigten zudem, dass Thioharnstoffe die Ugi-Reaktion asymmetrisch katalysieren können. In einer Initialstudie wurde ein *ee* von über 11% erreicht. Bemerkenswert war, dass selbst unter Bedingungen, die eine Ugi-Reaktion normalerweise unmöglich machen, im Beisein des Katalysators eine Produktbildung nachgewiesen werden konnte, was die katalytische Fähigkeit der Thioureas unterstreicht.

Zusammenfassend legt diese Arbeit den Grundstein für weitere Untersuchungen zur Etablierung von Thioharnstoffen als Katalysatoren in asymmetrischen Isocyanid-basierten Multikomponentenreaktionen. Die vielversprechenden Ergebnisse dieser Studie sollen weitere Forschung in diesem Bereich inspirieren und das Anwendungsspektrum von Thioharnstoffen als vielseitige Organokatalysatoren erweitern.

Table of Content

Chapter 1 Introduction

Catalysis is an essential part of the modern chemical industry and one of its primary driving forces. It is estimated that approximately 90% of global chemical production involves at least one catalytic step.[1-5] The impressive dominance of catalysed reactions on an industrial scale is due to the significant advantages compared to uncatalysed reactions. By providing an alternative, energetically favourable reaction pathway, catalysts enable many chemical reactions to occur under conditions that are industrially practical, particularly with respect to applied pressures and temperatures.[1] Thereby, the overall efficiency is enhanced while reduced energy consumption improves the sustainability of the process. Furthermore, catalysts are also frequently used on a laboratory scale, facilitating a wide range of research activities.

In today's world, catalysts are indispensable across many industrial sectors, playing a key-role in the production of transportation fuels, as well as for the production of bulk and fine chemicals. Additionally, catalysts are crucial for pollution prevention, either by enabling reaction pathways that outcompete the formation of toxic by-products or by reducing pollutants through end-of-pipe solutions, such as those used in automotive and industrial exhaust systems.[1] Notably, catalysis is also of tremendous economic importance, as it is estimated that industrial processes involving at least one catalytic step contribute to approximately one-quarter of the gross domestic product in developed countries worldwide.[1,2] At the turn of the century in 2000, the global market for catalysts was valued at around 10 billion USD.[1,2] More than 20 years later, in 2023, the global catalyst market had already grown to 31.1 billion USD and is expected to continue expanding at a compound annual growth rate (CAGR) of 4.4% from 2024 to 2030.[6] The rising demand for catalysts is driven by manufacturers worldwide seeking to enhance process optimisation, improve yields, reduce costs, and save energy. Additional growth originates from increased applications in chemical synthesis, petroleum refining, polymer synthesis, petrochemicals, and environmental initiatives.[6]

Beyond the obvious economic interests in catalysis, it represents a vibrant and multidisciplinary research field spanning numerous areas, particularly inorganic and organic chemistry, biochemistry, theoretical chemistry, material science, and engineering.[1,2] Catalysis has played a significant role throughout human history, with the earliest documented man-made catalyst dating back to the 18th century.[1,2,7]

However, the ongoing pursuit of better solutions and more efficient synthetic processes will necessitate continued research in the field.[1,2] Increasing pressure to improve synthetic processes — particularly in terms of yield and selectivity — will arise in response to the global challenges of our time, such as climate change,[8-10] man-made pollution,[11-14] a growing world population,[15] and the rising demand for consumer products,[16] to name but a few.

On the other hand, increasingly stringent environmental mandates (e.g. the reduction of NO_x, SO_x, and carbon dioxide emissions) have created and will continue to create a more pressing need for cleaner and more sustainable methods of chemical production.[17] According to Sheldon: "the application of stoichiometric inorganic reagents is a main waste cause in fine chemical manufacturing".[18] Consequently, alternative and preferably catalytic synthesis pathways are essential to conserve resources and minimise waste production.[18] In general, a process or a technology can be termed as "greener" or "more sustainable — compared to pre-existing strategies" — if the application of toxic and hazardous reagents and solvents, as well as the generation of large quantities of waste and by-products, is reduced.[1,18] For this purpose, a set of sustainable principles in chemistry has been outlined in the "Twelve Principles of Green Chemistry" by Anastas *et al*., which serves as a valuable guide.[19] Catalytic synthesis routes can often fulfil many of these criteria.[1,20]

Despite the decisive significance of catalytic processes in the economy, industry and sustainable technologies, one area of application is of particular importance for this project. In asymmetric catalysis (or enantioselective catalysis), a chiral catalyst intervenes in the reaction by providing an alternative reaction pathway — one that leads to the preferential formation of a specific stereoisomer of the product. The spatial arrangement in three dimensions at the molecular level is crucial and can be as influential as the chemical nature of the molecule's functional groups themselves.[21-24] Furthermore, life itself depends on molecular chirality.[25,26] Not only are the essential biopolymers — which are associated with life — based on chiral monomers, but many physiological phenomena also depend on the interactions of chiral molecules.[26] Moreover, it becomes particularly interesting when host molecules interact unequally with two enantiomeric guest molecules, often resulting in distinct physiological effects.[27,28] For instance, while some enantiomers may differ in smell or taste others can produce different, and sometimes severe, effects.[27,29]

The reason for this is that the absolute configuration determines how chiral receptors in the human body interact with a chemical compound.[25] Consequently, stereoisomerism is of utmost importance in pharmacology, as more than 50% of all commercial drugs today contain at least one stereogenic centre — a figure that is likely to increase in the future.[28]

History provides a particularly tragic example of how two enantiomers of the same drug can have dramatically different effects on the human body. The drug THALIDOMIDE, originally developed as a sedative, became widely available in the 1960s.[21,25,29,30] THALIDOMIDE was sold as a racemic mixture, with devastating consequences: while the (*R*)-enantiomer possesses the intended sedative properties, the (*S*)-enantiomer is teratogenic, causing severe malformations in foetuses.[25,31] This tragedy highlighted the critical role of stereoisomerism in drug design.

Despite this, by the 1990s, approximately 90% of all synthetic chiral drugs were still sold as racemic mixtures, underscoring the challenges of synthesising enantiopure compounds.[25,32] In most cases, enantiomerically pure compounds were derived from racemic mixtures through methods such as chromatographic resolution. Alternatively, compounds from the chiral pool —such as amino acids, carbohydrates, terpenes, or alkaloids — were used as precursors to produce enantiopure products.[25] On the other hand, the stereoselective transformation of prochiral compounds remains the most elegant method for enantioselective synthesis. On the contrary, the majority of industrial production still relies heavily on biochemical or biological methods.[25] As a result, organic synthesis aims to develop methods for producing compounds with precisely defined stereochemistry from prochiral starting material while reducing dependence on biological or chiral pool-derived approaches.[21]

This work focuses on the stereoselective execution of isocyanide-based multicomponent reactions (IMCRs), specifically the Passerini-3 component reaction (Passerini-3CR) and the Ugi-4 component reaction (Ugi-4CR). These multicomponent reactions enable the synthesis of α-acyloxy amides (Passerini) and peptide-like α-acylamino amides (Ugi). Both ICMRs are well-suited for diversity-oriented synthesis in drug discovery, as they allow the rapid generation of large libraries of potentially pharmacologically active molecules.[33] Although the reactions have been known for many years — since their discoveries in 1921 (Passerini)[34] and 1959 (Ugi)[35] — a truly enantioselective catalytic version of these reactions was only published recently. The Bin Tan group used chiral phosphoric acids (CPA) successfully as catalyst in 2015 for the Passerini and 2018 for the Ugi reaction.[33,36] While numerous catalysts are now available for asymmetric uni- or bimolecular reactions with high enantioselectivity, developing effective catalysts for asymmetric IMCRs has historically been a challenge.[37,38] The breakthrough achieved by Bin Tan and colleagues addressed several long-standing drawbacks, yet the asymmetric catalysis of IMCRs remains a significant hurdle, with only one catalyst class currently known to function effectively. Furthermore, the CPA-catalysed IMCRs have some limitations inherent to the catalyst class

used. CPA catalyst possess C_2-symmetry to provide a chiral pocket around the central phosphorus atom. The respective building blocks necessary to achieve this require tedious functionalisation and generate high amounts of waste.[39] Additionally, commercially available CPAs are extremely expensive, therefore limiting their application.[39] Furthermore, in the Passeri procedure, they require different conditions for various substrates and primarily involve bulky substrates.[36]

This project seeks to expand the scope of catalysts for asymmetric IMCRs by exploring thioureas. These small-molecule organocatalysts are well-known for their ability to activate substrates through hydrogen-bonding interactions.[40] They are a class of organocatalysts that are inexpensive, easily synthesised from chiral-pool compounds, bench-stable, metal-free, moisture-insensitive, and capable of catalysing reactions under mild conditions. Thioureas have demonstrated catalytic activity in various reactions, including asymmetric syntheses,[41] Diels-Alder reactions,[42-44] Michael additions,[45-48] Henry reactions,[49,50] acetalization,[51,52] Mannich-type reactions[53-57] and ring-opening polymerisations (ROP).[58,59] Consequently, the aim of this project is to further establish thioureas as viable alternatives for asymmetric IMCRs and to evaluate their catalytic performance in such reactions.

Chapter 2 Theoretical background

2.1 Catalysis – principles and historic developments

The earliest forms of catalytic processes were practised for thousands of years by early human societies across the globe, often without realising it.[7] Much of the impact of catalytic processes was evident in food and beverage production, as the creation of wine and beer, for instance, relied on the fermentation of grapes or grains respectively — a process catalysed by enzymes.[60,61] Furthermore, the production of other goods such as cheese, soap, sulphuric acid, and ether also depended on catalytic processes.[3]

One of the earliest recorded examples of catalysis dates back to 1552, when Valerius Cordus observed that the conversion of alcohol to ether could be accelerated by the presence of small amounts of sulphuric acid.[7,62] Other early accounts of catalytic effects include a report by Antoine Augustin Parmentier in 1781, describing the fermentation of starch into alcohol when treated with potassium hydrogen tartrate or acetic acid.[63] More historic examples of catalytic processes were given by Sigismund Konstantin Kirchhoff, who noted in 1811, that the mineral acids used to convert starch into gum, dextrin, and raisin sugar were not consumed in the reaction.[64] Another example is the discovery of Sir Humphry Davy in 1817, that the combustion of coal gas with oxygen was accelerated by the presence of a glowing platinum wire at temperatures far below ignition.[65,66]

Finally, the first general theory emerged, that incorporated these and many other observations of accelerated chemical reaction. This theory was published in 1835 by Jöns Jakob Berzelius.[67] He also coined the term *catalysis*, derived from the Greek words "$\kappa\alpha\tau\alpha$" (down) and "$\lambda\upsilon\sigma\iota\varsigma$" (solution, loosening).[67] Most remarkably, Berzelius recognised the common feature of all the aforementioned reactions: in each case, a foreign substance, distinct from the actual starting materials of the reaction, was required. Furthermore, these additional substances were never consumed during the process.[5,68] A more universally valid definition of catalysis was provided by Wilhelm Ostwald in 1894: "Catalysis is the acceleration of a slow chemical process by the presence of a foreign material".[69,70] Ostwald's investigations into catalysis, chemical equilibria, and reaction velocities earned him the Nobel Prize in Chemistry in 1909.[71]

In other words, catalysis can be described as a process in which a substance, known as the catalyst, accelerates the rate of a chemical reaction without alteration of the thermodynamic equilibrium. The reaction is accelerated because the catalyst forms chemical bonds with the reactants or intermediates, thereby altering the transition state of the reaction and providing

an alternative, energetically favourable reaction pathway.[72] Conversely, a substance is termed an *inhibitor* if its presence in the reaction mixture has the opposite effect, leading to a reduction in the reaction rate.[73] Moreover, catalysis is described as a cyclic process (see **Scheme 1**). In this process, the catalyst bonds with the reactants "**A**" and "**B**" before the reaction occurs. The catalyst facilitates the reaction, leading to the formation of the product "**P**", which remains temporarily attached to the catalyst. In the final step, the catalyst and product separate, allowing the catalyst subsequently to initiate another catalytic cycle.[1]

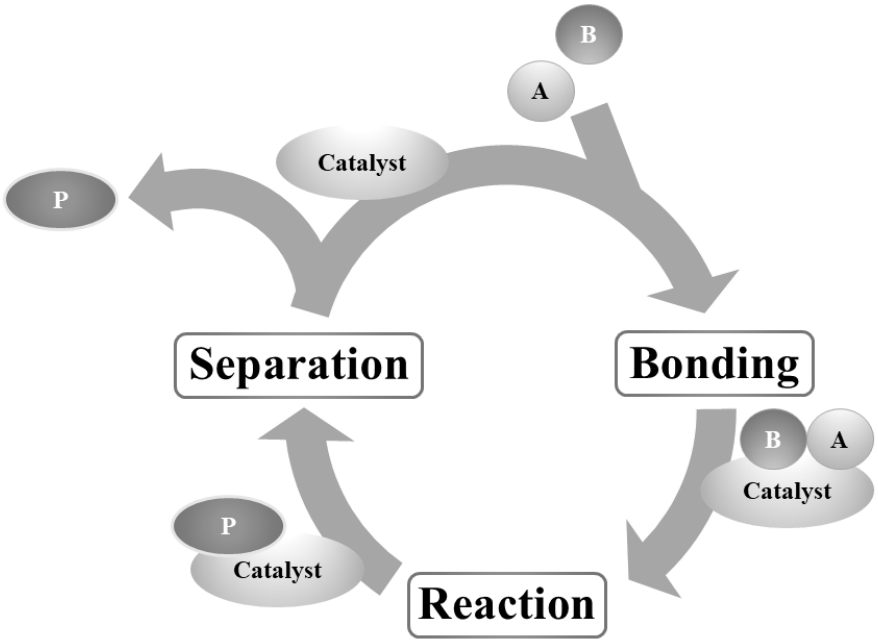

Scheme 1 A model catalytic cycle according to Kakaei *et al.*, illustrating the elementary steps of the cycle of bonding, reaction and separation.[1]

The catalyst functions as both a reactant and a product of the reaction, emerging unchanged and unconsumed.[72] Consequently, only small amounts of the catalyst are required, as it can repeatedly transform large quantities of reactants by continuously reinitiating the catalytic cycle.[70] The efficiency of a catalyst can be quantified using the Turnover Frequency (TOF) and the Turnover Number (TON). According to Martin *et al.*, there is significant controversy surrounding the precise definitions of TOF and TON.[74] They propose that the TOF represents the number of catalytic cycles performed by the catalyst per unit of time. TOF° refers to the standard Turnover Frequency, where TOF is measured under typical reaction conditions to facilitate comparison.[74]

Additionally, the TON is calculated by multiplying the TOF by the catalyst's lifetime, thus specifying the maximum utility of a catalyst under defined reaction conditions.[74] It quantifies the total number of catalytic cycles that occur at the active catalytic site over a given period — until the catalyst's activity declines (end of lifetime).[74] Notably, a catalyst's lifetime is not infinite, as it can decompose or become deactivated through processes such as poisoning, where irreversible binding with side products or other substances occurs.[75-77]

Scheme 1 illustrates a generic energy diagram, showing the uncatalysed reaction pathway (dashed line) and the catalysed reaction pathway (continuous line). It is important to note that the catalytic pathway can be arbitrarily complex, potentially involving numerous transition states and various intermediates. Consequently, **Scheme 2** represents a significant simplification.

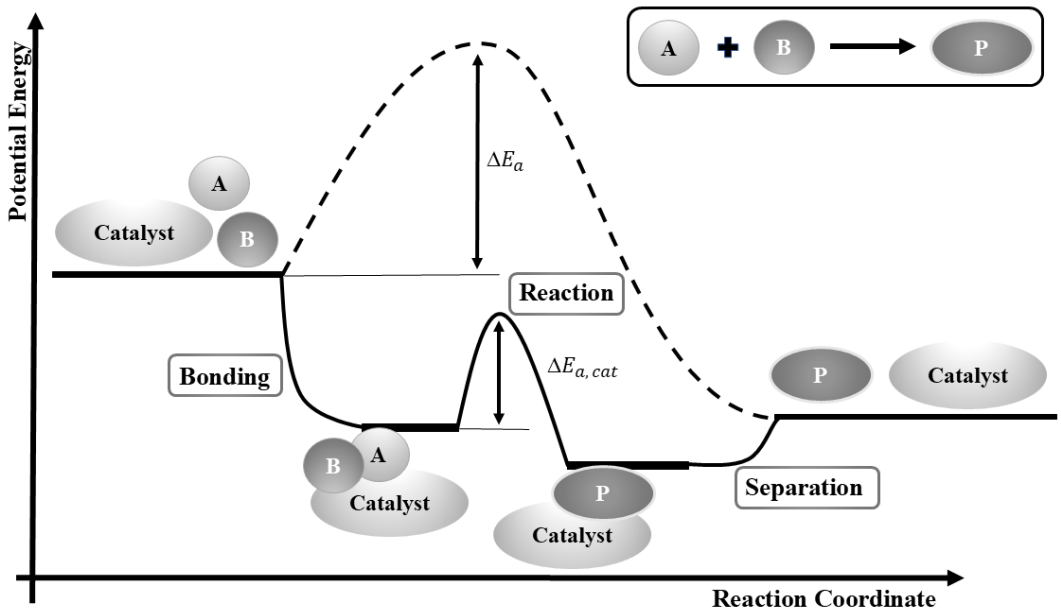

Scheme 2 A generic potential energy diagram of a model catalytic reaction according to Kakaei *et al.*,[1] in which the reactants "**A**" and "**B**" form the product "**P**". The Illustration compares the uncatalysed reaction pathway (dashed line) with the catalysed reaction pathway (continues line).

Often, the bonding between the reactants "**A**" and "**B**" and the catalyst is an exothermic process that occurs spontaneously. Due to its exothermic nature, the formation of a complex between the catalyst and reactants results in a lowered energy state in the potential energy diagram of the catalytic reaction.[1] After the reaction between "**A**" and "**B**" — while both are bound to the catalyst — took place, another lowered energy state is reached, in which the reaction product remains bound to the catalyst. To transition to this new energy state and

complete product formation, the activation energy $\Delta E_{a,\,cat}$ must be overcome. The highest point on the catalysed reaction pathway (continuous line) represents the transition state of the catalysed reaction. Comparatively, this transition state has a significantly lower activation energy barrier than that of the uncatalysed reaction pathway.[1]

The activation energy required can be calculated using the Arrhenius equation.[78]

$$k = A * \exp\left(\frac{-E_a}{RT}\right) \qquad \textit{(Eq. 1)}$$

In this context, k denotes the rate constant for any activation step, while E_a signifies the activation energy required for the reaction. The parameter A, known as the pre-exponential or frequency factor, represents the temperature-dependent product of the collision frequency and the steric factor, as explained by collision theory.[79] Furthermore, R stands for the universal gas constant, and T represents the absolute temperature. The reaction rate is accelerated because the presence of a catalyst provides an alternative reaction pathway with a comparably lower transition state energy. Consequently, more reactant molecules possess sufficient energy to reach the transition state, resulting in increased product formation.

In summary, catalysis is a kinetic effect. The thermodynamics of the reaction remain unchanged, as illustrated in **Figure 2**, where the reactants at the start of the reaction and the products of the catalysed reaction pathway are at the same energy states as in the uncatalysed reaction pathway. This indicates that the Gibbs free energy and the enthalpy are identical to those of the uncatalysed reaction.[1] Nonetheless, the presence of a catalyst can enable reactions that would otherwise not occur, or that would proceed at an extremely low rate in its absence. It is worth noting that a catalyst can also affect the reverse reaction, as the transition state energy is similarly lowered. However, while the energy barrier for the reverse reaction may be reduced, the activation of the reactant (which, in this case, is the product of the forward reaction) by the catalyst might not occur in the same way as in the forward reaction. As a result, this effect remains mostly undetected.[70] Another important point is that a catalyst can alter measurable quantities — such as formation of more product within a given time period — but by definition, a catalyst cannot change the reaction equilibrium.[80]

Generally, catalysts can vary significantly in size and shape: Catalysts have been described in literature ranging from single atom catalysts (SAC)[81-83] to molecules[1] and even much larger structures such as zeolites[84,85] and enzymes are known.[86,87] Moreover, catalysis can be categorised into three subdisciplines: homogeneous catalysis, heterogeneous catalysis, and

biocatalysis. In homogeneous catalysis, the catalyst and all reactants exist in the same phase, typically either in the gas or liquid phase.[88-92] In contrast, heterogeneous catalysis involves the catalyst being in a different phase from the reactants.[68] Most commonly, the catalyst is a solid in contact with either a gaseous atmosphere or a liquid reaction mixture. Heterogeneous catalysis primarily occurs on the surface of the catalytic material. To maximise efficiency, catalysts are often supported on nanometer-sized, inert materials to take advantage of their surface area. Additionally, porous materials are used to increase the available surface area.[93,94] The third subdiscipline is biocatalysis, which involves for instance enzymes.[95,96] These are highly specialised and efficient catalytic proteins that occur naturally in living cells. Each enzyme features an active site surrounded by a specifically shaped protein structure, which guides substrates to the catalytic centre. This mechanism is often described by the "lock-and-key" principle.[1]

2.1.1 Organocatalysis and asymmetric synthesis

Homogeneous catalysts can be divided into two subcategories: those containing a metal in their catalytically active site are classified as metal-organic catalysts, while those without any metal in their active site are classified as organocatalysts.[88]

Metalorganic catalysts have been extensively studied in the past. Their catalytic activity arises from the d-orbitals of the respective transition-metal and relies on substrate coordination to it.[5] Additionally, the selectivity and activity of the metal centre can be modified and tailored by its ligands, which are predominantly organic. Besides the coordination-interaction, metalorganic catalysts activate reactants through mechanisms such as ligand exchange, and/or insertion.[88] Today, metal-organic catalysts are widely used and have found numerous applications in industry.[97-100] The significance of metal-containing catalysts is highlighted by the numerous Nobel Prizes awarded for advancements in this dynamic field. Recipients include Ostwald (1909), Haber (1918), Bergius and Bosch (1931), Natta and Ziegler (1963), Fischer and Wilkinson (1973), Knowles, Noyori, and Sharpless (2001), as well as Chauvin, Grubbs, and Schrock (2005). Their contributions span a wide range of achievements, from the development of fundamental kinetic principles and industrial processes to the creation of innovative catalysts for hydrogenation, stereospecific polymerisations, enantioselective reactions, and olefin metathesis.[98]

Organocatalysis, on the other hand — initially overshadowed by the success of organometallic catalysts — experienced exponential growth in research activity from the

1990s onwards, driven by pioneering advances in metal-free asymmetric catalysis.[101] The first enantioselective organocatalytic reaction, however, was reported as early as 1971 — an asymmetric aldol reaction using a catalyst based on the amino acid proline.[102-105] Much progress has been made in the past decades and today, numerous important reactions for forming C-C and C-heteroatom bonds can be performed in the presence of organocatalysts — even asymmetrically. These include aldol-type reactions, such as the Morita-Baylis-Hillmann reaction, Henry reaction, Pictet-Spengler reaction, and Michael reactions — as well as Diels-Alder reactions and 1,3-dipolar cycloadditions.[45,47,50,106-112] Organocatalysts have also been applied in multi-component reactions (e.g., Strecker, Biginelli, and Mannich reactions).[55,113-115] Additionally, they have found applications in Claisen rearrangements, polycyclisations, acetalisation, and ring-opening polymerisations.[52,116-118] Furthermore, organocatalysis received recognition by the Nobel Prize Committee when List and MacMillan were awarded the Nobel Prize in Chemistry in 2021 for their contributions to this field.

The catalytic activity of organocatalysts generally relies on the formation of reactive covalently bonded intermediates between the catalyst and substrates or arises from hydrogen-bonded or ion-pair complexes.[5] For instance, in enamine- and iminium-based catalysis, the catalyst influences the LUMO and HOMO energies of carbonyl compounds through covalent bond formation.[88,119] Another example is the urea/thiourea induced polarisation of double-bonds *via* hydrogen-bonding interactions.[120-122] Furthermore, it has been discovered that bifunctional catalysts, such as phosphoric acids, are promising catalysts, which activate the substrate *via* Brønsted acidity as well as through Lewis-basic interactions.[123,124] Based on Lewis and Brønsted concepts, organocatalysts can further be categorised according to their behaviour as Lewis bases, Lewis acids, Brønsted acids, or Brønsted bases.[125] For instance, Lewis-basic catalysts initiate reactions *via* nucleophilic addition to an electrophilic substrate, while Lewis-acidic catalysts activate nucleophilic substrates in the reverse case. Brønsted acids and bases, on the other hand, influence reactions through (partial) protonation or deprotonation. Furthermore, organocatalysis can proceed through supramolecular interactions or reversible covalent bonding with the reactants.[125]

In comparison to transition-metal-based catalysts, the use of metal-free organocatalysts generally offers several advantages, including the often higher tolerance to moisture and atmospheric oxygen.[126-128] Consequently, inert conditions are usually unnecessary, significantly simplifying the reaction process.[89] Additionally, organocatalysts demonstrate better tolerance towards various functional groups within the reactants, enabling a broader

range of applications.[48,88,125,129] Notably, compared to enzymes and other bioorganic catalysts, they also tolerate a wider range of conditions.[22] From the financial perspective, transition-metal-containing catalysts are typically expensive and sometimes rely on scarce resources.[130] Many organometallic catalysts use metals such as ruthenium, rhodium, palladium, osmium, iridium, and platinum, which are present in the Earth's crust only in very limited amounts and require challenging and costly exploitation.[130] Most likely the situation will not improve and the scarcity of these metals is expected to worsen in the coming years[48,88,125,129] According to a report from the British Geological Society (2011), the supply of these metals, along with antimony, mercury and tungsten, is predicted to be at high risk.[131,132] These metals have also been coined as “strategic,” with both the United States of America and the European Union relying on the import of the majority of these. Alongside economic factors, the exploration and exploitation of such scarce metals raise environmental concerns, as one ounce of pure platinum is usually extracted from 40 tons of raw ore, which is mined at depths of up to 1 kilometre.[131]

Contrary to these circumstances, organocatalysts are often less expensive and straightforward to prepare. The separation of residual metals from products presents a significant challenge in metalorganic catalysis, as incomplete removal can result in toxicity concerns — particularly in pharmaceutical applications — and pose environmental disposal issues.[48,88,125,129] These concerns are reduced with the use of organocatalytic methods, simplifying the overall purification process. However, some limitations remain. Reactions involving organocatalysts often exhibit low efficiency in industrial applications, requiring large quantities of catalyst, relatively long reaction times, and separation procedures that are still more complex compared to heterogeneous catalysis.[88]

As previously described, organocatalysts are particularly effective in promoting asymmetric syntheses. An asymmetric synthesis is performed under reaction conditions that predominantly or exclusively favour the formation of one enantiomer or diastereomer.[31,133] As highlighted in the introduction, catalysis mediated by a homochiral catalyst is one strategy to influence the stereoselectivity of a reaction during the reaction.

Traditionally, reactions with prochiral compounds were conducted, and the enantiopure compounds were subsequently isolated through the separation of enantiomorphic crystals or fractional crystallisation of diastereomers. [134] Another method involves separating stereoisomers *via* chromatographic techniques, which exploit the differing interactions between the analyte and the chiral stationary phase. Both approaches are laborious and produce significant waste, particularly when only one enantiomer in a racemic mixture is

desired, with the other treated as a by-product. A more modern approach allows stereoselectivity to be influenced directly during the reaction through the use of chiral auxiliaries.[135,136] These auxiliaries are covalently attached to the reactant to control stereochemistry and are subsequently cleaved. While the formation of enantiomeric by-products can be suppressed or completely avoided, auxiliaries typically need to be used in stoichiometric amounts, requiring an additional cleavage step that generates considerable waste. Recycling these auxiliaries often demands a complex recycling system, and in some cases, they degrade after use and cannot be reused. Finally, reactions may simply employ homochiral molecules from the chiral pool. However, in this method, chirality is not generated during the reaction but is instead predetermined by the reactant. [31,137]

In contrast, asymmetric organocatalysis — where a catalytic amount of the catalyst is sufficient — represents an elegant and economically attractive approach to stereoinduction. Asymmetric synthesis mediated by an organocatalyst can be categorised into four distinct mechanisms of stereoinduction.[22,138]

1. Non-covalent interactions: Asymmetric reactions are facilitated by supramolecular interactions, such as nucleophilic or electrophilic interactions between the catalyst and the substrate, Van der Waals interactions, hydrogen bonding, or π-π interactions. The catalyst is not consumed, and regeneration is unnecessary. Covalent intermediate formation: The catalyst forms a reactive intermediate with the substrate, requiring regeneration for further reactions.

2. Phase transfer catalysis: A host-guest complex between the catalyst and substrate enables migration between two phases, where product formation occurs.

3. Reactions within molecular cavities: A catalyst's molecular cavity can differentiate substrates based on steric demands and shape, achieving higher reaction rates similar to Lewis acid or base activation.

Asymmetric reactions require highly ordered transition states, achieved through passive or dynamic substrate-catalyst interactions. Passive interactions for instance, include hydrophobic, hydrophilic, van der Waals, and electrostatic forces, while dynamic interactions involve direct interactions at reactive centres and functional groups. Hydrogen bonding between the substrate and the catalyst is particularly important in asymmetric catalysis, with energy contributions ranging from 0.5–15 kcal/mol for ordinary hydrogen bonds, to up to 15–60 kcal/mol for charge- or resonance-assisted hydrogen bonds (CAHB, RAHB).[139] These interactions stabilise reactive intermediates and transition states,

promoting the formation of rigid, three-dimensional structures — such as catalyst-substrate dimers.[22,140] Thus, organocatalysis often exhibits parallels to enzymatic catalysis.

To quantify the outcome of an enantioselective reaction and determine the proportion of enantiomers in a product mixture, either the enantiomeric ratio (*er*) or the enantiomeric excess (*ee*) is employed. Historically, enantiomeric excess was widely used and remains the predominant metric in literature. The *ee* represents the extent to which a mixture contains one enantiomer in greater abundance than the other.[141] It often corresponds to the optical purity of a compound as determined by polarimetry, which was the standard method at the time. Modern chromatographic and spectroscopic techniques have since been developed, offering higher precision in quantifying enantiomeric composition. Moss *et al*. defined the enantiomeric ratio as the percentage ratio of one enantiomer to the other.[133] The product ratio reflects the rate constants under kinetic control, while under thermodynamic control, it is determined by the equilibrium constants.[142]

2.1.2 Thiourea – organocatalysts and their hydrogen bonding interactions

Thioureas are the thio-analogues of ureas, in which the oxygen atom of the carbonyl group is substituted by a sulphur atom. Thioureas are categorised by their substitution pattern at the nitrogen atoms, with mono-, 1,1- and 1,3-di-, tri-, and tetra-substituted thioureas being observed. Thioureas are typically prepared by the addition reaction of amines to isothiocyanates.[143] The reactants are usually stirred in solution at room temperature or at slightly elevated temperatures to yield the respective thiourea.[144] This reaction tolerates a wide range of functional groups, and even less reactive aromatic amines can be used as reactants if a base is added[52] or increased pressure (0.6 GPa) is applied.[145] Using this method, mono-,[146] 1,3-di-,[147-149] and tri-substituted[150-152] thioureas can be synthesised.

The required isothiocyanates, on the other hand, are thio-analogues of isocyanates and are classically synthesised from amines using highly toxic reagents such as thiophosgene[143] or carbon disulphide (CS_2).[153,154] The Meier group recently proposed a method for generating isothiocyanates using elemental sulphur and an organobase catalyst, i.e. 1,8-diaza-bicyclo-[5.4.0]undec-7-ene (DBU) or others, to convert isocyanides to their respective isothiocyanates.[155] This approach can be extended further to yield the desired thiourea compound in a more sustainable fashion directly in a multicomponent reaction (MCR), by adding an amine to the respective mixture of isocyanide, DBU, and elemental sulphur.[41] Other commonly employed reaction methods for thiourea synthesis rely on the use of

CS_2[143,156] or thionylation reagents, such as thiophosgene,[52] bis(1-benzotriazolyl)-methanethion,[157] or phenyl chlorothionoformate.[158]

Thioureas are compounds that have found extensive applications. Their intrinsic properties include biological activity, making them useful in agriculture as fungicides,[159] herbicides,[160] or rodenticides.[161] Their biological activity is also utilised in medical applications, where they serve as anti-thyroid agents,[162] anti-tumour agents,[147] anti-epileptic agents,[163] anti-hypertonic agents,[164] or antioxidants.[147] Furthermore, they are used in dyes, photographic films, textiles, and plastics,[143] with anti-corrosive properties also being reported recently.[165] In addition, thioureas are employed as intermediates in heterocycle synthesis,[166-170] or for the synthesis of amidines,[171] guanidines,[172-174] or as ligands in metal-organic chemistry.[175-179] Notably, thioureas are valued for their ability to act as anion receptors *via* host-guest complexation,[180-183] and 1,3-disubstituted derivatives are particularly known for forming hydrogen bonds with numerous electron-donating substrates[40,184] — a property that has led to their extensive application over recent decades in the field of organocatalysis.

Hydrogen bonding is a non-covalent interaction between molecules and an important concept derived from nature, as it is observed, for instance, in ribonucleases, antibodies, and enzymes.[140,185] By investigating the working principles of enzymes, it became evident that their catalytic activity mostly does not involve strong Lewis-acidic groups, but is rather based on weak bonds between their active site and the substrate, accompanied by only a small change in the Gibbs free energy.[184] In other words, their catalytic activity and selectivity rely on hydrogen bonding and other non-covalent intermolecular interactions, such as hydrophobic interactions, aromatic π-stacking, van der Waals forces, and dipole-dipole interactions.[184]

Thioureas interact with the Lewis-basic functionality of the substrate by forming bidentate hydrogen bond interactions. The ability of double hydrogen bonding was first described in 1984 by Hine *et al*., who used X-ray crystallography to analyse 1,8-biphenylenediol.[186] In 1990, Kelly *et al*. successfully demonstrated the activation of the dienophile in a Diels-Alder reaction, achieved by double hydrogen bonding of a 1,8-biphenylenediol derivative to the carbonyl group of the dienophile.[187] In subsequent years, Etter *et al*. explored the hydrogen-bond-donating capacities of *N*,*N*-diphenylureas using X-ray crystal structure analysis for the co-crystallising product of diphenylureas with different guest acceptors.[188-190] This period also saw a number of influential publications on *N*,*N*-disubstituted ureas and thioureas. Among these was Wilcox's 1992 study on substituent effects in anion recognition and the supramolecular chemistry of *N*,*N*-disubstituted (thio)urea derivatives.[191] In 1994, Curran *et*

al. reported on the activation of sulfoxides by urea derivatives in a radical allylation and later also in the first Claisen rearrangement catalysed by *N*,*N*-diphenyl (thio)urea derivatives.[192]

After the catalytic activity of such organic molecules became more widely recognised, the Jacobsen group achieved another milestone by introducing (thio)urea catalysts in asymmetric catalysis. Jacobsen *et al*. demonstrated in 1998 that chiral bifunctional thiourea catalysts bearing an imine functionality were able to catalyse imine-based MCRs — such as the Strecker and Mannich reactions — in an asymmetric fashion.[55,115] **Figure 1** shows the (thio)urea derivatives used by the Etter, Curran and the Jacobsen group.

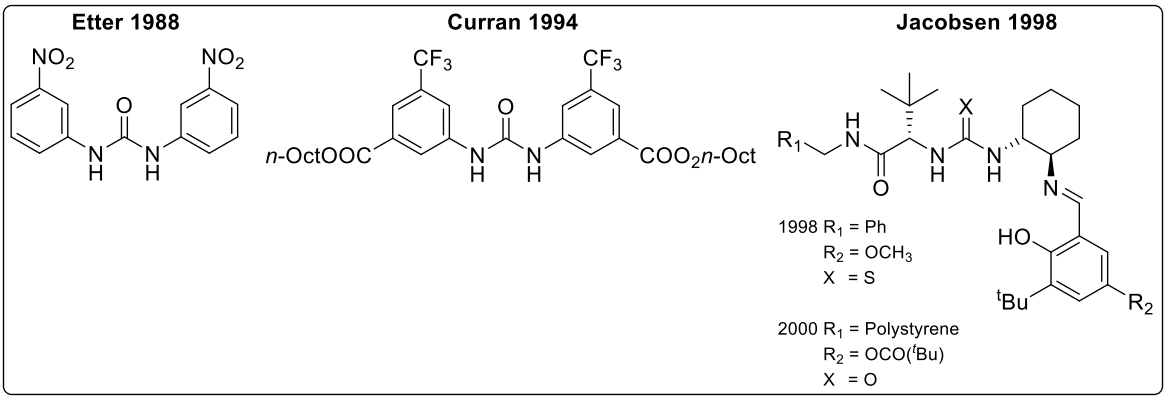

Figure 1 Illustration of important (thio)urea derivatives, which were investigated for their hydrogen-bonding abilities (Etter and Curran) as well as the first (thio)urea derivatives used in asymmetric catalysis (Jacobsen). The latter-named catalyst features solid support in its 2000 version, as it was bound to polystyrene in this modification — enabling catalyst recycling up to ten times.[193]

As the field of (thio)urea-mediated catalysis continued to expand, Schreiner *et al*. published an article in 2002, which provided a comprehensive guide to the structural design of (thio)urea catalysts.[42] Moreover, the highly active 3,5-bis(trifluoromethyl)phenyl moiety was introduced into the catalyst structure, a structural motif which was later coined as a privileged building block.[40,42]

The urea or thiourea group contains two N–H bonds (if not otherwise substituted), which enable double hydrogen-bond donor interactions, characteristic of these catalysts. This facilitates binding to hydrogen-bond acceptors such as carbonyl, carboxylic acid, sulphuric acid, and nitrate groups.[194] Furthermore, interactions of thioureas with imines have been reported.[195] Hydrogen bonding causes the electron density of the hydrogen-bond acceptor to shift towards the thiourea protons, ultimately resulting in a higher partial positive charge at the acceptor molecule and its activation.[43]

Based on these interactions, (thio)ureas can be categorised as catalysts that act as Lewis acids.[43,194] On the other hand, this activation mechanism has also been described as partial protonation, akin to Brønsted acidic catalysts, according to Seayad *et al.*[125] Supporting this hypothesis, Pápai *et al.* demonstrated through computational and experimental investigations that the Schreiner catalyst, for instance, possesses moderate Brønsted acidity, with a pK_a of 10.7.[121,196]

However, these hydrogen bonds are not particularly strong, and it is therefore unlikely that an ordinary thiourea would catalyse many reactions. For instance, the hydrogen bonding between a thiourea and a carbonyl compound exhibits a strength of approximately 7 kcal·mol^{-1} [194] at room temperature in dichloromethane. Consequently, entropic effects would most likely outcompete the exothermic effects of the binding.[40,42,43] Nevertheless, Schreiner *et al.* described several beneficial design principles, that greatly enhance the performance of such catalysts.[40,42,43]

To begin with, effective catalysis generally requires stabilisation of the transition state of a chemical reaction. In the case of (thio)ureas, this is achieved by partial protonation *via* hydrogen bonding. Although it can be advantageous for the overall performance of a chemical reaction if the catalyst stabilises the reactants or products, stabilisation of the transition state lowers its activation energy, ultimately accelerating the reaction.[59] Schreiner described that the hydrogen-bond donor capability of a (thio)urea can be enhanced by introducing electron-deficient aryl moieties adjacent to the thiourea group. **Scheme 3** illustrates several beneficial enthalpic and entropic effects of such electron-deficient aryl groups.

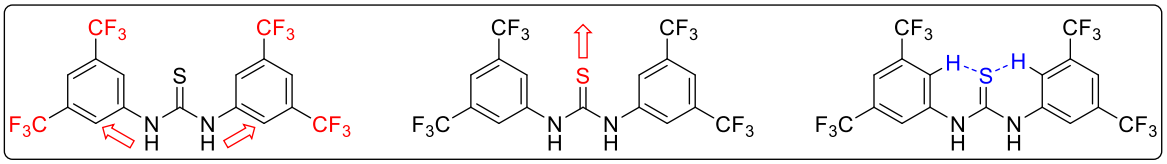

Scheme 3 Illustration of the enthalpic and entropic effects in the structure of Schreiner's catalyst. Enthalpic effects are coloured red, leading to polarisation of the N–H bonds and thereby improving the hydrogen-bond donor capabilities of the catalyst. This is achieved either through electron withdrawal (CF_3 group) or by enhanced polarisability (sulphur atom). The arrows indicate the direction in which the electron density is withdrawn. The intramolecular hydrogen bonds are coloured blue, enhancing the rigidity of the catalyst structure and facilitating substrate complexation by lowering the Gibbs free energy of complex formation—an entropic effect.[43]

Electron deficiency of the aryl group is achieved through the attachment of electron-withdrawing groups (EWGs), such as fluoro or trifluoromethyl groups. These groups

exhibit -M (mesomeric) and -I (inductive) effects, which reduce the electron density of the N-H bond of the (thio)urea. This results in a partial positive charge on the protons and an overall increase in the hydrogen-bonding strength of the molecules.[40,42,43] The hydrogen-bonding strength is most significantly enhanced when strong electron-withdrawing groups are attached in the *meta*-position. Some enhancement is also observed when EWGs are in the *para*-position, but to a lesser extent.[40,42,43] The positioning in the *meta*-position is particularly effective, as it causes less steric hindrance with the thiourea group compared to the *ortho*-position. Secondly, compared to *para*-positioning, two EWGs can be attached to the catalyst in the *meta*-position, while the difference in steric demands between *meta*- and *para*-positioning is negligible.

Furthermore, switching from urea to thiourea reduces the self-association of the catalyst due to the lower electronegativity of the sulphur atom. Sulphur in the thiourea group is a far weaker hydrogen-bond acceptor than oxygen in the urea group. Additionally, the solubility of thiourea is improved compared to urea, increasing the applicability of the catalyst. Additional electron-withdrawing effects are achieved with the thiourea group, as it has higher polarisability than its urea counterpart. This is due to the more efficient distribution of the partial negative charge on the sulphur atom compared to oxygen.[40,42] This further enhances the polarisation of the N–H bond in the thiourea group, increasing its hydrogen-bond donor capabilities. These capabilities are primarily determined by enthalpic effects, but the complexation of the catalyst with a suitable hydrogen-bond acceptor introduces an entropic contribution to the decrease in Gibbs free energy during the formation of the catalyst-substrate complex.

The strong electron-withdrawing effects of the CF_3 group attached to the aryl groups result in highly polarised aromatic protons in the *ortho*-position, which are prone to form intramolecular hydrogen bonds with the sulphur atom in the thiourea group. The diaryl-thiourea structure exhibits pronounced rigidity, with rotation limited by attractive intramolecular hydrogen bonds between the ortho hydrogen atoms on the aromatic rings and the Lewis-basic sulphur atom of the thiourea. This favours a nearly planar conformation of the thiourea. This preorganisation effect in the catalyst structure reduces the entropic penalty associated with complex formation between the catalyst and the substrate. The rigidity also facilitates catalysis by minimising the entropy loss that would otherwise result from the coordination of thiourea with its substrate, as the rotational degrees of freedom in the thiourea molecule are already restricted.[52,129,184,197]

Furthermore, due to the very low tendency of CF_3 groups to accept hydrogen bonds themselves, the catalyst is limited to forming intermolecular hydrogen bonds, which might otherwise reduce its catalytic activity. Moreover, Schreiner *et al*. suggest that binding interactions between the substrate and catalyst should not be excessively strong to avoid inhibition by the product.[40] Ultimately, Schreiner found that the *ortho*-hydrogen atoms — which are not incorporated into the intramolecular hydrogen-bonding of the catalyst — can form additional hydrogen-bonding interactions with Lewis-basic moieties in the substrate structure.[198] Considering all these adaptions to the original catalyst structure reported by Etter in 1988, *N*,*N*′-bis[3,5-bis(trifluoromethyl)phenyl]-thiourea (Schreiner's catalyst) emerged as an exceptionally active organocatalyst. It is widely regarded across various fields as a reference molecule for investigating the catalytic activities of hydrogen-bond donors, particularly thiourea catalysts.[52,129,184,197]

In summary, thioureas are a versatile class of organocatalysts, offering numerous advantages and applications. They can catalyse a wide range of reactions and even facilitate the catalysis of pH-sensitive substrates, as their hydrogen-bonding strength is not directly proportional to decreasing pK_a values.[199] Their synthesis is comparably uncomplicated and straightforward, with recent adaptations made towards more sustainable synthetic approaches.[41] Furthermore, it has been shown that thioureas can be immobilised on a solid phase, enabling catalyst recovery and reusability.[193]Additionally, catalytic activity has been reported even at very low catalyst loadings (0.001 mol%), achieving high TOF of up to 5700 h^{-1}.[197]

2.2 Multicomponent reactions (MCRs)

Multicomponent reactions (MCRs) are a class of reactions in which three or more starting materials react to form a single product, with several covalent bonds formed consecutively.[200,201] The products of MCRs usually incorporate most of the atoms from the reactants used, resulting in typically high atom economies (AE) — higher than 80%.[200,202,203] Most commonly, MCRs are conducted between three or four reactants, but higher-order MCRs involving up to eight different starting materials have also been reported.[204,205] MCRs are usually carried out in a one-pot fashion under mild conditions, offering facile reaction execution. Generally, MCRs fulfil various aspects of green chemistry, such as waste prevention, high yields, and excellent atom economy during synthesis.[201,202,206-208]

In addition, they offer significant advantages compared to bimolecular reactions — these advantages become especially apparent in multistep syntheses, or instance in the synthesis

procedures of natural compounds, where numerous subsequent reaction steps are typically required to obtain the final product.[200,209] Multicomponent reactions represent an elegant alternative to multistep procedures in the formation of complex products in organic synthesis by avoiding a sequence of consecutive reactions, especially considering that each of them would typically require subsequent purification. As a result, resources as well as time are saved tremendously.[210,211]

Reactant selection in MCRs is often modular, enabling the use of a vast scope of different moieties and resulting in a broad variety of potential products.[201,212] Moreover, MCRs represent a versatile tool in organic synthesis. Their application for the synthesis of large substance libraries for drug discovery in medicinal chemistry, as well as their use in polymer chemistry, has been reported.[200,213-216] Furthermore, the typically high yields achieved in MCRs, in addition to their other advantages, make them ideal candidates for the synthesis of sequence-defined macromolecules, where uniform macromolecules are generated through iterative synthesis.[217-220]

Generally, MCRs can be categorised into three subtypes based on their reaction mechanisms, as illustrated in **Scheme 4**.[200]

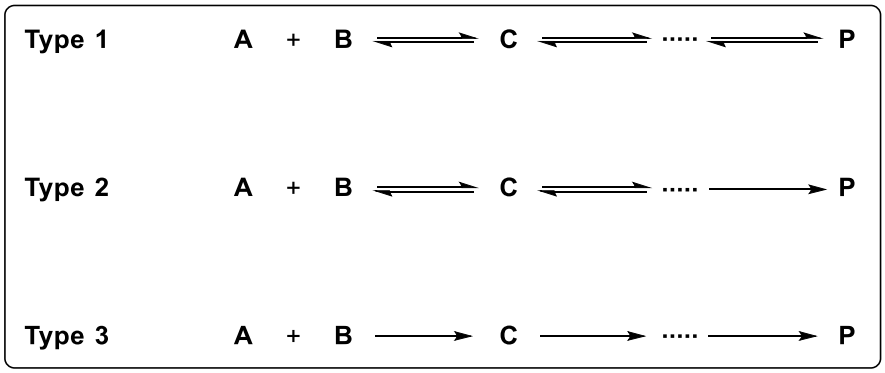

Scheme 4 Illustration of the three different types of multicomponent reactions. In **Type 1** all reaction steps are reversible, while in **Type 2** only the last step is irreversible. **Type 3** consists only of irreversible steps.[200]

Multicomponent reactions of **Type 1** involve dynamic equilibria among all species in the reaction system, including the starting compounds (**A** and **B**), intermediates (**C**), and products (**P**), as all reaction steps are reversible.[200] Since all the species are interconnected through equilibrium reactions, the reaction mixture inevitably contains a blend of all these species, making it challenging to isolate the product in high yields. Additionally, this type of MCR is highly prone to side reactions due to incomplete conversion. In contrast, **Type 2** MCRs also consists of reversible equilibrium steps for the individual reaction stages, but the

final step is irreversible.[200] This irreversibility offers a significant advantage for preparative synthesis by shifting the overall equilibrium towards the product. The irreversible step is often strongly exothermic — for example, the oxidation of a carbon atom in an isocyanide from C^{II} to C^{IV}, or processes such as ring closure reactions or aromatisation.[200] **Type 3** MCRs, on the other hand, consist exclusively of a sequence of irreversible reaction steps. These reactions are rarely observed under laboratory conditions but play a crucial role in enzymatic processes. In these cases, irreversibility is often mediated by thermodynamics or the use of adenosine triphosphate (ATP) as an energy source in living organisms.[200]

Notably, this classification into three types is not definitive, as the boundaries between them are fluid. Moreover, the classifications presented here is an idealisation of the underlying mechanisms.[200]

In **Figure 2** an overview of important MCRs is given in chronologic order, illustrating their versatility.

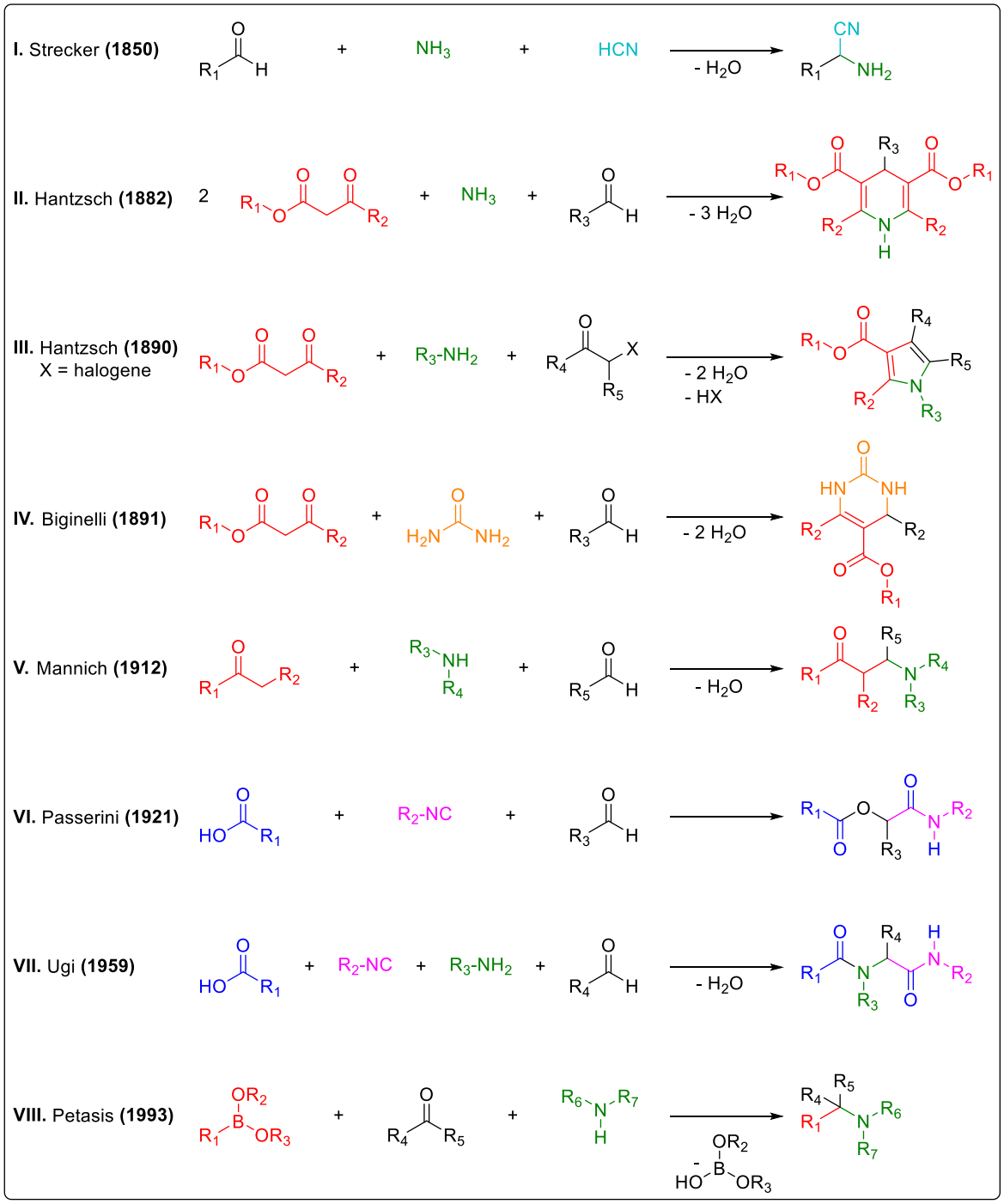

Figure 2 Chronological overview of important multicomponent reactions, according to Ugi *et al.*[200] For better visualisation, the starting materials are colour-coded and highlighted in the final product to emphasise their incorporation.

The Strecker synthesis (S-3CR) of α-amino acids, first described in 1850, is widely regarded as the earliest published multicomponent reaction.[221] The S-3CR involves a three-component

reaction between an aldehyde, ammonia, and hydrogen cyanide. This process initially forms an α-aminonitrile, which is then converted to the α-amino acid *via* hydrolysis in an acidic medium. Significant contributions to the synthesis of heterocycles were made by Hantzsch. In 1882, he reported his studies on pyridine derivatives,[222] and in 1890 his work on pyrrole derivatives demonstrated their accessibility through multicomponent reactions.[223]

In 1891, Biginelli introduced another multicomponent cyclo-condensation reaction (B-3CR), which converted esters of acetoacetic acid, aldehydes, and urea into 3,4-dihydro-pyrimidinones.[224] The Mannich reaction (M-3CR), described in 1912, involves a three-component reaction between an oxo-component (aldehyde or ketone), formaldehyde, and primary or secondary amines.[225] This reaction became highly influential in the total synthesis of natural products,[200] and was utilised in the synthesis of Tropinone — the first application of a MCR in the synthesis of natural products.[226] Later, in 1921, Passerini published the first multicomponent reaction using isocyanides as one of the starting materials, marking the emergence of a significant subgroup of isocyanide-based multicomponent reactions (IMCR).[34,211] In 1959, Ugi developed a four-component reaction involving an aldehyde, an amine, an isocyanide, and an acid component.[35] This work significantly expanded the scope of IMCRs. More recently, in 1993, Petasis modified the Mannich reaction by replacing enolisable carbonyl groups with boronic acids as nucleophiles to alkylate, vinylate, or arylate imines, establishing a distinct multicomponent reaction.[227,228]

2.2.1 Isocyanides

Isocyanide-based multicomponent reactions (IMCRs), including the Passerini and Ugi reactions, rely on the unique reactivity and intrinsic properties of isocyanides. IMCRs represent a subcategory of multicomponent reactions.[211,229] This chapter aims to discuss isocyanides and providing a comprehensive explanation of their reactivity, synthesis and applications. Detailed discussions of the Passerini and Ugi reactions are presented in **Chapters 2.2.2** and **2.2.3**, respectively.

Isocyanides, historically referred to as isonitriles, represent a substance class categorised by their extraordinary functional group. Notably, isocyanides are the only class of stable organic molecules, aside from stable carbenes, that feature a divalent carbon atom.[200] Isocyanides are renowned for their high α-acidity, their ability to form radicals, and their capacity to undergo α-additions.[200] Additionally, isocyanides can undergo polymerisation in the presence of a Lewis-acid catalyst.[200,230] Isocyanides exhibit a linear geometry and can be

represented by two distinct electronic structures: a carbenic structure and a zwitterionic structure (see **Scheme 5**).

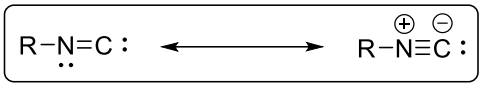

Scheme 5 Illustration of the electronic configurations of an isocyanide: The carbenic and the zwitterionic structure.

Historically, Nef *et al*. first described the electronic structure of isocyanides in their carbenic form, attributing this configuration to their ambivalent reactivity.[231] Later, a zwitterionic structure was proposed to explain observations from infrared spectroscopy and electron diffraction studies.[232] Additionally, high-level valence bond calculations suggest that the predominant electronic structure of isocyanides is carbenic. This configuration is energetically stabilised by the π-lone pair donor abilities of the nitrogen atom.[233]

The most remarkable property of isocyanides is the ability of the isocyanide carbon to act as both a nucleophile and an electrophile. This rare capability is shared only by carbenes and carbon monoxide.[200] Therefore, the typical reactions of isocyanides is an α-addition — a key-step in the mechanism of the Passerini-3CR and the Ugi-4CR. Here, the negative partial charge on the carbon enables the isocyanide to act as a nucleophile, after which it converts to an electrophile once the reaction is complete, allowing a nucleophilic attack at the same position.[200]

IMCRs can be subdivided into three subgroups based on their reaction mechanism. The underlying mechanisms of these subgroups are shown in **Figure 3**.

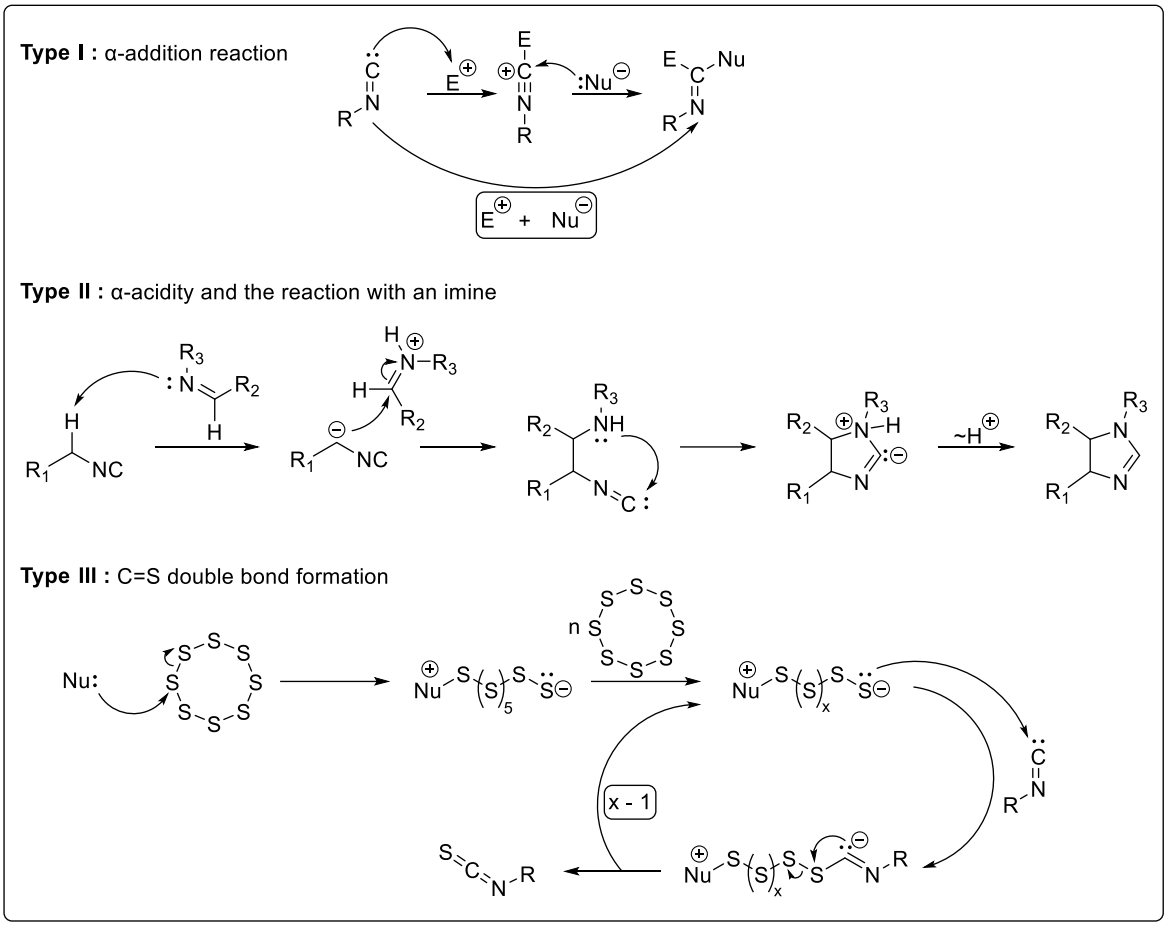

Figure 3 Illustration of the mechanistic pathways of various IMCR types: **Type I:** This pathway involves an α-addition mechanism on the isocyanide functional group, where the isocyanide reacts with an electrophile (E) and a nucleophile (Nu). **Type II:** This IMCR type is allowed by the high α-acidity of the α-CH_2 group next to the isocyanide functional group. Here, the reaction with an imine is depicted, with the formation of an imidazole. **Type III:** In this mechanism, a C=S double bond is formed. The process involves the activation of a chalcogen (e.g., elemental sulphur, S_8) by a base (Nu), producing a sulphur chain derivative. This activated sulphur compound subsequently reacts with the isocyanide carbon for the subsequent formation of an isothiocyanate.

IMCRs that involve an α-addition are classified as IMCRs of **Type I**.[144,234-237] The α-addition can either proceed concertedly or step-wise. The second type of IMCRs (**Type II**) relies on the α-acidity of the isocyanide carbon, which arises from the electron-withdrawing effect of the nitrogen atom. This effect is further amplified by the partial positive charge on the nitrogen. The α-CH_2 group's acidity can be enhanced by additional electron-withdrawing groups, such as tosylates or esters in α-position. In the presence of an imine, deprotonation generates a carbanion, which subsequently acts as a nucleophile, attacking the imine in a Mannich-reaction-like fashion. The hereby resulting nucleophilic amine subsequently attacks the isocyanide carbon. After a final proton transfer to the negatively charged, former isocyanide carbon, the product is generated. Overall, this reaction can be regarded as a formal [2+3] cycloaddition reaction.[144,238-241] IMCRs of **Type III** proceed through double bond formation between the isocyanide carbon and a chalcogen, such as sulphur or selenium.

If sulphur is used, it is generally assumed that the chalcogen is pre-activated by a base, forming a poly-sulphur anion chain, which then acts as a nucleophile and attacks the isocyanide. In this reaction, an isoseleno- or isothiocyanate is generated as product, while the elimination of one sulphur atom effectively shortens the poly-sulphur chain by one of its atoms (see **chapter 4.1.1.2** for further details).[144,242-244]

Isocyanides, which are isomers of cyanides,[245] were first synthesised accidentally in 1859 by Lieke.[246] During the alkylation of silver cyanide, he unexpectedly obtained allyl isocyanide alongside the anticipated cyanide. In 1869, Gautier was the first to describe the isomeric relationship between isocyanides and cyanides.[247] Two years earlier, Hoffmann had introduced a new method for synthesising isocyanides, which involved reacting primary amines with a base and chloroform.[248]

Initially, isocyanide chemistry received little attention, likely due to poor yields, complex procedures, and a lack of generalised methods for their synthesis. Additionally, isolating isocyanides was often challenging, especially due to difficulties in separating them from accompanying cyanides. The highly volatile nature of some isocyanides, coupled with their infamous and offensive odour, may also have discouraged researchers.[200,245] Interest in isocyanides increased significantly in 1921, when Passerini introduced his multicomponent reaction based on isocyanides.[34] This interest was further amplified in 1958 and 1960, when Ugi reported two synthesis procedures for isocyanides, which remain widely used today despite the availability of alternative methods.[155,249,250] Ugi's reliable methods begin with the formylation of primary amines to formamides, followed by dehydration in the presence of a base and a dehydrating agent to yield isocyanides.[251] Phosphorus oxychloride ($POCl_3$) is the most commonly used dehydration reagent today,[245,249] although recent studies suggest that 4-methylbenzene-1-sulfonyl chloride *(p*-TsCl) could serve as a more sustainable alternative.[155] In 2015, Dömling *et al*. discovered that the Leuckart-Wallach reaction is an efficient tool for the formation of *N*-formamides, which then can be transformed into isocyanides *via* a dehydration reaction.[252] **Figure 4** summarises the mentioned methods for isocyanide synthesis.

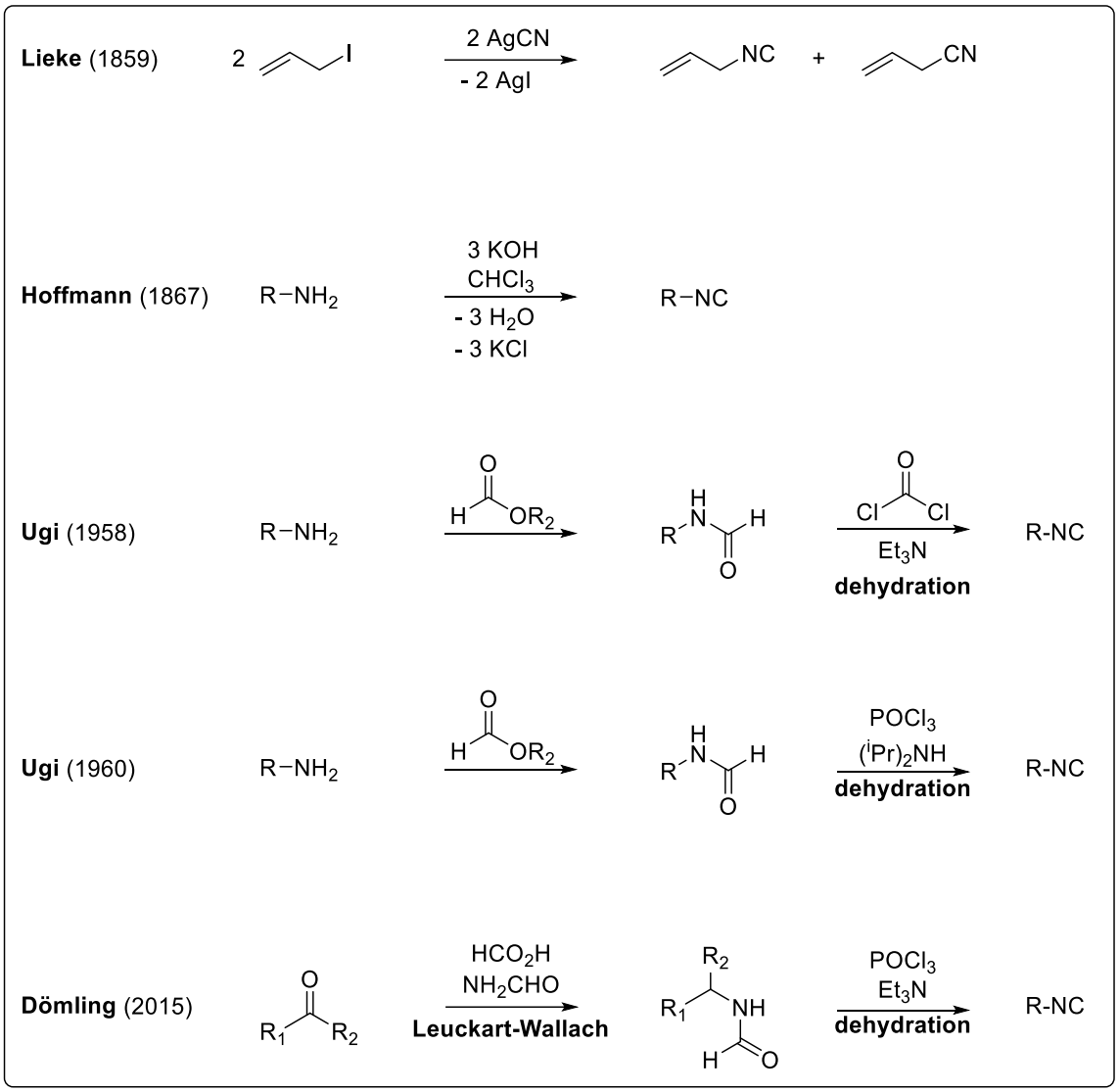

Figure 4 Selected important methods for isocyanide syntheses in chronological order.[246,248,251]

Furthermore, isocyanides are isolobal with carbon monoxide, which makes them highly valuable in organometallic chemistry.[253] Beyond their role as two-electron donor ligands in organometallic applications, isocyanides are prominently used in multicomponent reactions and are well-suited for synthesising nitrogen heterocycles.[200,254] Moreover, a variety of naturally occurring isocyanides have been identified. The first was discovered in 1950 by Rothe *et al*. in the fungal species *Penicillium notatum*.[255] This isocyanide was later utilised as the antibiotic xanthocillin. Many naturally occurring isocyanides exhibit antibiotic and fungicidal properties, making them useful in pharmaceutical applications. Most are derived from terpenes and found in marine sponges, although terrestrial isocyanides based on α-amino acids have also been identified.[249,256-259]

2.2.2 The Passerini-3 component reaction

The consecutive reaction involving an aldehyde, a carboxylic acid, and an isocyanide leading to a single product is known as the Passerini-three component reaction (Passerini-3CR). It is further recognized as the first-ever mentioned multicomponent reaction based on isocyanides (IMCR).[260] The "classic" Passerini-3CR, discovered in 1921 by its eponym Mario Passerini in Florence, Italy, involves the aforementioned reactants and results in the formation of α-acyloxy amides.[34,261] Similar to other multicomponent reactions, the Passerini-3CR is characterized by favourable features such as its simple execution under ambient conditions, leading to a complex product in one synthetic step.

Since the last step of the reaction involves the rearrangement towards the final product, which is an irreversible reaction step, the Passerini-3CR can be classified as a **Type 2 -** MCR.[200] This characteristic contributes to the high yields often obtained from this reaction, with quantitative yields not being uncommon. Furthermore, each atom of the starting materials is fully integrated into the final product of the Passerini-3CR. This signifies that the reaction demonstrates a perfect atom economy of 100% — at least in theory, since the Passerini-3CR is not entirely insusceptible for side reaction for instance if the aldehyde oxidises to the respective acid and afterwards competes with the other carboxylic acid in the reaction mixture. The following **Scheme 6** presents a proposed mechanism of the Passerini-3CR, which is commonly accepted today.

The reaction sequence starts by the activation of the oxo-component (here the aldehyde) by the carboxylic acid *via* hydrogen-bonding. The resulting dimeric structure undergoes an α-addition, the isocyanide acting as a nucleophile, adding to the carbonyl centre of the previously activated aldehyde. The isocyanide itself is attacked by the carboxylic acid, forming a cyclic transition state. The final step of the reaction involves an irreversible rearrangement, facilitating intramolecular transacylation, ultimately leading to the formation of the Passerini product - the α-acyloxy amide.

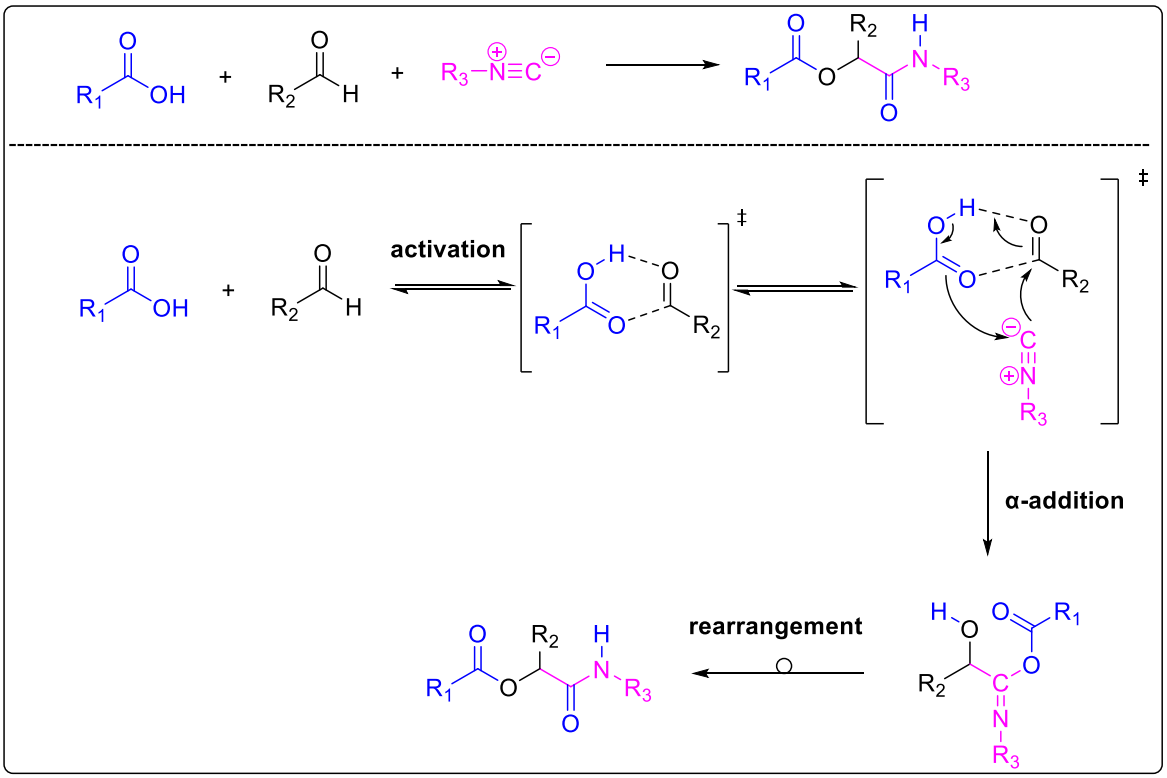

Scheme 6 Commonly accepted reaction mechanism of the Passerini-3 component reaction[261]

The reaction mechanism of the Passerini-3CR was refined twice in 2011 and in 2015 by the Morokuma group.[262,263] In both cases, density functional theory (DFT) calculations were carried out to propose a more detailed mechanism. Morokuma *et al.* first suggested the involvement of an additional molecule of carboxylic acid in the reaction mechanism.[262] This involvement was coined as the key factor for enhancing the reaction, since the additional carboxylic acid acts as a catalyst in the reaction, thus effectively lowering the activation energy barrier of the transition state.[262] According to the calculations, the resulting reduction in energy barrier facilitates the rearrangement process, leading to enhanced product formation. Consequently, Morokuma *et al.* stated that the Passerini-3CR can be seen as a four-component reaction due to the significant energy difference and the pronounced benefits conferred by the additional carboxylic acid.[262] In subsequent investigations in the following years, the Morokuma group validated these findings through further DFT calculations, which were extended to include solvation effects. Their results confirmed the existence of the previously debated nitrilium-ion as an intermediate in the Passerini-3CR.[263] The complete revised mechanism is depicted in **Figure 5**.

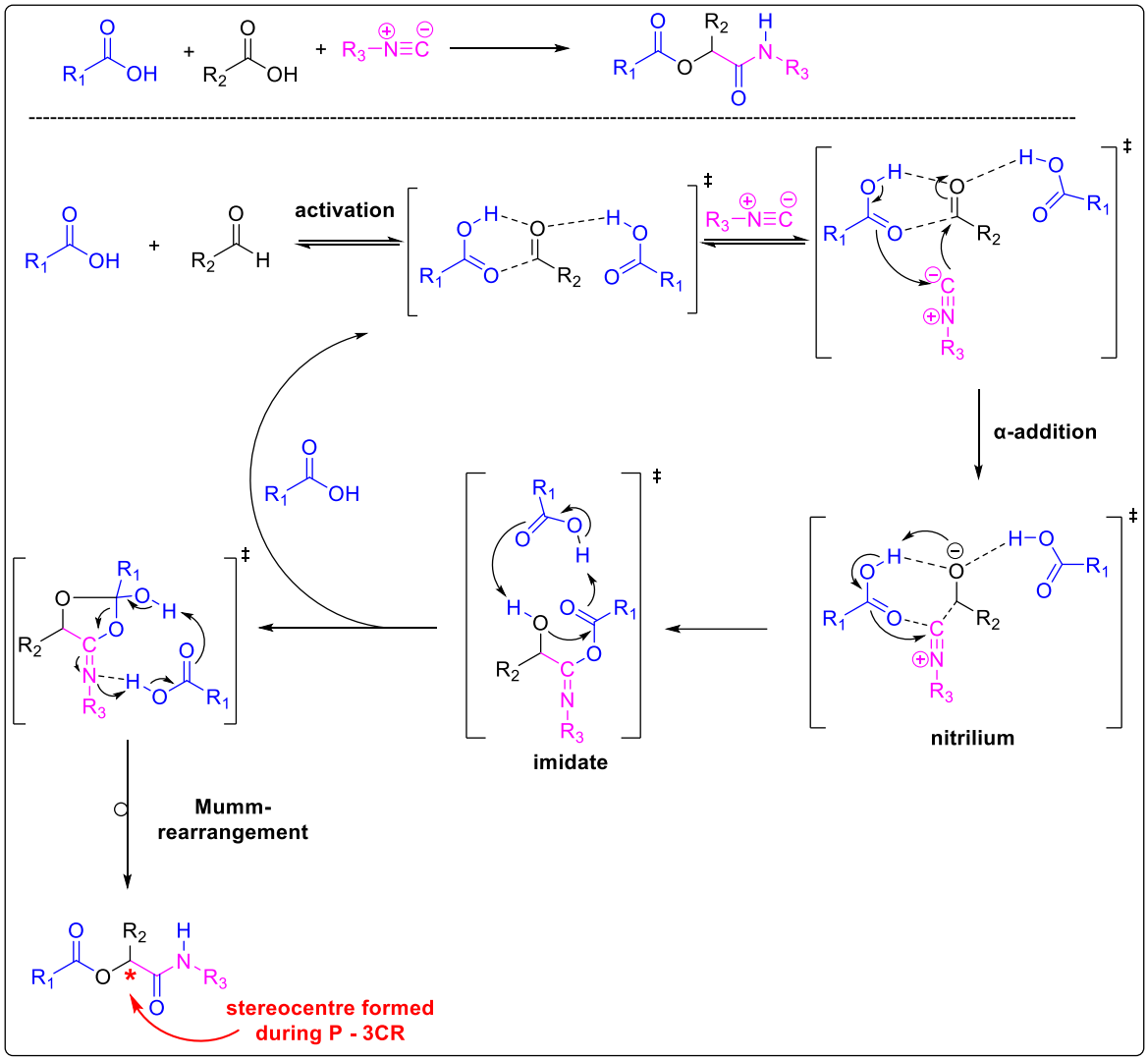

Figure 5 Revised reaction mechanism of the Passerini-3CR based on quantum-chemical calculations[263]

In 2021, the Passerini reaction celebrated its 100th anniversary. However, achieving an asymmetric version of the reaction continues to pose a formidable challenge. The Passerini reaction leads to the generation of a new stereogenic centre, if unsymmetric oxo-components are used as reactants. Generally, the addition of nucleophiles in a catalytic and enantioselective fashion to carbonyl- or imine C-atoms represents a well-established procedure.[264] However, if isocyanides are employed as nucleophilic species, the process faces several challenges to overcome.[261]

For instance, when employing Multicomponent Reactions (MCR), the catalytic reaction pathway consistently competes with a non-catalysed reaction pathway, i.e. with a racemic background reaction. The Passerini-3CR represents a spontaneous process that proceeds smoothly even under non-optimal reaction conditions, making it highly challenging to be

outcompeted through a catalytic pathway. Furthermore, the complexity of a reaction with more than two reactants[33] and the inherent challenges in achieving stereo control over the alpha-addition of isocyanides by the most logical activation of an aldehyde by a Lewis acid[265] can result in undesired interactions with the isocyanide.[261,264,266]

Despite these hurdles, the first approach towards an enantioselective Passerini-3CR was described in 2003 by Denmark *et. al.*[267] It is important to note that silicon tetrachloride, a weak Lewis acid, was used instead of a carboxylic acid, leading to a "truncated" two component Passerini reaction, yielding α-hydroxyamide. This Lewis acid was catalytically activated by chiral bisphosphoroamide, which led to the formation of a silicon cation, which then binds to the aldehyde, enabling the subsequent stereoselective α-addition on the isocyanide. The intermediate nitrilium ion is then trapped by chloride, which is the only nucleophile available in the reaction mixture. Thus, the landmark work of Denmark *et. al.* represents a two-component Passerini reaction to yield an imidoyl chloride and also the first catalytic, enantioselective α-addition on isocyanides.[267]

In the same year, Dömling *et. al.* reported the outcomes of extensive screenings involving a great variety of Lewis acid/ligand combinations, aiming for stereo induction in the Passerini-3CR.[268] In this context, they identified a Ti(IV)–TADDOL complex as the best performing chiral catalyst. Their work represents the first catalytic approach of the “classic” three component Passerini reaction.[261] However, their catalytic systems suffered from low turnover numbers and only moderate enantiomeric excess was achieved and typically equimolar amounts of the Ti(IV)–TADDOL complex were needed.[268] In the following year, the research group of Schreiber *et al.* documented the effective application of tridentate bis(oxazolinyl)pyridine (pybox)-Cu(II) - Lewis acid complex in substoichiometric amounts (0.2 equivalents) as a catalyst for the Passerini-3CR.[269] This approach led to high enantiomeric excess (60% to 98%) and satisfactory yields, provided that bidentate coordinating aldehydes and dry conditions were employed. In 2008, Zhu and co-workers achieved good to excellent enantiomeric excess by employing a (Salen)Al(III)Cl complex as Lewis acid catalyst, also when using nonchelating aldehydes.[266] In this approach, only aliphatic aldehydes were tolerated, while an argon atmosphere and cryogenic temperatures were required.

It took an additional 7 years for the first organocatalytic enantioselective Passerini-3CR to emerge, when Bin Tan *et al.* obtained excellent results using a chiral phosphoric acid (CPA) to influence the stereochemistry of the Passerini-3CR. According to their proposition, the remarkable results were achieved by formation of a hetero-dimeric, hydrogen-bonded

complex between the acid component and the CPA. Consequently, the acidity of the CPA might have increased, while the nucleophilicity of the carboxylate was enhanced for the attack on the nitrilium intermediate.[36] Although remarkable results were achieved, the procedure requires long reaction times and different conditions according to the substrates employed in the reaction. Furthermore, it was mostly investigated for the employment of bulky substrates (especially the carboxylic acid) in order to obtain high enantioselectivities.[36,270]

Notably, until today, the substitution of aldehydes with ketones remains an unexplored gap in the literature, yet to be addressed.[270]

2.2.3 The Ugi-4 component reaction

The Ugi-4 component reaction (Ugi-4CR) was discovered in 1959 by Ivar Karl Ugi.[35] This MCR is closely related to the Passerini-3 component reaction, which was discovered 28 years earlier.[34,271] The classic version of the Ugi reaction combines an aldehyde, a carboxylic acid, an amine, and an isocyanide in a consecutive reaction to form a single product, with the elimination of one molecule of water.[35,200] The Ugi-4CR facilitates the simultaneous formation of multiple bonds (C—C and C—N) in a single reaction, leading to the formation of α-aminoacyl amide derivatives in its classic version.[35] Additionally, the Ugi reaction enables the synthesis of peptide-like structures due to the two amide bonds formed in the product during the reaction.

The Ugi-4CR offers a wide range of applications and impresses with the variety of reactants that can be utilised, resulting in abroad spectrum of possible products to be generated. These features make it particularly suitable for the straightforward generation of compound libraries. Owing to the peptide-like structures with two amide bonds, the Ugi reaction enables the creation of potentially bioactive molecules, many of which may exhibit pharmaceutical application possibilities.[38,213,271-273] For example, in addition to aldehydes, ketones can also be used as oxo-components.[200] Alongside primary and secondary amines, hydrazines,[274] hydrazides,[275] sulfonamides,[276] and ureas[277] are also used in the Ugi-4CR.[271] Apart from carboxylic acids, numerous compounds can substitute the acidic component in this reaction. For instance, hydrazoic acids,[278] (thio)cyanates,[279] phenols[280] and also water[212] and many other compounds are applicable.[200,201] To this day, the Ugi-4CR remains one of the most important and popular multicomponent reactions alongside the Passerini reaction, primarily due to the high degree of structural diversity it offers.[38,281]

Generally, the Ugi-4CR can be carried out under mild conditions. The MCR can be conducted smoothly at room temperature or even at lower temperatures, in solution or using solid-phase synthesis. Most commonly, the Ugi-4CR is performed in polar protic solvents, such as low molecular weight alcohols (e.g., methanol); however, it can also be carried out in polar aprotic solvents, such as chloroform, DCM, dioxane, DMF, or THF. High concentrations (0.5–3 M) in the reaction solution are advantageous and generally lead to an enhanced reaction rate and high conversion.[200] Furthermore, it has been reported that a precondensation reaction between the amine and the oxo-component can result in an increased yield of the reaction.[272] Two plausible mechanisms are discussed in the literature. Both reaction paths (**A** and **B**) are presented in **Figure 6**:

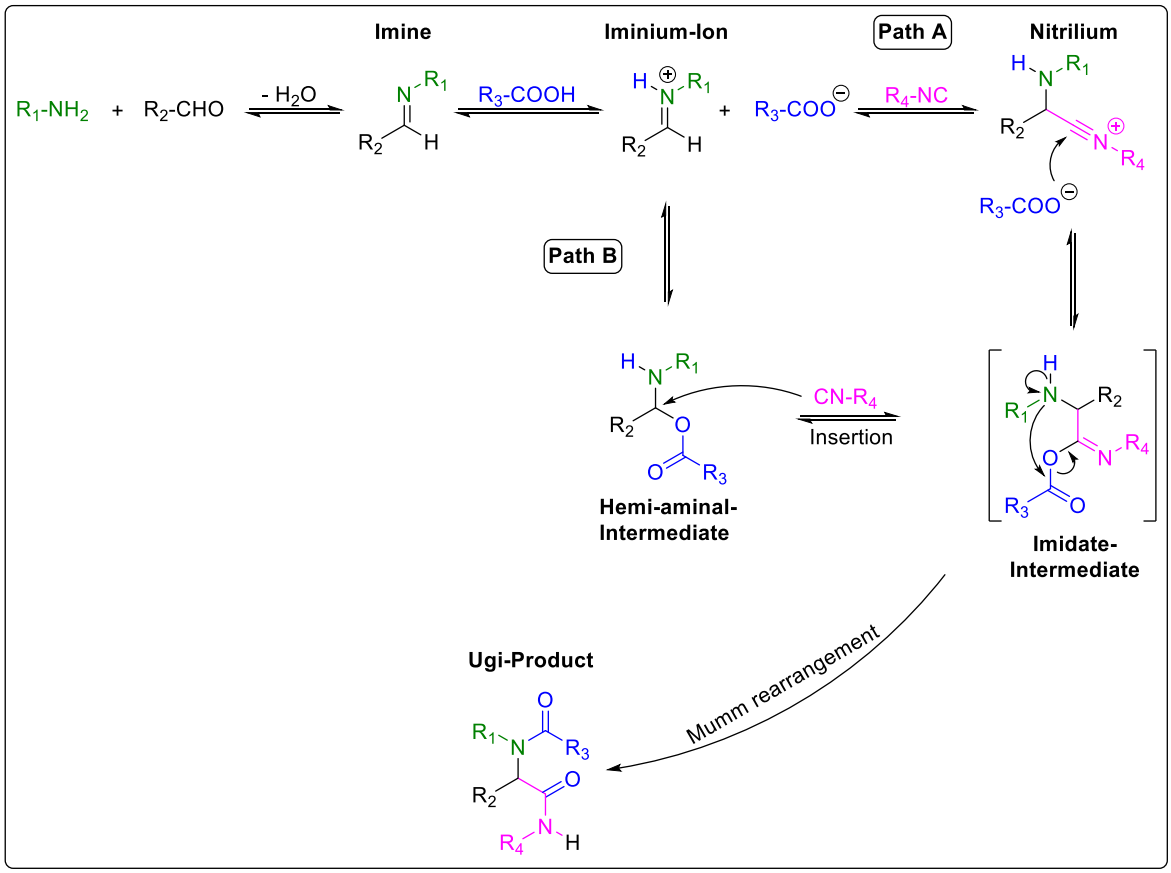

Figure 6 Illustration of the mechanisms of the Ugi-4CR, which includes two plausible reaction pathways, which were both proposed by Ugi himself (1961 **path A**[282] and 1997 **path B**[283]).

In 1961, Ugi proposed a mechanism for the MCR following reaction **path A**. This pathway begins with a condensation reaction between the oxo-component — an aldehyde in **Scheme 9** — and the amine, resulting in the formation of the corresponding imine and the elimination of one molecule of water.[200,282] In the subsequent step, the imine is protonated

by the carboxylic acid, forming an iminium-ion, resulting in the activation of the carbonyl compound for a nucleophilic attack, which is carried out by the isocyanide. The electrophilicity of the iminium-ion can be further enhanced by the addition of a Lewis acid as catalyst.[200] The nucleophilic attack of the isocyanide results in the formation of a nitrilium-ion, which subsequently reacts with the carboxylate anion towards the imidate intermediate. The last reaction step for the formation of the Ugi product is the exothermic, irreversible Mumm rearrangement. The irreversibility of the rearrangement is one of the driving forces of the Ugi-4CR (MCR of **Type 2**),[200] besides the exothermic oxidation of the C^{II} carbon atom of the isocyanide to the C^{IV} carbon of the amide bond in the product structure.[272,284,285]

In 1997, Ugi proposed another possible reaction **path B**, which starts in the same manner as **pathway A** until the iminium-ion is generated.[201,283] After its formation, the iminium-ion undergoes an addition reaction of the carboxylate anion instead of the isocyanide, which leads to the generation of a hemiaminal as a reaction intermediate. Subsequently, the hemiaminal reacts with the isocyanide in an insertion reaction to form the imidate as an intermediate. Afterwards, the imidate undergoes a Mumm rearrangement towards the final Ugi product in the same manner as in reaction **path B**.[283]

Both mechanistic pathways have been examined closely in the past. For instance, the imidate was confirmed as a reaction intermediate by Faggi *et al*. in 2010, as they succeeded in isolating stable adducts before the final rearrangement step occurred.[285,286] Then, in 2012, the research group of Fleurat-Lessard utilised density functional theory computation to simulate the reaction mechanism of the Ugi-4CR.[284] Hereby, they found a mechanism that is in close accordance with the original reaction **pathway A**, which was proposed by Ugi in 1961.[282] They further found that the energetically preferred reaction pathway is highly dependent on solvent effects. **Figure 7** presents a segment of the energy diagram from the DFT calculations for the Ugi-4CR. The diagram has been simplified, as following the formation of the imidate intermediate, the reaction mechanism is in accordance with Ugi's original proposed mechanism and proceeds directly to the Ugi product *via* a Mumm rearrangement.[284] The calculations of Fleurat-Lessard *et al*. include corrections of the zero-point energy (ZPE), to account for the minimum energy that is retained in a quantum mechanical system even at absolute zero temperature (0 K).

The studies on the mechanism were performed using methanol and toluene as solvents. For example, in protic polar solvents such as methanol, no protonation of the imine occurs; instead, the imine is activated through hydrogen bonding. Moreover, when the reaction is

conducted in toluene, the nitrilium ion **3** does not form at all and also transition state **TS-2** does not exist. According to their simulations, the formation of the imidate intermediate **4** is highly exothermic and can be considered an additional energetic driving force of the reaction, alongside the Mumm rearrangement. Furthermore, due to the highly exothermic nature of this reaction step in toluene, it can also be regarded as an irreversible step. During this transition, the carbon atom of the isocyanide group is exothermically oxidised from C^{II} to C^{IV} in the resulting amide bond.

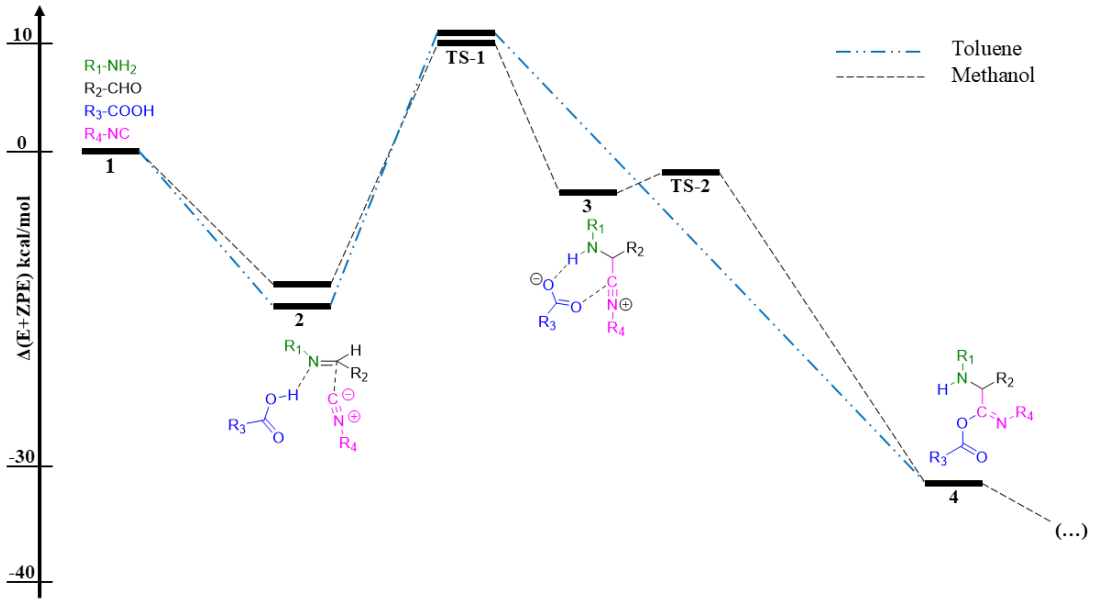

Figure 7 Section of the energy diagram of the reaction mechanism of the Ugi-4CR according to Fleurat-Lessard *et al.*[284] DFT-calculations, that include zero point energy (ZPE) corrections, were calculated at the M06-2X/6-31+G(d,p) level in toluene (blue line) and in methanol (black line).

The Ugi-4 component reaction is generally assumed to proceed non-ionically in non-polar solvents, whereas in polar protic solvents, hydrogen bonding plays a crucial role. These bonding interactions not only activate the imine, but also facilitate the Mumm rearrangement by promoting acyl transfer during the process.[272,284]

The research group of De Angelis *et al.* further investigated the mechanism using ESI-MS(/MS) measurements and concluded that Ugi's second proposed mechanism (**path B**) should be dismissed.[285] Overall, their findings align with the calculations by Fleurat-Lessard. In their ESI-MS(/MS) studies, most reaction intermediates were intercepted and structurally analysed; however, the easily ionised hemiaminal was never detected. On the other hand, their studies confirmed that the reaction proceeds *via* the nitrilium ion in the presence of polar protic solvents.[272,284,285]

Despite significant progress and new insights into the mechanism of the Ugi reaction, achieving its enantioselective execution has proven extremely challenging. According to Wang *et al*.,[264] the difficulties in performing isocyanide-based multicomponent reactions (IMCRs) in an asymmetric fashion can be summarised as follows:

First, under inappropriate reaction conditions, both the catalysed as well as the non-catalysed reaction pathway of the IMCRs compete with each other. For successful enantioselective catalysis, the non-catalysed reaction pathway must be suppressed. Secondly, chemoselective activation of the imine or carbonyl group — such as by a Lewis acid — is hindered by the presence of Lewis-basic components in the reaction mixture. The inherent complexity of multicomponent reactions, with their numerous reactants and intermediates, further complicates the control of regioselectivity and stereoselectivity. Third, organometallic catalysis in these reactions is problematic because isocyanides readily coordinate with metals. This not only reduces catalyst activity, but also depletes the available isocyanide from the reaction mixture. Fourth, the bidentate nature of the Passerini-3CR and Ugi-4CR products poses a challenge. The (organo)catalyst may become inhibited due to the kinetically unfavourable process of breaking the bidentate product-catalyst bond to form a monodentate bond with a reactant. This leads to low catalyst turnover frequencies (TOF). Finally, Wang *et al*. highlight the inherent complexity of the reaction mechanisms in multicomponent processes as a significant obstacle.[264]

The first enantioselective Ugi-4CR was reported by Bin Tan *et al*. in 2018 using chiral phosphoric acids (CPAs) as organocatalysts.[33] The CPA — with its higher acidity — outcompeted the carboxylic acid in the reaction mixture and effectively suppressed non-catalysed side reactions. Furthermore, the CPA simultaneously enhanced the nucleophilicity of the carboxylic acid in the Ugi reaction and increased the electrophilicity of the imine intermediate. This approach achieved enantiomeric excess of up to 99% and reaction conversions of up to 96%.[33] The respective catalysts are shown in **Figure 8**.

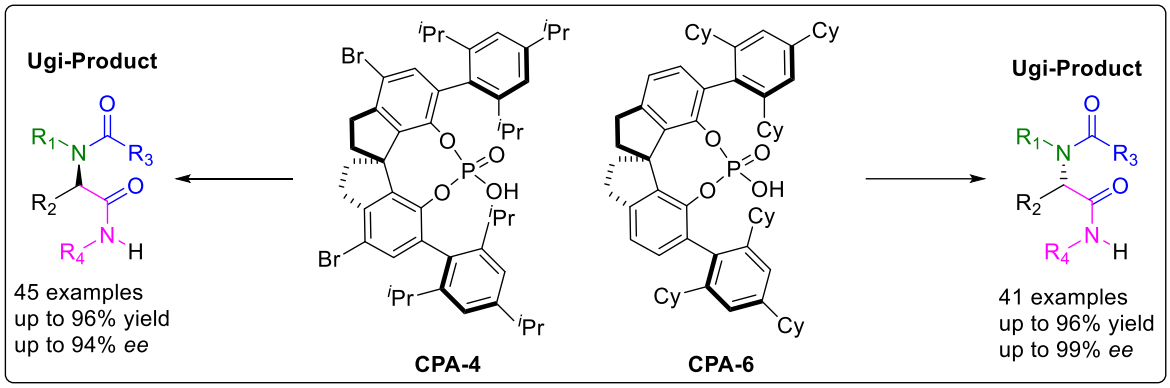

Figure 8 Chiral phosphor acid (CPA) catalysts utilised by the Bin Tan group in an enantioselective Ugi-4CR.[33]

Bin Tan's group also conducted DFT calculations, which confirmed that the α-addition on the isocyanide is the critical step of the reaction.[33,287] The study highlighted the crucial role of intermolecular non-covalent interactions in fostering stereoselectivity. For example, the cyclohexyl (Cy) groups in CPA-6 (see **Figure 8**) were shown to play a directing role for the aryl groups of the tested substrates, which leads to preferred formation of one conformation over the other in the transition state.[33,287]

The DFT calculations further revealed that the CPA catalyst first forms a heterodimer with the carboxylic acid. This heterodimer is then extended to a heterotrimer through coordination with the imine intermediate, setting the stage for the subsequent nucleophilic α-addition. The CPA catalyst acts as an organising agent within the transition state, effectively influencing stereoselectivity. Additionally, it facilitates the final Mumm rearrangement, leading to the formation of the Ugi product.[33,272]

2.3 Thiohydantoin

Since the MCR used to generate thiourea resulted in the formation of thiohydantoin in the presence of amino acid methyl esters, this chapter aims to provide a concise overview of these compounds, whose derivatives have been widely employed in medical research.

1,3-Imidazolidine-2,4-diones, also known as hydantoins, are molecules that contain a five-membered heterocycle that represents the oxidised form of imidazolidine with a cyclic urea core.[288] They further categorise a group of compounds which all contain the hydantoin substructure. The name "hydantoin" is derived from the original synthesis method utilised by Bayer AG, who synthesised them by hydrogenation of allantoin.[288] Their thio-analogue is named thiohydantoin accordingly, in which one or both carbonyl groups are replaced by a

thiocarbonyl group.[289,290] **Figure 9** shows the 1,3-diazacyclopentane core structure and its oxo- as well as thio-derivatives, and compares them to the 2-thioxoimidazolidin-4-one structure (2-thiohydantoin) and its derivatives.

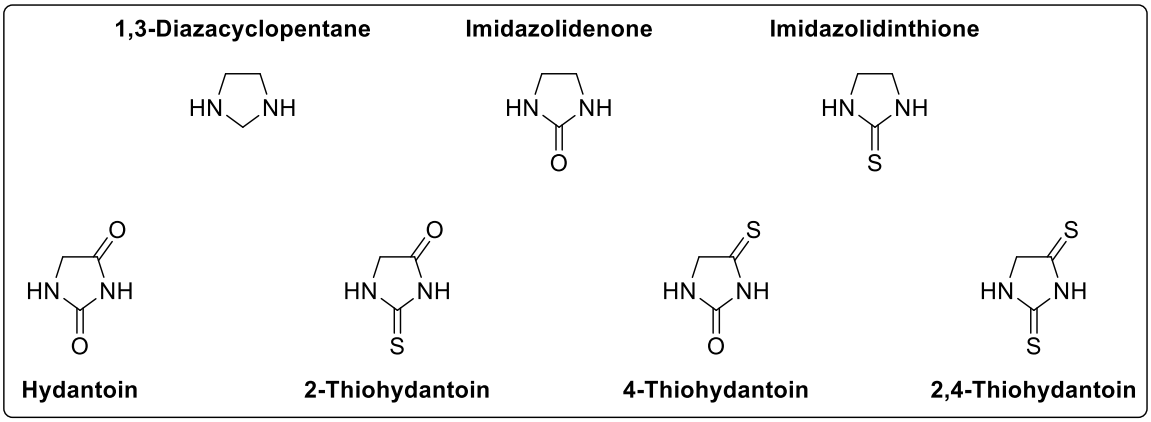

Figure 9 Illustration of the 1,3-diazacyclopentane core structure and its oxo- and thio-derivatives.[289]

The hydantoin core provides four positions that can be derivatised as well as two hydrogen-bond donor and acceptor positions each. The observed properties and activities of (thio)-hydantoins arise from the heterocyclic core and the different substituents attached to it.[291] The hydantoin and thiohydantoin structural motif is found in many products derived from nature, and due to their vast pharmacological activity, they attracted significant research interest.[292] Particularly, 2-thiohydantoin derivatives have been widely employed in pharmacological studies and have found broad application in drugs, as they exhibit antitumour activity,[293-297] antibacterial and antifungal activity,[298,299] antidiabetic and anticonvulsant activities,[300-303] anti-inflammatory,[304,305] adrenoceptor-modulating,[306-308] antiplatelet[309] and even anti-HIV activities.[310-313] Clinically approved drugs containing the (thio)hydantoin core include phenytoin,[314] mephenytoin,[315] ethotoin,[316] necrostatin-1[317] and fosphenytoin[304] as anticonvulsants; nitrofurantoin[305] and dantrium[318] as muscle relaxants; and nilutamide[319] and enzalutamide[320] as androgen receptor antagonists (see **Figure 10**).

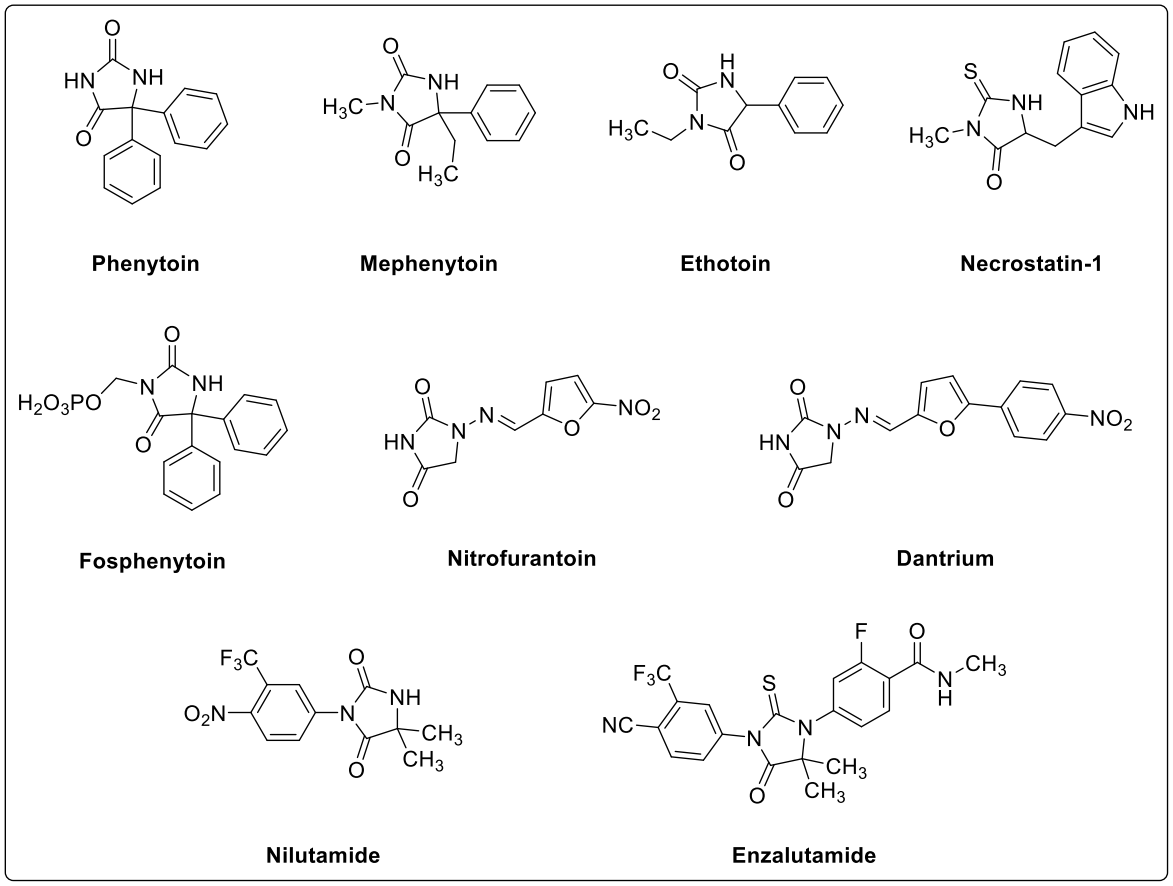

Figure 10 Selection of clinically approved drugs which contain the (thio)hydantoin structural motif.

According to Khodair *et al.*, (thio)hydantoins represent privileged scaffolds in drug discovery.[291] Furthermore, thiohydantoins are applied as reagents in herbicides and fungicides,[289] but they are also used in textile printing, in the production of resins and plastics, as catalysts for polymerisations, and in asymmetric Michael additions.[321,322] Additionally, (thio)hydantoins are applied in the cosmetic industry for skin hyperpigmentation treatments.[323] Moreover, enantiomerically pure thiohydantoins and hydantoins have been utilised as chiral auxiliaries and ligands in organometallic catalysis.[324,325]

(Thio)hydantoins can be obtained from nature, as they have been isolated from marine organisms.[326] In the literature, a multitude of methods for synthesising (thio)hydantoins are reported.[327-330] Traditional synthetic routes include Bucherer-Bergs,[331] Read,[332] and Blitz[333] reactions. Although these reactions were originally described for hydantoins, the synthesis of their thio-analogue, thiohydantoin, is carried out in the presence of thio-based reagents or by subsequent transformation of the hydantoin scaffold *via* thionation reactions

(e.g., Lawesson's method).[328,330,334] Alternatively, many synthetic routes involve approaches *via* iso(thio)cyanates to generate (thio)hydantoins.[290,328,335-340]

Other methods involve the usage of highly toxic reagents (e.g., cyanides) or harsh reaction conditions,[329] but MCRs such as the Ugi-4CR have also been reported to generate the (thio)hydantoin scaffold.[35,202,216,341] Additionally, transition-metal catalysed reactions,[342,343] microwave-assisted cyclisation reactions of carbamates[326] and flow synthesis methods have been published.[344] In 2015, Fang *et al*. described a mild method to convert enantiomerically pure thiourea and urea derivatives, which contain an amino acid group, into thiohydantoins and hydantoins, respectively.[292] This method provides an efficient way to enantioselectively synthesise (thio)hydantoins with good to high yields. Previously, racemisation had been a major issue when synthesising enantiomerically pure (thio)hydantoins.[345] The enantiomeric outcome of the reaction was highly dependent on the reaction conditions, including base addition, the chosen solvent, and the applied temperature.[292]

2.4 Coronaviruses – From discovery to modern pandemics

Since the Passerini reaction is valuable for producing bioactive peptidomimetics, investigations have been conducted, yielding Passerini-reaction-derived molecules that proved effective against coronaviruses.[346] Therefore, this chapter aims to provide a concise overview of this virus family, which has been highly prominent in the media in recent years.

On December 26, 2019, a man was hospitalised at the Central Hospital of Wuhan with symptoms including fever, chest tightness, unproductive cough, pain, and weakness that had persisted for a week.[347] An epidemiological investigation conducted by the Wuhan Centre for Disease Control and Prevention revealed that the patient had previously worked at a local indoor seafood market, where wild animals were also sold.[347,348] By late December 2019, several cases of pneumonia of unknown origin were reported in Wuhan, Hubei Province, China.[347,349] By January 3, 2020, the number of reported cases had risen to 44, prompting Chinese officials to notify the World Health Organisation (WHO).[347] On January 12, 2020, Chinese authorities announced the genetic sequence of the novel coronavirus, which was subsequently named 2019-novel coronavirus (2019-nCoV).[350]

Despite efforts to contain the virus, its spread was swift. On January 13, 2020, Thailand's Ministry of Public Health reported the first imported case. Just two days later, Japan's Ministry of Health, Labour and Welfare confirmed an imported case, followed by the Republic of Korea reporting its first case on January 20, 2020.[347,348] Within three months,

the novel virus had spread to 210 countries, with 1,727,602 confirmed cases and 105,728 deaths reported by April 10, 2020.[347] By November 12, 2024, the WHO recorded an overwhelming total of 7,074,400 deaths globally.[351]

The rapid spread of the virus was facilitated by interhuman transmission in a highly globalised world with extensive international travel, despite its zoonotic origin.[349] Many early cases in Wuhan were linked to visits to the seafood market, where the virus is believed to have originated. Initial studies on 2019-nCoV revealed that the genes of the novel virus are to 96.2% identical to bat CoV RaTG13 and that it shares 79.5% identity to previously reported SARS-CoV.[347,349,352] This distinction is attributed to mutations in its spike glycoproteins and nucleocapsid proteins, which enabled it to infect humans, even though its origin has been traced to bats.[349,353] The novel virus was later officially renamed Severe Acute Respiratory Syndrome Coronavirus 2 (SARS-CoV-2) by the Coronavirus Study Group, while the associated acute respiratory disease was designated Coronavirus Disease 2019 (COVID-19).[354]

Despite the devastating global pandemic outbreak of SARS-CoV-2, the virus is considered less pathogenic than some other members of its virus family, *Coronaviridae*, for instance SARS-CoV or MERS-CoV (Middle East Respiratory Syndrome).[355] In general, coronaviruses include a group of enveloped, positive-sense single-stranded RNA viruses within the order *Nidovirales*, which affect amphibians, birds, and mammals and can cause respiratory, enteric, hepatic, and neurological diseases of varying severity.[356,357]

The first human coronavirus (HCoV) was identified in the mid-1960s and was isolated from a person suffering from the common cold.[357] At that time, two species were detected: HCoV-229E and HCoV-OC43.[358,359] A distinctive characteristic of coronaviruses is their large genome, ranging from 27 to 32 kilobases, and their crown-like appearance under the electron microscope — a feature that inspired their name, derived from the Latin word *corona*, signifying crown or halo.[357] RNA viruses, including coronaviruses, evolve rapidly, with their evolution occurring on timescales of months or years.[360] Virus evolution notably occurs during replication in individual host cells, and mutations are disseminated through populations. Mutations are driven and constrained by natural selection. Additionally, successful transmission from one host to another introduces further complexity to viral evolution, as most mutations are propagated by chance without a selective advantage.[360]

After the identification of HCoV-229E and HCoV-OC43, it took nearly 40 years before another coronavirus was detected — one that caused severe acute respiratory syndrome (SARS).[352,361] Luckily, the aforementioned SARS-CoV was eradicated from the human

population through a highly effective global health response, which prevented its further spread.[357] Subsequently, it became evident that more coronaviruses affect humankind, and in 2004, HCoV-NL63 was identified, followed by HCoV-HKU1 in 2005.[362,363] Both of these newly identified viruses had been circulating in the human population for a long time, but were only recently discovered. Furthermore, only between 2006 and 2009, 16 new coronaviruses were detected in animals.[357] The great variety of newly discovered coronaviruses in animals underscores the urgent need for research, as zoonotic coronaviruses such as SARS-CoV (2002), MERS-CoV (2012), and SARS-CoV-2 (2019) have demonstrated the potential of this virus family to cause severe respiratory illnesses and pandemics. This highlights the necessity of vaccine and medication development to address future outbreaks and potential pandemics. Moreover, coronaviruses serve as important models for studying RNA virus evolution and recombination.

Chapter 3 Aim

The development of efficient catalysts for asymmetric synthesis is a central research area in chemistry. This study aims to explore the applicability of thiourea-based catalysts in the Passerini reaction and to optimise their stereoselectivity through systematic catalyst design studies and variation of reaction parameters. Furthermore, the study aims to provide an understanding of the thiourea-catalysed IMCRs and to pave the way for the development of more efficient catalysts in the future. The ultimate goal is to establish thioureas as effective catalysts for the asymmetric Passerini reaction, enabling the enantioselective synthesis of α-acyloxy amides with high yields. Following their successful application to the Passerini reaction, the catalytic concept will be extended to the closely related Ugi reaction, broadening the utility of thioureas as organocatalysts in the most prominent isocyanide-based multicomponent reactions (IMCRs).

IMCRs have historically posed significant challenges for achieving successful asymmetric catalysis, with only one known catalyst class thus far enabling enantioselective organocatalysis.[264,266,364] If thioureas could be established as enantioselective catalysts in these reactions, their scope of application would be greatly expanded to include the generation of diverse libraries of enantiopure substances, many of which may exhibit biological activity. This approach could address the limitations of existing catalysts, such as the CPAs developed by Bin Tan and colleagues, which have shown efficacy only with spatially demanding substrates in asymmetric Passerini reactions.[36]

Moreover, once a thiourea catalyst for the Passerini-3CR is successfully developed, its applicability will be investigated in the synthesis of potential antiviral agents targeting HCoV-229E and SARS-CoV-2. These compounds, which involve the Passerini reaction in their synthesis, would benefit from the use of enantioselective thiourea catalysts, since they would enable an investigation into how changes in diastereomeric composition influence antiviral efficacy.

To achieve these objectives, the thioureas required for this investigation will be synthesised using a route that aligns as closely as possible with the Twelve Principles of Green Chemistry.[19] If applicable, a MCR based on the method developed by Meier *et al.* will be utilised, ensuring a more sustainable and efficient approach to thiourea preparation.[41]

Chapter 4 Results and Discussion

This chapter is divided into three main sections, as follows: The first section, **Chapter 4.1 Synthesis of thiourea organocatalysts**, will focus on the synthesis of the thioureas used in this thesis. **Chapter 4.2 The asymmetric Passerini 3-component reaction** will cover investigations into the Passerini reaction in the presence of the previously synthesized thioureas. This section will provide details on their activity and selectivity, the required reaction conditions, and the possibilities and limitations of this approach. Finally, **Chapter 4.3 The asymmetric Ugi 4-component reaction** will present the initial investigations into the respective reaction.

4.1 Synthesis of thiourea organocatalysts

Many thiourea derivatives required for the subsequent catalytic screening of the isocyanide-based multicomponent reactions (Passerini-3CR and the Ugi-4CR) were synthesised according to a literature procedure of Meier *et. al.*,[41] which is based on results obtained by Al-Mourabit *et al.*,[244] extending the procedure reported by Lipp *et al.*[242] This synthesis method applies elemental sulphur, an isocyanide and an aliphatic amine in a multicomponent reaction (MCR) to form the respective thiourea at ambient to moderate temperatures, resulting in high yields under generally mild conditions.[244] The MCR approach stands out due to its simplicity and its atom economy. Additionally, highly toxic reagents can mostly be avoided or in the special case of isothiocyanates, they are only generated *in-situ*.[41] Therefore, this MCR represents a viable alternative towards typical thiourea synthesis, since other established synthetic pathways[244] often include the addition of amines to isothiocyanates,[145] thiophosgene,[365] carbon disulfide[156] and other thioacylating reagents, such as trifluoroacetic anhydride.[366]

The amines used for the thiourea synthesis were primarily chosen according to their commercial availability to facilitate the rapid generation of a small library of thiourea catalysts for the subsequent catalytic screening. Chiral amines were used to implement a chiral building block into the structure of the catalyst. Furthermore, several amines containing bulky aromatic groups were tested for their influence on the catalyst's steric properties. Moreover, (1*R*, 2*R*)-cyclohexane-1,2-diamine allowed the synthesis of bifunctional chiral organocatalysts that contain two thiourea moieties, each adjacent to the

cyclohexyl ring-structure. Further, under correctly chosen conditions, the functionalisation of only one amino group within this diamine allows for the synthesis of a bifunctional thiourea with a nucleophilic tertiary amine moiety, as established by Takemoto *et al*.[367]

This MCR approach to a more sustainable generation of thiourea organocatalysts utilises elemental sulphur, which is both non-toxic and bench-stable. Additionally, it is inexpensive, even at high levels of purity, and readily available as a by-product of the petroleum industry, with approximately 78 million metric tons produced in 2020.[368] Although elemental sulphur itself does not possess a high reactivity, it can be activated in the presence of Lewis acids or Lewis bases — such as aliphatic amines — due to their strong interaction with elemental sulphur.[244,369] The reaction can be conducted smoothly even if the isocyanides and amines used are sterically demanding.

It was further intended to implement dimethyl 5-isocyanioisophthalate as an alternative building block for thiourea organocatalysts. This aromatic isocyanide, which includes two electron-withdrawing ester groups in *meta*-position, was already introduced by Meier *et. al.,* [41] as alternative building block to the often used bis(trifluoromethyl)phenyl moiety. When comparing both electron-deficient aromatic building-blocks, the bis(trifluoromethyl)phenyl group leads to thioureas with higher H-bond-donor capabilities,[41] but one advantage of the diester as building block is its improved sustainability and tuneability regarding the ester group.[144,192] For instance, long alkyl-chains at the ester group can possibly enhance solubility of the thiourea in non-polar organic solvents.[41]

Thioureas based on the bis(trifluoromethyl)phenyl moiety have been previously recognized as containing a privileged building block, and indeed, most of the thiourea catalysts reported in the literature follow this structural motive.[198,370,371] Typically, thioureas incorporating the bis(trifluoromethyl)phenyl moiety can be synthesized by reacting commercially available bis(trifluoromethyl)phenylisothiocyanate with the respective amine.[143,372] Meier *et al.* described a procedure in which thioureas bearing the bis(trifluoromethyl)phenyl group are also synthesized *via* the MCR approach. In this method, 3,5-bis(trifluoromethyl) isocyanobenzene is generated from the corresponding formamide and used directly, without further purification, in the subsequent reaction with elemental sulphur and an amine to form the thiourea. While this method is preferable from a sustainability perspective, its practical implementation is challenging due to the high reactivity and moisture sensitivity of the isocyanide, making it laborious to handle and resulting in lower yields (26%, based on the amount of formamide used).[41] Therefore, for improved practicality and ease of handling, the

route *via* isothiocyanate was chosen to efficiently obtain various thioureas bearing the bis(trifluoromethyl)phenyl group.

In the following two chapters, the synthesis of thiourea organocatalysts is described in more detail. Either the MCR approach using elemental sulphur is employed, or the route *via* bis(trifluoromethyl)phenyl isothiocyanate is chosen.

4.1.1 Multicomponent reaction strategy for thiourea synthesis

4.1.1.1 Precursor synthesis - dimethyl 5-isocyanoisophthalate

One aim of this thesis is to implement dimethyl 5-isocyanioisophthalate as an alternative, more sustainable building block for thiourea organocatalysts. In the following section, a synthesis strategy is presented in **Scheme 8**, based on the work of Meier *et. al.*[41,144]

This synthetic strategy begins with 5-aminoisophthalic acid as the starting material. In the first step, 5-aminoisophthalic acid is converted into the corresponding methyl ester (**1**) using thionyl chloride and methanol. The resulting dimethyl 5-aminoisophthalate (**1**) is then transformed into dimethyl 5-formamidoisophthalate (**2**) through an amidation reaction with formic acid. Subsequently, a dehydration reaction is performed to convert the formamide into dimethyl 5-isocyanoisophthalate (**3**). Diisopropylamine and phosphorus oxychloride are used for this dehydration step.

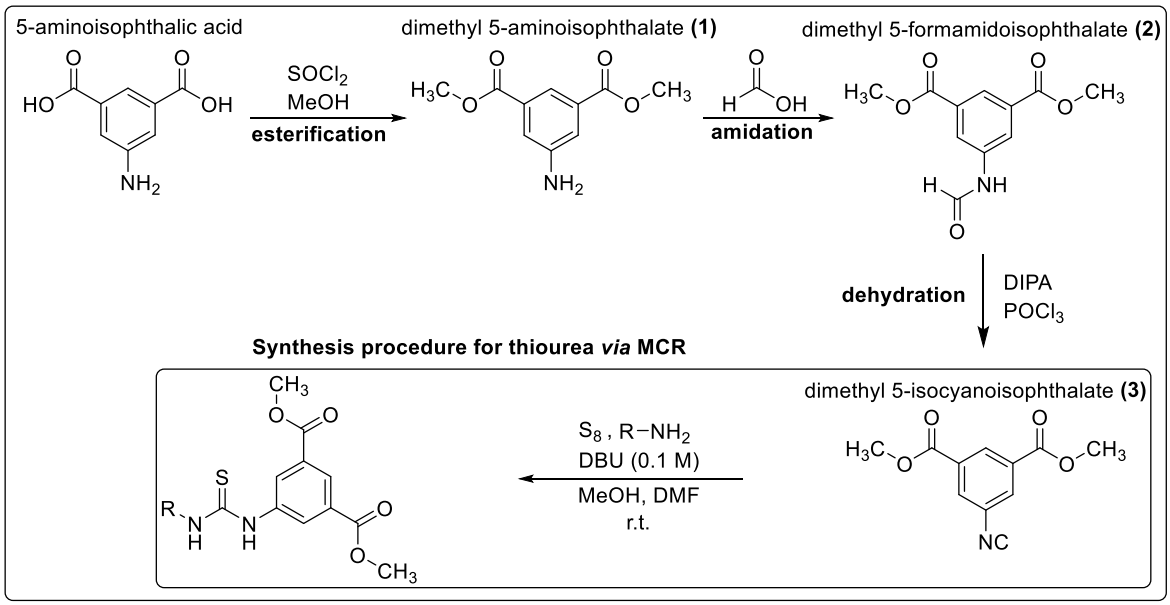

Scheme 8 Overview of the synthetic strategy to synthesise thioureas *via* the MCR approach using 5-aminoisophthalic acid as starting material. First, the precursor isocyanide is generated, and then applied in the MCR.[41,144]

Esterification of 5-aminoisophthalic acid

Dimethyl 5-aminoisophthalate (**1**) was synthesised *via* an esterification reaction following the protocol of Hosangadi *et. al*.[373] This protocol used thionyl chloride and methanol for the esterification, resulting in good chemoselectivity for aromatic carboxylic acids in the presence of aromatic amino groups.

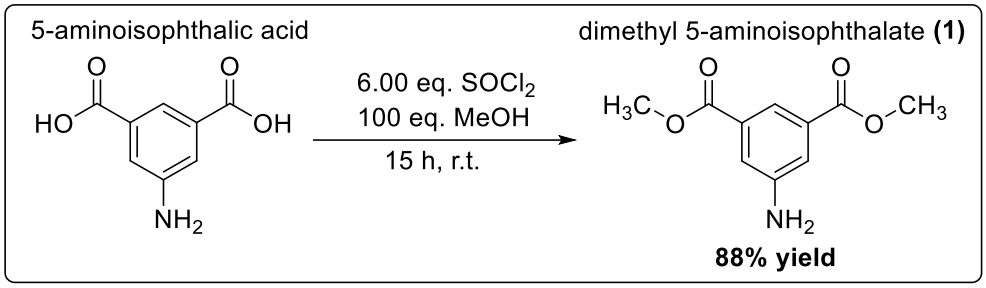

Scheme 9: Esterification reaction of 5-aminoisophthalic acid towards dimethyl 5-aminoisophthalate **(1)**.

The reaction was carried out at room temperature and stirred for 15 hours overnight. The workup included neutralizing the crude product mixture using potassium carbonate and sodium bicarbonate, which is necessary for amino-substituted aromatic esters.[373] Therefore, the pH was adjusted to 8–9. Dimethyl 5-aminoisophthalate (**1**) was obtained in a yield of 88%. Further purification steps were avoided, as the crude product had sufficient purity for subsequent reactions. Product formation und purity were proven by proton NMR analysis.

Amidation of dimethyl 5-aminoisophthalates

The second step of the isocyanide synthesis is an amidation reaction according to the synthesis protocol of Dhake *et al.*[374] using formic acid as presented in **Scheme 10**.

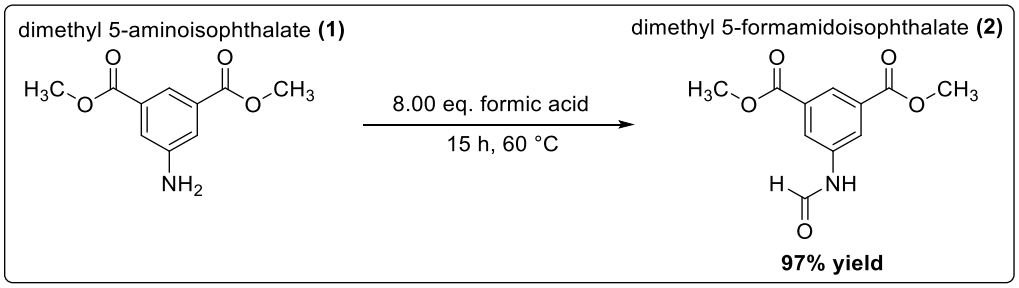

Scheme 10 Amidation reaction of dimethyl 5-aminoisophthalate **(2)** using formic acid to generate the formamide **(3)**.

The reaction was stirred for 15 hours at 60 °C. After 20 minutes, the reaction mixture solidified, making stirring impossible. Nonetheless, the reaction continued and resulted in a high yield of 97% for dimethyl 5-formamidoisophthalate (**2**). Proton NMR analysis was then used to determine the successful conversion of dimethyl 5-aminoisophthalate (**1**) to the respective amide (**2**). No further purification steps were performed after the evaporation of the excess formic acid.

This reaction procedure represents a relatively simple yet effective approach for the generation of formamides. Many different strategies for N-formylation can be found in the literature, utilising various reagents, such as chloral,[375] formic acid-EDCL,[376] CDMT[377] or KF-alumina and other solid-supported reagents.[378,379] As summarised by Rahman *et al*.,[380] these methods include the application of toxic or expensive reagents and many methods lead to several by-products or are only suitable for aromatic amines. Both Rahman and Dhake found that it is possible to only use formic acid in slight excess (1.20 – 1.50 eq.) at elevated temperatures (60 – 80 °C) to convert the amine into the formamide.[374,380] The method used for formylation is generally well suited for aromatic, alicyclic and aliphatic amines and led to good to excellent yields, while not affecting many other sensitive functionalities.[380] Since electron-donating groups in aryl amines were found to enhance the effectiveness of the reaction[380] and ester substituents are moderately deactivating, the reaction of dimethyl 5-aminoisophthalate (**1**) with formic acid was conducted overnight for 15 hours until full conversion was achieved. The reactions were monitored *via* TLC analysis.

Dehydration of dimethyl 5-formamidoisophthalates

In the final step of the precursor synthesis, the isocyanide was generated by dehydration of the respective dimethyl 5-formamidoisophthalates (**2**), following the reaction protocol of Nickisch *et. at*.[41,144] An overview of the reactions is provided in **Scheme 11**. In the previous

two reaction steps, purification by column chromatography was avoided. However, after this final step in the synthesis of isocyanides, final purification was achieved only after column chromatography, resulting in a yield of 62% of the respective isocyanide (**3**) in the final reaction step.

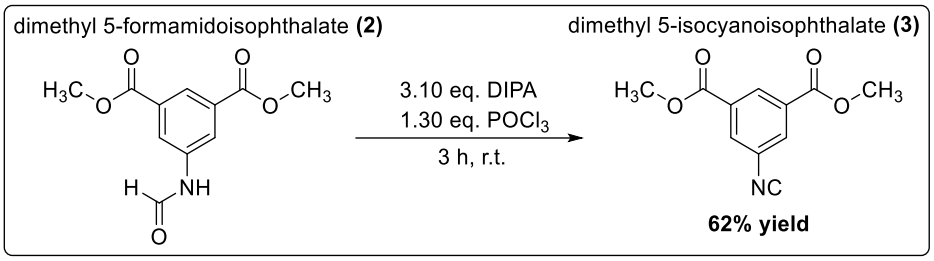

Scheme 11: Dehydration reaction of dimethyl 5-formamidoisophthalate **(2)** using phosphor oxychloride as dehydration agent to generate the respective isocyanide **(3)**.

Recent progress toward synthesising isocyanides in a more sustainable manner was reported by Meier *et. al*.[155] They compared different known methods for generating isocyanides from various *N*-formamides and found that 4-methylbenzene-1-sulfonyl chloride (*p*-TsCl) is a superior dehydrating agent compared to phosphorus oxychloride in terms of green chemistry.[155] *p*-TsCl is also easier to handle due to its lower reactivity, while still producing comparably high yields. Unfortunately, this promising procedure is limited to aliphatic formamides, as high yields were not obtained for sterically demanding or aromatic formamides.[41,155] As a result, the standard procedure using phosphorus oxychloride was employed here to dehydrate the formamide, yielding the respective isocyanide with a yield of 62%. Considering the three reaction steps, an overall yield of 53% was achieved for isocyanide (**3**) after final purification *via* column chromatography.

4.1.1.2 Synthesis of thioureas *via* the MCR

Subsequently to the precursor synthesis, a small library of thioureas was generated using the two aforementioned reaction pathways. For the first pathway, an overview is given in **Scheme 12**. The MCR approach is based on the synthetic protocols from Al-Mourabit *et al.*[244] and Meier *et al*.[41]

Scheme 12: Multicomponent reaction for thiourea synthesis using elemental sulphur, an amine and an isocyanide.[41,244]

According to Al-Mourabit *et al.*, the multicomponent reaction leading to the thiourea catalysts is initiated by the activation of elemental sulphur by the aliphatic amine **[b]**.[244] The proposed reaction mechanism is presented in **Figure 11**.

The reaction mechanism starts with the activation of elemental sulphur by the amine **[b]**. This initial step results in the formation of a zwitterionic ammonium polysulfide chain **[d]**. The chain length is not fixed and is influenced by factors such as temperature, concentration, and the sulphur-to-amine ratio.[244] The zwitterionic form **[d]** of the ammonium polysulfide chain coexists with its neutral form **[d']**. The negatively charged species is highly nucleophilic due to the combined effects of the anionic charge and the alpha effect of the polysulfane chain. The reaction can then proceed either *via* a concerted pathway or *via* a stepwise pathway, as shown in **Figure 11**. In both cases, the carbenoid carbon atom of the isocyanide is attacked by the nucleophilic zwitterionic ammonium polysulfide chain, leading ultimately to the formation of thiourea **[c]**. Additionally, the reaction releases a cyclic polysulfide with one fewer sulphur atom as a byproduct of thiourea formation.

In the stepwise pathway, an intermediate isothiocyanate **[e]** is formed, which subsequently reacts with an amine in the reaction mixture to yield thiourea **[c]**. Alternatively, a reaction pathway described by Al-Mourabit *et al.* suggests that the initiation step involves nucleophilic addition of the isocyanide **[a]** to elemental sulphur, leading to the formation of a nitrilium intermediate **[f]**. The nitrilium then reacts with an amine, resulting in the desired thiourea **[c]**.[244]

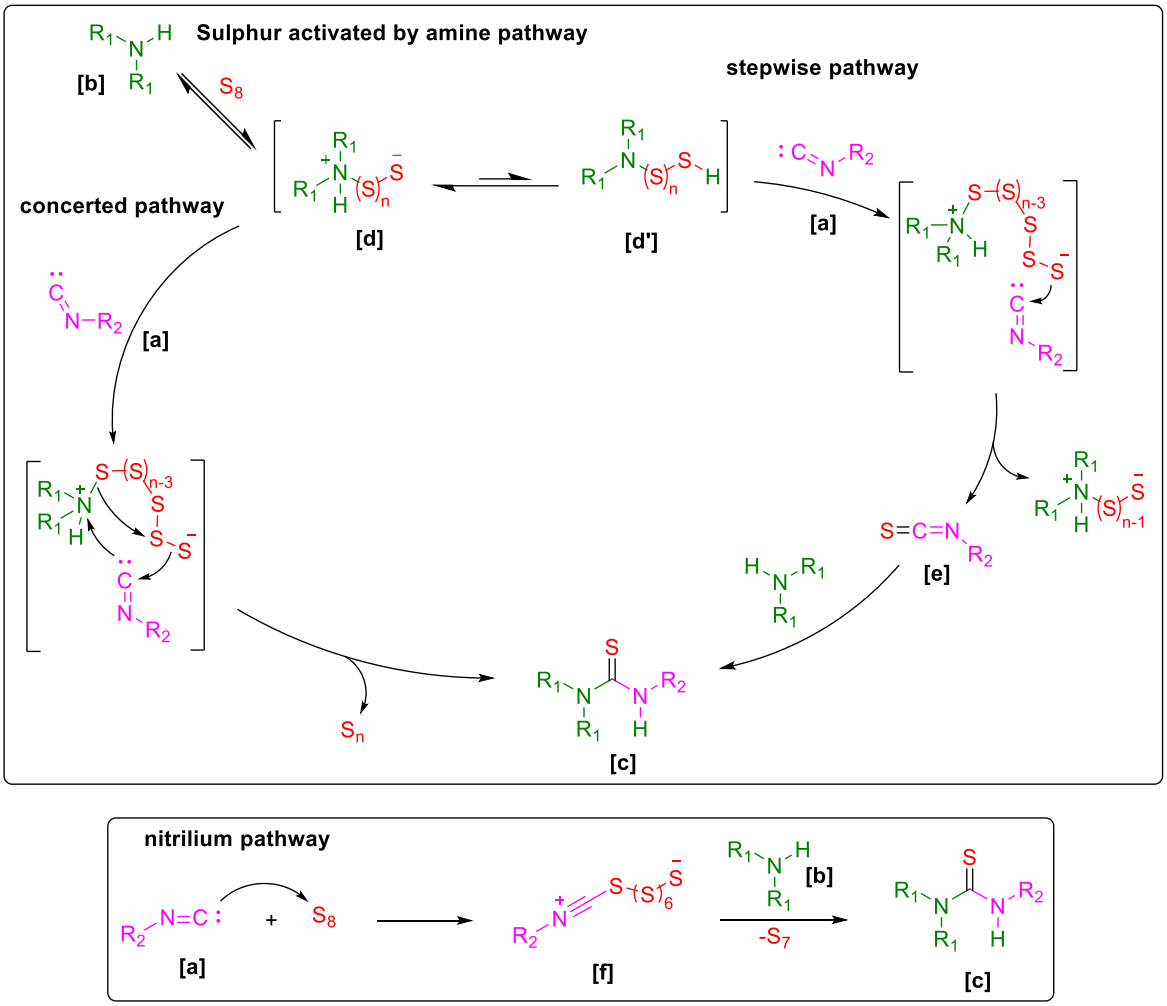

Figure 11 Proposed mechanism of the multicomponent reaction, which leads to the formation of thioureas, according to Al-Mourabit *et al.*[244]

In **Figure 12**, a selection of thioureas is presented, synthesised *via* MCR procedure, and later employed in the catalytic screening of isocyanide-based MCRs.

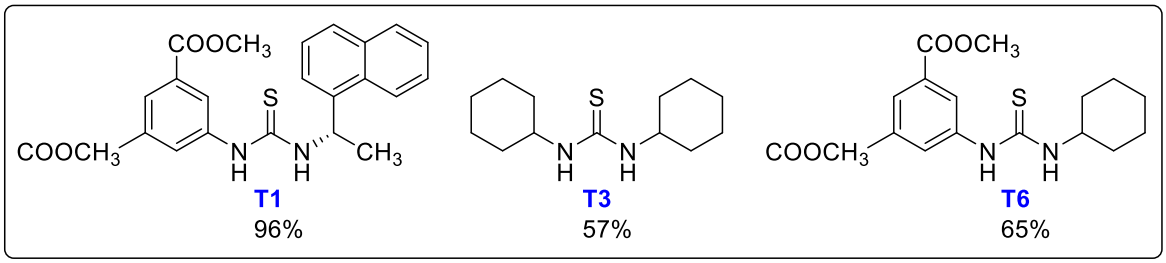

Figure 12 Overview of the thioureas synthesised *via* a multicomponent reaction using elemental sulphur, an amine, and an isocyanide. The thioureas are ordered according to their use in the catalytic screenings. An overview which includes all synthesised thioureas is given in **Figure 19** and **Figure 20** in **Chapter 4.2.1.3**. The respective yields from their synthesis are shown below their labelling. Detailed reaction conditions are shown in **Chapter 6 Experimental**.

Using this multicomponent reaction, yields of up to 96% — in the case of thiourea **T1** — were achieved. Since dimethyl 5-isophthalate (**3**) was poorly dissolved in methanol, dimethyl formamide (DMF) was added to the reaction mixture as a co-solvent, producing a homogeneous mixture and resulting in a concentration of the mixture of 1 M for the isocyanide. Typically, multicomponent reactions benefit from higher concentrations.[212] Moreover, Nickisch *et al*. reported that the reaction is also feasible in bulk, which could enhance its sustainability.[144] However, these reaction conditions were sometimes problematic due to restricted stirring and reactant solubility and were therefore avoided.[144]

In the MCR, the other reactants were used in minimal excess, sulphur in 1.12 equivalents, corresponding to the required amount of sulphur atoms, and the respective amine in 1.10 equivalents, which proved sufficient to achieve high yields.[41,144] Elevated temperatures were largely unnecessary, as full conversion was typically achieved at room temperature.

The non-nucleophilic organobase 1,8-diazabicyclo[5.4.0]undec-7-ene (DBU) was added at a concentration of 0.1 M to activate sulphur and start the reaction, if the amine used in the reaction was insufficient for effective sulphur activation. The activation of sulphur is often visually noticeable, as the reaction mixture turns a dark brown colour.[381] After the addition of DBU, a colour change occurred immediately.

For **T6**, purification by column chromatography may have led to product loss. **T3** was obtained by precipitation, and it is likely that some product remained in the liquid residue. Further attempts to recover more product were not carried out. Additionally, no DBU catalyst was used in the synthesis of **T3**, and the reaction was conducted in bulk. After full addition of all reactants, the meanwhile solidified reaction mixture was dissolved in ethanol. The mixture was then kept stirring overnight while the product precipitated.

4.1.2 Synthesis of thiourea *via* bimolecular reaction

Thioureas containing the bis(trifluoromethyl)phenyl moiety were prepared *via* a bimolecular reaction between the commercially available bis(trifluoromethyl)phenylisothiocyanate and the respective amine as shown in **Scheme 13**.

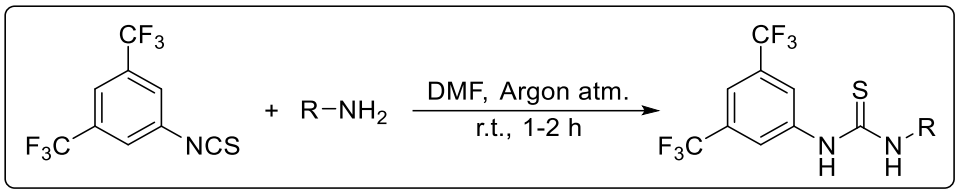

Scheme 13 Overview of the reaction conditions applied to synthesise thioureas bearing the bis(trifluoromethyl)phenyl moiety. The detailed reaction conditions are presented in **Chapter 6 Experimental**.

The reaction proceeds through the nucleophilic addition of the amine to the electrophilic carbon atom in the isothiocyanate structure. This results in the formation of a zwitterionic intermediate, which then undergoes an amine-catalysed prototropic rearrangement, yielding the thiourea product, as shown in **Figure 13**.

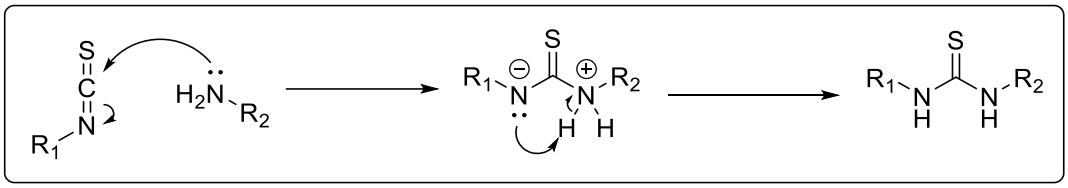

Figure 13 Proposed reaction mechanism of the bimolecular thiourea synthesis according to Satchell *et al.*[382]

The thioureas prepared in such manner are presented in **Figure 14**. Generally, the method is well suited to synthesise a great variety of thioureas with synthetic simplicity. Moderate to high yields were obtained (compare **Table 1**). The reactions were carried out in DMF at a concentration of 0.5 M with regard to the amine and under an inert argon atmosphere. Typically, the reaction proceeded fast within 1 - 2 hours at room temperature to nearly full conversion according to TLC monitoring. Since thioureas usually represent bench-stable and non-sensitive compounds, the purification of the crude product was mostly carried out the next day after overnight stirring of the reaction mixture. In the case of **T12,** difficulties to separate the product from the non-reacted starting materials occurred during the purification process. π-π – staking interactions between the thiourea and the non-reacted reactants might have caused the difficulties and therefore, lower yields were obtained after column chromatography, as shown in **Figure 14**.

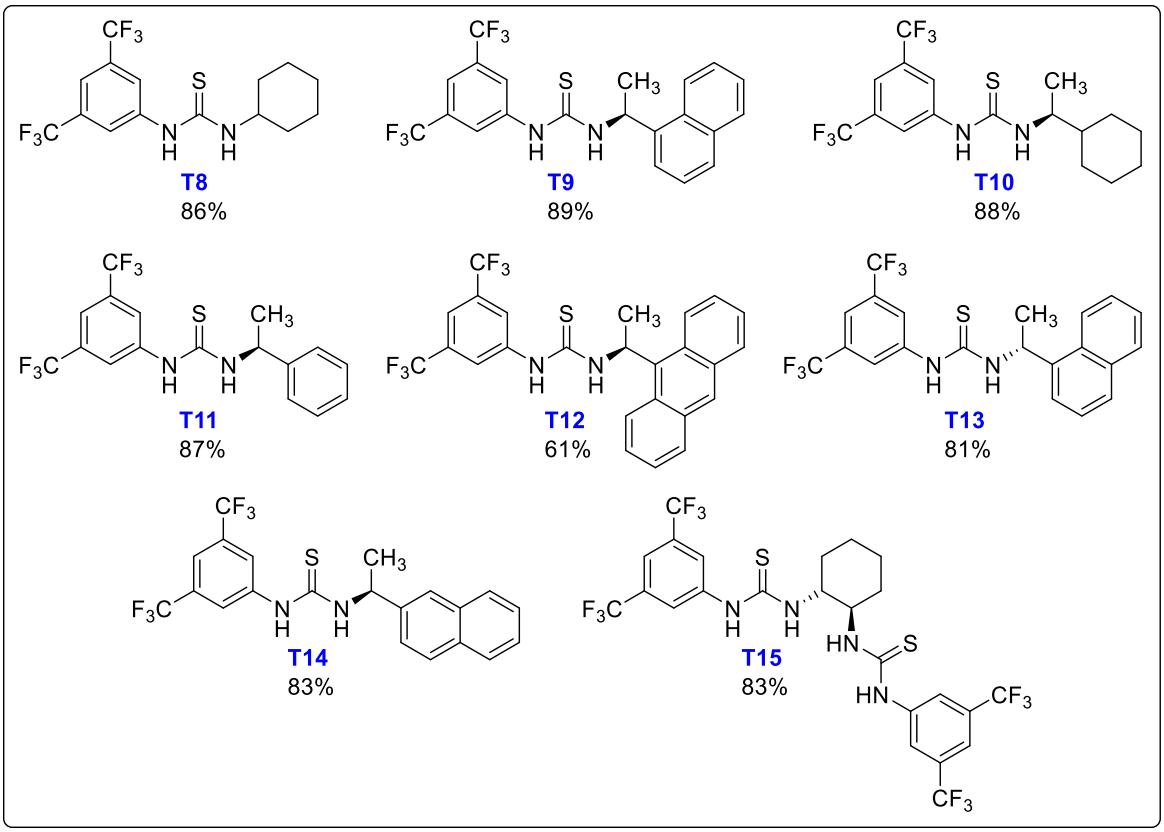

Figure 14 Set of thioureas that were synthesised through the reaction between an isothiocyanate and an amine. All reactions were conducted at room temperature with 1.10 eq. of bis(trifluoromethyl)phenylisothiocyanate as reactant and with 1.00 eq. of the respective amine in dimethylformamide (DMF) with a concentration of 0.5 M in regard of the isothiocyanate and under an argon atmosphere.

4.1.3 Novel MCR approach for thiohydantoin synthesis

This chapter is based on results by Simon Werling and Felix Lukas. The practical course "Vertiefungspraktikum" of Simon Werling and the bachelor thesis of Felix Lukas were both co-supervised by the author of this thesis. In each case, the objective was to perform preliminary investigations towards a more sustainable synthesis of thiohydantoins *via* a multicomponent reaction. The author of this thesis developed the synthetic procedures, planned the experiments, and assisted in evaluating the results. This chapter provides a brief overview of the synthetic procedure, and a concise summary of the findings.

Originally, it was anticipated that amines derived from chiral pool compounds would be chosen for the synthesis of thioureas.[137] The incorporation of naturally occurring amino acid-derived amines into the catalyst structure is motivated by the aim of employing more sustainable chiral building blocks to enhance the overall sustainability of the synthesis of the catalysts.
In this context, methyl *L*-tryptophanate, derived from the chiral pool compound *L*-tryptophan, exemplifies this strategy.

Thus, the synthesis of thiourea **4** was attempted; however, instead of the anticipated thiourea formation, an intramolecular ring-closing process occurred during the reaction, yielding the corresponding thiohydantoin **5**, as shown in **Scheme 14**. Many attempts to synthesise a thiourea incorporating α-amino acid methyl esters using the elemental sulphur-based multicomponent reaction were carried out and proved impractical. It is assumed that the intermediate thiourea product consistently underwent an intramolecular ring closure, forming thiohydantoin each time. Still, this outcome presents a promising approach of generating thiohydantoins through a multicomponent reaction without the use of toxic sulphur-transfer agents such as thiophosgene, its derivatives, or carbon disulphide.[383]

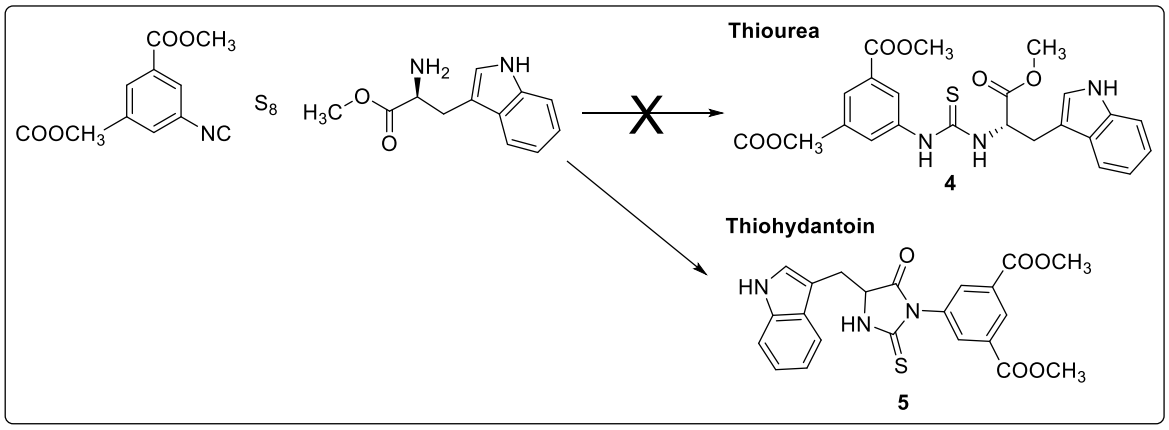

Scheme 14 The MCR of elemental sulphur, dimethyl 5-isocyano isophthalate and methyl *L*-tryptophanate resulting in a thiohydantoin compound instead of the targeted thiourea.

The assumed ring-closing reaction that generates thiohydantoin could proceed through two plausible mechanisms. To simplify the investigation into reaction optimization, more simple reactants were chosen. **Scheme 15** illustrates the reaction between dodecyl isocyanide, elemental sulphur, and methyl *L*-leucinate, selected for the screening setup.:

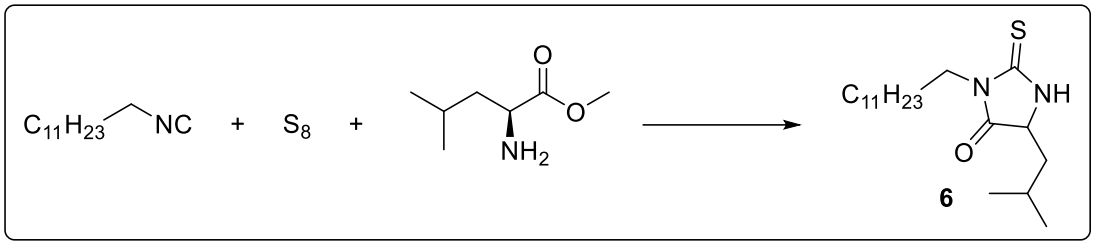

Scheme 15 Model reaction of the optimisation of the reaction conditions aiming for a more sustainable thiohydantoin synthesis *via* a MCR approach. The reaction involves dodecyl isocyanide, elemental sulphur and methyl *L*-leucinate as reactants.

Scheme 16 shows the first suggested mechanism using these reactants, which involves the formation of a thiourea as an intermediate. Subsequently, the carbonyl carbon atom is attacked intramolecularly, resulting in the elimination of methanol as the ring closes, forming thiohydantoin.[321]

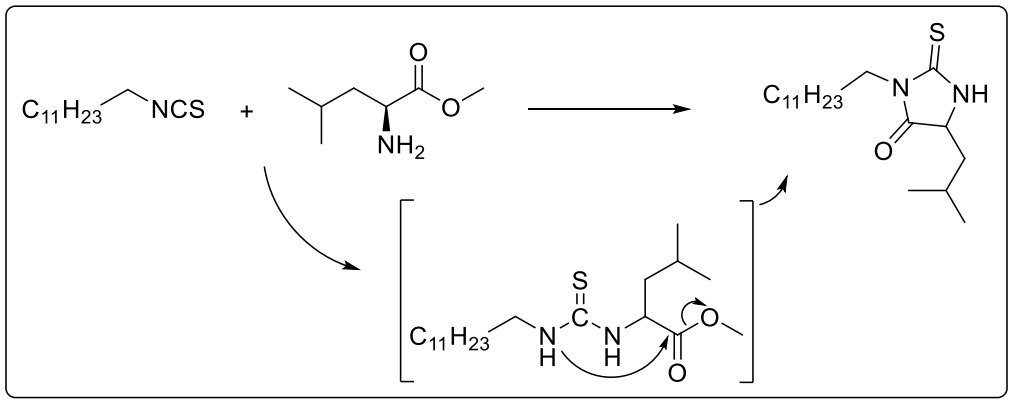

Scheme 16 Depiction of one plausible reaction mechanism for thiohydantoin formation according to Juaristi *et al.*[321] To present a more streamlined mechanism, the reaction is shown starting from the isothiocyanate intermediate rather than the isocyanide, as the MCR generates the isothiocyanate as an intermediate.

The second plausible reaction mechanism is shown in **Scheme 17**. This pathway occurs according to the literate known Edmann-degradation and also includes the formation of a

thiourea intermediate. However, in this case the sulphur atom of the thiourea moiety intramolecularly attacks the ester group, generating an isothiourea, which can subsequently undergo a rearrangement reaction to form thiohydantoin.[321,384,385] The rearrangement reaction depends on the chosen reaction conditions, but under prolonged reaction times the thiohydantoin was described to be the dominant product.[321]

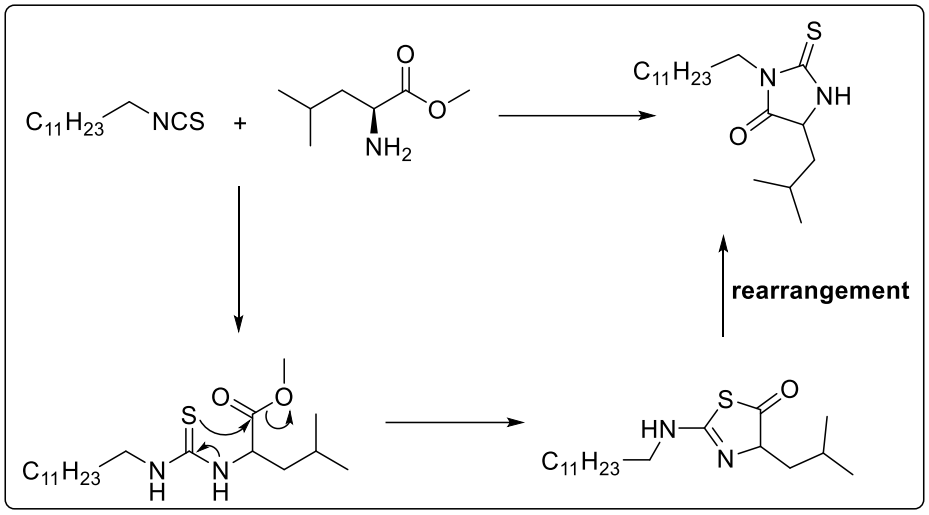

Scheme 17 Second plausible reaction mechanism of the thiohydantoin formation. This reaction mechanism is described according to the Edman-degradation.[321]

Notably, in both illustrations of the reaction mechanisms, the final thiohydantoin product is shown without stereochemical information, even though the starting amino acid methyl ester is a chiral compound. The formation of the heterocycle likely leads to racemization of the thiohydantoin product. This assumption is based on a procedure described by Fang *et al*., in which a similar thiohydantoin ring-closing reaction under comparable conditions (polar aprotic solvent and base) resulted in 90% enantiomeric excess *(ee*) at -60 °C, but only 14% *ee* at -20 °C.[292] The original screening method for optimising reaction conditions was carried out at slightly elevated temperatures (40 °C). Furthermore, according to Fang *et al*., achieving significant enantiomeric excess requires very strong bases, such as sodium hydride (NaH).[292,386]

The initial attempt to synthesise a thiohydantoin followed a two-step synthetic procedure, as illustrated in **Figure 15**. The primary objective was to produce a sufficient quantity of thiohydantoin **6** to establish a calibration curve for GC analysis, enabling reaction monitoring of optimisation screenings. Moreover, this two-step procedure was used as a comparative approach to evaluate the advantages of the MCR method. Additionally, it

benefited from prior investigations by the Meier group, which developed a more sustainable synthesis of isothiocyanates.[383]

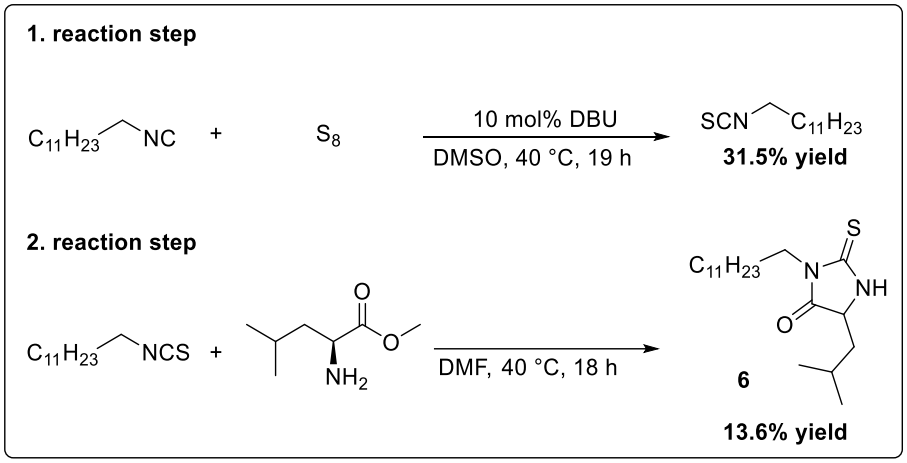

Figure 15 Overview of the initial two-step procedure for thiohydantoin synthesis. Equimolar amounts of reactants were used in both reaction steps. In the first step, dodecyl isocyanide is converted to the corresponding isothiocyanate following a modified procedure from Meier *et al.*[383] In the second step, thiohydantoin is synthesised under the same conditions in which the ring-closing towards thiohydantoin was initially observed.

Each step required purification *via* column chromatography, resulting in significant waste generation and increased labour. First, dodecyl isocyanide was converted to the corresponding isothiocyanate following a literature-described procedure.[383] Unfortunately, only 32% yield were achieved, compared to 87% yield reported under similar conditions.[383] The literature method employed Cyrene® as the solvent, while DMSO was used in this work as a polar aprotic alternative.

In the next step, the isothiocyanate was reacted with methyl *L*-leucinate in DMF to yield the thiohydantoin **6** with a yield of 14%. Overall, this multistep approach produced a total yield of 4.3%. The unexpectedly low yield was surprising, as reactions between isothiocyanates and amino acid methyl esters are well-established in the literature for thiohydantoin synthesis.[328,387] The low yield motivated the development of a multicomponent reaction approach as an alternative. The primary focus was on enhancing the yield, followed by simplifying the procedure, improving sustainability, and avoiding the use of toxic, highly reactive isothiocyanates by generating them *in situ*.

The multicomponent reaction approach was subsequently investigated using equimolar ratios of the reactants and the organobase 1,8-diazabicyclo[5.4.0]undec-7-ene (DBU) to accelerate the reaction in the initial attempt. The optimisation focused on several reaction

conditions, including solvent choice, base selection, temperature, concentration, and catalyst concentration. After multiple screenings to improve the sustainability of the MCR, following the solvent and base guides provided by GSK, the following conditions — which are summarised in **Scheme 18** — were identified.[388-390]

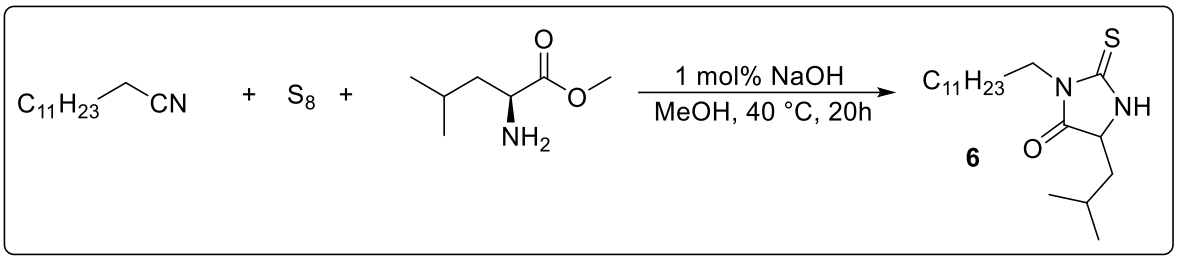

Scheme 28 Overview of the optimised reaction conditions for a synthetic MCR approach towards thiohydantoin.

The procedure presented here represents a clear improvement over the earlier two-step synthesis with its low yield, though it still leaves room for further optimization. The solvent was switched to methanol, which presents fewer environmental concerns than DMSO or DMF according to the GSK solvent selection guide.[388,390] Additionally, methanol's lower boiling point allows for easier removal from the product, unlike the higher-boiling DMF or DMSO. The thiohydantoin product was observed to precipitate rapidly from methanol at lower temperatures (-20 °C) or at high concentrations, enabling easier purification and significantly reducing waste compared to chromatographic purification methods. Furthermore, a more sustainable base catalyst, NaOH, was identified to replace DBU.[389] The reaction proceeds efficiently with NaOH at a low concentration of 1 mol%. Yields up 61% were obtained *via* the MCR approach — a substantial improvement over the initial system. In conclusion, a reaction procedure with satisfactory yields was identified, avoiding the use of toxic sulphur-transfer agents and generating isothiocyanates *in situ*. Future research should focus on improving the overall yield of this reaction while maintaining its mild conditions and environmentally friendly reagents. Additionally, the versatility of this novel approach can be further validated by screening a range of isocyanides and amino acid methyl esters for thiohydantoin synthesis.

4.1.4 Chapter summary – Synthesis of the thiourea catalysts

A selection of thioureas was synthesised for subsequent catalytic screening. A more sustainable synthetic approach *via* a multicomponent reaction to generate a variety of thioureas was used where possbile.[41] If the MCR was not feasible, the respective thioureas were obtained instead by a straightforward bimolecular reaction between isothiocyanates and amines. While this bimolecular approach with commercially available reactants provided a quick and efficient synthesis method, the MCR represents a more sustainable alternative. For instance, it avoids the use of highly hazardous reagents, producing toxic isothiocyanates only *in situ*.[41] Furthermore, it was demonstrated that this MCR, involving elemental sulphur and isocyanides, could also be adapted to synthesise thiohydantoins when the usual amine is replaced with an amino acid methyl ester. This reaction was optimised to enable the synthesis of thiohydantoins in a straightforward procedure, achieving yields of up to 61%. Nonetheless, the versatility of this reaction procedure remains to be further demonstrated.

4.2 Investigation into the asymmetric Passerini-3CR

This chapter provides a concise summary of the results from investigations into the Passerini three component reaction in the presence of thioureas as organocatalysts. Initial screenings revealed that thioureas are notably effective in catalysing the Passerini-3CR. The focus then shifted towards the asymmetric conduction of the Passerini reaction, prompting a detailed investigation. First, a design study of thioureas as organocatalysts was conducted to gain insight into their mode of action, specifically how they influence the stereo induction in the reaction mechanism. Subsequently, attention was given to optimizing reaction conditions to enhance catalyst performance. Finally, a substrate screening was performed to assess the scope and limitations of this organocatalytic approach.

A special thanks go to Aaron Seider, who, under the co-supervision of the author of this thesis, contributed significantly to the experimental work related to the substrate scope of the thiourea-catalysed Passerini-3CR (see **Chapter 4.2.4.2**). This work was performed during his role as an assistant researcher at the Institute of Organic Chemistry (IOC) at KIT. The author of this thesis was responsible for supervising the project, planning the experiments, and evaluating the results.

4.2.1 Initial screening and design study of thiourea organocatalysts

4.2.1.1 The model reaction and analytical methods

The Passerini-3CR is a reaction that proceeds smoothly even under non-optimal uncatalysed reaction conditions, making it highly challenging to outperform this *via* a catalytic pathway.[266] Therefore, the model reaction was intentionally designed to yield comparatively low outputs and overall poor performance. For instance, the reaction rate can be influenced by factors such as the reactant concentration, choice of solvent, temperature, or stoichiometry, to name a few. This ensures that the catalytic effects are visible, as the catalytic reaction pathway consistently competes with a non-catalysed reaction pathway that remains unaffected by the catalyst.[36] For the initial screening, a model reaction incorporating acetic acid, octanal, and benzyl isocyanide was selected for investigation (see **Scheme 19**). The reactants were used in equimolar ratios.

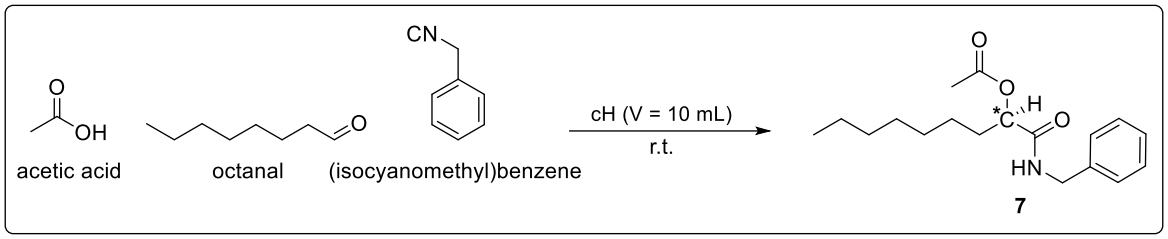

Scheme 19 Model reaction for the screening of the Passerini-3 component reaction. The reaction was conducted in cyclohexane with a concentration of 0.025 mol×L^{-1}.

The reactions were conducted at room temperature using cyclohexane as solvent with a concentration of 0.025 mol* L^{-1}. Typically, Passerini-3CR are conducted in high concentration in polar aprotic solvents (compare **chapter 2.2.2**) such as dichloromethane, tetrahydrofuran, ethyl acetate or diethylether.[261] Cyclohexane, a non-polar aprotic solvent, was deliberately chosen to avoid optimal reaction conditions and to prevent interference with the hydrogen bonding of a potential thiourea catalyst due to protic solvent conditions.[198] The standard reaction procedure for the investigation of the Passerini-3CR used the aforementioned reaction conditions and was conducted as follows: Tetradecane, the internal standard — a substance inert under the reaction conditions, which allows for screening and quantification *via* gas chromatography — was weighed into a 10 mL crimp-vial. Tetradecane, being a liquid, was added using a micropipette. If deviations between the intended and actual mass of the internal standard occurred, a correction factor k_c was calculated and applied during the calculation of the concentration of the Passerini product at a given reaction time. Subsequently, a thiourea catalyst was added to the vial, followed by dilution with 10 mL of cyclohexane. The aldehyde was then added, and the mixture was stirred for 5 minutes to ensure homogeneity. A first sample was taken using a micropipette, serving as the t_0-sample, to monitor the conversion of the aldehyde over time.

Next, the carboxylic acid was added, and the mixture was again stirred for 5 minutes to ensure homogeneity. The isocyanide was then added, followed by another t_0-sample — this time to monitor the conversion of the isocyanide. After the isocyanide addition, the vial was sealed, and the reaction was stirred at room temperature. The first sample for GC analysis was taken after two hours of reaction time, with additional samples taken at 20 and 44 hours. The reaction mixture was then quenched by dilution with ethyl acetate, and the solvent was evaporated until the volume was reduced to 1.5 mL. The resulting mixture was then purified directly by column chromatography to obtain the pure product.

The Passerini reaction forms a single stereogenic centre (respective carbon atom is highlighted as **C*** in **Scheme 18**) during the nucleophilic α-addition of the isocyanide on the aldehyde. The aim is to influence this reaction step asymmetrically through interaction with chiral thiourea organocatalysts. To quantify the effectiveness of such a thiourea catalyst, the obtained Passerini products were subjected to chiral HPLC analysis, which provides the enantiomeric excess (*ee*) of one of the resulting enantiomers.

For monitoring of the conversion and yield of the reaction, gas chromatography was used as analytical tool. Therefore, a calibration curve of the Passerini product 1-(benzylamino)-1-oxononan-2-yl acetate **7** was created using the internal standard (IS) tetradecane. The calibration curve enables the analysis of multiple reactions without the requirement of prior purification of the crude product *via* column chromatography, thereby saving both time and resources. Six samples of varying concentrations were measured three times each by GC to establish the calibration curve.

Each sample contained different amounts of the Passerini product but a constant amount of the internal standard. Tetradecane provided high signal intensity per substance amount when detected by a flame ionization detector (FID), which was used as detector in the GC analysis. For each sample, specific volumes of stock solutions of both the Passerini product and the IS in ethyl acetate were added to a measuring flask and further diluted with ethyl acetate to a total volume of 1.5 mL. The exact composition of each sample and the corresponding GC analysis results are summarised in **Table 1**. The resulting calibration curve is shown in **Figure 16**.

The GC analysis yielded different ratios of the area values for the Passerini product ($A_{Passerini}$) and the internal standard (A_{IS}) for each sample. The arithmetic mean ($\bar{X}$) of the area ratios was calculated based on three measurements for each sample.

Table 1 Sample preparation for GC calibration

sample	$\frac{n_{Passerini}}{n_{IS}}$	$c_{Passerini}$ $\left[10^{-3}\frac{mol}{L}\right]$	c_{IS} $\left[10^{-3}\frac{mol}{L}\right]$	$\frac{c_{Passerini}}{c_{IS}}$	$\overline{X}\left(\frac{A_{Passerini}}{A_{IS}}\right)$
1	1.40	4.70	3.36	1.40	1.480
2	1.20	4.03	3.36	1.20	1.314
3	1.00	3.36	3.36	1.00	1.015
4	0.80	2.69	3.36	0.80	0.807
5	0.60	2.02	3.36	0.60	0.608
6	0.40	1.34	3.36	0.40	0.399
7	0.30	1.01	3.36	0.30	0.288
8	0.20	0.67	3.36	0.20	0.208
9	0.10	0.34	3.36	0.10	0.103

Each sample contained a constant concentration of the internal standard tetradecane and varying concentrations of the Passerini product (**7**). The resulting signal ratios in the chromatograms, corresponding to these different concentrations, are represented by the arithmetic mean ($\overline{X}$) calculated from three measurements for each sample.

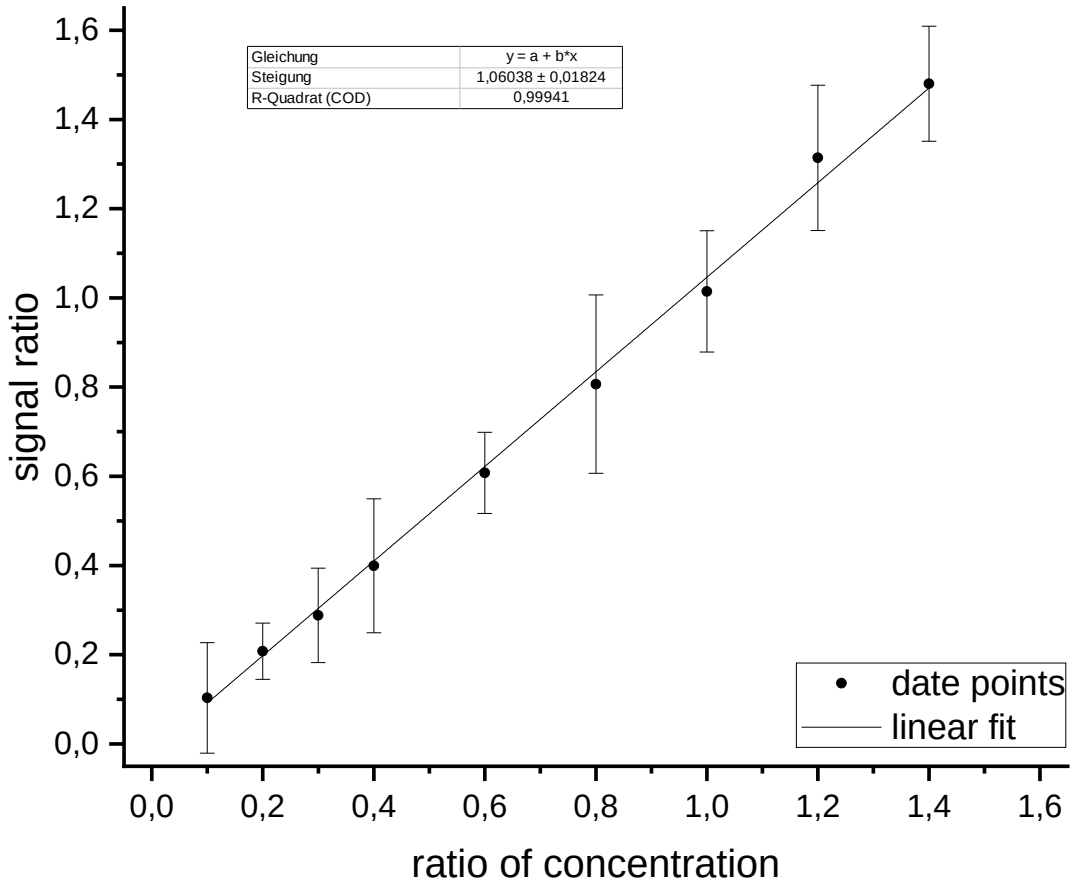

Figure 16 Calibration curve of the Passerini product (**7**) using an internal standard (IS). The curve was generated by applying a linear fit through the origin, based on nine measured data points. Each sample was measured three times, and the arithmetic mean ($\overline{X}$) was used to construct the calibration curve.

The measured samples fitted the calibration well and the deviations were marginal, resulting in a high coefficient of determination (COD) of 0.99941. The COD quantifies the degree of linear correlation, with a value of 1.0 indicating that the data is perfectly represented by the regression line. With the calibration established, the concentration of the Passerini product in an unknown sample $c_{Passerini}$ can now be determined using equation *Eq. 2*:

$$c_{Passerini} = \frac{(k_c * c_{IS}) * \left(\frac{A_{Passerini}}{A_{IS}}\right)}{s} \qquad \textit{(Eq. 2)}$$

$k_c =$ The correction factor for the internal standard accounts for minor deviations between the intended and actual mass during the weighing process. This factor is calculated by dividing the measured mass of the internal standard by its intended mass, ensuring the signal ratio is adequate to the concentration ratio.

$c_{IS} =$ The concentration of the internal standard IS which is present in the sample.

$\frac{A_{Passerini}}{A_{IS}} =$ The ratio of the integral signals of the Passerini product and the IS which is obtained by the GC-measurement.

$s =$ The slope of the calibration curve $= 1.06038$

To validate the accuracy of the calibration, one test reactions (*vide infra*) was worked up *via* column chromatography, and the obtained yield was compared to the yield calculated using the calibration. After purification, 23.7% of the Passerini product (**7**) was obtained, while the GC analysis predicted a yield of 24.9%. The relative deviation of 4.7% demonstrates that the calibration provided results with satisfactory accuracy — keeping in mind, that the purification *via* column chromatography led to loss of product. A deviation of less than 5% is acceptable, as it allows for continuous monitoring of conversion and yield without the need for prior product purification. The lower yield after purification can partly be attributed to product loss during the purification process itself.

4.2.1.2 Initial findings – The start of the investigation

The initial reactions aimed to assess the general effectiveness of thiourea compounds as an organocatalyst under this reaction setup. For this purpose, the catalysts were first used in substoichiometric amounts, specifically 20 mol%. Later in this research (see **Chapter 4.2.2.7**), efforts were made to reduce the catalyst loading for reasons of sustainability, while demonstrating its effectiveness with truly catalytic quantities. However, 20 mol% was chosen initially to ensure that a possible catalytic effect would be detectable. Thiourea catalysts **T1** and **T2** (shown in **Figure 17**) were selected for the initial tests.

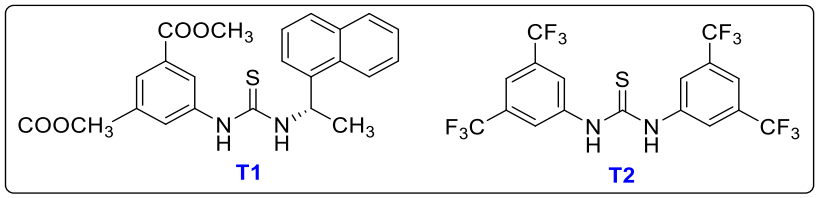

Figure 17 Selection of thiourea organocatalysts for the initial screening of the Passerini-3CR.

Thiourea **T1** was synthesised *via* the MCR approach using elemental sulphur.[41] **T1** contains electron-withdrawing methyl ester groups in the *meta*-position of the aryl ring, a feature previously studied in the Meier group.[41] This modification was considered a valuable alternative to the well-established bis(trifluoromethyl)phenyl group of Schreiner's thiourea **T2**.[41,198] Meier *et al*. demonstrated that thioureas with methyl ester groups in the *meta*-position of the aryl ring result in significantly strong hydrogen bond donors.[41] Quantification of hydrogen bond donor strength was performed using phosphorus-NMR analysis, following a protocol adapted from Franz *et al*., with triethyl phosphine oxide ($POEt_3$) as the hydrogen bond acceptor.[391] Originally, Hilt *et al*. showed that catalytic activity could be correlated to phosphorus-NMR results in the presence of a suitable hydrogen bond acceptor.[392] Meier *et al*. found that a thiourea similar to **T2**, but containing methyl ester groups instead of trifluoromethyl groups, exhibited a 19% reduction in hydrogen bond donor strength, but represented a more sustainable alternative synthesis route.[41]

In this initial screening, three reactions were conducted following the procedure outlined in **Chapter 4.2.1.1**, hereafter referred to as the "**standard screening procedure**." One reaction was performed without a catalyst, serving as a reference, while one of the other two reactions was carried out in the presence of **T1**, a thiourea based on commercially available (*S*)-(−)-1-(1-naphthyl)ethylamine. The other reaction was carried out in presence of **T2** as

benchmark catalyst. **T2** is a well-known thiourea named after its inventor, Peter Schreiner.[40,42] The initial results are summarised in **Table 2**.

Table 2 Results from the initial screening of the Passerini-3CR depicted in **Scheme 19.**

Entry	Catalyst	Yield 2h [%]	Yield 20h [%]	Yield 44h [%]
P-01	-	5.1	26.8	43.2
P-02	T1	4.9	25.5	40.5
P-03	T2	38.6	59.0	67.0

The reactions were carried out in cyclohexane at a concentration of 0.025 mol×L^{-1} following the **standard screening procedure**. The thioureas were used in amounts of 20 mol%.

The uncatalysed reaction (**P-01**) yielded 43.2% after 44 hours, while a slightly lower yield of 40.5% was obtained in the presence of 20 mol% of **T1** as the catalyst. Notably, a 67% yield was achieved in the presence of **T2**. In relative perspective, there was a 55% increase in yield by incorporating the highly electron-deficient thiourea **T2**. Furthermore, comparing thioureas **T1** and **T2**, it is highly likely that stronger electron-withdrawing groups (EWG) are essential for effective catalysis under given conditions. The employed 3,5-bis(trifluoromethyl)phenyl-group was broadly discussed in literature and designated as a **privileged building block** for thiourea organocatalysts.[198] It is conceivable that the catalyst performance of **T2** is influenced not only by the two electron-deficient aryl moieties, but also by the strong electron-withdrawing ability of the trifluoromethyl groups. Therefore, the following chapter on the design study of thiourea catalysts will take this into account and explore this aspect in greater detail.

4.2.1.3 Design study of the thiourea catalyst

After obtaining promising results from the initial screening, further investigation into the catalyst design was pursued. A potential thiourea catalyst for the asymmetric Passerini-3CR is depicted in **Figure 13**. At the centre of the catalyst is the thiourea functional group, which interacts with the reactants and intermediates through hydrogen bonding, ultimately stabilising the transition state.[40] (Compare **Chapter 2.1.2**)

To the left of the thiourea group, an electron-deficient aryl moiety is positioned to enhance the hydrogen bond donor capabilities of the catalyst. The first experiment of this chapter explored which electron-withdrawing groups promote catalytic behaviour. Additionally, the thiourea is bound to a chiral scaffold, which influences the spatial arrangement of the

catalyst, reactants, and intermediates in the transition state, possibly enabling asymmetric synthesis. The second set experiments in this chapter was conducted to emphasise this aspect.

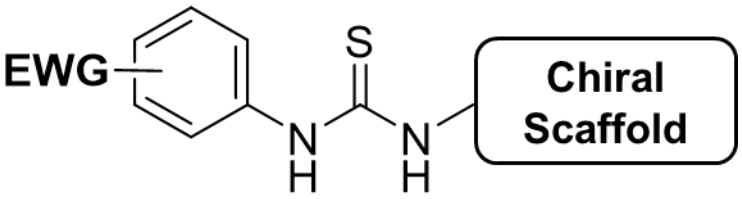

Figure 18 An archetype for the design study of a thiourea catalyst for the Passerini-3CR.

For the first experiment, thioureas with a cyclohexyl moiety attached to one side of the thiourea group and a phenyl ring with varying EWGs in the *para* or *meta* position (except for thiourea **T3**, which has another cyclohexyl ring) were selected. The aim was to determine whether a highly electron-deficient thiourea is necessary for catalytic activity in the Passerini reaction. Thiourea **T4** does not possess any EWG at its aryl moiety and can therefore serve as reference for the other thioureas that include EWGs, while thiourea **T3** serves for comparison between aromatic and aliphatic building blocks. The results of this screening series are summarised in **Table 3**, and the thioureas used for the subsequent screenings, including **T1** and **T2** for completeness, are shown in **Figure 19**.

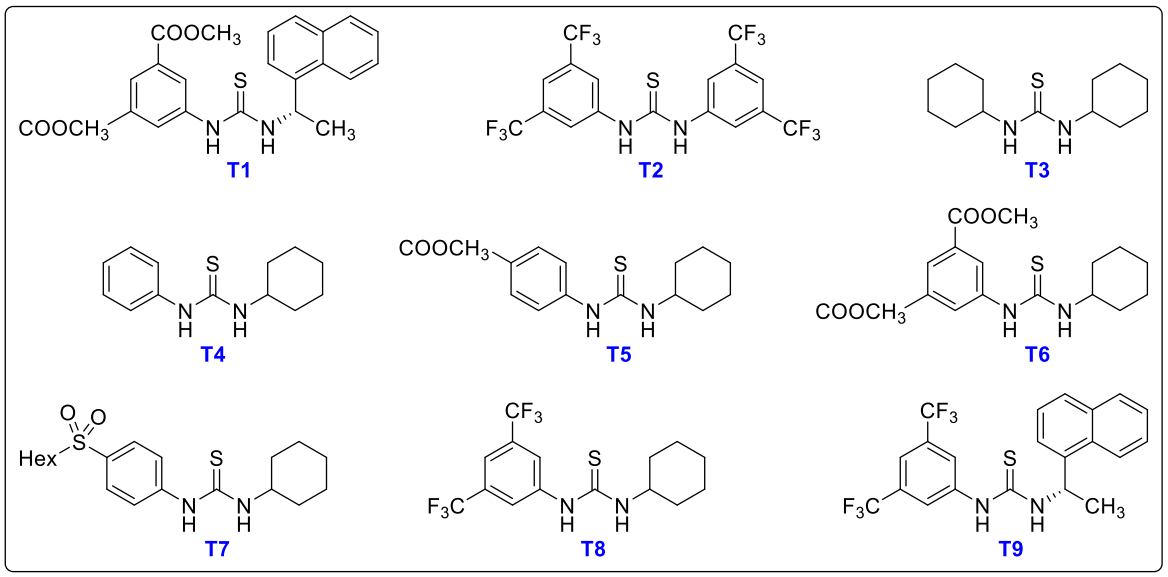

Figure 19 A selection of thioureas used in the first screening of Passerini-3CR to conduct the catalyst design study.

Most of the thioureas presented in **Figure 19** were synthesised using the procedures described in **Chapter 4.1**, unless they were purchased commercially (**T2**) or provided by coworkers. Special thanks go to **Dr. Clara Scheelje**, who previously synthesised thioureas **T4**, **T5** and **T7**.[393,394] With her permission, the author was pleased to include them in this study, as they fit perfectly into the screening series.

Table 3 Investigation of the electronic configuration of thiourea organocatalysts for Passerini-3CR, as shown in **Scheme 19**.

Entry	Catalyst	Yield 2h [%]	Yield 20h [%]	Yield 44h [%]	*ee* [%]
P-01	-	5.1	26.8	43.2	0
P-02	T1	4.9	25.5	40.5	1.5
P-03	T2	38.6	59.0	67.0	-
P-04	T3	4.8	31.6	45.9	-
P-05	T4	4.9	31.0	44.5	-
P-06	T5	3.8	25.3	38.4	-
P-07	T6	4.8	32.2	47.0	-
P-08	T7	4.7	31.9	44.9	-
P-09	T8	17.3	48.7	57.9	-
P-10	T9	21.0	51.1	58.5	7.0

The reactions were carried out in cyclohexane at a concentration of 0.025 mol×L^{-1} following the **standard screening procedure**. For reasons of compatibility, previous results were included as well. The thioureas were used in amounts of 20 mol%. For achiral thiourea catalysts, no chiral HPLC analysis was carried out.

Comparing the results from the GC screening, it becomes clear that thioureas **T3**–**T7** had only a marginal impact on the yields obtained after 44 hours of reaction time. In those cases, yields were comparable to those of the uncatalysed reaction (**P-01**). Notably, thiourea **T6**, which features two methyl ester groups in the *meta*-position, showed a relative increase of 8% in yield compared to **P-01**. In contrast, thiourea **T5** resulted in a 13% decrease in yield compared to **P-01** after 44 hours. The difference between thioureas **T5** and **T6** is attributed to the hydrogen bonding strength, which results from the strong electron-withdrawing groups in the *meta*-position of the aryl ring. This is further confirmed by the ^{31}P-NMR measurements by Meier *et al*., who found that, for instance, thiourea **T6** has a 51% higher donor capability than **T5**.[41] This higher donor capability correlates with greater catalytic activity.[41] At this point, it can be speculated whether thiourea **T5** might also bind to one of the substrates without enhancing the overall reaction rate, but rather leading to passivation.

Upon inspecting **P-09** in the presence of thiourea **T8**, a notable increase in reactant conversion and yield was observed. The catalyst exhibited high activity early in the reaction, achieving a yield of 17.3% after just two hours — a 3.4-fold increase compared to the reaction without a thiourea catalyst. As the reaction progressed, a yield of 57.9% was recorded after 44 hours, representing a significant 34% relative increase.

These results confirm that the Passerini-3CR benefits greatly from thioureas with strong hydrogen-bonding capabilities, particularly when the thiourea bears a 3,5-bis(trifluoromethyl)phenyl group, as seen in Schreiner's thiourea **T2**. This finding was further corroborated by **P-02** and **P-10**, the latter containing a chiral building block derived from naphthalene. The two thioureas, **T1** and **T9**, differed in their EWGs at the aryl moiety: **T1** featured methyl ester groups, while **T9** had trifluoromethyl groups. **T9** exhibited significantly higher activity and yields, and, notably, an enantiomeric excess of 7.0% was observed. This suggests that strong hydrogen-bonding capabilities are crucial for effective catalyst design and that stereo induction with thioureas following the catalyst design shown in **Figure 18** is possible.

Since **T2**, **T8**, and **T9** — each bearing the strong 3,5-bis(trifluoromethyl)phenyl group — consistently enhanced reaction performance, it was concluded that incorporating a chiral building block into the thiourea catalyst, rather than a second electron-deficient aryl moiety, would be sufficient for designing a catalyst capable of both accelerating the reaction and inducing stereo control. This approach holds promise for achieving the ultimate goal of developing thiourea as a useful catalyst for asymmetric Passerini-3 component reaction.

After obtaining promising initial results — including a small *ee* — with thiourea **T9**, the influence of the chiral polycyclic aromatic building block of the thiourea catalyst was systematically explored. Four thioureas were synthesised and tested as catalysts, as illustrated in **Figure 20**. These thioureas vary in the size of the polycyclic aromatic ring, ranging from benzyl to anthracene. Additionally, **T10** was included to serve as a direct comparison to **T11**, allowing for the investigation of the influence of an aromatic π-system. This exploration aimed to discern whether possible π-π stacking interactions or the flat structure of the aromatic ring, as compared to the chair conformation of cyclohexane, have an impact. The summarised results can be found in **Table 4**.

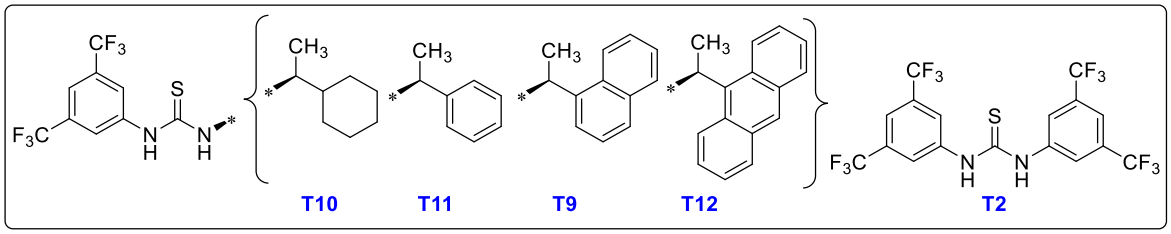

Figure 20 Selection of thiourea organocatalyst for the catalyst design study which bear aliphatic or aromatic ring structures.

Table 4 Results from the investigation of the of the Passerini-3CR depicted in **Scheme 19** using chiral thiourea organocatalysts bearing aliphatic or aromatic ring structures.

Entry	Catalyst	Yield 2h [%]	Yield 20h [%]	Yield 44h [%]	*ee* [%]
P-01	-	5.1	26.8	43.2	0
P-03	T2	38.6	59.0	67.0	-
P-11	T10	19.2	52.9	64.5	0.5
P-12	T11	24.6	55.4	65.3	3.3
P-10	T9	21.0	51.1	58.5	7.0
P-13	T12	27.6	63.9	74.6	11.6

The reactions were carried out in cyclohexane at a concentration of 0.025 mol×L^{-1} following the **standard screening procedure**. For reasons of compatibility, previous results were included as well. The thioureas were used in amounts of 20 mol%. For achiral Schreiner thiourea **T2** no chiral HPLC analysis was carried out.

A distinct trend is evident upon reviewing the results from **Table 4**, indicating that an aromatic ring structure outperforms the respective aliphatic derivative if the entries **P-11** and **P-12** are compared for their enantioselectivity. In both cases, high yields, comparable to Schreiner's thiourea **T2** after 44h were measured, but only **T11** demonstrated the ability to induce enantioselectivity to a small yet significant extent of 3.3%. The *ee* value of 0.5% from entry **P-11** is negligible and within experimental errors. As we progress to naphthalene and anthracene derivatives of the catalyst, it becomes apparent that the size of the aromatic building block is crucial. The introduction of more spatially demanding aromatic groups near the thiourea moiety leads to increased steric hindrance. In addition to this observation, the highest yield was achieved in the presence of **T12**, surpassing even Schreiner's thiourea **T2**. Furthermore, **T12** yielded the highest enantiomeric excess of 11.6%.

It is noteworthy that the yield of entry **P-10** is lower after 44 hours compared to the corresponding other entries. This can be attributed to the laboratory temperature during the reactions. Unfortunately, the laboratory lacks adequate insulation in the summer months, resulting in a room temperature that was 4 °C higher for reactions **P-11** to **P-13** than for the other approaches (usually the room temperature ranges from 19 - 21 °C throughout the year). This higher temperature may explain the increased yields observed.

In summary, an initial understanding of catalyst design was achieved, highlighting two crucial structural motifs: (i) the highly electron-deficient 3,5-bis(trifluoromethyl)phenyl group, and (ii) chiral polycyclic aromatic building blocks of increased size. These elements have proven pivotal for catalyst design. With this initial success and promising results from the first screening, the focus of the investigation shifted towards the reaction conditions of the Passerini-3CR. The aim was to gain a deeper understanding of the working principles of thiourea organocatalysts in the Passerini reaction, as well as to identify reaction conditions that drive the MCR towards higher yields and greater enantioselectivities, while suppressing the uncatalysed background reaction.

4.2.2 Optimisation of the reaction conditions of the Passerini–3CR

This chapter aims to systematically explore the optimal reaction conditions for the Passerini reaction in the presence of thiourea catalysts, with the goal of improving both yield and enantioselectivity. The investigation began with a kinetic study, based on the hypothesis that these catalysts exhibit high activity in the early stages of the reaction. Understanding these kinetics may provide valuable insights for future research. Following the kinetic study, the solvent used in the **standard screening procedure** was revised, as cyclohexane proved suboptimal for low-temperature reactions. Subsequently, low-temperature screenings were conducted, while the next step involved examining the stoichiometry and the order of reactant addition to the reaction mixture. Finally, the addition of additives, along with a study on catalyst concentration, was explored. These adjustments were aimed at enhancing reaction performance and minimising catalyst usage, contributing to a more sustainable approach.

It is noteworthy that thiourea **T9** was consistently used during the optimisation process, despite being less effective than its anthracene counterpart, **T12**. This choice was made purely for cost-effectiveness, as the amines required for synthesising the two thioureas differ significantly in price. It was assumed that both catalysts would perform similarly under the given conditions, with **T12** being superior in terms of yield and enantioselectivity.

4.2.2.1 Investigation into the kinetics of the Passerini-3CR

The catalytic activity of thiourea (**T9**) was screened, focusing on the initial stages of the reaction, as it was inferred that the thiourea is primarily active in the first few minutes and hours, with its activity decreasing later on. This assumption was made in regard of the results

from **Table 4**, in which the relative difference between catalysed and no-catalysed reaction was most pronounced in the beginning. The kinetic study included experiments conducted without a catalyst as a reference, and with 20% and 100% molar equivalents of **T9**, respectively. A more detailed GC screening of the concentration evolution of the Passerini product was conducted to gain further insights into the catalyst's behaviour. **Figure 21** illustrates the evolution of the yield over time graphically, while the summarised results can be found in **Table 5**. Typically, the yield data over time plots exhibit a fast growth in the beginning, followed by decreasing product formation due to depleting concentration of the reactants. The grey dataset displayed in **Figure 21** represents conditions without any catalyst, while the red and blue curves correspond to conditions with 20 mol% and 100 mol% of the **T9** catalyst, respectively.

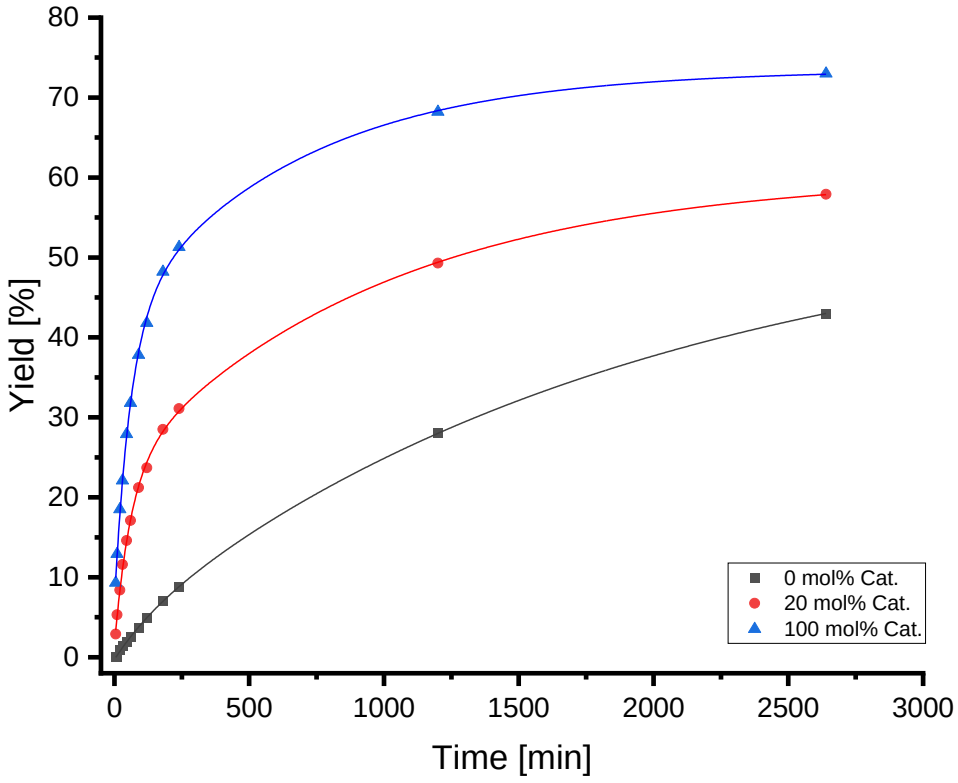

Figure 21 Evolution of the yield of the Passerini-3CR over time. The dataset represents conditions without any catalyst, and with 20 mol% and 100 mol% of thiourea **T9**, respectively.

Table 5 Kinetic study on the Passerini-3CR, as shown in **Scheme 19**.

Entry	**Catalyst**												
	T9	5 min	10 min	20 min	30 min	45 min	60 min	90 min	2 h	3 h	4 h	20 h	44 h

P-14	-	0.0	0.0	0.9	1.4	1.9	2.5	3.7	4.9	7.1	8.8	28.0	43.0
P-15	20 mol%	2.9	5.3	8.4	11.6	14.6	17.1	21.2	23.7	28.5	31.1	49.3	57.9
P-16	100 mol%	9.3	12.9	18.5	22.1	27.9	31.8	37.8	41.8	48.2	51.3	68.2	73.0

The reactions employed acetic acid, octanal and benzyl isocyanide in equimolar ratios. The reactions were carried out in cyclohexane at a concentration of 0.025 $mol \times L^{-1}$. The yield of the Passerini reaction was determined by gas chromatography (GC) and is based on the implementation of tetradecane as internal standard.

Reviewing the outcomes of the kinetic screening, it became evident that elevated catalyst loadings correspond to increased conversions of the reactants and higher yields. However, as the reaction advanced, a decreasing reaction rate was observed. This phenomenon is likely attributed to a decreasing concentration of reactants and very typical for chemical batch reactions. Multicomponent reactions, such as the Passerini-3CR, are generally disadvantaged by the depletion of reactant concentrations and benefit greatly from high concentrations on the contrary.[200] Recent developments in investigating the mechanism of the Passerini reaction using density functional theory (DFT) suggested that carboxylic acid not only participates in the reaction as a reactant, but also effectively catalyses product formation through hydrogen bonding.[262,263] The authors further asserted that in the absence of additional carboxylic acid molecules, the energy barrier for product formation in the Mumm rearrangement is so substantial that the reaction might not proceed effectively.[262,263] Consequently, optimising reactant concentrations becomes crucial for achieving high yields in the Passerini-3CR, but is counterproductive for the goal of catalysed stereoselective Passerini-3CRs due to increased background reactions at increased substrate concentrations.

The results from the catalytic screening can be summarised as follows: In the initial phase, a clear catalytic effect can be observed. In the reference reaction, the first Passerini product was detected by GC analysis after 20 minutes of reaction time, yielding a signal corresponding to 0.9% yield. In contrast, reactions with 20 mol% **T9** resulted in 8.4% yield, and those with 100 mol% in 18.5% yield, respectively. The trajectory of the curve clearly illustrates this, with the slope being significantly steeper in the presence of the catalyst.

While it became evident that the Passerini reaction performs significantly better in the presence of thiourea **T9**, particularly in the early stages, another approach was undertaken to determine whether this enhanced catalytic effect also leads to higher enantioselectivity. This experiment followed the same procedure as **P-15** but was interrupted and quenched after two hours, followed by workup and product isolation. A sample for chiral HPLC analysis was then prepared from the isolated product. Additionally, to investigate whether the purification process has an impact on the experimental outcome, another run was

conducted in which purification was avoided, and a crude sample was extracted for analysis and comparison. The results are presented in **Table 6**.

Table 6 Influence of the reaction time onto the enantioselectivity of the Passerini-3CR depicted in **Scheme 19**.

Entry	Catalyst	Yield 2h [%]	Yield 20h [%]	Yield 44h [%]	*ee* [%]
P-01	-	5.1	26.8	43.2	0
P-10	T9	21.0	51.1	58.5	7.0
P-17	T9	20.6	-	-	5.9
P-18	T9	20.9	-	-	5.6

The reactions were carried out in cyclohexane at a concentration of 0.025 mol×L^{-1} following the **standard screening procedure**. For reasons of compatibility, previous results were included as well. The thioureas were used in amounts of 20 mol%. Approach **P-17** was intersected after two hours, purified and submitted to chiral HPLC analysis. From **P-18**, a crude sample was submitted to chiral HPLC analysis after two hours reaction time.

While enhanced conversion and higher yields in the presence of thiourea were confirmed, no improvement in enantioselectivity within the first two hours was observed. It was found that purification *via* column chromatography (**P-17**) had no effect on the experimental outcome of the reaction, as the results were nearly identical to that of **P-18**, where the crude sample was analysed. If compared to **P-10**, where chiral HPLC was performed after 44 hours and an *ee* of 7.0% was measured, slightly lower *ee* values of 5.9% and 5.6% were obtained after 2 hours, respectively.

These results indicated that the thiourea catalyst not only promotes the reaction pathway leading to a specific enantiomer, but also facilitates other reaction pathways that result in a racemic Passerini product. In other words, there are at least three potential reaction pathways under the given conditions. First, the reaction can proceed without the involvement of the thiourea, but this pathway is kinetically outcompeted by the other two pathways influenced by the catalyst. In the presence of thiourea, the reaction can either proceed towards racemic product formation or towards an enantioselective product formation. Notably, both pathways appear to occur simultaneously, likely due to the small or no difference in their activation energy barriers, as both pathways involve thiourea.

According to Gawley *et al.*,[395] this kinetic behaviour can be approximated as follows: assuming that the reaction and its selectivity are under kinetic control, the starting material A can either react to form product B, in which only one enantiomer is generated (depending on the catalyst used), or react to form a racemic mixture of products, C. The reaction rates are given in the subsequent equation*s* — following kinetic for 1st order reactions: k_1 and k_2 represent the rate constants for the formation of B and C, respectively.

$$\frac{d[B]}{dt} = k_1[A] \qquad \textit{(Eq. 3)}$$

$$\frac{d[C]}{dt} = k_2[A] \qquad \textit{(Eq. 4)}$$

From transition state theory, the rate constants are put into equation with the transmission coefficient κ (which is usually taken as unity), the Boltzmann constant k_B, the absolute temperature T, the Plack constant h, the gas constant R and the free energies $\Delta G_B^{\ddagger}$ and $\Delta G_C^{\ddagger}$ of the activation for the generation of B and C, respectively.

$$k_1 = \frac{\kappa k_B T}{h} e^{\left(-\frac{\Delta G_B^{\ddagger}}{RT}\right)} \qquad \textit{(Eq. 5)}$$

$$k_2 = \frac{\kappa k_B T}{h} e^{\left(-\frac{\Delta G_C^{\ddagger}}{RT}\right)} \qquad \textit{(Eq. 6)}$$

In a first approximation, the transmission coefficients are assumed to be equal at a given temperature. The product ratio can then be calculated as follows:

$$\frac{B}{C} = \frac{k_1}{k_2} = e^{-\frac{\Delta\Delta G^{\ddagger}}{RT}} \qquad \textit{(Eq. 7)}$$

The difference in the activation energy for each process $\Delta\Delta G^{\ddagger}$ is described as:

$$\Delta\Delta G^{\ddagger} = \Delta G_B^{\ddagger} - \Delta G_C^{\ddagger} \qquad \textit{(Eq. 8)}$$

Technically, the equation is only valid for a unimolecular reaction in the gas phase.[395] However, it can be used to illustrate that the product ratio — specifically, the ratio between enantiomer B, obtained from the asymmetric reaction pathway *via* thiourea, and the racemic product mixture C, also generated through thiourea but *via* racemic catalytic pathway — depends on the energy difference between the activation energy barriers of the two pathways (denoted here as $\Delta\Delta G^{\ddagger}$). In a first approximation it is valid to utilise these equations for 1st order reaction rates to describe the Passerini-3CR, since the MCR is

conducted at low reactant concentration, typically at 0.025 mol×L^{-1} in the **standard screening procedure**.

It is conceivable that achieving higher enantioselectivity in the thiourea-catalysed Passerini reaction requires a more significant difference in the activation energy barriers between the multiple possible reaction pathways. At least one of these pathways leads to the preferred formation of one enantiomer. It is required that the thiourea catalyst stabilises the corresponding transition state, thus altering its activation energy.

Here, the rotation of functional groups within the catalyst may play a crucial role, as this phenomenon generates different conformations or orientations of the catalyst. One specific orientation of the rotating group could lead to a favourable conformation of the catalyst, ultimately resulting in enantiomeric excess.

4.2.2.2 Investigation into the thiourea catalysed reaction mechanism

This chapter aims to provide a deeper understanding of the role of a thiourea catalysts in the Passerini reaction, offering initial insights into mechanistic investigations. Emphasis is placed on the different conformations and orientations of the catalyst, as these are assumed to significantly impact the stereoselectivity of the thiourea-catalysed Passerini reaction. The author expresses gratitude to Sonia Dhull from the Wenzel group at the Institute of Nanotechnology (INT) at KIT, who calculated the different rotamers of thioureas **T9** and **T12** and their respective energies using density functional theory (DFT). This ongoing collaboration seeks to elucidate the reaction mechanism of the Passerini reaction in the presence of thiourea organocatalysts.

The initial findings from these DFT calculations indicate that the thiourea catalyst likely interacts with the aldehyde during the reaction. This activation mode for thiourea with aldehydes is literature know.[40-42,194,396] The thiourea — capable of donating hydrogen bonds — interacts with the oxygen atom of the aldehyde's carbonyl group, forming a dual hydrogen-bonding complex that increases the electrophilicity of the carbonyl carbon, therefore fostering nucleophilic attacks. By binding to the carbonyl oxygen, the thiourea catalyst stabilises the transition state of the reaction, reducing the activation energy. Furthermore, thiourea — while bound to the aldehyde — might direct the nucleophile to approach from a specific orientation, favouring the formation of one enantiomer over another.

Figure 22 illustrates the plausible hydrogen-bonded dimer between aldehydes and thioureas, as well as a plausible transition state in which nucleophilic α-addition of the isocyanide to the aldehyde occurs while bound to thiourea. Thiourea **T9** (indicated in orange) was chosen to exemplify this interaction. The carboxylic acid likely interacts with the thiourea–aldehyde heterodimer via hydrogen bonding during the α-addition process.

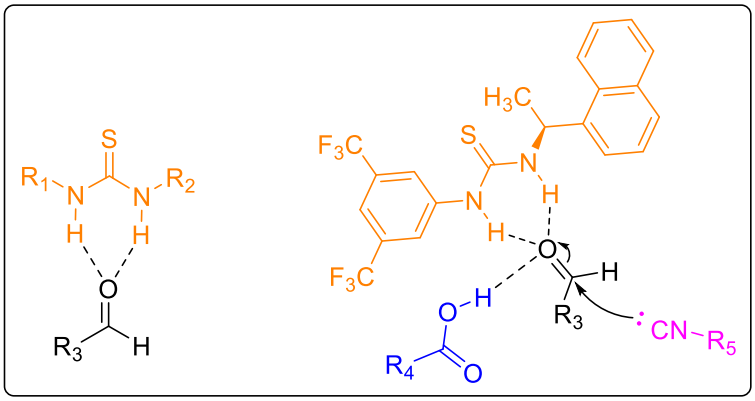

Figure 22 Plausible activation mode of a thiourea organocatalyst and an aldehyde, in which a hydrogen-bound complex is generated. While bound to thiourea, an enhancement of electrophilicity of the aldehyde is expected. Additionally, a plausible transition state of the α-addition of the isocyanide in presence of thiourea catalyst **T9** (here in orange colour) is shown.

To support the DFT calculations, ^{1}H-NMR and ^{19}F-NMR experiments were carried out to gain a better understanding of the potential operational mechanism of a thiourea catalyst. For the proton NMR experiments, all the reactants (octanal, acetic acid and benzyl isocyanide) and the respective Passerini product were measured in deuterated cyclohexane in absence as well as in the presence of the thioureas **T2** and **T9**. This investigation sought to uncover if any shift in their respective NMR peaks indicating a changed chemical surrounding, might unveil a potential favoured binding mode of the thiourea with any of the reactants — with special focus on the aldehyde.

Unfortunately, the thioureas exhibited insolubility in cyclohexane, preventing the investigation into peak shifts during the experiment. This discovery was unexpected, given that previous reaction screenings had consistently occurred in cyclohexane, and both catalysts had previously rendered a homogeneous solution, albeit after a minimum of 10 minutes of reaction time. Please note that the NMR experiments were carried out previous to the identification of *n*-hexane as a better solvent choice. Interestingly, during the NMR experiment, the thioureas displayed complete solubility when octanal or the Passerini product was present, suggesting the formation of substantial hydrogen bonding between the carboxylic oxygen atoms of these species and the respective thioureas. This complexation

potentially facilitated solubilisation in cyclohexane. It was hypothesised that the thiourea might have been carried into solution while bound to the aldehyde or the product. Notably, this effect was absent when the acid or the isocyanide was present. In summary, deuterated cyclohexane proved to be a poor choice for the experiment design, since no NMR could be measured due to solubility issues. On the other hand, these solubility issues hint to the preferred hydrogen-bonding interactions between thiourea and the aldehyde or product in non-polar solvents.

Subsequently, the experiments were replicated in deuterated DMSO for effectively solubilising thioureas. These experiments were exemplarily carried out with Schreiner's thiourea **T2**. Intriguingly, when measuring thiourea **T2** alongside acetic acid, the detection of the acidic proton peak at 11.95 ppm ceased (compare **Figure 23**). It was previously reported that thiourea catalysts could benefit from additional acid components by forming a dimeric complex, resulting in augmented yields and enantiomeric excesses during asymmetric synthesis.[397] The disappearance of the peak suggests the formation of a dimer between the thiourea and the carboxylic acid anion.

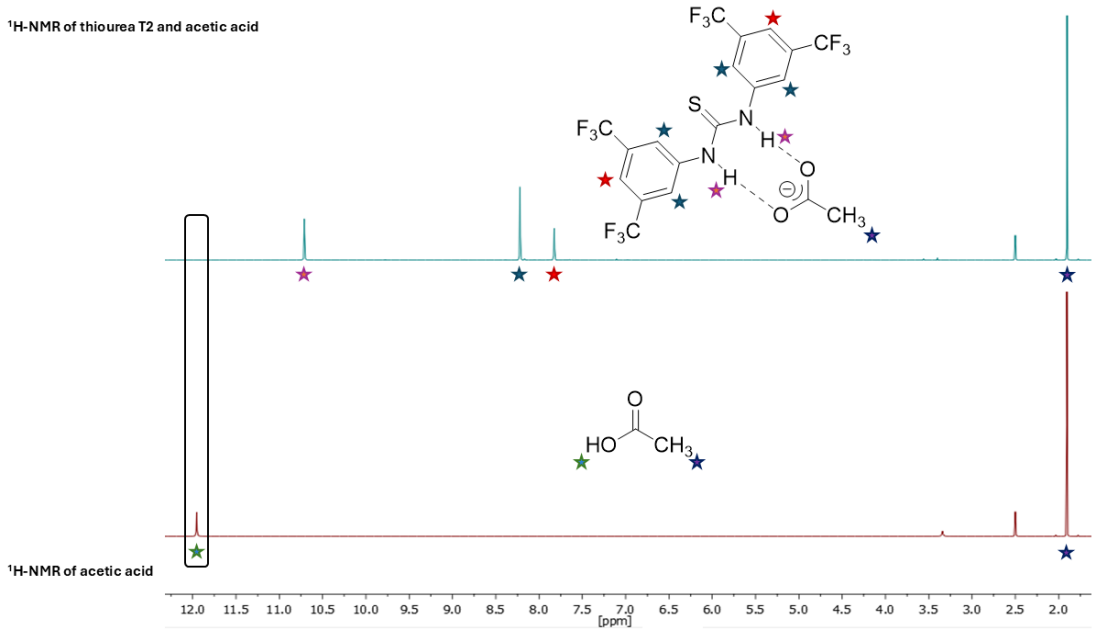

Figure 23 ^{1}H-NMR of acetic acid (lower spectrum) and of an equimolar mixture of thiourea **T2** and acetic acid (upper spectrum). Both NMR spectra were measured in deuterated DMSO. The acidic proton peak at 11.95 ppm ceased completely in presence of **T2**, indicating the possible formation of the shown hydrogen bonded complex.

Furthermore, the thiourea-*N*-*H* peak shifted slightly ($\Delta\delta$ = 0.015 ppm) when measuring thiourea **T2** with the Passerini product or the aldehyde. To exemplify this peak shift,

Figure 24 shows the interaction of octanal and thiourea **T2**. One the other hand, no detectable peak shift was observed in the presence of the isocyanide.

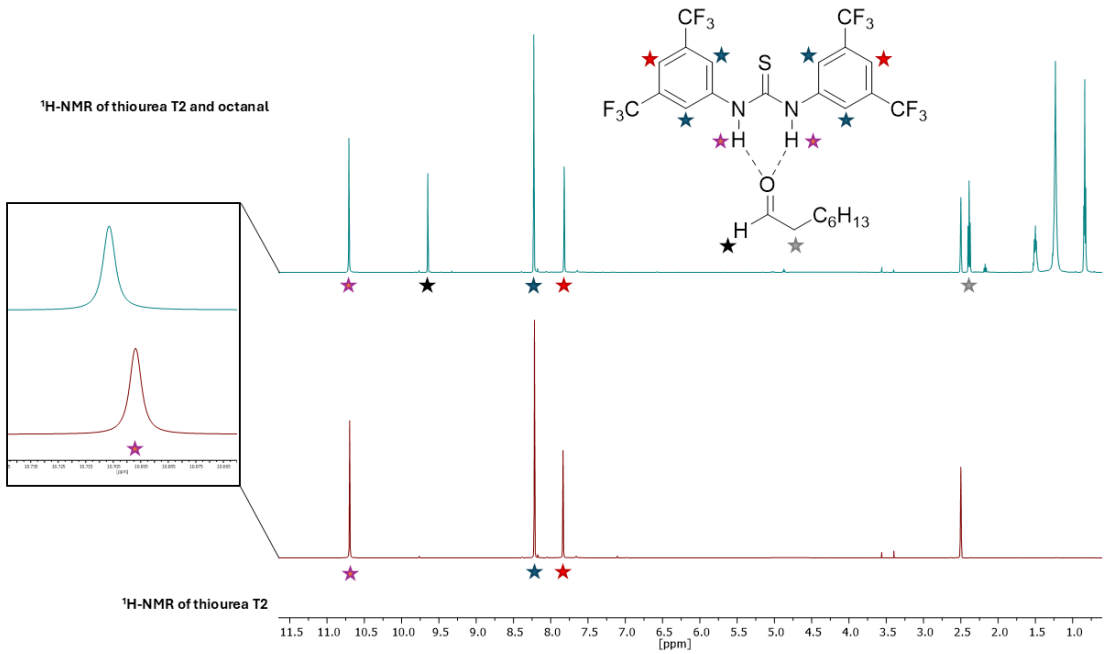

Figure 24 ^{1}H-NMR of thiourea **T2** (lower spectrum) and of an equimolar mixture of thiourea **T2** and octanal (upper spectrum). Both NMR spectra were measured in deuterated DMSO. Slight peak shifts were noticeable.

Subsequently, ^{19}F-NMR experiments (See **Figure 25**) were conducted to investigate if complexation has an impact on the chemical shift of the fluorine atoms incorporated into the catalyst structure. 2,2,2-Trifluoroethanol was used as an internal standard and in all cases marginal peak shifts were observed, but the most significant shifts were recorded when measuring alongside acetic acid ($\Delta\delta$ = 0.06 ppm) or the aldehyde ($\Delta\delta$ = 0.17 ppm).

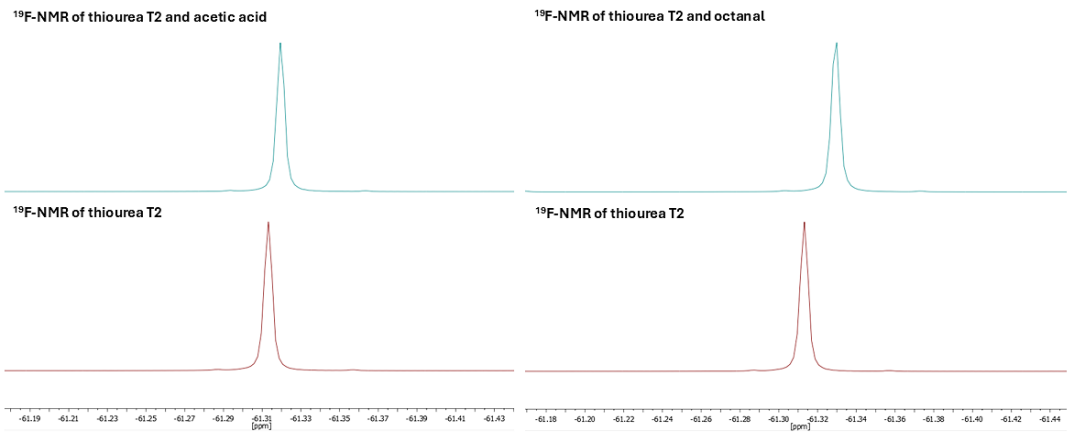

Figure 25 ^{19}F NMR spectra of equimolar mixtures of thiourea **T2** with either acetic acid (top left spectrum) or the aldehyde (top right spectrum). The bottom spectra show thiourea **T2** alone under the same conditions. All spectra were recorded with 2,2,2-trifluoroethanol as the internal standard.

Collectively, based on the outcomes from both NMR experiments, it can be argued that thiourea likely engages in hydrogen bonding interactions with both the acid and the aldehyde in the Passerini-3CR. On the other hand, a higher affinity of thiourea **T2** towards the aldehyde was detected, since stronger peak shifts were observed during the ^{19}F-NMR experiments. This suggests that the thiourea catalyst, in accordance with the DFT calculations, complex the aldehyde, subsequently guiding the isocyanide through secondary intermolecular interactions (e.g., steric, hydrogen-bonding, π – π - interactions) during the nucleophilic addition. Alternatively, it is still conceivable that the formation of a 1:1 complex between thiourea and acid significantly influences the reaction, potentially enhancing the acidity of the acid.[397]

During the screening of the Passerini-3CR with thiourea as an organocatalyst, it became apparent that the reaction benefits from its presence, leading to higher yields, an accelerated reaction rate, and small enantiomeric excesses. It is assumed that previously employed thiourea catalysts are limited in their ability to inflict significant stereochemical control on the Passerini product. Additionally, it is proposed that the thiourea catalysts used here possess rotational freedom in certain structural parts, which reduces their overall rigidity and leads to the formation of various rotamers. In **Figure 26**, the thiourea catalyst **T9** and **T12** are shown. It is proposed that the hydrogen atom on the aryl group forms a hydrogen bond with the sulphur atom (indicated by a purple dashed line), increasing rigidity in the catalyst.[40,370] Furthermore, it is assumed that the bulky naphthyl group can rotate around the bond between carbon atoms 13 and 14, with additional rotation possible between nitrogen atom 15 and carbon atom 13. It is conceivable that thiourea **T12** behaves accordingly. This results in a series of potential rotamers of the respective catalyst.

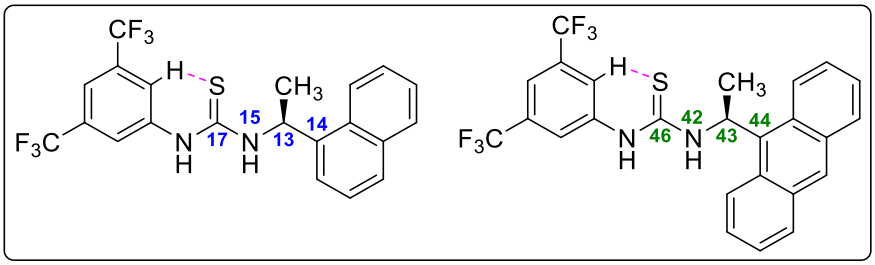

Figure 26 Thiourea **T9**, here shown with atom labels (blue colour) and intramolecular hydrogen bonding interaction between the *ortho*-hydrogen and the sulphur atom creating rigidity in the catalyst structure.[129] Accordingly, thiourea **T12** is also shown with atom labels (green colour) and intramolecular hydrogen bonding.

Figure 27 shows the relative energy diagram of **T9** as a function of the torsion angle. Density functional theory calculations provided by Sonia Dhull simulated the rotation around the C_{13}-N_{15} bond in the dihedral angle of thiourea **T9** (C_{17}-N_{15}-C_{13}-C_{14}) in the gas phase, assuming the rest of the molecule remains rigid.

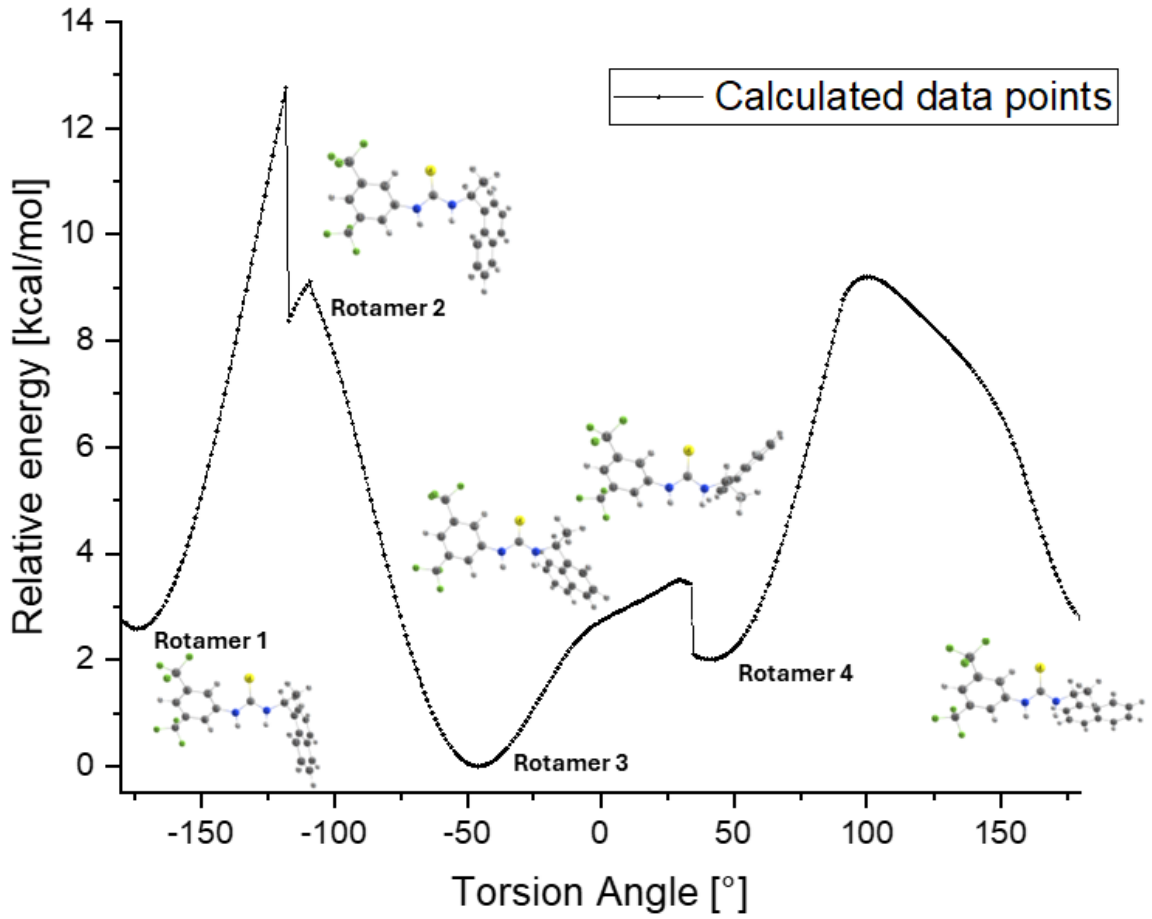

Figure 27 Relative energy diagram as a function of the torsion angle calculated for thiourea **T9** in the gas phase. All catalyst rotamers are optimised using the B3LYP functional with the D3(BJ) dispersion correction and the 6-31G(d,p) basis set. The temperature was set at 298 K.

The variation of the torsion angle led to the identification of four plausible rotamers of thiourea **T9**, shown in **Figure 27**. According to calculations by the Wenzel group, only **Rotamer 3** —which has the lowest relative energy — facilitates successful stereoselective induction in the Passerini reaction. Upon examining the energy diagram, a chiselled, jagged curve is observed. The torsion angle was incrementally altered by 1° in each step. It can therefore be assumed that the curve would appear much smoother if infinitesimally smaller steps were used in the calculation; however, this approach was not feasible due to the resulting infinite calculation time. Instead of carrying out a rigid scan of the potential surface, another approach could be to apply a relaxed scan, which optimises the geometry after each rotation step, resulting in a smoother curve in the diagram. Generally, the energy differences between the rotamers were found to be small, with the largest difference being less than 11 kcal/mol. This suggests that multiple rotamers of **T9** likely coexist under the given reaction conditions (e.g., room temperature).

Figure 28 shows the relative energy diagram of **T12** as a function of the torsion angle, which was calculated accordingly to the energy diagram of **T9**. Here, only two rotamers were identified.

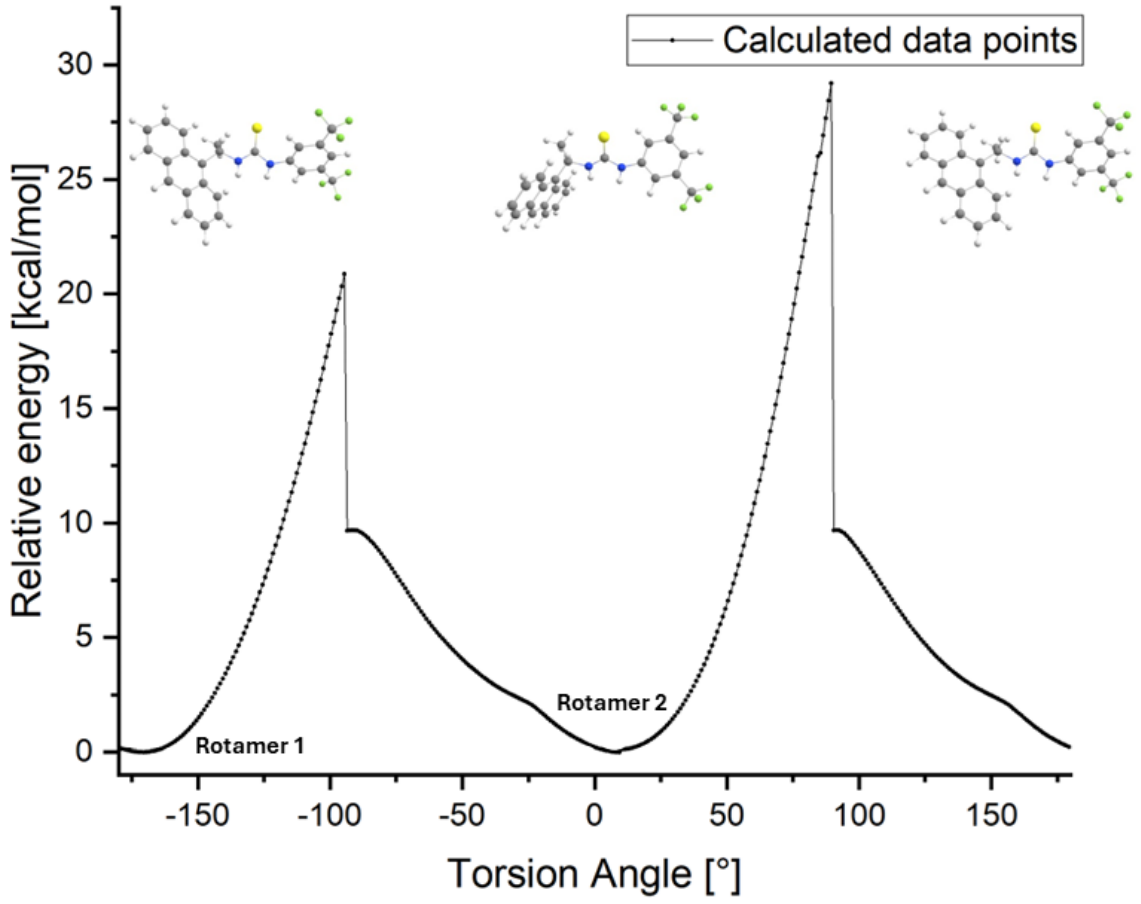

Figure 28 The three possible rotamers of **T12** if the rotation around the C–N bond angle is simulated *via* DFT calculations in the gas phase. All catalyst rotamers are optimised using the B3LYP functional with the D3(BJ) dispersion correction and the 6-31G(d,p) basis set. The temperature was set at 298 K.

The simulation for thiourea **T12** revealed two possible rotamers, with relative energy differences between 22 and 27 kcal/mol, indicating a more restricted rotation (energy-wise) compared to thiourea **T9**. This effect is likely due to the greater steric demands of the anthryl-group. Additionally, reduced rotational freedom results in a more rigid catalyst, which explains **T12**'s superior performance and higher enantioselectivity obtained in the Passerini reaction. The larger anthryl-group — compared to the naphthyl group in **T9** — provides better shielding of the reaction plane, effectively limiting the isocyanide's approach to the aldehyde (while bound to thiourea **T12**) to fewer orientations. Comparing the

optimised structures of the catalysts (Rotamer 3 of **T9**, and Rotamer 2 of **T12**), both the naphthyl- (**T9**) as well as the anthryl-group (**T12**) shield the downside of the thiourea functionality. While the larger anthryl-group is also able to shield the front and the back space, the smaller naphthyl-group is only able to shield one of them. This restriction likely favours a configuration that leads to the preferred formation of one enantiomer over the other.

Generally, the rotation of various functional groups in a catalyst can have multiple effects. For instance, the orientation may be responsible for stabilising the transition state that leads to one enantiomer by lowering the activation energy of that pathway, making it kinetically more favourable.[40] Ultimately altering the energy landscape can have tremendous influence on the reaction outcome. Several factors influence transition state stabilisation, such as non-covalent interactions (e.g., hydrogen bonding, π-π stacking, or van der Waals forces) and steric effects that can block certain reaction pathways. Since rotation is a dynamic phenomenon that may be influenced by reaction conditions (such as temperature), it is crucial for future research to investigate these factors to gain a better understanding of the mechanism of thiourea catalysis in the Passerini reaction.

4.2.2.3 Exploring the choice of solvent for the Passerini-3CR

Another crucial parameter for the reaction outcome is the choice of solvent for the chemical reaction.[398] The solvent can directly affect the conversion as well as the selectivity of the asymmetric reaction.[398] Generally, solvent effects arise from properties such as polarity, dielectric constant, coordination ability, or hydrogen bonding ability, to name a few. The previously employed cyclohexane has proven to be a versatile solvent in the initial investigations of the catalytic abilities of thiourea in the Passerini-3CR. Unfortunately, cyclohexane possesses a disadvantage. Cyclohexane has a rather high melting point of 6.7 °C, which makes its usage at low temperatures below its melting point impossible. At the same time, asymmetric catalysis often benefits from lower temperatures with regard to enantioselectivity.[395,398] Therefore, an investigation was performed to find another suitable solvent for the catalytic screening. Since the Passerini-3CR benefits from polar aprotic solvents and it is generally faster in a low-polarity medium, it is often conducted in dichloromethane, ethyl acetate, diethyl ether, and tetrahydrofuran.[261,263] The solvents used for the screening were chosen with respect to their melting points, which should be as low as possible to allow later screenings at low temperatures. Furthermore, aprotic solvents that are either non-polar (*n*-hexane, toluene) or slightly to moderately polar (dichloromethane)

were chosen. Additionally, chloroform was tested. Besides the selection of the solvent, the **standard screening conditions** were used. **Table 7** summarises the findings from the screening and allows a comparison between the thiourea-catalysed reactions (entry **P-10** to **P-23**) and highlights the catalytic effect on the yield of the Passerini product and the enantioselectivity.

Table 7 Screening of the Passerini-3CR, as shown in **Scheme 19**, with various solvents.

Entry	Catalyst	Solvent	Solvent m.p.	Yield [%]			*ee* [%]
			[°C]	2h	20h	44h	
P-01	-	Cyclohexane	6.7	5.1	26.8	43.2	0
P-10	T9	Cyclohexane	6.7	23.7	49.3	57.9	7.0
P-20	T9	Toluene	- 95	2.2	16.0	26.6	3.8
P-21	T9	Dichlormethane	- 97	2.7	19.0	32.3	0.2
P-22	T9	*n*-Hexane	- 95	20.1	42.6	57.4	9.3
P-23	T9	Chloroform	- 63	3.5	21.6	35.5	0.6

The reactions employed acetic acid, octanal and benzyl isocyanide in equimolar ratios at the standard screening conditions. The reactions were carried out in the respective solvent at a concentration of 0.025 mol×L^{-1}. The product yield was calculated based on GC-analysis and the *ee* was measured by chiral HPLC after 44 hours of reaction time.

By reviewing the obtained results of the solvent screening, *n*-hexane was determined as the solvent of choice for future catalytic screenings. The reaction conducted in *n*-hexane resulted in a comparable yield to the catalytic reaction in cyclohexane (**P-10**) with 57.4%. Furthermore, compared to entry **P-10**, the reaction in *n*-hexane initially led to lower yields after 2 hours and also after 20 hours of reaction time. However, after prolonged reaction times, the difference between these two approaches (**P-10** and **P-22**) became negligible, with only a 0.5% difference in total.

Thus, in terms of conversion and yield, both solvents are interchangeable. However, with regard to the enantioselectivity, *n*-hexane is more favourable. The change from cyclohexane to *n*-hexane led to a relative increase in enantioselectivity of 22%. Furthermore, *n*-hexane is a better solvent choice for further catalytic screening due to its much lower melting point of -95 °C. The difference in their melting points is accompanied by the slightly lower polarity of *n*-hexane, when compared to cyclohexane.[399]

The other tested solvents did not lead to an improvement in the reaction outcome. None of them resulted in higher yields, and they were outperformed by the non-catalysed reaction, which was conducted in cyclohexane (**P-01**). Furthermore, chlorinated solvents such as dichloromethane and chloroform had a negative influence on the catalyst's behaviour, as no

significant enantiomeric excess was measured. The use of toluene resulted in a much slower reaction, with only 26.6% yield after 44 hours, but it produced a small *ee* of 3.8%, making it only half as effective as the original approach in cyclohexane. It can be speculated whether the dipole moments of the solvents interfere with the transition state of the α-addition in the Passerini reaction, as both chlorinated solvents possess a dipole moment, as does toluene, albeit weaker. As a consequence, *n*-hexane was selected as the solvent of choice for all subsequent screenings under standard conditions.

4.2.2.4 Investigations into the reaction temperature

The influence of the reaction temperature on both yield and enantioselectivity was investigated to test the hypothesis that lowering the reaction temperature might suppress the background reaction that does not follow the catalytic pathway. For instance, a reduced temperature could limit the rotation of the polycyclic aromatic building block of the thiourea catalyst, due to the lower energy available. This might stabilise the most energetically favoured rotamer of the thiourea, leading to a more rigid structure of the organocatalyst and potential suppression of racemic catalytic pathways (compare **Chapter 4.2.2.2**). Furthermore, the increased rigidity could improve the spatial arrangement of the catalyst and reactants, potentially resulting in enhanced enantioselectivity in the process. Therefore, a screening series was performed (as summarised in **Table 8**) covering the temperature range from room temperature to -40 °C in steps of 20 °C.

Table 8 Screening of the Passerini-3CR, as shown in **Scheme 19**, at lower temperatures.

Entry	Catalyst	Solvent	Temperature [°C]	Yield 2h [%]	Yield 20h [%]	Yield 44h [%]	*ee* [%]
P-22	T9	*n*-hexane	r.t.	19.8	42.6	57.4	9.3
P-24	-	*n*-hexane	0	1.4	12.1	23.4	0.7
P-25	T9	*n*-hexane	0	6.8	35.9	47.9	11.9
P-26	-	*n*-hexane	- 20	0	5.6	14.8	0.8
P-27	T9	*n*-hexane	- 20	2.1	18.8	35.3	11.6
P-28	-	*n*-hexane	- 40	0	2.5	5.8	0.7
P-29	T9	*n*-hexane	- 40	1.4	8.6	16.5	10.7

The reactions employed acetic acid, octanal and benzyl isocyanide in equimolar ratios. The reactions were carried out in *n*-hexane at a concentration of 0.025 mol×L^{-1}. The product yield was calculated based on GC-analysis and the *ee* was measured by chiral HPLC after 44 hours of reaction time.

Given the nature of slight variations in enantiomeric excess — often within a range of approximately 1 percent due to measurement inaccuracies or integration discrepancies in peak analysis *via* ORIGINLAB — it is reasonable to believe that the entries without catalyst employment resulted in no discernible excess of either enantiomer.

The results show that temperatures lower than -20 °C did not result in improvements in enantioselectivity or overall yield. In fact, comparative analysis after 44 hours between **P-27** and **P-29** demonstrated a 114% difference in relative yield. An equal result is obtained by comparing the approaches conducted at -20 °C (**P-27**) and 0 °C (**P-25**) with only a negligible difference in enantioselectivity, but a 36% higher yield in relative terms at 0 °C. Hence, for subsequent screenings at low temperatures, 0 °C emerges as the optimal choice, representing the best combination of yield and enantioselectivity.

According to Gawley *et al*., the previously discussed equation *(Eq. 7)* (**Chapter 4.2.2.1**) for the product ratio of a reaction under kinetic control can explain why lower temperatures did not lead to improved enantioselectivity.[395]

$$\frac{B}{C} = \frac{k_1}{k_2} = e^{-\frac{\Delta\Delta G^{\ddagger}}{RT}} \qquad (Eq.\ 7)$$

Temperature effects must be included in the equation, as the free energy is temperature-dependent. The following equation demonstrates the relationship of Gibbs free energy (G) with reaction enthalpy (H) and entropy (S):

$$\Delta G = \Delta H - T\Delta S \qquad \textit{(Eq. 9)}$$

The combination of *Eq. 7* and *Eq. 9* leads to *Eq. 10*, where $\Delta\Delta H$ and $\Delta\Delta S$ represent the differences in enthalpy and entropy for the activation energy barriers for the formation of B and C, respectively.

$$\frac{B}{C} = \frac{k_1}{k_2} = (e^{-\frac{\Delta\Delta H^{\ddagger}}{RT}})(e^{\frac{\Delta\Delta S^{\ddagger}}{R}}) \qquad \textit{(Eq. 10)}$$

It is important to note that *Eq. 10* indicates that only the enthalpy term is temperature-dependent. According to Gawley *et al.*, enthalpy contributions dominate in many stereoselective reactions, though this is not always the case.[395] On the other hand, it is crucial to remember the approximations made with these equations. Additionally, the logarithm of *Eq. 10* results in a modified form of the Eyring equation:

$$\ln\frac{k_1}{k_2} = -\frac{\Delta\Delta H^{\ddagger}}{RT} + \frac{\Delta\Delta S^{\ddagger}}{R} \qquad \textit{(Eq. 11)}$$

Plotting $ln(k_1/k_2)$ versus $1/T$ often results in non-linear behaviour across a wide temperature range, and the modified Eyring plot shows a maximum for enantioselectivity, known as the inversion temperature.[395] Below and above this inversion temperature, lower enantioselectivities are observed. Assuming this, one can infer that in the thiourea-catalysed Passerini reaction, the inversion temperature lies between 0 °C and -20 °C, as suggested by empirical data. Generally, lower temperatures can be beneficial for enantioselectivity, as they help control the conformational flexibility of the catalyst and reaction intermediates, particularly by restricting the rotation of the bulky naphthyl-group in the catalyst.

4.2.2.5 Exploring the impact of stoichiometry on the Passerini-3CR

To explore the impact of the stoichiometry of the reactants, several reactions were carried out with altered stoichiometry, in which one or two of the reactants were used in excess. All other reaction parameters remained consistent, with 20 mol% of the **T9** as catalyst added to the reaction mixture. The results from this screening are summarised in **Table 9**.

Table 9 Screening the impact of the stoichiometry on the Passerini reaction, as shown in **Scheme 19**.

Entry	Stoichiometry Acid : Aldehyde : Isocyanide	Yield 2h [%]	Yield 20h [%]	Yield 44h [%]	*ee* [%]
P-22	1 : 1 : 1	19.8	42.6	57.4	9.3
P-30	2 : 1 : 1	27.2	63.6	73.9	10.7
P-31	1 : 2 : 1	30.5	67.7	77.9	12.3
P-32	1 : 1 : 2	29.5	65.8	76.0	11.4
P-33	2 : 2 : 1	37.6	85.0	96.5	7.6
P-34	2 : 1 : 2	35.8	79.9	90.6	9.5
P-35	1 : 2 : 2	42.2	89.7	97.9	10.4

All reactions used acetic acid, octanal and benzyl isocyanide as reactants and were conducted in presence of **T9** as organocatalyst. The reactions were carried out in *n*-hexane at a concentration of 0.025 mol×L^{-1}.

Entry **P-22** serves as a reference point, employing equimolar ratios of the reactants. A clear trend emerges when compared to other reactions: using two equivalents of one reactant significantly enhances the yield (**P-30** to **P-32**). This effect is further amplified when two reactants are used in excess, leading to nearly quantitative results. For example, entry **P-35**, which used higher amounts of isocyanide and aldehyde, achieved yields of 97.9%. Similarly, entry **P-33**, where both the acid and aldehyde were used with two equivalents each, yielded 96.5%. These enhanced yields can be explained by the shift in reaction equilibria towards product formation, in line with Le Chatelier's principle.

However, using higher amounts of two reactants also resulted in lower enantiomeric excesses. Notably, when only one reactant was added in excess (entry **P-31**), the best outcome in terms of yield was achieved in this screening series, reaching 77.9% — a relative increase of 36% compared to **P-22** with equimolar ratios. Additionally, entry **P-31** exhibited the highest enantioselectivity, with an *ee* of 12.3%, representing a relative increase of 32%.

In general, the best results in terms of enantioselectivity were obtained when the carboxylic acid was present in a smaller amount compared to the other reactants (compare **P-31** and **P-32**). This suggests that the uncatalysed background reaction was slightly suppressed, as a smaller amount of acid — compared to the other reactants — had to compete with the catalyst for product formation. These findings align with the proposal from the Morokuma group, which suggests that the Passerini reaction can be viewed as a four-component reaction, in which the carboxylic acid acts both as a reactant and as a catalyst, now in greater competition with the thiourea catalyst.[262]

This effect is more pronounced when higher amounts of aldehyde are used (**P-31**) instead of isocyanide (**P-32**), which led to the hypothesis that the thiourea catalyst binds to the aldehyde *via* hydrogen bonding, thereby enabling the catalytic pathway by enhancing the aldehyde's electrophilicity. With higher amounts of aldehyde present in the reaction mixture, this effect is more visible and higher enantioselectivities were achieved. This hypothesis was confirmed by DFT calculations conducted by the Wenzel group (Institute of Nanotechnology, KIT) during an ongoing collaborative study, which has yet to be published. Wenzel *et al*. found that thiourea is most likely to bind to the aldehyde at the beginning of the reaction.

4.2.2.6 Impact of adding the acid component over an extended period

In further tests, a theory was investigated, which stated that the addition of the carboxylic acid over an extended time period can affect stereoselectivity favourably.[266] For this purpose, the carboxylic acid was added over a period of 2 hours using a syringe pump to ensure that, at the beginning of the reaction, only a very small amount of the acid was present. This could potentially help suppress the uncatalysed racemic Passerini reaction, which competes with the catalysed reaction pathway involving thiourea. This concept was previously investigated by Wang *et al*., who reported that such a delayed addition led to higher enantioselectivities in their approach to the enantioselective Passerini-3CR.[266] The following **Table 10** compares this method with the conventional enantioselective Passerini-3CR under the standard setup.

Table 10 Investigation into a delayed addition of the carboxylic acid to reaction mixture of the Passerini reaction, as shown in **Scheme 19**.

Entry	Catalyst	Notes	Yield 2h [%]	Yield 20h [%]	Yield 44h [%]	*ee* [%]
P-36		-	3.5	25.4	41.8	0
P-22	T9	-	20.1	42.6	57.4	9.3
P-37	T9	acid added over time period of 2h	15.4	46.9	56.1	12.6

The reactions were carried out according to the **standard screening procedure** at room temperature at a concentration of 0.025 mol×L^{-1} in *n*-hexane. The reactants were added in equimolar ratios and in case of **P-37**, the carboxylic acid was added over a prolonged time period of 2 hours.

It is evident that the reaction in which the carboxylic acid was added over a period of two hours (**P-37**) performed almost as well in terms of yield as the reaction where all reactants were present from the beginning (**P-22**). Additionally, the reaction **P-37** outperformed the reaction conducted without a catalyst (**P-36**), achieving a 34% higher yield after 44 hours.

The approaches **P-22** and **P-37** showed differences in performance during the first two hours, which can be attributed to the lower concentration of the acid component in the early stages of **P-37**. Due to the syringe pump's gradual addition, the full initial concentration of the acid component was only reached after two hours, resulting in a 33% lower yield compared to **P-22** during this period. However, as the reaction progressed, this initial disparity diminished, and comparable yields were eventually measured.

Notably, **P-37** exhibited a 36% improvement in enantioselectivity compared to **P-22**, with a total enantiomeric excess of 12.6%. This clearly indicates that the addition procedure over a long time period in the beginning of the reaction can help suppress the uncatalysed reaction pathway to some extent.

To further explore this effect, another reaction (**P-38**) was conducted, where the carboxylic acid was added over a prolonged period of four hours using a syringe pump. Enantioselectivity was also monitored during this experiment, with samples taken from the crude mixture and analysed *via* chiral HPLC over the first four hours to track the enantiomeric excess. The corresponding results are presented in **Table 11**.

Table 11 Addition of the carboxylic acid over a time period of four hours to the Passerini reaction, as shown in **Scheme 19**.

Entry	Yield 2h [%]	Yield 20h [%]	Yield 44h [%]	*ee* 1h [%]	*ee* 2h [%]	*ee* 3h [%]	*ee* 4h [%]	*ee* 44h [%]
P-38	10.1	48.8	54.8	15.5	15.2	14.8	14.4	12.3

The reactions were carried out at room temperature at a concentration of 0.025 mol×L^{-1}. The reactants were added in equimolar ratios and if not otherwise stated using the **standard screening procedure**. The carboxylic acid was added over a prolonged period of four hours using a syringe pump.

The extended addition time resulted in a slower reaction at the beginning, as indicated by the yield progression. Due to the slow addition, the yield of the Passerini product was only 10.1% after 2 hours of reaction time. This represents a relative decrease of 52% compared to the approach with a 2-hour addition time (**P-37**), and a 100% decrease compared to the approach where the carboxylic acid was added all at once at the start of the reaction (**P-22**). However, comparable yields were ultimately achieved over the long term, suggesting that the effect of extended reactant addition is more pronounced early in the reaction, but diminishes after 20 hours.

The delayed addition of the acid component also influenced the enantioselectivity of the reaction. After just one hour, an *ee* value of 15.5% was measured, representing a 67% relative

increase compared to the approach where all of the carboxylic acid was added at the beginning (**P-22**). However, the *ee* values decreased over time, and after 44 hours, the same result was obtained as in the 2-hour addition approach (**P-37**). The investigation suggests that higher enantioselectivity can generally be achieved when a lower amount of carboxylic acid is present in the reaction mixture, as it was the case in the early stages when the acid was slowly added.

Furthermore, these results align with findings from the altered stoichiometry experiments, where the best outcomes were observed when the aldehyde and isocyanide were used in higher amounts relative to the carboxylic acid. With both approaches pointing in the same direction, one objective for future research could be to investigate the concentration of the reaction mixture. In both the altered stoichiometry procedure and the approach involving slow carboxylic acid addition, a total concentration of 0.025 M was used. This low concentration was initially chosen to ensure that the catalytic activity was visible for the analytical devices and to slow down the uncatalysed background reaction.

It may be worth investigating whether a slow addition of carboxylic acid over a longer period would yield better results if the overall concentration of the reaction mixture were higher. The hypothesis is that small portions of acid, when added, would react more quickly with the other reactants to form the Passerini product. This would likely proceed through the catalytic pathway, as the thiourea catalyst would be present as well to promote the reaction and previous results state, that the catalytic pathway generally outcompetes the non-catalysed in terms of kinetics. As a result, the small portions of acid would react promptly, rather than remaining in the mixture where they might catalyse the background reaction through a non-catalytic pathway, in which according to Morokuma two molecules of the carboxylic acid are necessary for product formation.[262] Also, the catalytic effect might even improve if at the same time the addition time is extended further. Until then, this procedure represents a promising tool for enhancing the enantioselectivity of the Passerini-3CR in the presence of thioureas as organocatalysts.

4.2.2.7 Exploring the impact of additional drying agents in the reaction mixture

This screening series follows the description of Tan and Liu *et al*.[36] that drying agents in the reaction mixture positively influence the chemical yield and asymmetric induction of the Passerini-3CR. Therefore, commonly used drying agents and molecular sieves were added in the respective approaches to investigate their performance. The results are summarised in **Table 12**.

Table 12 Exploring the impact of drying agents in the reaction procedure of the Passerini-3CR, as shown in **Scheme 19.**

Entry	Catalyst	Additive	Yield 2h [%]	Yield 20h [%]	Yield 44h [%]	*ee* [%]
P-36		-	3.5	25.4	41.8	0
P-22	T9	-	20.1	42.6	57.4	9.3
P-39	T9	$MgSO_4$	17.6	46.7	56.3	14.1
P-40	T9	Na_2SO_4	16.0	45.8	54.0	14.4
P-41	T9	MS-3Å	19.7	50.6	60.0	10.0
P-42	T9	MS-4Å	18.4	48.8	58.1	9.8

The reactions were carried out at room temperature at a concentration of 0.025 mol×L^{-1}. The reactants were added in equimolar ratios and if not otherwise stated using the **standard screening procedure**. **P-39** and **P-40**, each used 0.1 g of manganese or sodium salt respectively, while also 0.1 g of molecular sieves (MS) were used in **P-41** and **P-42**.

Comparing the yields that were measured, all approaches using conventional drying agents performed very similarly to approach **P-22**, which did not employ drying agents. Only approach **P-41**, in the presence of molecular sieves MS-3Å, performed slightly better, giving a 5% increased yield compared to **P-22**. The reaction in the presence of Na_2SO_4 performed slightly worse than **P-22**, with a decrease of 6% in yield after 44 hours of reaction time.

More interestingly, drying agents indeed tend to have a beneficial effect on the enantioselectivity of the reaction. This effect was only marginally visible in the presence of molecular sieves in approaches **P-41** and **P-42** but was highly noticeable when sodium and magnesium sulphate salts were used. In both cases, the enantiomeric excess slightly exceeded 14%, leading to increases of 52% (**P-39**) and 55% (**P-40**) in enantiomeric excess, respectively. Such a significant effect was unexpected. One possibility is that the salt ions help stabilize the transition state of the α-addition, contributing to higher enantioselectivities. Another explanation lies in the nature of thiourea catalysts. Their catalytic potential stems from their ability to act as hydrogen bond donors.[184] It is plausible that the use of drying agents created drier conditions within the reaction mixture, reducing the presence of trace water residues. This would minimise any hydrogen bonding interactions with residual water,

creating a less disruptive environment for the thiourea catalyst to function more effectively as a hydrogen bond donor. Consequently, this may have led to improved overall performance. Further research is needed to explore this phenomenon in greater depth.

4.2.2.8 Investigation into the catalyst concentration

In this screening series, the required catalyst concentration to observe a catalytic effect was investigated. Several reactions were performed with varying catalyst concentrations reaching from 1 to 100 mol%, while maintaining standard screening conditions for all other variables. Reactant conversion and yield were monitored using GC analysis, and the stereoselective outcome was determined after 44 hours *via* chiral HPLC. The results are summarised in **Table 13**, which also includes previous data for better comparability.

Table 13 Exploring the impact of different amounts of catalyst on the Passerini reaction, as shown in **Scheme 19**.

Entry	Catalyst [mol%]	Yield 2h [%]	Yield 20h [%]	Yield 44h [%]	*ee* [%]
P-36	0	3.5	25.4	41.8	0
P-43	1	5.8	31.2	47.4	2.3
P-44	5	11.4	40.0	54.6	6.8
P-45	10	14.8	43.0	54.3	8.8
P-22	20	20.1	42.6	57.4	9.3
P-46	100	22.5	68.9	79.8	11.8

The reactions were carried out at room temperature at a concentration of 0.025 mol×L^{-1}. The reactants were added in equimolar ratios and if not otherwise stated using the **standard screening procedure**. Different amounts of thiourea **T9** were used. The exact amount is shown in the table.

Reviewing the data from the catalyst concentration screening, it became evident that even at a catalyst concentration of only 1 mol% (**P-43**), a slight catalytic effect was noticeable. Compared to entry **P-36**, which was conducted without any thiourea, a 13% higher yield was observed after 44 hours, along with a modest enantiomeric excess of 2.3%. When comparing catalyst concentrations between 5 and 20 mol% (**P-44**, **P-45**, and **P-22**), it became clear that higher catalyst concentrations primarily impacted the yield of the Passerini product within the first 2 hours of the reaction. Subsequently, comparably high yields were achieved. For instance, after 44 hours each showing at least a 29% increase over the uncatalysed reaction.

In contrast, when 100 mol% of thiourea **T9** was used (**P-46**), the catalyst's effect on yield was marginal after the first 2 hours, with a yield of 22.5% compared to 20.1% in **P-22**. On the other hand, the high catalyst concentration led to yields reaching 79.8% after 44 hours,

representing an approximate 100% increase compared to **P-36**. In terms of enantioselectivity, a clear trend emerged: higher amounts of thiourea resulted in higher enantiomeric excesses, with **P-46** showing up to 11.8% *ee* with 100 mol% **T9**.

Given the previous hypothesis that thiourea **T9** catalyses the Passerini-3CR *via* multiple pathways — leading either to one enantiomer or a racemic mixture — the results from this concentration screening align with that theory. As more catalyst is introduced, the reaction rate increases, resulting in higher yields, but only a portion of the accelerated product generation contributes to stereoselective product formation.

In summary, catalytic effects were observed under the given conditions even with low catalyst concentrations of 1 mol%. However, for future investigations, 20 mol% of thiourea will continue to be used until a more comprehensive understanding of the entire catalytic process is obtained and higher enantioselectivities in general are achievable. The use of 20 mol% ensures the catalytic effect is clearly detectable while still using a moderate, substoichiometric amount of catalyst. It is noteworthy that the utilised thiourea catalyst can be easily recovered from the reaction mixture through purification by column chromatography with a recovery rate of 93%. It is assumed, that this number can even be higher if the gradient of the chromatographic purification process is adapted. Unless stated otherwise, the crude product is typically purified using a gradient of cyclohexane and ethyl acetate. During this process, the thiourea is readily separated from other fractions and can be isolated for future use.

4.2.3 A screening series of thiourea catalysts with similar structural features

The optimization of the reaction conditions provided valuable insights into the mechanism of the asymmetric Passerini-3CR in the presence of thiourea catalysts. Subsequently, a screening series was conducted to further investigate the impact of stereoisomerism (**T13**) and regioisomerism (**T14**) of the isomers of the previously employed thiourea **T9**. **Figure 29** shows the respective thioureas **T13** and **T14**, which were previously synthesized and are now being used for direct comparison with **T9**. The catalysts were tested under standard reaction conditions, and the results are presented in **Table 14**. For better comparability also previous results are included.

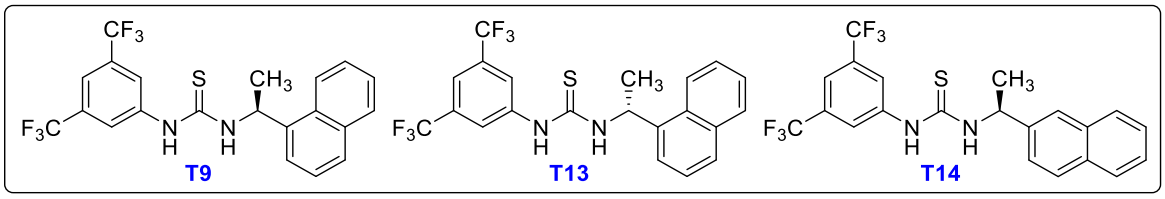

Figure 29 Thiourea organocatalysts that follow the same structural motif as **T9** represent stereo and regioisomers of **T9**.

Table 14 Investigation into thiourea catalysts with similar structural features in the standard set up of the Passerini-3CR, as shown in **Scheme 19**.

Entry	Catalyst	Yield 2h [%]	Yield 20h [%]	Yield 44h [%]	*ee* [%]
P-36	-	3.5	25.4	41.8	0
P-22	T9	20.1	42.6	57.4	-9.3
P-47	T13	20.5	51.4	62.7	7.9
P-48	T14	23.3	49.8	58.9	-5.4

The reactions were conducted at room temperature with a concentration of 0.025 mol×L^{-1} following the standard screening conditions. Negative *ee* values were obtained when the second of the two enantiomeric peaks in the chromatogram showed a greater response in the presence of the catalyst, resulting in a higher integration value for this peak. Positive *ee* values indicate that the first enantiomeric peak had a higher integration value.

The screening series with regio- and stereoisomers of thiourea **T9** confirmed that altering the stereochemistry of the catalyst from the *S*-derivative (**T9**) to the *R*-derivative (**T13**) directly influences the stereochemistry of the Passerini product. While the reaction yields two enantiomeric peaks detectable in chiral HPLC analysis, *S*-thiourea **T9** favours the formation of the second enantiomer (represented by the second enantiomeric peak in chiral HPLC analysis), whereas *R*-thiourea **T13** promotes the preferred generation of the first enantiomer (represented by the first enantiomeric peak). This allows for direct control over the stereochemical outcome of the Passerini reaction by selectively choosing the stereochemistry of the catalyst.

Additionally, an investigation was conducted to assess the extent to which regioisomerism influences catalyst design. To facilitate this, the regioisomer **T14** was introduced as an organocatalyst for comparison with thiourea **T9** (compare **Figure 30**).

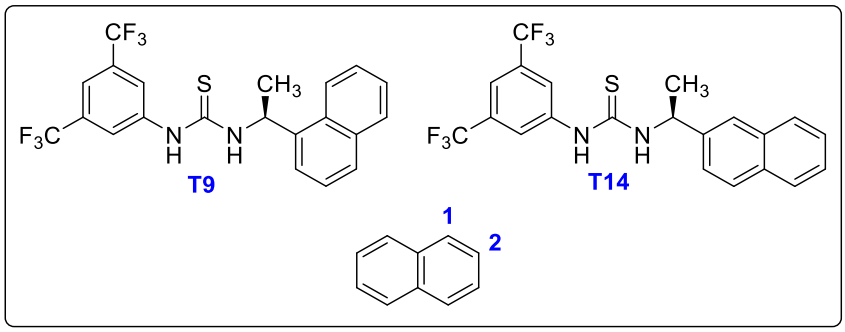

Figure 30 Thiourea organocatalysts **T9** and **T14**: Variations in positioning of the naphthyl group.

It was found that connecting the naphthalene group at the 2-position towards the thiourea (**T14**) is less effective for catalyst design. This reduced effectiveness is likely due to decreased shielding of one plane of the catalyst compared to when the naphthalene group is connected to the thiourea *via* the 1-position (**T9**). The steric bulk of naphthalene, when connected to thiourea at the 1-position, may provide better shielding of the reactive plane, resulting in a more favourable orientation for catalytic activity. Additionally, the rotation of the naphthyl group may be more hindered, leading to a more rigid structure for the catalyst.

4.2.4 Investigation into the reactant variability of the Passerini-3CR

Despite several advancements in catalyst design and reaction conditions, improvements in the stereoselective Passerini-3CR remained modest. In a comparison with the approach of the Bin Tan group, a key difference represents the choice of reactants. Bin Tan *et al*., who used chiral phosphoric acid as an organocatalyst for their asymmetric Passerini reaction, predominantly employed bulky and spatially demanding reactants (e.g., triphenylacetic acid as opposed to the acetic acid used in this thesis) to achieve high enantioselectivities up to 99%.[36]

To ensure that the stereochemical outcomes in this thesis are not constrained by the choice of reactants, a systematic study was conducted. The aim was to identify structural motifs of the reactants that are essential for achieving good enantiomeric excess. For this purpose, reactants of increased steric hindrance compared to the so far used acetic acid, octanal and benzyl isocyanide were investigated, such as phenylacetic acid, cyclohexyl isocyanide, and benzaldehyde. Additionally, the screening series involved using previously selected thiourea catalysts in Passerini-3CR reactions with those bulkier reactants, in order to validate earlier

results and trends when one substituent was exchanged with a bulkier option, for instance phenylacetic acid instead of acetic acid.

For comparison, please refer to previous chapters where the results of the investigation into the impact of the size of the polycyclic aromatic building block are summarised in **Table 5**, while the influence on the stereo- and regioisomerism of catalyst **T9** is shown in **Table 15**. Furthermore, **Table 8** contains entry **P-22**, which serves as a reference for the catalytic performance of thiourea **T9** under standard screening conditions in the solvent *n*-hexane (e.g. 57.4% yield and 9.3% ee after 44 hours of reaction time).

4.2.4.1 Validation of previous results with bulkier reactants

Impact of the carboxylic acid

This screening series focused on the exchange of the carboxylic acid to a spatially more demanding option. The reactions were carried out according to the **standard screening procedure** in *n*-hexane at room temperature. Phenylacetic acid, octanal, and benzyl isocyanide were used as reactants, as illustrated in **Scheme 20**. The subsequent **Table 15** summarises the results of the respective screening series:

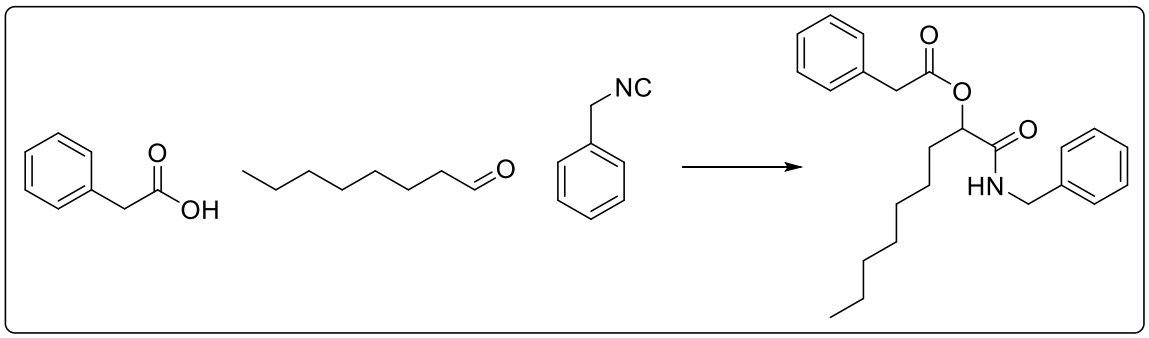

Scheme 20 Reaction scheme of the Passerini-3CR involving phenylacetic acid, octanal and benzyl isocyanide.

Table 15 Investigation into sterically demanding reactants – phenylacetic acid.

Entry	Catalyst	Conversion 2h [%]	Conversion 44h [%]	*ee* [%]
P-49	-	10.8	63.6	0.3
P-50	T10	30.9	75.0	0.7
P-51	T11	40.7	82.7	0.8
P-52	T9	37.4	75.4	7.7
P-53	T12	38.6	80.6	13.1
P-54	T13	35.7	77.7	6.4
P-55	T14	29.8	72.8	0.1

The reactions were carried out according to the **standard screening procedure** in *n*-hexane at a concentration of 0.025 mol×L^{-1}. Phenylacetic acid, octanal and benzyl isocyanide were used as reactants. Since no calibration for the GC existed, the reaction progress was measured by screening the conversion of the aldehyde. For this purpose, tetradecane served as an internal standard and was added to the reaction mixture.

Please note that in this approach, no calibration was performed for the GC used to monitor reaction progress. Here, the progress is expressed by the conversion of the aldehyde component, calculated using tetradecane as an internal standard. Nonetheless, the aldehyde conversion can serve as a reference to approximate reaction progress. This is legitimate, since no major side reactions that would consume the aldehyde were observed in previous experiments. The primary focus of this screening series was on enantioselectivity.

Overall, the results obtained are consistent with earlier findings and support the conclusions from the outcomes of the screening series involving acetic acid. However, notable discrepancies arise with catalysts **T11** and **T14**. For instance, the use of **T11** did not result in a significant enantiomeric excess when phenylacetic acid was used, unlike the approach with acetic acid, which achieved a 3.3% enantiomeric excess (entry **P-12**, **Table 5**). The most significant deviation was observed with **T14** in entry **P-55**, where no enantioselectivity was obtained, in contrast to the 5.1% achieved in the acetic acid approach (**P-48**). This difference highlights the crucial role of the positioning of the naphthyl group in the thiourea organocatalyst. It is conceivable that steric repulsion occurred between the phenyl group in phenylacetic acid and the naphthyl group attached to thiourea **T14** at the 2-position, preventing stereoinduction. Notably, a catalytic effect was observed in **P-55** regarding the conversion of the aldehyde, in comparison with the uncatalysed reaction **P-49**.

Another notable difference from previous findings is the slightly poorer performance of **T9** compared to the acetic acid approach in *n*-hexane, which resulted in a higher *ee* value of 9.3% (entry **P-22**, **Table 8**). It seems that the smaller, less sterically demanding acetic acid was more suitable for achieving higher enantioselectivities. A possible explanation is that

thiourea **T9**, the aldehyde, and the isocyanide create a spatial arrangement in the transition state of the α-addition of the isocyanide to the aldehyde compare (**Figure 22** in **Chapter 4.2.2.2**). In this arrangement, it may be advantageous for the carboxylic acid to be smaller in order to fit into the cavity of the hydrogen-bonded complex created by the other reactants and the catalyst.

However, thiourea **T12** achieved higher enantioselectivity compared to the 11.6% in Entry **P-13** when phenylacetic acid was used, resulting in an *ee* of 13.1%. It should be noted that approach **P-13** was conducted in cyclohexane, and therefore direct comparison with **P-53** is challenging due to solvation effects, which are likely to play a crucial role in the reaction outcome.

Impact of the aldehyde

The screening involving benzaldehyde was initially omitted due to a lack of reaction progress, leading to the conclusion that the Passerini-3CR does not proceed effectively with benzaldehyde as it was also reported by Wang *et al.*[266] However, later investigations showed that the reaction with benzaldehyde is possible, albeit very slow and with poor yields. A more detailed investigation into the impact of the aldehyde is provided in **Chapter 4.2.4.2**.

Impact of the isocyanide

Next, screening focused on the exchange of the isocyanide towards a spatially more demanding option. The reactions were carried out again according to the **standard screening procedure** in *n*-hexane at room temperature. Acetic acid, octanal, and cyclohexyl isocyanide were used as reactants, as illustrated in **Scheme 21**. The subsequent **Table 16** summarises the results of the respective screening series:

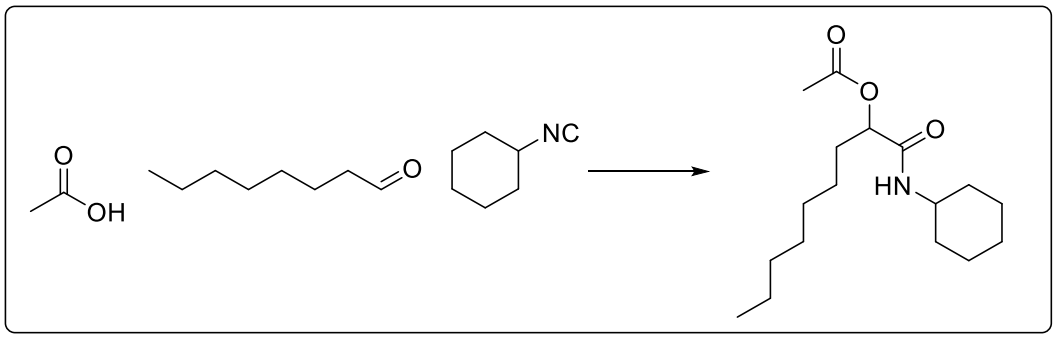

Scheme 21 Reaction scheme of the Passerini-3CR involving acetic acid, octanal and cyclohexyl isocyanide.

Table 16 investigation into sterically demanding reactants – cyclohexyl isocyanide

Entry	Catalyst	Conversion 2h [%]	Conversion 44h [%]	*ee* [%]
P-56	-	5.1	50.7	0.4
P-57	T10	27.1	71.2	3.5
P-58	T11	33.8	74.1	6.6
P-59	T9	30.4	67.7	13.7
P-60	T12	34.2	75.6	19.3
P-61	T13	32.7	75.5	7.0
P-62	T14	37.3	76.6	6.0

The reactions were carried out according to the **standard screening procedure** in *n*-hexane at a concentration of 0.025 mol×L^{-1}. Acetic acid, octanal and cyclohexyl isocyanide were used as reactants in all approaches. Since no calibration for the GC existed, the reaction progress was measured by screening the conversion of the aldehyde. For this purpose, tetradecane serves as an internal standard and was added to the reaction mixture.

Also here, the reaction progress was monitored by measuring the aldehyde conversion, which was assessed across all approaches using GC screening. A distinct catalytic effect was observed in the presence of the thiourea organocatalyst, leading to aldehyde conversions ranging from 68% to 77% after 44 hours of reaction. In contrast, without the thiourea catalyst, only 50.7% conversion was observed in entry **P-56**.

Overall, the results from both GC analysis and chiral HPLC are consistent with earlier findings and support the conclusions drawn from the screening of the different thiourea catalyst. The results from the screening series presented in **Table 5** were confirmed, this time with overall better catalyst performance with regard to the obtained enantiomeric excess. Reviewing the measurements, improved enantioselectivities were obtained in the presence of the thiourea organocatalysts **T9** and **T12** in relative perspective to previous results.

Entry **P-60** is particularly noteworthy, as the best results were achieved with **T12**, resulting in an *ee* value of 19.3% and an aldehyde conversion of 75.6% after 44 hours of reaction,

marking the most favourable outcome thus far. It is conceivable that the spatial arrangement in the transition state was both influenced by the bulky reactant cyclohexyl isocyanide and the steric demands of the catalyst and further the catalysts ability to shield the reaction plane.

Figure 31 presents a comparison between the HPLC measurements using a chiral column conducted without any thiourea catalyst (entry **P-56**, black line) and those with **T12** (entry **P-60**, red line). A decrease in the first peak, accompanied by an increase in the second peak compared to the uncatalysed reaction, is evident.

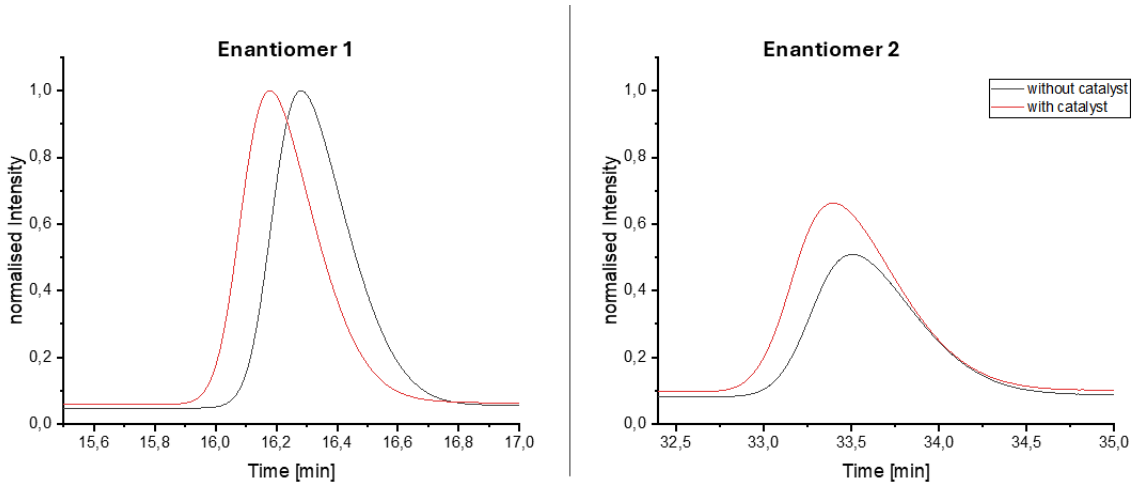

Figure 31 Comparison of entry **P-56** (black line), which was carried out without thiourea catalyst and **P-60** (red line), which was carried out in presence of 20 mol% thiourea **T12**. Usage of thiourea **T12** led to the observation, that the second enantiomer peak is growing in its intensity. For better clarity, the respective peaks are presented in a zoomed-in view and the peaks are normalised.

Previous results (refer to **Table 4**) were validated by the catalyst screening in the presence of bulkier carboxylic acids and isocyanides. It was concluded that, in addition to the rigidity of the catalyst and the restricted rotation of its functional groups (refer to **Chapter 4.2.2.2**), the choice of reactants has a major impact on the stereoselectivity of the thiourea-catalysed Passerini reaction. Therefore, the following chapter aims to explore this matter in greater depth by conducting a substrate screening.

4.2.4.2 Investigation into the substrate scope of the thiourea-catalysed Passerini–3CR

The following investigations aimed at determining the limitations of the substrate choices and at identifying the types of reactants that enhance enantioselectivity. For this purpose, both aliphatic as well as aromatic compounds were selected. Additionally, first efforts were made by selecting aldehyde and carboxylic acid substrates with varying electronic properties, being either electron-rich or electron-poor. Furthermore, substrates with different steric demands were employed to compare the influence of spatial arrangement on each reactant in the P – 3CR. Since completely new compounds were generated, the determination of the reactions yield *via* the GC calibration was not applicable and therefore the conversion of the aldehyde or the isocyanide was used to monitor the reactions progress. Usually both reactants showed good detectability by GC, which uses an FI-detector, and their conversion was easily determinable with the employment of an internal standard and the method of t_0-sampling. For all substrate screenings, the cost-efficient but less powerful thiourea catalyst **T9** was used, despite the more promising enantioselectivities obtained with its anthryl-counterpart, **T12**.

Structural variation of the isocyanide

Since the substitution of benzyl isocyanide with cyclohexyl isocyanide had the greatest effect on the stereochemical outcome of the reaction so far, the initial screening aimed to further investigate steric effects. For comparison, results from earlier screenings are also included in the **Table 17**. **Figure 32** shows the investigated isocyanide compounds.

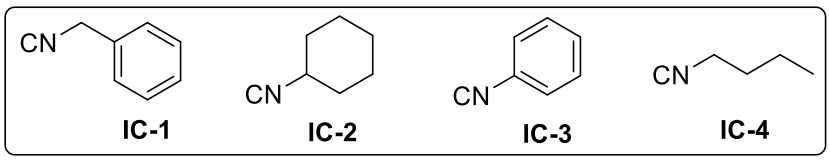

Figure 32 Selection of isocyanides employed in the screening series for structural variation of the Passerini compound.

Benzyl isocyanide (IC-1) is the standard isocyanide used in the screening procedure and serves as a reference. Cyclohexyl isocyanide (IC-2) and phenyl isocyanide (IC-3) are used to explore the steric impact when the isocyano functional group is positioned closer to the bulky element. By comparing IC-2 and IC-3, potential electronic effects of the aryl moiety versus the aliphatic cyclohexyl group can be examined. *n*-Butyl isocyanide (IC-4), a less-sterically hindered aliphatic isocyanide, is intended to determine whether steric effects

influence the reaction at all. The results of the respective screening series are summarised in **Table 17**.

Table 17 Investigation into structural variations of the isocyanide

Entry	Isocyanide	Catalyst	Conversion 2h [%]	Conversion 20h [%]	Conversion 44h [%]	*ee* [%]
P-36	IC-1	-	3.5	25.4	41.8	0.2
P-22	IC-1	T9	19.8	42.6	57.4	9.3
P-56	IC-2	-	5.1	-	50.7	0.4
P-59	IC-2	T9	30.4	-	67.7	13.7
P-63	IC-3	-	0.8	4.0	7.6	0.3
P-64	IC-3	T9	3.4	20.6	33.6	13.9
P-65	IC-4	-	5.5	32.9	57.3	0.3
P-66	IC-4	T9	28.8	59.7	69.6	9.7

The reactions were carried out according to the standard screening protocol in *n*-hexane at a concentration of 0.025 mol×L^{-1}. The Passerini reaction uses acetic acid, octanal and the respective isocyanide mentioned in the table in equimolar ratios. Since no calibration for the GC existed, the reaction progress was measured while screening the conversion of the aldehyde. Therefore, an internal standard was added to the reaction mixture. The enantiomeric excess was determined by chiral HPLC.

Upon analysing the data of the isocyanide screening, it becomes evident that isocyanides IC-1 and IC-4 resulted in comparable enantioselectivities. In each case, they were lower than those of IC-2 and IC-3, which also showed comparable results to each other. This circumstance might be explained by the R-CH_2-spacer present between the isocyano-functional group and the sterically demanding rest (R-group) in IC-1 and IC-4. There was no difference in stereoselectivity in the entries **P-22** and **P-66** and between the aliphatic chain of isocyano butane (IC-4) and the phenyl group of benzyl isocyanide (IC-1), respectively.

However, the isocyanides IC-1 and IC-4 differed in their reactivity. IC-4 was more reactive, resulting in a higher conversion (69.6% after 44 hours), a trend confirmed by the also aliphatic cyclohexyl isocyanide (IC-2), which led to similarly high reactant conversions of 67.7%. It becomes apparent that aliphatic isocyanides generally lead to higher conversions and product yields than aromatic (IC-3) or aromatic-containing isocyanides (IC-1). For instance, IC-1 led to a conversion of 57.4% after 44 hours, while IC-3 yielded only 33.6% of converted aldehyde in the same period. These results are in accordance with previous publications by Tron *et al.*[400] and Mayr *et al.*,[401] who investigated into the nucleophilicity of aliphatic and aromatic isocyanides — with aliphatic isocyanides being more nucleophile in general.

It should be noted that the above discussed values for reactant conversions were derived from reactions in the presence of **T9** as a catalyst. In the absence of **T9**, the values are significantly lower, while in the presence of **T9** a catalytic effect on the conversion was observed in all approaches. The most remarkable effect is observed when employing IC-3 as a reactant; here, almost no conversion occurs in the absence of the catalyst (**P-63**), with conversion still below 8% even after 44 hours. Interestingly, this approach led to the highest *ee*-value of 13.9%, very comparable to the 13.7% of the aliphatic cyclohexyl isocyanide (IC-2).

Overall, the results indicate that a presence of an aromatic moiety in direct proximity to the isocyano-group has a significant impact on the reactant performance and is disadvantageous for product formation in uncatalysed the Passerini-3CR, thus reducing background reaction and leading to a high observed *ee* value in the presence of catalyst. Generally, it appears that the enantioselective step of the α-addition of the isocyanide is determined primarily by the spatial arrangement of the substrates, rather than by intermolecular interactions between aromatics during the reaction. It is conceivable that the electronic properties of an aryl-ring in close proximity of the isocyano group negatively affects the nucleophilicity of the isocyanide, resulting in lower reactivity. Contrary, the influence of the aromatic ring-system on the isocyano-group in benzyl isocyanide (IC-1) is assumed to much lower influence, due to the spacer in between.

Structural variation of the carboxylic acid

The following screening series was caried out in order to investigate the opportunities and limitations of using different carboxylic acids as reactants. **Table 18** summarises the results of this respective screening series. For comparison, recent results from earlier experiments are also included in **Table 18**. **Figure 33** shows the investigated carboxylic acids (CA):

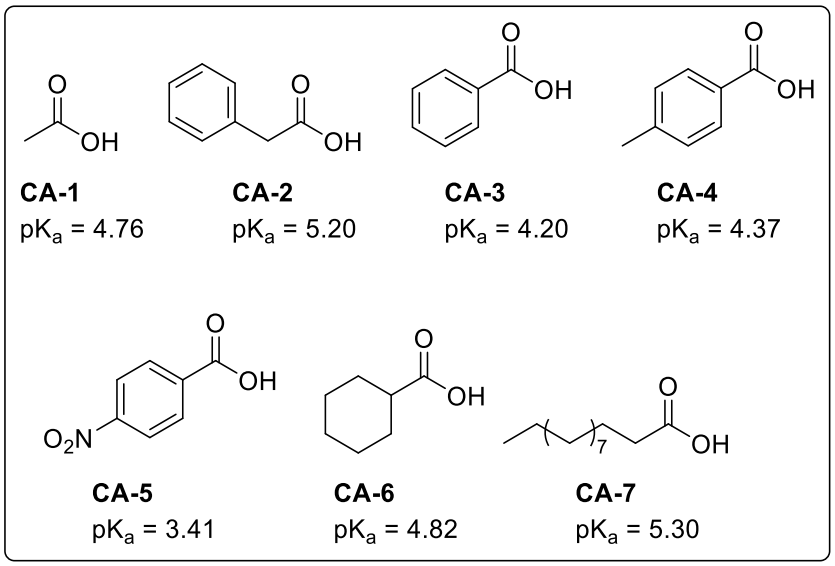

Figure 33 Selection of carboxylic acids used in the screening series for structural variation of the Passerini compound. Furthermore, the pk_a values of the respective acids in water under standard conditions are shown.

Table 18 Investigation into structural variations of the carboxylic acid

Entry	Carboxylic Acid	Catalyst	Conversion 2h [%]	Conversion 20h [%]	Conversion 44h [%]	*ee* [%]
P-36	CA-1	-	3.5	25.4	41.8	0.2
P-22	CA-1	T9	19.8	42.6	57.4	9.3
P-49	CA-2	-	10.8	n.a.	63.6	0.3
P-52	CA-2	T9	37.4	n.a.	75.4	7.7
P-67	CA-3	-	4.9	50.2	70.8	0.5
P-68	CA-3	T9	28.6	58.9	70.8	7.5
P-69	CA-4	-	1.8	11.5	45.2	n.a.
P-70	CA-4	T9	20.1	51.1	62.6	n.a.
P-71	CA-5	-	1.0	7.1	29.1	n.a.
P-72	CA-5	T9	4.1	23.6	42.6	n.a.
P-73	CA-6	-	0.7	9.9	20.3	n.a.
P-74	CA-6	T9	18.8	49.7	60.4	n.a.
P-75	CA-7	-	1.9	15.8	28.7	n.a.
P-76	CA-7	T9	20.2	51.1	61.7	n.a.

The reactions were carried out according to the standard screening protocol in *n*-hexane at a concentration of 0.025 mol×L^{-1}. The Passerini reaction uses benzyl isocyanide, octanal and the respective carboxylic acid mentioned in the table in equimolar ratios. Since no calibration for the GC existed, the reaction progress was measured while screening the conversion of the aldehyde. Therefore, an internal standard was added to the reaction mixture. The enantiomeric excess was determined by chiral HPLC.

In this screening series, both aliphatic (CA-1, CA-2, CA-6, CA-7) and aromatic carboxylic acids (CA-3 – CA-5) were selected. Additionally, aromatic carboxylic acids with varying

electronic properties, either electron-rich (CA-4) or electron-poor (CA-5), were used. Furthermore, substrates with different steric demands at the β-position of the acid were employed.

Unfortunately, much of the data from the chiral HPLC analysis was not obtainable due to difficulties in performing the analysis, which often resulted in poor resolution. In most cases, the respective Passerini products were not observed by the UV/Vis detector of the HPLC system, preventing quantification of the enantiomers. Missing analytical data is marked as not applicable (n.a.) in **Table 18**. As a result, not all aspects of the substrate scope with respect to the enantioselectivity of the reaction can be discussed. However, analysis *via* gas chromatography was still possible and provided valuable insights into the behaviour of the reactants under the respective reaction conditions and in the presence of a thiourea catalyst.

Interestingly, despite the limited data, the relatively small and non-sterically demanding acetic acid (CA-1) gave the highest enantioselectivity of all approaches after a reaction time of 44 hours, achieving 9.3% enantiomeric excess. Both the approaches using phenylacetic acid (CA-2) and benzoic acid (CA-3) resulted in slightly lower enantioselectivity, yielding 7.7% and 7.5% respectively.

It can be speculated that sterically demanding building blocks, such as the phenyl ring, at neither the α-position (CA-3) nor the β-position (CA-2) of the carboxylic acid have much influence on the stereochemistry, especially when combined with sterically non-demanding reactants such as octanal and benzyl isocyanide. Also in the mechanism postulated by Morokuma *et al*.,[262,263] the enantioselectivity of the Passerini-3CR arises from the spatial arrangement of the reactants during the transition state of the α-addition to the isocyanide, with the acid hydrogen-bonded to the aldehyde, forming a dimeric complex. It is possible that if the spatial arrangement of all the reactants is non-demanding, then the nature of the carboxylic acid is of limited importance. Further confirmation of this hypothesis requires additional results in line with this observation. Future screening series should compare a relatively non-demanding carboxylic acid (such as CA-1) with a more sterically demanding one (e.g., CA-6) in a more complex spatial environment where both the aldehyde and isocyanide are also sterically demanding. Additionally, as previously suggested, it may even be advantageous for the carboxylic acid to be relatively small and sterically non-demanding in order to fit into a hypothetical cavity created by thiourea **T9** while binding to the aldehyde during the transition state of the α-addition of the isocyanide. Consequently, sterically more demanding carboxylic acids may be unfavoured, resulting in a less-favoured catalytic pathway that competes with the non-catalysed reaction. To validate such assumptions, DFT

calculations should be carried out in the future, to address such specific spatial arrangement in the transition state of the α-addition.

Upon reviewing the data from the GC screening and comparing the obtained conversion values with the pK_a of the respective acids, no correlation appears. For instance, *para*-nitrobenzoic acid (CA-5), with the lowest pK_a value of all tested carboxylic acids (3.41), led to a conversion of only 29.1% after 44 hours of reaction time without catalyst. In comparison, phenylacetic acid (CA-2), with a pK_a of 5.2, led to the second-best conversion value (63.6%). It was initially speculated that higher acidity is correlated with stronger hydrogen-bonding interactions between the substrates and resulting activation of the aldehyde. However, the conversion rates with respect to the employed carboxylic acid do not seem to follow any discernible trend.

Nonetheless, in nearly all cases, a catalytic effect was observed, with higher aldehyde conversions measured during the GC analysis. The only exception was benzoic acid (CA-3), where the catalytic effect was visible only at the beginning of the reaction but diminished over longer reaction times (44 hours), resulting in the same conversion as non-catalytic reactions. Interestingly, when derivatives of benzoic acid with electron-donating functional groups (CA-4) or electron-withdrawing functional groups (CA-5) were used as reactants, neither a benefit nor a disadvantage was observed in terms of reaction progress. In both cases, lower conversions were measured. One possible explanation is that both carboxylic acids (CA-4 and CA-5) were poorly soluble in the reaction mixture, and even after 44 hours, a suspension was still visually observed. Due to poor solubility, lower reactivity and reduced reactant conversion can be assumed. Unsubstituted benzoic acid (CA-3) on the other hand, dissolved better in the reaction media, resulting in a clear reaction mixture after 20 hours of reaction time.

Structural variation of the aldehyde

In this screening series, both aliphatic (AL-1) and aromatic aldehydes (AL-2, AL-3) were selected. Additionally, electron-deficient aromatic aldehydes (AL-3) were investigated, as their enhanced electrophilicity was expected to facilitate the α-addition of the isocyanide. From previous screenings with aromatic benzaldehyde, it was known that aromatic aldehydes appeared to be less reactive or non-reactive under the given conditions. Therefore, this screening series aimed to explore the potential for substituting aliphatic, sterically non-demanding aldehydes like octanal (AL-1) with aromatic aldehydes from the outset. **Figure 34** shows the aldehydes used, while **Table 19** summarises the results of the aldehyde

screening. For comparison, recent results from earlier screenings are also included in **Table 19**.

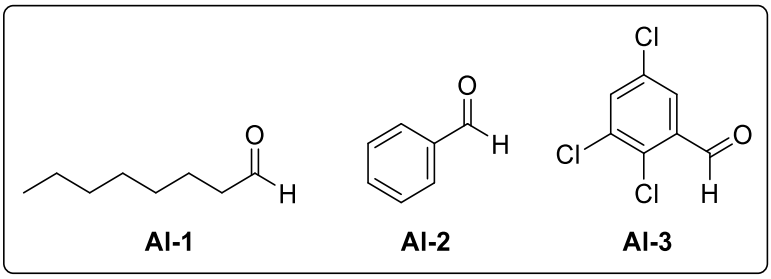

Figure 34 Selection of aldehydes employed in the screening series for structural variation of the Passerini compound.

Table 19 Investigation into structural variations of the aldehyde

Entry	Aldehyde	Catalyst	Conversion 2h [%]	Conversion 20h [%]	Conversion 44h [%]	*ee* [%]
P-36	Al-1	-	3.5	25.4	41.8	0.2
P-22	Al-1	T9	19.8	42.6	57.4	9.3
P-77	Al-2	-	0	0.9	2.6	0.1
P-78	Al-2	T9	1.6	15.7	21.5	9.8
P-79	Al-3	-	1.1	11.1	21.1	0.0
P-80	Al-3	T9	5.8	40.0	54,1	4.0

The reactions were carried out according to the standard screening protocol in *n*-hexane at a concentration of 0.025 mol×L^{-1}. The Passerini reaction uses benzyl isocyanide, acetic acid and the respective aldehyde mentioned in the table in equimolar ratios. Since no calibration for the GC existed, the reaction progress was measured while screening the conversion of the isocyanide. Therefore, an internal standard was added to the reaction mixture. The enantiomeric excess was determined by chiral HPLC.

Benzaldehyde was previously used as a reactant — an approach not mentioned in **Table 19** —with nearly no reactant conversion, even after 10 days of reaction time in the presence of thiourea **T9**. **P-77** and its catalysed version, **P-78**, were conducted in the same manner as the previous attempt. In that earlier attempt, very little conversion was measured, and no effort was made to isolate the products for HPLC analysis to gather information on the stereoselectivity of the reaction. This time, the reactions proceeded more smoothly, and to a small extent, product formation was observed when the organocatalyst was present in the reaction mixture. For example, after 44 hours, a conversion of 21.5% was achieved, while the uncatalysed reaction yielded only 2.6% conversion in the same period.

One possible explanation is the seasonal fluctuation of ambient temperature during the experiments. The unlabelled attempt not included in the table was conducted in February at a room temperature of 19°C, whereas **P-77** and **P-78** were carried out in June at 24°C. This temperature difference may be sufficient to explain the much better performance of **T9** in the second attempt using benzaldehyde as the reactant.

Additionally, one could hypothesise that the uncatalysed reaction is nearly completely suppressed in **P-78**, suggesting that higher enantioselectivities should be achievable. However, HPLC analysis showed an enantiomeric excess of only 9.8%, which was only marginally higher than with octanal in entry **P-22**. This result again suggests that, besides the steric demands of the carboxylic acid, the steric demands of the aldehyde have little influence on the overall enantioselectivity of the thiourea-catalysed Passerini reaction — at least under the given conditions and with reactants exhibiting low to moderate steric demands, such as acetic acid or benzyl isocyanide.

The electron-deficient aldehyde (AL-3) performed much better under the given conditions. Nearly the same isocyanide conversion as in entry **P-78** was measured when AL-3 was used, but without catalyst presence (see **P-79**). In the presence of the catalyst, a conversion of 54.1% was observed, suggesting that electron-deficient aromatic aldehydes react more smoothly than benzaldehyde. This effect can be attributed to the electron density of the aromatic ring, which influences the electrophilicity of the aldehyde, enhancing or reducing its reactivity towards α-addition by nucleophiles, depending on whether the aldehyde contains electron-donating or electron-withdrawing groups.

Moreover, in the presence of thiourea **T9**, both aliphatic octanal (AL-1) and electron-deficient AL-3 resulted in nearly similar isocyanide conversions (57.4% and 54.1%, respectively). However, octanal was more reactive in the early stages of the reaction (see 2 hour measurements), and in the absence of thiourea, octanal yielded nearly twice the conversion rates of AL-3.

Wang *et al*. have previously noted that aromatic aldehydes are less reactive, or not reactive at all, in the Passerini reaction, although no specific explanation was provided for this observation.[266] Here, it was demonstrated that electron-deficient aromatic aldehydes can indeed react in the classic Passerini-3CR, whereas ordinary aromatic aldehydes show very low reactivity in the absence of a thiourea catalyst (**P-77**).

The reaction with AL-3 resulted in only 4% *ee*, compared to 9.3% in the standard reaction using aliphatic octanal (**P-22**) and 9.8% with benzaldehyde (**P-78**). Since AL-3 is more

reactive than benzaldehyde, it is plausible that the uncatalysed background reaction is more pronounced, thereby lowering the overall enantioselectivity of the reaction.

To conclude, the choice of reactants has a significant influence on the thiourea-catalysed Passerini-3CR, as demonstrated by the use of various carboxylic acids, aldehydes, and isocyanides, each with distinct properties such as aliphatic, aromatic, sterically hindered, or electronic characteristics. The most notable result was that, under the given reaction conditions with thiourea **T9**, the choice of isocyanide had the greatest impact on stereoselectivity. The best results were obtained when the sterically demanding feature was in the α-position of the isocyano functional group. The choice of aldehyde had the most pronounced effect on reactant conversion, with aromatic and non-electron-poor aromatic aldehydes performing inferior. However, the investigation of the impact of the carboxylic acid remains incomplete due to the missing data from chiral HPLC analysis. This limitation highlights the fact that established methodologies for reaction monitoring cannot always be adapted for every reaction in a screening series, as the methodology is dependent on each Passerini compound's ability to absorb UV/Vis light. Despite these challenges, the substrate screening clearly indicated that thiourea catalysts like **T9** can accelerate the Passerini reaction and enhance product formation for a variety of substrates, showcasing their versatility. The catalyst’s effect on stereoselectivity is limited and works best for sterically demanding reactants. It is hypothesised that catalysts with more rigidity in their structure and restricted rotation of their chiral building blocks may achieve higher enantioselectivities. The potential of thioureas as catalysts for the classic Passerini reaction has been clearly demonstrated.

4.2.5 Cumulative optimisation of the reaction conditions

In this chapter, the research focuses on combining previously identified beneficial reaction conditions with the ultimate goal of developing an adapted procedure for future thiourea-catalysed Passerini reactions, aiming to achieve enhanced performance with high yields and high enantioselectivities.

The **standard screening procedure** was modified as follows: The reactants acetic acid, octanal, and benzyl isocyanide were used in a 1:2:1 ratio. The substrate screening was chronologically conducted after the optimisation the reaction conditions. Consequently no reactant from the original screening procedure was substituted by better choices revealed from the substrate screening. Additionally, a temperature of -20 °C was chosen, as it had shown improvements in stereoselectivity. At the time these cumulative adapted reaction conditions were applied, the results from the screening at 0 °C were not yet available. Therefore, the reactions were conducted at -20 °C, even though 0 °C would likely have been more advantageous for conversion and yield while maintaining similarly high *ee* values. The most effective thiourea catalysts, **T9** and **T12**, were used in this screening series to enable direct comparison. The respective reactions, **P-81** and **P-82** are summarised in **Table 20**.

Table 20 Comparison of the performance of the **T9** and **T12** catalysts at lower temperatures.

Entry	Catalyst	Temperature [°C]	Yield 2h [%]	Yield 20h [%]	Yield 44h [%]	*ee* [%]
P-81	T9	- 20	3.7	26.8	49.4	13.7
P-82	T12	- 20	10.2	24.0	50.3	14.3

The reactions were performed using acetic acid, octanal, and benzyl isocyanide in a reactant ratio of 1:2:1. The reactions took place at -20 °C with a concentration of 0.025 mol×L^{-1} in *n*-hexane. Both catalysts were used at a loading of 20 mol%. The product yield was calculated based on GC-analysis and the *ee* was measured by chiral HPLC after 44 hours of reaction time.

In both reactions, comparable yields were obtained after 44 hours, with a slightly higher enantioselectivity (*ee*-value of 14.3%) in the presence of **T12**. Generally, both thiourea catalysts, **T9** and **T12**, benefitted from the modified reaction conditions and resulted in nearly identical catalyst performance under the given reaction conditions.

Previously, using catalyst **T12**, 74.6% of the Passerini product was formed after 44 hours with an *ee* of 11.6% under standard screening conditions (in cyclohexane, with equimolar reactant ratios and at room temperature — see entry **P-13**, **Table 4**). In this instance, the *ee* value improved by 23% compared to the previous result, although the yield decreased by a significant 48%.

The reaction using thiourea **T9** (**P-81**) showed an even more pronounced improvement under the modified conditions compared to standard conditions (entry **P-22**, **Table 7**). The *ee* value increased by 47%, meaning **T9**'s performance improved twice as much as **T12**'s in this screening setup, although the yield decreased by 16%.

Subsequently, another approach was taken to combine all reaction conditions that had shown to benefit the stereoselectivity of the Passerini-3CR. Several adjustments were made compared to **P-81** and **P-82**: Benzyl isocyanide (IC-1) was replaced with cyclohexyl isocyanide (IC-2), as the latter had produced up to 47% higher *ee* in relative perspective (Compare substrate screening, **Table 17**). Isocyanobenzene (IC-3) was discarded due to lower aldehyde conversion observed in its presence. Acetic acid and octanal were retained, as no other carboxylic acid or aldehyde tested provided improved enantioselectivities and yields above 57% simultaneously (compare **P-22**, **Table 18** and **19**). The aldehyde was again used in twofold excess, which resulted in 36% higher yields and 32% improved *ee* values (compare **P-31**, **Table 9**). Additionally, 0.1 g of Na_2SO_4 was added as a drying agent and the reaction was conducted at 0 °C, based on previously observed positive effects (compare **Chapter 4.2.2.4** and **4.2.2.7**). Finally, acetic acid was added last, delivered *via* a syringe pump over a 4-hour period, as prolonged addition time of the carboxylic acid proved to be beneficial for the enantioselectivity (compare **Chapter 4.2.2.6**).

This time only catalyst **T12** was used, since the overall performance is better in terms of enantioselectivity compared to the others tested. The results of this screening are summarised in **Table 21**.

Table 21 Performance of **T12** at improved reaction conditions

Entry	Catalyst	Temperature [°C]	Conversion 2h [%]	Conversion 20h [%]	Conversion 44h [%]	*ee* [%]
P-83	T12	0	16.6	54.4	64.8	15.8

The reaction was performed using acetic acid, octanal, and cyclohexyl isocyanide in a reactant ratio of 1:2:1. The reactions took place at 0 °C with a concentration of 0.025 mol×L^{-1} in *n*-hexane. The catalyst was used at a loading of 20 mol%. The isocyanide conversion was calculated based on GC-analysis and the *ee* was measured by chiral HPLC after 44 hours of reaction time. The conversion of the isocyanide was monitored to determine the reaction progress since no calibration for this specific Passerini product exists. Na_2SO_4 was used as drying agent and the acid was added over a 4-hour interval.

As observed, the reaction outcome shows an 11% improvement in enantioselectivity (*ee* value) compared to entry **P-82**, with an isocyanide conversion of 64.8% after 44 hours. However, while enantioselectivity improved compared to **P-82**, a much lower *ee* value was obtained when compared to **P-60** (see **Table 16**), which was carried out under the original standard screening setup and yielded an *ee* value of 19.3%. The attempt to combine various

previously beneficial adaptations did not lead to an overall improvement in the presence of **T12**.

This could be attributed to several factors. Previous optimisation efforts were conducted using **T9**, largely due to cost considerations. It was assumed that **T12** would perform similarly under conditions optimised for **T9**, but this was the first time these conditions were applied to **T12**, so differences in performance are not entirely unexpected.

By comparing the data with **P-82**, where only temperature and stoichiometry were altered from the standard setup, it suggests that temperature has a greater influence on the catalyst's performance. In both **P-83** and **P-82**, **T12** was used at 0 °C and -20 °C respectively, and while stereoselectivity improved, the increase was not as substantial as anticipated and stays even below the 19.3% *ee* in entry **P-60** (**Table 16**). A possible explanation is that **T12** may perform better at higher temperatures. While lower temperatures often benefit enantioselectivity by controlling the conformational flexibility of the catalyst and intermediates, the inversion temperature for **T12** could be closer to room temperature, which might explain the lower enantioselectivity in **P-83** compared to **P-60**.[395]

It was mistakenly assumed that the thiourea catalysts **T12** and **T9** would perform equally well under the given reaction conditions and that **T12** would also benefit from the modifications made to the reaction conditions to enhance the performance of **T9** during the optimisation screenings. Therefore, future research should focus on modifying the reaction conditions specifically for **T12**, altering only one variable at a time to better understand the effect of each condition on stereoselectivity and reaction performance.

4.2.6 Passerini compounds as antiviral agents against coronaviruses

The Passerini reaction typically yields acyclic depsipeptides — peptides in which one or more amide groups are replaced by corresponding esters. From a medicinal standpoint, these products are generally less appealing due to the lability of ester groups under physiological conditions.[261] Nevertheless, the Passerini reaction is valuable in producing bioactive peptidomimetics and is an important tool in combinatorial chemistry, enabling easy access to large molecular libraries with potential candidates for drug discovery.[346] Additionally, this reaction simplifies synthetic routes toward bioactive molecules with complex structures.[346]

For example, the Passerini reaction is utilized in the precursor synthesis of telaprevir, an antiviral drug developed by VERTEX PHARMACEUTICALS and JOHNSON & JOHNSON for treating hepatitis C genotype 1.[346] Furthermore, the Passerini reaction is essential for synthesising halichonadin H, which demonstrates *in vivo* antitumor activity in mice and *in vitro* anticancer activity against human cancer cells.[346] Another notable application is in the synthesis of eurystatin A, a 13-membered macrocyclic natural product typically isolated from *Streptomyces eurythermus* R353-21, which shows potential as an inhibitor of the serine protease prolyl endopeptidase (PEP).[346]

During an ongoing collaboration with researchers at Twincore, a Passerini product previously synthesised in the Meier group was found to exhibit antiviral activity against HCoV-229E and SARS-CoV-2. The following section presents a structure-response study in which the author of this thesis participated. The author wishes to express gratitude to Dr. Phillip Bohn for his mentorship and to Natalie Köhler of Twincore for conducting the dose-response and single-point experiments. Additionally, the author thanks Aaron Seider and Florian Dicks, who contributed to the experimental work as assistant researchers under the author's supervision at the Institute of Organic Chemistry (IOC) at KIT. The author was responsible for project supervision, experimental planning, and result evaluation. Please note that this chapter contains unpublished data, which will be presented with limited details. For example, the chemical structures of the hit compounds are not shown in their entirety

A synthetic strategy for the hit compound in the medicinal study is shown in **Figure 35**. First, the precursor — a carboxylic acid — is synthesised *via* an MCR. This precursor was previously synthesised by Dr. Philipp Bohn and provided to the author of this thesis. The precursor is then utilised as reactant in a Passerini-3CR to yield structural variations of the hit-compound.

One objective of this project was to synthesise various derivatives of the hit compound **X7523** in which the aldehyde chain length was systematically shortened. Twincore then conducted a structure-response investigation to assess the impact of these chain-length variations on biological activity and effectiveness against coronaviruses. Another objective was to assess whether the diastereomeric composition of the hit-compound influences its antiviral activity. Since one step in the synthesis of **X7523** involves a Passerini reaction, it was also aimed to utilise thiourea catalysts to perform this reaction step and directly impact the diastereomeric composition of the hit-compound.

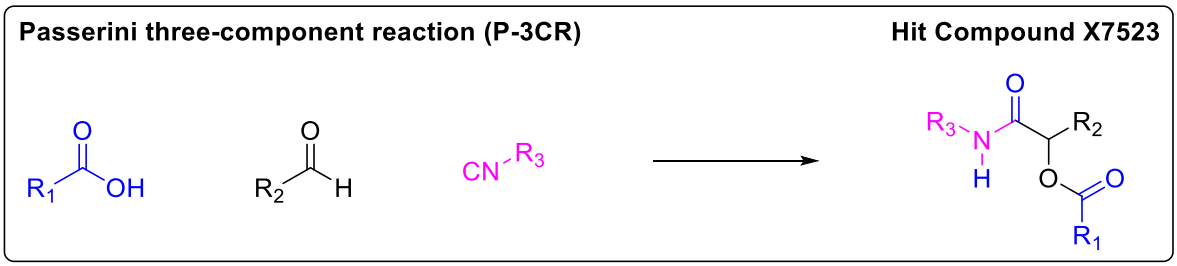

Figure 35 Synthesis strategy for the Hit-Compound **X7523** and its derivatives.

Figure 36 shows the dose-response measurement for the hit compound **X7523** against HCoV-229E. This study is conducted to determine how varying doses of the compound affect the organism and trigger a response, ultimately identifying the optimal dose for maximum therapeutic effectiveness. Such testing is essential in drug development, as it provides dosage recommendations while assessing the effectiveness and safety of new drugs.

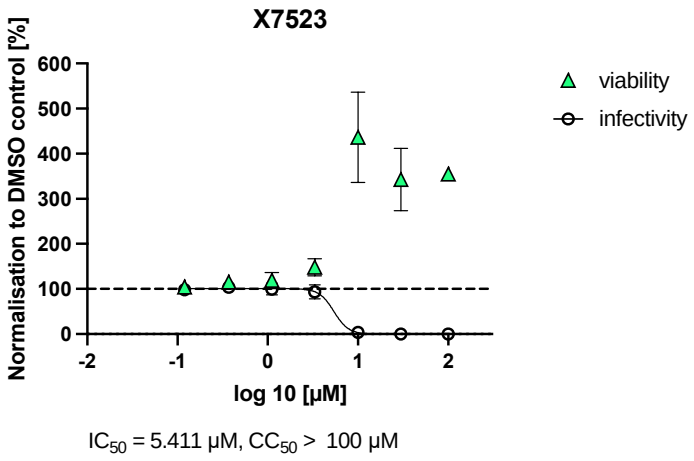

Figure 36 Dose-response measurement of the Hit-compound **X7523** against HCoV-229E.

The x-axis of the diagram represents the dosage used, which is displayed on a logarithmic scale in micromoles. The corresponding response is shown on the y-axis, expressed as a percentage normalized to a DMSO control. This normalisation means that responses measured at different drug doses are adjusted relative to a control sample treated only with DMSO, establishing a baseline at 100%. In pharmacology, IC_{50} and CC_{50} values are essential parameters for evaluating a compound's effectiveness and toxicity. IC_{50}, or "Inhibitory Concentration 50%," denotes the concentration needed to inhibit a specific biological or biochemical function by 50%. For compound **X7523**, a concentration of 5.411 µM was sufficient to achieve 50% inhibition of HCoV-229E. Another key parameter, CC_{50}, stands for "Cytotoxic Concentration 50%" and indicates the concentration required to induce cytotoxicity (cell death) in 50% of cells. Here, concentrations above 100 µM were necessary to reach 50% cytotoxicity, suggesting that **X7523** exhibits low toxicity at the tested concentrations, which may indicate its safety for therapeutic use.

The dose-response plot also illustrates infectivity as a downward-sloping curve, with infectivity decreasing as dosage increases until it reaches 0%. Additionally, the plot reflects host cell viability, which first rises with increasing **X7523** dosage until a certain concentration is reached (compare **Figure 36**). A combination of high host cell viability and low infectivity is generally favourable, as it implies that the compound reduces viral infectivity without harming the viability of host cells.

Subsequently, structural derivatives of **X7523** were synthesised to evaluate how their structure reflects in their antiviral activity. The Passerini reaction leading to the target product encountered significant solubility challenges, which substantially limited the reaction rate and achievable yield. Consequently, several adaptations to the reaction protocol were implemented to enhance product formation. For instance, it was necessary to use a solvent mixture of DCM and DMF to address the poor solubility of the carboxylic acid precursor, while still maintaining suitable conditions for the Passerini reaction. Additionally, an elevated reaction temperature of 60 °C was required to keep the reaction time within the time frame of 2 days, as the reaction proceeded slowly at room temperature, with poor conversions observed by TLC analysis even after extended periods of over 7 days.

Another adjustment involved carrying out the reaction at a concentration of 1 M relative to the carboxylic acid precursor, as the MCR only progressed under these conditions. Besides poor solubility, it is suspected that steric factors of the precursor also played a limiting role. Ultimately, the other reactants — the isocyanide and the respective aldehyde — had to be used in a 3.00-fold excess to make use of Le Chatelier's principle and drive the reaction

toward product formation. Combining all modifications to the reaction protocol, yields up to 92% were achieved.

Additionally, the use of a highly electron-deficient thiourea organocatalyst was investigated to further enhance product formation and to evaluate the utility of thioureas as catalysts in this reaction set-up, with the ultimate goal of achieving control over the stereoselectivity of the Passerini reaction step. Schreiner's thiourea **T2** was employed at 0.20 equivalents as a catalyst, but this had no effect; TLC monitoring over a 48-hour period, along with product isolation, revealed no evidence of catalytic activity. In all cases, regardless of whether the thiourea was present, similarly low product yields in the single-digit range were obtained. Compared to previous findings in **Chapter 4.2**, the solvents used here (DCM and DMF) do not favour thiourea catalysis, which performs best in non-polar solvents like cyclohexane and *n*-hexane. The poor performance of thiourea in this specific case suggests that using thiourea to influence the stereoselectivity and achieve diastereomer-enriched samples of the hit compound **X7523** may be of limited effectiveness.

However, under the author's supervision, the following structural derivatives of **X7523** were synthesised using aliphatic aldehydes ranging from hexanal to propanal. These derivatives were obtained in yields ranging from 39% to 92%, as shown in **Figure 37**.

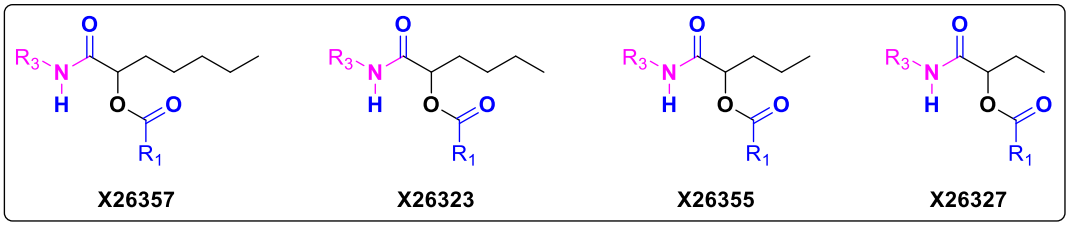

Figure 37 Structural derivatives of the hit compound **X7523** with varying aliphatic chain length resulting from different aldehydes (black colouration) used for product formation.

Subsequently dose-response and single point measurements were conducted of the newly synthesised structure derivatives and they were compared to dose-response measurements using Remdesivir — the first antiviral agent approved for SARS-CoV-2 treatment.[402-404] The respective dose-response measurements are shown in **Figure 38** and the single point measurements are shown in **Figure 39**.

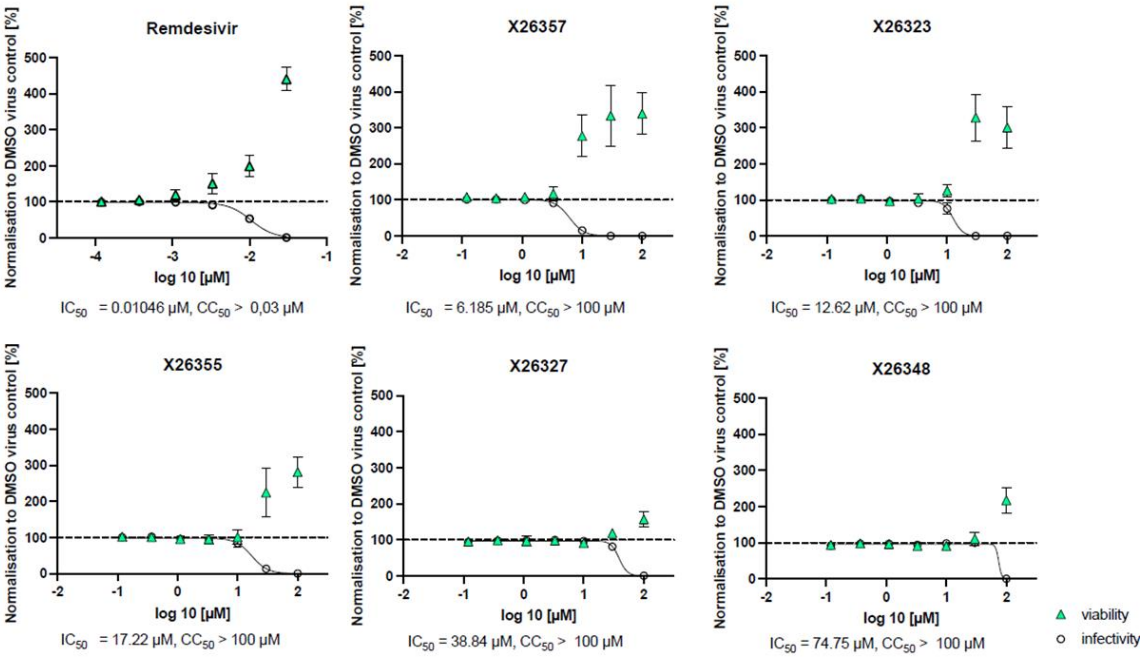

Figure 38 Dose-response measurements of Remdesivir, **X26357**, **X26323**, **X26355**, **X26327**, **X26348** against HCoV-229E

Upon reviewing the data obtained from the dose-response measurements, it is evident that the approved antiviral agent Remdesivir significantly outperforms the other compounds tested, particularly regarding the dosage needed to achieve 50% inhibition (IC_{50} = 0.01046 µM). However, it is worth noting that Remdesivir is a drug that has already undergone extensive optimisation and approval, whereas the Passerini compounds are still in the early stages of testing. Nevertheless, these compounds show potential as future drug alternatives once fully optimised and tested.

A clear trend is observable: as the alkyl chain length of the aldehyde used to synthesise the Passerini product decreases, a higher dosage is required to reach IC_{50}. Generally, the compounds' effectiveness appears to diminish with shorter alkyl chains, and lower host cell viabilities are observed at these reduced chain lengths. Additionally, compound **X26348**, synthesised using acetaldehyde, was included in these measurements. This compound, previously synthesised by Dr. Philipp Bohn and sent to Twincore for medicinal testing, aligns well with the trend showing that shorter alkyl chain lengths result in decreased effectiveness.

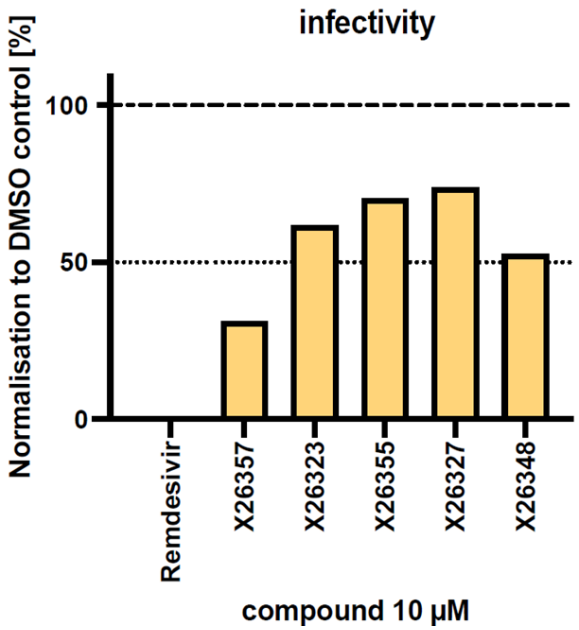

Figure 39 Single-point experiment of the Passerini products against SARS-CoV-2 and comparison with Remdesivir.

Additionally, the respective Passerini products were tested against SARS-CoV-2 using single-point measurements. In these experiments, only one concentration (10 µM) was applied to trigger a response. For Remdesivir, this represents an exceptionally high dosage (compared to its IC_{50} of 0.01046 µM against HCoV-229E), so it is unsurprising that 0% infectivity was achieved. Nonetheless, antiviral activity was also observed for the Passerini products, as shown in the plot. With the exception of compound **X26348** — featuring the shortest alkyl chain length derived from acetaldehyde — longer alkyl chain lengths led to compounds with greater activity and effectiveness against SARS-CoV-2, resulting in a reduction to approximately 66% infectivity compared to the DMSO control, as seen with Passerini compound **X26357**.

Certainly, further adaptations and optimisations of the Passerini compounds are needed to support effective drug development against coronaviruses. However, these initial tests have already demonstrated activity in this very early stage of medicinal studies. The next step will be further structural optimisation of the compounds to enhance antiviral activity while maintaining low toxicity toward host cells. To this end, additional structural variations and derivative synthesis are planned. Given that these compounds contain ester groups, which are known to be labile under physiological conditions, one option might be to replace them with more stable amide or ether groups, potentially resulting in compounds with improved stability and effectiveness.[261]

4.2.7 Chapter Conclusion

To summarise, the investigation into the asymmetric Passerini reaction in the presence of thiourea organocatalysts has demonstrated significant advancements in understanding and optimising the reaction's stereoselectivity. Catalyst design studies were carried out, and the successful incorporation of the bis(trifluoromethyl)phenyl group as a key structural element on one side of the thiourea moiety was confirmed. Introducing chiral building blocks adjacent to the thiourea moiety, which include bulky polycyclic aromatic groups — particularly the anthryl-moiety — proved highly effective. These building blocks likely create an enzyme-like cavity, shielding one plane of the reaction, guiding the isocyanide to attack the aldehyde in a stereospecific manner, leading to enantiomeric excesses.

However, despite these advancements, the stereoselectivity of the reaction remains limited, with the best result so far achieving an enantiomeric excess of 19.3% in the presence of thiourea **T12**. The primary issue appears to be the flexibility of certain chiral building blocks, particularly with regard to the rotation of the polycyclic aromatic group, which compromises the catalyst's rigidity and prevents more consistent enantiomeric control.

Further optimisation of reaction conditions was explored to improve both yields and enantiomeric excesses, leading to a better understanding of how different factors affect stereoselectivity. New procedures for screening conditions were developed, offering refined approaches for future studies. Additionally, the investigation into the reactant scope demonstrated the potential versatility of the catalyst, with the aim of broadening its application to various carboxylic acids, aldehydes, and isocyanides.

Furthermore, medical studies on compounds obtained through a Passerini reaction were conducted, and initial results demonstrated their effectiveness against coronaviruses, specifically HCoV-229E and SARS-CoV-2. The original aim was to obtain diastereomer-enriched Passerini compounds using a thiourea organocatalyst. Unfortunately, the reaction conditions required by the reactants rendered thiourea ineffective as a catalyst. However, future investigations may reveal reaction conditions that enable successful thiourea catalysis.

4.3 Investigation into the asymmetric Ugi-4 component reaction

After demonstrating that a thiourea catalyst can accelerate the Passerini-3CR and achieve small enantiomeric excesses up to 19.3%, the idea arose to investigate its application in the Ugi-4 component reaction (Ugi-4CR), a multicomponent reaction related to the Passerini reaction. In both reactions, the key transition state that leads to stereoselectivity involves an α-addition on the isocyanide component.[263,285] In the case of the Ugi-4CR, this addition occurs on the imine, which can be considered a nitrogen analogue of a carbonyl compound.[405,406] Both imines (in the Ugi-4CR) and aldehydes (in the classical Passerini reaction) undergo nucleophilic attacks by isocyanides, and in both cases, it is known that thiourea interacts with aldehydes as well as imines.[195,197,200,407]

Nziko *et al.* performed *ab initio* calculations to investigate the interactions of thiourea with imines and found that many stable dimeric coordination complexes (CC) were possible.[195] Particularly for the simplest imine, CH_2NH, which was investigated, five possible dimers (**CC1–5**) were obtained, as presented in **Scheme 22**. Likewise, the simplest possible thiourea was considered for the calculations.

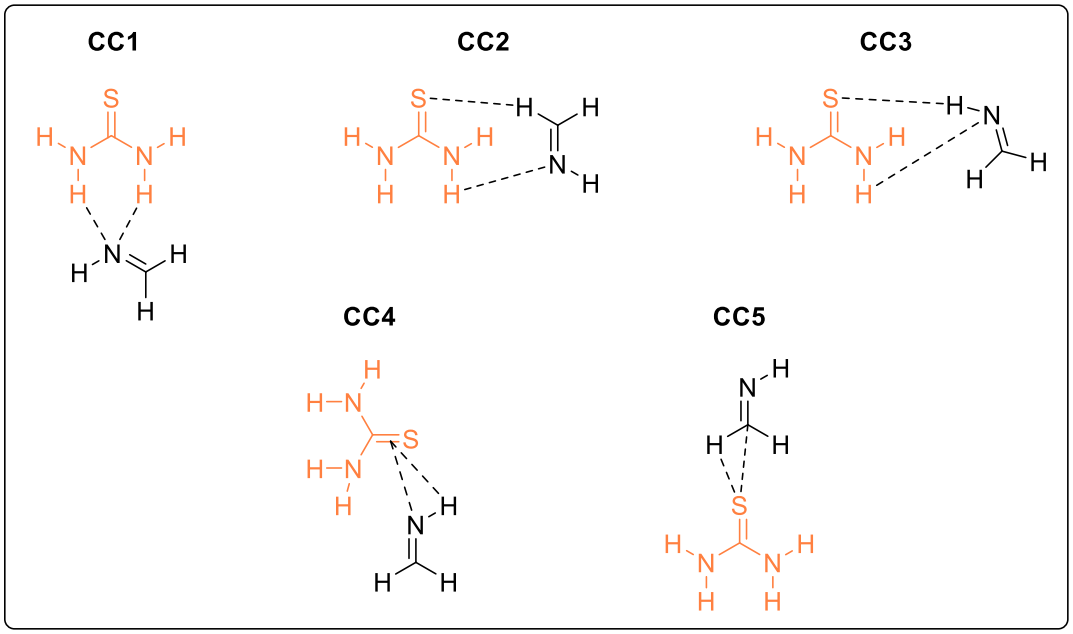

Scheme 22: Overview of the multitude of possible activation modes of the Ugi-4 component reaction mediated by a thiourea. (**CC1 – 5**), which were calculated by Nziko *et al.*[195]

The dimeric structures **CC1** and **CC2** were found to have almost identical energies. **CC1** is characterised by two equivalent NH--N hydrogen bonds (HB) from thiourea to the nitrogen atom of the imine, which acts as a proton acceptor. According to the molecular electrostatic potential (MEP), this interaction type represents the bond between the most positively charged and most negatively charged parts of the respective molecules. This results in a binding energy of 9.66 kcal/mol for the dimer **CC1**. With an energy of 9.65 kcal/mol, the dimer **CC2** has an almost identical energy and is therefore just as likely to be encountered during the reaction. This dimer is characterised by a linear NH--N HB and an elongated and weaker CH--S HB. In the dimer **CC3**, the coordination occurs at a 20° angle, and the sulphur atom of thiourea binds to the proton of the imine *via* NH--S HB. This results in slightly less favourable binding conditions and a lower energy of 9.17 kcal/mol. The two activation modes, **CC4** with 5.23 kcal/mol and **CC5** with only 1.90 kcal/mol, are significantly less stable and thus less likely to be encountered.

Nziko *et al.* described how a thiourea can specifically interact with an imine. Coordination to the imine is of crucial importance for the asymmetric execution of the Ugi-4CR. By coordination of the thiourea catalyst to the imine, a directing effect on the subsequent α-attack of the nucleophilic isocyanide can be achieved, thus decisively influencing the stereoselectivity of the reaction. Furthermore, recent investigations by the Meier group indicate that electron-deficient thioureas can catalyse the Ugi-4CR.[41] As consequence, it seemed natural to explore a thiourea-catalysed asymmetric Ugi-4CR.

4.3.1 Finding a model reaction for the catalytic screening and first results

The catalytic effect observed in previous research of the Meier group was particularly evident in the presence of the well-known Schreiner catalyst, which features two electron-deficient bis(trifluoromethyl)phenyl groups adjacent to the thiourea moiety.[41,198] Consequently, this commercially available thiourea was selected as the organocatalyst for the initial screenings.

For the Ugi-4CR screening, benzoic acid, *p*-toluidine, 4-methoxybenzaldehyde, and *tert*-butyl isocyanide were chosen as the reactants. The reactants and the reaction product (*N*-(2-(*tert*-butylamino)-1-(4-methoxyphenyl)-2-oxoethyl)-*N*-(*p*-tolyl)benzamide) **8** are depicted in **Scheme 23**.

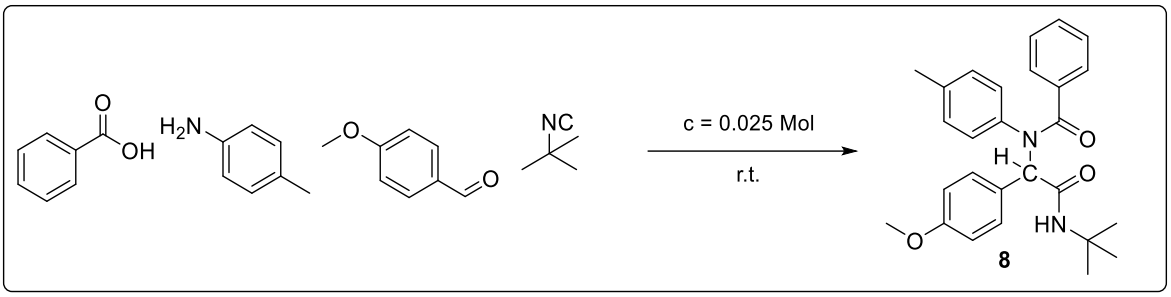

Scheme 23 Overview of the model reaction for the screening of the Ugi-4CR.

The other reaction conditions were aligned with those previously used in the investigation of the Passerini-3CR. The catalyst was added in 20 mol% at the beginning of the reaction, while the other reactants were introduced in equimolar amounts. The reaction was conducted in 10 mL of solvent (*n*-hexane, methanol or dichloromethane) at an overall concentration of 0.025 mol×L^{-1}. The aldehyde and amine were added after the catalyst, along with the internal standard tetradecane, to monitor the reaction progress *via* GC analysis. The mixture was then diluted with 10 mL of the respective solvent and stirred for one hour to allow for imine precondensation, potentially suppressing the Passerini-3CR side reaction. Following this, the carboxylic acid and finally afterwards, the isocyanide were added to initiate the Ugi-4CR. The reaction progress was monitored by GC analysis at 16, 20, and 44 hours.

To investigate the most suitable solvent for catalytic screening, test reactions were performed. For each chosen solvent, two reactions were conducted — one in the presence of the thiourea catalyst and the other without it — to directly assess the catalyst's influence. The following solvents were selected: *n*-hexane, as previous studies found it optimal for thioureas in the Passerini-3CR; methanol, which is known to be a good solvent for Ugi-4CR and also suppresses the Passerini side reaction,[200,263] and dichloromethane, as it was the solvent of choice in the Bin Tan group's studies on asymmetric Ugi-4CR catalysed by chiral phosphoric acids.[33] The following **Table 22** summarises the results from the solvent screening:

Table 22 Solvent screening for the Ugi-4CR.

Entry	Solvent	Catalyst	Yield 16h [%]	Yield 20h [%]	Yield 44h [%]	P – 3CR detectable?
U-01	*n*-hexane	-	0.0	0.0	0.0	No
U-02	*n*-hexane	T2	15.8	16.7	18.6	Yes
U-03	Methanol	-	3.3	30.5	47.9	No
U-04	Methanol	T2	31.9	35.7	45.9	No
U-05	DCM	-	0.0	1.1	2.6	No
U-06	DCM	T2	14.0	14.9	17.3	Yes

The reactions were carried out in the respective solvent at a concentration of 0.025 mol×L^{-1}. The reaction progress was monitored *via* GC analysis. Therefore, an internal standard (tetradecane) was added to the reaction mixture.

From the obtained data, it can be reasoned that *n*-hexane as well as dichloromethane are suitable solvents for further investigation, as reactions in both showed no (in *n*-hexane) to negligible product formation (in dichloromethane) when no catalyst was used. In contrast, when Schreiner's catalyst was present, product yields of 17.3% (in dichloromethane) and 18.6% (in *n*-hexane) were measured by GC analysis. The catalytic effect was also visible in methanol, but only in the early stages of the reaction. After 16 hours, a product yield of 31.9% was obtained in the presence of the catalyst, whereas the non-catalysed reaction only resulted in a 3.3% yield. However, in the later stages, the catalytic effect became less pronounced, and after 44 hours, the non-catalysed reaction in methanol outperformed the catalysed one by a slight margin of 4% in relative terms.

The Passerini side-product was only detected in *n*-hexane and dichloromethane, and only in the presence of the catalyst. In both cases, the imine intermediate was detected in high concentrations, suggesting that imine precondensation occurs early in the reaction. The catalyst appears to not only facilitate the desired reaction outcome, as the Ugi product was only formed in *n*-hexane and to a much greater extent in dichloromethane when the catalyst was present, but it also enables the formation of the Passerini side-product in both cases. This implies that the catalyst interacts with the reactants and intermediates (such as the imine[200]), enabling alternative reaction pathways *via* hydrogen bonding, which ultimately leads to both product and side-product formation.

Based on these observations, one potential direction for further screening is the suppression of the side reaction. Since both the Ugi and Passerini reactions use the same reactants, apart from the amine, it is crucial to ensure that imine precondensation occurs almost to a full extent, preventing the aldehyde from reacting to form the Passerini product. This might be achieved by using more reactive components that favour imine formation, or by extending

the condensation time until complete conversion is achieved. However, a limitation is that the condensation reaction between the amine and aldehyde is reversible.[405,406] This issue could potentially be circumvented by the addition of drying agents, which would remove water molecules and thus prevent the reverse reaction to amine and aldehyde. To finalize the initial investigation of the thiourea-catalysed Ugi-4CR, it was decided to further use *n*-hexane as solvent of choice, since product formation was only possible in presence of the highly electron-deficient 1,3-bis[3,5-bis(trifluoromethyl)phenyl]thiourea, leading to the assumption that the stereoselective outcome of the reaction can be affected to a higher extend if the reaction can only proceed through a catalytic pathway.

4.3.2 Screening of the Ugi-4CR in presence of chiral thiourea catalysts

After proving that electron-deficient thiourea organocatalysts bearing the 3,5-bis(trifluoromethyl)phenyl group were effective, future investigations aimed to explore thiourea catalysts incorporating a chiral building block to achieve stereoselective induction during product formation. To carry out these investigations, the same thioureas previously used in the screening series of the Passerini-3CR were employed again. Accordingly, the four thioureas **T9** – **T12** were tested as catalysts in the Ugi-4CR as well. The respective catalysts are illustrated again in **Figure 40.**

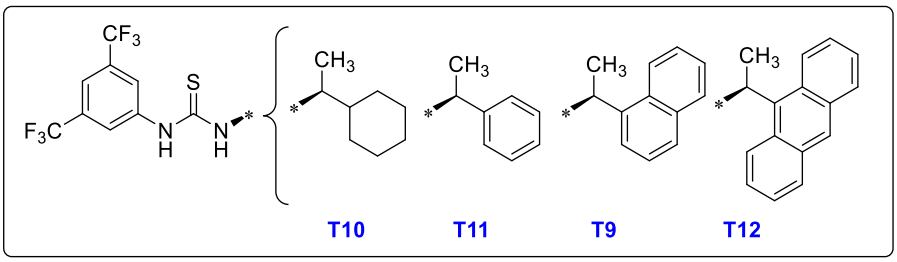

Figure 40 Thiourea organocatalyst bearing aliphatic or aromatic ring structures for the screening of the Ugi-4CR.

As previously mentioned, these thioureas vary in the size of the polycyclic aromatic ring, ranging from benzene to anthracene. Additionally, **T10** was designed to serve as a direct comparison to **T11**, allowing for the investigation of the direct influence of an aromatic π-system. The aforementioned thioureas were used at 20 mol% in the model Ugi-4CR, and the summarised results can be found in **Table 23** and compared to the previous results in presence of Schreiners thiourea **T2** and the uncatalysed reaction.

Table 23 Catalytic screening of the Ugi-4CR with chiral thioureas

Entry	Catalyst	Yield 2h [%]	Yield 20h [%]	Yield 44h [%]	*ee* [%]
U-01	-	-	0.0	0.0	0.0
U-02	T2	-	16.7	18.6	0.0
U-07	T10	1.2	4.0	4.9	6.3
U-08	T11	2.1	7.1	8.6	7.7
U-09	T9	1.3	6.3	8.2	10.3
U-10	T12	5.1	4.2	5.9	5.4

The reactions were carried out in the respective solvent at a concentration of 0.025 mol×L^{-1}. The reaction progress was measured *via* GC analysis. Therefore, an internal standard (tetradecane) was added to the reaction mixture.

The first notable feature of the screening series is that all thiourea catalysts containing only one 3,5-bis(trifluoromethyl)phenyl group were clearly inferior to Schreiner's thiourea (**T2**) in terms of yield. The chiral thioureas did catalyse the reaction to some extent, as product formation was detectable — unlike in the non-catalysed reaction. However, after 44 hours of reaction time, only 4.9% to 8.6% yield was obtained. This indicates that only thiourea organocatalysts capable of forming strong hydrogen-bond interactions with the substrates and intermediates can effectively catalyse the reaction. Schreiner's thiourea, bearing two 3,5-bis(trifluoromethyl)-phenyl groups, exhibits stronger hydrogen-bond donor capabilities and remains the benchmark for thiourea catalysts in the Ugi-4CR.

More importantly, the chiral thioureas used in this study were indeed able to induce enantiomeric excess, achieving *ee* values between 6.3% and 10.3% in this initial screening. By comparison, aromatic building blocks showed a slight advantage, with higher enantioselectivity observed when considering the results from entries **U-07** and **U-08**. The thiourea containing an aromatic phenyl group (**T11**) yielded a slightly higher *ee* value of 1.4%, which represents a 22% increase relative to its aliphatic counterpart (**T10**). On the other hand, it can be assumed that the difference of 1.4% is in the range of measurement inaccuracies and consequently it is conceivable that the catalysts performance is not determined by the bulky building block being aromatic or aliphatic. Further investigations are required considering this occurrence. However, the best results were obtained with thiourea **T9**, which contains a naphthyl group, achieving an *ee* value of 10.3%.

The trend observed in the screening of the Passerini-3CR, where higher enantioselectivities were obtained using thioureas with larger polycyclic aromatic ring systems (see **Chapter**

4.2), was not replicated here. The thiourea containing an anthryl-group (**T12**) yielded an *ee* value of only 5.4%. Furthermore, this approach led to the detection of the Passerini product after just 2 hours, as analysed by GC. Compared to the other chiral thioureas, not only was a lower enantiomeric excess obtained with **T12**, but also a lower yield, with the most intense signals corresponding to side products. In the other approaches, the Passerini product was detectable only after 44 hours, suggesting that **T12** exhibits a reactivity less favourable for the Ugi-4CR under these reaction conditions. For further investigation, it is recommended that the Passerini side product be synthesized and isolated so that GC calibration can be performed. This would allow for quantification of the signal intensity, making future investigations easier.

At this stage, it has become evident that chiral thioureas are indeed capable of inducing stereoselectivity in the Ugi-4CR, a promising result that opens exciting opportunities for future research. To date, only one organocatalytic pathway for enantioselective Ugi-4CR with high enantioselectivities has been reported,[33] and the chiral phosphoric acids used in that case represent the only class of organocatalyst able to catalyse the isocyanide-based MCR in an asymmetric fashion. By further developing thiourea catalysts, the range of catalysts for isocyanide-based MCRs would be expanded, potentially allowing for a wider variety of reactants and reaction conditions.

4.3.3 Usage of bifunctional thiourea organocatalysts

After obtaining promising initial results with the chiral thioureas, the idea emerged to test a bifunctional thiourea containing two 3,5-bis(trifluoromethyl)phenyl groups to enhance reactivity, while also incorporating a chiral structural motif. A thiourea that combines both of these features is Nagasawa's bis-thiourea **T13**, originally developed for asymmetric Baylis-Hillman reactions.[111] This catalyst contains two thiourea groups, each adjacent to a 3,5-bis-(trifluoromethyl)phenyl group, with both thiourea groups separated by a chiral scaffold derived from 1,2-diaminocyclohexane, as shown in **Figure 41**.

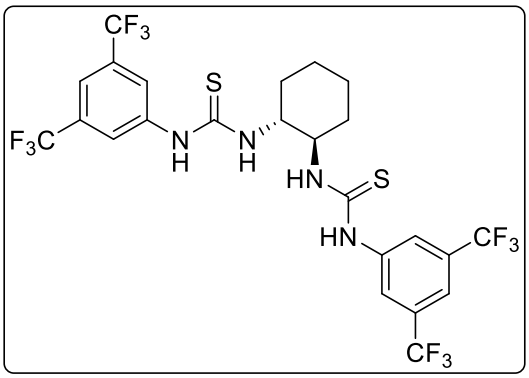

Figure 41 Nagasawa's bis-thiourea **T13**, here in *R,R*-conformation.

To further investigate into this theory, Nagasawa's thiourea was used at 20 mol% in the model Ugi-4CR and the summarised results can be found in **Table 24**. The used thiourea was previously synthesised in in *R,R*-conformation.

Table 24 Screening of the Ugi-4CR with chiral bis-thioureas

Entry	Catalyst	Yield 2h [%]	Yield 20h [%]	Yield 44h [%]	*ee* [%]
U-01	-	-	0.0	0.0	0.0
U-11	T13	5.9	9.9	11.2	11.2

The reactions were carried out in the respective solvent at a concentration of 0.025 mol×L^{-1}. The reaction progress was measured *via* GC analysis. Therefore, an internal standard was added to the reaction mixture.

The results shown in **Table 24** are promising. Using Nagasawa's bis-thiourea as an organocatalyst led to enhanced yields and higher enantioselectivities compared to the previous results in **Table 23**. The bis-thiourea outperforms the previously employed chiral thioureas, in terms of conversion surpassed only by Schreiner's thiourea **T2**. Additionally, the Passerini side product was still detected, but with less intense signals compared to the approach using **T12** as catalyst. Furthermore, a in relative perspective 9% higher *ee* value was achieved, when compared to the approach using the naphthyl-group-containing thiourea (**T9**).

In this case, one has to argue that Nagasawa's bis-thiourea **T13** may induce stereochemical information not merely through steric hindrance while hydrogen-bound to one reactant — as is suspected with **T9** and its derivatives — but potentially by hydrogen bonding with more than one reactant or intermediate during the course of the reaction. This could organise the spatial arrangement in the key transition state *via* a hydrogen-bonding network. This theory

would be intriguing to explore further through DFT calculations of the transition state in future research.

The next step in empirical research involved investigating the imine precondensation at the start of the Ugi-4CR. By extending the condensation time to 2 hours, the aldehyde and amine had more time to react and form the imine. Additionally, it was anticipated that the reverse reaction of the condensation could be further hindered by the addition of drying agents. Following the successful results from the Passerini-3CR screening in the presence of Na_2SO_4, 100 mg of Na_2SO_4 was added at the beginning of the next reaction attempt. This amount equals three times the theoretical amount required to absorb the water molecules formed during the condensation. The results are presented in **Table 25** below.

Table 25 Improving the reaction conditions of the asymmetric Ugi-4CR in presence of Nagasawa's bis-thiourea

Entry	Catalyst	Yield 2h [%]	Yield 20h [%]	Yield 44h [%]	*ee* [%]
U-11	T13	5.9	9.9	11.2	11.2
U-12	T13	5.1	7.6	8.1	8.9

The reactions were carried out in the respective solvent at a concentration of 0.025 mol×L^{-1}. The reaction progress was monitored *via* GC analysis. Therefore, an internal standard (tetradecane) was added to the reaction mixture. To the reaction mixture of entry **U-12**, 100 mg of Na_2SO_4 were added at the beginning of the reaction and the precondensation time was elongated to two hours in total.

Interestingly, attempts to improve the reaction outcome in terms of yield and enantioselectivity (*ee* values) were unsuccessful and led to worse results. The effort to suppress the Passerini side reaction did not yield the desired improvement; instead, a 38% lower yield and a 25% lower *ee* value — both relative to the previous approach — were obtained. The addition of the drying agent and the extended precondensation time increased the formation of imine at the beginning of the reaction. A GC sample taken immediately after the addition of the isocyanide revealed that the aldehyde conversion was 6% higher than in the approach without drying agents. The aldehyde conversion was used here as an indirect measure of imine formation, as the imine was not isolated beforehand, and no GC calibration for it exists. However, this is a reasonable comparison since, without the addition of isocyanide, neither the Passerini nor the Ugi reaction could have occurred at the time the GC sample was taken. The only possible reaction outcome at this stage would be the formation of the intermediate imine. Interestingly, throughout the later stages of the reaction, the Passerini side product was never detected via GC analysis, indicating that the chosen

reaction conditions successfully suppressed the side reaction. However, this suppression did not lead to an improvement in the overall results of the Ugi reaction.

One possible explanation for the outcome is temperature. Both reaction approaches were conducted at room temperature. Unfortunately, during the summer, room temperature can vary, as the laboratory lacks sufficient insulation to maintain a consistent temperature throughout the year. For instance, during the approach in entry **U-12**, the room temperature was measured at 26 °C, while during approach **U-11**, it was 3 °C lower. Surprisingly, the higher room temperature in **U-12** resulted in a lower yield, which is counterintuitive.

This discrepancy might be explained by the reaction mechanism. It has previously been shown that the Ugi-4CR cannot proceed under the given reaction conditions unless a sufficiently electron-deficient thiourea catalyst is present; only then does product formation occur in *n*-hexane. It is plausible that the alternative reaction pathway facilitated by Nagasawa's bis-thiourea also has a relative high activation energy barrier. Therefore, it is conceivable that this bis-thiourea might perform better at higher reaction temperatures, potentially leading to improved results — both in terms of yield and enantioselectivity — in approach **U-12**. It was already previously discussed that the inversion temperature of a enantioselective reaction might be found counterintuitively at higher temperatures — this might be the case here as well.[395] Furthermore, it cannot be excluded that the addition of Na_2SO_4 as drying agent might influence the reaction outcome in terms of yield and enantioselectivity while it proved to be effective to supress the Passerini side-reaction, thought. Clearly more research regarding this is necessary and future investigations should screen various drying agents for their effectiveness.

4.3.4 The asymmetric Ugi-4CR: Chapter summary

This study has shown that the previously successful thiourea catalysts can also influence the Ugi reaction. Both isocyanide-based multicomponent reactions — Passerini and Ugi — share key mechanistic features, and thiourea organocatalysts are well-known for facilitating nucleophilic attacks on aldehydes and imines. This preliminary investigation establishes a solid foundation for future research. Further exploration could unlock the full potential of thiourea-catalysed Ugi reactions, potentially adding a thiourea as a new organocatalyst to the list of truly enantioselective catalysts for the Ugi reaction. Such advances would broaden the scope of applications and enhance the possibilities offered by asymmetric Ugi reactions.

As with the screening of the Passerini reaction, future work should focus on developing thiourea catalysts with more rigid structures to improve stereoselectivity. Notably, the thioureas tested here may face similar limitations as in the Passerini reaction. Further, enhancing the reactivity of imines — given that aldehydes are known to react more rapidly — would improve reactant conversion, increase yields, and help to suppress Passerini side reactions.[408]

In addition, further investigation into the use of drying agents is necessary to determine the optimal conditions. Careful optimisation of reaction parameters in general is also crucial, and this is expected to yield valuable insights into thiourea-catalysed isocyanide-based MCRs.

Chapter 5 Conclusion and outlook

This study demonstrated that thioureas can act as effective catalysts for the Passerini-3CR and Ugi-4CR. In both IMCRs, a significant increase in yield was observed in the presence of thioureas, with pronounced reaction acceleration and increased product formation observed particularly at the initial stages. The impact on reaction yield was dependent on the chosen reactants and reaction conditions. However, in all Passerini reactions studied, utilising diverse aldehydes, carboxylic acids, and isocyanides, a catalytic effect was consistently observed. Similarly, a catalytic effect on product formation was noted in the thiourea-catalysed Ugi reaction, although only a single model reaction was investigated without varying the reactants. Future experiments are needed to confirm whether this catalytic effect extends to a broader range of reactants in the Ugi-4CR. Notably, in the Ugi reaction, solvent selection played a critical role in suppressing the uncatalysed background reaction while still enabling the reaction to proceed in the presence of a thiourea catalyst. This strategic choice of reaction conditions opens possibilities for exclusively catalysed reaction pathways, which could lead to high enantiomeric excesses.

However, in the thiourea-catalysed Ugi reaction, the Passerini reaction as side reaction was observed. This suggests that the thiourea catalyst facilitates both IMCRs under the given reaction conditions. Importantly, the Passerini by-product was not detected in the absence of a catalyst. Future experiments should aim to optimise the reaction conditions to further supress side reaction by controlling the imine pre-condensation, which would limit the possibility of aldehyde-based Passerini reaction to occur.

In summary, this study provides a fundamental basis for further investigations into thiourea-catalysed Ugi-4CRs. It is anticipated that with further optimisation of catalysts and reaction conditions, thioureas could be established as an alternative class of organocatalysts alongside chiral phosphoric acids (CPAs). Preliminary experiments already achieved an enantiomeric excess of 11.2%, an encouraging result for future research.

The thiourea-catalysed Passerini-3CR also showed great promise. A systematic study of catalyst design identified key features enabling enantioselective catalysis of the Passerini-3CR. Notably, thiourea catalysts benefited from aryl substituents with strong electron-withdrawing properties. The literature-recognised bis(trifluoromethyl)phenyl group, when incorporated into the catalyst framework, significantly improved catalytic activity regarding yield and enantioselectivity (e.g., **P-02** and **P-10**, **Table 3**). This suggests that the enhanced

hydrogen bond donor capability of thioureas, attributed to electron-withdrawing substituents, strengthens hydrogen bonding with reactants in the transition state, thereby achieving higher enantioselectivities. Large and sterically demanding building blocks also proved beneficial in catalyst design. The incorporation of an anthryl group, for example, produced the most catalytically active thiourea, **T12**. Moreover, the stereoselectivity of thiourea was found to directly influence the preferred enantiomer in the Passerini reaction (e.g., **Table 14**), demonstrating that selecting a thiourea with appropriate chirality can theoretically enable enantioselective synthesis of the desired enantiomer.

Catalyst **T12** achieved the highest *ee* reported thus far in thiourea-catalysed Passerini reactions, with an enantiomeric excess of 19.3% observed when sterically demanding isocyanides such as cyclohexyl isocyanide were utilised (e.g., **P-60**, **Table 16**). Furthermore, the catalytic effect was evident with a wide range of reactants, including aromatic and aliphatic isocyanides, carboxylic acids, and aldehydes. Among the carboxylic acids tested, both electron-rich and electron-poor aromatic derivatives were included, with pK_a values ranging from 3.41 to 5.30. Notably, aromatic aldehydes such as benzaldehyde showed a remarkable reactivity in the presence of thioureas (e.g., **P-77** and **P-78**, **Table 19**), with nearly tenfold increased conversion in the presence of a thiourea catalyst compared to negligible conversion without it.

Reaction condition optimisation further highlighted the influence of lower temperatures (e.g., 0 °C, **Table 8**), the use of drying agents (e.g., Na_2SO_4, **Table 12**), and non-polar solvents (e.g., *n*-hexane, **Table 7**). Prolonged addition of carboxylic acids positively impacted enantio-selectivity (e.g., **Table 10**), and catalytic effects were observed even at low catalyst concentrations of 0.01 equivalents (e.g., **Table 13**).

In summary, this work underscores the promising potential of thioureas as organocatalysts in the Passerini-3CR. Through careful adjustment of reaction conditions and the selection of suitable reactants, both catalytic activity and enantioselectivity can be enhanced. Future studies should focus on refining catalyst structures. DFT calculations conducted in collaboration with the Wenzel group (INT, KIT) revealed that thioureas exist in multiple conformations at room temperature due to rotational freedom. Since rigid catalysts are generally advantageous for stabilising transition states, investigating the impact of increased rigidity on catalytic performance should be a priority in future catalyst design.

Additionally, structure-property relationships of Passerini products were explored. Passerini products with varying aliphatic chain lengths were synthesised and tested for their effectiveness against coronaviruses, including HCoV-229E and SARS-CoV-2, in

collaboration with Twincore. It was hypothesised that the diastereomeric composition of the products, influenced by thiourea catalysis, might affect antiviral activity. However, suboptimal reaction conditions — resulting from poor solubility and low reactivity of certain reactants — hindered the application of thiourea catalysis in this context. Future work should redesign the synthesis plan to prioritise thiourea-catalysed Passerini reactions, allowing for subsequent functionalisation of the Passerini product — to yield the final antiviral compound — in controlled diastereomeric composition.

The synthesis of a diverse range of thioureas, achieved through both more sustainable multicomponent approaches and efficient bimolecular reactions, provided a versatile library for catalytic screening. The multicomponent reaction pathway, which utilises elemental sulphur and avoids the use of highly toxic reagents, highlights the potential of more sustainable synthetic methodologies in modern catalysis. Furthermore, an investigation into extending the versatility of the MCR to synthesise thiohydantoins demonstrated its adaptability, achieving yields of up to 61%. Future research should aim to expand the reactant scope and improve yields to fully unlock the potential of this MCR to synthesis thiohydantoin — a class of compounds widely used in medicinal chemistry .

Finally, this study has provided valuable insights into the role of thiourea catalysts, paving the way for future research in asymmetric catalysis and the application of isocyanide-based multicomponent reactions.

Chapter 6 Experimental

6.1 Methods

6.1.1 Chemicals

Unless otherwise noted, all solvents and reagents were used as received without further purification. Dichloromethane was pre-distilled.

(±)-α-methyl-1-naphthalenemethylamine (98%, ACROS ORGANICS), (1*R*,2*R*)-(−)-1,2-diamino-cyclohexane (96%, ABCR CHEMICALS), (1*R*,2*R*)-(−)-1,2-diamino-cyclohexane (98%, FISHER CHEMICALS), (1*R*,2*R*)-(+)-1,2-diphenyl-ethylendiamine (96%, TCI CHEMICALS), (1*R*,2*R*)-(+)-1,2-diaminocyclohexane (97%, FISHER CHEMICALS), (1*R*,2*R*)-(+)-1,2-diaminocyclohexane (99%, ACROS ORGANICS), (1*S*,2*R*)-(−)-cis-1-amino-2-indanol (99%, SIGMA ALDRICH), (1*S*,2*S*)-(+)-1,2-diamino-cyclohexane (97%, FISHER CHEMICALS), (1*S*,2*S*)-cyclohexane-1,2-diamine (96%, CHEMPUR), (*R*),(*R*)-diaminocyclohexane (99%, ACROS ORGANICS), (*R*)-(+)-α-4-dimethylbenzylamine (99%, SIGMA ALDRICH), (*R*)-(+)-α,4-dimethylbenzylamine (98%, SIGMA ALDRICH), (*S*)-(−)-1-(1-naphthyl)-ethylamine (98%, CHEMPUR), (*S*)-(−)-1-(2-naphthyl)-ethylamine (97%, CHEMPUR), (*S*)-(−)-1-(1-naphthyl)-ethylamine (98%, FISHER CHEMICALS), (*S*)-(-)-1-phenylethylamine (98%, FISHER CHEMICALS), (*S*)-(+)-1-cyclohexylethylamine (98%, TCI CHEMICALS), (*S*)-(+)-α-methyl-1-naphthalenemethylamine (>99%, FLUOROCHEM), (*S*)-2-[[3,5-bis(trifluoromethyl)phenyl]-thioureido]-*N*-benzyl-*N*,3,3-trimethylbutanamide (97%, SIGMA ALDRICH), 1-(1-naphthyl)-ethylamine (98%, FISHER CHEMICALS), 1-(4-methylphenyl)-ethylamine (96%, SIGMA ALDRICH), 1-(4-methylphenyl)-ethylamine (99%, SIGMA ALDRICH), 1,3-bis[3,5-bis(trifluoromethyl)-phenyl]thiourea (98%, FISHER CHEMICALS), 1-hexanol (98%, SIGMA ALDRICH), 1-(anthracen-9-yl)ethanamine (99%, MERCK), 1-(4-methylphenyl)-ethylamine (96%, SIGMA ALDRICH), 2-propanol (99.5%, FISHER CHEMICALS), 2,6-diamino-pimelic acid (98%, FISHER CHEMICALS), 3,5-bis(trifluormethyl)phenylisothiocyanate (98%, CHEMPUR), 3-phenylpropionic acid (97%, FISHER CHEMICALS), 4-nitroaniline (99%, SIGMA ALDRICH), 5-aminoisophthalic acid (98%, SIGMA ALDRICH), acetic acid (99.7% FISHER CHEMICALS), benzyl isocyanide (98%, FISHER CHEMICALS), biphenyl (99%, ALFA AESAR), bis(bis-3,5-(trifluoromethyl)phenyl) thiourea (>98%, TCI CHEMICALS), Boc-Pro-OH (98%, CHEMPUR), Boc-Trp-OH (97%, CHEMPUR), Boc-Val-OH (98%, CHEMPUR), chloroform-d ($CDCl_3$, 99.8 atom %D, ARMAR CHEMICALS), cyclohexyl isocyanide (99%, ACROS ORGANICS), Cyrene™ (98%, SIGMA ALDRICH), deuterated cyclohexane (99%, ABCR CHEMICALS), dichloromethane (HPLC

grade, VWR CHEMICALS), diisopropylamine (99%, ABCR CHEMICALS), dimethyl sulfoxide (>99.7%, FISHER CHEMICALS), dimethyl sulfoxide-d6 (DMSO-d6, 99.9 atom %D, SIGMA ALDRICH), formaldehyde (37%, FISHER CHEMICALS), formic acid (99%, ACROS ORGANICS), *L*-cysteine-methylester-hydrochlorid (98%, TCI CHEMICALS), *L*-histidine methylester dihydrochloride (98%, FISHER CHEMICALS), *L*-leucin-methylester hydrochlorid (98%, FISHER CHEMICALS), *L*-phenylalanin-methylester hydrochlorid (96%, TCI CHEMICALS), *L*-tert-leucin (97%, CHEMPUR), *L*-threonine methylester hydrochloride (99%, FISHER CHEMICALS), *L*-tryptophane-methylester hydrochlorid (99%, FISHER CHEMICALS), methanol (HPLC grade, VWR CHEMICALS), n-hexane (HPLC grade, VWR CHEMICALS), *N*-Boc-*L*-tert-leucine (98%, CHEMPUR), pentanal (98%, MERCK), phosphorus oxychloride (99%, SIGMA ALDRICH), potassium carbonate (99%, FISHER CHEMICALS), sodium chloride (>99.5%, FISHER CHEMICALS), sodium hydrogen carbonate (>99%, ROTH), sodium sulphate (water free, BERND KRAFT), sulphur (elemental, technical grade, SIGMA ALDRICH), tetradecane (99%, FISHER CHEMICALS), thionyl chloride (98%, SIGMA ALDRICH).

6.1.2 Instruments and Characterisation Methods

6.1.2.1 Column Chromatography

TLC silica gel F254 (SIGMA ALDRICH) was used. The respective solvents were employed in HPLC-purity grade unless otherwise noted.

6.1.2.2 Gas Chromatography (GC)

Gas chromatography (GC) measurements were performed on an AGILENT 8860 gas chromatography instrument with a HP-5 column (30 m × 0.32 mm × 0.25 µm) and a flame ionisation detector (FID). Samples were prepared by dissolving 0.5 −3 .0 mg of compound in 1.5 mL of ethyl acetate. All samples were filtered *via* syringe filter (polytetrafluoroethylene, 13 mm diameter, 0.2 µm pore size, AGILENT) prior to measurement to avoid plug-ging of injection setup or the column. The heating program was as follows: Initial temperature at 100 °C, heating to 250 °C with a rate of 15 $K \times min^{-1}$, retaining 250 °C for 4 min, heating to 300 °C with a rate of 20 $K \times min^{-1}$, retaining 300 °C for 4 min. The injector transfer line temperature was set to 220 °C. Measurements were performed with a split ratio of 20:1 using nitrogen as make-up gas and helium as carrier gas with a flow rate of 1.87 $mL \times min^{-1}$.

6.1.2.3 High-Performance Liquid Chromatography (HPLC)

Analysis of the enantiomeric excess was conducted using an AGILENT HPLC 1100 series system with a G1322A degasser, a G1211A pump, a G1313A autosampler, a G1316A column oven, and a G1315B diode array system. A CHIRALPAK AD-H (4.6 × 250 mm, 5 µm particle size) column was used as stationary phase while solvent mixtures of *n*-hexane/isopropanol or *n*-hexane/ethanol with HPLC-grade were used as mobile phase.

6.1.2.4 Infrared Spectroscopy (IR)

Infrared spectra (IR) were recorded on a BRUKER Alpha-p instrument applying ATR-technology (ATR = Attenuated Total Reflection) in a frequency range from 3998 to 374 cm^{-1}. The band intensities were characterized in relation to the most intense signal as follows: vs = very strong, s = strong, m = medium, w = weak, vw = very weak. In addition, broad signals were expressed by the term: br = broad.

6.1.2.5 Mass Spectrometry (MS)

A mass spectrometer (THERMO FISHER SCIENTIFIC) equipped with a HESI II probe was employed to record high resolution electrospray ionization–MS (ESI-MS). Calibration was carried out in the m/z range 74–1.822 using premixed calibration solutions (THERMO FISHER SCIENTIFIC). A constant spray voltage of 4.7 kV and a dimensionless sheath gas of 5 were employed. The S-lens RF level was set to 62.0, while the capillary temperature was set to 250 °C. All samples were dissolved at a concentration of 0.05 $mg \times mL^{-1}$ in a mixture of THF and MeOH (3:2) doped with 100 µmol sodium trifluoroacetate and injected with a flow of 5 $\mu L \times min^{-1}$. High resolution mass spectra (HMRS) were recorded with electron impact ionization (EI) were recorded on a GC-TOF. Fast atom bombardment (FAB) mass spectra were recorded on a Finnigan MAT 95 instrument. The protonated molecule ion is expressed by the term: [(M + H+)].

6.1.2.6 Nuclear Magnetic Resonance (NMR)

^{1}H and ^{13}C NMR spectra were recorded on BRUKER Advance DPX spectrometers (Billerica, MA) with a 5-mm dual proton/carbon probe (300, 400, 500 MHz ^{1}H/ 75.5 or 126 MHz ^{13}C) and on BRUKER Advance III with a 5-mm z-gradient cryogenically cooled probe head (CPTCI, 600 MHz ^{1}H/ 75.5 MHz). The chemical shift for ^{1}H-NMR spectra were reported in ppm relative to TMS (0 ppm) or to the solvent signal $CDCl_3$ at 7.26 ppm and DMSO-d_6 at

2.50 ppm. ^{13}C-NMR spectra were reported in ppm relative to the central signal of the triplet for $CDCl_3$ at 77.16 ppm and of the septet for DMSO-d_6 at 39.52 ppm. Data for ^{1}H-NMR were reported as follows: multiplicity (s = singlet, d = doublet, t = triplet, q = quartet, m = multiplet, b = broad), coupling constant (Hz), integration, and assignment. Furthermore, 2D NMR methods e.g. heteronuclear single quantum coherence (HSQC) and correlated spectroscopy (COSY) were carried out, if necessary, for signal assignment and structure elucidation. If conformers (rotamers) of a substance could be observed due to restricted rotation, all species which could be assigned were clearly labelled with additional appendices (a, b, c. etc.). Hereby, the main conformer was labelled with the appendix “a”, the second conformer with appendix “b” and so on.

6.1.2.7 Thin Layer Chromatography (TLC)

For TLC analysis, precoated aluminium foils with fluorescence indicator from MERCK (TLC Silica gel 60, F254, layer thickness: 0.25 mm) were employed as stationary phase. The spots were firstly visualised by fluorescence quenching under UV-light (λ = 254 nm), fluorescence (λ = 365 nm) and then by staining with Seebach reagent: solution of 2.50g cerium (IV) sulfate tetrahydrate ($Ce(SO_4)_2 \cdot 4\ H2O$), 6.25g ammonium heptamolybdate tetrahydrate ($(NH_4)_6Mo_7O_{24} \cdot 4\ H2O$), 225 mL water and 25.0 mL concentrated sulfuric acid. Depending on the reagent, also a vanillin staining solution (solution of 15 g vanillin and 2.5 ml concentrated sulfuric acid in 250 ml ethanol) or a $KMnO_4$ staining solution (1.5 g $KMnO_4$, 10.0 g K_2CO_3, 1.25 mL of 10% NaOH, 200 mL H_2O) was used to visualise the signals.

6.2 Experimental procedures

6.2.1 Synthetic procedures for the precursors

Synthesis of dimethyl 5-amino-isophthalate (1)

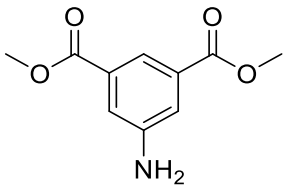

In a 250 mL round-bottom flask 3.00 g of 5-aminoisophthalic acid (16.56 mmol, 1.00 eq.) was dissolved in 65.4 mL of methanol. The reaction mixture was then cooled in an ice bath to 0 °C. Then 7.2 mL thionyl chloride (11.82 g, 99.36 mmol, 6.00 eq.) was added slowly and dropwise. Subsequently the mixture was stirred at room temperature overnight. Afterwards the mixture was neutralized with potassium carbonate and saturated sodium hydrogen carbonate solution. The pH-value was then adjusted to 8 – 9 with potassium carbonate. 200 mL of each DCM and distilled water were added to the mixture to redissolve the precipitated salts. The organic phase was separated, and the aqueous solution was then extracted three times with DCM. The combined organic phases were dried over sodium sulphate and were then filtered off. After evaporation of the solvent under reduced pressure the pure product dimethyl 5-amino-isophthalate (3.05 g, 14.6 mmol) was obtained as yellow-brownish solid (yield = 88 %).

^{1}H-NMR (400 MHz, DMSO-d_6) δ/ppm = 7.65 (s, 1H, ^{1}), 7.42 (s, 2H, ^{2}), 5.74 (s, 2H, ^{3}), 3.84 (s, 6H, ^{4}).

^{13}C-NMR (101 MHz, DMSO-d_6) δ/ppm = 166.5, 150.0, 131.1, 118.6, 117.1, 52.6.

HRMS-EI-MS m/z: [M] calculated for [$C_{10}H_{11}NO_4$] = 209.0688, found: 209.0696.

IR (ATR platinum diamond) ν/cm^{-1} = 3458 (m), 3421 (vw), 3365 (m), 3322 (vw), 3223 (vw), 2952 (w), 1697 (vs), 1627 (m), 1602 (m), 1434 (s), 1353 (s), 1279 (m), 1257 (s), 1242 (vs), 1189 (m), 1127 (m), 1094 (w), 1014 (s), 989 (m), 919 (w), 895 (m), 884 (m), 852 (vw), 841 (vw), 788 (vw), 751 (s), 726 (m), 673 (w), 582 (w), 551 (w), 539 (w), 529 (w), 516 (w), 502 (w), 492 (w), 485 (w), 473 (w), 430 (w).

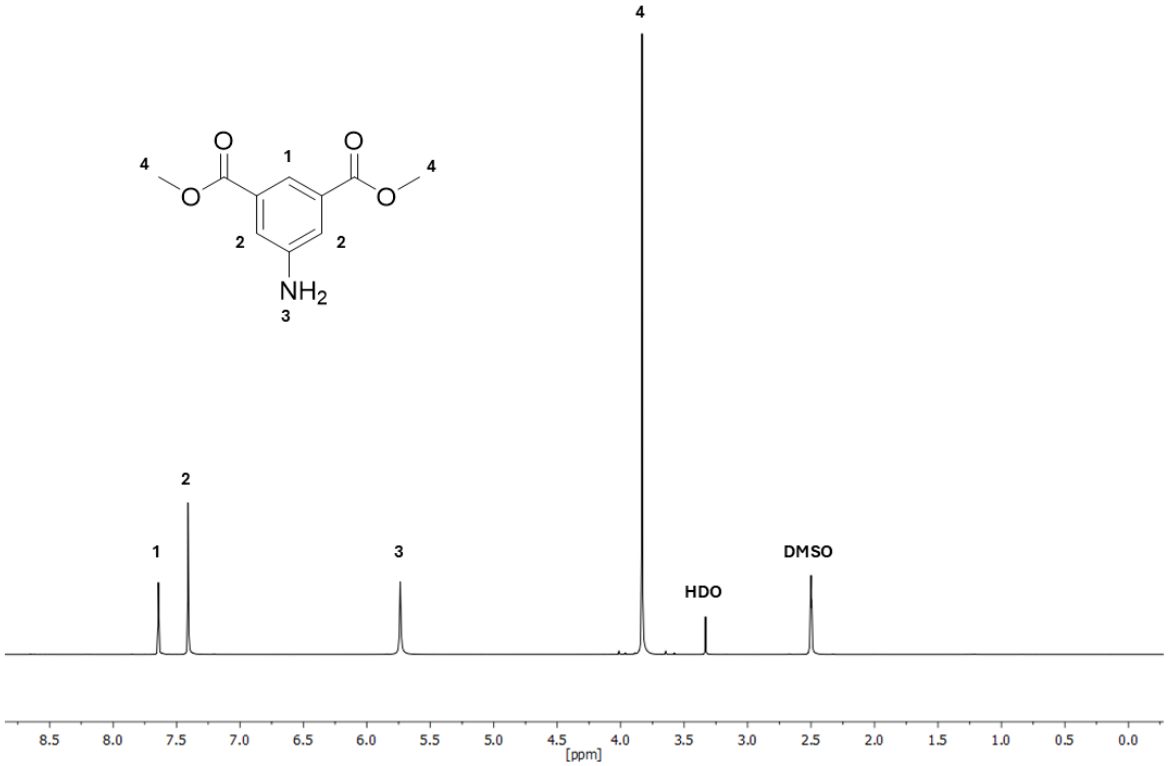

Supplementary Figure 1 ^{1}H-NMR of dimethyl 5-aminoisophthalate measured in DMSO-d_6 plotted as signal intensity versus chemical shift in ppm.

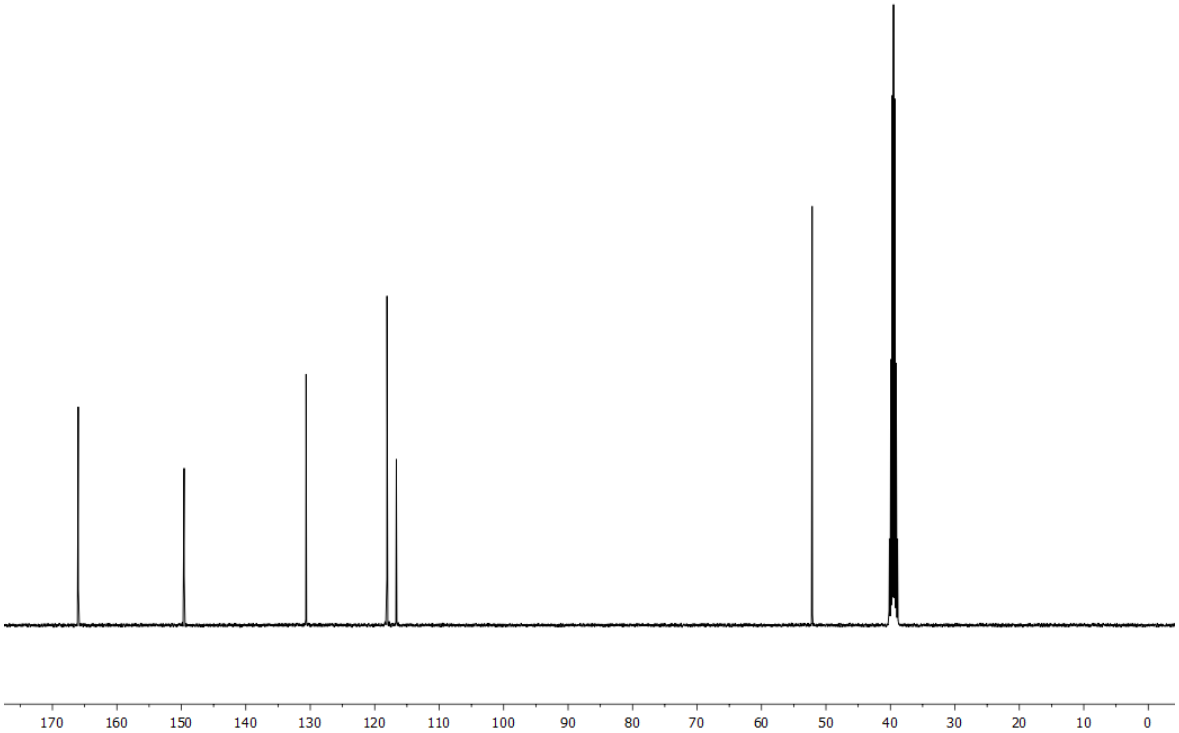

Supplementary Figure 2 ^{13}C-NMR of dimethyl 5-aminoisophthalate measured in DMSO-d_6 (septet signal at 39.52 ppm) and plotted as signal intensity versus chemical shift in ppm.

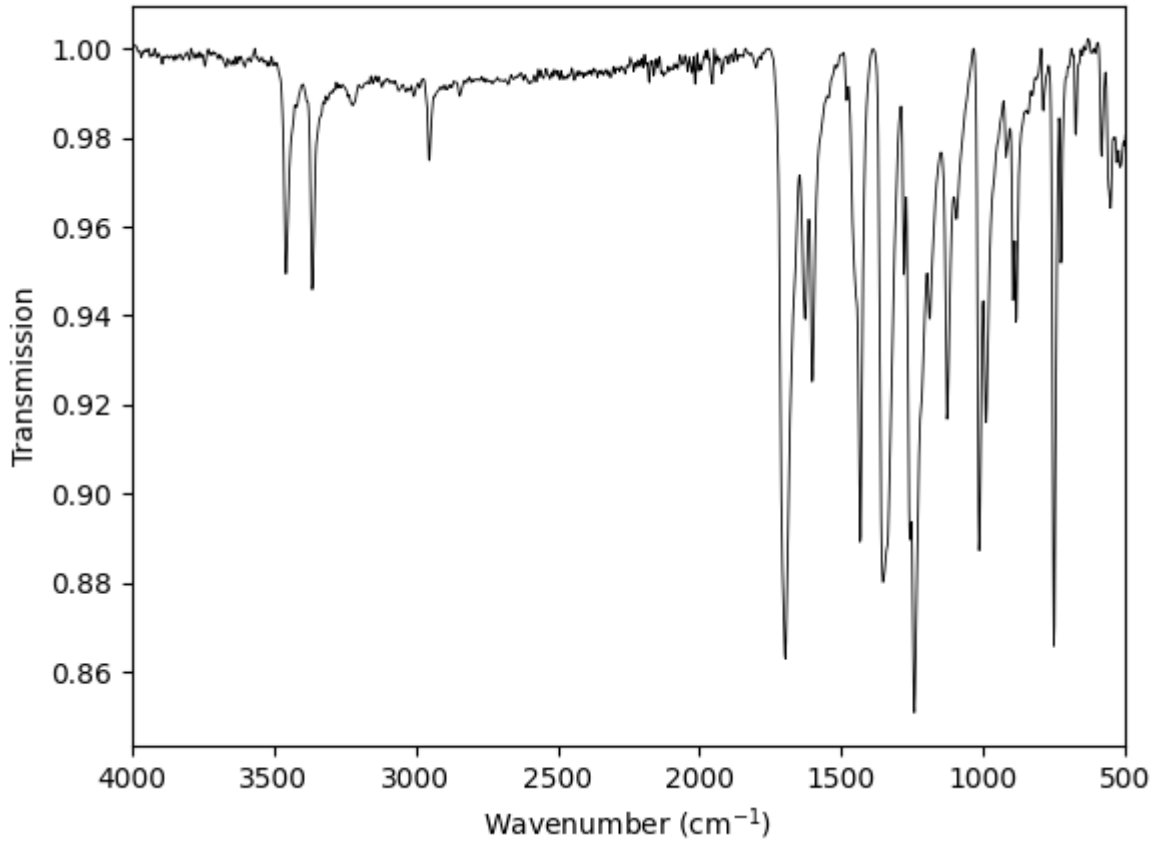

Supplementary Figure 3 IR-spectra of dimethyl 5-aminoisophthalate.

Synthesis of dimethyl 5-formamidoisophthalate (2)

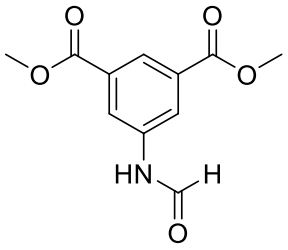

In a 10 mL round-bottom flask, which was equipped with a Dimroth condenser, 3.05 g of dimethyl 5-aminoisophthalate (**1**) (14.57 mmol, 1.00 eq.) and 4.4 mL formic acid (5,36 g, 116.52 mmol, 8.00 eq.) were added. The reaction mixture was then stirred for 15 hours at 60 °C until full conversion was indicated by TLC analysis. Subsequently the excess formic acid was evaporated under reduced pressure to obtain the product dimethyl 5-formamidoisophthalate as white solid in a yield of 97 % (3.36 g, 14.19 mmol).

^{1}H-NMR (400 MHz, DMSO-d_6) δ/ppm = 10.61 (s, 1H, ^{1}), 8.43 (s, 2H, ^{2}), 8.37 (d, J = 1.8 Hz, 1H, ^{3}), 8.14 (s, 1H, ^{4}), 3.89 (s, 6H, ^{5}).

^{13}C-NMR (101 MHz, DMSO-d_6) δ/ppm = 165.1, 160.2, 139.1, 130.7, 124.3, 123.5, 52.5.

HRMS-EI-MS m/z: [M] calculated for [$C_{11}H_{11}NO_5$] = 237.0637, found: 237.0629.

IR (ATR platinum diamond) ν/cm^{-1} = 3316 (w), 3275 (vw), 3069 (vw), 2960 (w), 2929 (vw), 2919 (vw), 1732 (m), 1707 (s), 1689 (s), 1602 (m), 1520 (w), 1452 (m), 1438 (m), 1421 (w), 1401 (m), 1339 (s), 1316 (m), 1281 (w), 1267 (m), 1246 (vs), 1209 (s), 1135 (s), 1111 (m), 1033 (w), 1014 (m), 983 (m), 926 (w), 919 (w), 899 (m), 884 (m), 850 (w), 804 (w), 782 (vw), 751 (vs), 730 (s), 722 (s), 693 (s), 666 (w), 586 (s), 555 (w), 459 (w) .

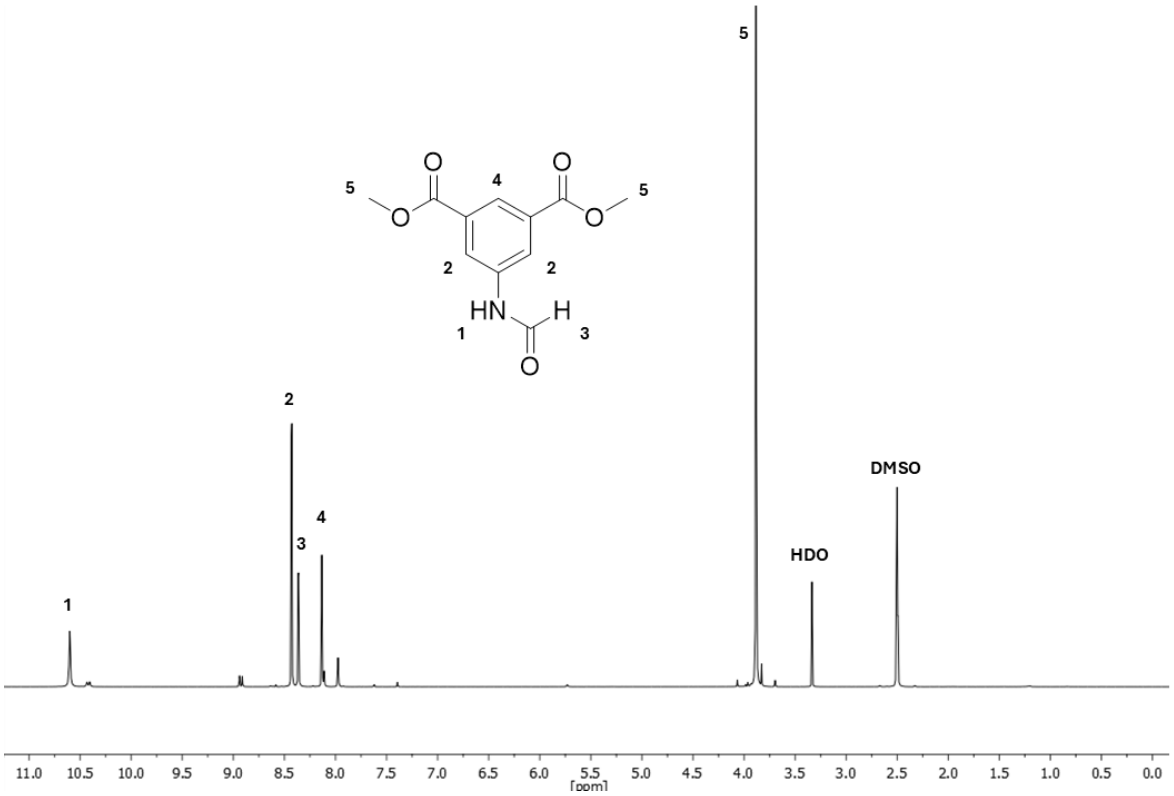

Supplementary Figure 4 ^{1}H-NMR of dimethyl 5-formamidoisophthalate measured in DMSO-d_6 plotted as signal intensity versus chemical shift in ppm. The NMR sample was taken from the crude product. The unlabelled signals are residues from formic acid.

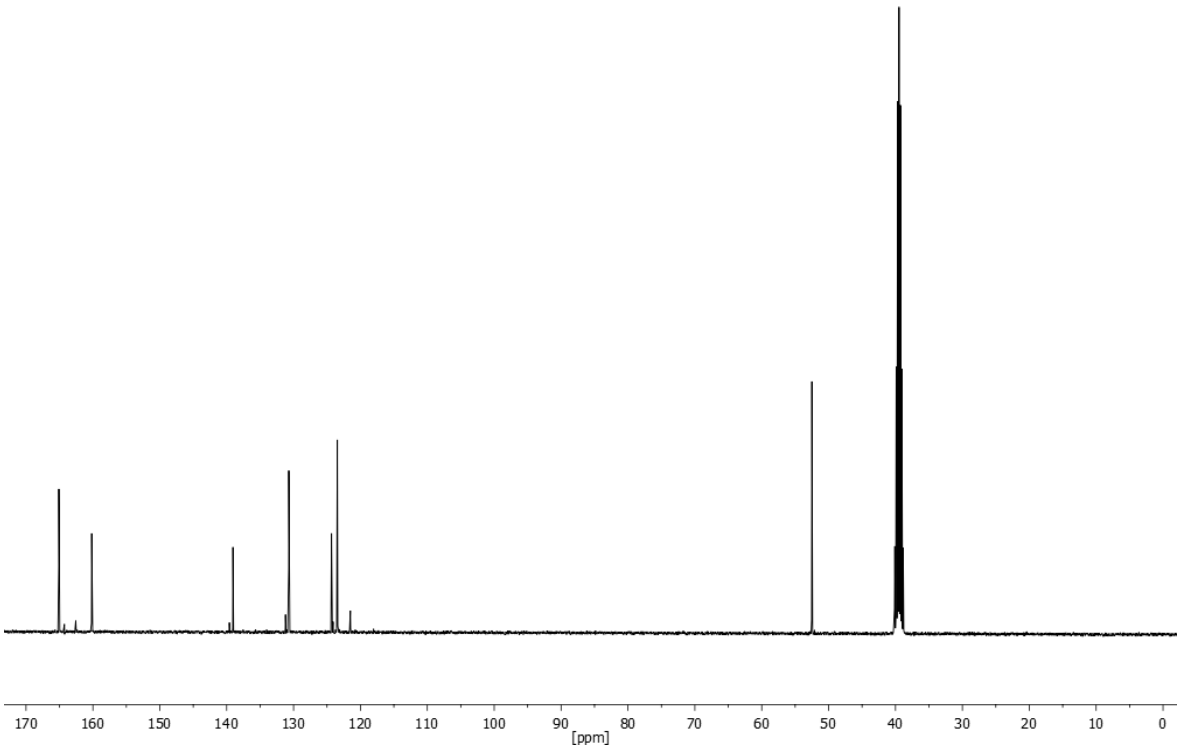

Supplementary Figure 5 ^{13}C-NMR of dimethyl 5-formamidoisophthalate measured in DMSO-d_6 (septet signal at 39.52 ppm) and plotted as signal intensity versus chemical shift in ppm.

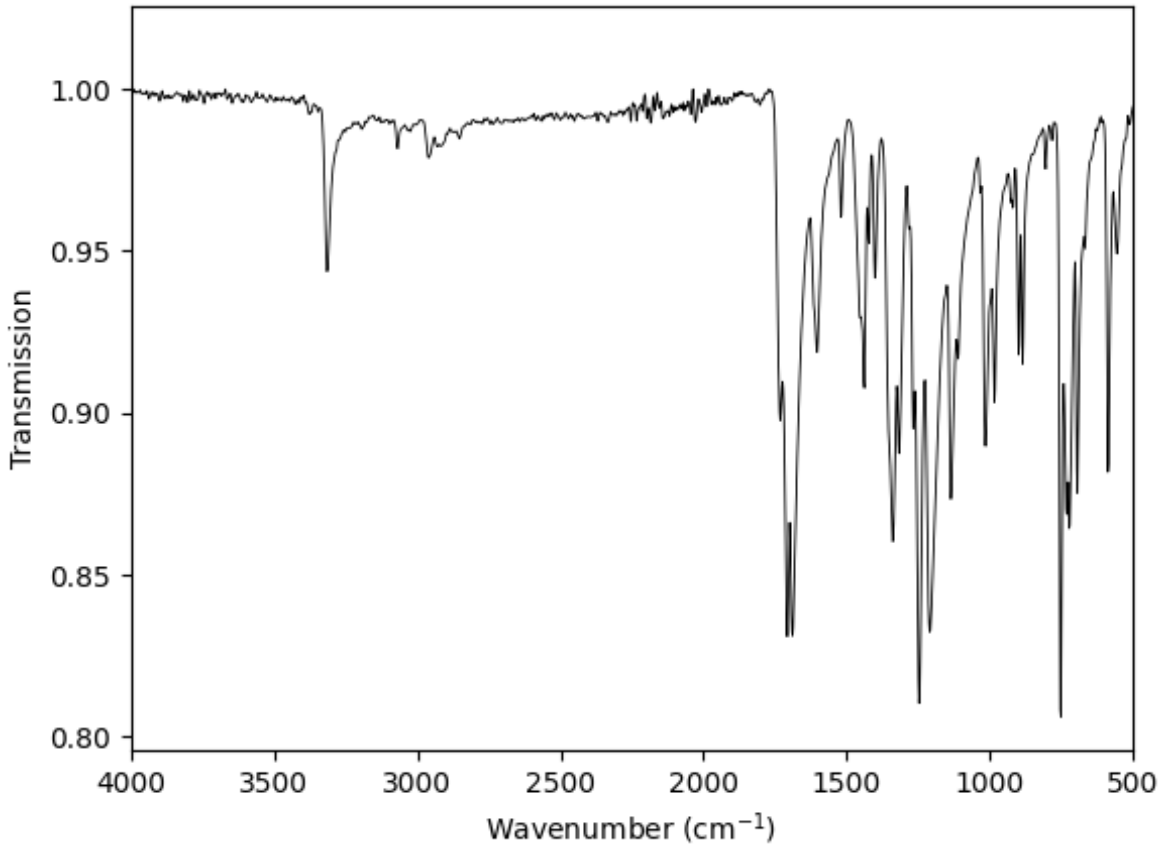

Supplementary Figure 6 IR-spectra of dimethyl 5-formamidoisophthalate.

Synthesis of dimethyl 5-isocyanoisophthalate (3)

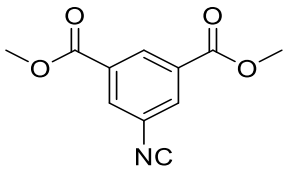

In a 100 mL round-bottom flask, which was equipped with a dimroth condenser, 3.296 g 5-formamidoisophthalate (**2**) (13.896 mmol, 1.00 eq.) was dissolved in 46.3 mL DCM. 6.05 mL diisopropyl amine (4.36 g, 43.08 mmol, 3.10 eq.) was added and the mixture was cooled in an ice-bath to 0 °C. Subsequently 1.65 mL phosphorous oxychloride (2.77 g, 18.07 mmol, 1.30 eq.) was added slowly and dropwise and the reaction mixture was then stirred at room temperature for three hours. Afterwards, the reaction mixture was quenched with 50 mL saturated sodium hydrogen carbonate solution and was stirred for further 15 min until gas formation ceased. Subsequently the organic phase was separated, and the aqueous phase was extracted three times with DCM. The combined organic phases were dried over sodium sulphate and were filtered off. The solvent was then evaporated under reduced pressure. The pure product dimethyl 5-isocyanoisophthalate was obtained as white solid in a yield of 62 % (1.88 g, 8.57 mmol) after column chromatography (cyclohexane / ethyl acetate 9:1). R_f-value (cyclohexane / ethyl acetate 9:1) = 0.23 visualised by UV quenching (254nm) or by treatment with staining vanillin solution (yellow - orange).

^{1}H-NMR (400 MHz, DMSO-d_6) δ/ppm = 8.28 (s, 1H, ^{1}), 8.12 (d, J = 1.5 Hz, 2H, ^{2}), 3.72 (s, 6H, ^{3}).

^{13}C-NMR (101 MHz, DMSO-d_6) δ/ppm = 163.9, 131.9, 131.0, 130.2, 52.9.

HRMS-EI-MS m/z: [M] calculated for [$C_{11}H_9NO_4$] = 219.0532, found: 219.0525.

IR (ATR platinum diamond) ν/cm^{-1} = 3085 (m), 3050 (vw), 3026 (vw), 3009 (vw), 2956 (w), 2923 (w), 2851 (w), 2791 (vw), 2781 (vw), 2135 (m), 2067 (w), 2061 (vw), 1726 (vs), 1623 (m), 1576 (w), 1539 (vw), 1454 (w), 1432 (s), 1349 (w), 1316 (s), 1286 (m), 1259 (m), 1238 (s), 1203 (s), 1172 (s), 1119 (m), 1107 (s), 983 (s), 932 (m), 917 (m), 880 (s), 798 (w), 784 (w), 767 (w), 749 (vs), 726 (m), 687 (w), 664 (m), 636 (w), 588 (w), 551 (w), 465 (m), 411 (w).

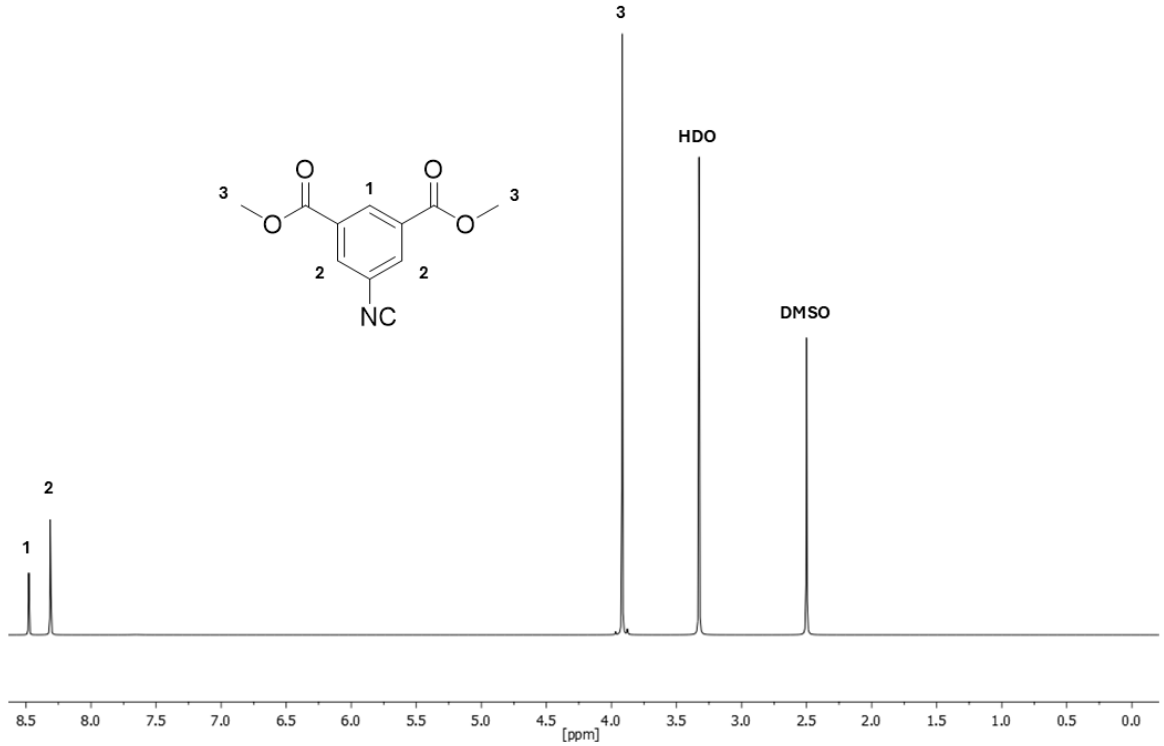

Supplementary Figure 7 ^{1}H-NMR of dimethyl 5-isocyanoisophthalate measured in DMSO-d_6 plotted as signal intensity versus chemical shift in ppm.

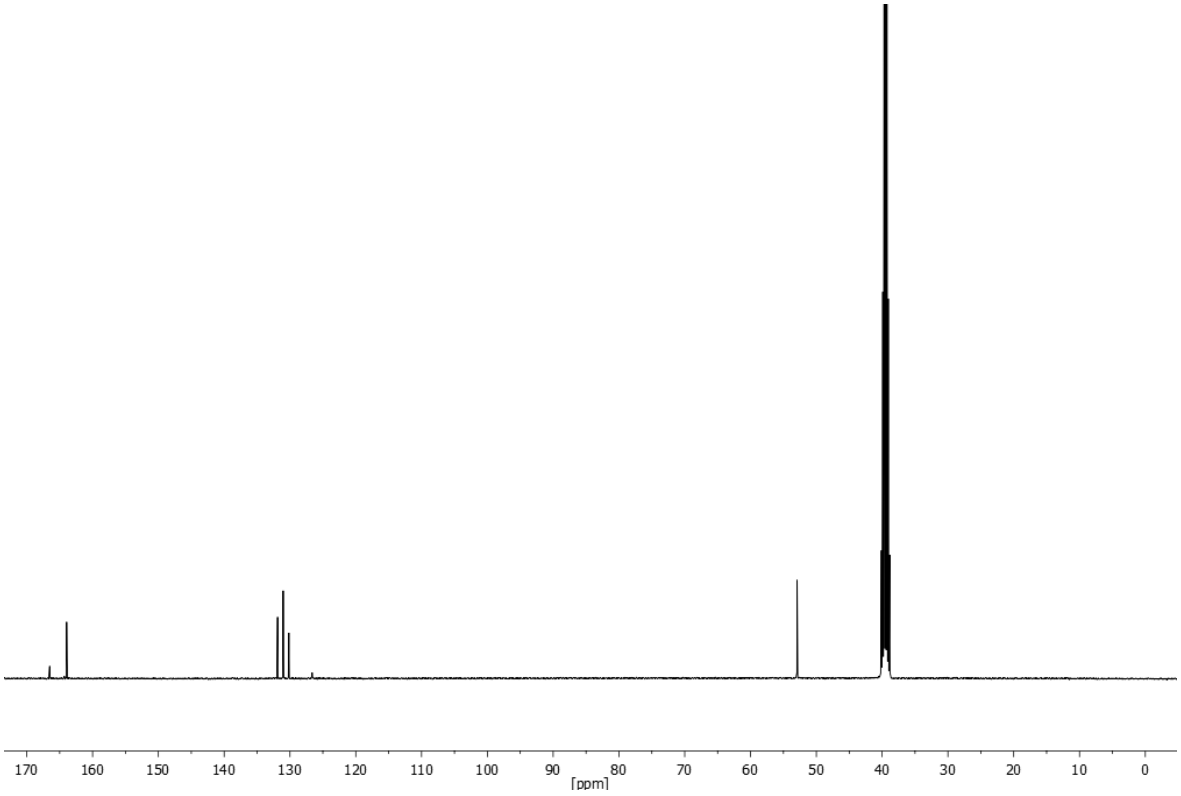

Supplementary Figure 8 ^{13}C-NMR of dimethyl 5-isocyanoisophthalate measured in DMSO-d_6 (septet signal at 39.52 ppm) and plotted as signal intensity versus chemical shift in ppm.

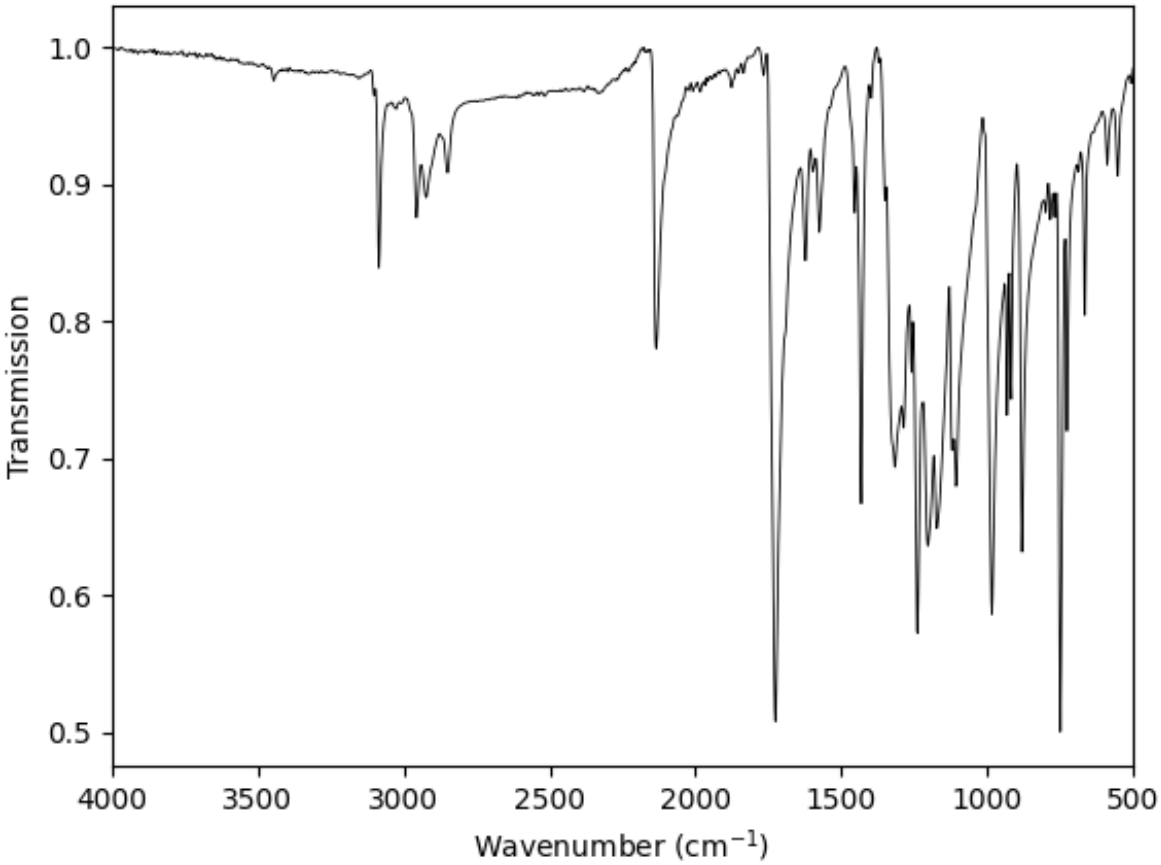

Supplementary Figure 9 IR-spectra of dimethyl 5-isocyanoisophthalate.

6.2.2 Synthesis of thiourea organocatalysts

Please note, thiourea **T2** was purchased commercially (FISHER CHEMICALS) while the thioureas **T4**, **T5** and **T7** were provided by **Dr. Clara Scheelje**, who previously synthesised them according to literature.[393,394] With her permission, the author was pleased to include them in his investigations.

6.2.2.1 General procedure for the synthesis of thioureas *via* MCR

A literature procedure according to Nickisch *et al.* was applied.[144] Elemental sulphur (0.14 eq., corresponds to 1.12 eq. of sulphur atoms) was suspended in methanol (1.0 M corresponding to n(isocyanide)) in a crimp vial. Subsequently, the respective amine (1.10 eq.) was added, and a dark brownish reaction mixture was usually observed. Subsequently, the isocyanide (1.00 eq.) was added, the crimp vial sealed, and the reaction mixture was stirred at room temperature until full conversion was observed by TLC. If the reaction did not proceed smoothly under the aforementioned conditions, 1,8-Diazabicyclo(5.4.0)undec-7-ene (DBU) — a organobase — was applied to catalyse the ring opening reaction of elemental sulphur and foster the reaction rate. Subsequently, the solvent was removed under reduced pressure. The crude product was washed with methanol at 60 °C for several minutes and then left to cool down to room temperature. After filtration and washing with minimal amount of methanol, the solvent was evaporated and the pure product was obtained. Deviations of this procedure are highlighted in the respective section.

Synthesis of thiourea T1

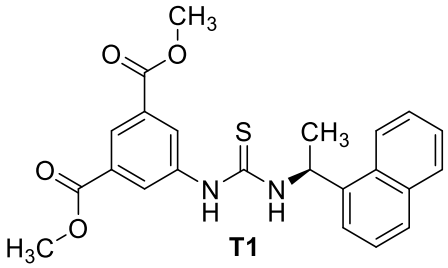

The synthesis was performed according to the general procedure for thioureas. Therefore, 220 mg of dimethyl 5-isocyanoisophthalate (1.00 mmol, 1.00 eq.), 37 mg elemental sulphur (0.14 mmol, 0.14 eq.) and 178 µL (*S*)-1-(naphthalen-1-yl)ethan-1-amine (189 mg, 1.10 mmol, 1.10 eq.) were used. The reactants were dissolved in a mixture of 1 mL MeOH and 1 mL DMF. Further 15 µL 1,8-diazabicyclo[5.4.0]undec-7-en (15.2 mg, 0.10 mmol, 0.10 eq.) were added and the mixture was stirred at room temperature for two hours until full conversion was observed *via* TLC analysis. After filtration and washing with minimal amount of methanol, the solvent was evaporated, and the pure product dimethyl (*S*)-5-(3-(1-(naphthalen-1-yl)ethyl)-thioureido)isophthalate was obtained as a white solid in a yield of 91% (384 mg, 0.91 mmol).

^{1}H-NMR (400 MHz, DMSO-d_6) δ/ppm = 9.80 (s, 1H, ^{1}), 8.53 (d, J = 7.3 Hz, 1H, ^{2}), 8.38 (s, 2H, ^{3}), 8.23 – 8.12 (m, 2H, ^{4}), 8.02 – 7.84 (m, 2H, ^{5}), 7.66 – 7.50 (m, 4H, ^{6}), 6.43 – 6.18 (m, 1H, ^{7}), 3.87 (s, 6H, ^{8}), 1.65 (d, J = 6.8 Hz, 3H, ^{9}).

^{13}C-NMR (101 MHz, DMSO-d_6) δ/ppm = 179.7, 165.2, 140.9, 138.9, 133.4, 130.6, 130.2, 128.7, 127.7, 126.8, 126.4, 125.7, 125.4, 124.3, 123.3, 122.9, 52.5, 49.0, 20.4.

HRMS-FAB-MS m/z: [M] calculated for [$C_{23}H_{23}N_2O_4S^+$] = 423.5068, found: 423.1375.

IR (ATR platinum diamond) $\tilde{\nu}$/cm^{-1} = 3322 (w), 3314 (w), 3289 (w), 3277 (w), 3258 (vw), 3250 (vw), 3242 (vw), 3211 (vw), 3055 (vw), 3042 (vw), 3013 (vw), 3005 (vw), 2989 (vw), 2972 (w), 2950 (w), 2929 (w), 1724 (s), 1598 (w), 1514 (m), 1436 (m), 1397 (w), 1372 (w), 1333 (m), 1240 (vs), 1119 (m), 1107 (m), 1033 (w), 1024 (w), 1000 (m), 950 (w), 926 (w), 901 (w), 876 (w), 796 (m), 778 (m), 757 (s), 732 (w), 716 (m), 701 (w), 681 (w), 650 (w), 640 (w), 582 (w), 564 (w), 549 (w), 533 (w), 516 (w), 483 (w), 469 (w), 457 (w), 448 (w), 436 (w).

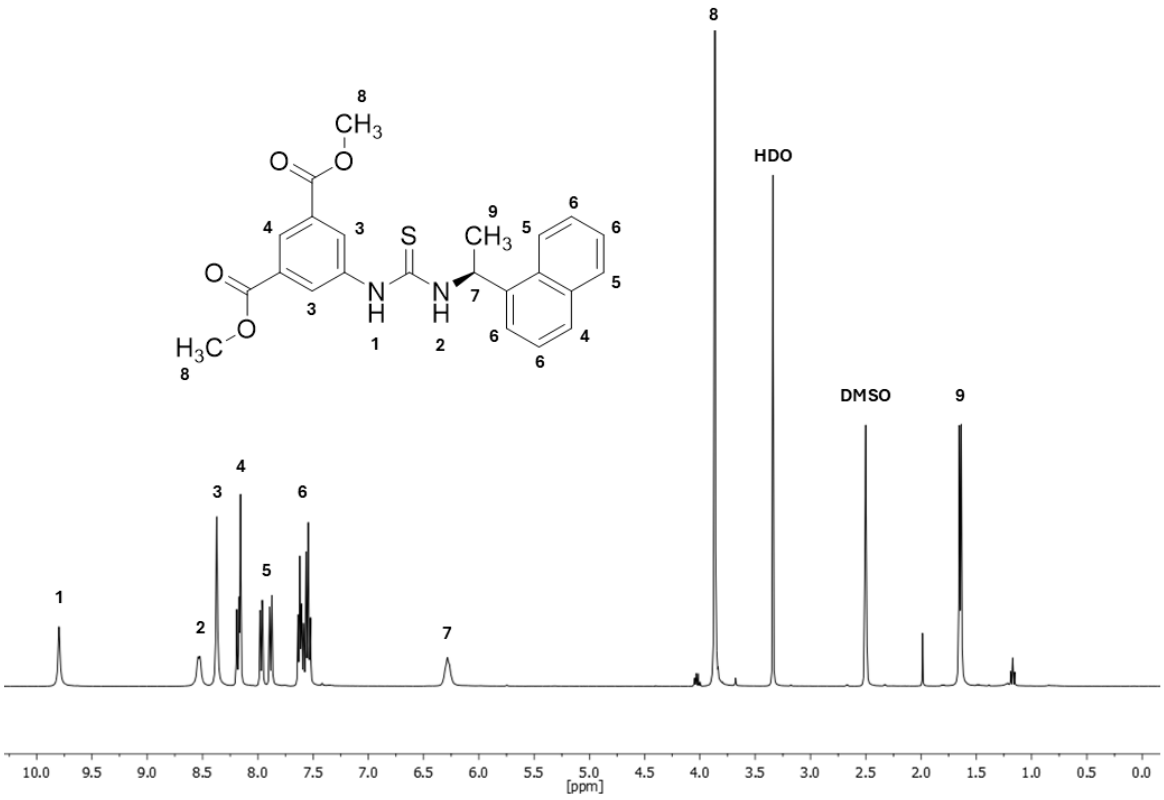

Supplementary Figure 10 ^{1}H-NMR of dimethyl (*S*)-5-(3-(1-(naphthalen-1-yl)ethyl)-thioureido)isophthalate measured in DMSO-d_6 plotted as signal intensity versus chemical shift in ppm. Unlabelled residues are caused by ethyl acetate.

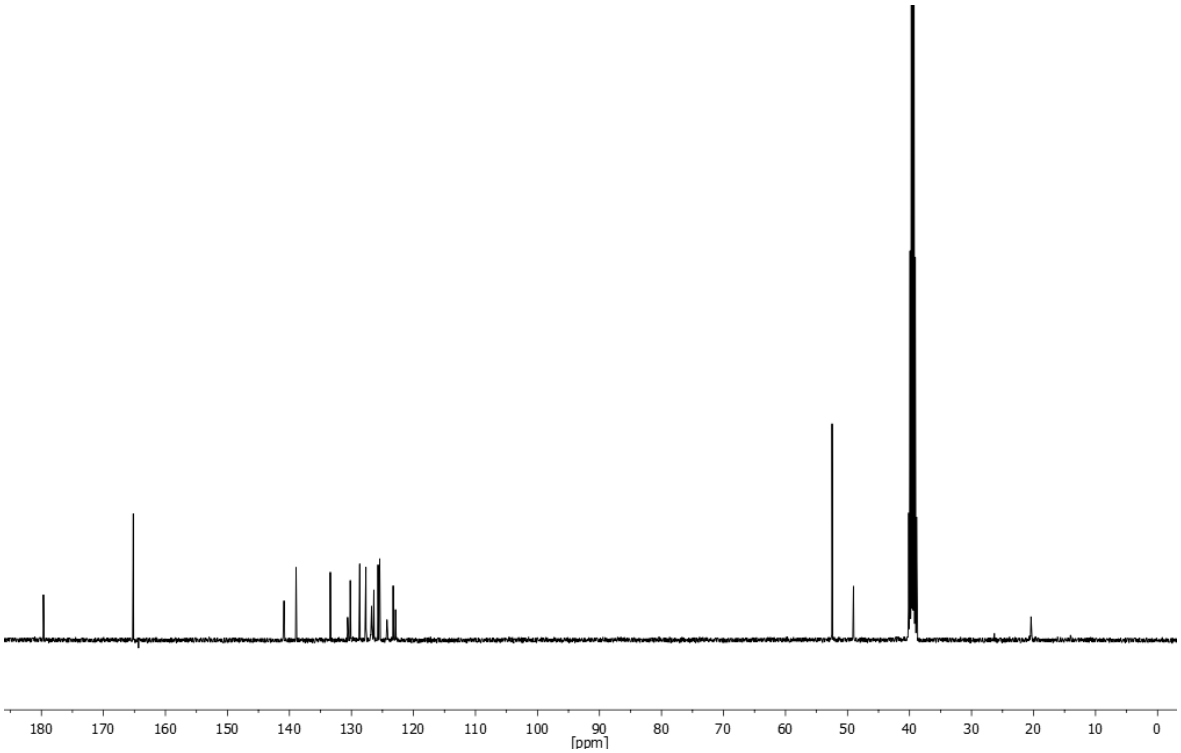

Supplementary Figure 11 ^{13}C-NMR of dimethyl (*S*)-5-(3-(1-(naphthalen-1-yl)ethyl)-thioureido)isophthalate measured in DMSO-d_6 (septet signal at 39.52 ppm) and plotted as signal intensity versus chemical shift in ppm.

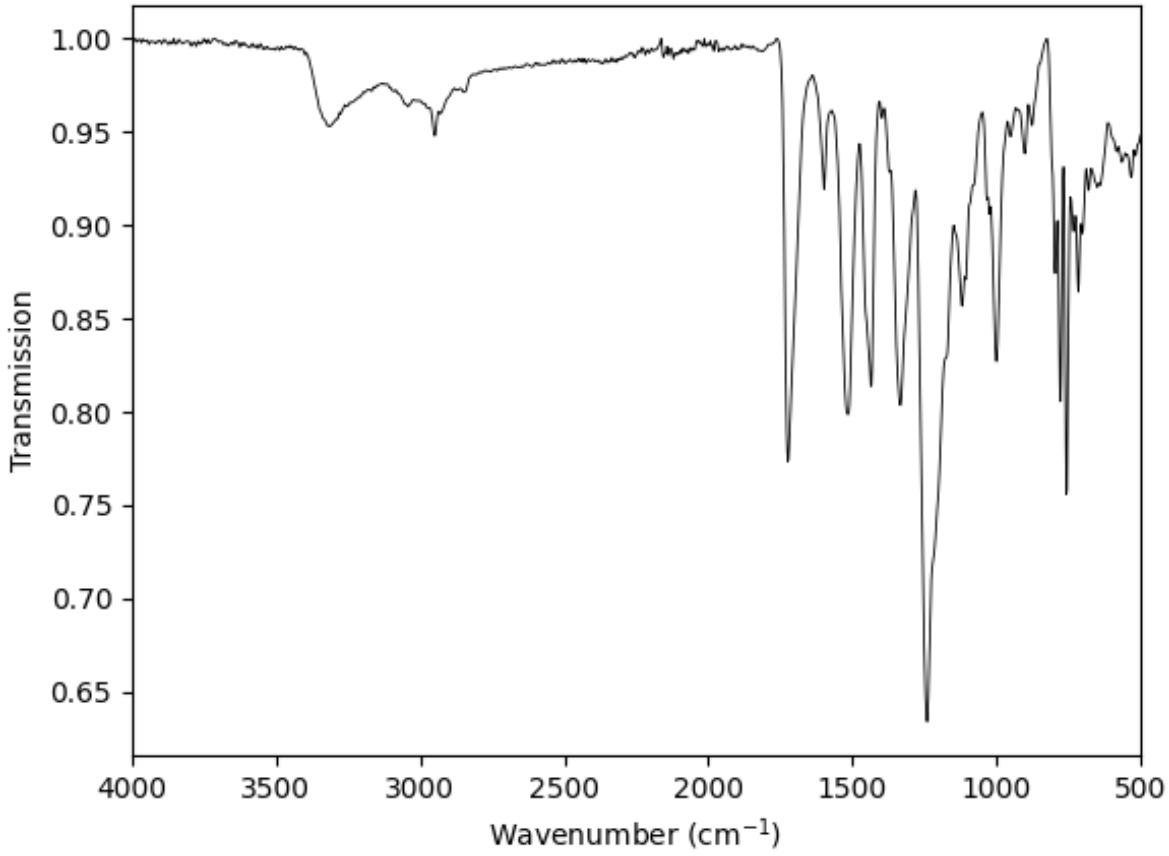

Supplementary Figure 12 IR-spectra of dimethyl (*S*)-5-(3-(1-(naphthalen-1-yl)ethyl)-thioureido)isophthalate.

Synthesis of thiourea T3

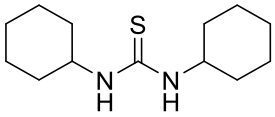

The reaction was conducted in bulk in a 10 mL crimp vial. To the vial, 225 µL of cyclohexyl isocyanide (200 mg, 1.83 mmol, 1.00 eq.), 231 µL of cyclohexylamine (200 mg, 2.02 mmol, 1.10 eq.), and 65.7 mg of elemental sulphur (256 µmol, 0.14 eq.) were added. The reaction mixture was stirred at room temperature for 5 minutes. Then, 1.5 mL of ethanol was added, and the resulting mixture was stirred overnight while the product precipitated. The crude product was then filtered using a frit and washed with ethanol (1 × 0.5 mL). After removal of the remaining solvent, the pure product 1,3-dicyclohexylthiourea was obtained as a colourless solid (250 mg, 1.04 mmol) in a yield of 57%. Further product could be obtained by repeating the purification steps from the obtained mother liquor, but this was not performed here.

Rf = 0.37 in cyclohexane/ethyl acetate (4:1), visualised *via* UV quenching at 254 nm and vanillin staining solution.

^{1}H-NMR (400 MHz, DMSO-d_6) δ/ppm = 7.06 (d, J = 8.0 Hz, 2H, ^{1}), 4.17 – 3.76 (m, 2H, ^{2}), 1.95 – 1.73 (m, 4H, ^{3}), 1.75 – 1.41 (m, 8H, ^{4}), 1.38 – 0.95 (m, 8H, ^{5}).

^{13}C-NMR (101 MHz, DMSO-d_6) δ/ppm = 180.5, 51.9, 32.8, 25.7, 25.0.

HRMS-EI-MS m/z: [M] calculated for $[C_{13}H_{25}N_2S]^+$ = 241.17330, found: 241.17302.

IR (ATR platinum diamond) ν/cm^{-1} = 3291 (m), 2925 (s), 2851 (m), 2797 (w), 2791 (w), 2783 (w), 2750 (vw), 2655 (vw), 1551 (vs), 1504 (vs), 1465 (w), 1450 (m), 1409 (m), 1378 (w), 1360 (m), 1341 (m), 1323 (m), 1306 (w), 1296 (w), 1275 (m), 1255 (m), 1226 (s), 1185 (m), 1154 (m), 1111 (m), 1090 (w), 1076 (w), 1051 (w), 1028 (w), 983 (m), 887 (m), 847 (w), 815 (w), 788 (w), 771 (m), 658 (w), 588 (s), 549 (s), 527 (s), 490 (w), 481 (w), 461 (w), 446 (w).

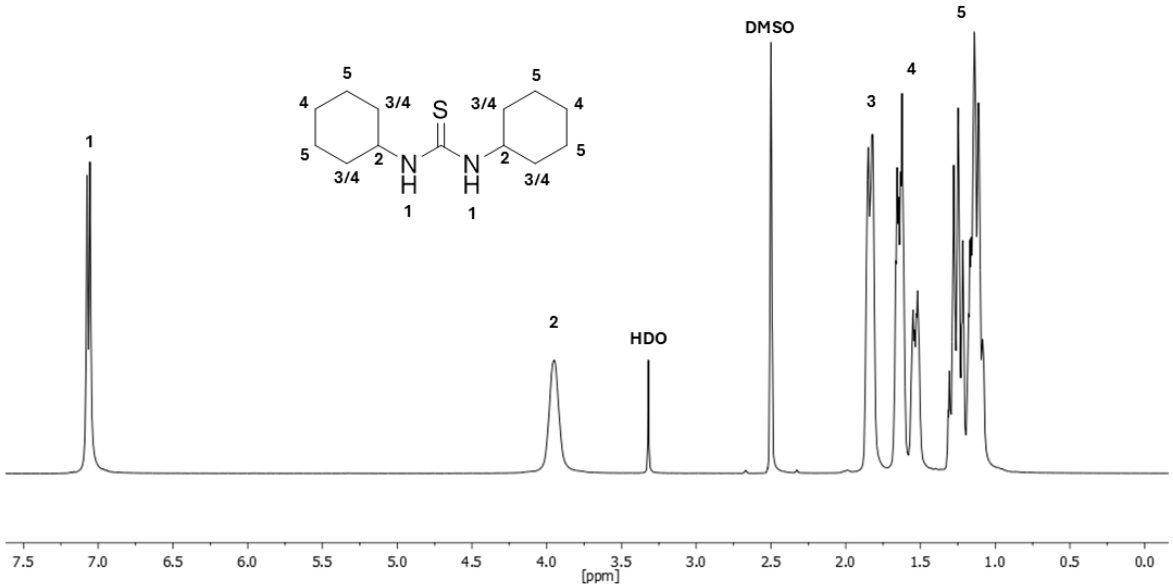

Supplementary Figure 13 ^{1}H-NMR of 1,3-dicyclohexylthiourea.measured in DMSO-d_6 plotted as signal intensity versus chemical shift in ppm.

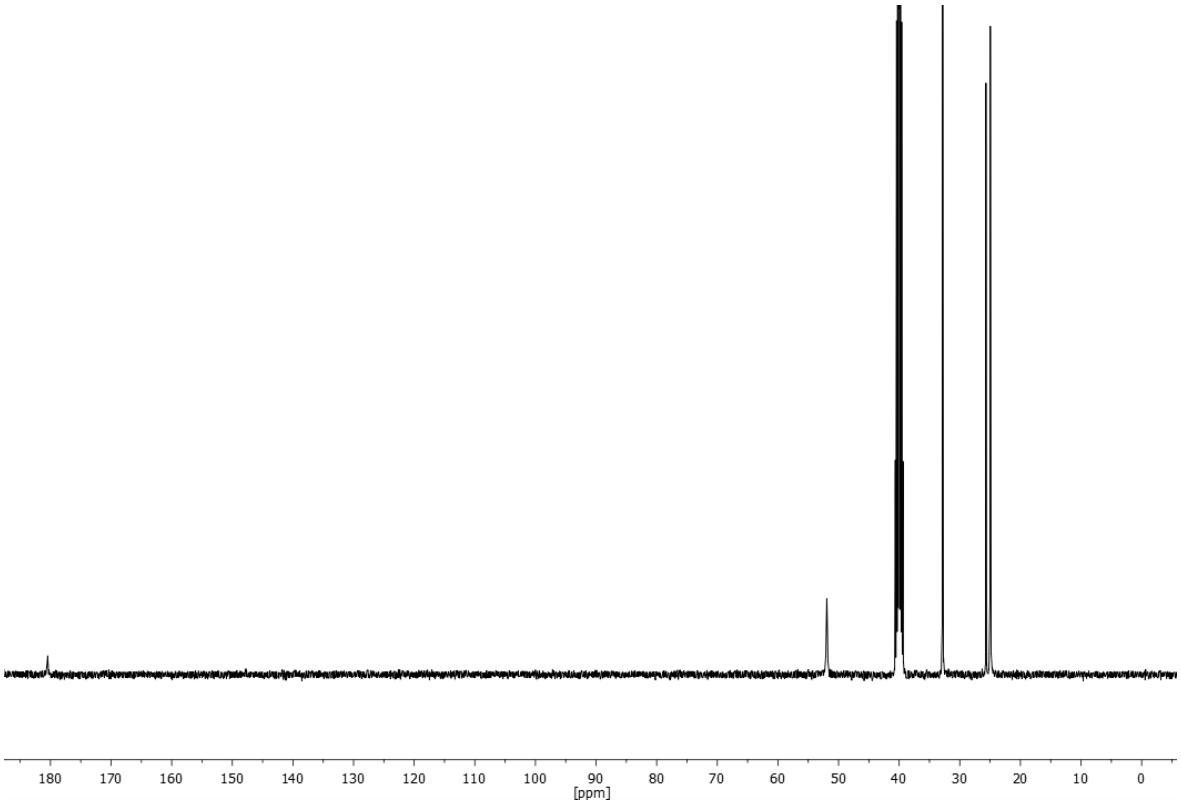

Supplementary Figure 14 ^{13}C-NMR of 1,3-dicyclohexylthiourea measured in DMSO-d_6 (septet signal at 39.52 ppm) and plotted as signal intensity versus chemical shift in ppm.

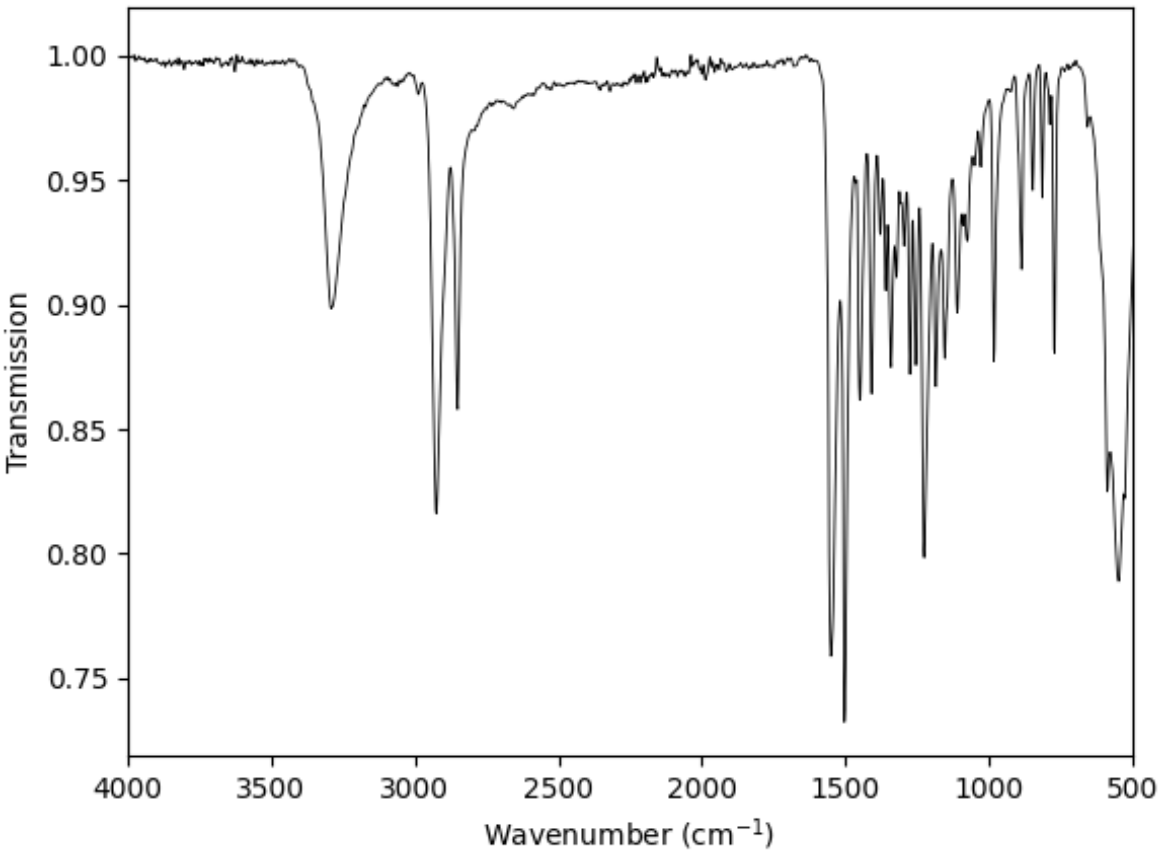

Supplementary Figure 15 IR-spectra of 1,3-dicyclohexylthiourea.

Synthesis of thiourea T6

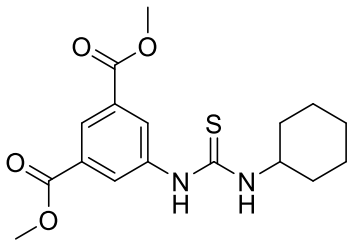

The reaction was conducted in a 10 mL crimp vial. In the vial, 400 mg of 5-isocyano dimethylisophthalate (1.82 mmol, 1.00 eq.), 230 µL of cyclohexylamine (199 mg, 2.01 mmol, 1.10 eq.), and 65.5 mg of elemental sulphur (255 µmol, 0.14 eq.) were suspended in 2 mL of methanol (0.9 M corresponding to n(isocyanide)). Since the isocyanide possesses low solubility in methanol, 2 mL of DMF were added until full solubility was achieved. Further, 30 µL of DBU (30.6 mg, 0.201 mmol, 0.11 eq.) were added to catalyse the reaction. The reaction mixture was stirred at room temperature overnight. Subsequently, the solvent was evaporated under reduced pressure. The concentrate was purified *via* column chromatography using silica gel and eluting with a gradual solvent mixture of cyclohexane / ethyl acetate (4:1 to 2:1). The pure product *N*-(5-(Dimethylisophtalate))-*N*'-cyclohexyl thiourea was obtained as a colourless solid (412 mg, 1.18 mmol) in a yield of 65%.

Rf = 0.38 in cyclohexane/ethyl acetate (2:1), visualised *via* UV quenching at 254 nm and vanillin staining solution.

^{1}H-NMR (400 MHz, DMSO-d_6) δ/ppm = 9.71 (s, 1H, [1]), 8.38 (s, 2H, [2]), 8.15 (s, 1H, [3]), 7.91 (s, 1H, [4]), 4.09 (s, 1H, [5]), 3.89 (s, 6H, [6]), 2.00 – 1.08 (m, 10H, [7]).

^{13}C-NMR (101 MHz, DMSO-d_6) δ/ppm = 179.8, 165.7, 141.5, 130.6, 55.4, 53.0, 52.6, 32.2, 25.6, 24.9.

HRMS-EI-MS m/z: [M] calculated for $[C_{17}H_{23}N_2O_4S]^+$ = 351.13730, found: 351.13705.

IR (ATR platinum diamond) $\tilde{\nu}$/cm^{-1} = 3330 (m), 3164 (w), 3127 (w), 3094 (w), 3018 (w), 2980 (w), 2946 (w), 2927 (m), 2913 (m), 2855 (w), 2847 (w), 2773 (vw), 1728 (s), 1711 (s), 1598 (m), 1530 (vs), 1448 (m), 1436 (s), 1382 (w), 1343 (s), 1312 (m), 1302 (m), 1261 (s), 1249 (vs), 1195 (s), 1183 (s), 1144 (s), 1123 (m), 1109 (s), 1053 (w), 1028 (w), 996 (s), 981 (m), 928 (w), 907 (m), 893 (m), 880 (w), 852 (w), 821 (w), 792 (m), 757 (s), 722 (m), 689 (m), 664 (m), 631 (s), 605 (m), 592 (w), 572 (w), 547 (m), 510 (w), 483 (w), 455 (w), 432 (w).

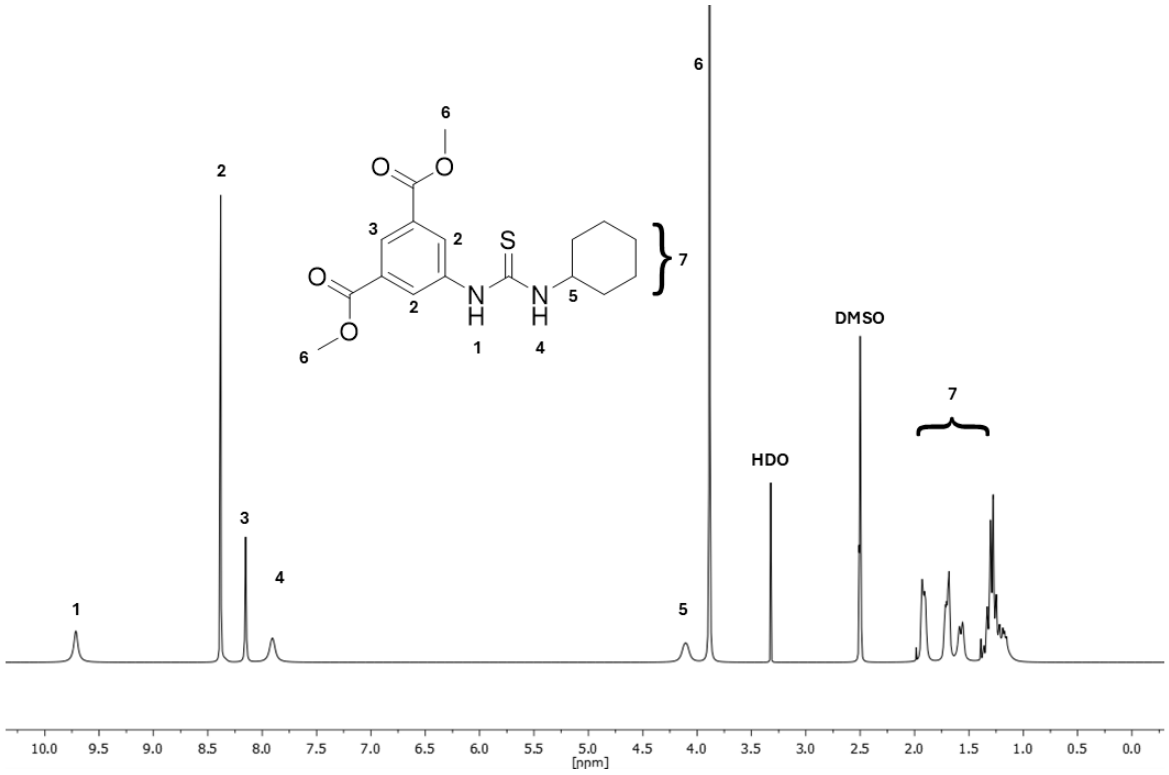

Supplementary Figure 16 ^{1}H-NMR of *N*-(5-(Dimethylisophtalate))-*N*'-cyclohexyl thiourea.measured in DMSO-d_6 plotted as signal intensity versus chemical shift in ppm.

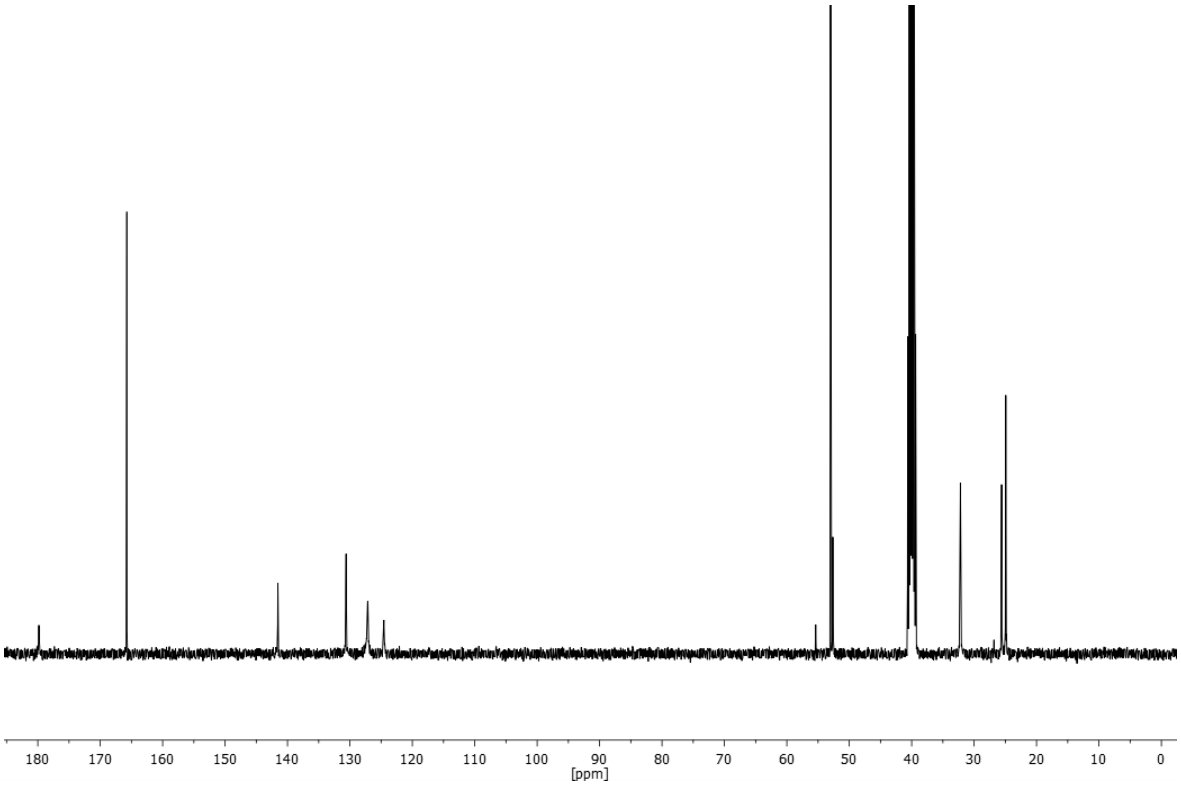

Supplementary Figure 17 ^{13}C-NMR of *N*-(5-(Dimethylisophtalate))-*N*'-cyclohexyl thiourea measured in DMSO-d_6 (septet signal at 39.52 ppm) and plotted as signal intensity versus chemical shift in ppm.

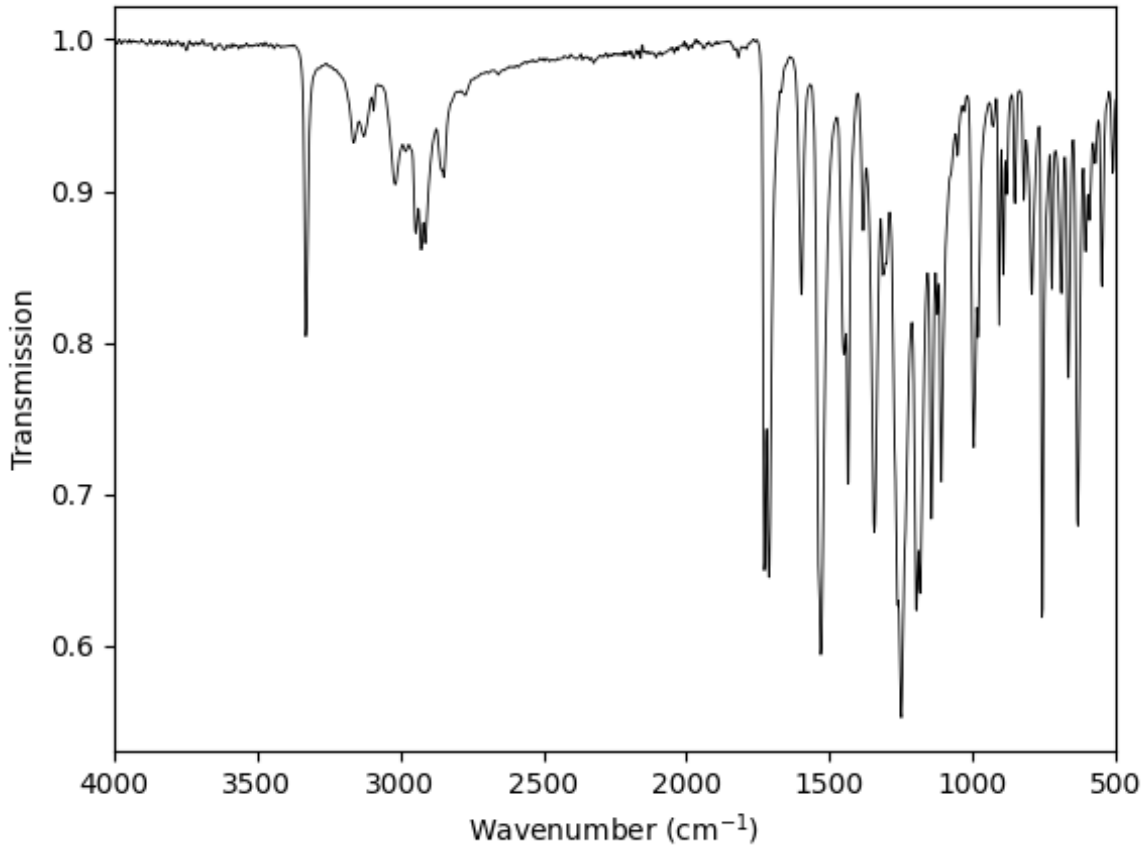

Supplementary Figure 18 IR-spectra of *N*-(5-(Dimethylisophtalate))-*N*'-cyclohexyl thiourea.

Synthesis of thiourea T8

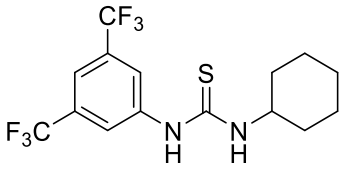

The reaction was conducted in a 10 mL crimp vial. 231 µL cyclohexylamine (198.4 mg, 2.00 mmol, 1.10 eq.) and ethyl acetate (3 mL) were initially introduced. Subsequently, 331 µL 1-isothiocyanato-3,5-bis(trifluoromethyl)benzene (493.1 mg, 1.82 mmol, 1.00 eq.) was added. To monitor the reaction, thin-layer chromatography (TLC) was performed, using a solvent mixture of cyclohexane and ethyl acetate in a 2:1 ratio. After 5 hours, the reaction was complete. Following this, water and ethyl acetate were added (10 mL each). The aqueous phase was extracted with ethyl acetate (2 × 25 mL) and then washed with water (2 × 25 mL). After drying over sodium sulphate, the solvent was removed under reduced pressure. Finally, the crude product was purified *via* column chromatography (cyclohexane/ethyl acetate, 2:1). The product, 1-(3,5-bis(trifluoromethyl)phenyl)-3-cyclohexylthiourea, was obtained as a white solid (577 mg, 1.56 mmol) in a yield of 86%.

Rf = 0.72 in cyclohexane/ethyl acetate (2:1), visualised *via* UV quenching at 254 nm and vanillin staining solution.

^{1}H-NMR (500 MHz, DMSO-d_6) δ/ppm = 9.85 (s, 1H, ^{1}), 8.24 (s, 2H, ^{2}), 8.15 (s, 1H, ^{3}), 7.70 (s, 1H, ^{4}), 4.11 (s, 1H, ^{5}), 1.95 – 1.14 (m, 10H, ^{6}).

^{13}C-NMR (126 MHz, DMSO-d_6) δ/ppm = 179.6, 142.5, 130.9, 130.7, 130.4, 130.2, 127.0, 124.8, 122.7, 120.5, 52.8, 32.0, 25.6, 24.9.

HRMS-EI-MS m/z: [M] calculated for $[C_{15}H_{17}F_6N_2S]^+$ = 371.10111, found: 371.10125.

IR (ATR platinum diamond) ν/cm^{-1} = 3281 (vw), 3190 (vw), 3164 (w), 3038 (w), 3001 (w), 2933 (w), 2859 (w), 1553 (m), 1524 (s), 1467 (m), 1438 (w), 1382 (m), 1364 (m), 1345 (m), 1337 (m), 1269 (s), 1244 (m), 1177 (s), 1125 (vs), 1107 (s), 1039 (m), 1024 (w), 1004 (w), 993 (w), 940 (m), 905 (w), 889 (s), 874 (w), 862 (w), 847 (m), 753 (w), 718 (m), 706 (m), 679 (s), 617 (w), 588 (w), 570 (w), 551 (w), 516 (w).

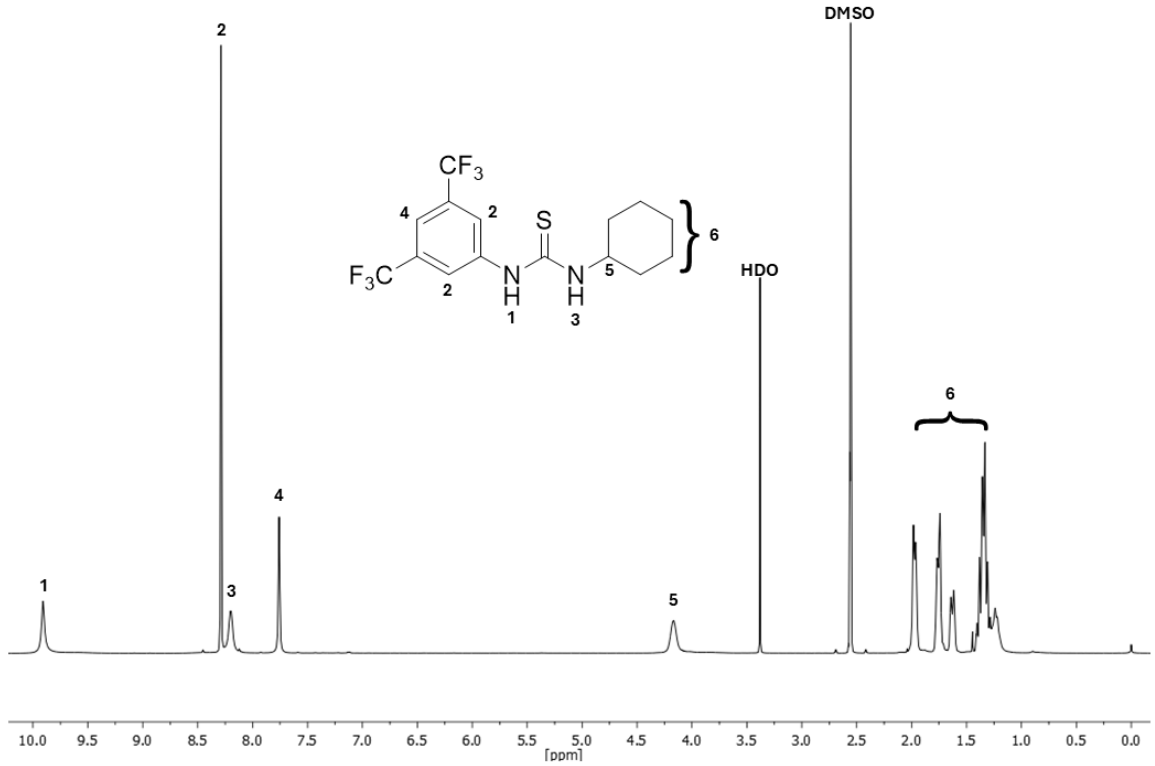

Supplementary Figure 19 ^{1}H-NMR of 1-(3,5-bis(trifluoromethyl)phenyl)-3-cyclohexylthiourea.measured in DMSO-d_6 plotted as signal intensity versus chemical shift in ppm.

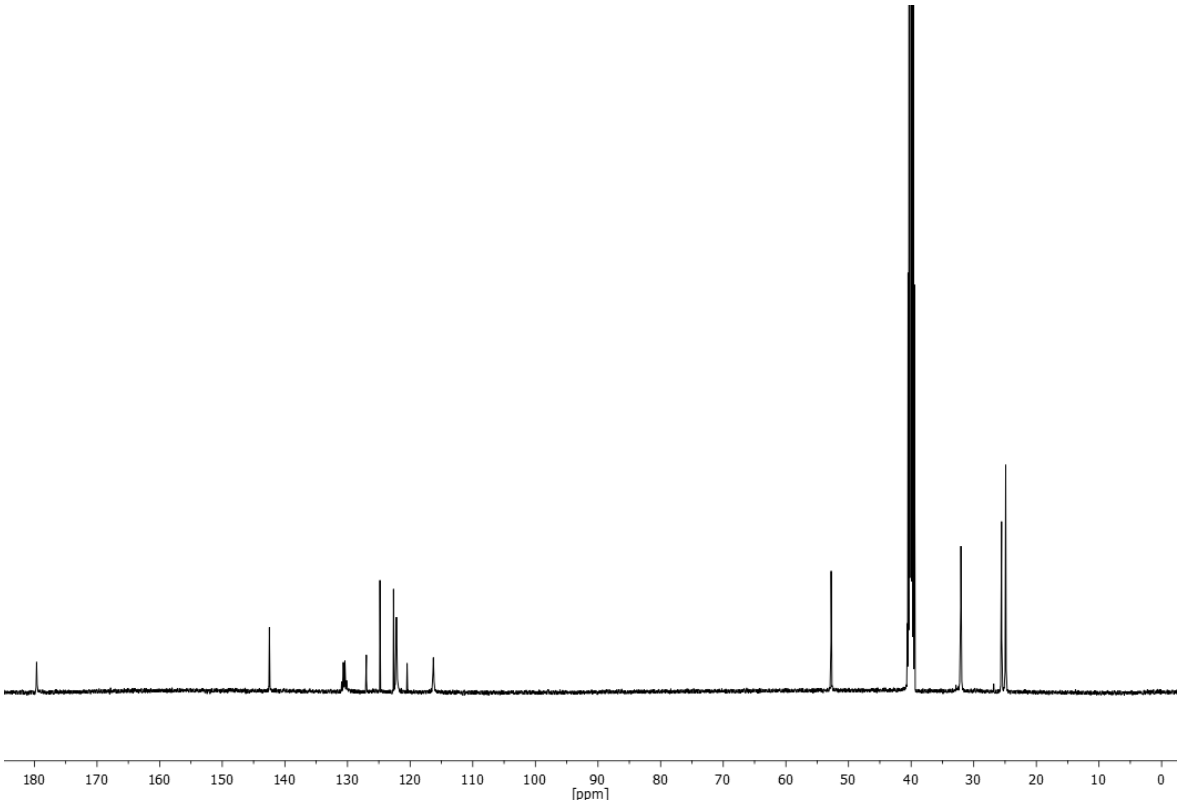

Supplementary Figure 20 ^{13}C-NMR of 1-(3,5-bis(trifluoromethyl)phenyl)-3-cyclohexylthiourea measured in DMSO-d_6 (septet signal at 39.52 ppm) and plotted as signal intensity versus chemical shift in ppm.

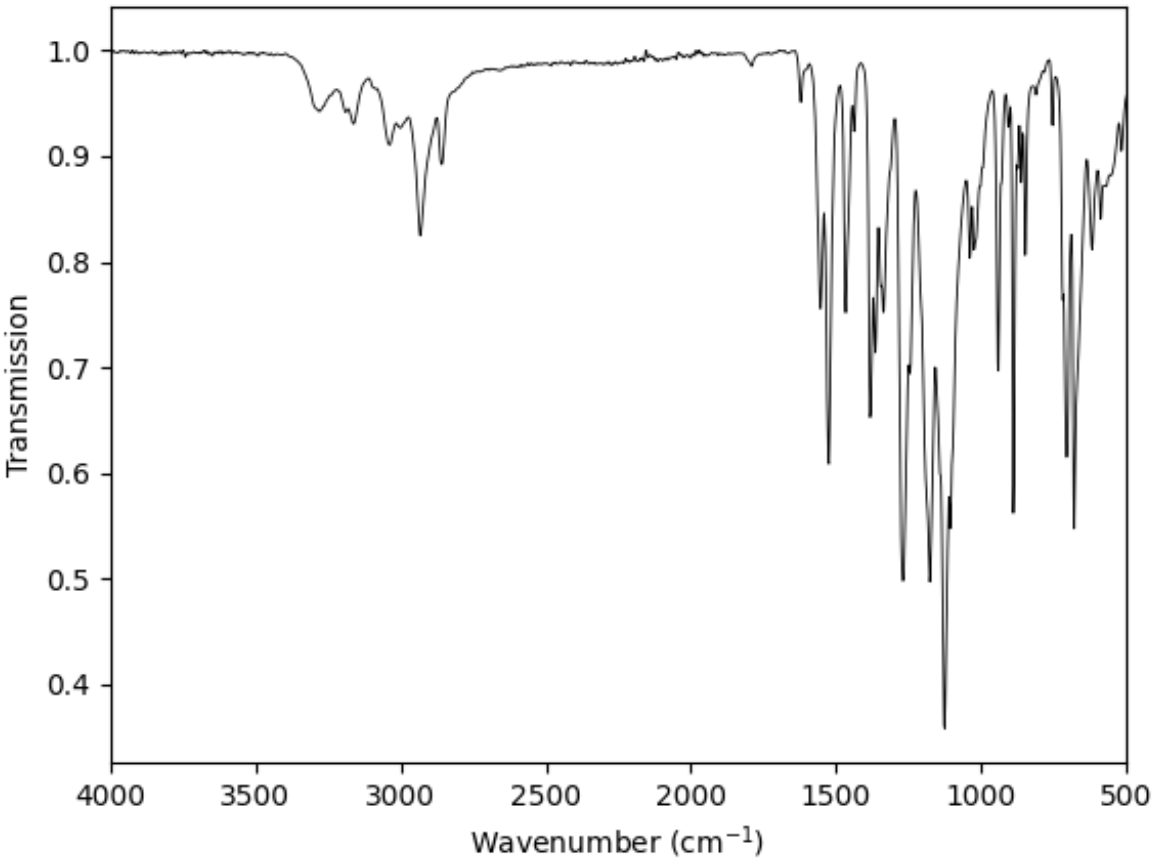

Supplementary Figure 21 IR-spectra of 1-(3,5-bis(trifluoromethyl)phenyl)-3-cyclohexylthiourea.

Synthesis of thiourea T9

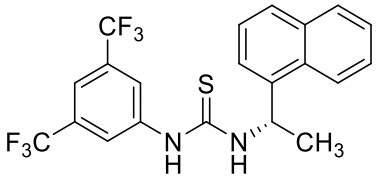

The reaction was conducted in a 10 mL crimp vial. 1.41 mL (*S*)-1-(naphthalen-1-yl)ethan-1-amine (1.50 g, 8.76 mmol, 1.00 eq.) and dimethylformamide (5 mL) were initially introduced. Subsequently, 1.75 mL 1-isothiocyanato-3,5-bis(trifluoromethyl)benzene (2.61 g, 9.63 mmol, 1.10 eq.) was added. To monitor the reaction, thin-layer chromatography (TLC) was performed, using a solvent mixture of cyclohexane and ethyl acetate in a 6:1 ratio. After 4 hours, the reaction was complete. The solvent was removed under reduced pressure. Finally, the crude product was purified *via* column chromatography (cyclohexane/ethyl acetate, 6:1). The product, (*S*)-1-(3,5-bis(trifluoromethyl)phenyl)-3-(1-(naphthalen-1-yl)ethyl)thiourea, was obtained as a white solid (3.44 g, 7.79 mmol) in a yield of 89%.

Rf = 0.23 in cyclohexane/ethyl acetate (6:1), visualised *via* UV quenching at 254 nm and vanillin staining solution.

^{1}H-NMR (400 MHz, DMSO-d_6) δ/ppm = 9.93 (s, 1H, ^{1}), 8.77 (d, J = 7.8 Hz, 1H, ^{2}), 8.24 – 8.14 (m, 3H, ^{3}), 7.97 (d, J = 8.0, 1H, ^{4}), 7.89 (d, J = 8.1 Hz, 1H, ^{5}), 7.70 (s, 1H, ^{6}), 7.65 – 7.51 (m, 4H, ^{7}), 6.36 – 6.19 (m, 1H, ^{8}), 1.65 (d, J = 6.8 Hz, 3H, ^{9}).

^{13}C-NMR (101 MHz, DMSO-d_6) δ/ppm = 179.9, 142.4, 139.1, 133.9, 129.2, 128.3, 126.9, 126.2, 125.9, 125.0, 125.0, 123.7, 123.5, 122.3, 49.6, 20.6.

HRMS-EI-MS m/z: [M] calculated for $[C_{21}H_{17}F_6N_2S]^+$ = 443.10111, found: 443.10314.

IR (ATR platinum diamond) $\tilde{\nu}$/cm^{-1} = 3238 (vw), 3089 (vw), 3081 (vw), 3067 (vw), 3050 (vw), 1555 (w), 1528 (m), 1471 (m), 1376 (m), 1337 (m), 1273 (s), 1240 (m), 1226 (m), 1205 (w), 1168 (s), 1123 (vs), 1109 (s), 1074 (m), 1035 (w), 1020 (w), 1000 (w), 971 (m), 930 (w), 913 (w), 882 (m), 860 (w), 847 (w), 798 (m), 780 (m), 751 (vw), 734 (w), 718 (m), 699 (m), 679 (s), 656 (w), 619 (w), 539 (m), 516 (m), 461 (w), 436 (w), 405 (w).

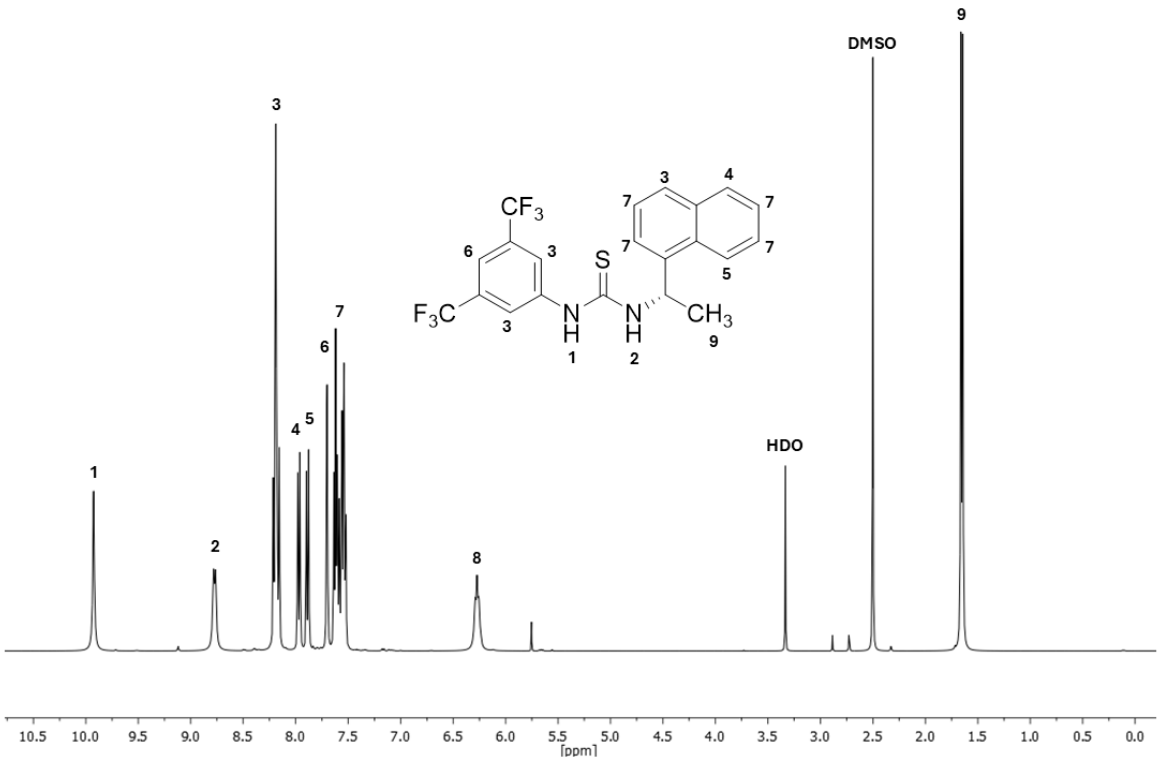

Supplementary Figure 22 ^{1}H-NMR of (*S*)-1-(3,5-bis(trifluoromethyl)phenyl)-3-(1-(naphthalen-1-yl)ethyl)thiourea measured in DMSO-d_6 plotted as signal intensity versus chemical shift in ppm.

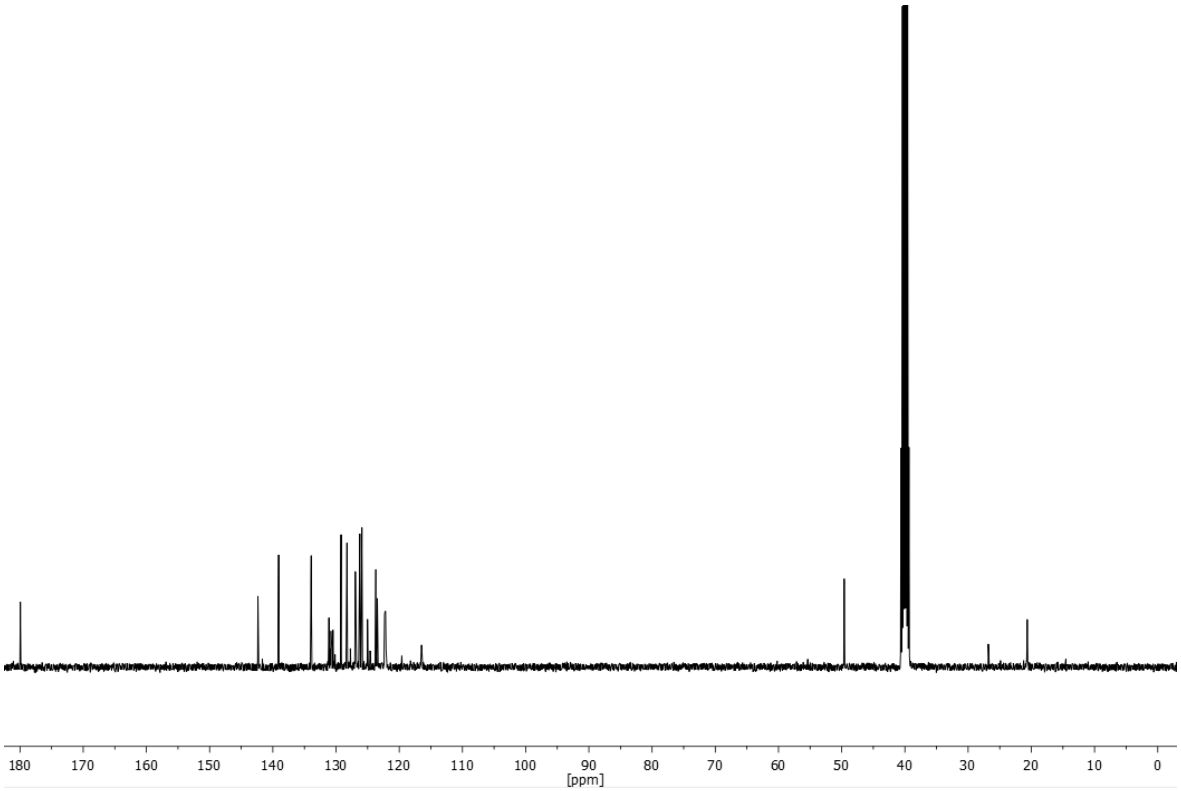

Supplementary Figure 23 ^{13}C-NMR of (*S*)-1-(3,5-bis(trifluoromethyl)phenyl)-3-(1-(naphthalen-1-yl)ethyl)thiourea measured in DMSO-d_6 (septet signal at 39.52 ppm) and plotted as signal intensity versus chemical shift in ppm.

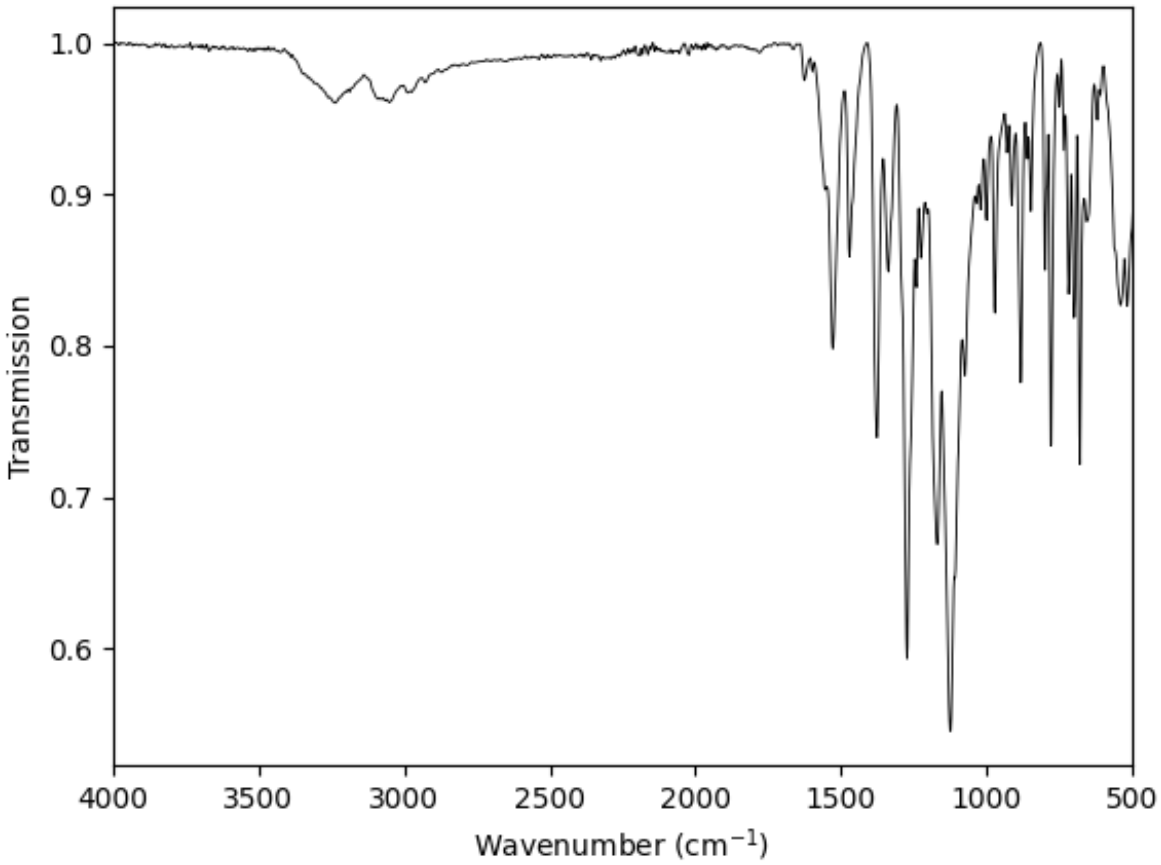

Supplementary Figure 24 IR-spectra of (*S*)-1-(3,5-bis(trifluoromethyl)phenyl)-3-(1-(naphthalen-1-yl)ethyl)thiourea.

Synthesis of thiourea T10

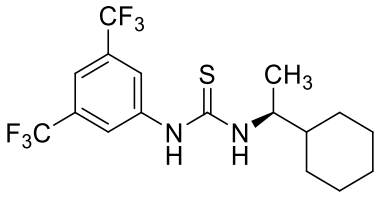

The reaction was conducted in a 10 mL crimp vial. 234 µL (*S*)-1-cyclohexylethan-1-amine (200 mg, 1.57 mmol, 1.00 eq.) and dimethylformamide (2 mL) were initially introduced. Subsequently, 286 µL 1-isothiocyanato-3,5-bis(trifluoromethyl)benzene (426 mg, 1.57 mmol, 1.00 eq.) was added. To monitor the reaction, thin-layer chromatography (TLC) was performed, using a solvent mixture of cyclohexane and ethyl acetate in a 4:1 ratio. After 4 hours, the reaction was complete. The solvent was removed under reduced pressure. Finally, the crude product was purified *via* column chromatography (cyclohexane/ethyl acetate, 4:1). The product, (*S*)-1-(3,5-bis(trifluoromethyl)phenyl)-3-(1-cyclohexylethyl)-thiourea, was obtained as a white solid (552 mg, 1.39 mmol) in a yield of 88%.

Rf = 0.42 in cyclohexane/ethyl acetate (4:1), visualised *via* UV quenching at 254 nm and vanillin staining solution.

^{1}H-NMR (400 MHz, DMSO-d_6) δ/ppm = 9.85 (s, 1H, ^{1}), 8.24 (s, 2H, ^{2}), 8.08 (d, J = 8.6 Hz, 1H, ^{3}), 7.69 (s, 1H, ^{4}), 4.37 – 4.16 (m, 1H, ^{5}), 1.89 – 0.90 (m, 14H, ^{6}).

^{13}C-NMR (101 MHz, DMSO-d_6) δ/ppm = 180.2, 142.5, 131.1, 130.7, 130.4, 130.1, 125.1, 122.4, 122.0, 54.3, 42.6, 29.4, 29.1, 26.4, 26.2, 26.1, 17.2.

HRMS-EI-MS m/z: [M] calculated for $[C_{17}H_{20}F_6N_2S]^+$ = 399.13241, found: 399.13246.

IR (ATR platinum diamond) $\tilde{\nu}$/cm^{-1} = 3223 (w), 3061 (w), 2983 (w), 2972 (w), 2931 (w), 2851 (w), 1547 (m), 1537 (m), 1467 (w), 1460 (w), 1450 (w), 1380 (m), 1347 (m), 1308 (w), 1271 (s), 1242 (m), 1183 (s), 1170 (s), 1154 (m), 1127 (vs), 1107 (s), 1068 (w), 1045 (w), 1026 (w), 1000 (m), 977 (m), 934 (w), 907 (vw), 889 (s), 847 (w), 749 (w), 712 (m), 699 (m), 681 (s), 617 (w), 586 (w), 557 (w), 535 (w), 514 (w), 504 (w).

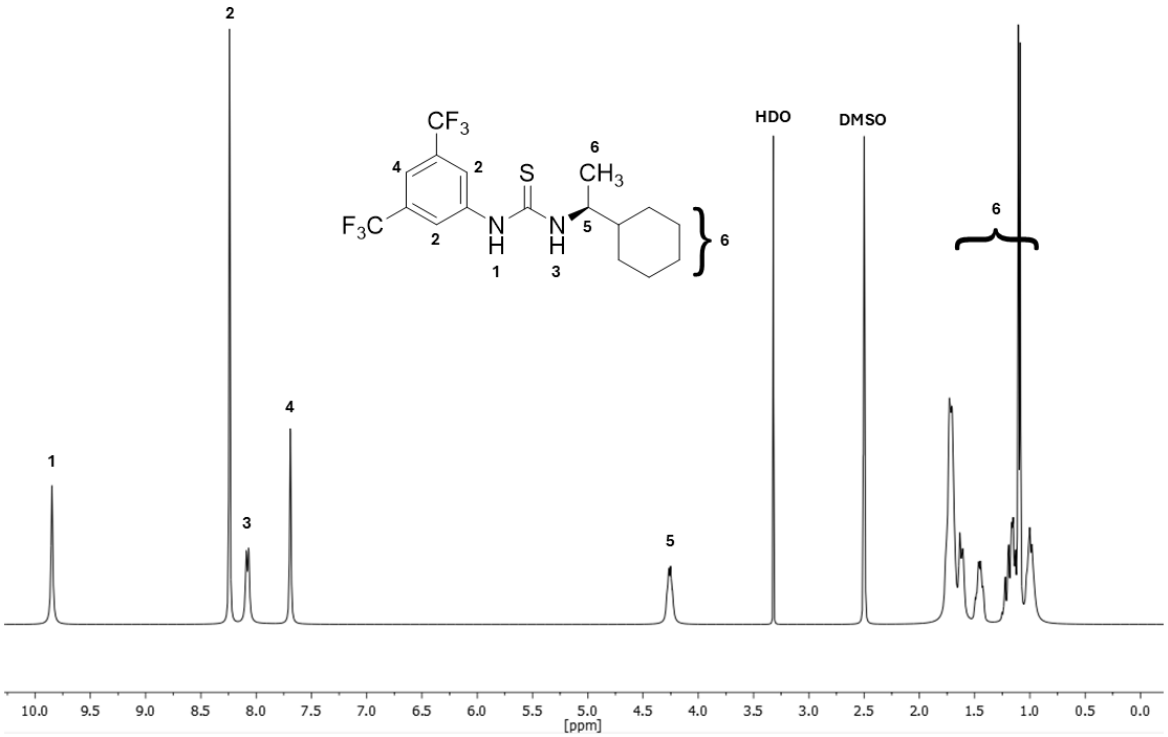

Supplementary Figure 25 ^{1}H-NMR of (*S*)-1-(3,5-bis(trifluoromethyl)phenyl)-3-(1-cyclohexylethyl)thiourea measured in DMSO-d_6 plotted as signal intensity versus chemical shift in ppm.

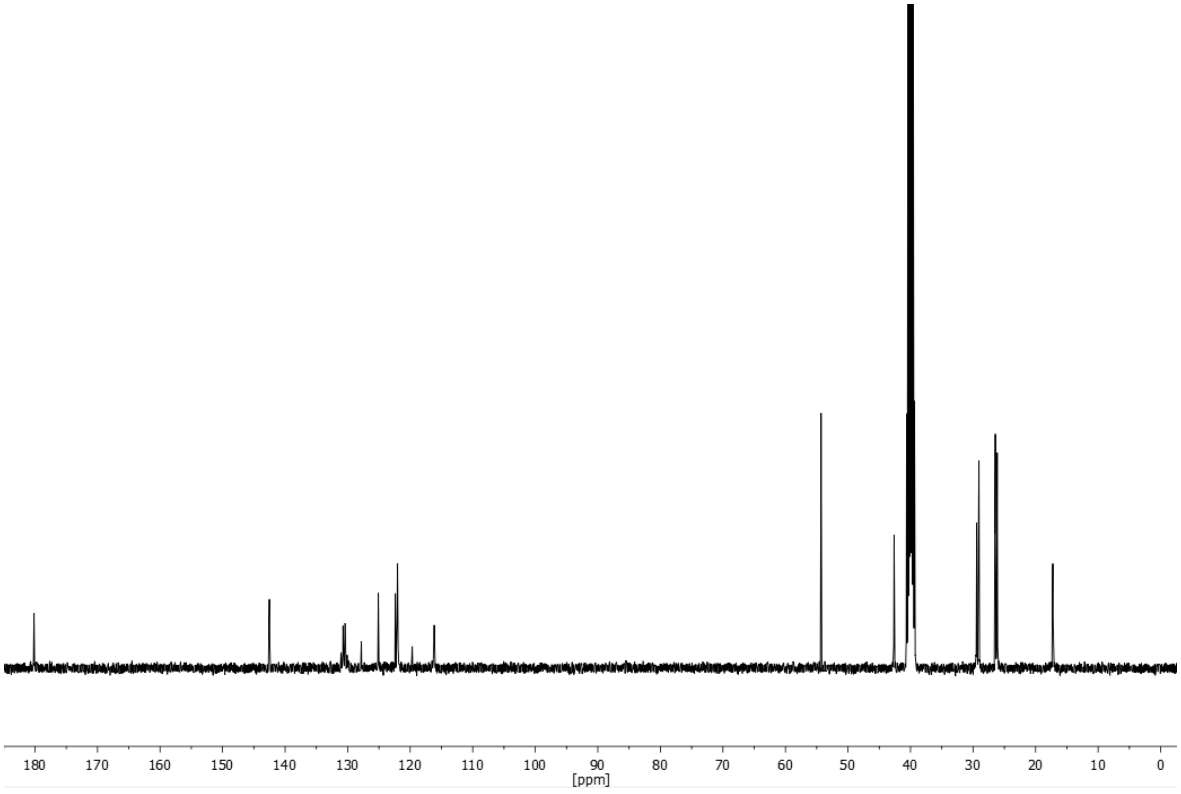

Supplementary Figure 26 ^{13}C-NMR of (*S*)-1-(3,5-bis(trifluoromethyl)phenyl)-3-(1-cyclohexylethyl)thiourea measured in DMSO-d_6 (septet signal at 39.52 ppm) and plotted as signal intensity versus chemical shift in ppm.

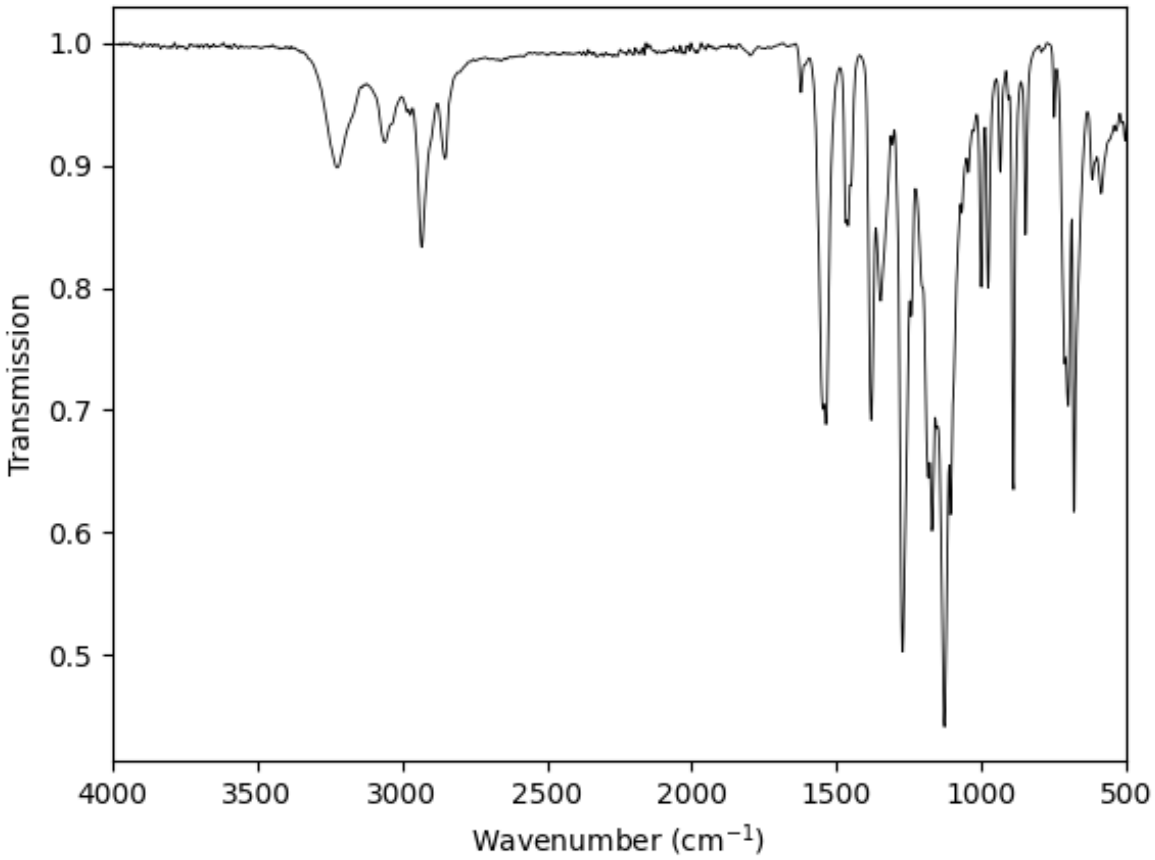

Supplementary Figure 27 IR-spectra of (*S*)-1-(3,5-bis(trifluoromethyl)phenyl)-3-(1-cyclohexylethyl)thiourea.

Synthesis of thiourea T11

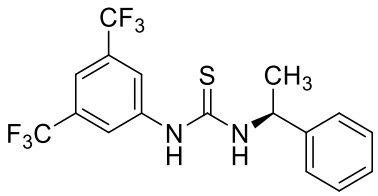

The reaction was conducted in a 10 mL crimp vial. 211 µL (*S*)-1-phenylethan-1-amine (200 mg, 1.65 mmol, 1.00 eq.) and dimethylformamide (2 mL) were initially introduced. Subsequently, 300 µL 1-isothiocyanato-3,5-bis(trifluoromethyl)benzene (447 mg, 1.65 mmol, 1.00 eq.) was added. To monitor the reaction, thin-layer chromatography (TLC) was performed, using a solvent mixture of cyclohexane and ethyl acetate in a 6:1 ratio. After 4 hours, the reaction was complete. The solvent was removed under reduced pressure. Finally, the crude product was purified *via* column chromatography (cyclohexane/ethyl acetate, 6:1). The product, (*S*)-1-(3,5-bis(trifluoromethyl)phenyl)-3-(1-phenylethyl)-thiourea, was obtained as a white solid (551 mg, 1.40 mmol) in a yield of 87%.

Rf = 0.35 in cyclohexane/ethyl acetate (6:1), visualised *via* UV quenching at 254 nm and vanillin staining solution.

^{1}H-NMR (400 MHz, DMSO-d_6) δ/ppm = 9.95 (s, 1H, [1]), 8.70 (d, J = 7.4 Hz, 1H, [2]), 8.23 (s, 2H, [3]), 7.71 (s, 1H, [4]), 7.44 – 7.33 (m, 4H, [5]), 7.31 – 7.20 (m, 1H, [6]), 5.70 – 5.45 (m, 1H, [7]), 1.50 (d, J = 6.9 Hz, 3H, [8]).

^{13}C-NMR (101 MHz, DMSO-d_6) δ/ppm = 180.2, 143.8, 142.4, 131.1, 130.8, 130.4, 130.1, 128.8, 127.4, 126.7, 125.1, 122.4, 60.2, 53.3, 22.1, 21.2.

HRMS-EI-MS m/z: [M] calculated for $[C_{17}H_{15}F_6N_2S]^+$ = 393.08546, found: 393.08574.

IR (ATR platinum diamond) ν/cm^{-1} = 3231 (w), 3223 (w), 3164 (w), 3087 (vw), 3036 (w), 2997 (w), 2976 (w), 1541 (s), 1497 (w), 1469 (w), 1458 (w), 1380 (m), 1331 (m), 1275 (s), 1220 (m), 1129 (vs), 1107 (s), 1063 (w), 1039 (w), 1022 (m), 1002 (w), 975 (m), 905 (w), 891 (s), 847 (m), 796 (w), 769 (w), 740 (w), 703 (s), 695 (s), 679 (s), 617 (w), 586 (w), 566 (w), 533 (m), 522 (w), 514 (m), 455 (w)

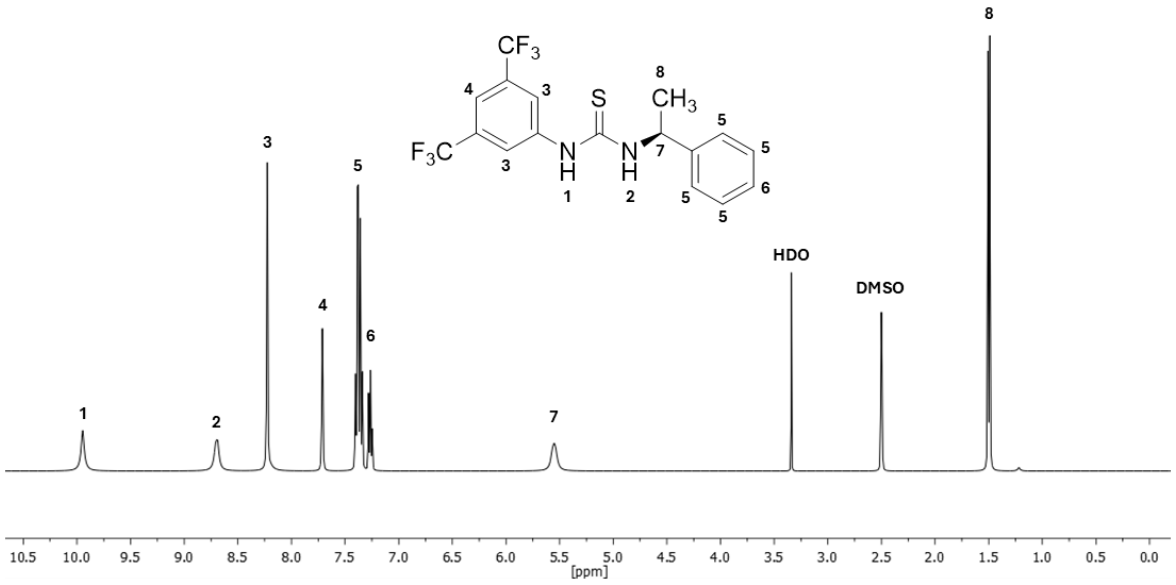

Supplementary Figure 28 ^{1}H-NMR of (*S*)-1-(3,5-bis(trifluoromethyl)phenyl)-3-(1-phenylethyl)thiourea measured in DMSO-d_6 plotted as signal intensity versus chemical shift in ppm.

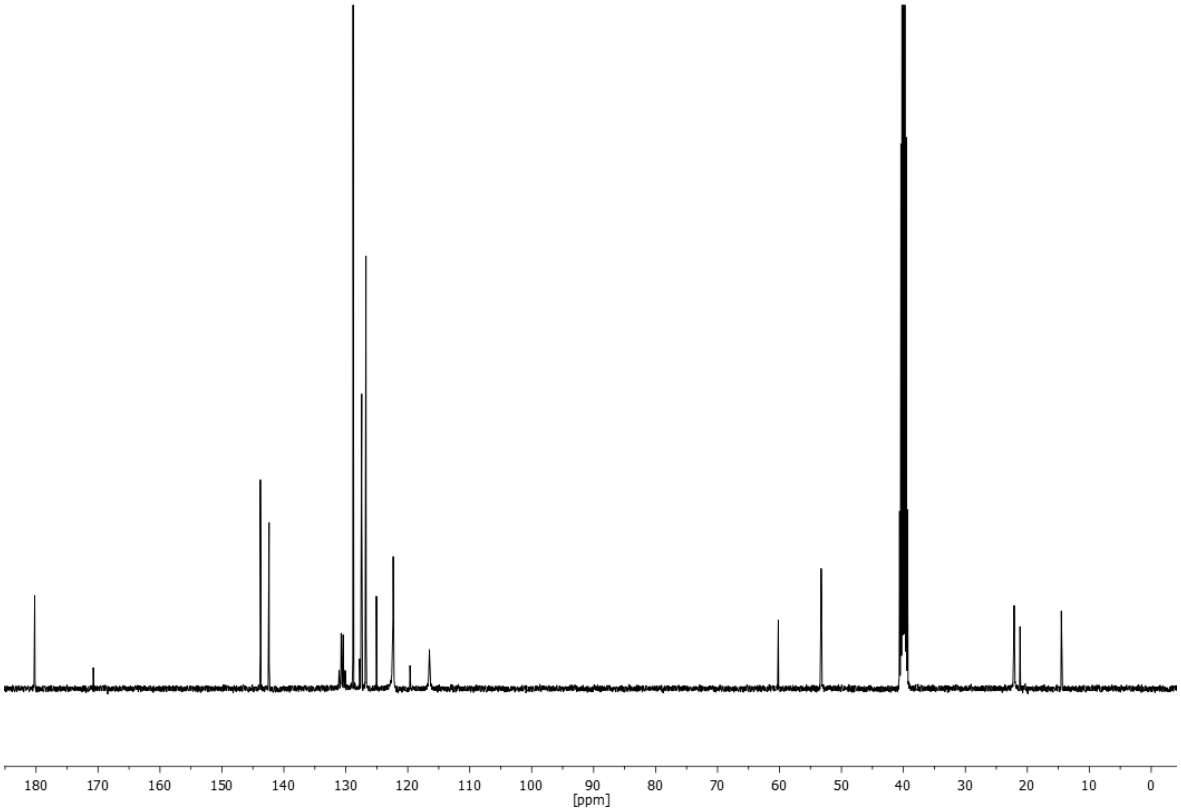

Supplementary Figure 29 ^{13}C-NMR of (*S*)-1-(3,5-bis(trifluoromethyl)phenyl)-3-(1-phenylethyl)thiourea measured in DMSO-d_6 (septet signal at 39.52 ppm) and plotted as signal intensity versus chemical shift in ppm.

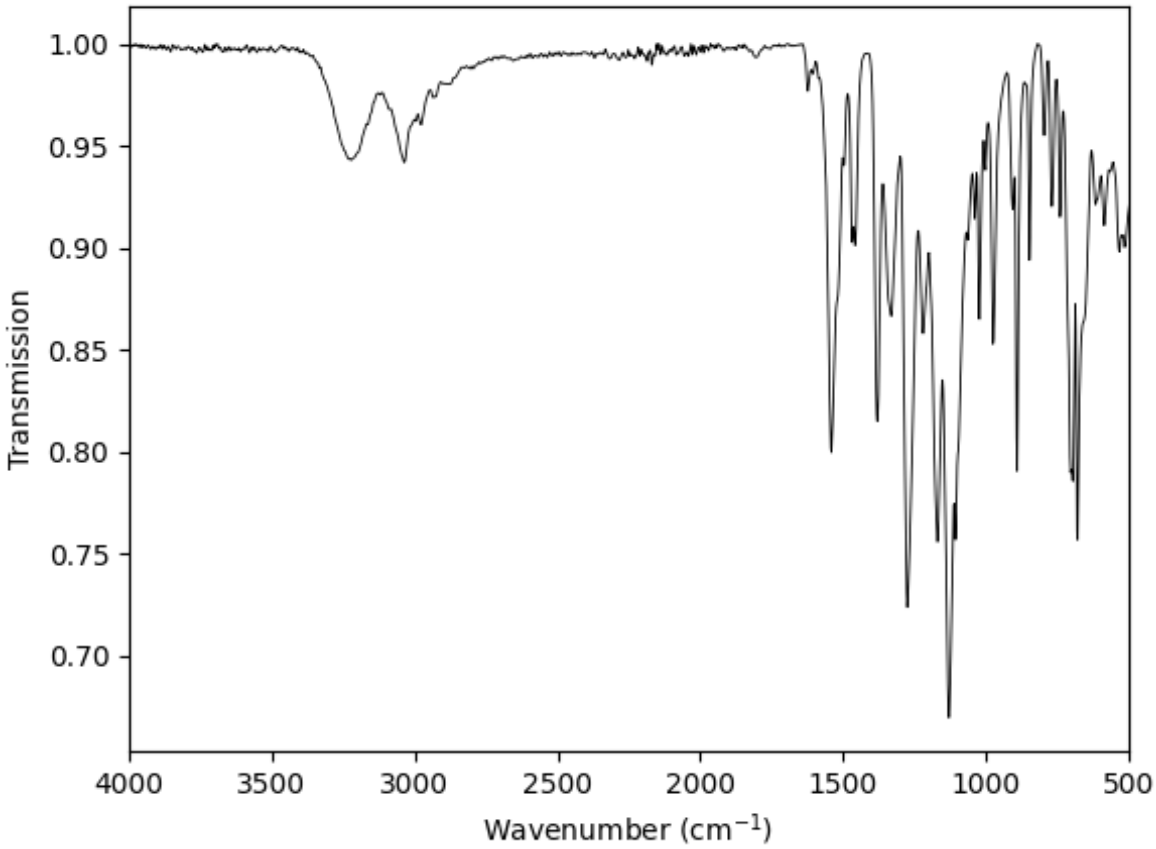

Supplementary Figure 30 IR-spectra of (*S*)-1-(3,5-bis(trifluoromethyl)phenyl)-3-(1-phenylethyl)thiourea.

Synthesis of thiourea T12

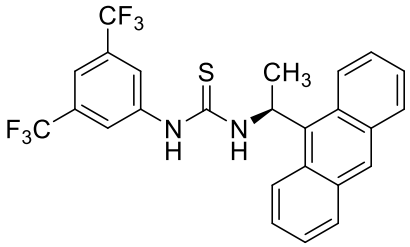

The reaction was conducted in a 10 mL crimp vial. 1.00 g (*S*)-1-(anthracen-9-yl)ethan-1-amine (4.52 mmol, 1.00 eq.) and dimethylformamide (10 mL) were initially introduced. Subsequently, 904 µL 1-isothiocyanato-3,5-bis(trifluoromethyl)benzene (1.35 g, 4.97 mmol, 1.10 eq.) was added. To monitor the reaction, thin-layer chromatography (TLC) was performed, using a solvent mixture of cyclohexane, toluene and ethyl acetate in a 7:2:1 ratio. After 4 hours, the reaction was complete. The solvent was removed under reduced pressure. Finally, the crude product was purified *via* column chromatography (cyclohexane/toluene/ethyl acetate, 7:2:1). The product, (*S*)-1-(1-(anthracen-9-yl)ethyl)-3-(3,5-bis(trifluoromethyl)phenyl)thiourea, was obtained as a white solid (1.36 g, 2.75 mmol) in a yield of 61%.

Rf = 0.23 in cyclohexane/toluene/ethyl acetate (7:2:1), visualised *via* UV quenching at 254 nm and vanillin staining solution.

^{1}H-NMR (400 MHz, DMSO-d_6) δ/ppm = 10.13 (s, 1H, [1]), 9.10 (d, J = 6.4 Hz, 1H, [2]), 8.76 – 8.50 (m, 3H, [3]), 8.25 (s, 2H, [4]), 8.13 (d, J = 8.4 Hz, 2H, [5]), 7.70 (s, 1H, [6]), 7.65 – 7.46 (m, 4H, [7]), 7.13 – 6.96 (m, 1H, [8]), 1.92 (d, J = 7.1 Hz, 3H, [9]).

^{13}C-NMR (101 MHz, DMSO-d_6) δ/ppm = 180.5, 142.3, 134.5, 131.8, 130.8, 130.4, 129.9, 129.1, 128.2, 126.5, 125.4, 125.0, 124.9, 122.3, 122.3, 49.4, 21.7.

HRMS-EI-MS m/z: [M] calculated for $[C_{25}H_{19}F_6N_2S]^+$ = 493.11676, found: 493.11623.

IR (ATR platinum diamond) ν/cm^{-1} = 3264 (vw), 3252 (vw), 3244 (w), 3092 (vw), 3079 (vw), 1528 (m), 1473 (m), 1460 (w), 1380 (s), 1339 (m), 1273 (vs), 1240 (m), 1226 (m), 1170 (s), 1127 (vs), 1109 (s), 1076 (m), 1035 (w), 1020 (w), 1002 (w), 973 (m), 913 (w), 882 (m), 860 (w), 847 (w), 800 (m), 780 (s), 751 (w), 734 (w), 718 (m), 699 (m), 679 (m), 656 (w), 621 (w), 539 (m), 518 (m), 463 (w), 436 (w), 405 (w).

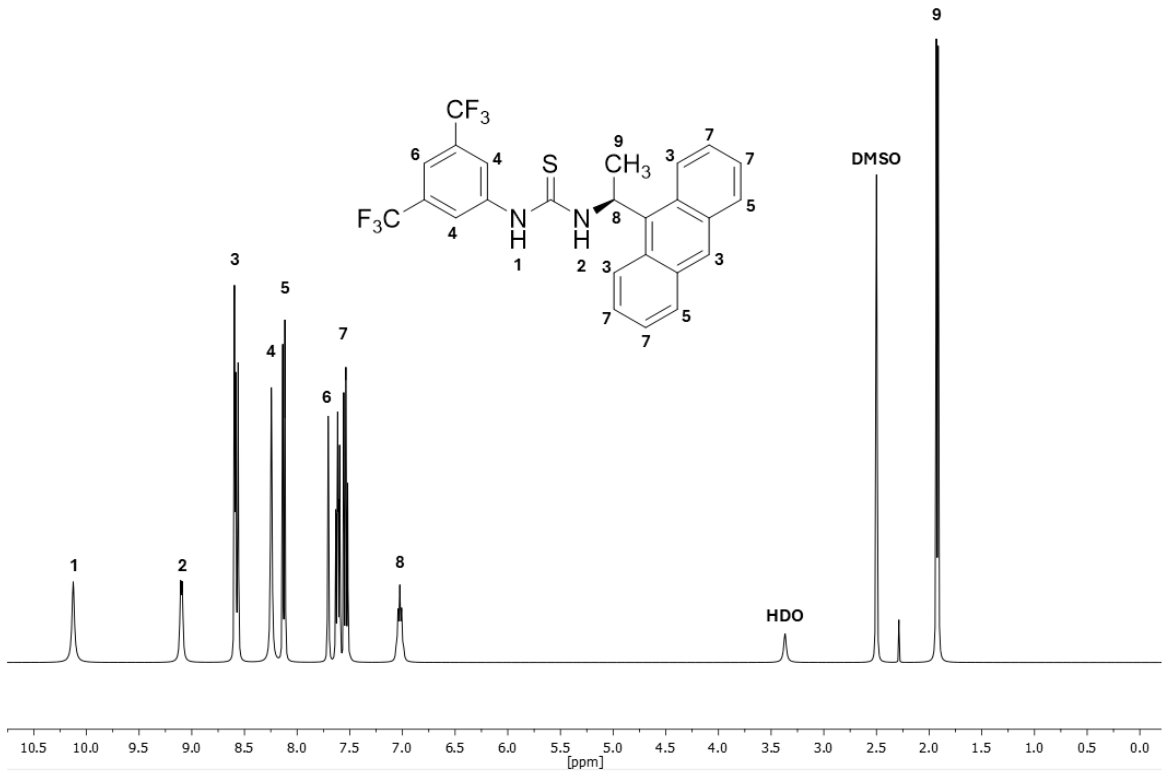

Supplementary Figure 31 ^{1}H-NMR of (*S*)-1-(1-(anthracen-9-yl)ethyl)-3-(3,5-bis(trifluoromethyl)phenyl)thiourea measured in DMSO-d_6 plotted as signal intensity versus chemical shift in ppm.

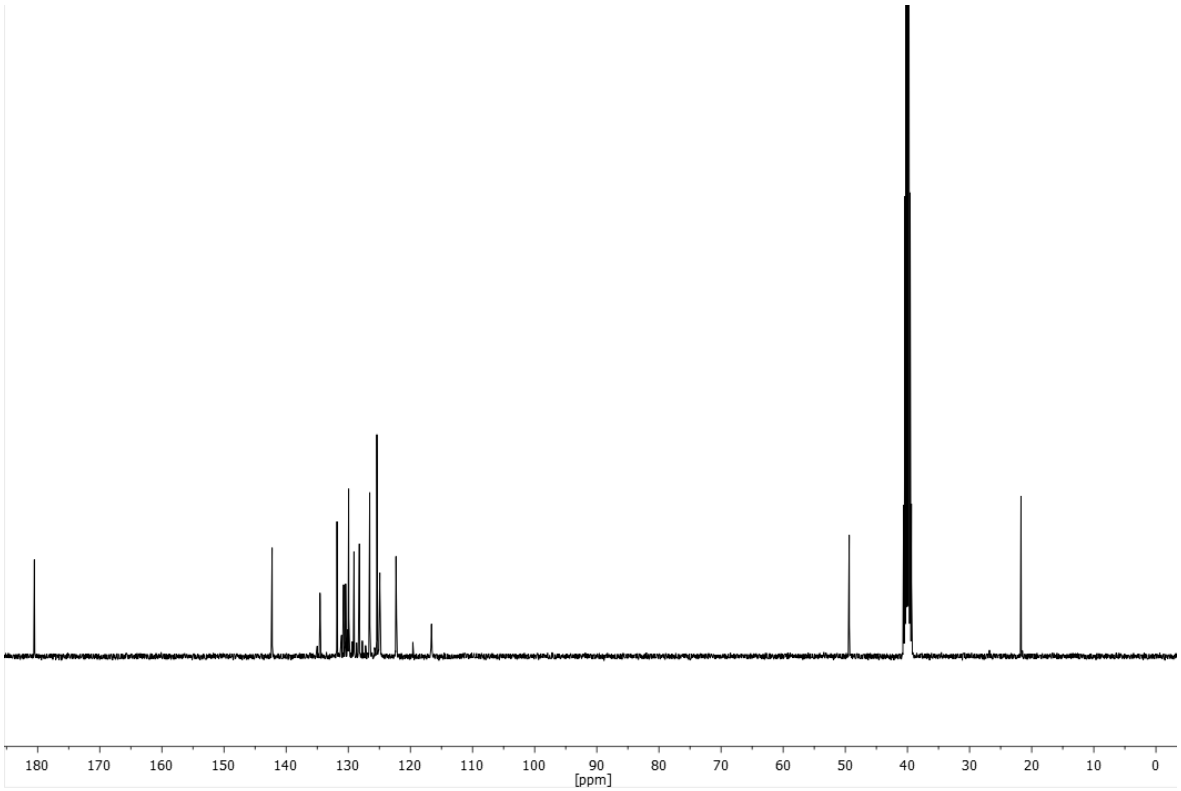

Supplementary Figure 32 ^{13}C-NMR of (*S*)-1-(1-(anthracen-9-yl)ethyl)-3-(3,5-bis(trifluoromethyl)phenyl)thiourea measured in DMSO-d_6 (septet signal at 39.52 ppm) and plotted as signal intensity versus chemical shift in ppm.

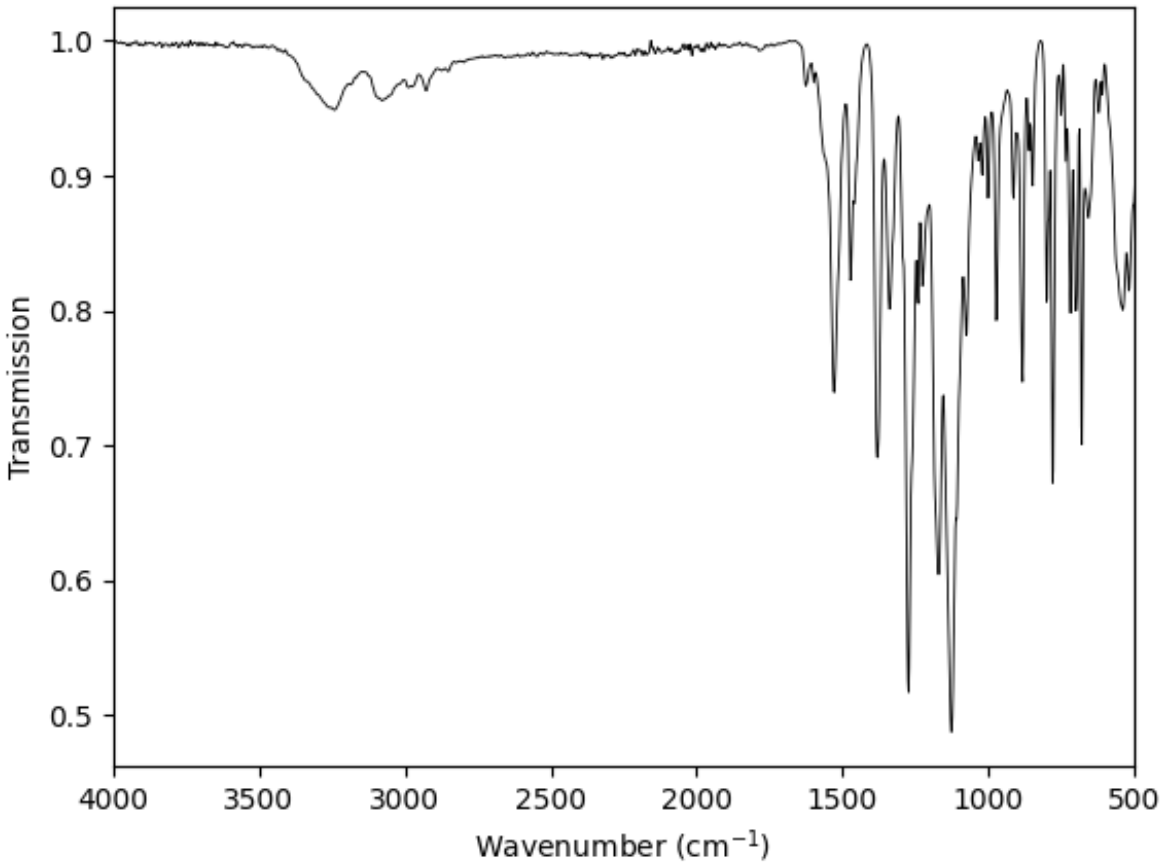

Supplementary Figure 33 IR-spectra of (*S*)-1-(1-(anthracen-9-yl)ethyl)-3-(3,5-bis(trifluoromethyl)phenyl)thiourea.

Synthesis of thiourea T13

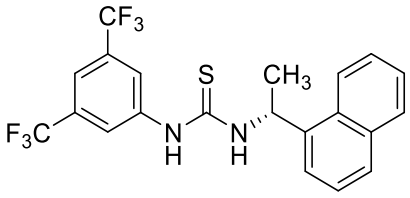

The reaction was conducted in a 10 mL crimp vial. 937 µL (*R*)-1-(naphthalen-1-yl)ethan-1-amine (1.00 g, 5.84 mmol, 1.00 eq.) and dimethylformamide (10 mL) were initially introduced. Subsequently, 1.17 mL 1-isothiocyanato-3,5-bis(trifluoromethyl)benzene (1.74 g, 6.42 mmol, 1.10 eq.) was added. To monitor the reaction, thin-layer chromatography (TLC) was performed, using a solvent mixture of cyclohexane and ethyl acetate in a 6:1 ratio. After 4 hours, the reaction was complete. The solvent was removed under reduced pressure. Finally, the crude product was purified *via* column chromatography (cyclohexane/ethyl acetate, 6:1). The product, (*R*)-1-(3,5-bis(trifluoromethyl)phenyl)-3-(1-(naphthalen-1-yl)ethyl)thiourea, was obtained as a white solid (2.089 g, 4.72 mmol) in a yield of 81%.

Rf = 0.23 in cyclohexane/ethyl acetate (6:1), visualised *via* UV quenching at 254 nm and vanillin staining solution.

^{1}H-NMR (400 MHz, DMSO-d_6) δ/ppm = 9.93 (s, 1H, ^{1}), 8.77 (d, J = 7.9 Hz, 1H, ^{2}), 8.28 – 8.11 (m, 3H, ^{3}), 7.97 (d, J = 8.1 Hz, 1H, ^{4}), 7.89 (d, J = 8.1 Hz, 1H, ^{5}), 7.70 (s, 1H, ^{6}), 7.68 – 7.47 (m, 4H, ^{7}), 6.36 – 6.20 (m, 1H, ^{8}), 1.65 (d, J = 6.8 Hz, 3H, ^{9}).

^{13}C-NMR (101 MHz, DMSO-d_6) δ/ppm = 179.9, 142.4, 139.1, 133.9, 131.1, 130.8, 129.2, 128.3, 126.9, 126.2, 125.9, 125.0, 123.7, 123.5, 122.3, 49.6, 26.8, 20.6.

HRMS-EI-MS m/z: [M] calculated for $[C_{21}H_{17}F_6N_2S]^+$ = 443.10111, found: 443.10098.

IR (ATR platinum diamond) ν/cm^{-1} = 3264 (vw), 3252 (vw), 3244 (w), 3092 (vw), 3079 (vw), 1528 (m), 1473 (m), 1460 (w), 1380 (s), 1339 (m), 1273 (vs), 1240 (m), 1226 (m), 1170 (s), 1127 (vs), 1109 (s), 1076 (m), 1035 (w), 1020 (w), 1002 (w), 973 (m), 913 (w), 882 (m), 860 (w), 847 (w), 800 (m), 780 (s), 751 (w), 734 (w), 718 (m), 699 (m), 679 (m), 656 (w), 621 (w), 539 (m), 518 (m), 463 (w), 436 (w), 405 (w).

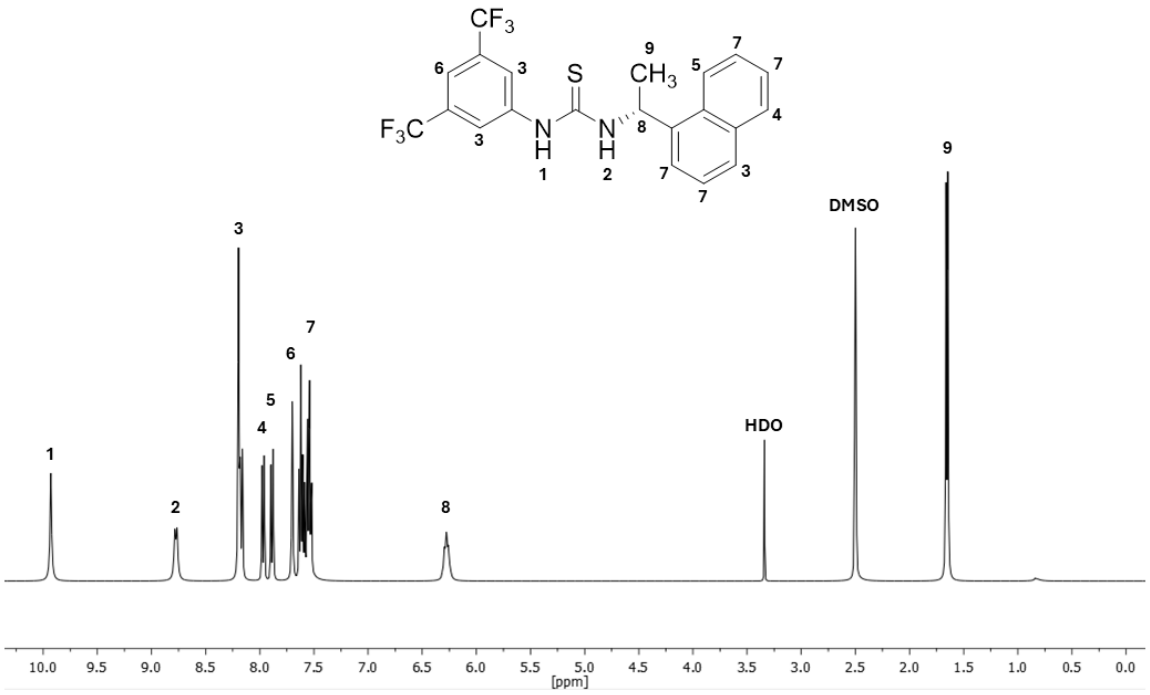

Supplementary Figure 34 ^{1}H-NMR of (*R*)-1-(3,5-bis(trifluoromethyl)phenyl)-3-(1-(naphthalen-1-yl)ethyl)thiourea measured in DMSO-d_6 plotted as signal intensity versus chemical shift in ppm.

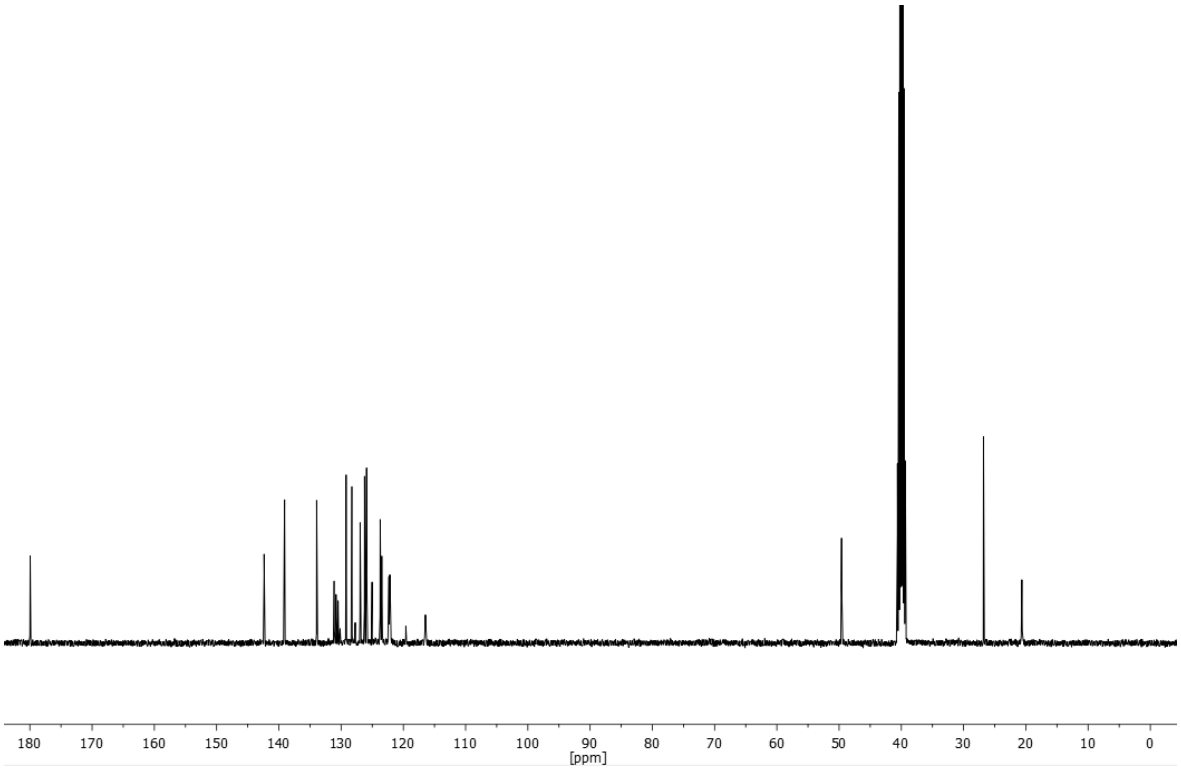

Supplementary Figure 35 ^{13}C-NMR of (*R*)-1-(3,5-bis(trifluoromethyl)phenyl)-3-(1-(naphthalen-1-yl)ethyl)thiourea measured in DMSO-d_6 (septet signal at 39.52 ppm) and plotted as signal intensity versus chemical shift in ppm.

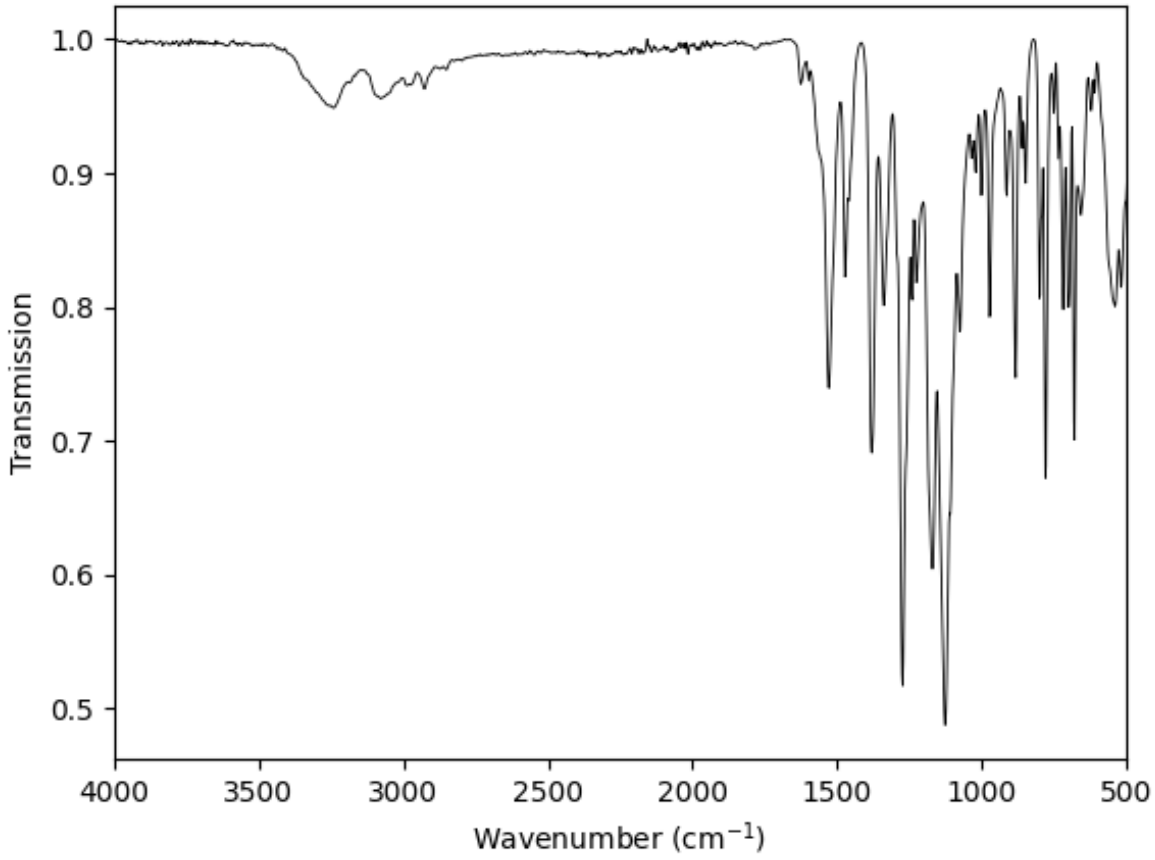

Supplementary Figure 36 IR-spectra of (*R*)-1-(3,5-bis(trifluoromethyl)phenyl)-3-(1-(naphthalen-1-yl)ethyl)thiourea.

Synthesis of thiourea T14

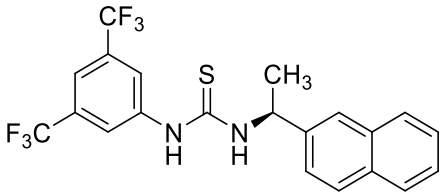

The reaction was conducted in a 10 mL crimp vial. 937 µL (*S*)-1-(naphthalen-2-yl)ethan-1-amine (1.00 g, 5.84 mmol, 1.00 eq.) and dimethylformamide (10 mL) were initially introduced. Subsequently, 1.17 mL 1-isothiocyanato-3,5-bis(trifluoromethyl)benzene (1.74 g, 6.42 mmol, 1.10 eq.) was added. To monitor the reaction, thin-layer chromatography (TLC) was performed, using a solvent mixture of cyclohexane and ethyl acetate in a 6:1 ratio. After 4 hours, the reaction was complete. The solvent was removed under reduced pressure. Finally, the crude product was purified *via* column chromatography (cyclohexane/ethyl acetate, 6:1). The product, (*S*)-1-(3,5-bis(trifluoromethyl)phenyl)-3-(1-(naphthalen-2-yl)ethyl)thiourea, was obtained as a white solid (2.141 g, 4.84 mmol) in a yield of 83%.

Rf = 0.23 in cyclohexane/ethyl acetate (6:1), visualised *via* UV quenching at 254 nm and vanillin staining solution.

^{1}H-NMR (400 MHz, DMSO-d_6) δ/ppm = 10.02 (s, 1H,[1]), 8.83 (d, J = 7.9 Hz, 1H, [2]), 8.25 (s, 2H, [3]), 7.95 – 7.86 (m, 4H, [4]), 7.72 (s, 1H, [5]), 7.61 – 7.55 (m, 1H, [6]), 7.55 – 7.44 (m, 2H, [7]), 5.78 – 5.70 (m, 1H, [8]), 1.60 (d, J = 6.9 Hz, 3H, [9]).

^{13}C-NMR (101 MHz, DMSO-d_6) δ/ppm = 180.3, 142.4, 141.4, 133.3, 132.7, 131.1, 130.8, 130.5, 130.1, 128.5, 128.2, 128.0, 127.8, 126.7, 126.2, 125.5, 125.1, 124.9, 122.4, 53.5, 22.1.

HRMS-EI-MS m/z: [M] calculated for $[C_{21}H_{17}F_6N_2S]^+$ = 443.10111, found: 443.10088.

IR (ATR platinum diamond) ν/cm^{-1} = 3252 (w), 3244 (w), 3145 (vw), 3129 (vw), 3096 (w), 3052 (w), 2980 (w), 1623 (w), 1600 (w), 1528 (m), 1471 (m), 1458 (m), 1378 (s), 1339 (m), 1273 (vs), 1226 (m), 1170 (s), 1123 (vs), 1107 (s), 1080 (m), 1045 (m), 1026 (w), 1000 (w), 977 (m), 950 (w), 884 (m), 856 (m), 850 (m), 817 (m), 747 (m), 718 (m), 699 (m), 679 (s), 654 (m), 621 (w), 592 (w), 576 (w), 570 (w), 537 (w), 518 (w), 475 (m).

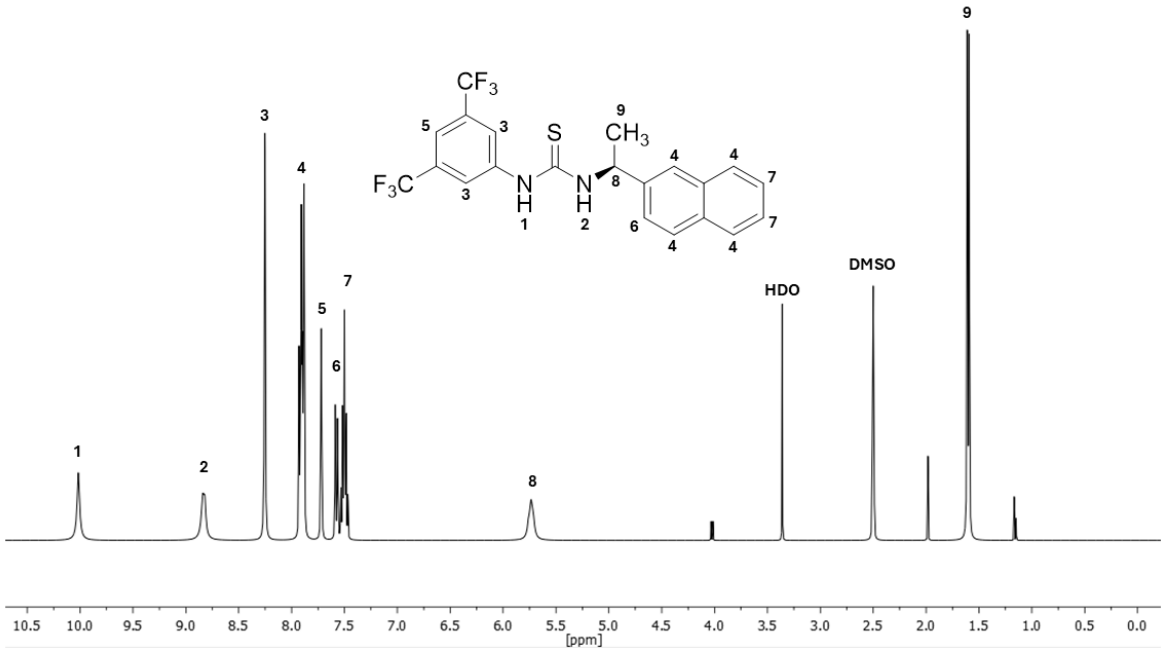

Supplementary Figure 37 ^{1}H-NMR of (*S*)-1-(3,5-bis(trifluoromethyl)phenyl)-3-(1-(naphthalen-2-yl)ethyl)thiourea measured in DMSO-d_6 plotted as signal intensity versus chemical shift in ppm. Unlabelled peaks are assigned to ethyl acetate.

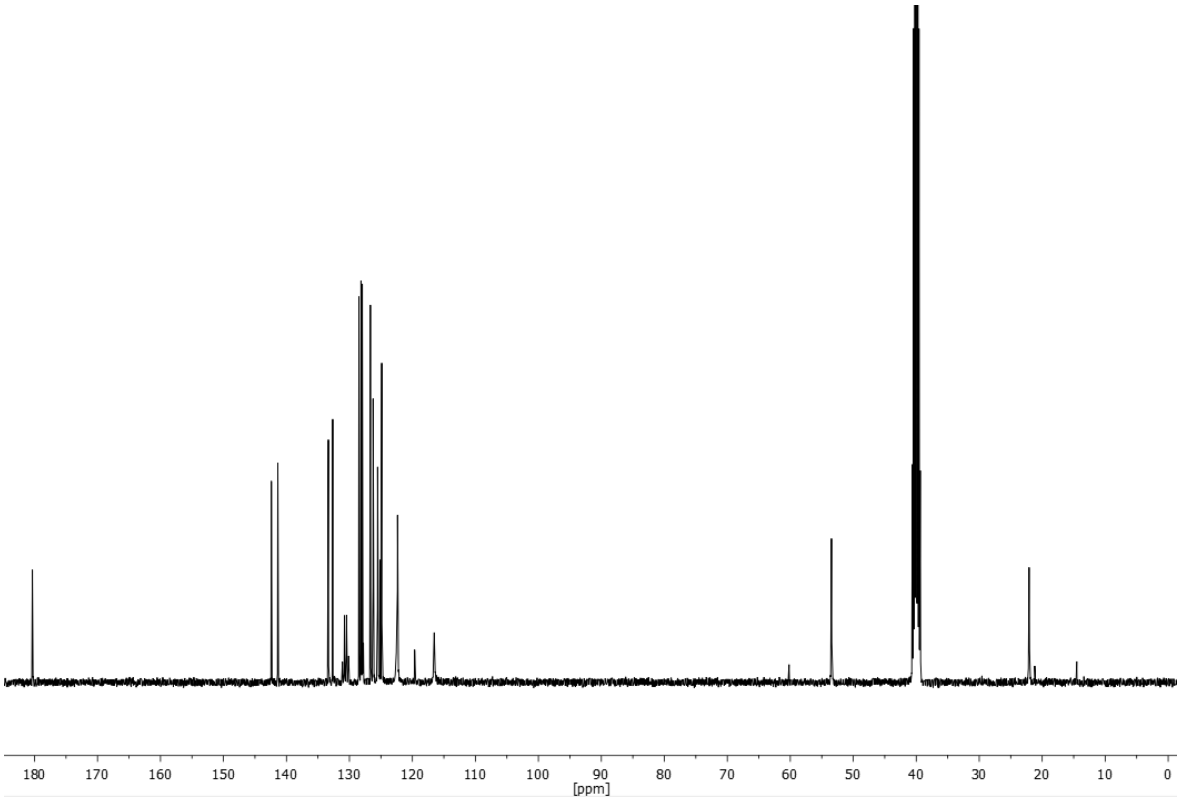

Supplementary Figure 38 ^{13}C-NMR of (*S*)-1-(3,5-bis(trifluoromethyl)phenyl)-3-(1-(naphthalen-2-yl)ethyl)thiourea measured in DMSO-d_6 (septet signal at 39.52 ppm) and plotted as signal intensity versus chemical shift in ppm.

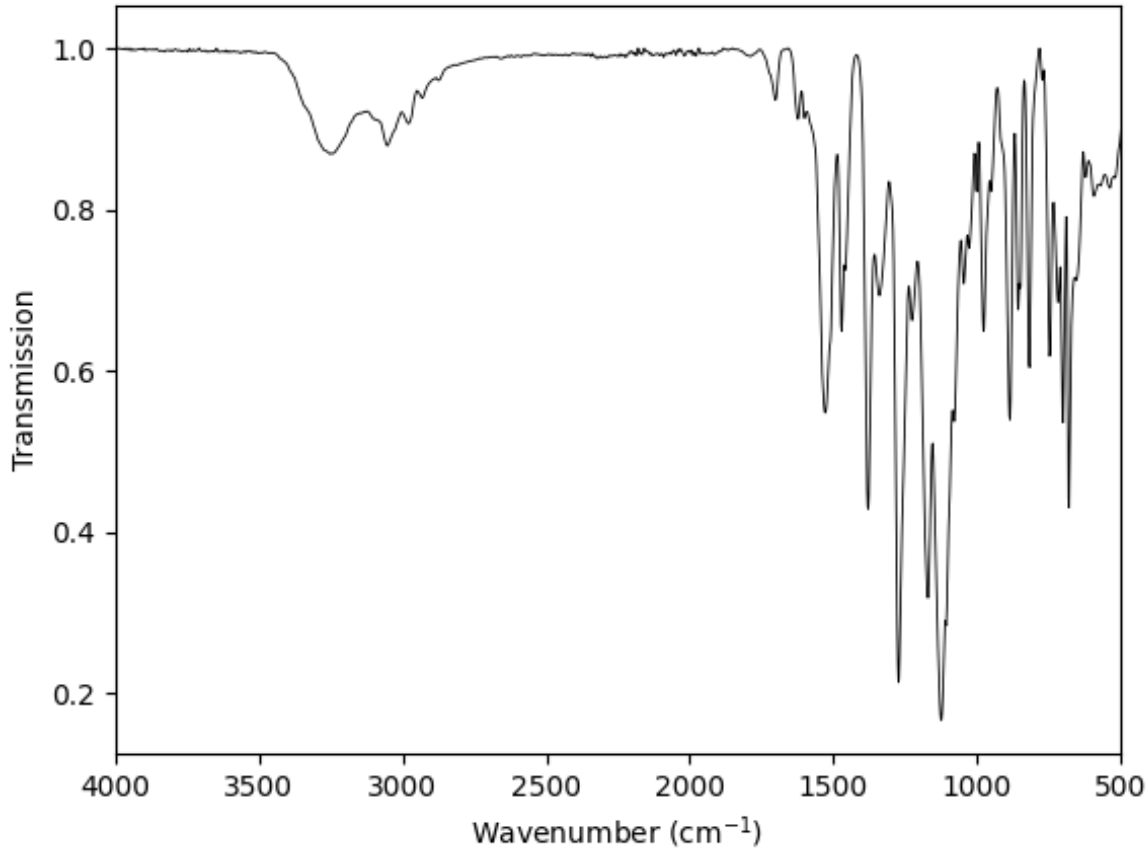

Supplementary Figure 39 IR-spectra of (*S*)-1-(3,5-bis(trifluoromethyl)phenyl)-3-(1-(naphthalen-2-yl)ethyl)thiourea.

Synthesis of thiourea T15

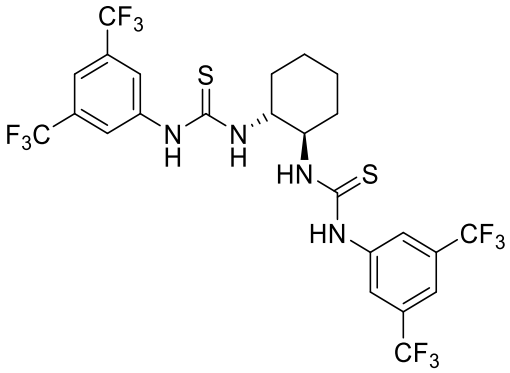

The reaction was conducted in a 10 mL crimp vial. 158 µL (1*R*,2*R*)-cyclohexane-1,2-diamine (150 mg, 1.31 mmol, 1.00 eq.) and dimethylformamide (2 mL) were initially introduced. Subsequently, 478 µL 1-isothiocyanato-3,5-bis(trifluoromethyl)benzene (712 mg, 2.62 mmol, 2.00 eq.) was added. To monitor the reaction, thin-layer chromatography (TLC) was performed, using a solvent mixture of cyclohexane and ethyl acetate in a 2:1 ratio. After 3 hours, the reaction was complete. The solvent was removed under reduced pressure. Finally, the crude product was purified *via* column chromatography (cyclohexane/ethyl acetate, 2:1). The product, 1,1'-((1*R*,2*R*)-cyclohexane-1,2-diyl)bis(3-(3,5-bis(trifluoromethyl)phenyl)-thiourea) was then obtained as a white solid (612 mg, 0.80 mmol) in a yield of 71%.

Rf = 0.61 in cyclohexane/ethyl acetate (2:1), visualised *via* UV quenching at 254 nm and vanillin staining solution.

^{1}H-NMR (400 MHz, DMSO-d_6) δ/ppm = 10.13 (s, 2H, [1]), 8.26 – 8.07 (m, 6H, [2]), 7.69 (s, 2H, [3]), 4.34 (s, 2H, [4]), 2.19 (s, 2H, [5]), 1.78 – 1.65 (m, 2H, [6]), 1.38 – 1.23 (m, 4H, [7]).

^{13}C-NMR (101 MHz, DMSO-d_6) δ/ppm = 180.5, 142.1, 131.1, 130.8, 130.5, 130.1, 127.7, 125.0, 122.3, 119.6, 57.3, 31.6, 24.7.

HRMS-EI-MS m/z: [M] calculated for $[C_{24}H_{21}F_{12}N_4S_2]^+$ = 657.10105, found: 657.10147.

IR (ATR platinum diamond) $\tilde{\nu}$/cm^{-1} = 3262 (w), 3246 (w), 3233 (w), 3225 (w), 3211 (w), 3194 (w), 3153 (vw), 3141 (vw), 3124 (vw), 3114 (vw), 3085 (vw), 3059 (w), 2941 (w), 1687 (w), 1623 (vw), 1537 (m), 1471 (m), 1458 (w), 1380 (m), 1347 (w), 1273 (vs), 1214 (m), 1172 (s), 1125 (vs), 1107 (s), 1043 (m), 1002 (w), 977 (w), 956 (m), 884 (m), 847 (w), 755 (vw), 720 (m), 701 (m), 679 (s), 656 (m), 613 (w), 597 (w), 574 (w), 549 (w), 535 (w), 525 (w), 516 (w), 465 (w).

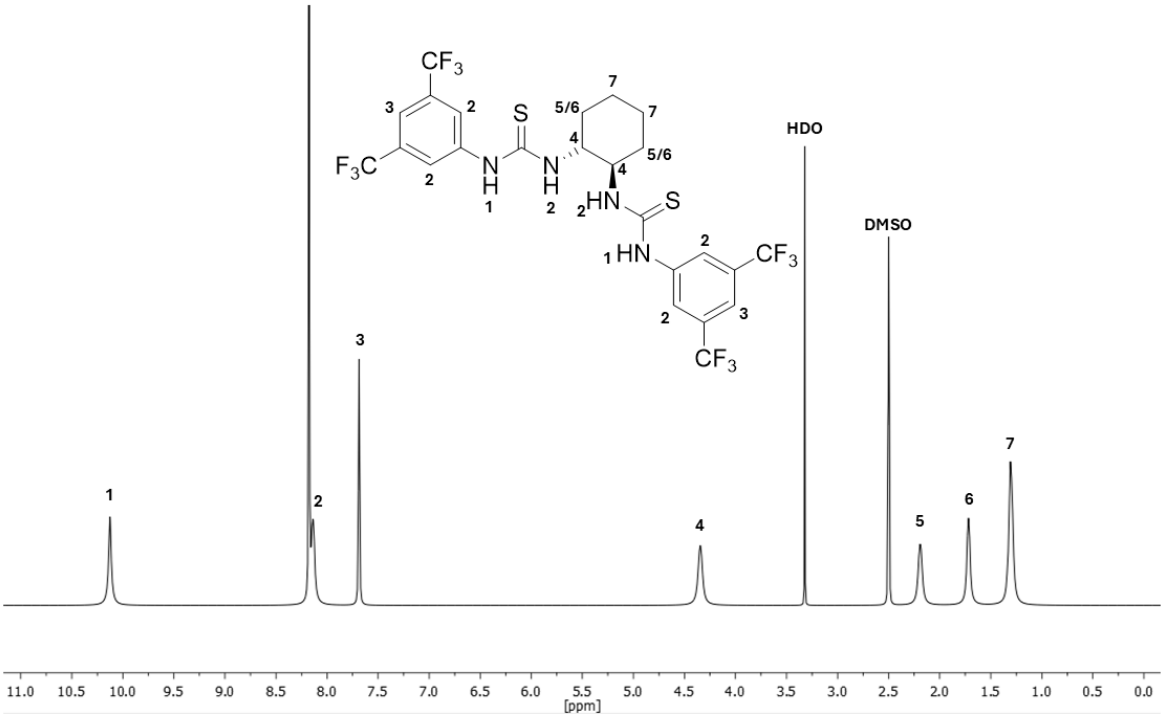

Supplementary Figure 40 ^{1}H-NMR of 1,1'-((1*R*,2*R*)-cyclohexane-1,2-diyl)bis(3-(3,5-bis(trifluoromethyl)phenyl)-thiourea) measured in DMSO-d_6 plotted as signal intensity versus chemical shift in ppm. Unlabelled peaks are assigned to ethyl acetate.

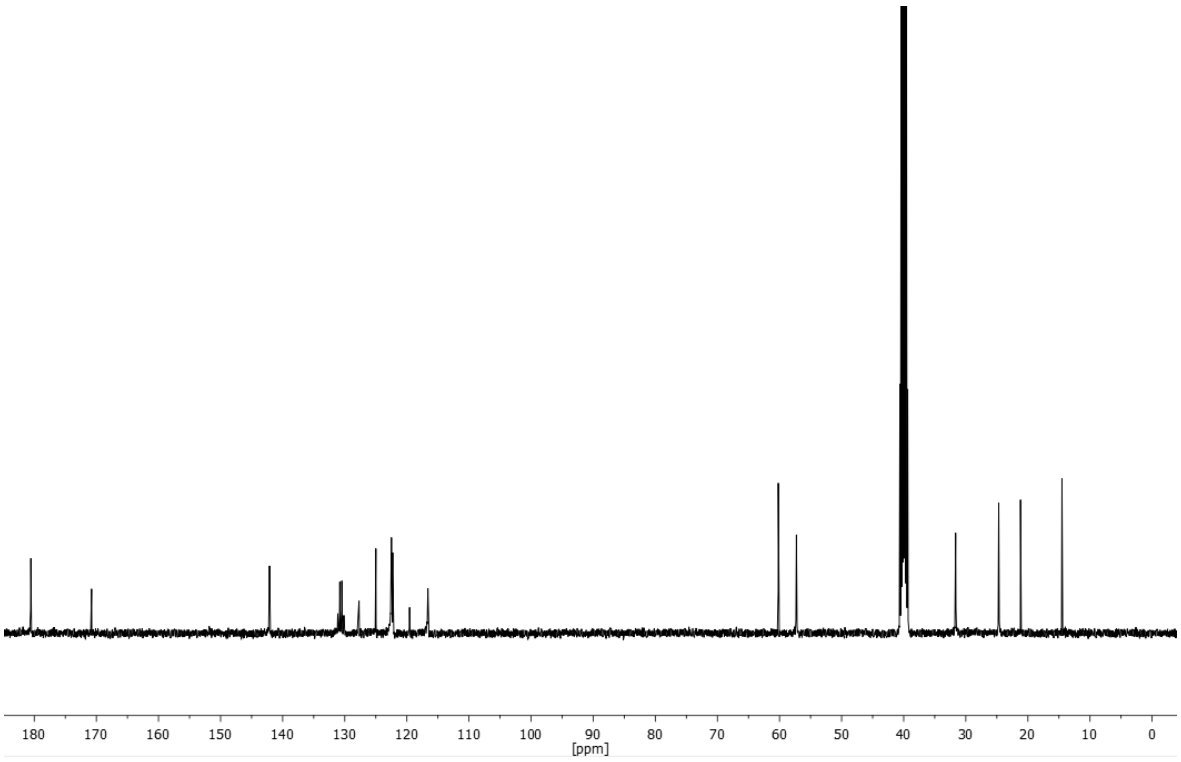

Supplementary Figure 41 ^{13}C-NMR of 1,1'-((1*R*,2*R*)-cyclohexane-1,2-diyl)bis(3-(3,5-bis(trifluoromethyl)phenyl)-thiourea) measured in DMSO-d_6 (septet signal at 39.52 ppm) and plotted as signal intensity versus chemical shift in ppm.

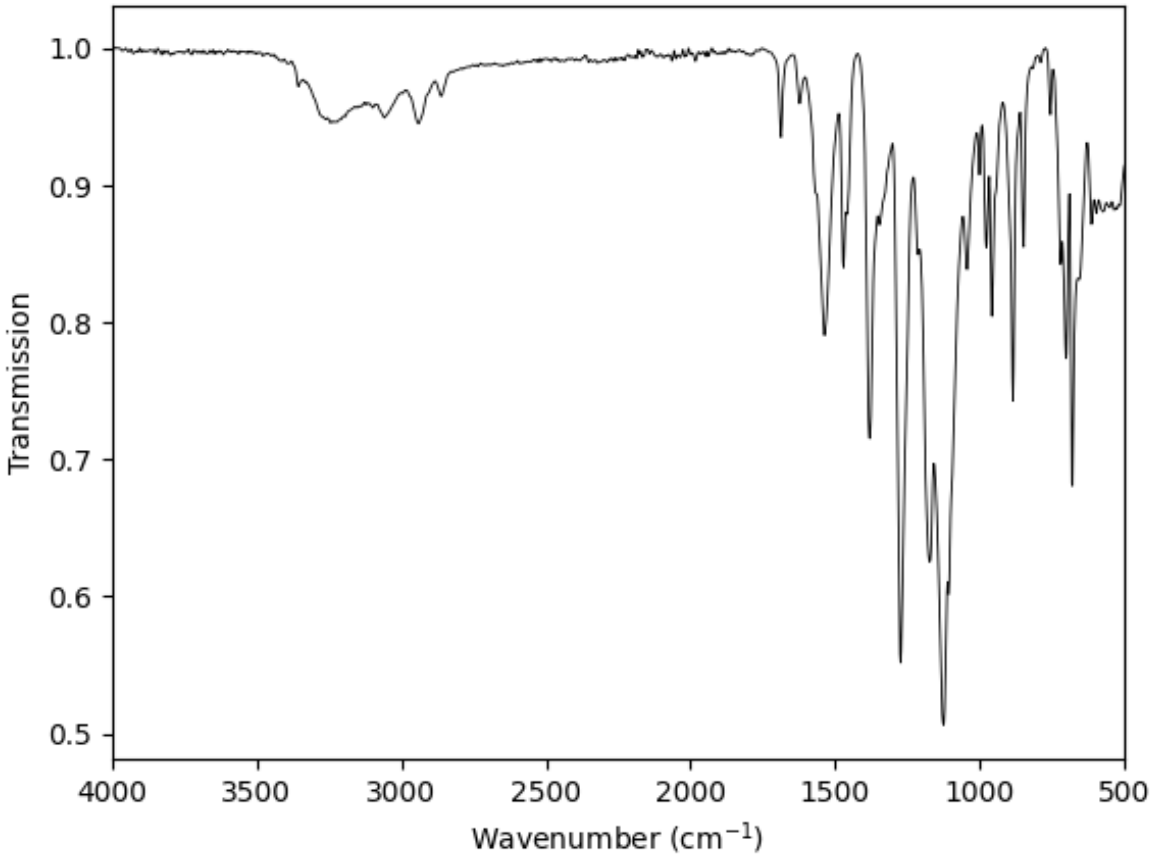

Supplementary Figure 42 IR-spectra of 1,1'-((1*R*,2*R*)-cyclohexane-1,2-diyl)bis(3-(3,5-bis(trifluoromethyl)phenyl)-thiourea).

6.2.3 Synthesis procedures for thiohydantoins

This chapter is based on previously published results by Simon Werling. The "Vertiefer" thesis of Simon Werling was co-supervised by the author of this thesis. The author of this thesis developed the synthetic procedures, planned the experiments, and assisted in evaluating the results.

Synthesis of 5-isobutyl-2-thioxo-3-tridecylimidazolidin-4-one

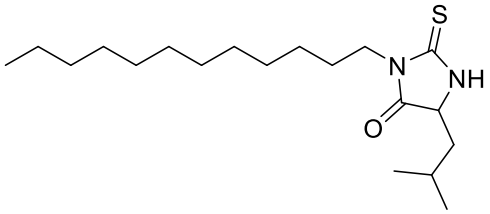

The reaction was conducted in a 10 mL crimp vial which was charged with 0.14 equivalents of elemental sulphur (corresponding to 1.12 equivalents of sulphur atoms). Subsequently, 73.2 µL of 1-isocyanododecane (75.0 mg, 0.38 mmol, 1.00 eq.) was added to the reaction mixture. MeOH was then added to achieve a concentration of 0.2 M for 1-isocyanododecane. Afterwards, 52.0 mg of previously deprotonated methyl *L*-leucinate (0.42 mmol, 1.10 eq.) were added, along with 0.01 equivalents of a NaOH as base catalyst. The reaction mixture was stirred at 40 °C overnight. After solvent evaporation, the crude product was purified by column chromatography using a graduate solvent mixture of cyclohexane and ethyl acetate in a 17:3 ratio. The pure product 5-isobutyl-2-thioxo-3-tridecylimidazolidin-4-one was obtained as white powder (79.0 mg, 0.23 mmol) with a yield of 61%.

Rf = 0.29 in cyclohexane/ethyl acetate 17/3 visualised *via* UV quenching at 254 nm and $KMnO_4$ staining solution

^{1}H-NMR (400 MHz, DMSO-d_6) δ/ppm = 10.38 (s, 1H, [1]), 4.25 (dd, J = 8.6, 4.9 Hz, 1H, [2]), 3.70 – 3.53 (m, 2H, [3]), 1.91 – 1.77 (m, 1H, [4]), 1.61 – 1.41 (m, 4H, [5]), 1.23 (s, 18H, [6]), 0.93 – 0.79 (m, 9H, [7]).

^{13}C-NMR (101 MHz, DMSO-d_6) δ/ppm = 182.9, 175.6, 57.7, 31.8, 29.5, 29.5, 29.5, 29.4, 29.4, 29.3, 29.2, 29.1, 29.0, 27.6, 26.5, 24.4, 24.4, 22.6, 22.0, 14.4.

HRMS-EI-MS m/z: [M] calculated for $[C_{19}H_{37}N_2OS]^+$ = 341.26211, found: 341.26133

IR (ATR platinum diamond) ν/cm^{-1} = 3182 (m), 2999 (w), 2962 (m), 2950 (m), 2915 (s), 2874 (m), 2849 (s), 1742 (vs), 1705 (w), 1520 (vs), 1467 (m), 1440 (m), 1415 (m), 1388 (m),

1370 (m), 1360 (m), 1345 (s), 1335 (s), 1318 (m), 1292 (m), 1275 (m), 1255 (s), 1238 (m), 1216 (w), 1191 (m), 1172 (m), 1131 (s), 1082 (m), 1035 (w), 1004 (w), 983 (w), 971 (w), 932 (w), 884 (w), 858 (w), 843 (w), 792 (vw), 761 (w), 751 (w), 722 (m), 693 (m), 652 (m), 621 (m), 594 (m), 551 (vw), 514 (w), 506 (w), 494 (m), 469 (m), 426 (w), 405 (w).

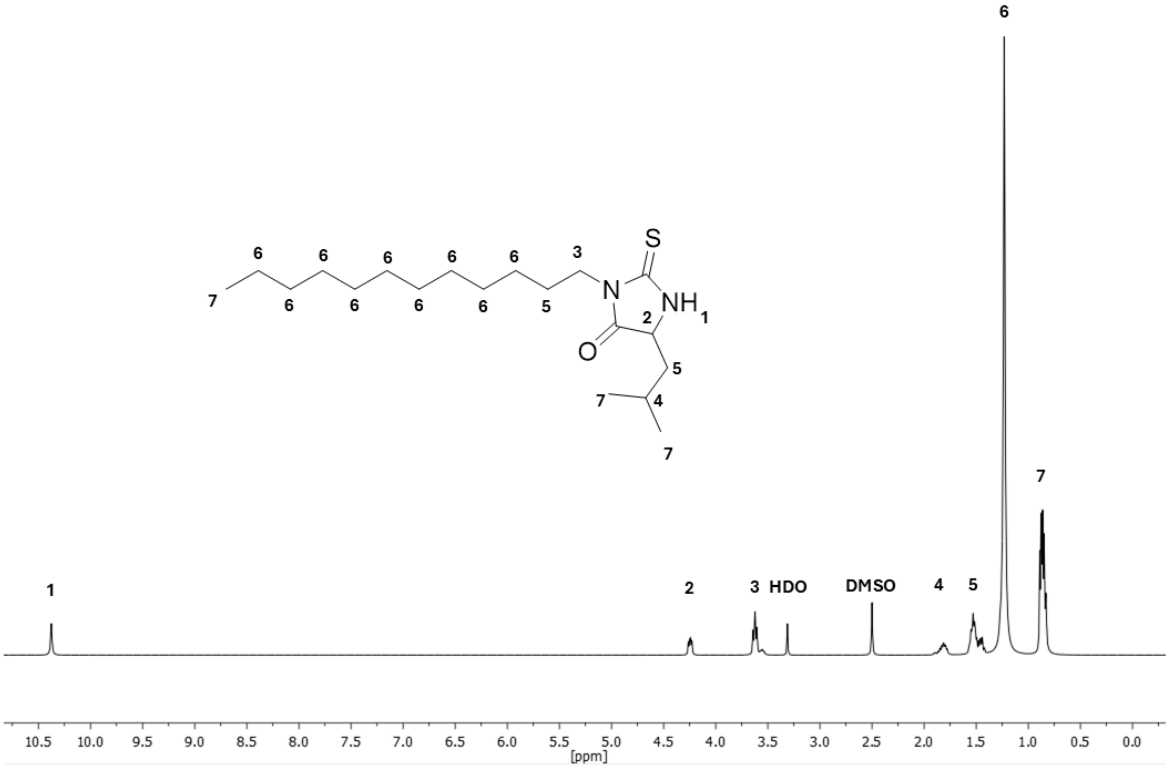

Supplementary Figure 43 ^{1}H-NMR of 5-isobutyl-2-thioxo-3-tridecylimidazolidin-4-one measured in DMSO-d_6 plotted as signal intensity versus chemical shift in ppm.

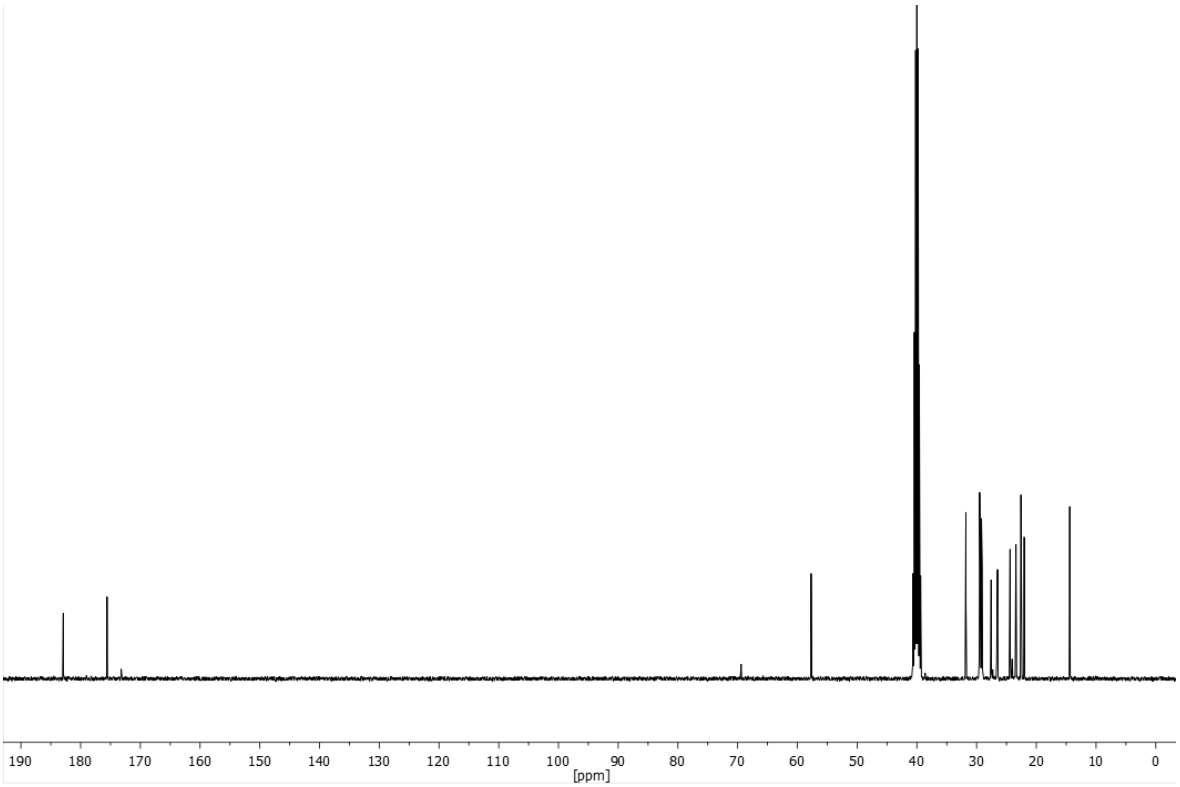

Supplementary Figure 44 ^{13}C-NMR of 5-isobutyl-2-thioxo-3-tridecylimidazolidin-4-one measured in DMSO-d_6 (septet signal at 39.52 ppm) and plotted as signal intensity versus chemical shift in ppm.

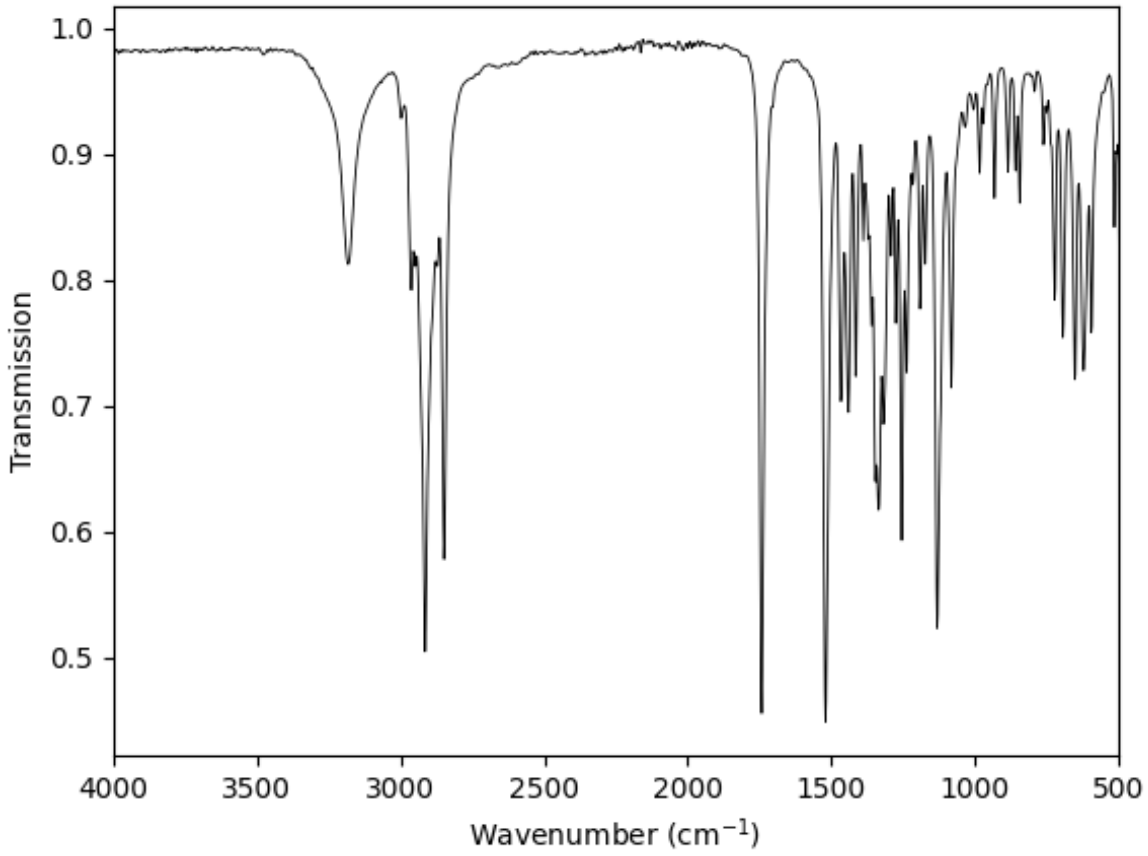

Supplementary Figure 45 IR-spectra of 5-isobutyl-2-thioxo-3-tridecylimidazolidin-4-one.

Synthesis of dimethyl 5-(4-((1H-indol-3-yl)methyl)-5-oxo-2-thioxoimidazolidin-1-yl)-isophthalate

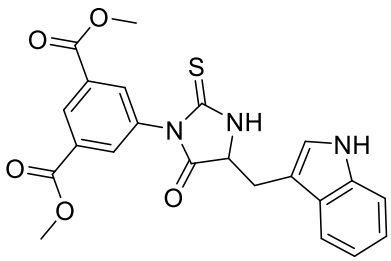

The reaction was conducted in a 10 mL crimp vial which was charged with 0.14 equivalents of elemental sulphur (corresponding to 1.12 equivalents of sulphur atoms). Subsequently, 83.2 mg of dimethyl 5-isocyanoisophthalate (0.38 mmol, 1.00 eq.) was added to the reaction mixture. MeOH was then added to achieve a concentration of 0.2 M for dimethyl 5-isocyanoisophthalate. Afterwards, 91.6 mg of previously deprotonated methyl *L*-tryptophanate (0.42 mmol, 1.10 eq.) were added, along with 0.01 equivalents of a NaOH as base catalyst. The reaction mixture was stirred at 40 °C overnight. After solvent evaporation, the crude product was purified by column chromatography using a graduate solvent mixture of cyclohexane and ethyl acetate in a 1:1 ratio. The pure product 5-(4-((1H-indol-3-yl)methyl)-5-oxo-2-thioxoimidazolidin-1-yl)-isophthalate was obtained as white powder (94.9 mg, 0.22 mmol) with a yield of 57%.

Rf = 0.44 in cyclohexane/ethyl acetate 1/1 visualised *via* UV quenching at 254 nm and $KMnO_4$ staining solution

^{1}H-NMR (400 MHz, DMSO-d_6) δ/ppm = 10.99 (d, J = 2.4 Hz, 1H, ^{1}), 10.73 (s, 1H, ^{2}), 8.41 (d, J = 1.6 Hz, 1H, ^{3}), 7.61 (s, 2H, ^{4}), 7.54 (d, J = 7.9 Hz, 1H, ^{5}), 7.37 (d, J = 8.2 Hz, 1H, ^{6}), 7.17 (d, J = 2.4 Hz, 1H, ^{7}), 7.08 (t, J = 7.0, Hz, 1H, ^{8}), 6.97 (t, J = 7.0 Hz, 1H, ^{9}), 4.73 (t, J = 4.6 Hz, 1H, ^{10}), 3.89 (s, 6H, ^{11}), 3.41 – 3.21 (m, 2H, ^{12}).

^{13}C-NMR (101 MHz, DMSO-d_6) δ/ppm = 182.0, 174.3, 165.0, 136.4, 134.6, 134.0, 131.1, 129.8, 127.5, 125.1, 121.5, 119.0, 118.9, 111.8, 107.3, 60.9, 53.1, 26.9.

HRMS-EI-MS m/z: [M] calculated for $[C_{22}H_{20}N_3O_5S]^+$ = 438.11182, found: 438.11190

IR (ATR platinum diamond) ν/cm^{-1} = 3349 (w), 3289 (w), 3227 (m), 3166 (w), 3131 (w), 3122 (w), 3100 (w), 3071 (w), 3063 (w), 3050 (w), 3034 (w), 3007 (w), 2952 (w), 2904 (w), 2871 (vw), 2859 (vw), 2851 (vw), 2845 (vw), 1757 (m), 1699 (s), 1621 (w), 1602 (w), 1512 (s), 1450 (m), 1432 (s), 1395 (m), 1351 (s), 1312 (s), 1269 (s), 1246 (vs), 1232 (s), 1201 (s), 1174 (s), 1158 (s), 1129 (m), 1105 (m), 1092 (m), 1059 (m), 1035 (m), 1008 (w), 989 (m),

952 (m), 928 (w), 907 (w), 889 (m), 874 (w), 839 (w), 823 (w), 794 (m), 755 (m), 745 (vs), 724 (m), 701 (s), 666 (s), 638 (s), 627 (s), 594 (m), 572 (m), 555 (m), 535 (m), 522 (w), 512 (m), 483 (w), 465 (w), 424 (s).

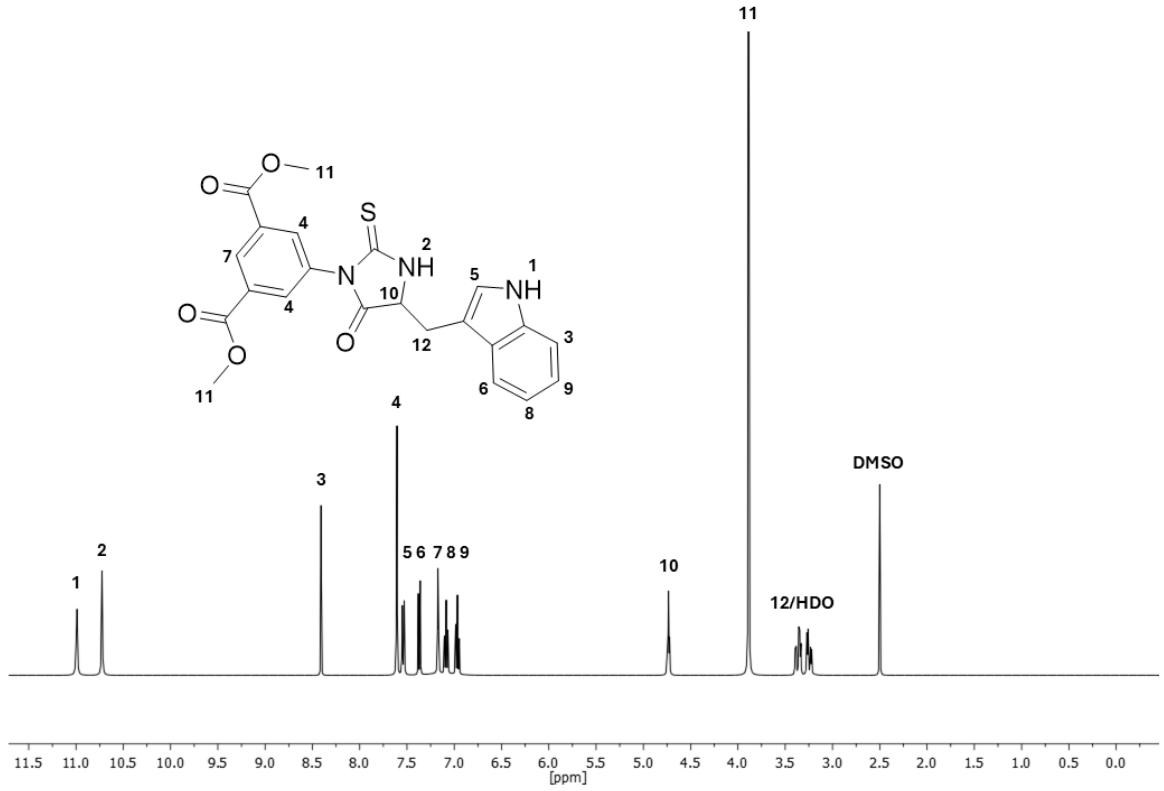

Supplementary Figure 46 ^{1}H-NMR of dimethyl 5-(4-((1H-indol-3-yl)methyl)-5-oxo-2-thioxoimidazolidin-1-yl)-isophthalate measured in DMSO-d_6 plotted as signal intensity versus chemical shift in ppm.

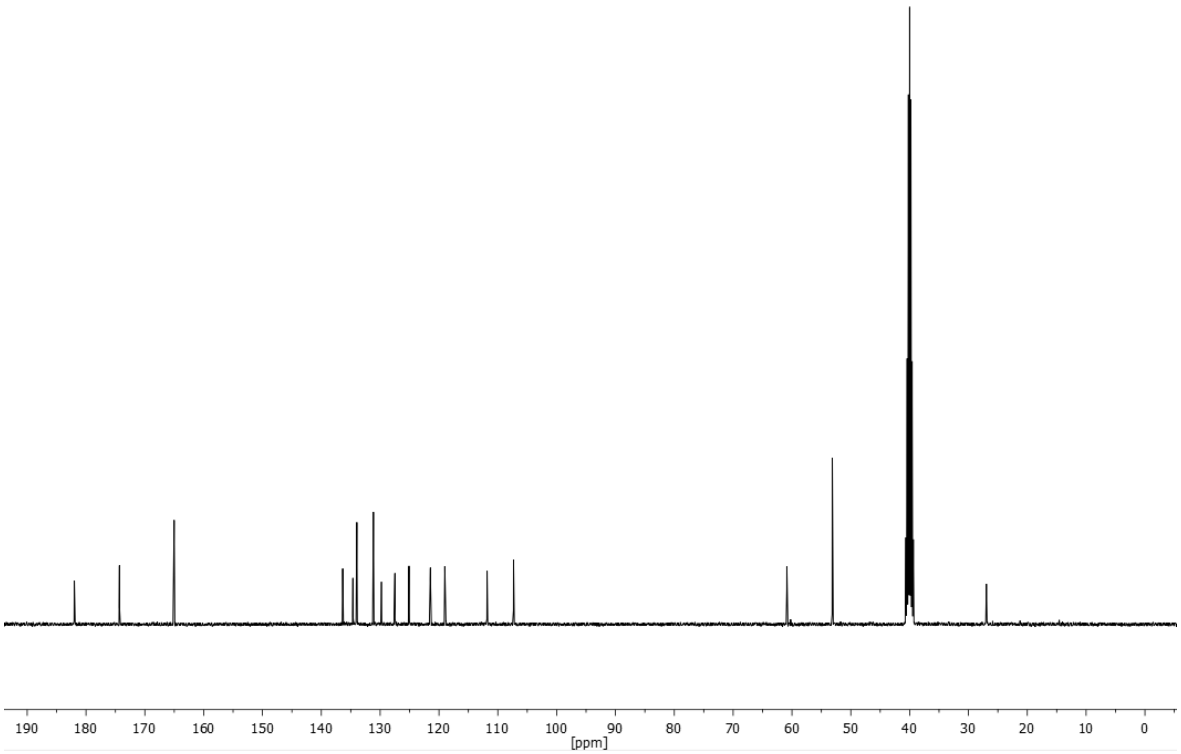

Supplementary Figure 47 ^{13}C-NMR of 5-(4-((1H-indol-3-yl)methyl)-5-oxo-2-thioxoimidazolidin-1-yl)-isophthalate measured in DMSO-d_6 (septet signal at 39.52 ppm) and plotted as signal intensity versus chemical shift in ppm.

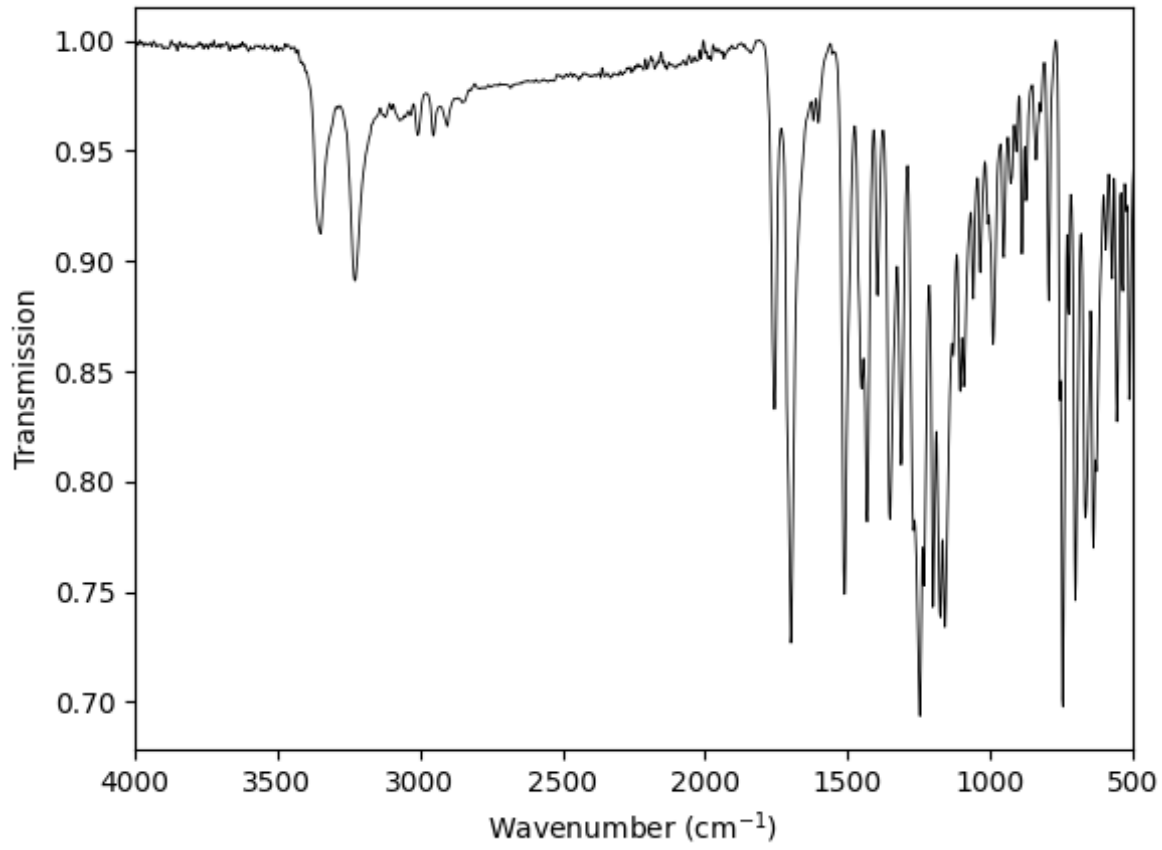

Supplementary Figure 48 IR-spectra of 5-(4-((1H-indol-3-yl)methyl)-5-oxo-2-thioxoimidazolidin-1-yl)-isophthalate.

6.2.3.1 Optimisation of the reaction conditions for thiohydantoin generation *via* a MCR

The following table presents all the reaction conditions screened to identify the optimal conditions for thiohydantoin generation:

Supplementary Table 1 Summary of the screening of the MCR for conditions suitable for thiohydantoin generation:

E	S	T [°C]	B	C_B [eq.]	C_I [mol/L]	Y_{1h} [%]	Y_{2h} [%]	Y_{3h} [%]	Y_{4h} [%]	Y_{20h} [%]	Y_{70h} [%]
1	*n*-hexane	40	DBU	0.1	0.2	1.7	2.3	3.1	-	2.9	-
2	Toluene	40	DBU	0.1	0.2	0	0	0.8	-	1.0	-
3	DMC	40	DBU	0.1	0.2	-	3.7	-	-	6.6	-
4	DCM	40	DBU	0.1	0.2	1.5	2.0	2.4	-	4.9	-
5	THF	40	DBU	0.1	0.2	0	1.0	1.0	-	1.6	-
6	2-MeTHF	40	DBU	0.1	0.2	0	0.8	-	-	1.1	-
7	GBL	40	DBU	0.1	0.2	-	2.5	-	-	4.1	-
8	Cyrene®	40	DBU	0.1	0.2	-	0	-	-	13.9	-
9	Isopropanol	40	DBU	0.1	0.2	5.0	18.7	27.8	-	52.4	-
10	EtOH	40	DBU	0.1	0.2	0	4.2	-	-	47.1	-
11	MeOH	40	DBU	0.1	0.2	0	0	-	-	65.5	-
12	Ethyl acetate	40	DBU	0.1	0.2	1.3	1.5	1.6	-	2.2	-
13	Acetone	40	DBU	0.1	0.2	1.6	2.8	3.7	-	12.4	-
14	DMF	40	DBU	0.1	0.2	3.7	4.3	4.4	-	7.7	-
15	DMSO	40	DBU	0.1	0.2	28.4	42.5	52.6	-	65.3	-
16	Water	40	DBU	0.1	0.2	0	0	-	-	1.5	-
17	DMSO	40	-	0.1	0.2	-	26.8	-	-	49.0	-
18	DMSO	40	NMI	0.1	0.2	-	25.4	-	-	44.6	-
19	DMSO	40	DABCO	0.1	0.2	-	30.1	-	-	49.6	-
20	DMSO	40	DMAP	0.1	0.2	-	23.5	-	-	41.7	-
21	DMSO	40	K_2CO_3	0.1	0.2	-	33.9	-	-	53.2	-
22	DMSO	40	DIPEA	0.1	0.2	-	17.2	-	-	36.2	-
23	DMSO	40	TEA	0.1	0.2	-	27.2	-	-	48.6	-
24	DMSO	40	DIPA	0.1	0.2	-	19.9	-	-	41.1	-
25	DMSO	40	TMG	0.1	0.2	-	20.9	-	-	39.4	-
26	DMSO	40	DBN	0.1	0.2	-	27.8	-	-	42.4	-
27	DMSO	40	DBU	0.1	0.2	-	42.5	-	-	65.3	-
28	DMSO	40	TBD	0.1	0.2	-	31.4	-	-	41.5	-
29	DMSO	40	NaOH	0.1	0.2	-	21.5	-	-	44.5	-
30	DMSO	40	KO^{t}Bu	0.1	0.2	-	25.3	-	-	40.7	-
31	MeOH	40	-	0.1	0.2	0	0	0	0	-	-
32	MeOH	40	DABCO	0.1	0.2	0	0	0	0	-	-
33	MeOH	40	DMAP	0.1	0.2	0	0	0	0	-	-
34	MeOH	40	K_2CO_3	0.1	0.2	0	1.8	3.6	8.6	-	-
35	MeOH	40	TEA	0.1	0.2	0	0	0	0	-	-
36	MeOH	40	DBN	0.1	0.2	0	1.0	3.1	12.0	-	-
37	MeOH	40	NaOH	0.1	0.2	2.2	14.9	35.3	55.0	-	64.6
38	MeOH	20	NaOH	0.1	0.2	0	0	0	-	24.1	-
39	MeOH	30	NaOH	0.1	0.2	0	0	0	-	51.0	-
40	MeOH	50	NaOH	0.1	0.2	0	1.1	2.8	-	15.3	-
41	MeOH	60	NaOH	0.1	0.2	2.5	7.9	21.3	-	44.9	-
42	MeOH	70	NaOH	0.1	0.2	4.7	9.3	11.1	-	26.2	-
43[a]	MeOH	40	NaOH	0.1	0.4	0	13.8	23.3	-	-	-
44[a]	MeOH	40	NaOH	0.1	0.8	0	11.6	-	-	-	-
45[a]	MeOH	40	NaOH	0.1	1.0	0	-	-	-	-	-
46	MeOH	40	NaOH	0.05	0.2	0	7.2	19.1	-	39.9	-
47	MeOH	40	NaOH	0.02	0.2	0	1.9	7.4	-	50.4	-
48	MeOH	40	NaOH	0.01	0.2	0	0	1.8	-	60.8	-

The reaction screening was conducted using dodecyl isocyanide, elemental sulphur, and *L*-methyl leucinate as reactants. Unless otherwise stated, a 10 mL crimp vial was equipped with a stirring bar and charged with 0.14 equivalents of elemental sulphur (equivalent to 1.12 equivalents of sulphur atoms). Subsequently, 1.00 equivalent of the tetradecane internal standard was added via an Eppendorf® pipette to facilitate monitoring of the reaction progress and determination of product yield by GC analysis. Next, 1.00 equivalent of 1-isocyanododecane was added to the reaction mixture, followed by the solvent to achieve a concentration of c(1-isocyanododecane) = 0.2 M. Subsequently, 1.10 equivalents of the pre-deprotonated amino acid methyl ester were added, and the solution was treated with 0.10 equivalents of a base catalyst. The reaction mixture was stirred at the respective screening temperature. GC samples were taken as outlined in the table, and the samples

were subsequently analysed by GC measurement. **E**: Entry; **S**: Solvent; **T**: Temperature; **B**: Base catalyst; $\mathbf{C_B}$: Base catalyst concentration in the reaction mixture; $\mathbf{C_I}$: Overall concentration based on the isocyanide reactant; **Y**: Product yield determined by GC analysis. In the concentration screening (enries are marked with a superscript letter "[a]"), product precipitation and solubility issues prevented adequate screening of the reaction progress by GC. Consequently, it was assumed that the initially choosen concentration c(1-isocyanododecane) = 0.2 M was most suited.

6.2.4 Synthetic procedures for the Passerini products (α-acyloxy amides)

6.2.4.1 General procedure for the synthesis of Passerini products

The general procedure for the synthesis of various Passerini products was carried out under non-optimal conditions. This procedure was used to screen the catalytic activity of thiourea organocatalysts. During the reaction, progress was monitored by GC analysis, with 100.8 µL samples taken at 2, 20, and 44 hours. The reaction was conducted in a 10 mL crimp vial. First, 1.00 equivalent of the respective aldehyde was dissolved in 10 mL of *n*-hexane, and the mixture was stirred for 5 minutes at room temperature to ensure homogeneity. Next, 1.00 equivalent of the respective carboxylic acid was added, and the mixture was stirred again for 5 minutes. Finally, 1.00 equivalent of the respective isocyanide was added. The crimp vial was then sealed, and the mixture was stirred for 44 hours at room temperature. Afterward, the reaction mixture was quenched by dilution with ethyl acetate, and the solvent was evaporated until the volume was reduced to 1.5 mL. The resulting mixture was purified directly via column chromatography to obtain the pure product.

Synthesis of 2-(benzylamino)-2-oxo-1-(2,3,6-trichlorophenyl)ethyl acetate

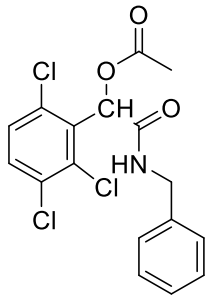

52.4 mg of 2,3,6-trichlorobenzaldehyde (250 µmol, 1.00 eq.), 14.3 µL of acetic acid (15.0 mg, 250 µmol, 1.00 eq.) and 30.4 µL of benzyl isocyanide (29.3 mg, 250 µmol, 1.00 eq.) were used in 10 mL n-hexane following the general procedure for the synthesis of Passerini products. The final product was obtained after purification *via* column chromatography (cyclohexane/ethyl acetate 98/2→55/45) and the pure product was obtained as a white powdery solid (29.7 mg, 78 µmol) with a yield of 31%.

Rf = 0.1 in cyclohexane/ethyl acetate 5/1 visualised *via* UV quenching at 254 nm and $KMnO_4$.

^{1}H-NMR (500 MHz, DMSO-d_6) δ/ppm = 8.79 (t, J = 6.2 Hz, 1H, ^{1}), 7.70 (d, J = 8.7 Hz, 1H, ^{2}), 7.54 (d, J = 8.7 Hz, 1H, ^{3}), 7.36 – 7.22 (m, 5H, ^{4}), 6.85 (s, 1H, ^{5}), 4.36 (ddd, J = 57.2, 15.1, 6.1 Hz, 2H, ^{6}), 2.14 (s, 3H, ^{7}).

^{13}C-NMR (126 MHz, DMSO-d_6) δ/ppm = 169.4, 166.2, 139.0, 134.4, 134.3, 133.9, 131.5, 131.5, 129.7, 128.2, 127.3, 126.8, 70.6, 42.4, 20.7.

HRMS-EI-MS m/z: [M] calculated for $[C_{17}H_{15}Cl_3NO_3]^+$ = 386.01120, found: 386.01026.

IR (ATR platinum diamond) ν/cm^{-1} = 3324 (w), 2950 (w), 2925 (w), 1748 (s), 1656 (s), 1609 (w), 1565 (w), 1534 (s), 1497 (w), 1454 (m), 1436 (m), 1388 (w), 1370 (m), 1360 (m), 1339 (w), 1316 (w), 1302 (w), 1279 (w), 1263 (w), 1220 (vs), 1193 (m), 1175 (s), 1133 (w), 1100 (m), 1082 (m), 1045 (s), 1020 (m), 1002 (w), 936 (w), 905 (w), 882 (w), 819 (s), 782 (w), 736 (m), 697 (vs), 675 (m), 627 (m), 599 (w), 590 (w), 576 (w), 547 (s), 529 (m), 502 (w), 485 (m), 450 (m), 403 (w)

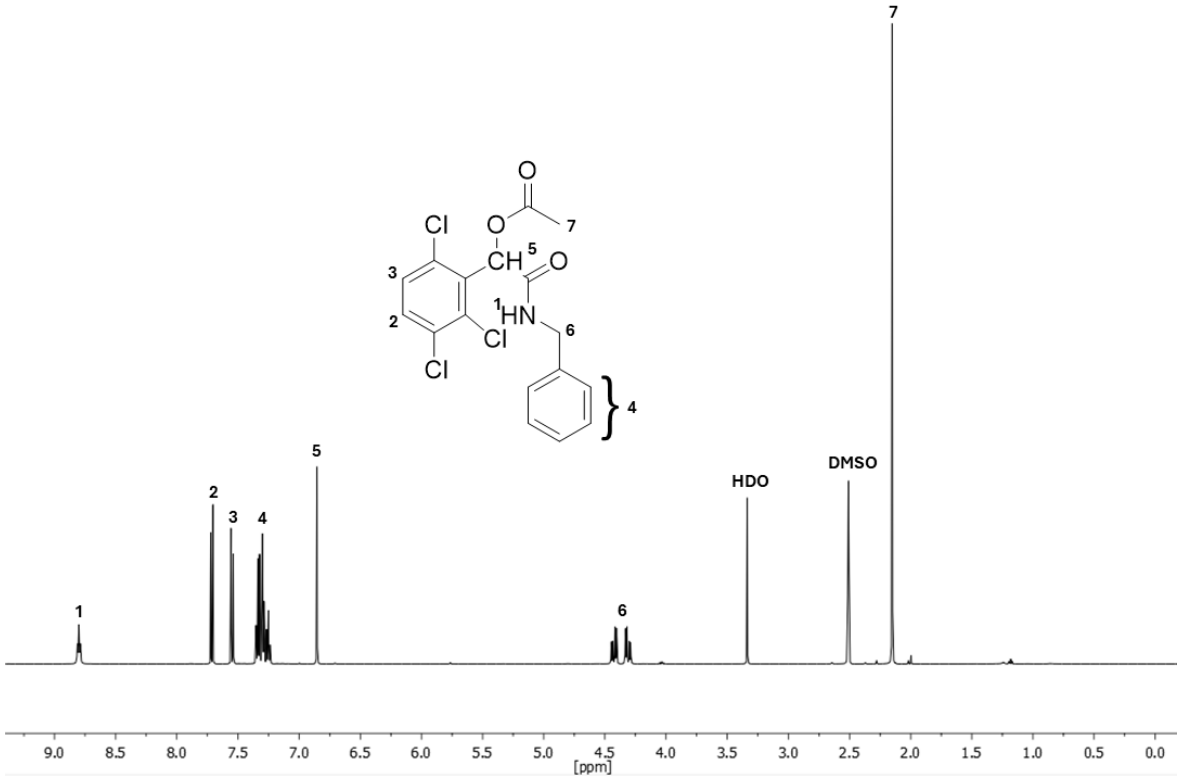

Supplementary Figure 49 ^{1}H-NMR of 2-(benzylamino)-2-oxo-1-(2,3,6-trichlorophenyl)-ethylacetate measured in DMSO-d_6 plotted as signal intensity versus chemical shift in ppm.

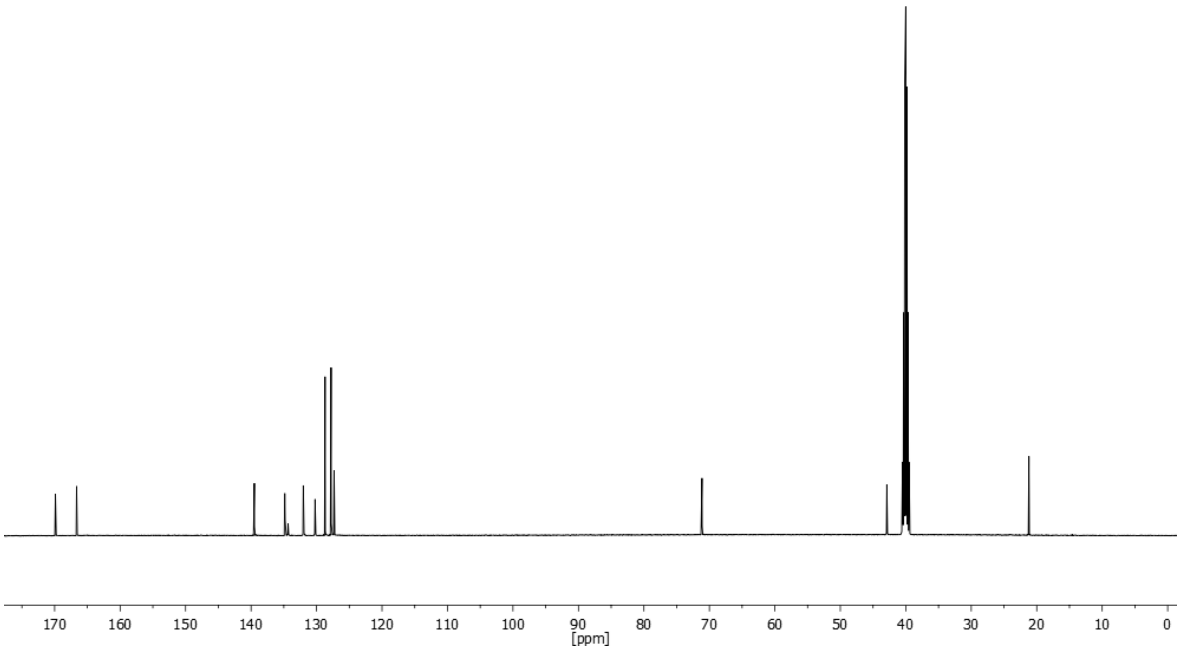

Supplementary Figure 50 ^{13}C-NMR of 2-(benzylamino)-2-oxo-1-(2,3,6-trichlorophenyl)-ethylacetate measured in DMSO-d_6 (septet signal at 39.52 ppm) and plotted as signal intensity versus chemical shift in ppm.

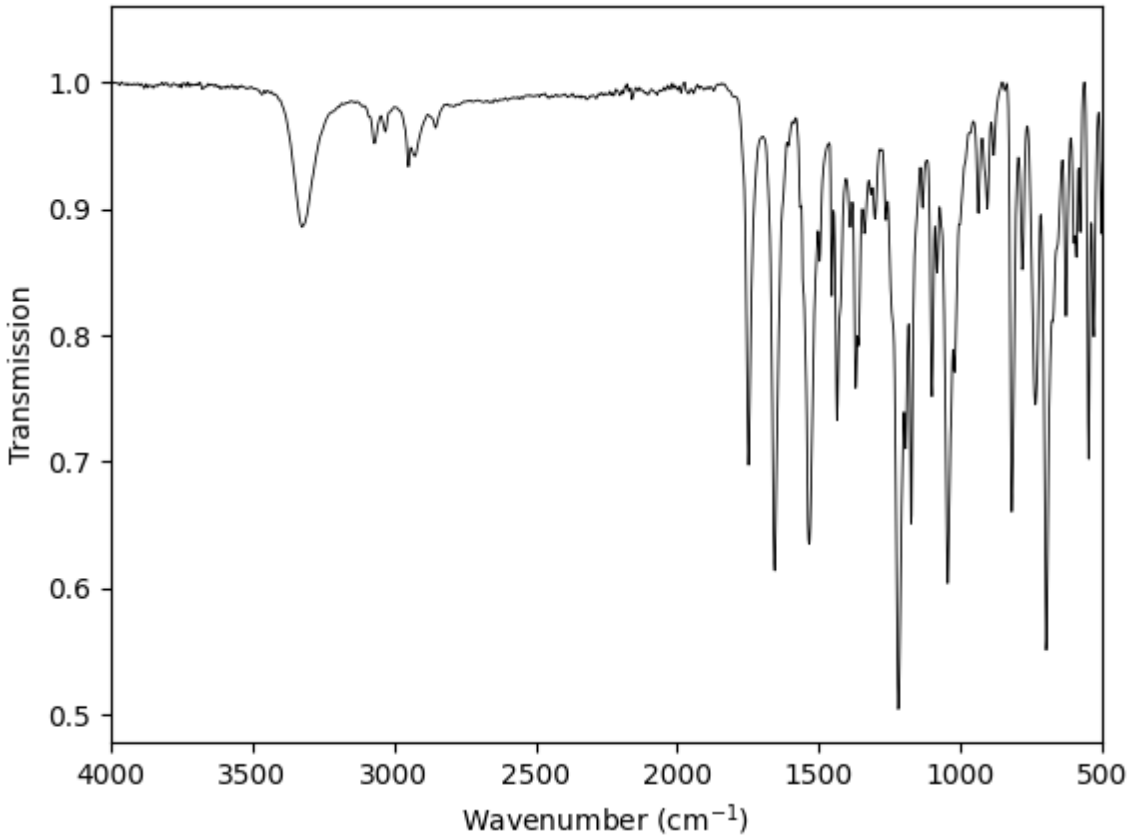

Supplementary Figure 51 IR-spectra of 2-(benzylamino)-2-oxo-1-(2,3,6-trichlorophenyl)-ethylacetate.

Synthesis of 2-(benzylamino)-2-oxo-1-phenylethyl acetate

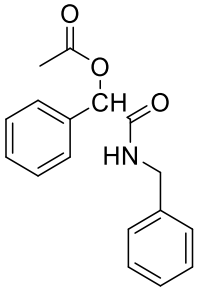

The reaction was conducted in a 10 mL crimp vial. 382 µL of benzaldehyde (397 mg, 3.74 mmol, 1.50 eq.) were dissolved in 2 mL n-hexane, and the mixture was stirred for 5 minutes at room temperature to ensure homogeneity. Then, 143 µL of acetic acid (150 mg, 2.50 mmol, 1.00 eq.) were added to the mixture, which was stirred again for 5 minutes to ensure homogeneity. Finally, 456 µL of benzyl isocyanide (439 mg, 3.74 mmol, 1.50 eq.) were added to the mixture. The crimp vial was then sealed, and the mixture was stirred for 44 hours at room temperature. Subsequently, the reaction mixture was quenched by dilution with ethyl acetate, and the volume was reduced by evaporating the solvent until 1.5 mL remained. This mixture was purified directly *via* column chromatography (cyclohexane/ethyl acetate 98/2→55/45) and the pure product was obtained as a white powdery solid (602 mg, 2.15 mmol) with a yield of 86%.

Rf = 0.11 in cyclohexane/ethyl acetate 5/1 visualised *via* UV quenching at 254 nm and $KMnO_4$.

^{1}H-NMR (500 MHz, DMSO-d_6) δ/ppm = 8.81 (t, J = 6.0 Hz, 1H, [1]), 7.53 – 7.46 (m, 2H, [2]), 7.42 – 7.34 (m, 3H, [3]), 7.30 – 7.24 (m, 2H, [4]), 7.24 – 7.19 (m, 1H, [5]), 7.18 – 7.13 (m, 2H, [6]), 5.89 (s, 1H, [7]), 4.37 – 4.21 (m, 2H, [8]), 2.14 (s, 3H, [9z]).

^{13}C-NMR (126 MHz, DMSO-d_6) δ/ppm = 170.3, 168.6, 139.5, 136.3, 129.1, 128.9, 128.7, 127.9, 127.4, 127.2, 75.6, 42.3, 21.2.

HRMS-EI-MS m/z: [M] calculated for $[C_{17}H_{18}NO_3]^+$ = 284.12812, found: 284.12782.

IR (ATR platinum diamond) ν/cm^{-1} = 3326 (m), 2925 (w), 1738 (s), 1701 (vw), 1658 (s), 1602 (w), 1586 (w), 1528 (s), 1495 (m), 1454 (m), 1434 (w), 1421 (w), 1374 (m), 1360 (w), 1347 (w), 1312 (w), 1294 (w), 1281 (w), 1251 (w), 1222 (vs), 1195 (m), 1160 (w), 1080 (w), 1074 (w), 1045 (s), 1028 (m), 975 (w), 934 (w), 924 (m), 876 (vw), 858 (w), 747 (m), 738 (m), 701 (s), 675 (m), 617 (m), 601 (m), 570 (m), 529 (m), 492 (w), 479 (w), 465 (w), 438 (w).

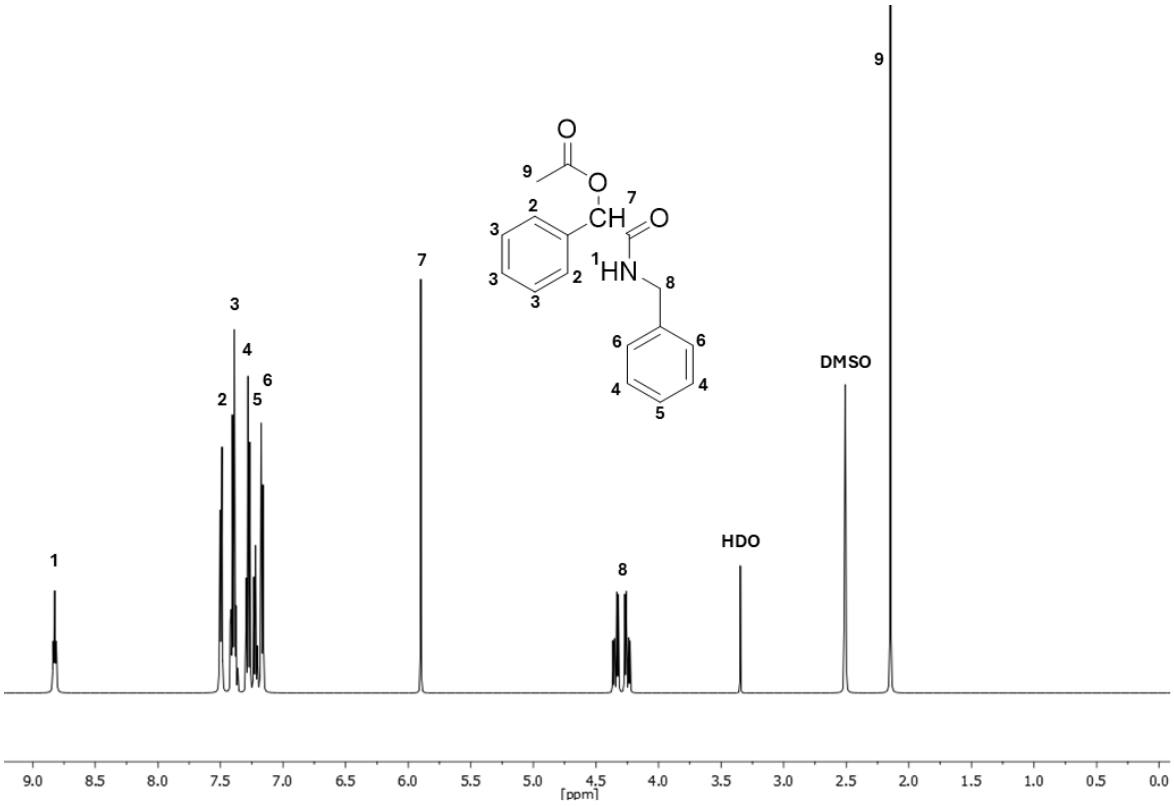

Supplementary Figure 52 ^{1}H-NMR of 2-(benzylamino)-2-oxo-1-phenylethyl acetate measured in DMSO-d_6 plotted as signal intensity versus chemical shift in ppm.

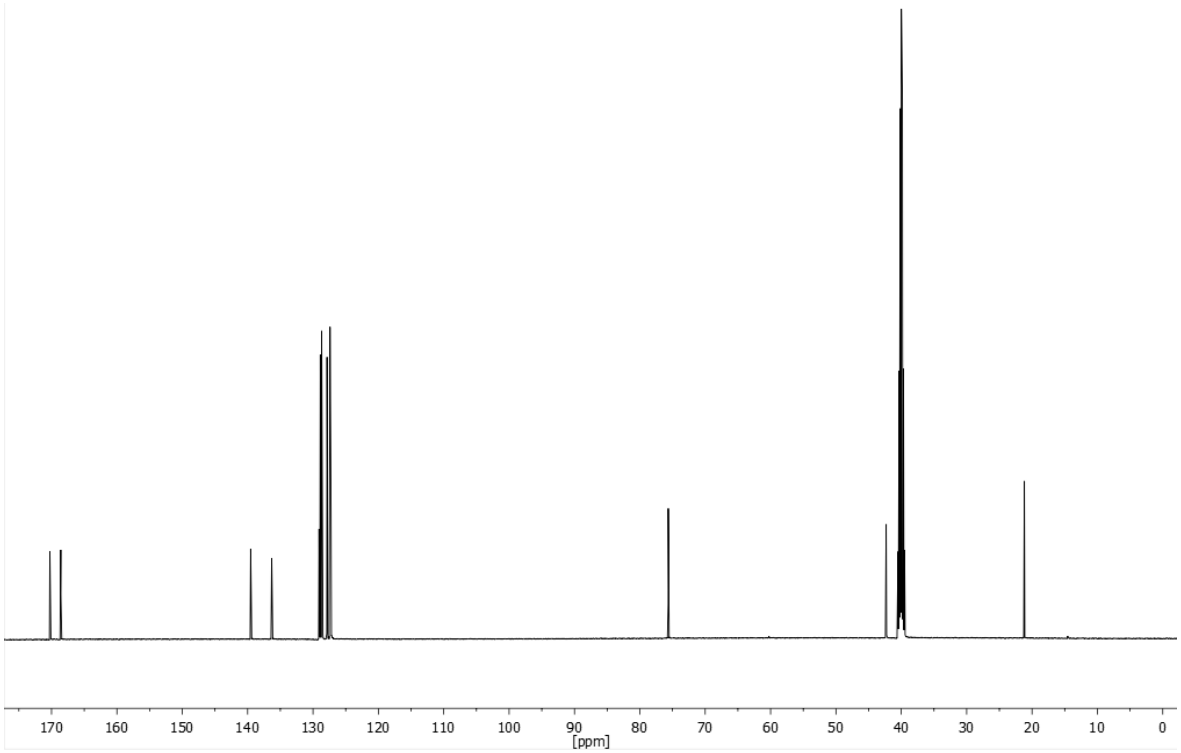

Supplementary Figure 53 ^{13}C-NMR of 2-(benzylamino)-2-oxo-1-phenylethyl acetate measured in DMSO-d_6 (septet signal at 39.52 ppm) and plotted as signal intensity versus chemical shift in ppm.

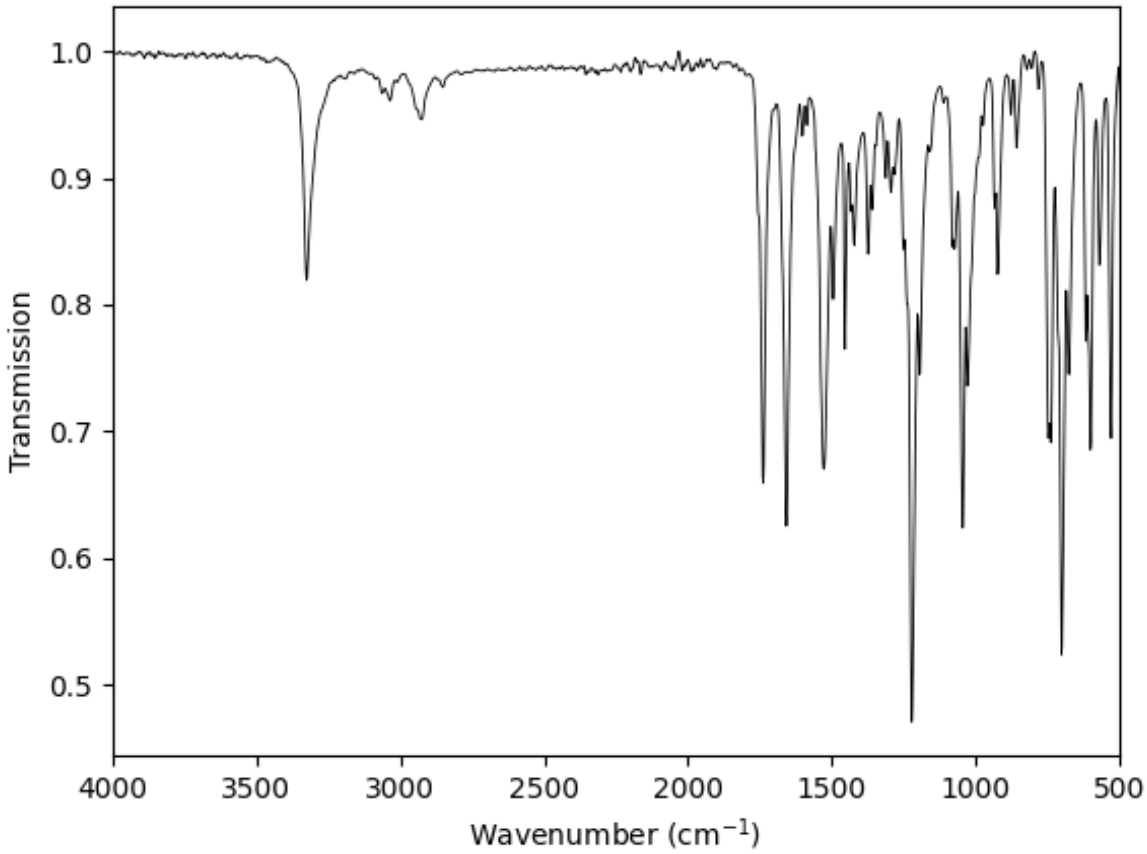

Supplementary Figure 54 IR-spectra of 2-(benzylamino)-2-oxo-1-phenylethyl acetate.

Synthesis of 1-(benzylamino)-1-oxononan-2-yl dodecanoate

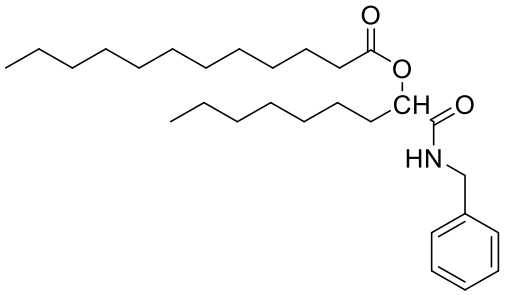

The reaction was conducted in a 10 mL crimp vial. 467 µL of octanal (384 mg, 2.99 mmol, 1.50 eq.) were dissolved in 1.5 mL n-hexane, and the mixture was stirred for 5 minutes at room temperature to ensure homogeneity. Then, 400 mg of dodecanoic acid (2.00 mmol, 1.00 eq.) were added to the mixture, which was stirred again for 5 minutes to ensure homogeneity. Finally, 364 µL of benzyl isocyanide (351 mg, 2.99 mmol, 1.50 eq.) were added to the mixture. The crimp vial was then sealed, and the mixture was stirred for 44 hours at room temperature. Subsequently, the reaction mixture was quenched by dilution with ethyl acetate, and the volume was reduced by evaporating the solvent until 1.5 mL remained. This mixture was purified directly *via* column chromatography (cyclohexane/ethyl acetate 8/1→6/1) and the pure product was obtained as a white powdery solid (791 mg, 1.77 mmol) with a yield of 89%.

Rf = 0.35 in cyclohexane/ethyl acetate 6/1 visualised *via* UV quenching at 254 nm and $KMnO_4$.

^{1}H-NMR (500 MHz, DMSO-d_6) δ/ppm = 8.49 (t, J = 6.1 Hz, 1H, ^{1}), 7.35 – 7.27 (m, 2H, ^{2}), 7.22 (dd, J = 7.8, 5.7 Hz, 3H, ^{3}), 4.90 (dd, J = 7.2, 5.4 Hz, 1H, ^{4}), 4.33 – 4.23 (m, 2H, ^{5}), 2.40 – 2.31 (m, 2H, ^{6}), 1.76 – 1.65 (m, 2H, ^{7}), 1.53 (p, J = 7.2 Hz, 2H, ^{8}), 1.25 (d, J = 8.9 Hz, 26H, ^{9}), 0.85 (t, J = 6.8 Hz, 6H, ^{10}).

^{13}C-NMR (126 MHz, DMSO-d_6) δ/ppm = 173.0, 170.0, 139.8, 128.7, 127.4, 127.2, 73.5, 42.2, 33.9, 31.9, 31.8, 31.6, 29.5, 29.5, 29.4, 29.2, 29.0, 29.0, 28.9, 28.9, 25.0, 24.9, 22.6, 22.5, 14.4, 14.4.

HRMS-EI-MS m/z: [M] calculated for $[C_{28}H_{48}NO_3]^+$ = 446.36287, found: 446.36263.

IR (ATR platinum diamond) $\tilde{\nu}$/cm^{-1} = 3299 (w), 3295 (w), 2954 (m), 2923 (vs), 2853 (s), 1742 (s), 1656 (s), 1606 (vw), 1532 (m), 1497 (w), 1465 (m), 1454 (m), 1436 (w), 1376 (w), 1362 (w), 1329 (w), 1294 (w), 1234 (m), 1156 (s), 1115 (m), 1078 (m), 1028 (w), 965 (vw), 722 (m), 697 (s), 619 (w), 599 (w), 481 (vw), 471 (vw), 459 (vw).

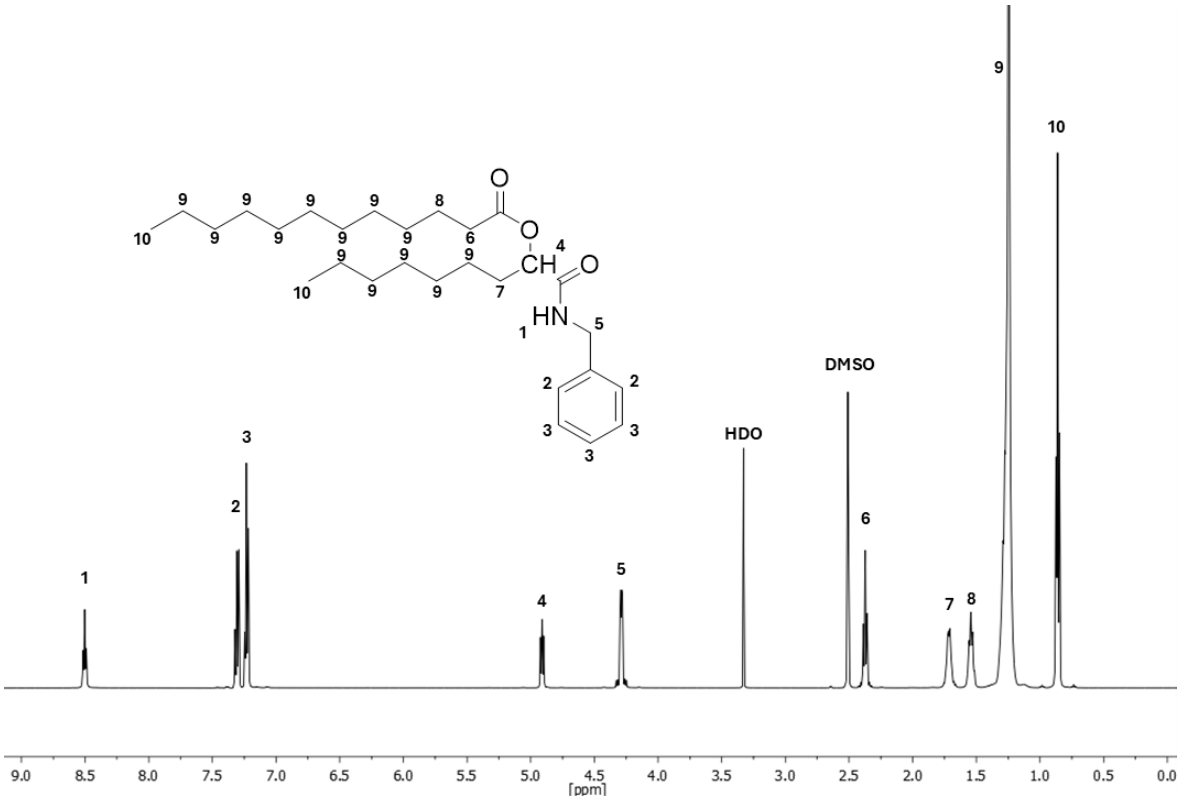

Supplementary Figure 55 ^{1}H-NMR of 1-(benzylamino)-1-oxononan-2-yl dodecanoate measured in DMSO-d_6 plotted as signal intensity versus chemical shift in ppm.

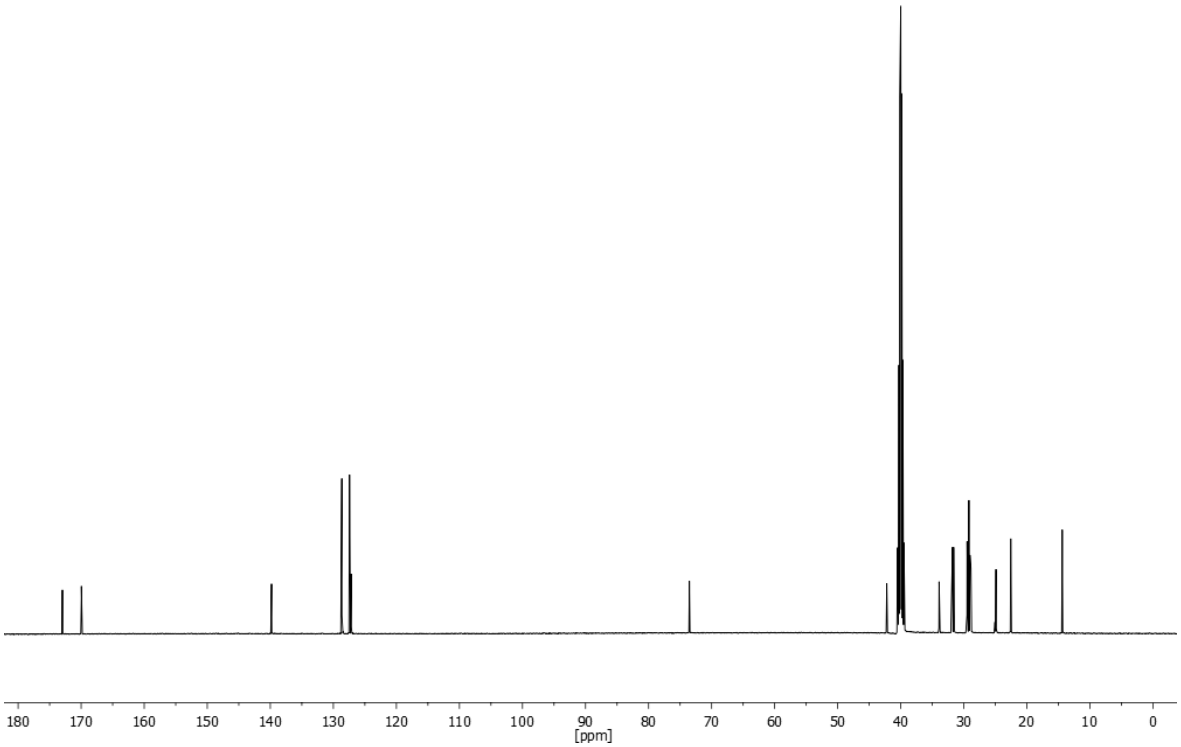

Supplementary Figure 56 ^{13}C-NMR of 1-(benzylamino)-1-oxononan-2-yl dodecanoate measured in DMSO-d_6 (septet signal at 39.52 ppm) and plotted as signal intensity versus chemical shift in ppm.

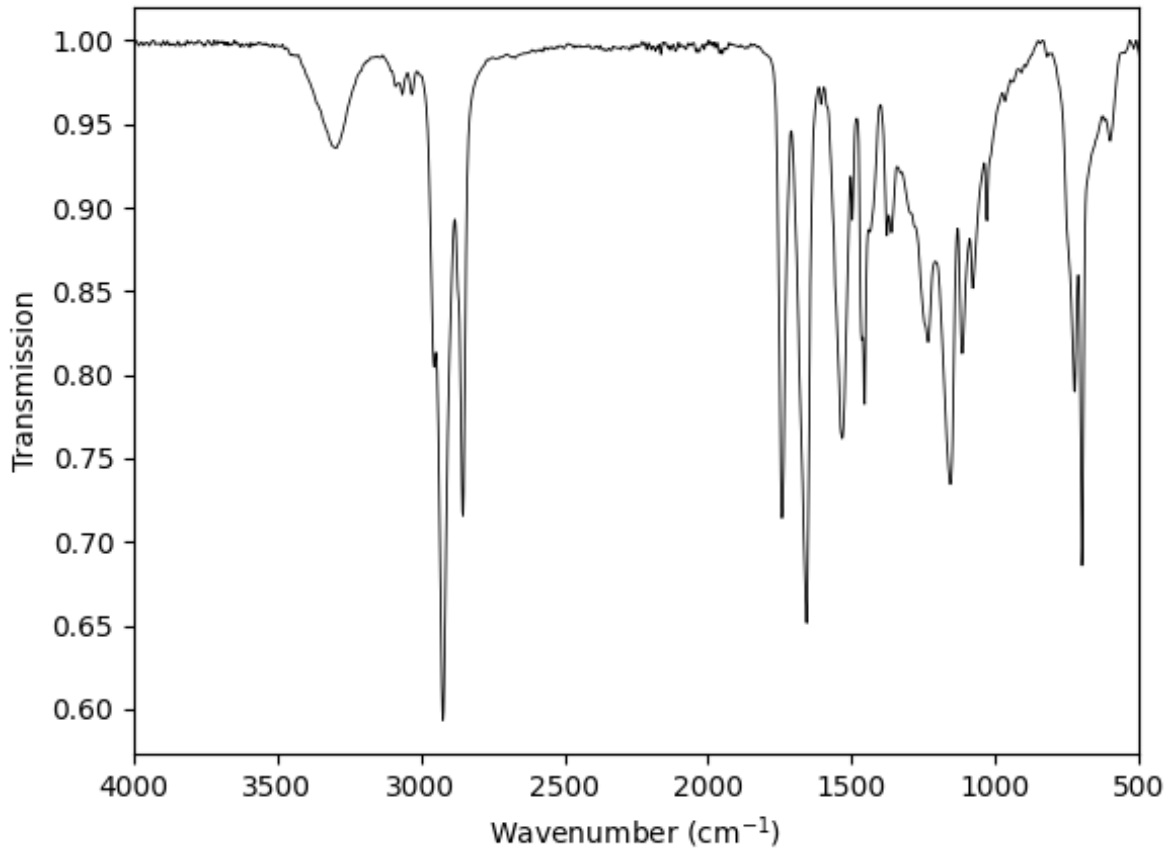

Supplementary Figure 57 IR-spectra of 1-(benzylamino)-1-oxononan-2-yl dodecanoate.

Synthesis of 1-(benzylamino)-1-oxononan-2-yl cyclohexanecarboxylate

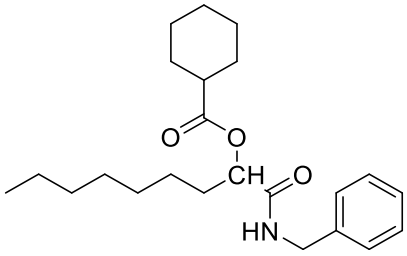

The reaction was conducted in a 10 mL crimp vial. 365 µL of octanal (300 mg, 2.34 mmol, 1.50 eq.) were dissolved in 1.5 mL n-hexane, and the mixture was stirred for 5 minutes at room temperature to ensure homogeneity. Then, 194 µL of acetic acid (200 mg, 1.56 mmol, 1.00 eq.) were added to the mixture, which was stirred again for 5 minutes to ensure homogeneity. Finally, 285 µL of benzyl isocyanide (274 mg, 2.34 mmol, 1.50 eq.) were added to the mixture. The crimp vial was then sealed, and the mixture was stirred for 44 hours at room temperature. Subsequently, the reaction mixture was quenched by dilution with ethyl acetate, and the volume was reduced by evaporating the solvent until 1.5 mL remained. This mixture was purified directly *via* column chromatography (cyclohexane/ethyl acetate 8/1→6/1) and the pure product was obtained as a white powdery solid (530 mg, 1.42 mmol) with a yield of 91%.

Rf = 0.16 in cyclohexane/ethyl acetate 6/1 visualised *via* UV quenching at 254 nm and $KMnO_4$.

^{1}H-NMR (500 MHz, DMSO-d_6) δ/ppm = 8.52 – 8.42 (m, 1H, [1]), 7.34 – 7.27 (m, 2H, [2]), 7.23 (td, J = 6.6, 1.7 Hz, 3H, [3]), 4.89 (dd, J = 7.1, 5.6 Hz, 1H, [4]), 4.32 – 4.23 (m, 2H, [5]), 2.45 – 2.35 (m, 1H, [6]), 1.89 – 1.77 (m, 2H, [7]), 1.76 – 1.63 (m, 4H, [8]), 1.61 – 1.51 (m, 2H, [9]), 1.42 – 1.13 (m, 14H, [10]), 0.85 (t, J = 6.9 Hz, 3H, [11]).

^{13}C-NMR (126 MHz, DMSO-d_6) δ/ppm = 175.0, 170.0, 139.8, 128.7, 127.4, 127.2, 73.5, 73.4, 42.4, 42.2, 31.9, 31.6, 31.6, 29.2, 29.0, 29.0, 29.0, 28.9, 28.9, 28.8, 28.7, 25.8, 25.3, 25.1, 25.0, 25.0, 24.9, 22.5, 22.5, 14.4, 14.4.

HRMS-EI-MS m/z: [M] calculated for $[C_{23}H_{36}NO_3]^+$ = 374.26897, found: 374.26852.

IR (ATR platinum diamond) ν/cm^{-1} = 3303 (w), 3297 (w), 3087 (vw), 3065 (vw), 3032 (vw), 2925 (vs), 2855 (s), 1736 (s), 1658 (vs), 1606 (w), 1586 (w), 1530 (s), 1497 (m), 1452 (s), 1376 (m), 1362 (w), 1331 (w), 1310 (m), 1298 (m), 1273 (w), 1244 (s), 1191 (m), 1162 (vs), 1129 (s), 1078 (m), 1055 (m), 1028 (m), 965 (w), 936 (vw), 895 (w), 845 (vw), 724 (m), 697 (vs), 619 (w), 603 (w), 479 (w), 459 (w).

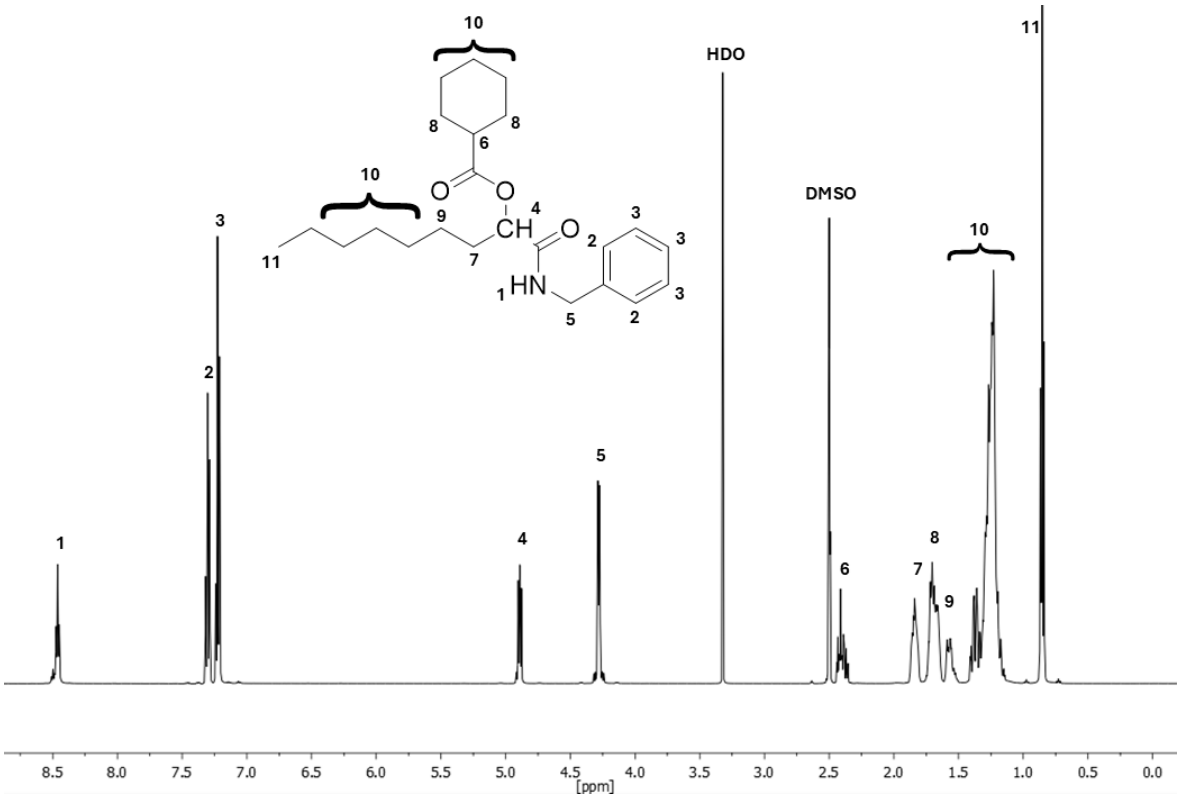

Supplementary Figure 58 ^{1}H-NMR of 1-(benzylamino)-1-oxononan-2-yl cyclohexanecarboxylate measured in DMSO-d_6 plotted as signal intensity versus chemical shift in ppm.

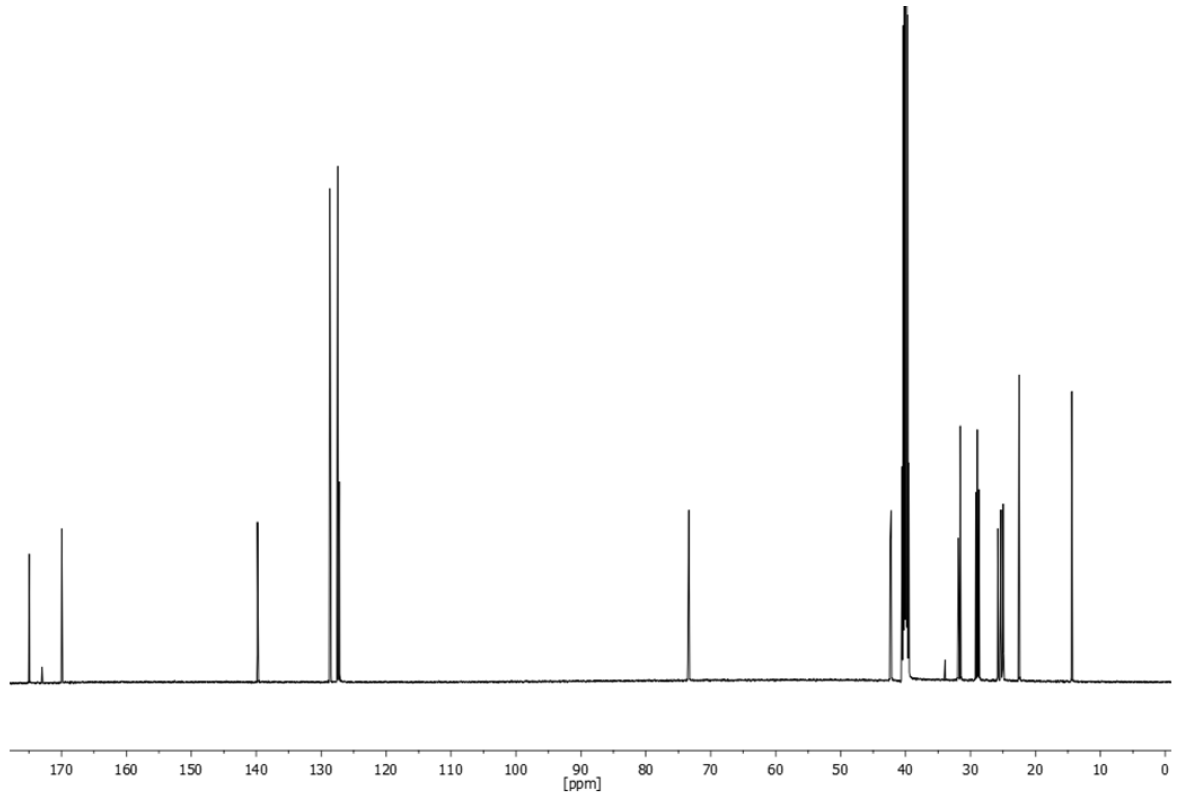

Supplementary Figure 59 ^{13}C-NMR of 1-(benzylamino)-1-oxononan-2-yl cyclohexanecarboxylate measured in DMSO-d_6 (septet signal at 39.52 ppm) and plotted as signal intensity versus chemical shift in ppm.

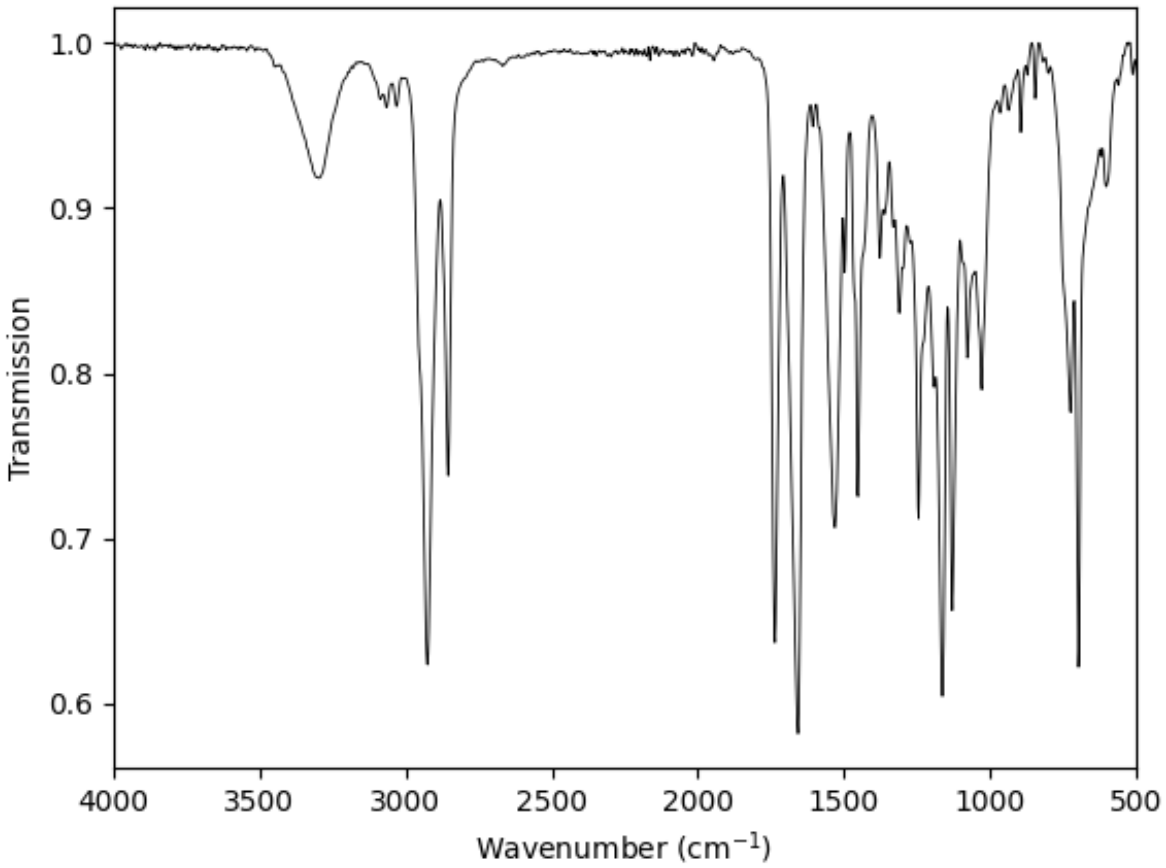

Supplementary Figure 60 IR-spectra of 1-(benzylamino)-1-oxononan-2-yl cyclohexanecarboxylate.

Synthesis of 1-(benzylamino)-1-oxononan-2-yl 4-nitrobenzoate

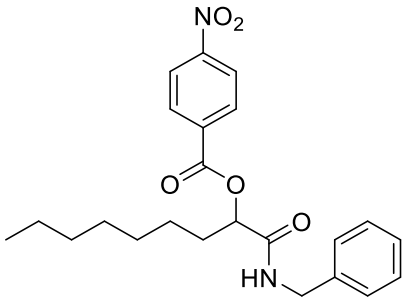

39.0 µL octanal (32.0 mg, 250 µmol, 1.00 eq.), 41.8 mg of 4-nitrobenzoic acid (250 µmol, 1.00 eq.) and 30.4 µL of benzyl isocyanide (29.3 mg, 250 µmol, 1.00 eq.) were used in 10 mL *n*-hexane following the general procedure for the synthesis of Passerini products. The final product was obtained after purification *via* column chromatography (cyclohexane/ethyl acetate 10/1→1/1) and the pure product was obtained as a white powdery solid (10.3 mg, 25 µmol) with a yield of 10%.

Rf = 0.13 in cyclohexane/ethyl acetate 6/1 visualised *via* UV quenching at 254 nm and $KMnO_4$.

^{1}H-NMR (500 MHz, DMSO-d_6) δ/ppm = 9.34 (d, J = 2.1 Hz, 1H, [1]), 7.94 – 7.87 (m, 2H, [2]), 7.35 (dq, J = 8.7, 2.1 Hz, 2H, [3]), 7.26 (dddd, J = 6.6, 5.1, 3.6, 2.0 Hz, 3H, [4]), 7.12 (dq, J = 7.2, 2.7 Hz, 2H, [5]), 5.25 (d, J = 3.4 Hz, 1H, [6]), 5.09 – 4.96 (m, 2H, [7]), 1.86 – 1.70 (m, 2H, [8]), 1.51 – 1.34 (m, 2H, [9]), 1.26 (m, 8H, [10]), 0.93 (t, J = 7.4, 3H, [11]).

^{13}C-NMR (126 MHz, DMSO-d_6) δ/ppm = 169.0, 165.4, 165.3, 152.2, 136.9, 130.1, 128.7, 128.7, 128.1, 127.2, 74.3, 65.3, 65.3, 54.4, 50.7, 34.2, 28.9, 18.6, 18.4, 14.4.

HRMS-EI-MS m/z: [M] calculated for $[C_{23}H_{29}N_2O_5]^+$ = 413.20710, found: 413.20659.

IR (ATR platinum diamond) ν/cm^{-1} = 3273 (m), 3112 (vw), 3087 (vw), 3079 (vw), 3059 (vw), 3032 (vw), 2925 (m), 2855 (m), 1732 (s), 1648 (s), 1606 (w), 1547 (m), 1524 (vs), 1497 (w), 1454 (m), 1436 (w), 1413 (w), 1378 (w), 1345 (s), 1323 (m), 1304 (m), 1275 (s), 1257 (s), 1242 (s), 1175 (w), 1142 (w), 1117 (s), 1103 (vs), 1072 (m), 1047 (w), 1028 (w), 1014 (m), 975 (vw), 952 (w), 872 (m), 843 (m), 784 (w), 761 (m), 740 (m), 714 (s), 695 (s), 580 (w), 508 (w), 487 (w), 465 (w)

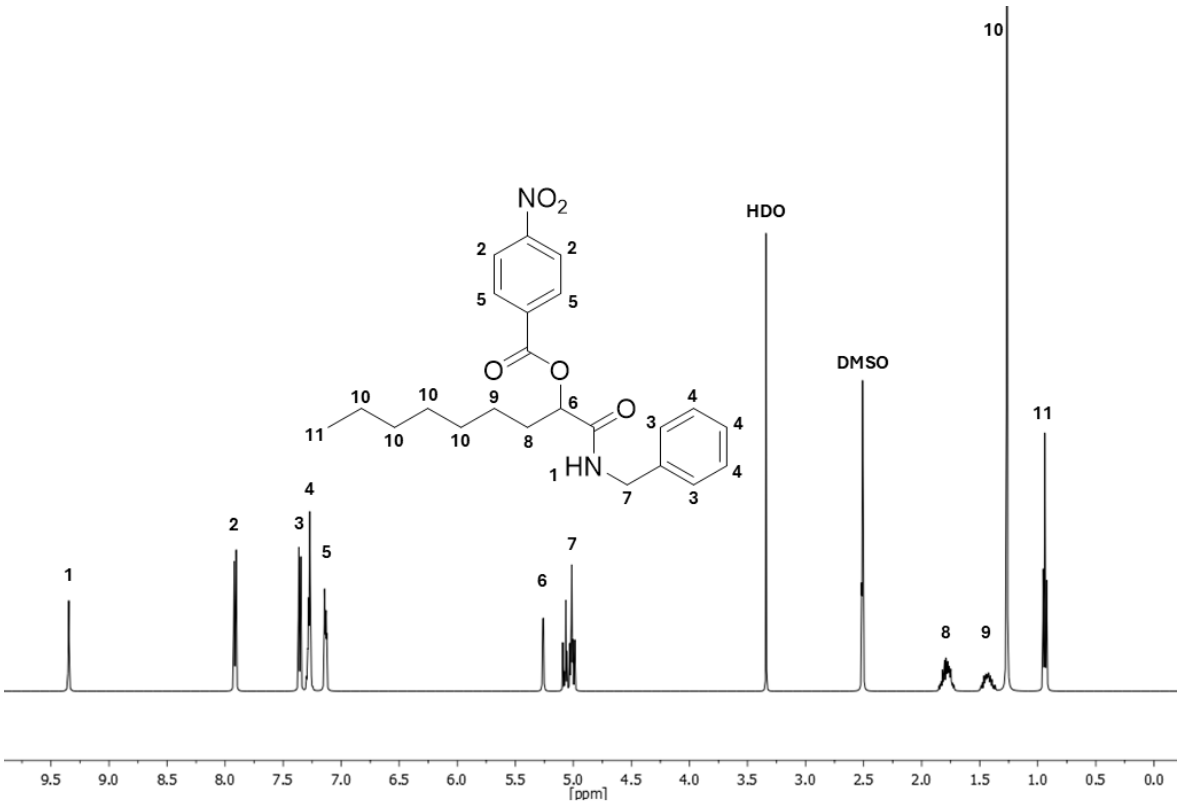

Supplementary Figure 61 ^{1}H-NMR of 1-(benzylamino)-1-oxononan-2-yl 4-nitrobenzoate measured in DMSO-d_6 plotted as signal intensity versus chemical shift in ppm.

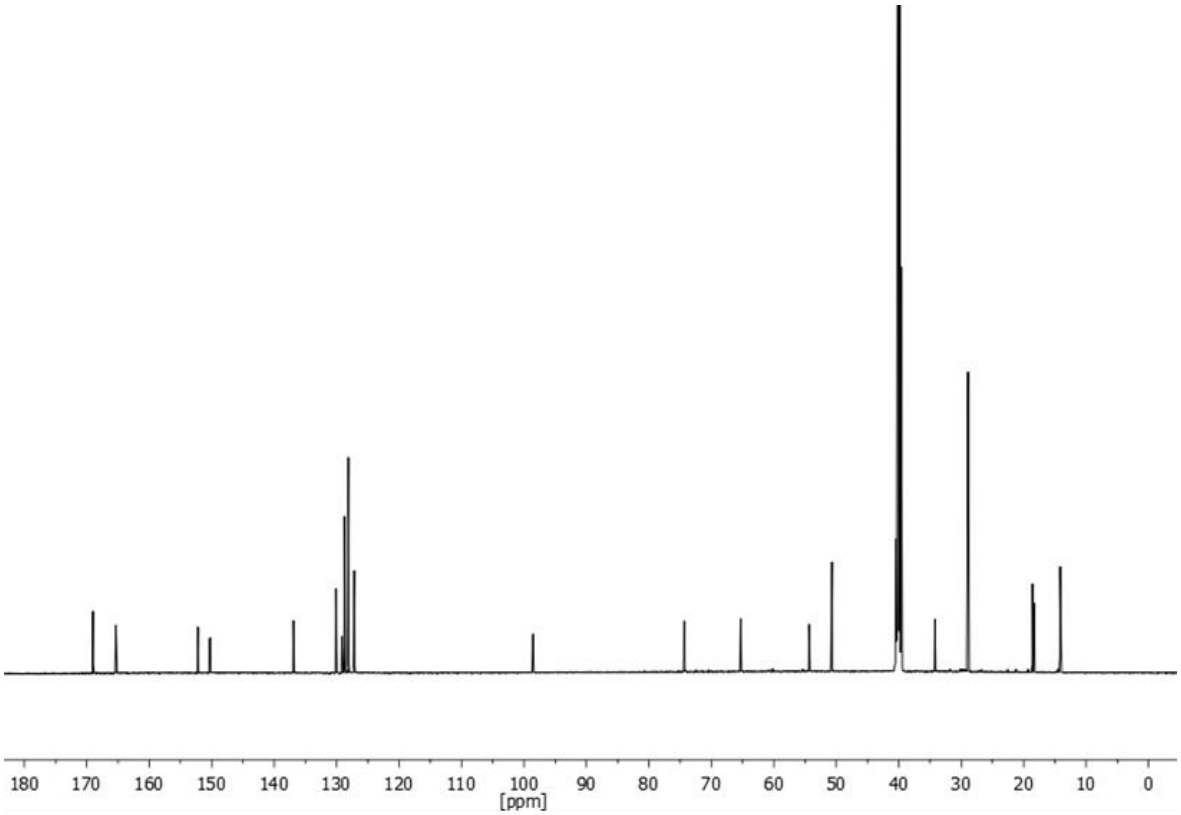

Supplementary Figure 62 ^{13}C-NMR of 1-(benzylamino)-1-oxononan-2-yl 4-nitrobenzoate measured in DMSO-d_6 (septet signal at 39.52 ppm) and plotted as signal intensity versus chemical shift in ppm.

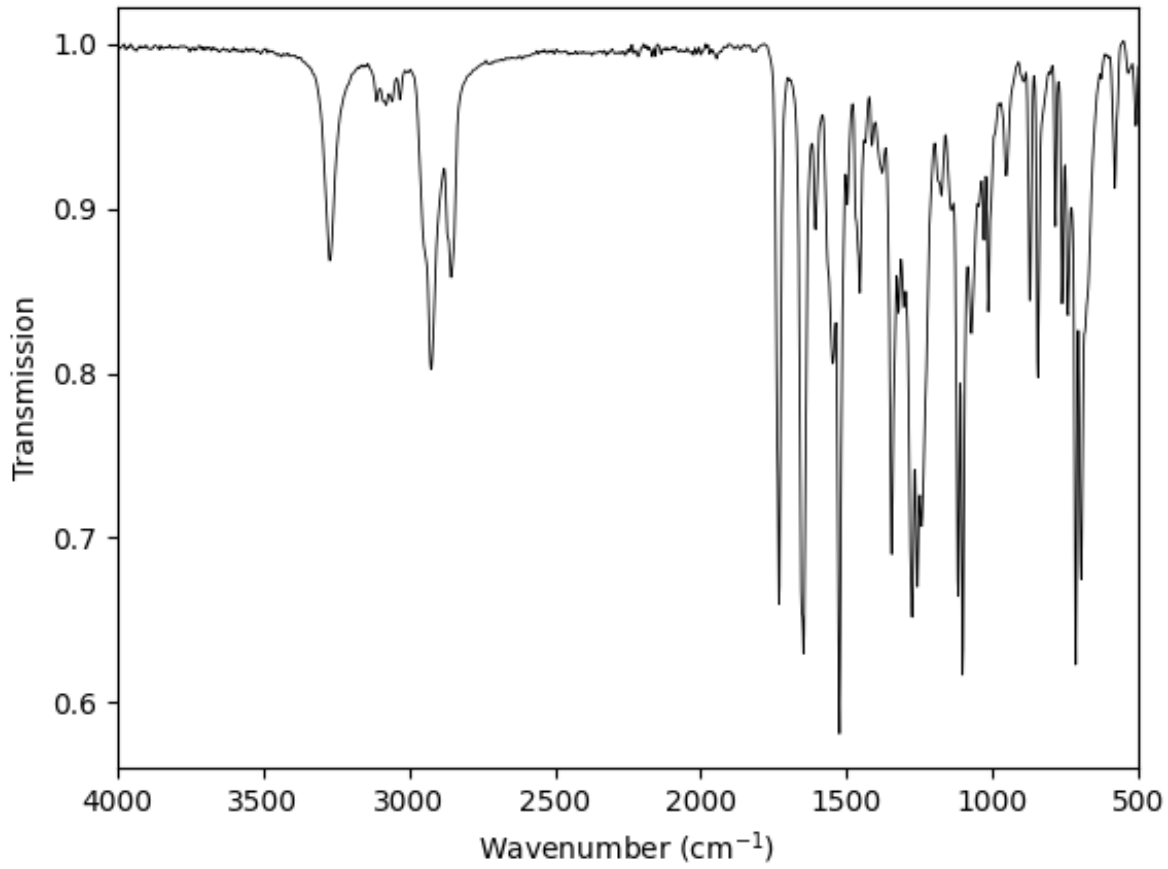

Supplementary Figure 63 IR-spectra of 1-(benzylamino)-1-oxononan-2-yl 4-nitrobenzoate.

Synthesis of 1-(benzylamino)-1-oxononan-2-yl 4-methylbenzoate

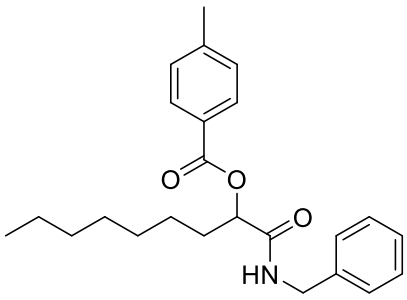

39.0 µL octanal (32.0 mg, 250 µmol, 1.00 eq.), 34.0 mg of 4-methylbenzoic acid (250 µmol, 1.00 eq.) and 30.4 µL of benzyl isocyanide (29.3 mg, 250 µmol, 1.00 eq.) were used in 10 mL *n*-hexane following the general procedure for the synthesis of Passerini products. The final product was obtained after purification *via* column chromatography (cyclohexane/ethyl acetate 10/1→1/1) and the pure product was obtained as a white powdery solid (11.9 mg, 30 µmol) with a yield of 12%.

Rf = 0.16 in cyclohexane/ethyl acetate 6/1 visualised *via* UV quenching at 254 nm and $KMnO_4$.

^{1}H-NMR (500 MHz, DMSO-d_6) δ/ppm = 8.64 (t, J = 6.0 Hz, 1H, [1]), 7.99 – 7.84 (m, 2H, [2]), 7.40 – 7.15 (m, 7H, [3]), 5.12 (dd, J = 7.1, 5.5 Hz, 1H, [4]), 4.31 (d, J = 6.0 Hz, 2H, [5]), 2.39 (s, 3H, [6]), 1.94 – 1.79 (m, 2H, [7]), 1.46 – 1.14 (m, 11H, [8]), 0.92 – 0.78 (m, 3H, [9]).

^{13}C-NMR (126 MHz, DMSO-d_6) δ/ppm = 169.4, 165.2, 143.8, 139.3, 129.5, 129.2, 128.2, 127.0, 127.0, 126.8, 126.7, 73.9, 31.1, 28.5, 24.6, 22.0, 21.2, 13.9.

HRMS-EI-MS m/z: [M] calculated for $[C_{24}H_{32}NO_3]^+$ = 382.23767, found: 382.23670.

IR (ATR platinum diamond) ν/cm^{-1} = 3285 (m), 3100 (vw), 3065 (vw), 3034 (vw), 2956 (w), 2921 (m), 2853 (m), 1726 (s), 1656 (vs), 1613 (m), 1563 (s), 1510 (w), 1495 (w), 1467 (w), 1454 (m), 1440 (m), 1407 (w), 1380 (w), 1358 (w), 1325 (w), 1304 (w), 1286 (m), 1261 (s), 1240 (s), 1207 (w), 1175 (m), 1156 (w), 1121 (s), 1109 (s), 1082 (m), 1068 (m), 1045 (w), 1028 (w), 1020 (m), 1008 (w), 971 (w), 965 (w), 954 (w), 911 (w), 864 (w), 841 (w), 833 (w), 751 (s), 724 (w), 699 (s), 640 (vw), 621 (w), 601 (m), 566 (vw), 490 (m), 473 (m), 428 (w), 420 (w).

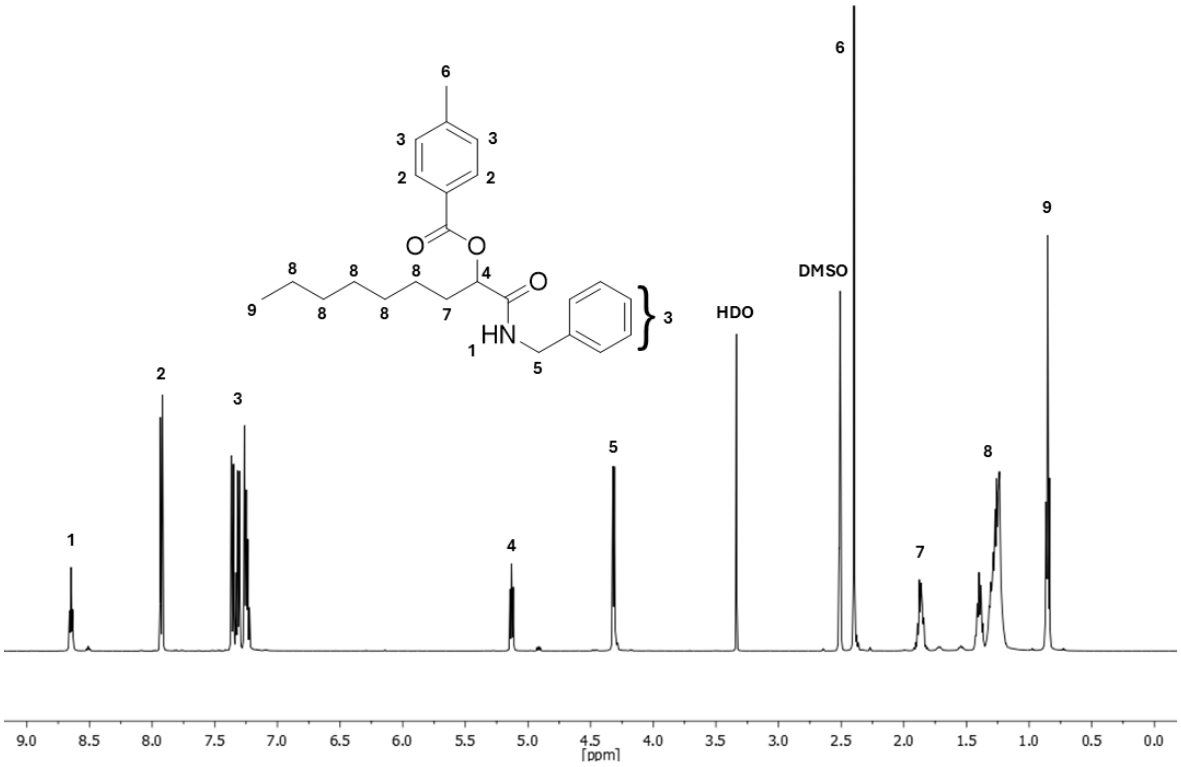

Supplementary Figure 64 ^{1}H-NMR of 1-(benzylamino)-1-oxononan-2-yl 4-methylbenzoate measured in DMSO-d_6 plotted as signal intensity versus chemical shift in ppm.

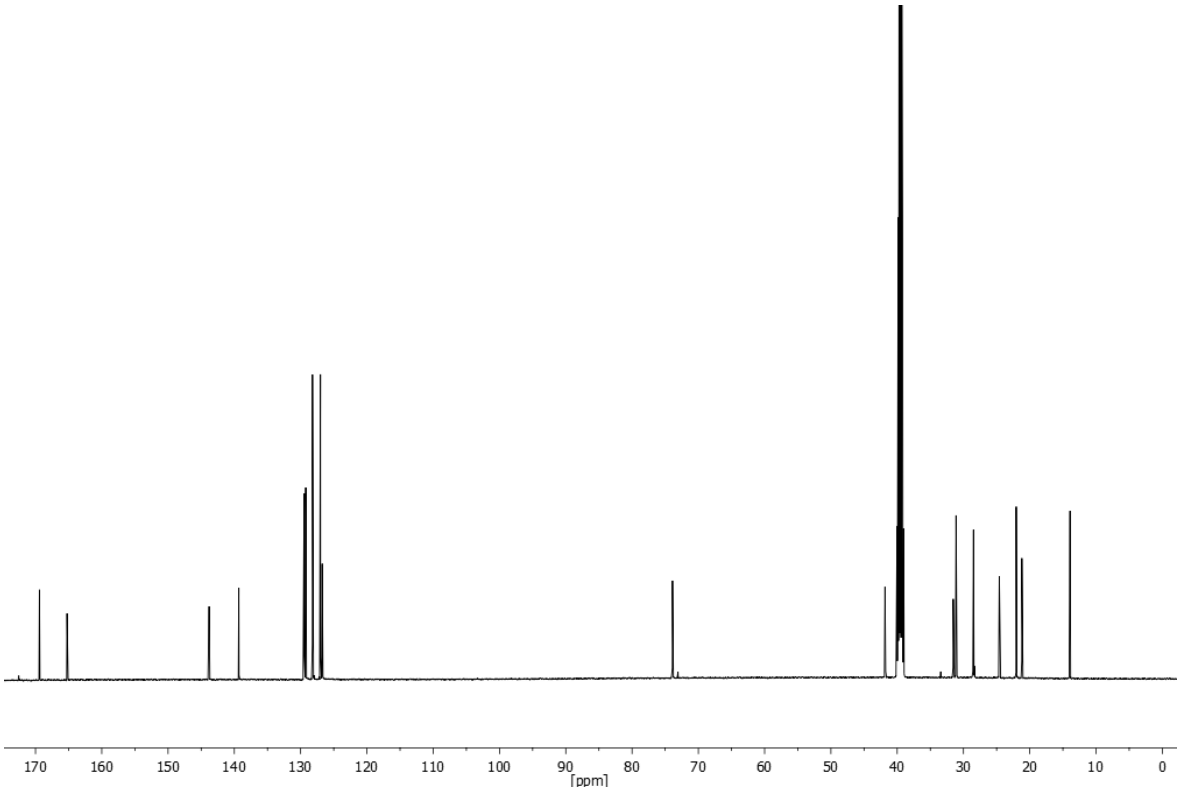

Supplementary Figure 65 ^{13}C-NMR of 1-(benzylamino)-1-oxononan-2-yl 4-methylbenzoate measured in DMSO-d_6 (septet signal at 39.52 ppm) and plotted as signal intensity versus chemical shift in ppm.

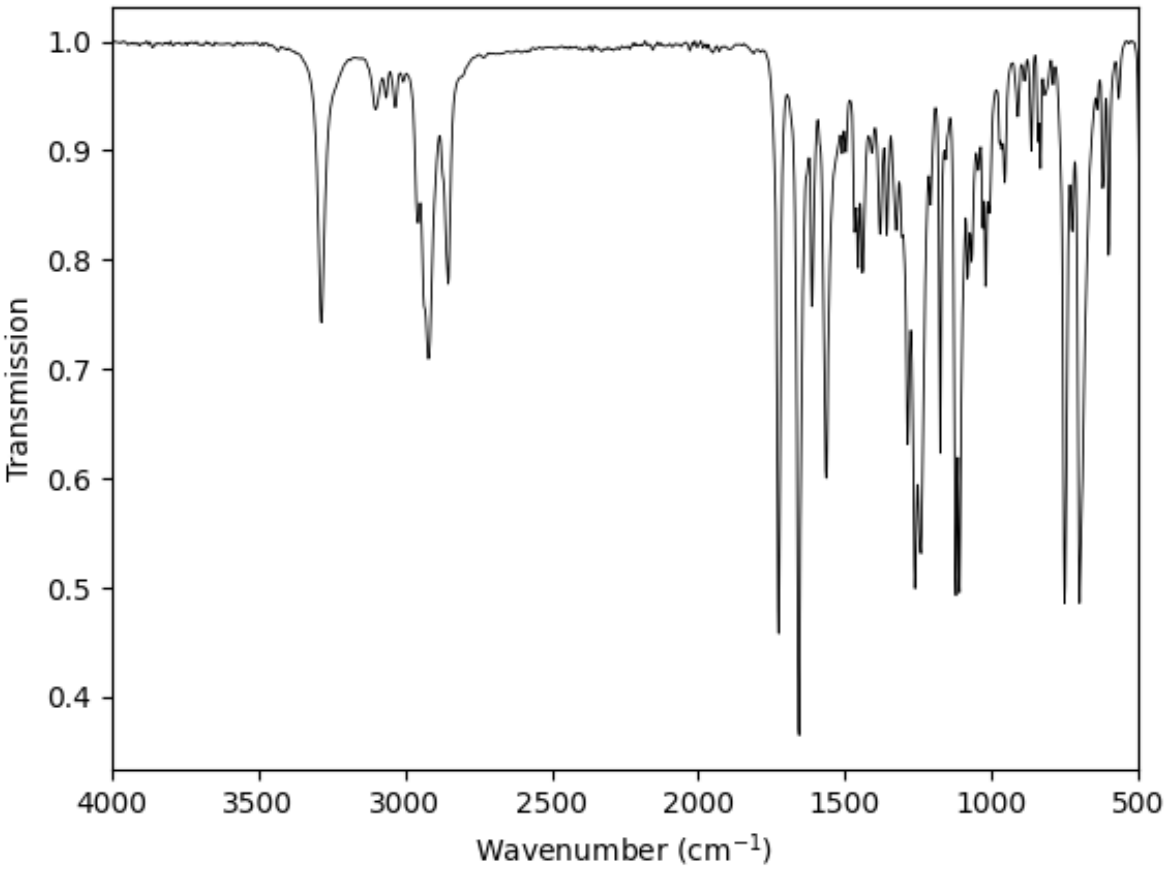

Supplementary Figure 66 IR-spectra of 1-(benzylamino)-1-oxononan-2-yl 4-methylbenzoate.

Synthesis of 1-(benzylamino)-1-oxononan-2-yl 4-methylbenzoate

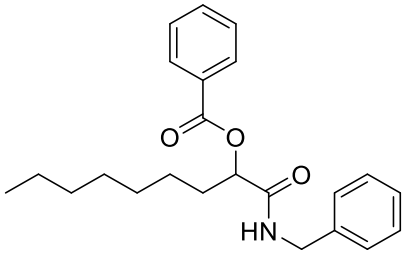

39.0 µL octanal (32.0 mg, 250 µmol, 1.00 eq.), 30.5 mg of benzoic acid (250 µmol, 1.00 eq.) and 30.4 µL of benzyl isocyanide (29.3 mg, 250 µmol, 1.00 eq.) were used in 10 mL *n*-hexane following the general procedure for the synthesis of Passerini products. The final product was obtained after purification *via* column chromatography (cyclohexane/ethyl acetate 10/1→1/1) and the pure product was obtained as a white powdery solid (4.9 mg, 12.5 µmol) with a yield of 5%.

Rf = 0.13 in cyclohexane/ethyl acetate 6/1 visualised *via* UV quenching at 254 nm and $KMnO_4$.

^{1}H-NMR (500 MHz, DMSO-d_6) δ/ppm = 8.66 (t, J = 6.0 Hz, 1H, ^{1}), 8.09 – 7.99 (m, 2H, ^{2}), 7.77 – 7.64 (m, 1H, ^{3}), 7.55 (t, J = 7.8 Hz, 2H, ^{4}), 7.36 – 7.18 (m, 5H, ^{5}), 5.15 (dd, J = 7.1, 5.4 Hz, 1H, ^{6}), 4.31 (d, J = 6.0 Hz, 2H, ^{7}), 1.95 – 1.81 (m, 2H, ^{8}), 1.40 (h, J = 7.7 Hz, 2H, ^{9}), 1.26 (tdd, J = 14.1, 10.7, 6.1 Hz, 9H, ^{10}), 0.89 – 0.78 (m, 3H, ^{11}).

^{13}C-NMR (126 MHz, DMSO-d_6) δ/ppm = 169.8, 165.7, 139.8, 134.0, 130.0, 129.9, 129.2, 128.7, 127.5, 127.2, 74.6, 42.3, 32.0, 31.6, 29.0, 29.0, 25.1, 22.5, 14.4.

HRMS-EI-MS m/z: [M] calculated for $[C_{23}H_{30}NO_3]^+$ = 368.22202, found: 368.22114.

IR (ATR platinum diamond) ν/cm^{-1} = 3281 (m), 3096 (vw), 3065 (vw), 2956 (w), 2935 (m), 2921 (m), 2853 (w), 1728 (s), 1658 (s), 1602 (w), 1565 (m), 1493 (w), 1467 (w), 1452 (m), 1436 (w), 1380 (w), 1356 (w), 1333 (w), 1314 (m), 1300 (w), 1284 (m), 1275 (m), 1257 (s), 1240 (s), 1175 (m), 1154 (w), 1148 (w), 1117 (s), 1082 (w), 1072 (m), 1047 (w), 1026 (m), 1002 (w), 989 (vw), 971 (vw), 954 (w), 907 (vw), 860 (w), 763 (w), 749 (m), 724 (w), 697 (vs), 685 (s), 619 (w), 605 (m), 566 (vw), 490 (m), 469 (w).

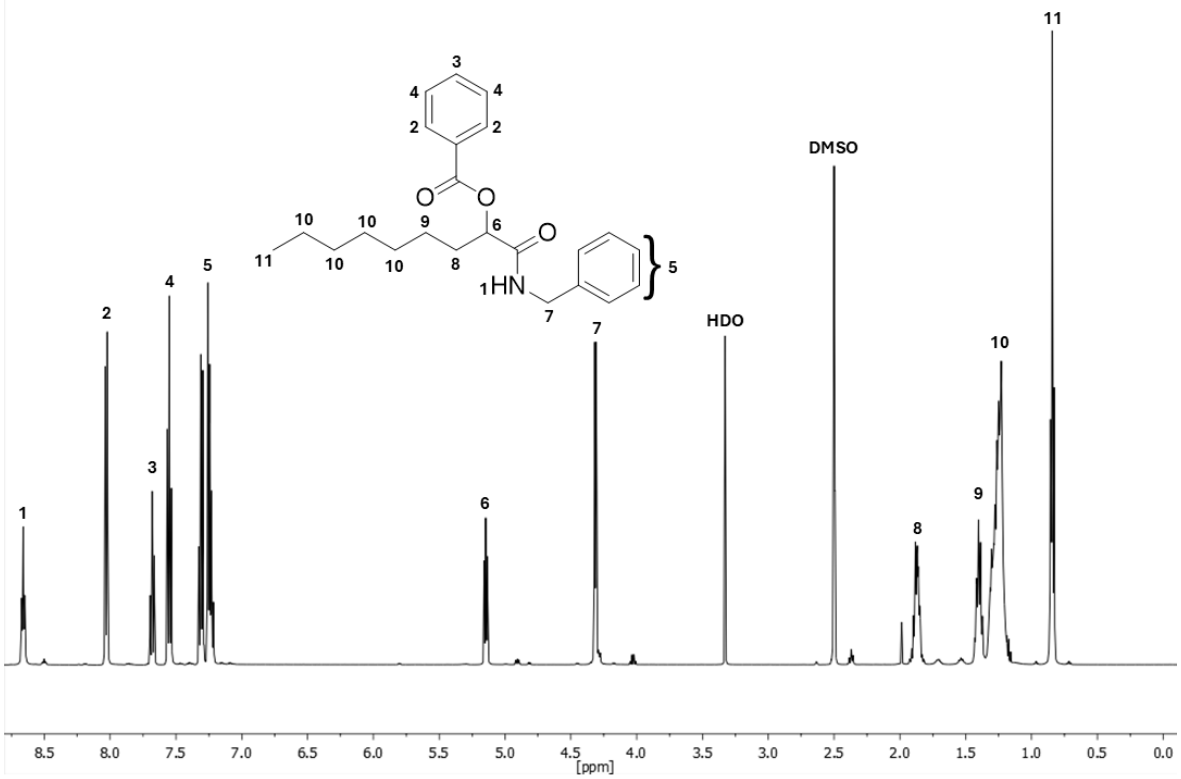

Supplementary Figure 67 ^{1}H-NMR of 1-(benzylamino)-1-oxononan-2-yl benzoate measured in DMSO-d_6 plotted as signal intensity versus chemical shift in ppm.

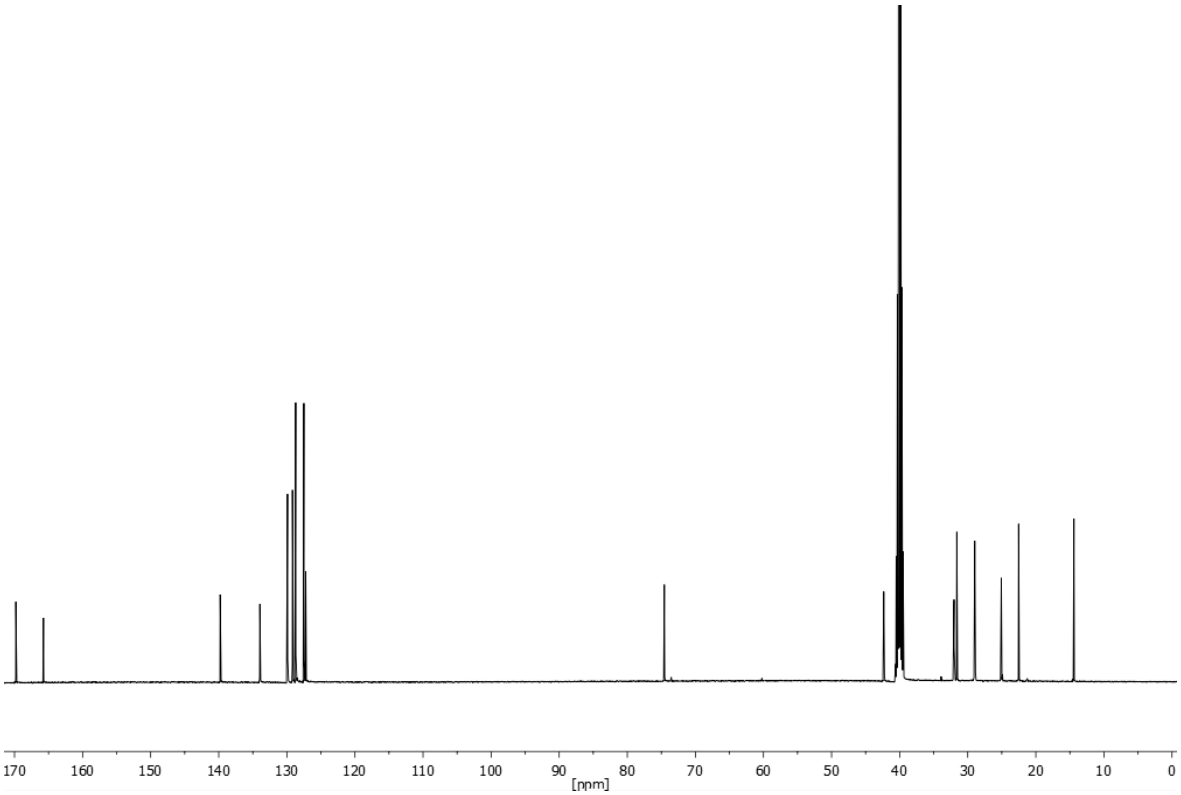

Supplementary Figure 68 ^{13}C-NMR of 1-(benzylamino)-1-oxononan-2-yl benzoate measured in DMSO-d_6 (septet signal at 39.52 ppm) and plotted as signal intensity versus chemical shift in ppm.

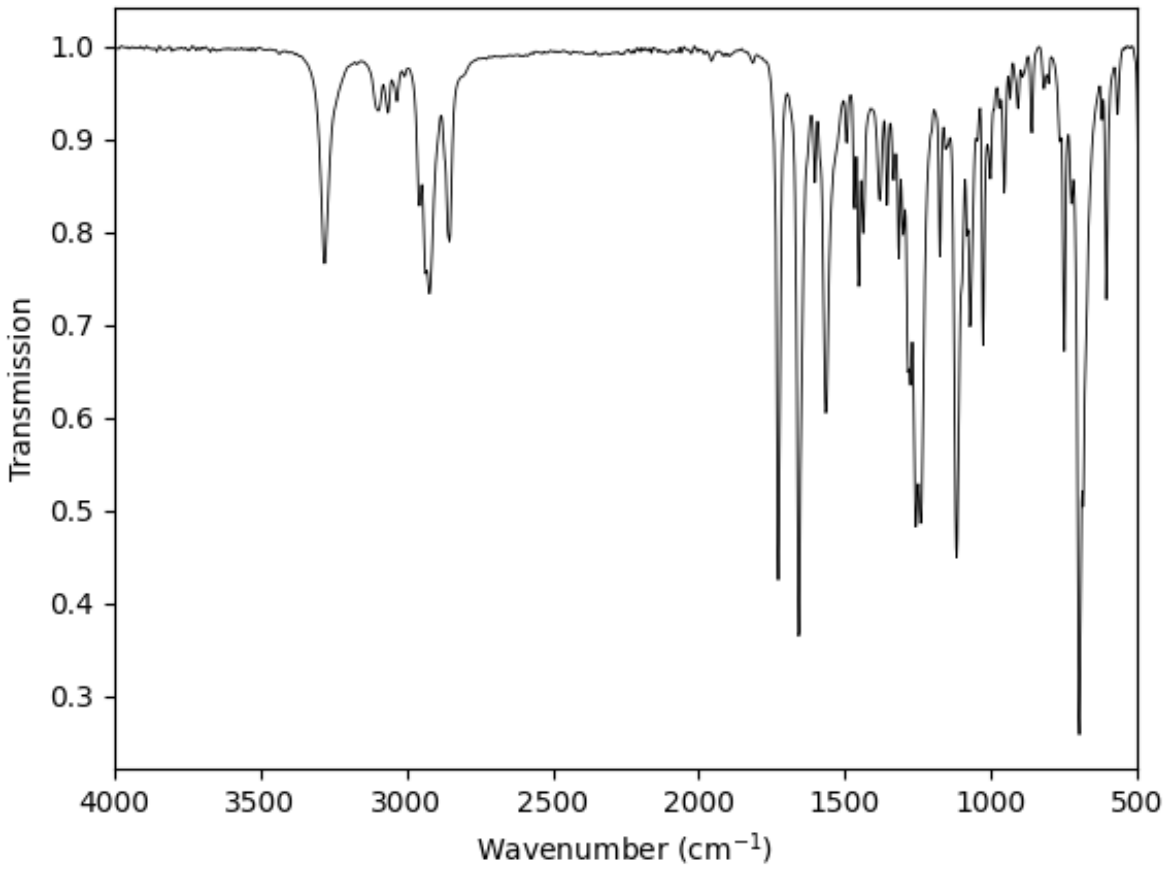

Supplementary Figure 69 IR-spectra of 1-(benzylamino)-1-oxononan-2-yl benzoate.

Synthesis of 1-oxo-1-(phenylamino)nonan-2-yl acetate

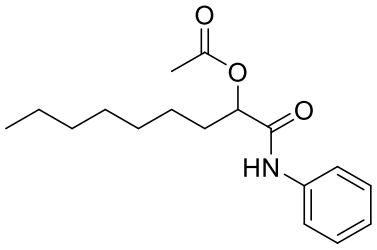

39.0 µL octanal (32.0 mg, 250 µmol, 1.00 eq.), 14.3 µL of acetic acid (15.0 mg 250 µmol, 1.00 eq.) and 25.3 µL of isocyanobenzene (25.8 mg, 250 µmol, 1.00 eq.) were used in 10 mL *n*-hexane following the general procedure for the synthesis of Passerini products. The final product was obtained after purification *via* column chromatography (cyclohexane/ethyl acetate 10/1→1/1) and the pure product was obtained as a white powdery solid (5.1 mg, 17.5 µmol) with a yield of 7%.

Rf = 0.08 in cyclohexane/ethyl acetate 6/1 visualised *via* UV quenching at 254 nm and $KMnO_4$.

^{1}H-NMR (500 MHz, DMSO-d_6) δ/ppm = 10.04 (s, 1H, [1]), 7.67 – 7.50 (m, 2H, [2]), 7.38 – 7.23 (m, 2H, [3]), 7.15 – 6.98 (m, 1H, [4]), 4.94 (dd, J = 7.4, 5.6 Hz, 1H, [5]), 2.09 (s, 3H, [6]), 1.85 – 1.71 (m, 2H, [7]), 1.48 – 1.15 (m, 10H, [8]), 0.91 – 0.79 (m, 3H, [9]).

^{13}C-NMR (126 MHz, DMSO-d_6) δ/ppm = 170.6, 168.7, 139.0, 129.2, 124.0, 119.9, 74.2, 31.8, 31.6, 29.1, 29.0, 25.1, 22.5, 21.1, 14.4.

HRMS-EI-MS m/z: [M] calculated for $[C_{17}H_{26}NO_3]^+$ = 292.19072, found: 292.18986.

IR (ATR platinum diamond) $\tilde{\nu}$/cm^{-1} = 3312 (w), 3303 (w), 3297 (w), 3289 (w), 3217 (vw), 3205 (vw), 3141 (vw), 3061 (vw), 2954 (m), 2925 (m), 2855 (m), 1746 (s), 1672 (s), 1619 (w), 1600 (s), 1539 (s), 1500 (m), 1465 (w), 1444 (s), 1372 (m), 1314 (m), 1228 (vs), 1179 (w), 1133 (w), 1121 (w), 1072 (m), 1045 (m), 950 (vw), 930 (w), 903 (w), 753 (s), 724 (w), 691 (s), 654 (w), 605 (w), 506 (w), 479 (w), 448 (vw).

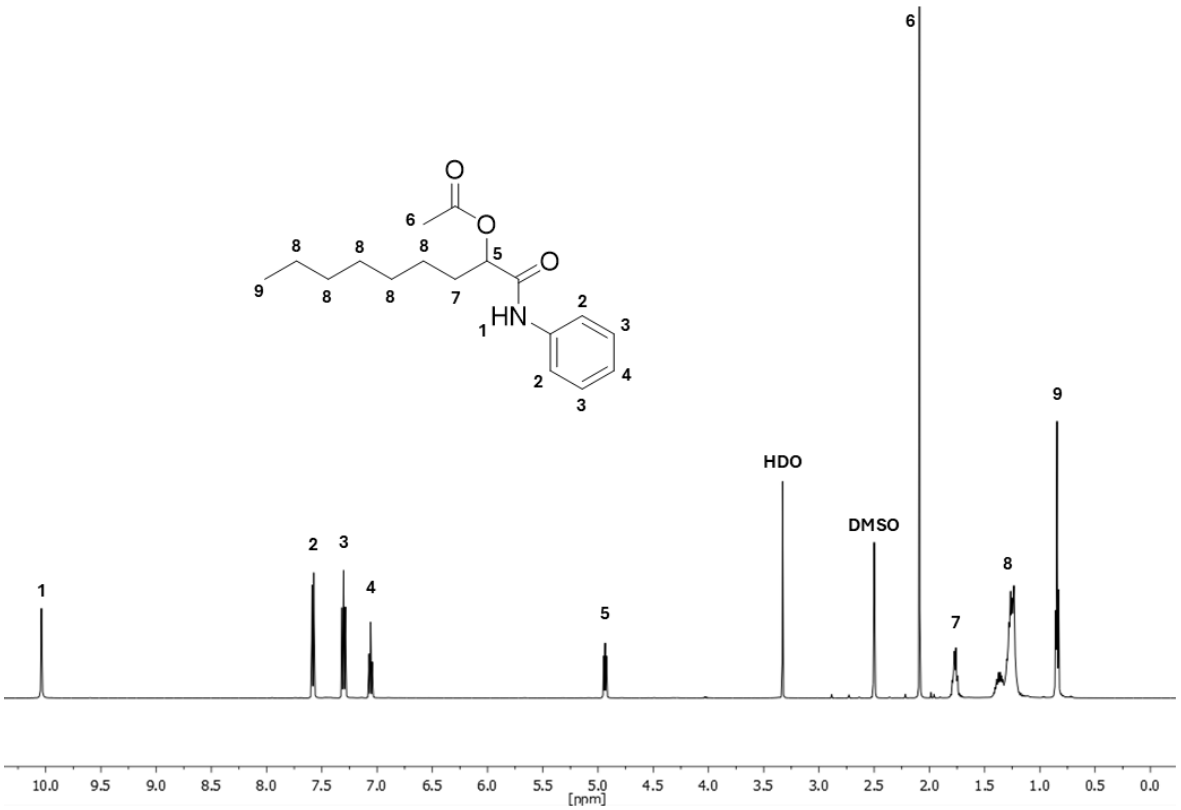

Supplementary Figure 70 ^{1}H-NMR of 1-oxo-1-(phenylamino)nonan-2-yl acetate measured in DMSO-d_6 plotted as signal intensity versus chemical shift in ppm.

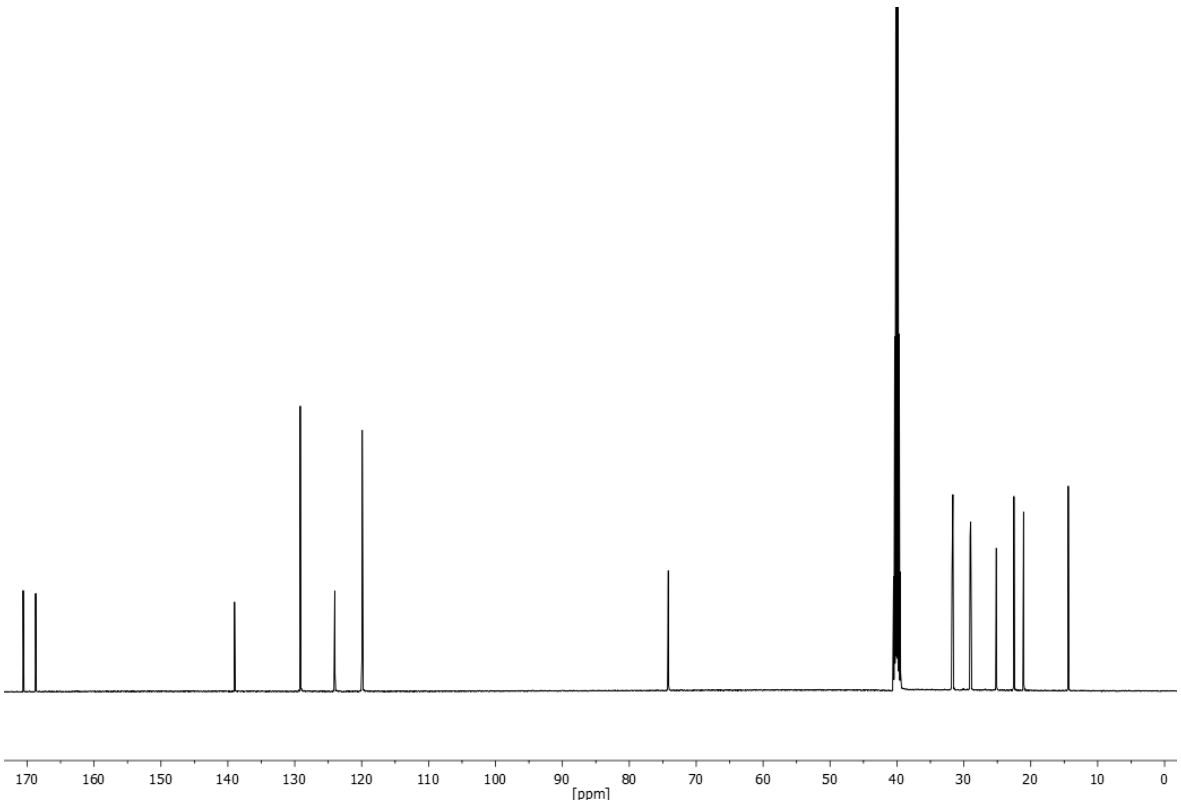

Supplementary Figure 71 ^{13}C-NMR of 1-oxo-1-(phenylamino)nonan-2-yl acetate measured in DMSO-d_6 (septet signal at 39.52 ppm) and plotted as signal intensity versus chemical shift in ppm.

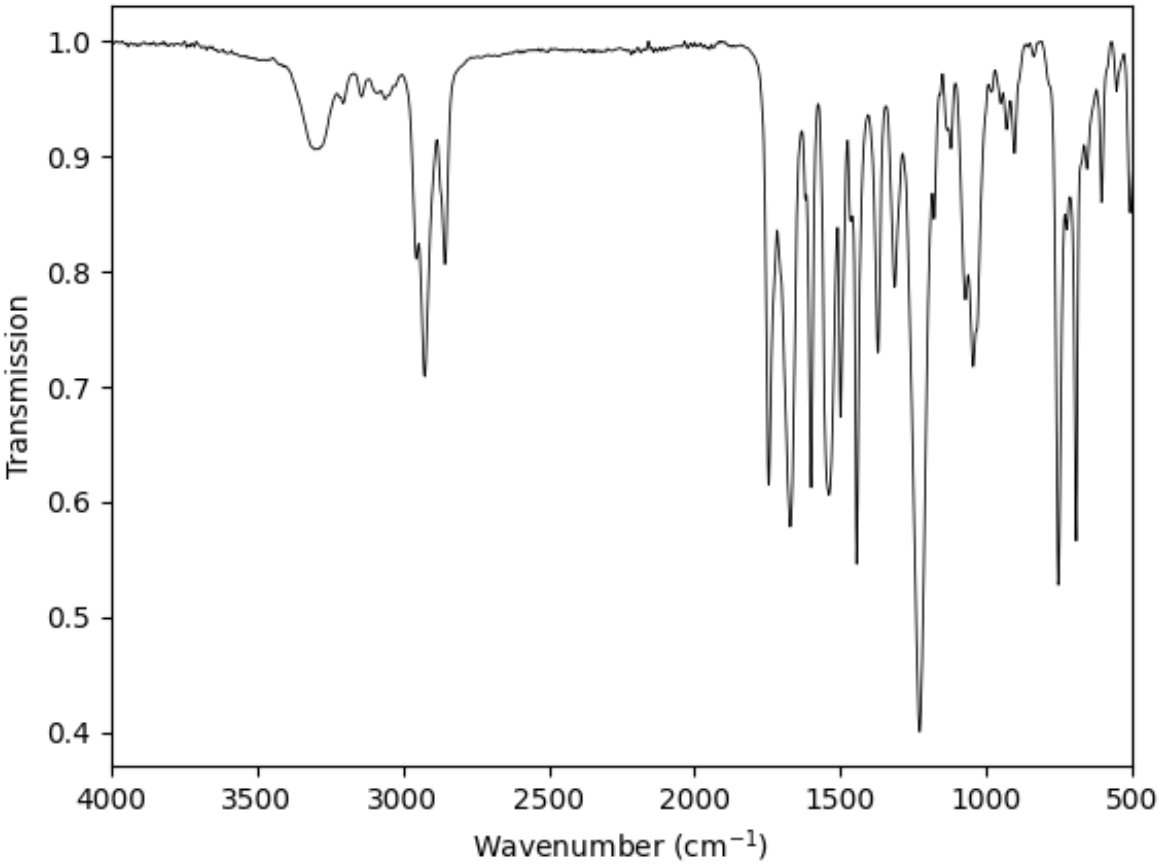

Supplementary Figure 72 IR-spectra of 1-oxo-1-(phenylamino)nonan-2-yl acetate.

Synthesis of 1-(butylamino)-1-oxononan-2-yl acetate

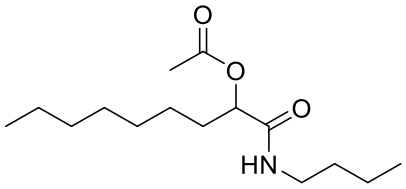

39.0 µL octanal (32.0 mg, 250 µmol, 1.00 eq.), 14.3 µL of acetic acid (15.0 mg 250 µmol, 1.00 eq.) and 25.3 µL of isocyanobenzene (25.8 mg, 250 µmol, 1.00 eq.) were used in 10 mL *n*-hexane following the general procedure for the synthesis of Passerini products. The final product was obtained after purification *via* column chromatography (cyclohexane/ethyl acetate 10/1→1/1) and the pure product 1-(butylamino)-1-oxononan-2-yl acetate was obtained as a white powdery solid (5.1 mg, 17.5 µmol) with a yield of 7%.

Rf = 0.08 in cyclohexane/ethyl acetate 6/1 visualised *via* UV quenching at 254 nm and $KMnO_4$.

^{1}H-NMR (500 MHz, DMSO-d_6) δ/ppm = 7.92 (t, J = 5.8 Hz, 1H, [1]), 4.85 – 4.73 (m, 1H, [2]), 3.11 – 2.96 (m, 2H, [3]), 2.05 (s, 3H, [4]), 1.72 – 1.58 (m, 2H, [5]), 1.44 – 1.32 (m, 2H, [6]), 1.34 – 1.16 (m, 12H, [7]), 0.91 – 0.82 (m, 6H, [8]).

^{13}C-NMR (126 MHz, DMSO-d_6) δ/ppm = 170.4, 169.6, 73.8, 38.4, 31.9, 31.6, 29.0, 29.0, 25.0, 22.5, 21.2, 19.9, 14.4, 14.1.

HRMS-EI-MS m/z: [M] calculated for $[C_{15}H_{30}NO_3]^+$ = 272.22202, found: 272.22180.

IR (ATR platinum diamond) $\tilde{\nu}$/cm^{-1} = 3287 (m), 3102 (w), 2954 (m), 2915 (m), 2869 (m), 2851 (m), 1740 (vs), 1656 (vs), 1567 (s), 1469 (m), 1444 (m), 1368 (s), 1329 (w), 1302 (w), 1271 (m), 1238 (vs), 1212 (m), 1150 (w), 1123 (w), 1086 (m), 1065 (m), 1043 (w), 1026 (m), 981 (w), 967 (w), 950 (w), 932 (w), 919 (w), 878 (w), 759 (w), 740 (w), 722 (w), 695 (m), 648 (w), 605 (w), 543 (vw), 457 (w).

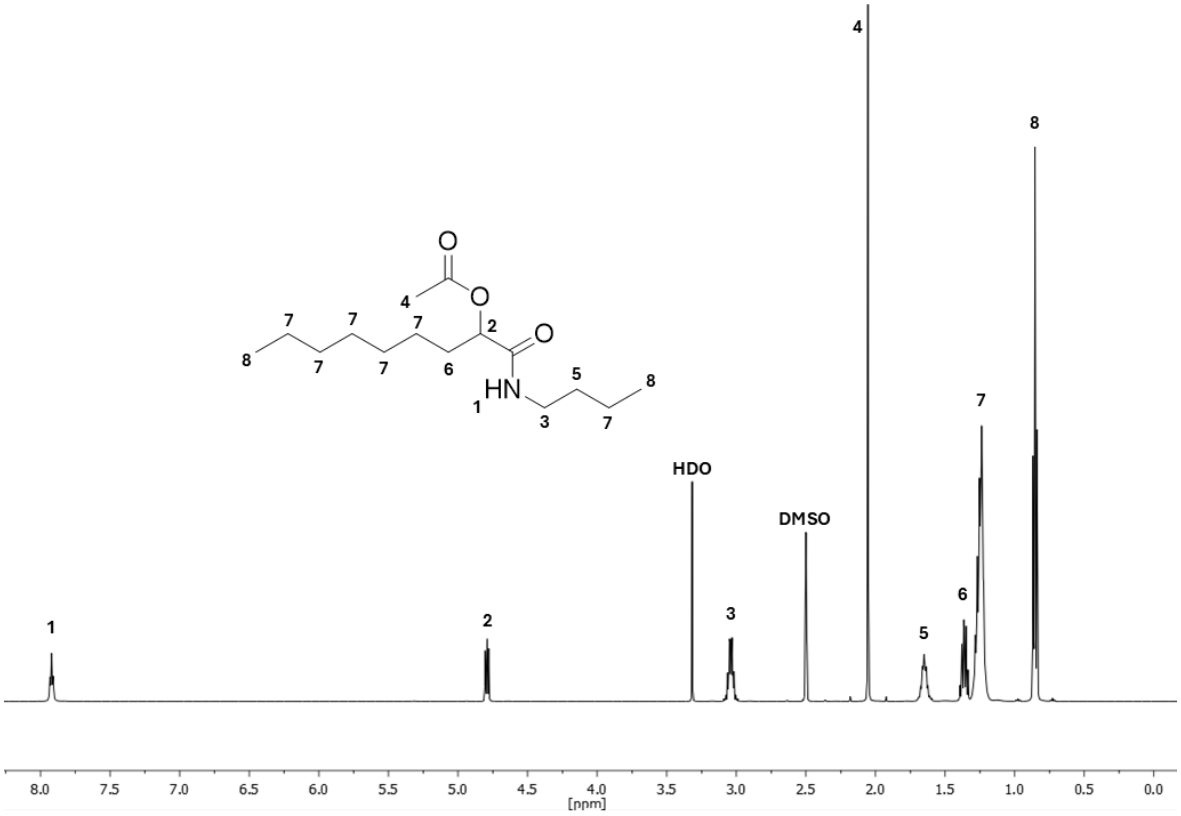

Supplementary Figure 73 ^{1}H-NMR of 1-(butylamino)-1-oxononan-2-yl acetate measured in DMSO-d_6 plotted as signal intensity versus chemical shift in ppm.

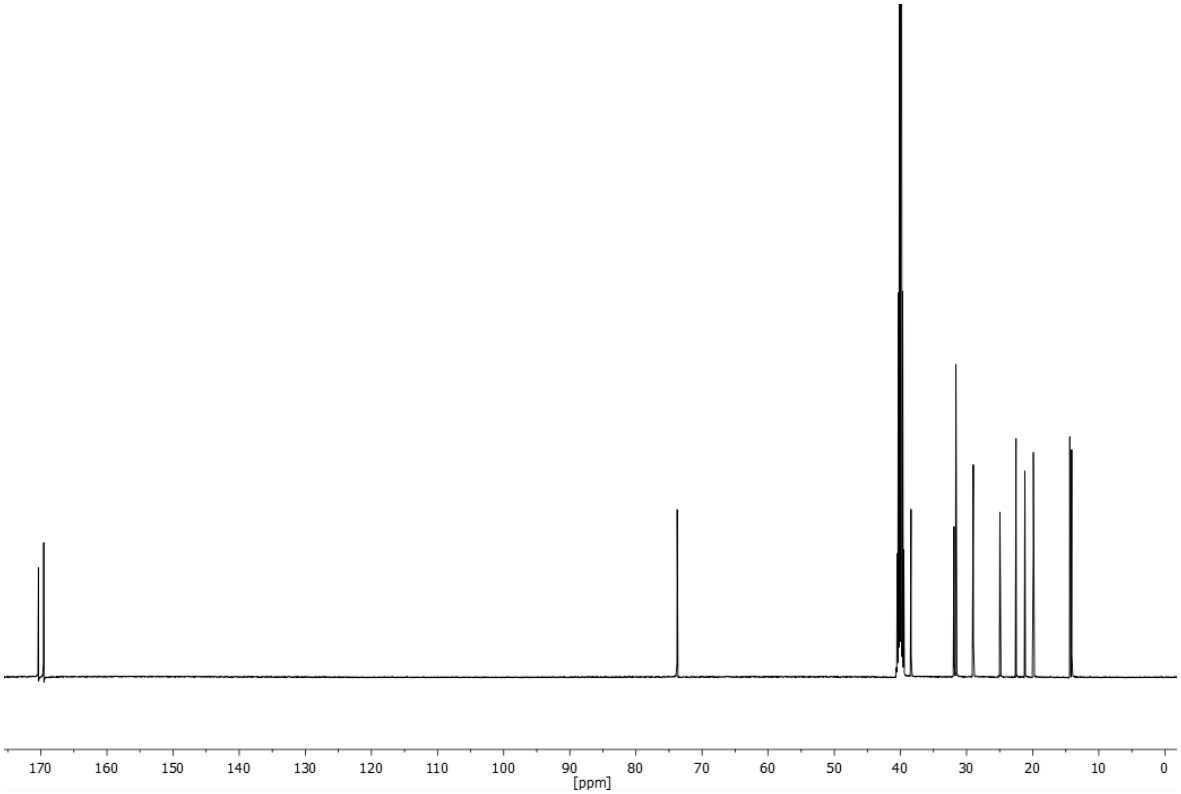

Supplementary Figure 74 ^{13}C-NMR of 1-(butylamino)-1-oxononan-2-yl acetate measured in DMSO-d_6 (septet signal at 39.52 ppm) and plotted as signal intensity versus chemical shift in ppm.

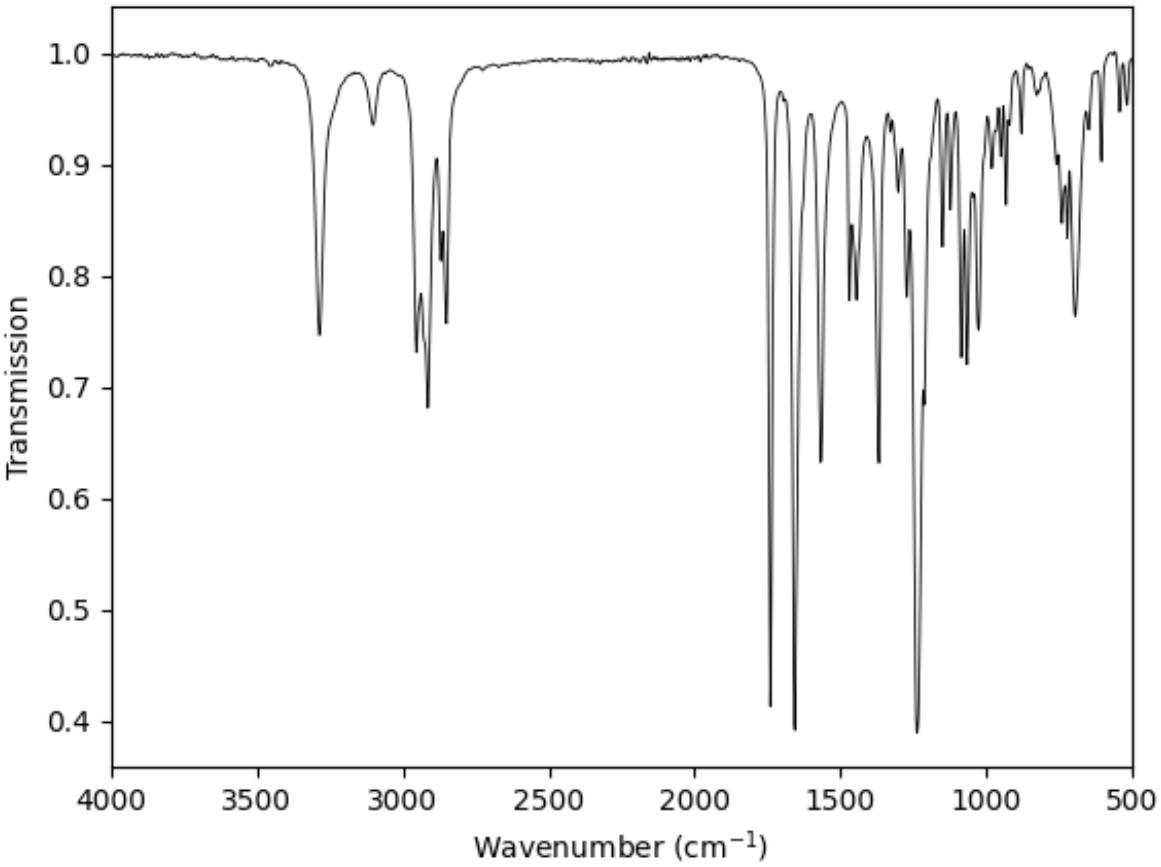

Supplementary Figure 75 IR-spectra of 1-(butylamino)-1-oxononan-2-yl acetate.

Synthesis of 1-(cyclohexylamino)-1-oxononan-2-yl acetate

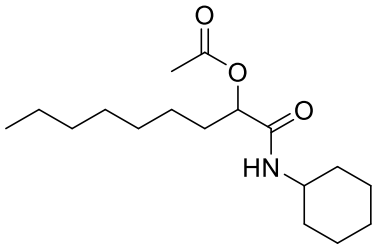

39.0 µL octanal (32.0 mg, 250 µmol, 1.00 eq.), 14.3 µL of acetic acid (15.0 mg 250 µmol, 1.00 eq.) and 31.1 µL of isocyanocyclohexane (27.3mg, 250 µmol, 1.00 eq.) were used in 10 mL *n*-hexane following the general procedure for the synthesis of Passerini products. The final product was obtained after purification *via* column chromatography (cyclohexane/ethyl acetate 10/1→1/1) and the pure product 1-(cyclohexylamino)-1-oxononan-2-yl acetate was obtained as a white powdery solid (15.6 mg, 52.5 µmol) with a yield of 21%.

Rf = 0.14 in cyclohexane/ethyl acetate 5/1 visualised *via* UV quenching at 254 nm and $KMnO_4$.

^{1}H-NMR (400 MHz, DMSO-d_6) δ/ppm = 7.78 (d, J = 8.0 Hz, 1H, [1]), 4.78 (t, J = 6.4 Hz, 1H, [2]), 3.65 – 3.43 (m, 1H, [3]), 2.04 (s, 3H, [4]), 1.82 – 1.47 (m, 8H, [5]), 1.38 – 1.05 (m, 16H, [6]), 0.86 (t, J = 6.6 Hz, 3H, [7]).

^{13}C-NMR (101 MHz, DMSO-d_6) δ/ppm = 170.3, 168.7, 73.7, 47.9, 32.7, 32.7, 31.9, 31.6, 29.0, 29.0, 25.6, 25.1, 25.0, 25.0, 22.5, 21.2, 14.4.

HRMS-EI-MS m/z: [M] calculated for $[C_{17}H_{31}NO_3]^+$ = 298.23767, found: 298.23733.

IR (ATR platinum diamond) ν/cm^{-1} = 3279 (m), 3094 (vw), 2927 (m), 2851 (m), 1744 (s), 1654 (vs), 1627 (w), 1561 (s), 1495 (vw), 1467 (w), 1444 (m), 1370 (m), 1331 (w), 1312 (w), 1261 (m), 1234 (vs), 1212 (m), 1189 (w), 1152 (m), 1123 (w), 1096 (m), 1074 (m), 1047 (w), 1026 (m), 983 (w), 948 (w), 930 (w), 893 (w), 876 (w), 819 (vw), 769 (w), 759 (w), 722 (w), 697 (m), 650 (w), 603 (w), 586 (w), 485 (w), 467 (w), 453 (vw), 446 (vw), 428 (m).

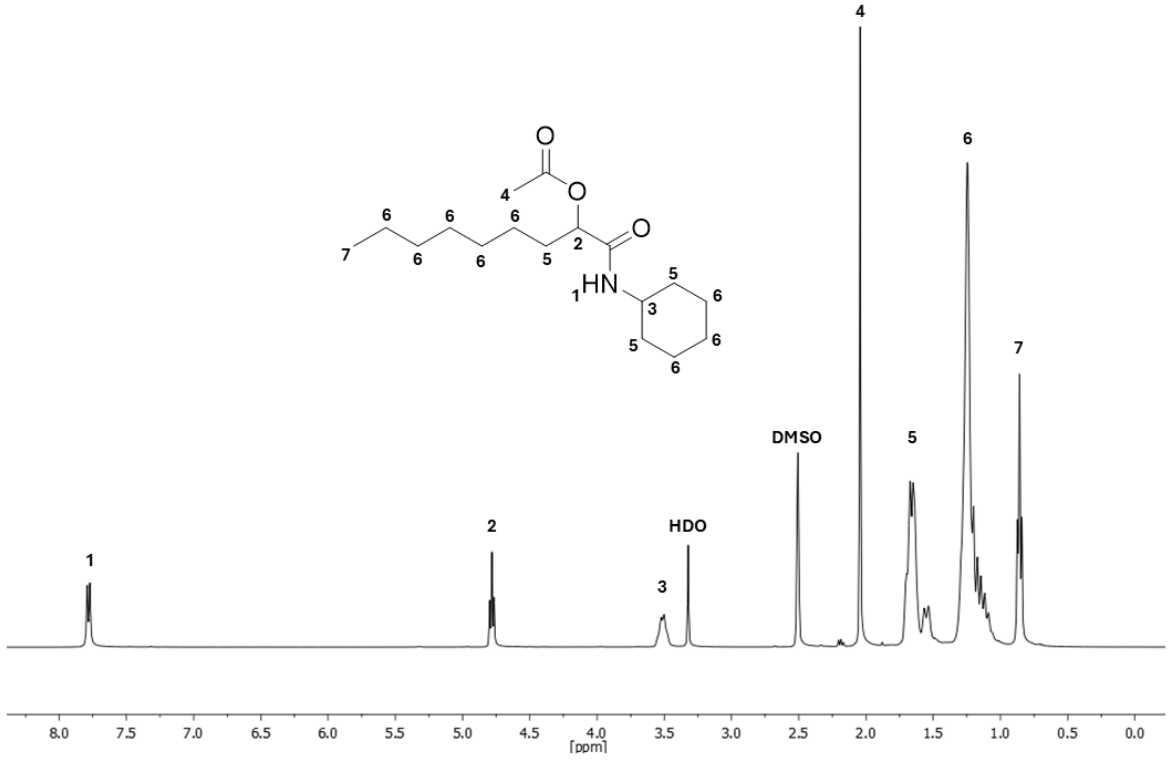

Supplementary Figure 76 ^{1}H-NMR of 1-(cyclohexylamino)-1-oxononan-2-yl acetate measured in DMSO-d_6 plotted as signal intensity versus chemical shift in ppm.

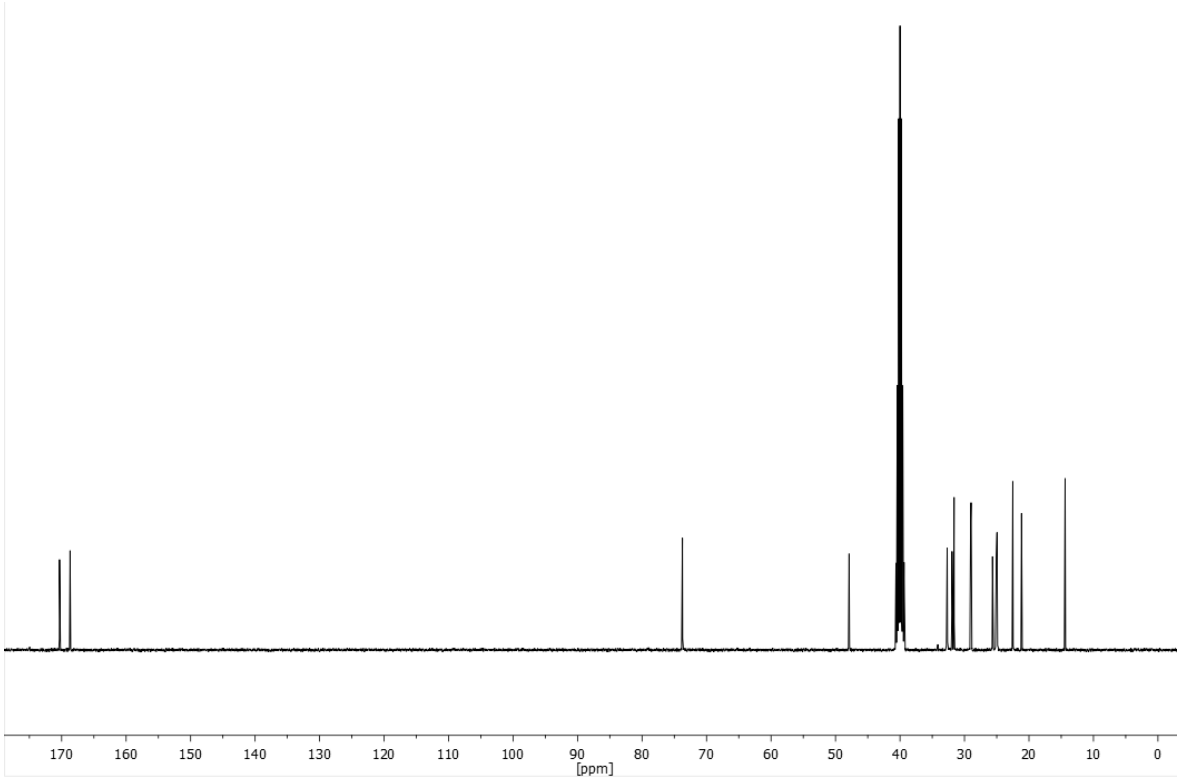

Supplementary Figure 77 ^{13}C-NMR of 1-(cyclohexylamino)-1-oxononan-2-yl acetate measured in DMSO-d_6 (septet signal at 39.52 ppm) and plotted as signal intensity versus chemical shift in ppm.

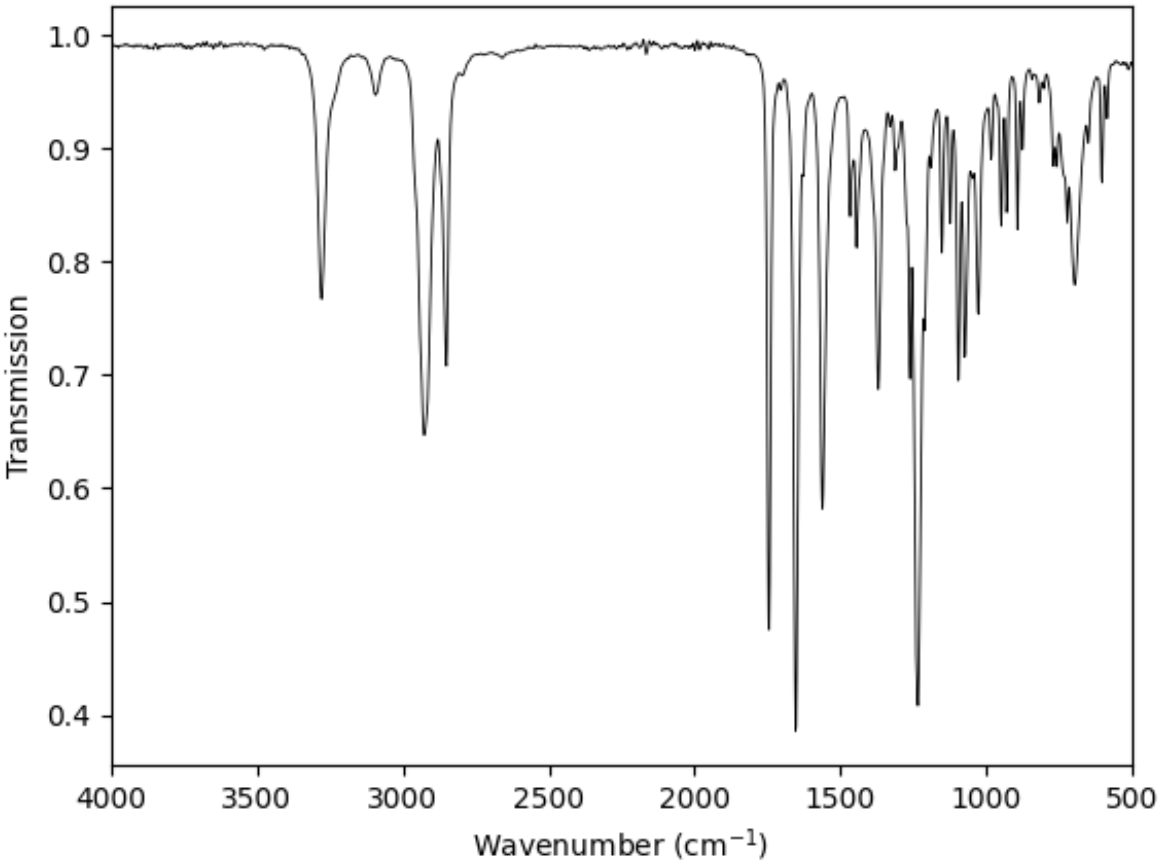

Supplementary Figure 78 IR-spectra of 1-(cyclohexylamino)-1-oxononan-2-yl acetate.

Synthesis of 1-(benzylamino)-1-oxononan-2-yl 2-phenylacetate

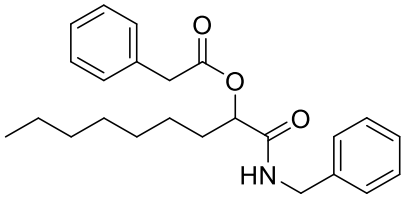

39.0 µL octanal (32.0 mg, 250 µmol, 1.00 eq.), 34.0 mg of phenylacetic acid (250 µmol, 1.00 eq.) and 30.4 µL of benzyl isocyanide (29.3 mg, 250 µmol, 1.00 eq.) were used in 10 mL *n*-hexane following the general procedure for the synthesis of Passerini products. The final product was obtained after purification *via* column chromatography (cyclohexane/ethyl acetate 10/1→1/1) and the pure product 1-(benzylamino)-1-oxononan-2-yl 2-phenylacetate was obtained as a white powdery solid (24.8 mg, 65 µmol) with a yield of 26%.

Rf = 0.15 in cyclohexane/ethyl acetate 5/1 visualised *via* UV quenching at 254 nm and $KMnO_4$.

^{1}H-NMR (400 MHz, DMSO-d_6) δ/ppm = 8.54 (t, J = 6.0 Hz, 1H, [1]), 7.40 – 7.17 (m, 10H,[2]), 4.92 (t, J = 6.4 Hz, 1H, [3]), 4.30 (d, J = 6.0 Hz, 2H, [4]), 3.85 – 3.69 (m, 2H, [5]), 1.81 – 1.65 (m, 2H, [6]), 1.34 – 1.15 (m, 10H, [7]), 0.92 – 0.79 (m, 3H, [8]).

^{13}C-NMR (101 MHz, DMSO-d_6) δ/ppm = 171.2, 169.8, 139.7, 134.7, 129.8, 128.8, 128.7, 127.5, 127.3, 127.2, 74.0, 42.3, 31.9, 31.6, 29.0, 28.9, 24.9, 22.5, 14.4.

HRMS-EI-MS m/z: [M] calculated for $[C_{24}H_{32}NO_3]^+$ = 382.24438, found: 382.23741.

IR (ATR platinum diamond) $\tilde{\nu}$/cm^{-1} = 3308 (w), 3297 (w), 3087 (vw), 3065 (w), 3032 (w), 2954 (m), 2925 (m), 2855 (m), 1740 (s), 1656 (s), 1604 (w), 1586 (w), 1530 (m), 1495 (m), 1454 (m), 1432 (w), 1376 (w), 1358 (w), 1329 (w), 1296 (w), 1240 (s), 1137 (s), 1076 (m), 1028 (m), 1006 (w), 969 (w), 946 (vw), 720 (s), 695 (vs), 648 (w), 619 (w), 597 (w), 566 (vw), 522 (w), 510 (w), 471 (w), 459 (w).

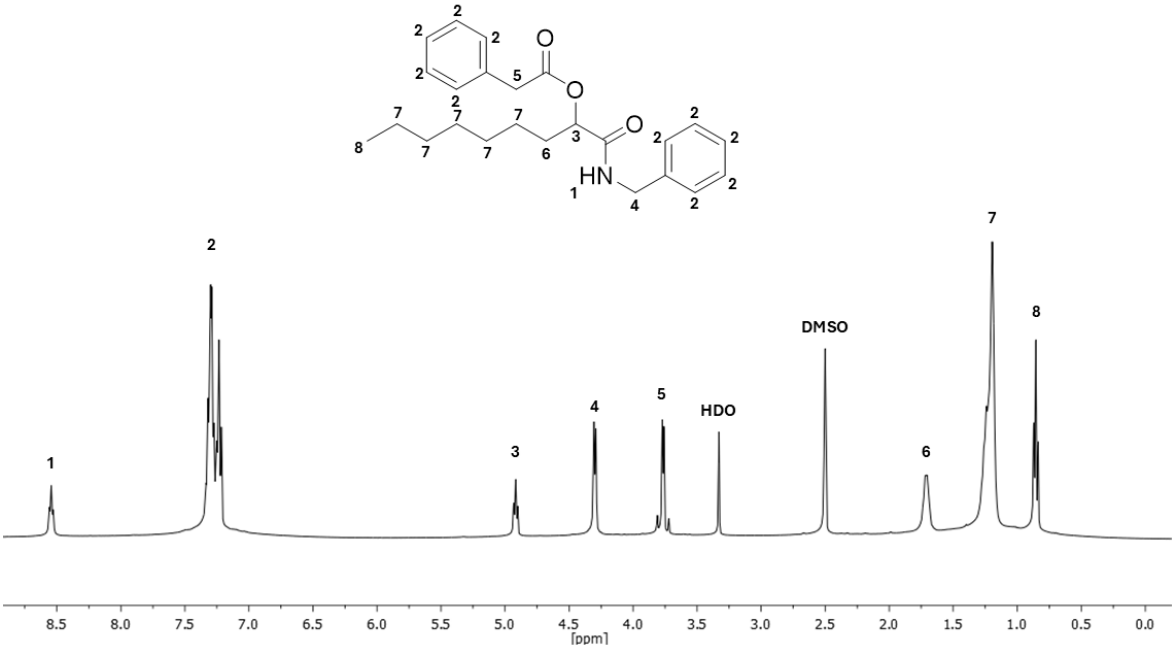

Supplementary Figure 79 ^{1}H-NMR of 1-(benzylamino)-1-oxononan-2-yl 2-phenylacetate measured in DMSO-d_6 plotted as signal intensity versus chemical shift in ppm.

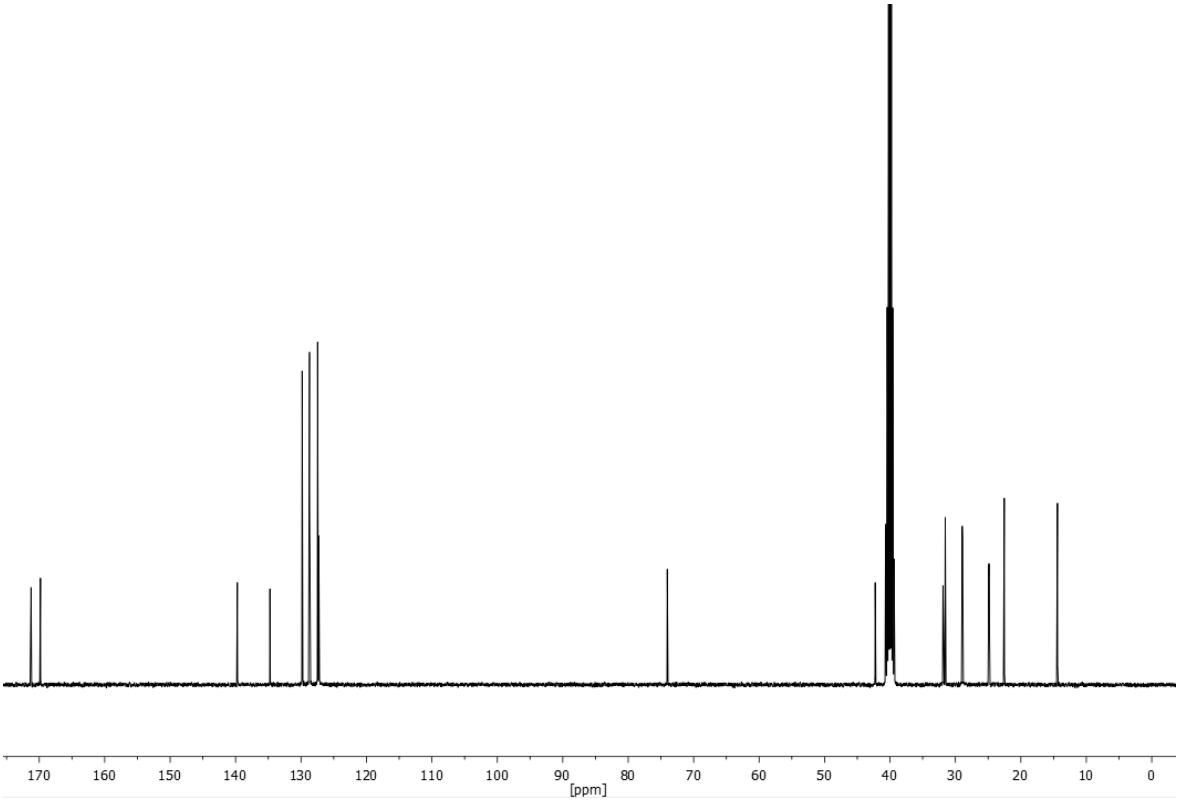

Supplementary Figure 80 ^{13}C-NMR of 1-(benzylamino)-1-oxononan-2-yl 2-phenylacetate measured in DMSO-d_6 (septet signal at 39.52 ppm) and plotted as signal intensity versus chemical shift in ppm.

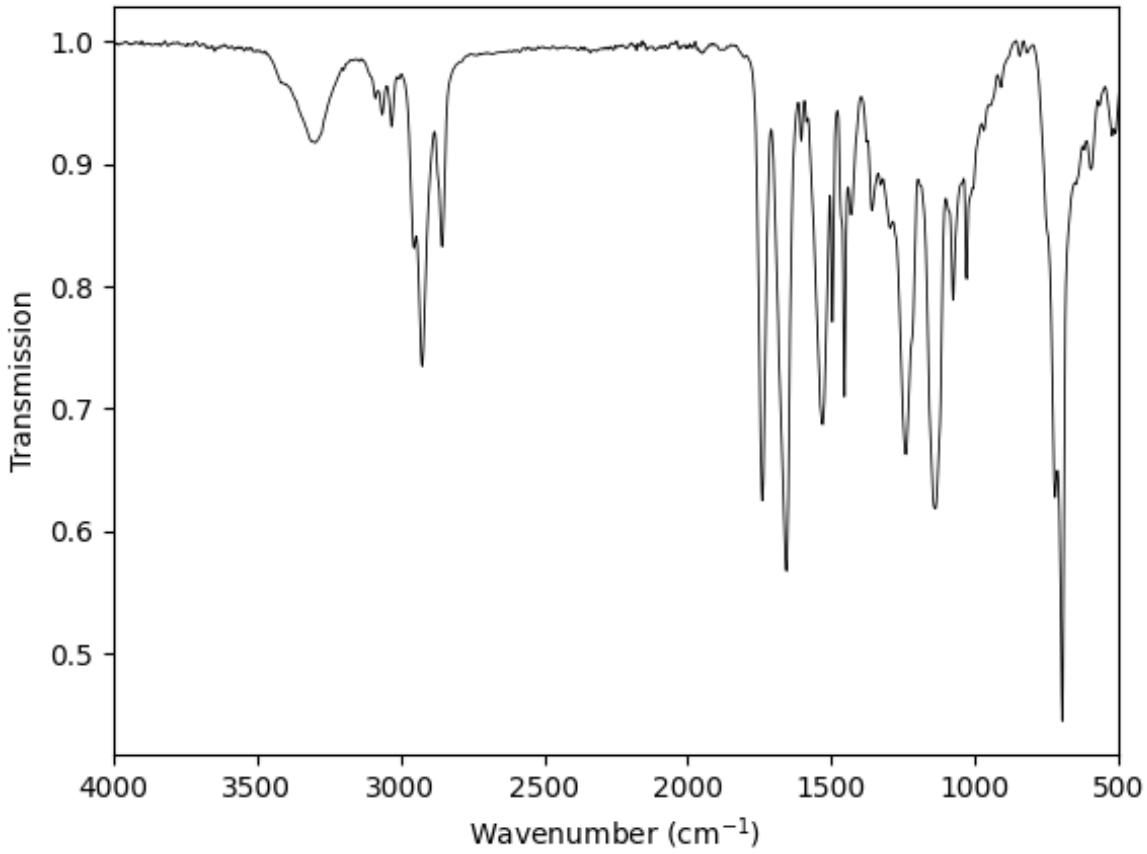

Supplementary Figure 81 IR-spectra of 1-(benzylamino)-1-oxononan-2-yl 2-phenylacetate.

Synthesis of 1-(benzylamino)-1-oxononan-2-yl acetate

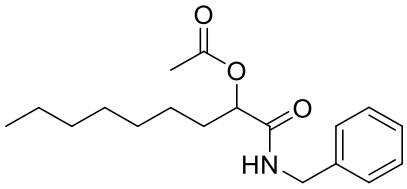

39.0 µL octanal (32.0 mg, 250 µmol, 1.00 eq.), 14.3 µL of acetic acid (15.0 mg, 250 µmol, 1.00 eq.) and 30.4 µL of benzyl isocyanide (29.3 mg, 250 µmol, 1.00 eq.) were used in 10 mL *n*-hexane following the general procedure for the synthesis of Passerini products. The final product was obtained after purification *via* column chromatography (cyclohexane/ethyl acetate 10/1→1/1) and the pure product 1-(benzylamino)-1-oxononan-2-yl acetate was obtained as a white powdery solid (23.7 mg, 77.5 µmol) with a yield of 31%.

Rf = 0.13 in cyclohexane/ethyl acetate 6/1 visualised *via* UV quenching at 254 nm and $KMnO_4$.

^{1}H-NMR (400 MHz, DMSO-d_6) δ/ppm = 8.54 (t, J = 6.1 Hz, 1H, [1]), 7.36 – 7.27 (m, 2H, [2]), 7.27 – 7.19 (m, 3H, [3]), 4.90 (t, J = 7.1 Hz, 1H, [4]), 4.37 – 4.22 (m, 2H, [5]), 2.09 (s, 3H, [6]), 1.79 – 1.65 (m, 2H, [7]), 1.34 – 1.18 (m, 10H, [8]), 0.87 (t, J = 6.8 Hz, 3H, [9]).

^{13}C-NMR (101 MHz, DMSO-d_6) δ/ppm = 170.5, 170.0, 139.8, 128.7, 127.5, 127.2, 73.8, 42.2, 31.9, 31.6, 29.0, 29.0, 25.0, 22.5, 21.2, 14.4.

HRMS-EI-MS m/z: [M] calculated for $[C_{18}H_{28}NO_3]^+$ = 306.20637, found: 306.20640.

IR (ATR platinum diamond) ν/cm^{-1} = 3299 (m), 3094 (vw), 3067 (vw), 2958 (w), 2943 (w), 2915 (m), 2871 (w), 2851 (m), 1738 (s), 1693 (w), 1662 (vs), 1606 (w), 1561 (m), 1500 (w), 1469 (w), 1454 (m), 1438 (m), 1372 (m), 1327 (w), 1314 (w), 1300 (w), 1271 (m), 1240 (vs), 1212 (m), 1148 (w), 1121 (w), 1086 (m), 1074 (m), 1049 (w), 1026 (m), 967 (w), 956 (w), 932 (w), 922 (w), 893 (vw), 876 (w), 819 (vw), 757 (w), 720 (s), 695 (s), 656 (m), 621 (w), 605 (m), 537 (w), 481 (w), 457 (m), 444 (w), 418 (w).

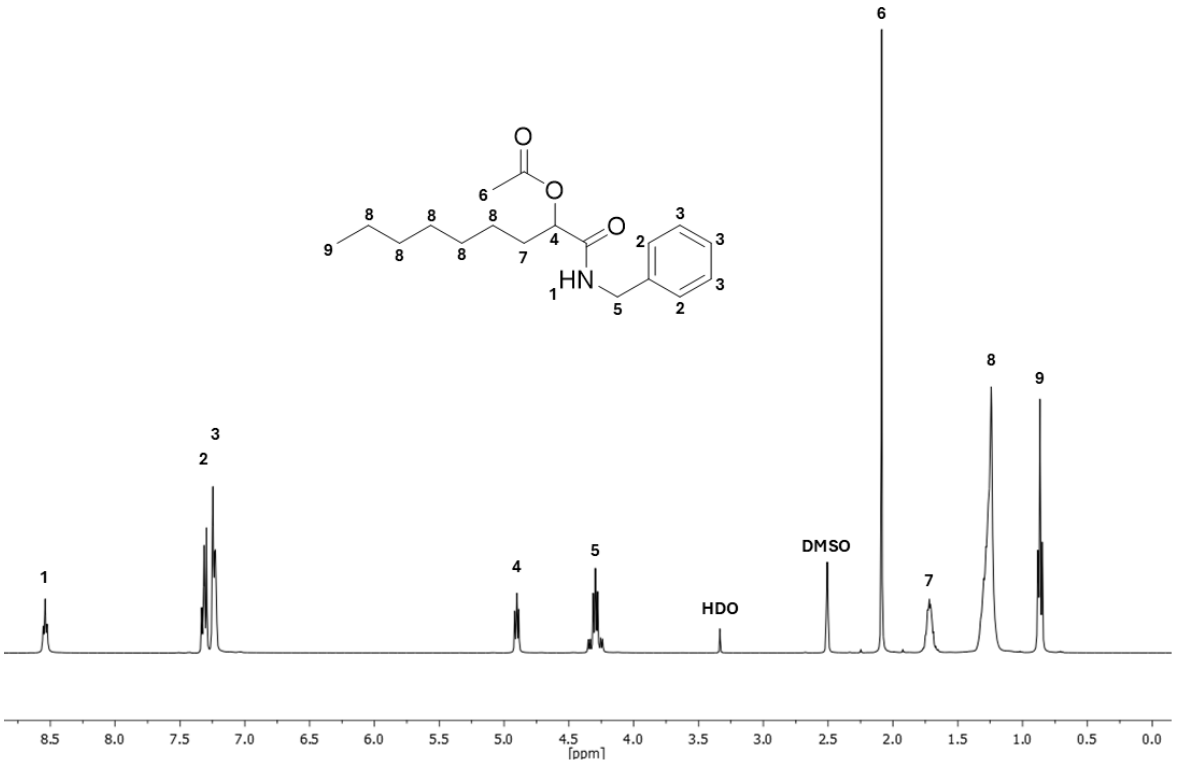

Supplementary Figure 82 ^{1}H-NMR of 1-(benzylamino)-1-oxononan-2-yl acetate measured in DMSO-d_6 plotted as signal intensity versus chemical shift in ppm.

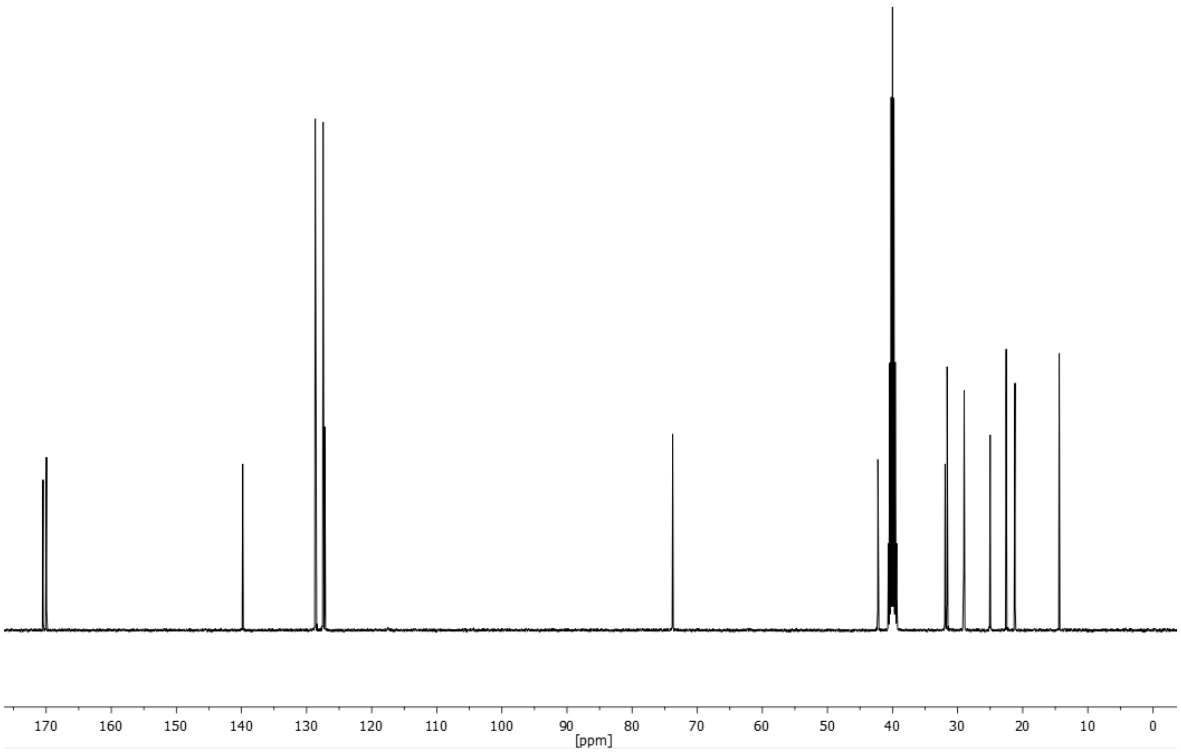

Supplementary Figure 83 ^{13}C-NMR of 1-(benzylamino)-1-oxononan-2-yl acetate measured in DMSO-d_6 (septet signal at 39.52 ppm) and plotted as signal intensity versus chemical shift in ppm.

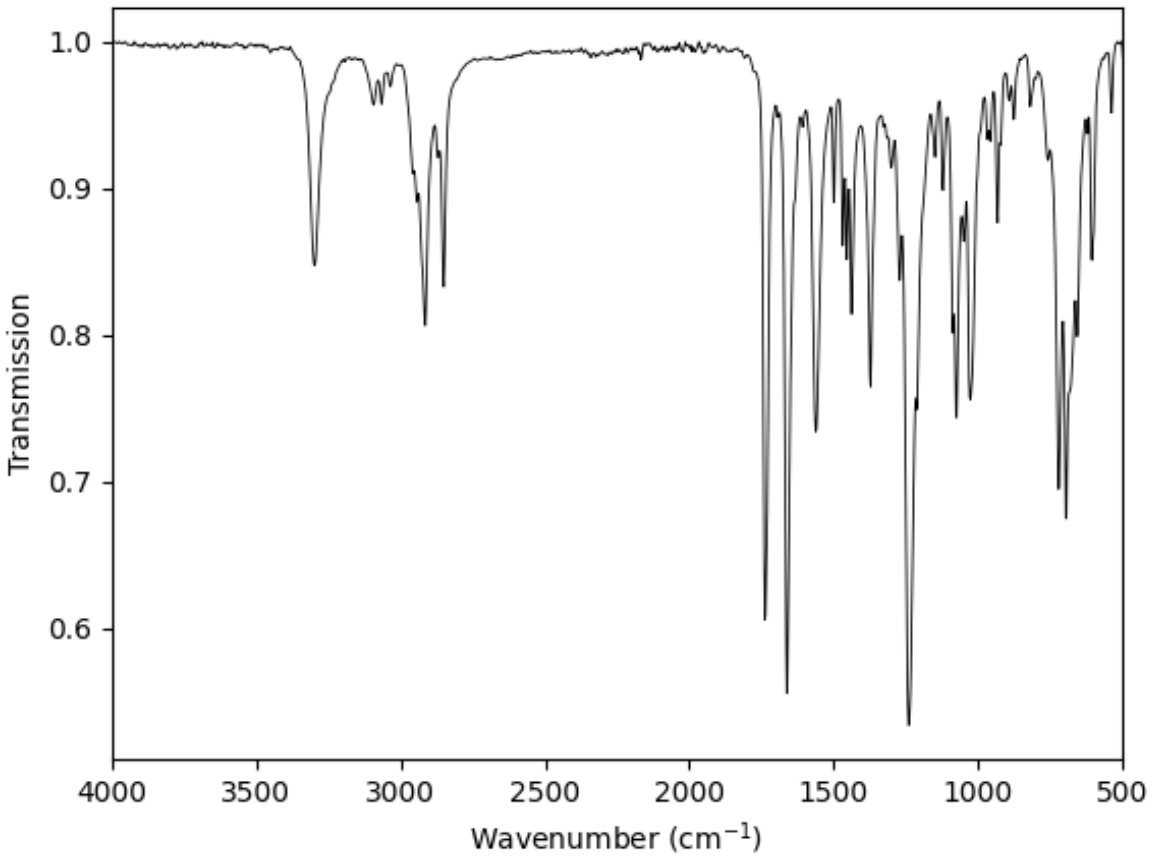

Supplementary Figure 84 IR-spectra of 1-(benzylamino)-1-oxononan-2-yl acetate.

6.2.5 Synthetic procedure for the Ugi product (bis-amide)

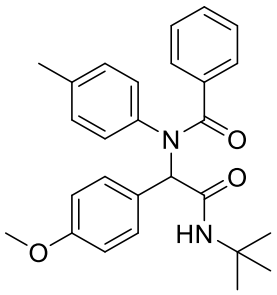

The reaction was conducted in a 10 mL crimp vial. First, 182 µL of 4-methoxybenzaldehyde (204 mg, 1.50 mmol, 1.50 eq.) and 161 mg of *p*-toluidine (1.50 mmol, 1.50 eq.) were dissolved in 5 mL MeOH and stirred for 1 hour at room temperature. Subsequently, 122 mg of benzoic acid (1.50 mmol, 1.50 eq.) and 140 µL of tert-butyl isocyanide (125 mg, 1.50 mmol, 1.50 eq.) were added. The vial was then sealed, and the mixture was stirred overnight. After completion, the solvent was evaporated under reduced pressure. The residue was purified by column chromatography on silica gel, eluting with a gradient of ethyl acetate/cyclohexane (9:1 to 5:1). The Ugi product, *N*-(2-(tert-butylamino)-1-(4-methoxyphenyl)-2-oxoethyl)-*N*-(*p*-tolyl)-benzamide, was obtained as a colourless solid (357 mg, 829 µmol), with a yield of 83%.

Rf = 0.10 in cyclohexane/ethyl acetate 5/1 visualised *via* UV quenching at 254 nm and $KMnO_4$ staining solution.

^{1}H-NMR (500 MHz, DMSO-d_6) δ/ppm = 7.68 (s, 1H, ^{1}), 7.21 – 7.11 (m, 5H, ^{2}), 7.06 – 7.02 (m, 2H, ^{3}), 6.91 (s, 2H, ^{4}), 6.78 – 6.69 (m, 4H, ^{5}), 6.17 (s, 1H, ^{6}), 3.65 (s, 3H, ^{7}), 2.05 (s, 3H, ^{8}), 1.26 (s, 9H, ^{9}).

^{13}C-NMR (101 MHz, DMSO-d_6) δ/ppm = 170.3, 169.8, 158.9, 138.4, 137.6, 136.0, 131.8, 131.2, 129.3, 128.6, 128.3, 128.2, 128.0, 113.7, 64.3, 55.4, 50.8, 28.9, 20.9.

HRMS-EI-MS m/z: [M] calculated for $[C_{27}H_{31}N_2O_3]^+$ = 431.23292, found: 431.23209.

IR (ATR platinum diamond) ν/cm^{-1} = 3340 (w), 3330 (w), 3316 (w), 3297 (w), 2962 (w), 2923 (w), 2869 (w), 2855 (w), 2841 (w), 1683 (m), 1627 (s), 1609 (m), 1576 (m), 1543 (m), 1510 (vs), 1452 (m), 1448 (m), 1378 (m), 1360 (s), 1329 (m), 1304 (m), 1294 (m), 1249 (s), 1226 (s), 1177 (s), 1148 (m), 1111 (w), 1076 (w), 1031 (m), 1002 (w), 959 (w), 930 (vw), 841 (w), 790 (m), 769 (w), 738 (w), 718 (m), 697 (s), 646 (w), 627 (m), 613 (w), 545 (m), 522 (m), 481 (w), 453 (w), 434 (w).

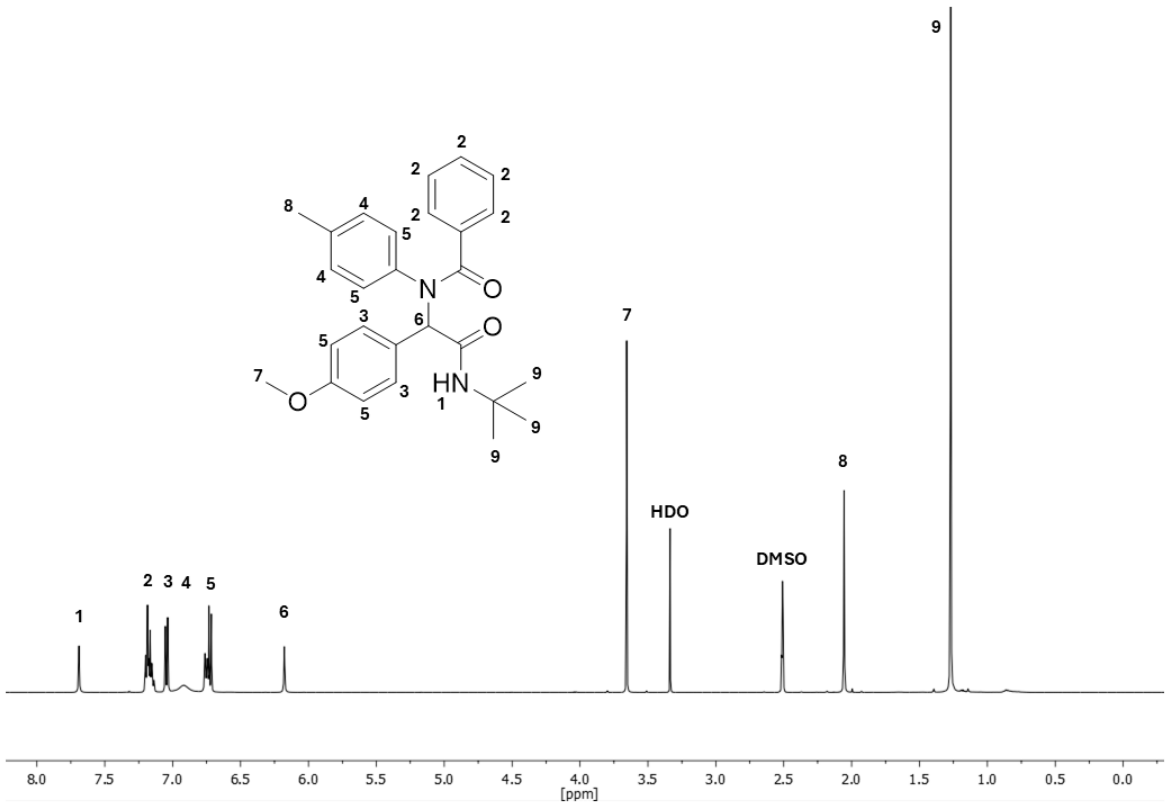

Supplementary Figure 85 ^{1}H-NMR of *N*-(2-(tert-butylamino)-1-(4-methoxyphenyl)-2-oxoethyl)-*N*-(p-tolyl)benzamide measured in DMSO-d_6 plotted as signal intensity versus chemical shift in ppm.

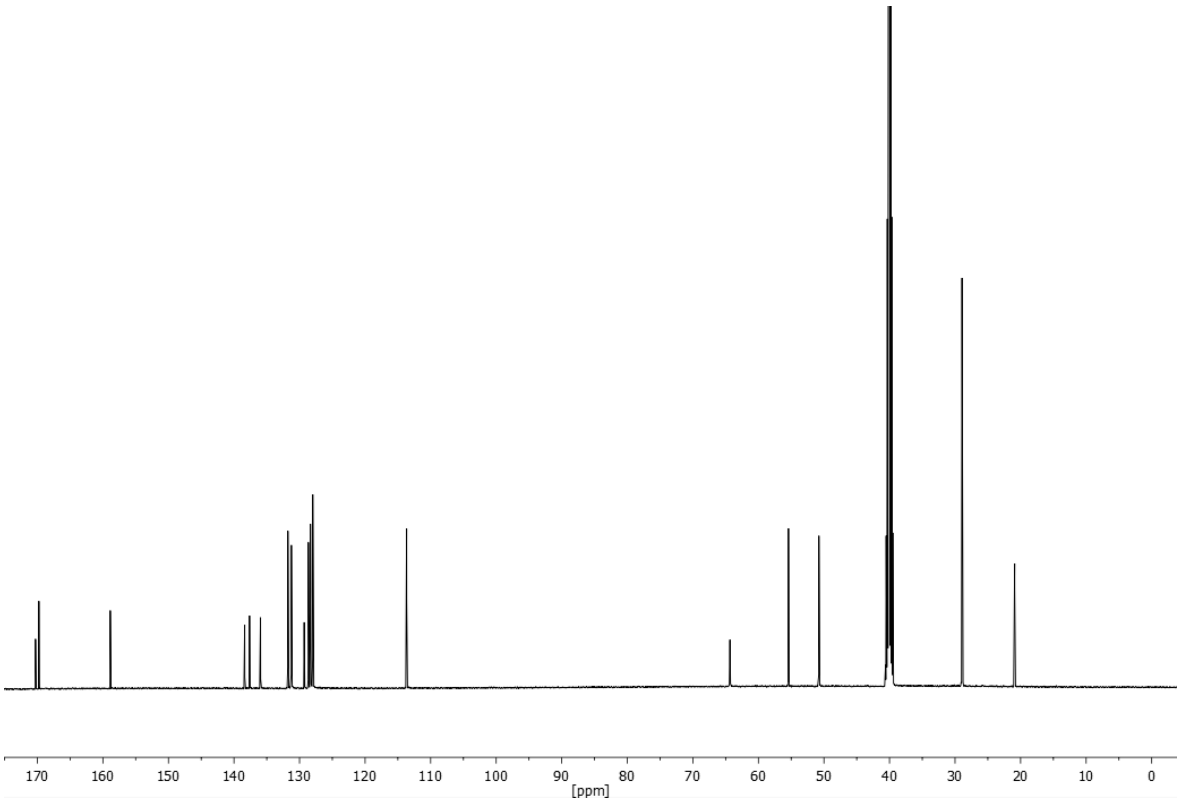

Supplementary Figure 86 ^{13}C-NMR of *N*-(2-(tert-butylamino)-1-(4-methoxyphenyl)-2-oxoethyl)-*N*-(*p*-tolyl)benzamide measured in DMSO-d_6 (septet signal at 39.52 ppm) and plotted as signal intensity versus chemical shift in ppm.

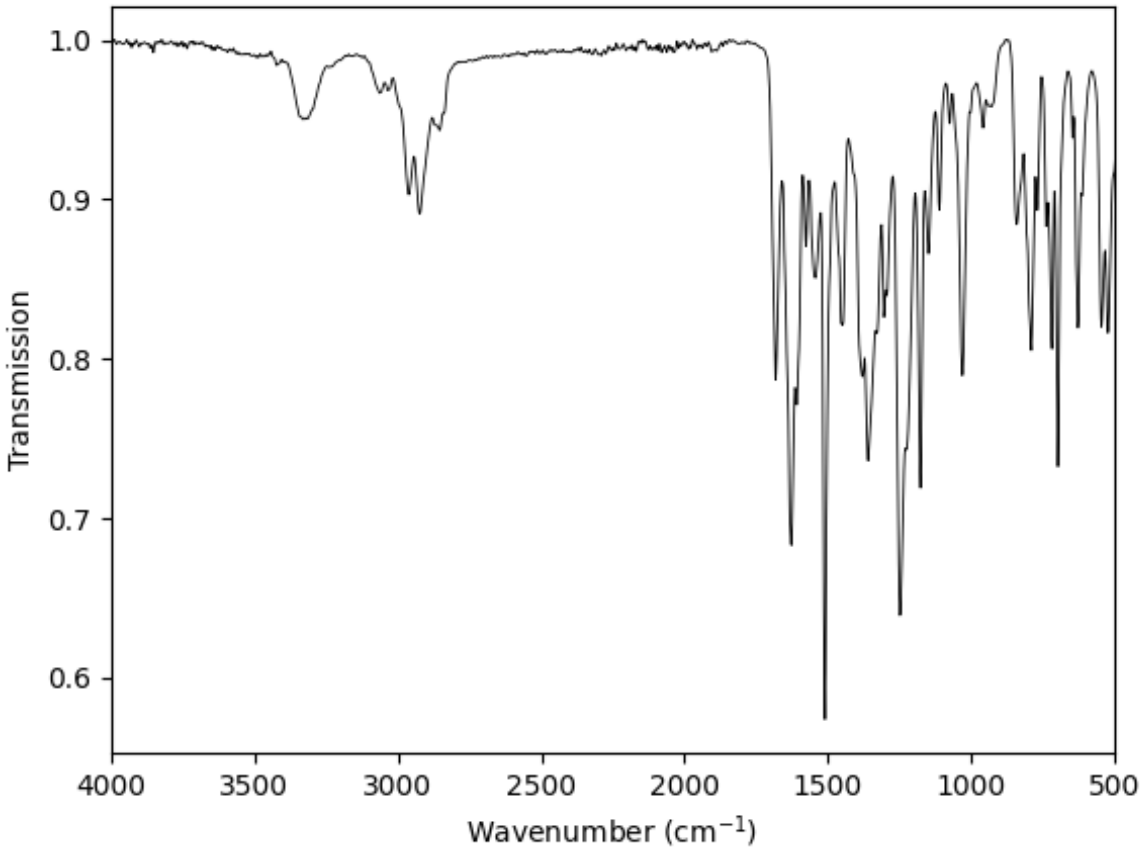

Supplementary Figure 87 IR-spectra of *N*-(2-(tert-butylamino)-1-(4-methoxyphenyl)-2-oxoethyl)-*N*-(*p*-tolyl)benzamide.

6.3 Quantitative analysis using HPLC: Methodology and results

This chapter presents the measurements from the screening of the Passerini and Ugi reactions. The enantiomeric excess was analysed using a THERMOFISHER Ultimate 3000 series HPLC system, connected to a THERMOFISHER QExactive Plus mass spectrometer. A CHIRALPAK AD-H column (4.6 × 250 mm, 5 µm particle size) was employed as the stationary phase. Unless otherwise stated, the standard procedure for the measurements was as follows: The mobile phase consisted of solvent mixtures of HPLC-grade *n*-hexane and ethanol. A gradient elution was typically used as follows: ethanol 2% to 10% over 0 to 40 minutes, held at 10% ethanol for 5 minutes, and then decreased from 10% to 2% ethanol over 45 to 50 minutes. The flow rate was set to 1.0 mL/min, and the UV/Vis detector monitored the absorbance at a wavelength of $\lambda = 215$ nm.

Sample preparation was carried out after purification of the analyte *via* column chromatography. The analyte was then dissolved in a solvent mixture of HPLC-grade *n*-hexane and ethanol in a ratio of 95:5. If solubility issues occurred, the ethanol content was increased until complete homogeneity of the mixture was achieved. The concentration of the sample was typically 0.1 mg/mL, and 10 µL of the analyte were injected into the analytical device by the HPLC autosampler. Prior to measurement, all samples were filtered using a syringe filter (polytetrafluoroethylene, 13 mm diameter, 0.2 µm pore size, AGILENT) to prevent clogging of the injection setup or column.

Supplementary Figure 88 Chiral HPLC spectrum of racemic P-01

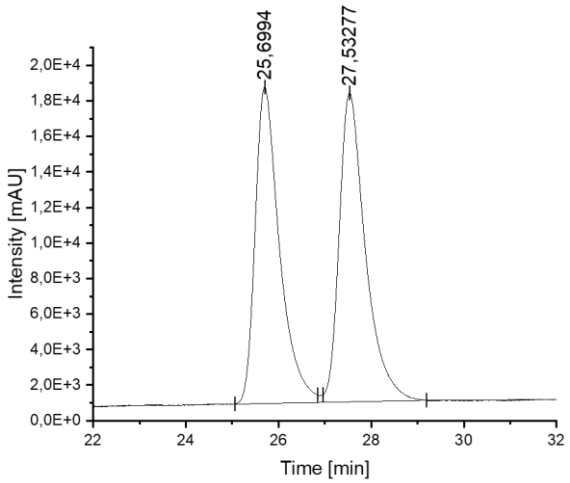

Peak	Time [min]	Area	Area %
1	25.699	11479.7	50.07
2	27.533	11446.4	49.93

The reactions used acetic acid, octanal and benzyl isocyanide in equimolar ratios. The reactions were carried out in cyclohexane at a concentration of 0.025 mol×L^{-1}. A crude sample from the reaction mixture was taken after 44 hours. The enantiomers of the crude product were separated on a Daicel Chiralpak AD-H using *n*-hexane and isopropanol in a gradient elution: isopropanol 2% to 10% over 0 to 40 minutes, increase to 70% isopropanol for 10 minutes, and then decreased from 70% to 2% isopropanol over 50 to 60 minutes.

Supplementary Figure 89 Chiral HPLC spectrum of P-02

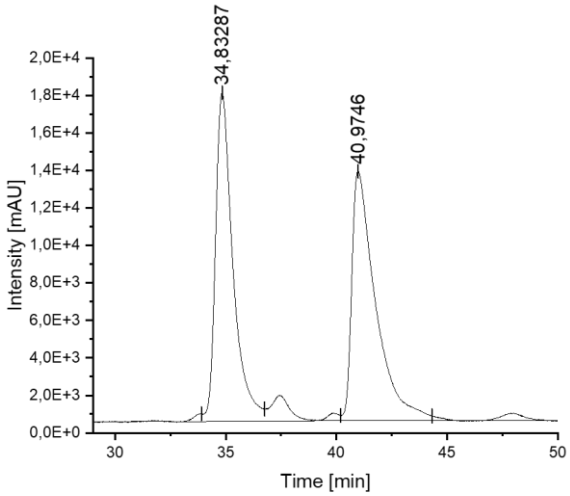

Peak	Time [min]	Area	Area %
1	34.833	16066.7	49.24
2	40.975	16560.3	50.76

The reactions used acetic acid, octanal and benzyl isocyanide in equimolar ratios. The reactions were carried out in cyclohexane at a concentration of 0.025 mol×L^{-1}. A crude sample from the reaction mixture was taken after 44 hours. The enantiomers of the crude product were separated on a Daicel Chiralpak AD-H using *n*-hexane and isopropanol in a gradient elution: isopropanol 2% to 5% over 0 to 80 minutes, held at 5% isopropanol for 10 minutes, then increase to 70% isopropanol in 20 minutes and then decreased from 70% to 2% isopropanol over 110 to 120 minutes.

Supplementary Figure 90 Chiral HPLC spectrum of P-10

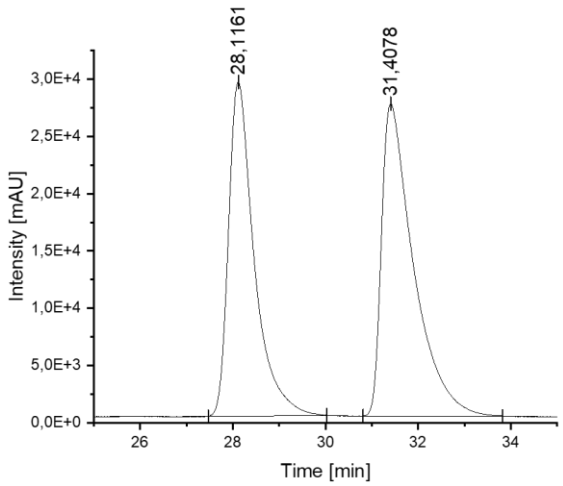

Peak	Time [min]	Area	Area %
1	28.116	18721.7	46.24
2	31.408	21769.8	53.76

The reactions used acetic acid, octanal and benzyl isocyanide in equimolar ratios. The reactions were carried out in cyclohexane at a concentration of 0.025 mol×L^{-1}. A crude sample from the reaction mixture was taken after 44 hours. The enantiomers of the crude product were separated on a Daicel Chiralpak AD-H using *n*-hexane and isopropanol in a gradient elution: isopropanol 2% to 5% over 0 to 40 minutes, increase to 70% isopropanol for 10 minutes, and then decreased from 70% to 2% isopropanol over 50 to 60 minutes.

Supplementary Figure 91 Chiral HPLC spectrum of P-11

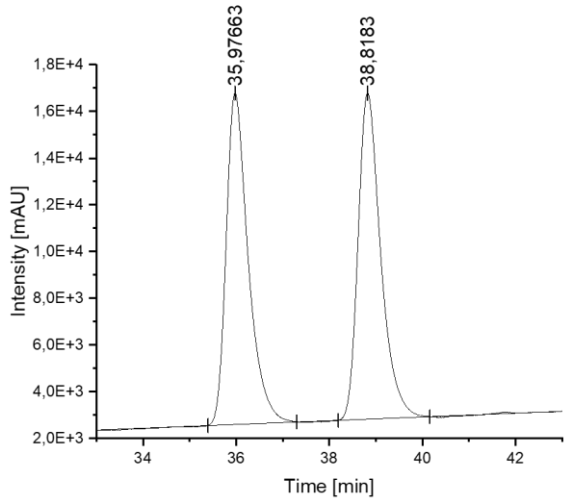

Peak	Time [min]	Area	Area %
1	35.977	7761.8	49.78
2	38.818	7832.5	50.22

The reactions used acetic acid, octanal and benzyl isocyanide in equimolar ratios. The reactions were carried out in cyclohexane at a concentration of 0.025 mol×L^{-1}. The product was purified after 44 hours and a sample was taken for chiral HPLC analysis. The enantiomers of the product were separated on a Daicel Chiralpak AD-H using *n*-hexane and ethanol in a gradient elution: ethanol 2% to 10% over 0 to 40 minutes, held at 10% ethanol for 5 minutes, and then decreased from 10% to 2% ethanol over 45 to 50 minutes.

Supplementary Figure 92 Chiral HPLC spectrum of P-12

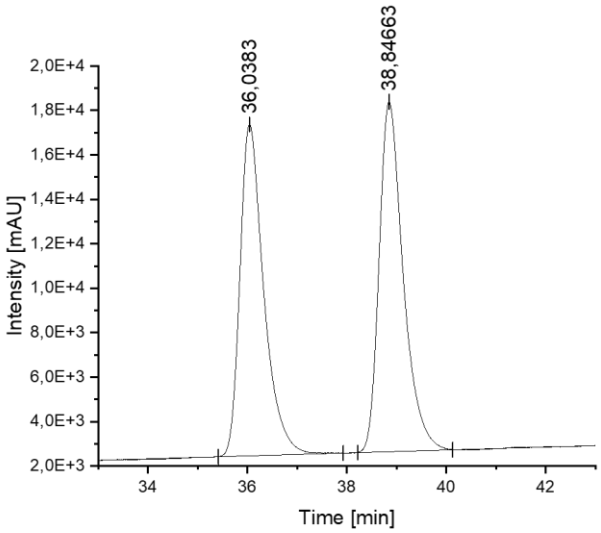

Peak	Time [min]	Area	Area %
1	36.038	8248.5	48.34
2	38.847	8815.3	51.66

The reactions used acetic acid, octanal and benzyl isocyanide in equimolar ratios. The reactions were carried out in cyclohexane at a concentration of 0.025 mol×L^{-1}. The product was purified after 44 hours and a sample was taken for chiral HPLC analysis. The enantiomers of the product were separated on a Daicel Chiralpak AD-H using *n*-hexane and ethanol in a gradient elution: ethanol 2% to 10% over 0 to 40 minutes, held at 10% ethanol for 5 minutes, and then decreased from 10% to 2% ethanol over 45 to 50 minutes.

Supplementary Figure 93 Chiral HPLC spectrum of P-13

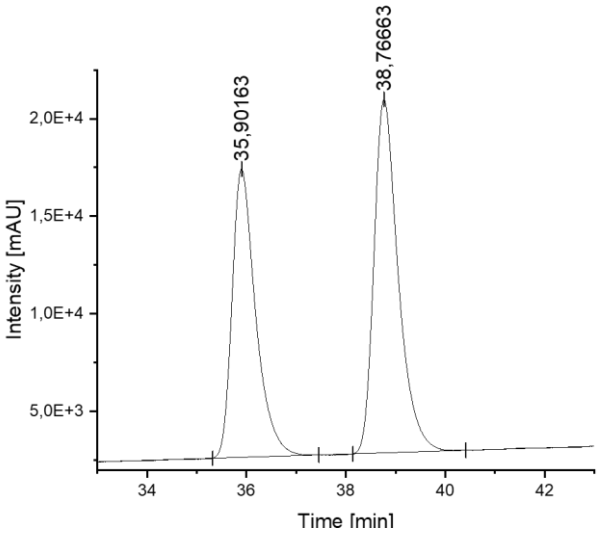

Peak	Time [min]	Area	Area %
1	35.902	8105.9	44.18
2	38.767	10239.9	55.82

The reactions used acetic acid, octanal and benzyl isocyanide in equimolar ratios. The reactions were carried out in cyclohexane at a concentration of 0.025 mol×L^{-1}. The product was purified after 44 hours and a sample was taken for chiral HPLC analysis. The enantiomers of the product were separated on a Daicel Chiralpak AD-H using *n*-hexane and ethanol in a gradient elution: ethanol 2% to 10% over 0 to 40 minutes, held at 10% ethanol for 5 minutes, and then decreased from 10% to 2% ethanol over 45 to 50 minutes.

Supplementary Figure 94 Chiral HPLC spectrum of P-17

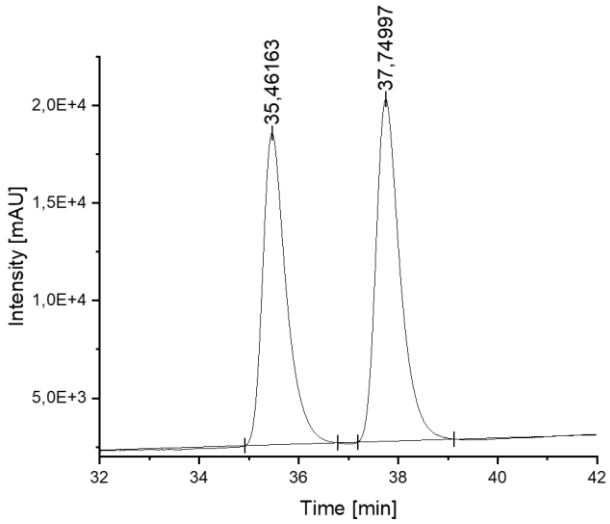

Peak	Time [min]	Area	Area %
1	35.462	8741.1	47.05
2	37.750	9836.9	52.95

The reactions used acetic acid, octanal and benzyl isocyanide in equimolar ratios. The reactions were carried out in cyclohexane at a concentration of 0.025 mol×L^{-1}. The product was purified after 44 hours and a sample was taken for chiral HPLC analysis. The enantiomers of the product were separated on a Daicel Chiralpak AD-H using *n*-hexane and ethanol in a gradient elution: ethanol 2% to 10% over 0 to 40 minutes, held at 10% ethanol for 5 minutes, and then decreased from 10% to 2% ethanol over 45 to 50 minutes.

Supplementary Figure 95 Chiral HPLC spectrum of P-18

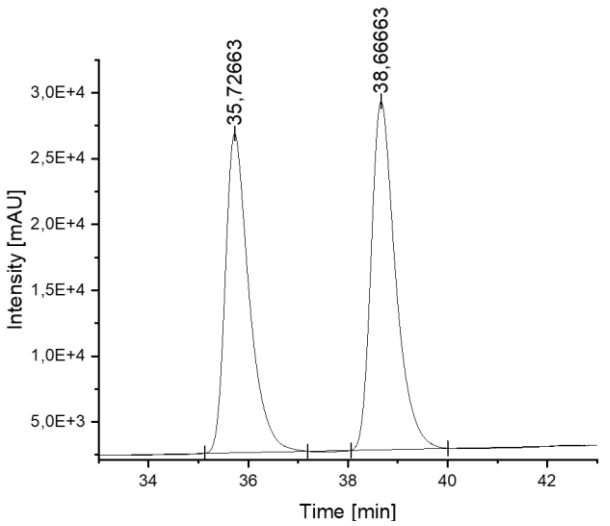

Peak	Time [min]	Area	Area %
1	35.727	13396.5	47.19
2	38.667	14991.9	52.81

The reactions used acetic acid, octanal and benzyl isocyanide in equimolar ratios. The reactions were carried out in cyclohexane at a concentration of 0.025 mol×L^{-1}. The product was purified after 44 hours and a sample was taken for chiral HPLC analysis. The enantiomers of the product were separated on a Daicel Chiralpak AD-H using *n*-hexane and ethanol in a gradient elution: ethanol 2% to 10% over 0 to 40 minutes, held at 10% ethanol for 5 minutes, and then decreased from 10% to 2% ethanol over 45 to 50 minutes.

Supplementary Figure 96 Chiral HPLC spectrum of P-20

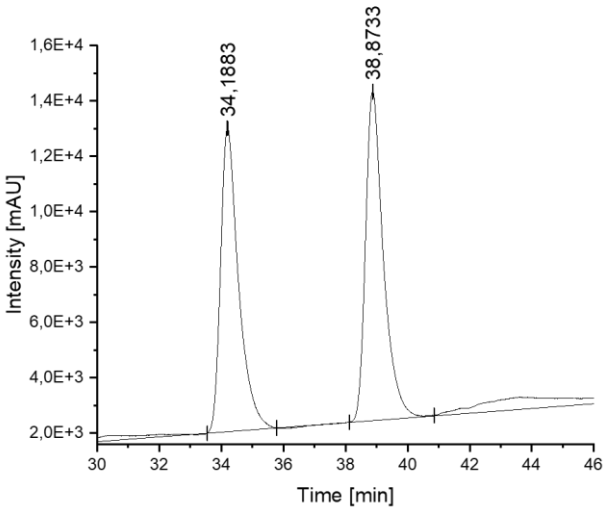

Peak	Time [min]	Area	Area %
1	34.188	7346.7	48.09
2	38.873	7929.2	51.91

The reactions used acetic acid, octanal and benzyl isocyanide in equimolar ratios. The reactions were carried out in toluene at a concentration of 0.025 mol×L^{-1}. The product was purified after 44 hours and a sample was taken for chiral HPLC analysis. The enantiomers of the product were separated on a Daicel Chiralpak AD-H using *n*-hexane and ethanol in a gradient elution: ethanol 2% to 10% over 0 to 40 minutes, held at 10% ethanol for 5 minutes, and then decreased from 10% to 2% ethanol over 45 to 50 minutes.

Supplementary Figure 97 Chiral HPLC spectrum of P-21

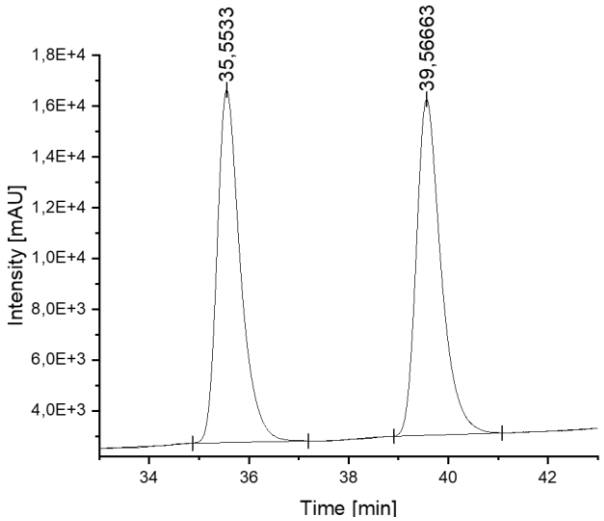

Peak	Time [min]	Area	Area %
1	35.553	7563.4	49.99
2	39.567	7565.6	50.01

The reactions used acetic acid, octanal and benzyl isocyanide in equimolar ratios. The reactions were carried out in dichloromethane at a concentration of 0.025 mol×L^{-1}. The product was purified after 44 hours and a sample was taken for chiral HPLC analysis. The enantiomers of the product were separated on a Daicel Chiralpak AD-H using *n*-hexane and ethanol in a gradient elution: ethanol 2% to 10% over 0 to 40 minutes, held at 10% ethanol for 5 minutes, and then decreased from 10% to 2% ethanol over 45 to 50 minutes.

Supplementary Figure 98 Chiral HPLC spectrum of P-22

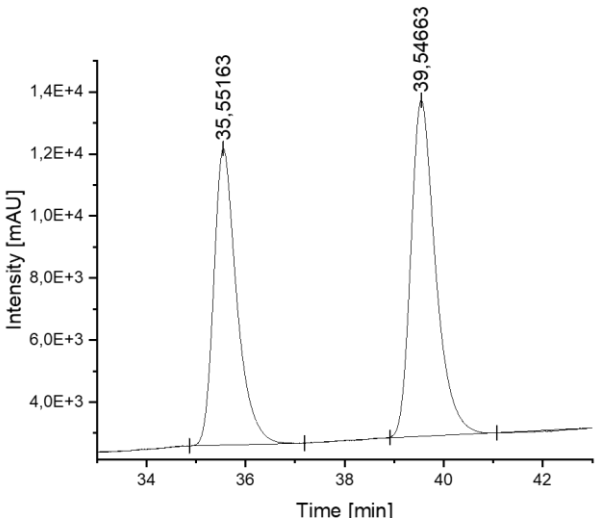

Peak	Time [min]	Area	Area %
1	35.552	5183.9	45.37
2	39.547	6243.0	54.63

The reactions used acetic acid, octanal and benzyl isocyanide in equimolar ratios. The reactions were carried out in *n*-hexane at a concentration of 0.025 mol×L^{-1}. The product was purified after 44 hours and a sample was taken for chiral HPLC analysis. The enantiomers of the product were separated on a Daicel Chiralpak AD-H using *n*-hexane and ethanol in a gradient elution: ethanol 2% to 10% over 0 to 40 minutes, held at 10% ethanol for 5 minutes, and then decreased from 10% to 2% ethanol over 45 to 50 minutes.

Supplementary Figure 99 Chiral HPLC spectrum of P-23

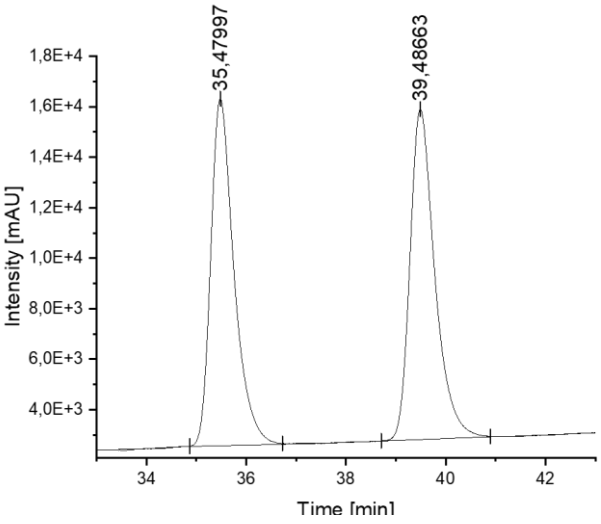

Peak	Time [min]	Area	Area %
1	35.480	7410.7	49.70
2	39.487	7500.5	50.30

The reactions used acetic acid, octanal and benzyl isocyanide in equimolar ratios. The reactions were carried out in chloroform at a concentration of 0.025 mol×L^{-1}. The product was purified after 44 hours and a sample was taken for chiral HPLC analysis. The enantiomers of the product were separated on a Daicel Chiralpak AD-H using *n*-hexane and ethanol in a gradient elution: ethanol 2% to 10% over 0 to 40 minutes, held at 10% ethanol for 5 minutes, and then decreased from 10% to 2% ethanol over 45 to 50 minutes.

Supplementary Figure 100 Chiral HPLC spectrum of racemic P-24

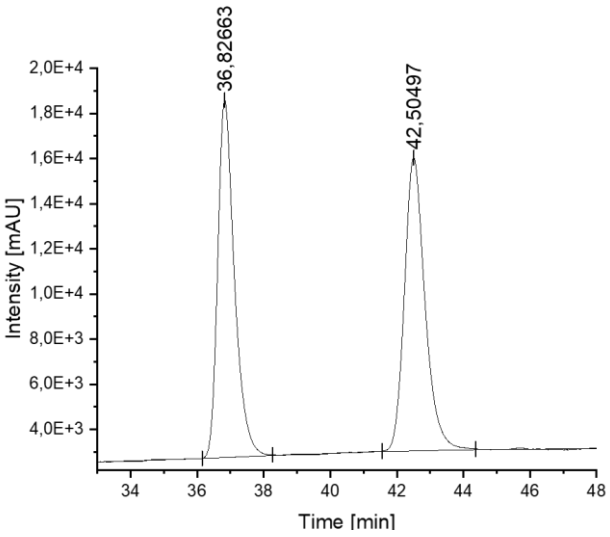

Peak	Time [min]	Area	Area %
1	36.827	9189.6	49.64
2	42.505	9323.0	50.36

The reactions used acetic acid, octanal and benzyl isocyanide in equimolar ratios. The reactions were carried out in *n*-hexane at a concentration of 0.025 mol×L^{-1}. The product was purified after 44 hours and a sample was taken for chiral HPLC analysis. The enantiomers of the product were separated on a Daicel Chiralpak AD-H using *n*-hexane and ethanol in a gradient elution: ethanol 2% to 5% over 0 to 40 minutes, held at 5% ethanol for 5 minutes, and then decreased from 5% to 2% ethanol over 45 to 50 minutes.

Supplementary Figure 101 Chiral HPLC spectrum of P-25

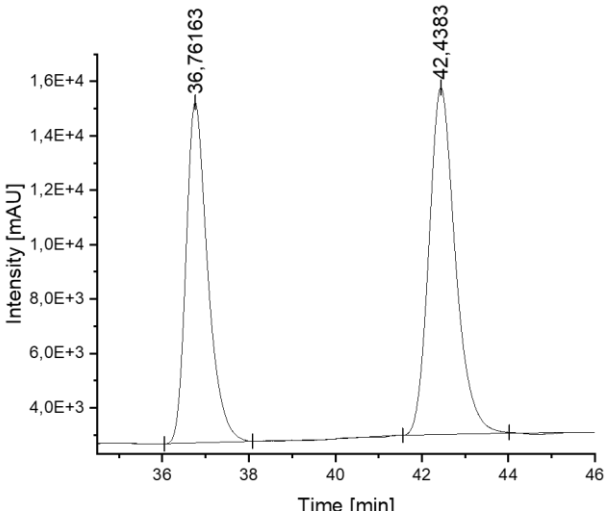

Peak	Time [min]	Area	Area %
1	36.762	7256.9	44.07
2	42.438	9023.9	55.93

The reactions used acetic acid, octanal and benzyl isocyanide in equimolar ratios. The reactions were carried out in *n*-hexane at a concentration of 0.025 mol×L^{-1}. The product was purified after 44 hours and a sample was taken for chiral HPLC analysis. The enantiomers of the product were separated on a Daicel Chiralpak AD-H using *n*-hexane and ethanol in a gradient elution: ethanol 2% to 5% over 0 to 40 minutes, held at 5% ethanol for 5 minutes, and then decreased from 5% to 2% ethanol over 45 to 50 minutes.

Supplementary Figure 102 Chiral HPLC spectrum of racemic P-26

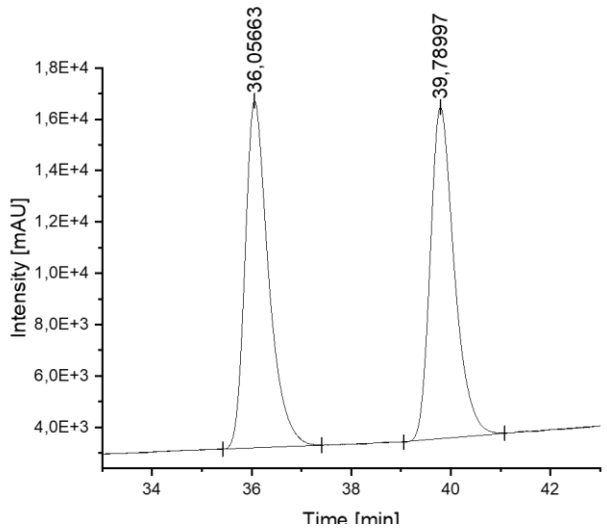

Peak	Time [min]	Area	Area %
1	36.057	7340.0	50.41
2	39.790	7219.8	49.59

The reactions used acetic acid, octanal and benzyl isocyanide in equimolar ratios. The reactions were carried out in *n*-hexane at a concentration of 0.025 mol×L^{-1}. The product was purified after 44 hours and a sample was taken for chiral HPLC analysis. The enantiomers of the product were separated on a Daicel Chiralpak AD-H using *n*-hexane and ethanol in a gradient elution: ethanol 2% to 10% over 0 to 40 minutes, held at 10% ethanol for 5 minutes, and then decreased from 10% to 2% ethanol over 45 to 50 minutes.

Supplementary Figure 103 Chiral HPLC spectrum of P-27

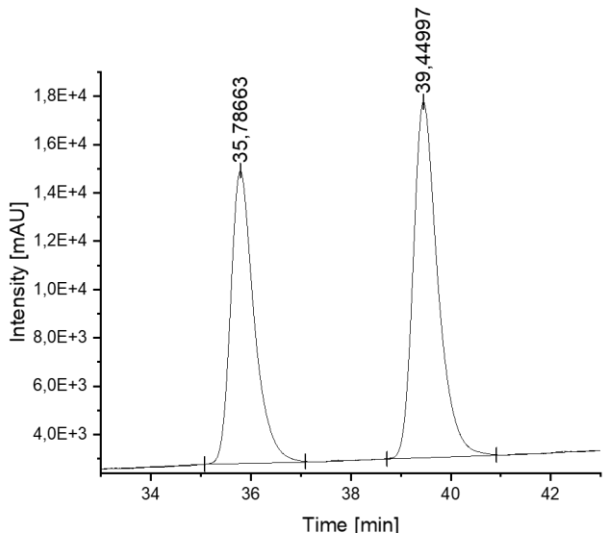

Peak	Time [min]	Area	Area %
1	35.787	6575.0	44.20
2	39.450	8301.8	55.80

The reactions used acetic acid, octanal and benzyl isocyanide in equimolar ratios. The reactions were carried out in *n*-hexane at a concentration of 0.025 mol×L^{-1}. The product was purified after 44 hours and a sample was taken for chiral HPLC analysis. The enantiomers of the product were separated on a Daicel Chiralpak AD-H using *n*-hexane and ethanol in a gradient elution: ethanol 2% to 10% over 0 to 40 minutes, held at 10% ethanol for 5 minutes, and then decreased from 10% to 2% ethanol over 45 to 50 minutes.

Supplementary Figure 104 Chiral HPLC spectrum of racemic P-28

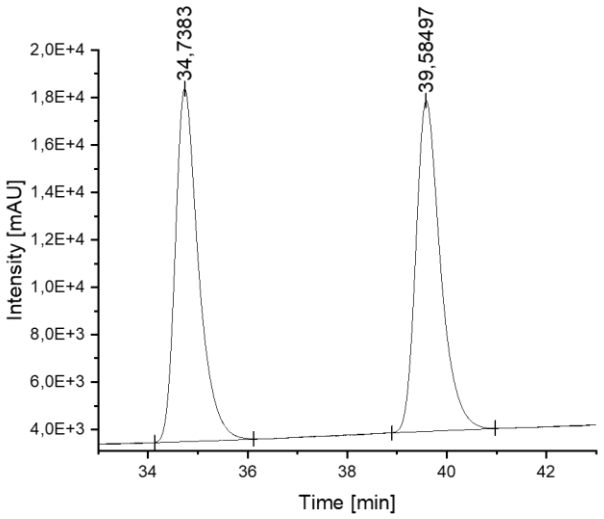

Peak	Time [min]	Area	Area %
1	34.738	7990.5	50.01
2	39.585	7988.1	49.99

The reactions used acetic acid, octanal and benzyl isocyanide in equimolar ratios. The reactions were carried out in *n*-hexane at a concentration of 0.025 mol×L^{-1}. The product was purified after 44 hours and a sample was taken for chiral HPLC analysis. The enantiomers of the product were separated on a Daicel Chiralpak AD-H using *n*-hexane and ethanol in a gradient elution: ethanol 2% to 10% over 0 to 40 minutes, held at 10% ethanol for 5 minutes, and then decreased from 10% to 2% ethanol over 45 to 50 minutes.

Supplementary Figure 105 Chiral HPLC spectrum of P-29

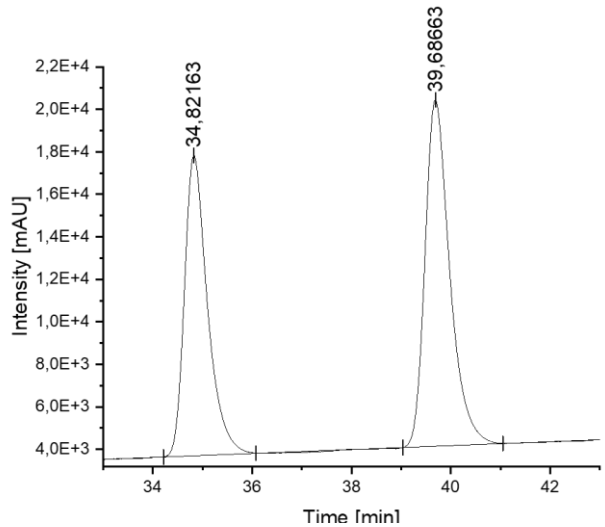

Peak	Time [min]	Area	Area %
1	34.822	7581.3	44.66
2	39.687	9394.6	55.34

The reactions used acetic acid, octanal and benzyl isocyanide in equimolar ratios. The reactions were carried out in *n*-hexane at a concentration of 0.025 mol×L^{-1}. The product was purified after 44 hours and a sample was taken for chiral HPLC analysis. The enantiomers of the product were separated on a Daicel Chiralpak AD-H using *n*-hexane and ethanol in a gradient elution: ethanol 2% to 10% over 0 to 40 minutes, held at 10% ethanol for 5 minutes, and then decreased from 10% to 2% ethanol over 45 to 50 minutes.

Supplementary Figure 106 Chiral HPLC spectrum of P-30

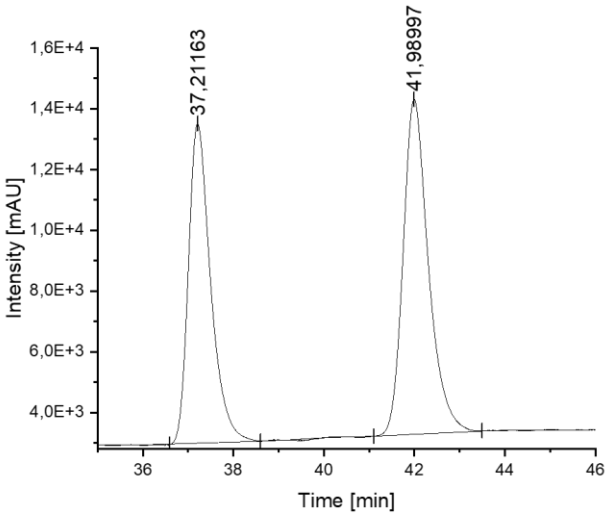

Peak	Time [min]	Area	Area %
1	37.212	7581.3	44.65
2	41.990	9394.6	55.35

The reactions used acetic acid, octanal and benzyl isocyanide. The reactions were carried out in *n*-hexane at a concentration of 0.025 mol×L^{-1}. The product was purified after 44 hours and a sample was taken for chiral HPLC analysis. The enantiomers of the product were separated on a Daicel Chiralpak AD-H using *n*-hexane and ethanol in a gradient elution: ethanol 2% to 8% over 0 to 40 minutes, held at 8% ethanol for 5 minutes, and then decreased from 8% to 2% ethanol over 45 to 50 minutes.

Supplementary Figure 107 Chiral HPLC spectrum of P-31

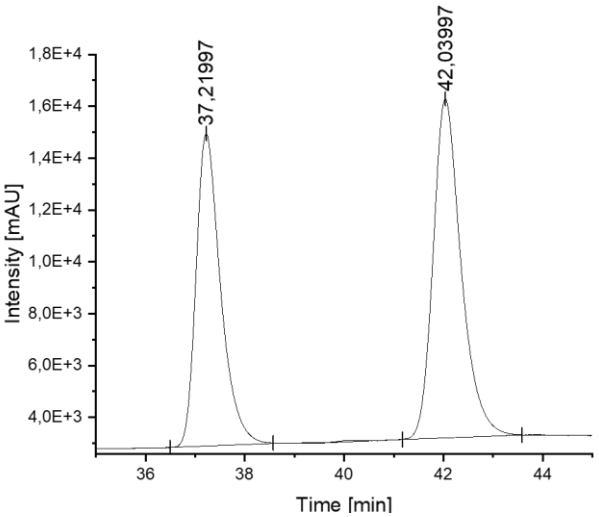

Peak	Time [min]	Area	Area %
1	37.220	6915.4	43.85
2	42.040	8855.1	56.15

The reactions used acetic acid, octanal and benzyl isocyanide. The reactions were carried out in *n*-hexane at a concentration of 0.025 mol×L^{-1}. The product was purified after 44 hours and a sample was taken for chiral HPLC analysis. The enantiomers of the product were separated on a Daicel Chiralpak AD-H using *n*-hexane and ethanol in a gradient elution: ethanol 2% to 8% over 0 to 40 minutes, held at 8% ethanol for 5 minutes, and then decreased from 8% to 2% ethanol over 45 to 50 minutes.

Supplementary Figure 108 Chiral HPLC spectrum of P-32

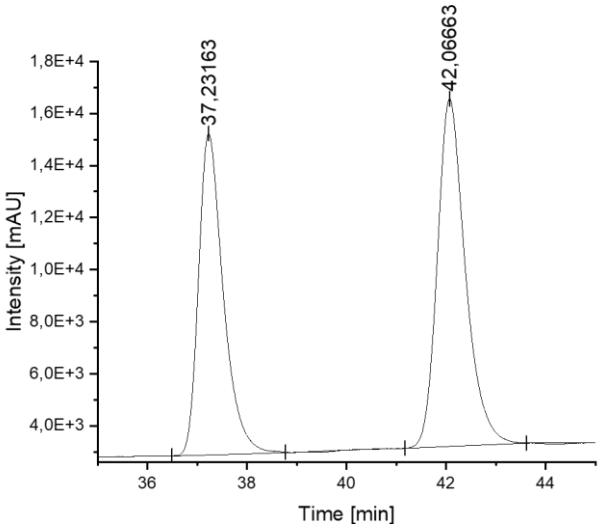

Peak	Time [min]	Area	Area %
1	37.232	7014.0	44.32
2	42.067	8813.0	55.68

The reactions used acetic acid, octanal and benzyl isocyanide. The reactions were carried out in *n*-hexane at a concentration of 0.025 mol×L^{-1}. The product was purified after 44 hours and a sample was taken for chiral HPLC analysis. The enantiomers of the product were separated on a Daicel Chiralpak AD-H using *n*-hexane and ethanol in a gradient elution: ethanol 2% to 8% over 0 to 40 minutes, held at 8% ethanol for 5 minutes, and then decreased from 8% to 2% ethanol over 45 to 50 minutes.

Supplementary Figure 109 Chiral HPLC spectrum of P-33

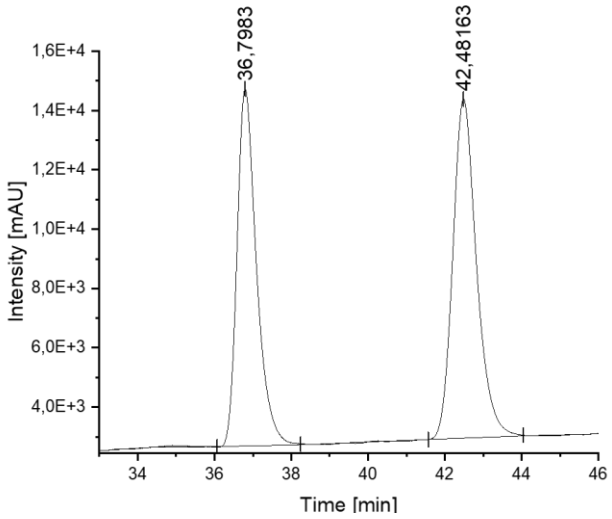

Peak	Time [min]	Area	Area %
1	36.798	7014.2	46.21
2	42.482	8163.3	53.79

The reactions used acetic acid, octanal and benzyl isocyanide. The reactions were carried out in *n*-hexane at a concentration of 0.025 mol×L^{-1}. The product was purified after 44 hours and a sample was taken for chiral HPLC analysis. The enantiomers of the product were separated on a Daicel Chiralpak AD-H using *n*-hexane and ethanol in a gradient elution: ethanol 2% to 8% over 0 to 40 minutes, held at 8% ethanol for 5 minutes, and then decreased from 8% to 2% ethanol over 45 to 50 minutes.

Supplementary Figure 110 Chiral HPLC spectrum of P-34

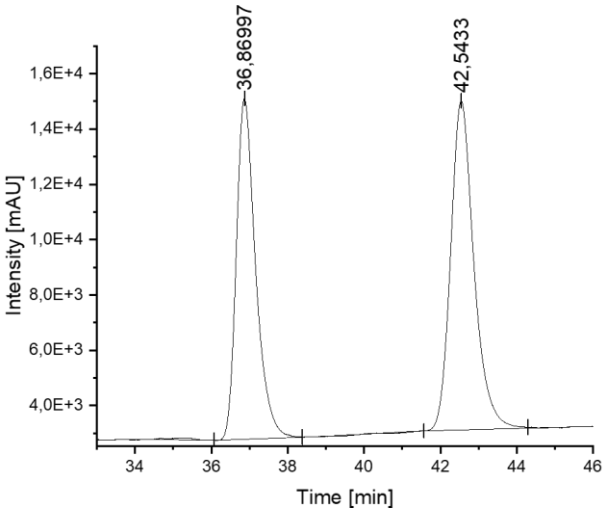

Peak	Time [min]	Area	Area %
1	36.870	6950.3	45.25
2	42.543	8408.7	54.75

The reactions used acetic acid, octanal and benzyl isocyanide. The reactions were carried out in *n*-hexane at a concentration of 0.025 mol×L^{-1}. The product was purified after 44 hours and a sample was taken for chiral HPLC analysis. The enantiomers of the product were separated on a Daicel Chiralpak AD-H using *n*-hexane and ethanol in a gradient elution: ethanol 2% to 8% over 0 to 40 minutes, held at 8% ethanol for 5 minutes, and then decreased from 8% to 2% ethanol over 45 to 50 minutes.

Supplementary Figure 111 Chiral HPLC spectrum of P-35

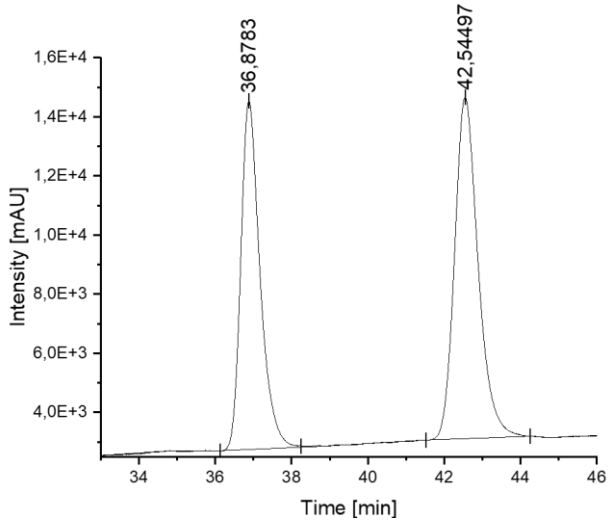

Peak	Time [min]	Area	Area %
1	36.878	6870.4	44.81
2	42.545	8463.3	55.19

The reactions used acetic acid, octanal and benzyl isocyanide. The reactions were carried out in *n*-hexane at a concentration of 0.025 mol×L^{-1}. The product was purified after 44 hours and a sample was taken for chiral HPLC analysis. The enantiomers of the product were separated on a Daicel Chiralpak AD-H using *n*-hexane and ethanol in a gradient elution: ethanol 2% to 8% over 0 to 40 minutes, held at 8% ethanol for 5 minutes, and then decreased from 8% to 2% ethanol over 45 to 50 minutes.

Supplementary Figure 112 Chiral HPLC spectrum of racemic P-36

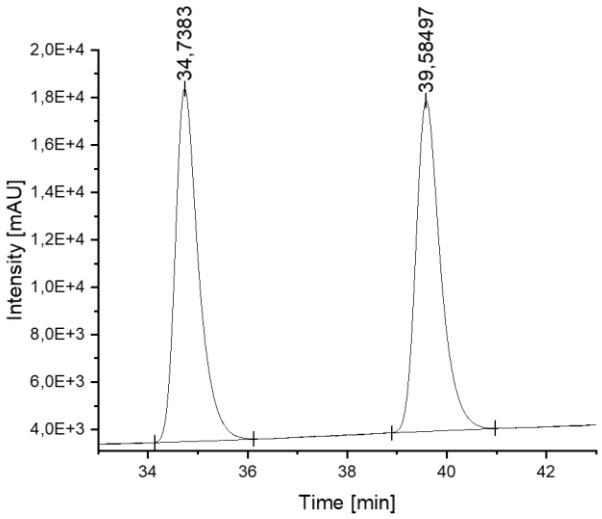

Peak	Time [min]	Area	Area %
1	34.738	8749.3	49.91
2	39.585	8779.4	50.09

The reactions used acetic acid, octanal and benzyl isocyanide in equimolar ratios. The reactions were carried out in *n*-hexane at a concentration of 0.025 mol×L^{-1}. The product was purified after 44 hours and a sample was taken for chiral HPLC analysis. The enantiomers of the product were separated on a Daicel Chiralpak AD-H using *n*-hexane and ethanol in a gradient elution: ethanol 2% to 10% over 0 to 40 minutes, held at 10% ethanol for 5 minutes, and then decreased from 10% to 2% ethanol over 45 to 50 minutes.

Supplementary Figure 113 Chiral HPLC spectrum of P-37

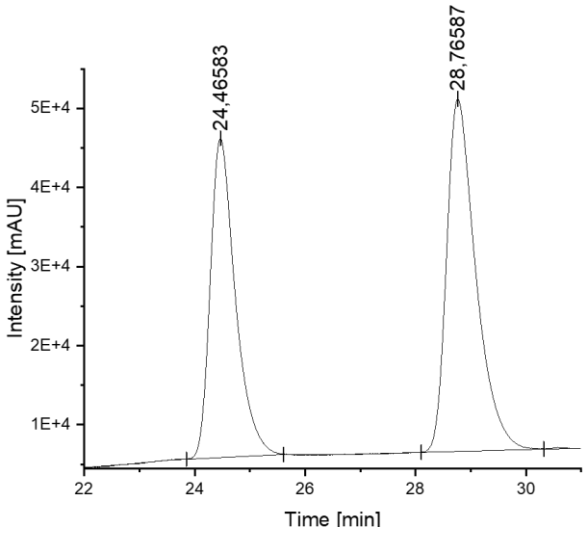

Peak	Time [min]	Area	Area %
1	24.466	21214.8	43.72
2	28.766	27306.1	56.28

The reactions used acetic acid, octanal and benzyl isocyanide in equimolar ratios. The reactions were carried out in *n*-hexane at a concentration of 0.025 mol×L^{-1}. The product was purified after 44 hours and a sample was taken for chiral HPLC analysis. The enantiomers of the product were separated on a Daicel Chiralpak AD-H using *n*-hexane and ethanol in a gradient elution: ethanol 5% to 10% over 0 to 40 minutes, held at 10% ethanol for 5 minutes, and then decreased from 10% to 5% ethanol over 45 to 50 minutes.

Supplementary Figure 114 Chiral HPLC spectrum of P-38 – 1 hour measurement

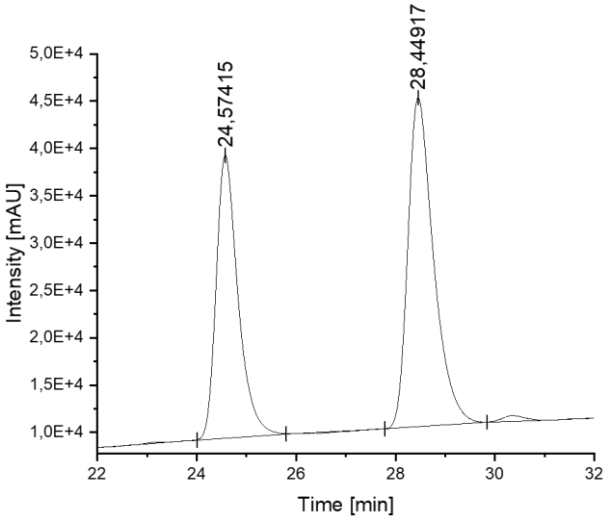

Peak	Time [min]	Area	Area %
1	24.574	15242.2	42.27
2	28.449	20814.6	57.73

The reactions used acetic acid, octanal and benzyl isocyanide in equimolar ratios. The reactions were carried out in *n*-hexane at a concentration of 0.025 mol×L^{-1}. A sample for chiral HPLC analysis was taken from the crude product after 4 hours. The enantiomers of the product were separated on a Daicel Chiralpak AD-H using *n*-hexane and ethanol in a gradient elution: ethanol 5% to 10% over 0 to 40 minutes, held at 10% ethanol for 5 minutes, and then decreased from 10% to 5% ethanol over 45 to 50 minutes.

Supplementary Figure 115 Chiral HPLC spectrum of P-38 – 2 hour measurement

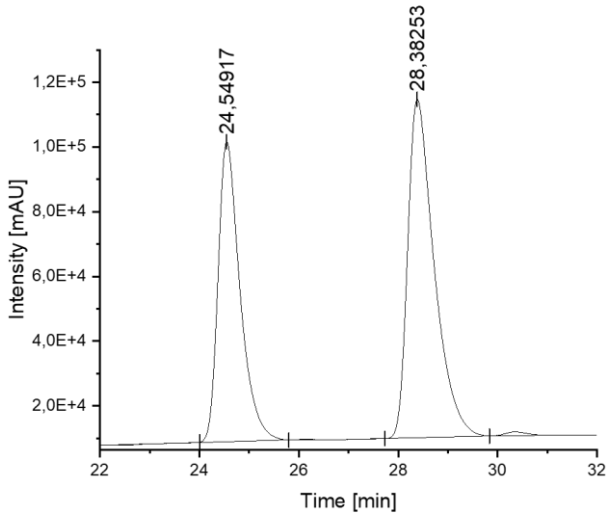

Peak	Time [min]	Area	Area %
1	24.549	47348.1	42.39
2	28.383	64343.8	57.61

The reactions used acetic acid, octanal and benzyl isocyanide in equimolar ratios. The reactions were carried out in *n*-hexane at a concentration of 0.025 mol×L^{-1}. A sample for chiral HPLC analysis was taken from the crude product after 4 hours. The enantiomers of the product were separated on a Daicel Chiralpak AD-H using *n*-hexane and ethanol in a gradient elution: ethanol 5% to 10% over 0 to 40 minutes, held at 10% ethanol for 5 minutes, and then decreased from 10% to 5% ethanol over 45 to 50 minutes.

Supplementary Figure 116 Chiral HPLC spectrum of P-38 – 3 hour measurement

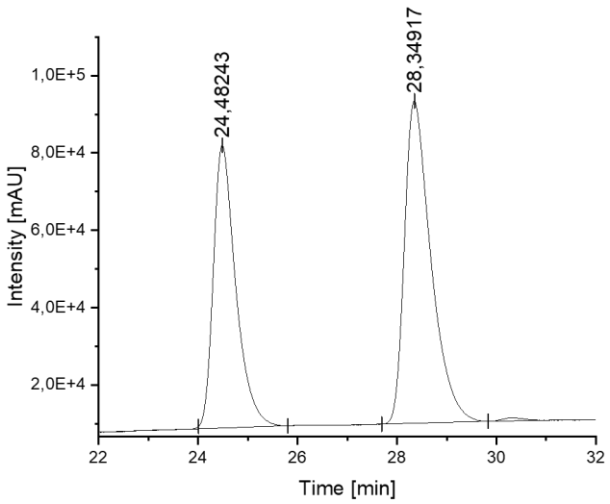

Peak	Time [min]	Area	Area %
1	24.482	38117.7	42.59
2	28.349	51385.7	57.41

The reactions used acetic acid, octanal and benzyl isocyanide in equimolar ratios. The reactions were carried out in *n*-hexane at a concentration of 0.025 mol×L^{-1}. A sample for chiral HPLC analysis was taken from the crude product after 4 hours. The enantiomers of the product were separated on a Daicel Chiralpak AD-H using *n*-hexane and ethanol in a gradient elution: ethanol 5% to 10% over 0 to 40 minutes, held at 10% ethanol for 5 minutes, and then decreased from 10% to 5% ethanol over 45 to 50 minutes.

Supplementary Figure 117 Chiral HPLC spectrum of P-38 – 4 hour measurement

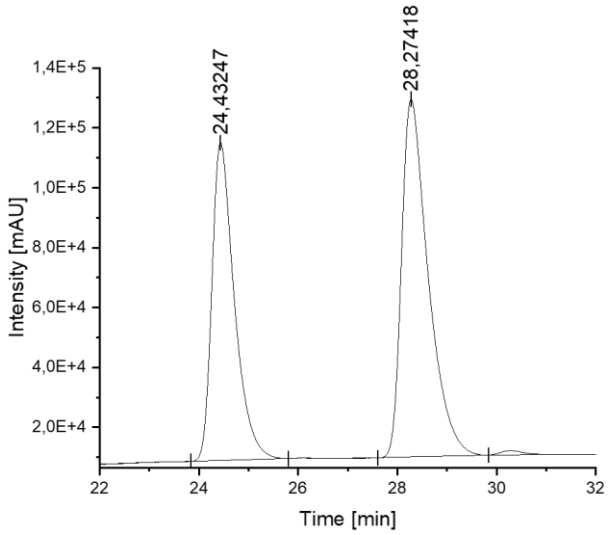

Peak	Time [min]	Area	Area %
1	24.433	55483.6	42.78
2	28.274	74200.4	57.22

The reactions used acetic acid, octanal and benzyl isocyanide in equimolar ratios. The reactions were carried out in *n*-hexane at a concentration of 0.025 mol×L^{-1}. A sample for chiral HPLC analysis was taken from the crude product after 4 hours. The enantiomers of the product were separated on a Daicel Chiralpak AD-H using *n*-hexane and ethanol in a gradient elution: ethanol 5% to 10% over 0 to 40 minutes, held at 10% ethanol for 5 minutes, and then decreased from 10% to 5% ethanol over 45 to 50 minutes.

Supplementary Figure 118 Chiral HPLC spectrum of P-38 – 44 hour measurement

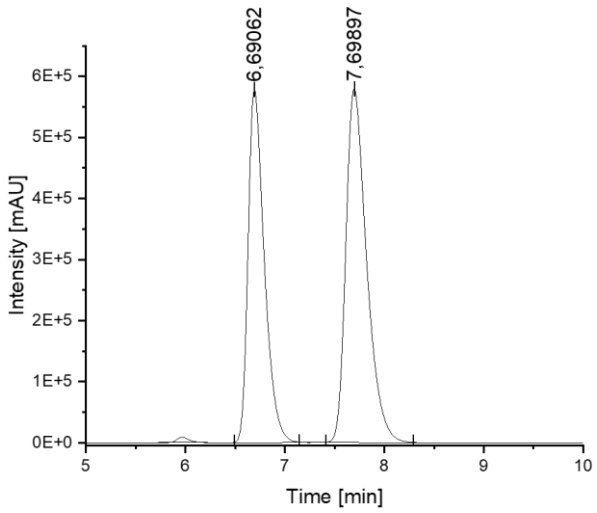

Peak	Time [min]	Area	Area %
1	6.691	109292.4	43.86
2	7.699	139893.4	56.14

The reactions used acetic acid, octanal and benzyl isocyanide in equimolar ratios. The reactions were carried out in *n*-hexane at a concentration of 0.025 mol×L^{-1}. The product was purified after 44 hours and a sample was taken for chiral HPLC analysis. The enantiomers of the product were separated on a Daicel Chiralpak AD-H using *n*-hexane and ethanol in a 9/1 eluent mixture for 40 minutes.

Supplementary Figure 119 Chiral HPLC spectrum of P-39

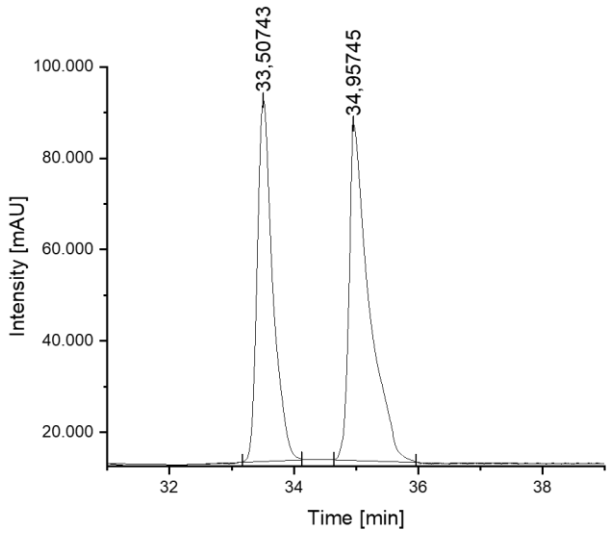

Peak	Time [min]	Area	Area %
1	33.507	1363238	42.94
2	34.957	1811800	57.06

The reactions used acetic acid, octanal and benzyl isocyanide in equimolar ratios. The reactions were carried out in *n*-hexane at a concentration of 0.025 mol×L^{-1}. The product was purified after 44 hours and a sample was taken for chiral HPLC analysis. The enantiomers of the product were separated on a Daicel Chiralpak AD-H using *n*-hexane and ethanol in a gradient elution: ethanol 2% to 10% over 0 to 35 minutes, held at 10% ethanol for 5 minutes, and then decreased from 10% to 2% ethanol over 40 to 50 minutes.

Supplementary Figure 120 Chiral HPLC spectrum of P-40

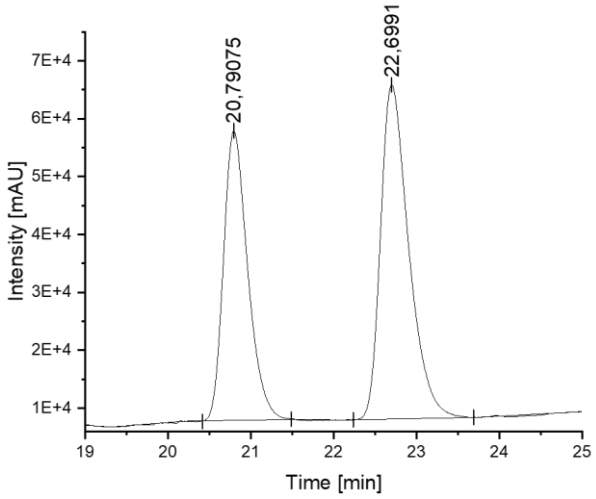

Peak	Time [min]	Area	Area %
1	20.791	17020.7	42.81
2	22.699	22733.8	57.19

The reactions used acetic acid, octanal and benzyl isocyanide in equimolar ratios. The reactions were carried out in *n*-hexane at a concentration of 0.025 mol×L^{-1}. The product was purified after 44 hours and a sample was taken for chiral HPLC analysis. The enantiomers of the product were separated on a Daicel Chiralpak AD-H using *n*-hexane and ethanol in a gradient elution: ethanol 6% to 10% over 0 to 40 minutes, held at 10% ethanol for 5 minutes, and then decreased from 10% to 2% ethanol over 40 to 50 minutes.

Supplementary Figure 121 Chiral HPLC spectrum of P-41

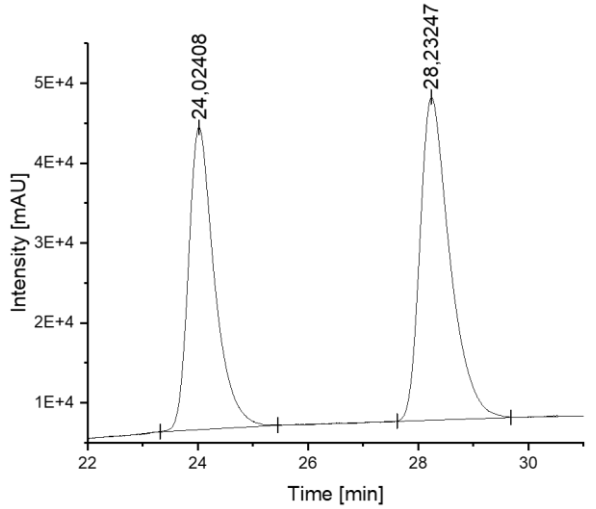

Peak	Time [min]	Area	Area %
1	24.024	20734.1	44.99
2	28.233	25355.1	55.01

The reactions used acetic acid, octanal and benzyl isocyanide in equimolar ratios. The reactions were carried out in *n*-hexane at a concentration of 0.025 mol×L^{-1}. The product was purified after 44 hours and a sample was taken for chiral HPLC analysis. The enantiomers of the product were separated on a Daicel Chiralpak AD-H using *n*-hexane and ethanol in a gradient elution: ethanol 5% to 10% over 0 to 40 minutes, held at 10% ethanol for 5 minutes, and then decreased from 10% to 2% ethanol over 40 to 50 minutes.

Supplementary Figure 122 Chiral HPLC spectrum of P-42

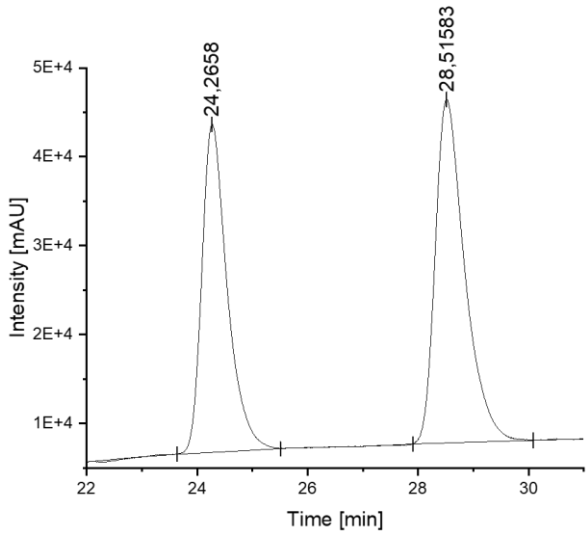

Peak	Time [min]	Area	Area %
1	24.266	19649.7	45.11
2	28.516	23914.2	54.89

The reactions used acetic acid, octanal and benzyl isocyanide in equimolar ratios. The reactions were carried out in *n*-hexane at a concentration of 0.025 mol×L^{-1}. The product was purified after 44 hours and a sample was taken for chiral HPLC analysis. The enantiomers of the product were separated on a Daicel Chiralpak AD-H using *n*-hexane and ethanol in a gradient elution: ethanol 5% to 10% over 0 to 40 minutes, held at 10% ethanol for 5 minutes, and then decreased from 10% to 2% ethanol over 40 to 50 minutes.

Supplementary Figure 123 Chiral HPLC spectrum of P-43

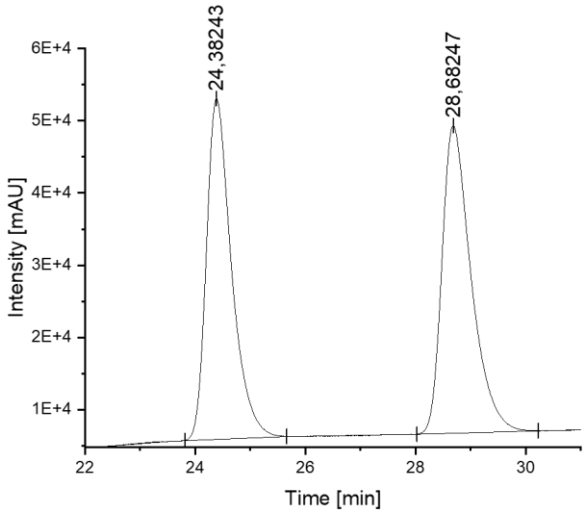

Peak	Time [min]	Area	Area %
1	24.382	24906.7	48.85
2	28.683	26084.3	51.15

The reactions used acetic acid, octanal and benzyl isocyanide in equimolar ratios. The reactions were carried out in *n*-hexane at a concentration of 0.025 mol×L^{-1}. The product was purified after 44 hours and a sample was taken for chiral HPLC analysis. The enantiomers of the product were separated on a Daicel Chiralpak AD-H using *n*-hexane and ethanol in a gradient elution: ethanol 5% to 10% over 0 to 40 minutes, held at 10% ethanol for 5 minutes, and then decreased from 10% to 2% ethanol over 40 to 50 minutes.

Supplementary Figure 124 Chiral HPLC spectrum of P-44

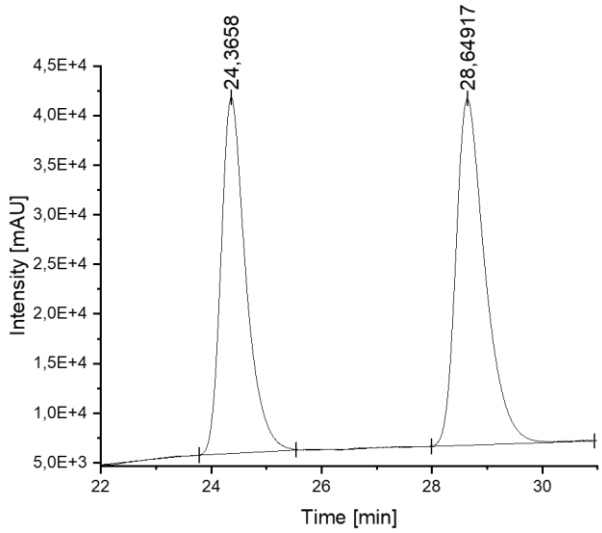

Peak	Time [min]	Area	Area %
1	24.366	18707.8	46.61
2	28.649	21430.2	53.39

The reactions used acetic acid, octanal and benzyl isocyanide in equimolar ratios. The reactions were carried out in *n*-hexane at a concentration of 0.025 mol×L^{-1}. The product was purified after 44 hours and a sample was taken for chiral HPLC analysis. The enantiomers of the product were separated on a Daicel Chiralpak AD-H using *n*-hexane and ethanol in a gradient elution: ethanol 5% to 10% over 0 to 40 minutes, held at 10% ethanol for 5 minutes, and then decreased from 10% to 2% ethanol over 40 to 50 minutes.

Supplementary Figure 125 Chiral HPLC spectrum of P-45

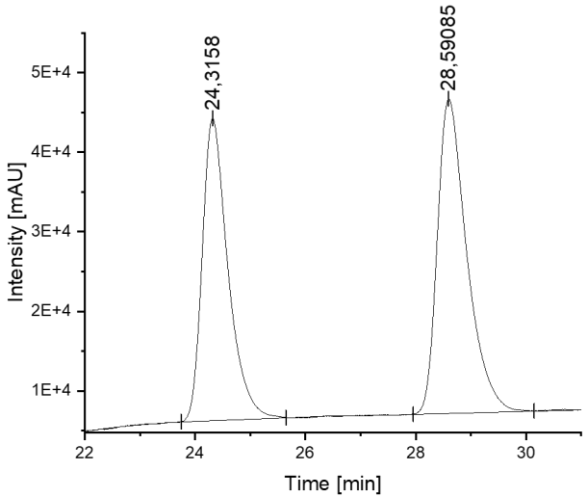

Peak	Time [min]	Area	Area %
1	24.316	20554.5	45.62
2	28.591	24497.6	54.38

The reactions used acetic acid, octanal and benzyl isocyanide in equimolar ratios. The reactions were carried out in *n*-hexane at a concentration of 0.025 mol×L^{-1}. The product was purified after 44 hours and a sample was taken for chiral HPLC analysis. The enantiomers of the product were separated on a Daicel Chiralpak AD-H using *n*-hexane and ethanol in a gradient elution: ethanol 5% to 10% over 0 to 40 minutes, held at 10% ethanol for 5 minutes, and then decreased from 10% to 2% ethanol over 40 to 50 minutes.

Supplementary Figure 126 Chiral HPLC spectrum of P-46

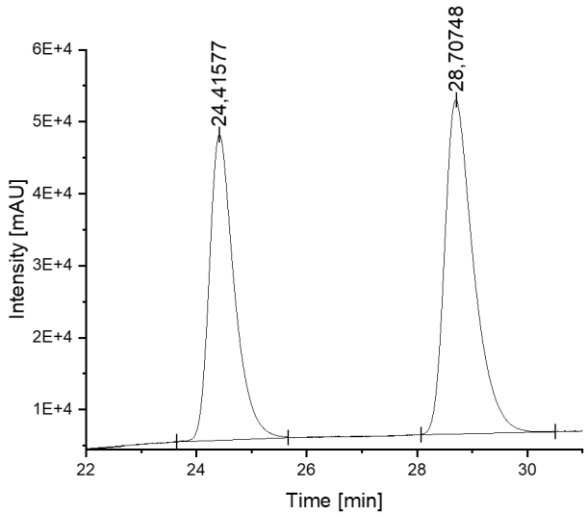

Peak	Time [min]	Area	Area %
1	24.416	22246.4	44.10
2	28.708	28194.9	55.90

The reactions used acetic acid, octanal and benzyl isocyanide in equimolar ratios. The reactions were carried out in *n*-hexane at a concentration of 0.025 mol×L^{-1}. The product was purified after 44 hours and a sample was taken for chiral HPLC analysis. The enantiomers of the product were separated on a Daicel Chiralpak AD-H using *n*-hexane and ethanol in a gradient elution: ethanol 5% to 10% over 0 to 40 minutes, held at 10% ethanol for 5 minutes, and then decreased from 10% to 2% ethanol over 40 to 50 minutes.

Supplementary Figure 127 Chiral HPLC spectrum of P-47

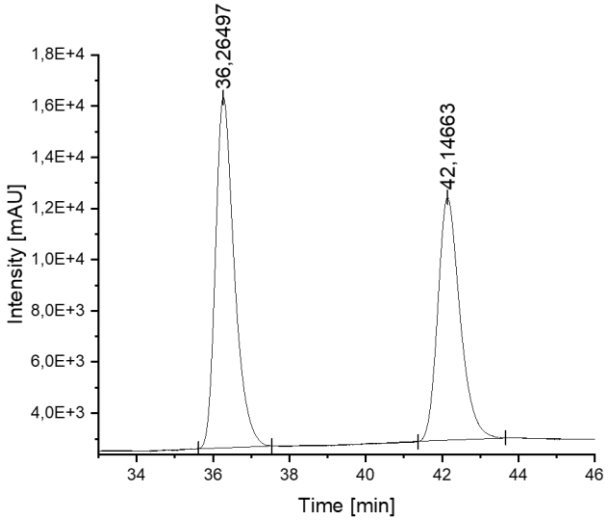

Peak	Time [min]	Area	Area %
1	36.265	7879.0	53.94
2	42.147	6728.1	46.06

The reactions used acetic acid, octanal and benzyl isocyanide in equimolar ratios. The reactions were carried out in *n*-hexane at a concentration of 0.025 mol×L^{-1}. The product was purified after 44 hours and a sample was taken for chiral HPLC analysis. The enantiomers of the product were separated on a Daicel Chiralpak AD-H using *n*-hexane and ethanol in a gradient elution: ethanol 2% to 8% over 0 to 40 minutes, held at 8% ethanol for 5 minutes, and then decreased from 8% to 2% ethanol over 40 to 50 minutes.

Supplementary Figure 128 Chiral HPLC spectrum of P-48

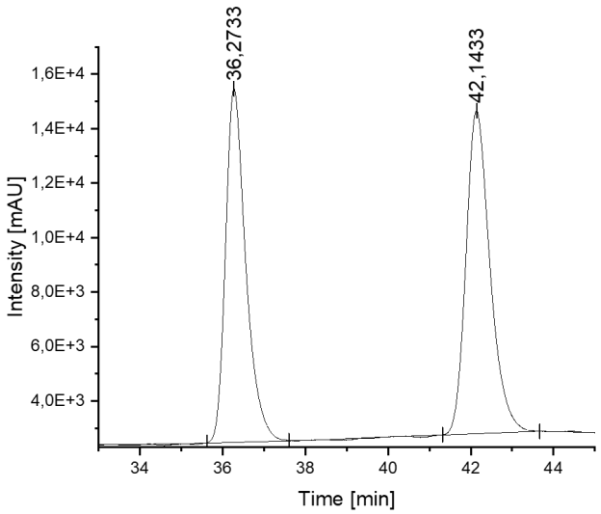

Peak	Time [min]	Area	Area %
1	36.273	7346.0	47.32
2	42.143	8179.4	52.68

The reactions used acetic acid, octanal and benzyl isocyanide in equimolar ratios. The reactions were carried out in *n*-hexane at a concentration of 0.025 mol×L^{-1}. The product was purified after 44 hours and a sample was taken for chiral HPLC analysis. The enantiomers of the product were separated on a Daicel Chiralpak AD-H using *n*-hexane and ethanol in a gradient elution: ethanol 2% to 8% over 0 to 40 minutes, held at 8% ethanol for 5 minutes, and then decreased from 8% to 2% ethanol over 40 to 50 minutes.

Supplementary Figure 129 Chiral HPLC spectrum of racemic P-49

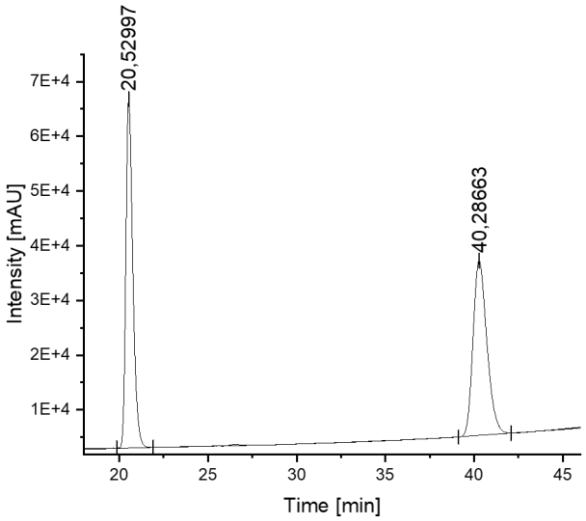

Peak	Time [min]	Area	Area %
1	20.530	28684.5	49.84
2	40.287	28868.8	50.16

The reactions used phenylacetic acid, octanal and benzyl isocyanide in equimolar ratios. The reactions were carried out in *n*-hexane at a concentration of 0.025 mol×L^{-1}. The product was purified after 44 hours and a sample was taken for chiral HPLC analysis. The enantiomers of the product were separated on a Daicel Chiralpak AD-H using *n*-hexane and ethanol in a gradient elution: ethanol 2% to 15% over 0 to 40 minutes, held at 15% ethanol for 5 minutes, and then decreased from 15% to 2% ethanol over 40 to 50 minutes.

Supplementary Figure 130 Chiral HPLC spectrum of P-50

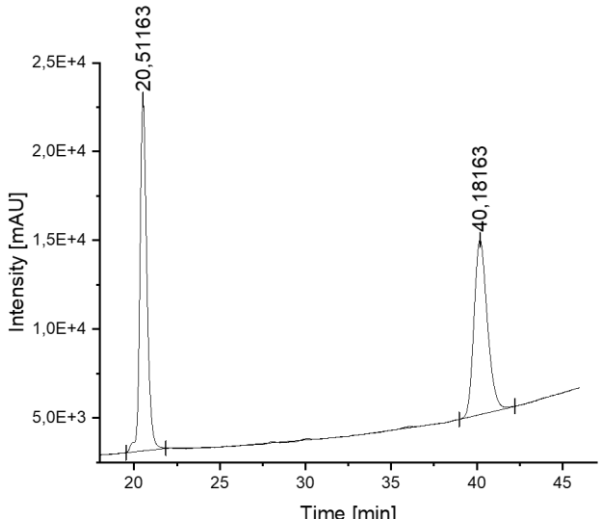

Peak	Time [min]	Area	Area %
1	20.512	9013.7	50.33
2	40.182	8894.0	49.67

The reactions used phenylacetic acid, octanal and benzyl isocyanide in equimolar ratios. The reactions were carried out in *n*-hexane at a concentration of 0.025 mol×L^{-1}. The product was purified after 44 hours and a sample was taken for chiral HPLC analysis. The enantiomers of the product were separated on a Daicel Chiralpak AD-H using *n*-hexane and ethanol in a gradient elution: ethanol 2% to 15% over 0 to 40 minutes, held at 15% ethanol for 5 minutes, and then decreased from 15% to 2% ethanol over 40 to 50 minutes.

Supplementary Figure 131 Chiral HPLC spectrum of P-51

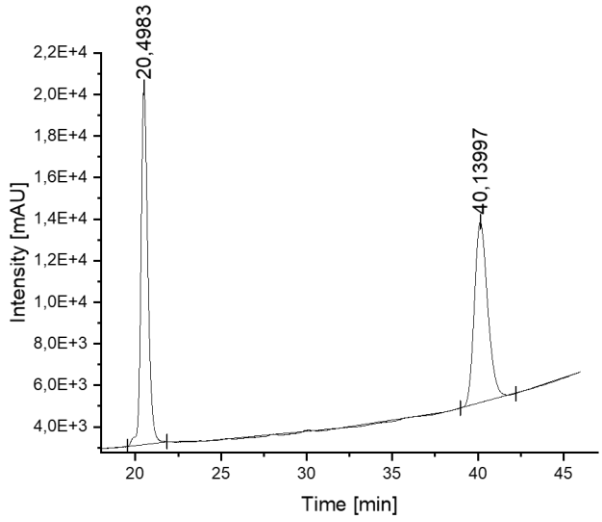

Peak	Time [min]	Area	Area %
1	20.498	7780.3	49.58
2	40.140	7913.3	50.42

The reactions used phenylacetic acid, octanal and benzyl isocyanide in equimolar ratios. The reactions were carried out in *n*-hexane at a concentration of 0.025 mol×L^{-1}. The product was purified after 44 hours and a sample was taken for chiral HPLC analysis. The enantiomers of the product were separated on a Daicel Chiralpak AD-H using *n*-hexane and ethanol in a gradient elution: ethanol 2% to 15% over 0 to 40 minutes, held at 15% ethanol for 5 minutes, and then decreased from 15% to 2% ethanol over 40 to 50 minutes.

Supplementary Figure 132 Chiral HPLC spectrum of P-52

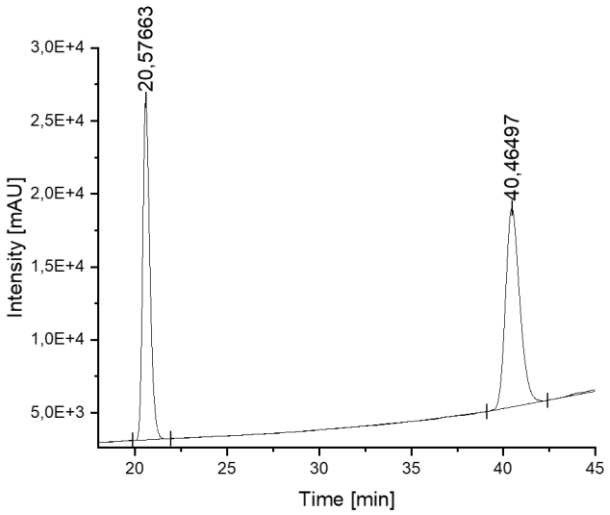

Peak	Time [min]	Area	Area %
1	20.577	10503.2	46.15
2	40.465	12253.3	53.85

The reactions used phenylacetic acid, octanal and benzyl isocyanide in equimolar ratios. The reactions were carried out in *n*-hexane at a concentration of 0.025 mol×L^{-1}. The product was purified after 44 hours and a sample was taken for chiral HPLC analysis. The enantiomers of the product were separated on a Daicel Chiralpak AD-H using *n*-hexane and ethanol in a gradient elution: ethanol 2% to 15% over 0 to 40 minutes, held at 15% ethanol for 5 minutes, and then decreased from 15% to 2% ethanol over 40 to 50 minutes.

Supplementary Figure 133 Chiral HPLC spectrum of P-53

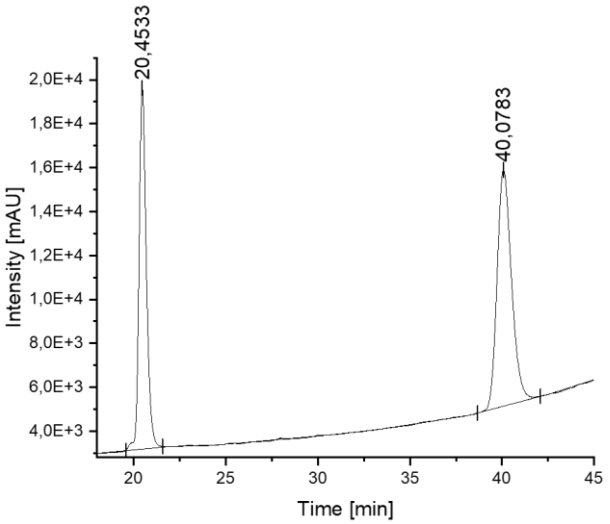

Peak	Time [min]	Area	Area %
1	20.453	7467.0	43.47
2	40.078	9708.5	56.53

The reactions used phenylacetic acid, octanal and benzyl isocyanide in equimolar ratios. The reactions were carried out in *n*-hexane at a concentration of 0.025 mol×L^{-1}. The product was purified after 44 hours and a sample was taken for chiral HPLC analysis. The enantiomers of the product were separated on a Daicel Chiralpak AD-H using *n*-hexane and ethanol in a gradient elution: ethanol 2% to 15% over 0 to 40 minutes, held at 15% ethanol for 5 minutes, and then decreased from 15% to 2% ethanol over 40 to 50 minutes.

Supplementary Figure 134 Chiral HPLC spectrum of P-54

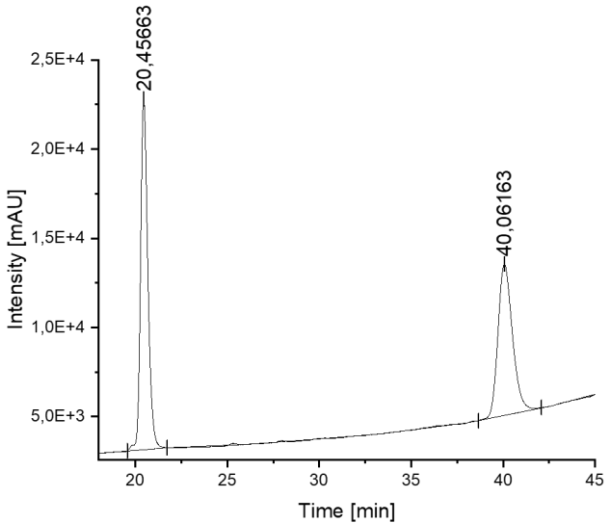

Peak	Time [min]	Area	Area %
1	20.457	8840.8	53.18
2	40.062	7782.3	46.82

The reactions used phenylacetic acid, octanal and benzyl isocyanide in equimolar ratios. The reactions were carried out in *n*-hexane at a concentration of 0.025 mol×L^{-1}. The product was purified after 44 hours and a sample was taken for chiral HPLC analysis. The enantiomers of the product were separated on a Daicel Chiralpak AD-H using *n*-hexane and ethanol in a gradient elution: ethanol 2% to 15% over 0 to 40 minutes, held at 15% ethanol for 5 minutes, and then decreased from 15% to 2% ethanol over 40 to 50 minutes.

Supplementary Figure 135 Chiral HPLC spectrum of P-55

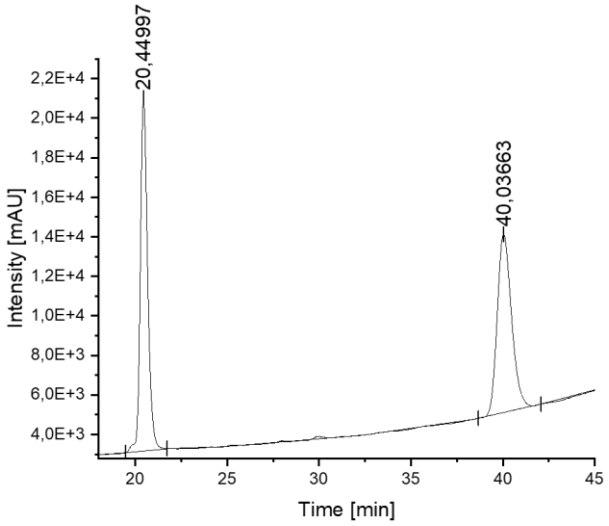

Peak	Time [min]	Area	Area %
1	20.450	8062.7	49.97
2	40.037	8071.7	50.03

The reactions used phenylacetic acid, octanal and benzyl isocyanide in equimolar ratios. The reactions were carried out in *n*-hexane at a concentration of 0.025 mol×L^{-1}. The product was purified after 44 hours and a sample was taken for chiral HPLC analysis. The enantiomers of the product were separated on a Daicel Chiralpak AD-H using *n*-hexane and ethanol in a gradient elution: ethanol 2% to 15% over 0 to 40 minutes, held at 15% ethanol for 5 minutes, and then decreased from 15% to 2% ethanol over 40 to 50 minutes.

Supplementary Figure 136 Chiral HPLC spectrum of racemic P-56

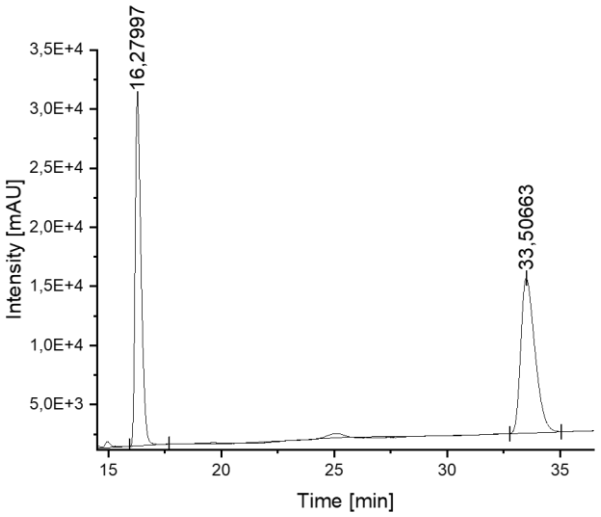

Peak	Time [min]	Area	Area %
1	16.280	9559.9	50.10
2	33.507	9520.3	49.90

The reactions used acetic acid, octanal and cyclohexyl isocyanide in equimolar ratios. The reactions were carried out in *n*-hexane at a concentration of 0.025 mol×L^{-1}. The crude product was analysed after 44 hours *via* chiral HPLC analysis. The enantiomers of the product were separated on a Daicel Chiralpak AD-H using *n*-hexane and ethanol in a gradient elution: ethanol 2% to 10% over 0 to 40 minutes, held at 10% ethanol for 5 minutes, and then decreased from 10% to 2% ethanol over 40 to 50 minutes.

Supplementary Figure 137 Chiral HPLC spectrum of P-57

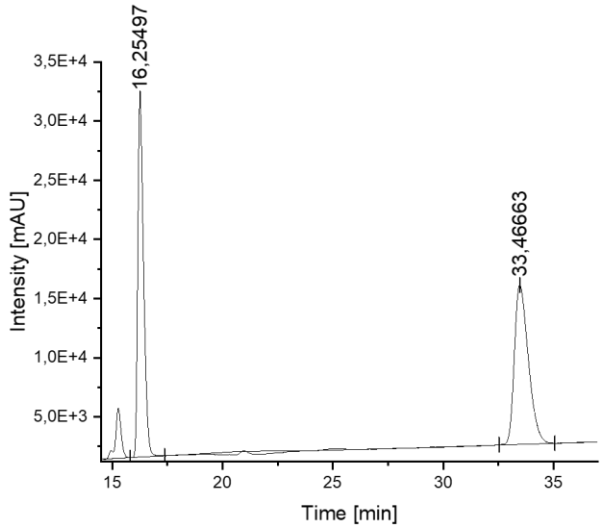

Peak	Time [min]	Area	Area %
1	16.255	9217.6	48.27
2	33.467	9878.3	51.73

The reactions used acetic acid, octanal and cyclohexyl isocyanide in equimolar ratios. The reactions were carried out in *n*-hexane at a concentration of 0.025 mol×L^{-1}. The crude product was analysed after 44 hours *via* chiral HPLC analysis. The enantiomers of the product were separated on a Daicel Chiralpak AD-H using *n*-hexane and ethanol in a gradient elution: ethanol 2% to 10% over 0 to 40 minutes, held at 10% ethanol for 5 minutes, and then decreased from 10% to 2% ethanol over 40 to 50 minutes.

Supplementary Figure 138 Chiral HPLC spectrum of P-58

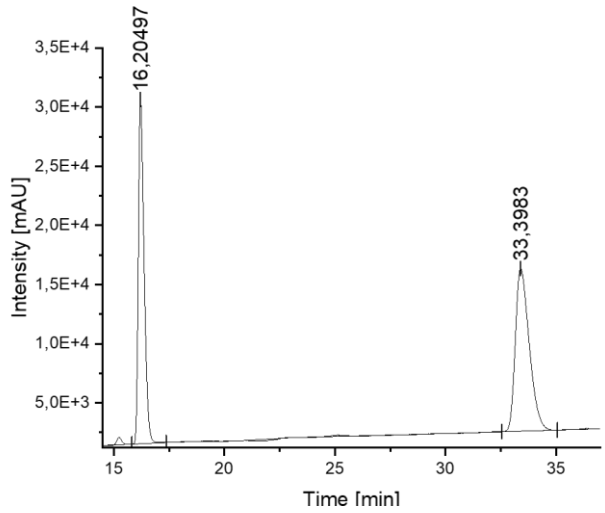

Peak	Time [min]	Area	Area %
1	16.205	8780.8	46.71
2	33.398	10018.7	53.29

The reactions used acetic acid, octanal and cyclohexyl isocyanide in equimolar ratios. The reactions were carried out in *n*-hexane at a concentration of 0.025 mol×L^{-1}. The crude product was analysed after 44 hours *via* chiral HPLC analysis. The enantiomers of the product were separated on a Daicel Chiralpak AD-H using *n*-hexane and ethanol in a gradient elution: ethanol 2% to 10% over 0 to 40 minutes, held at 10% ethanol for 5 minutes, and then decreased from 10% to 2% ethanol over 40 to 50 minutes.

Supplementary Figure 139 Chiral HPLC spectrum of P-59

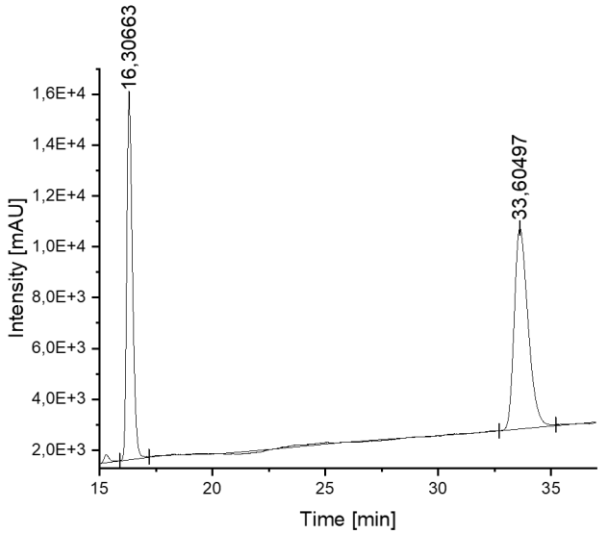

Peak	Time [min]	Area	Area %
1	16.307	8424.8	43.14
2	33.605	11123.6	56.86

The reactions used acetic acid, octanal and cyclohexyl isocyanide in equimolar ratios. The reactions were carried out in *n*-hexane at a concentration of 0.025 mol×L^{-1}. The crude product was analysed after 44 hours *via* chiral HPLC analysis. The enantiomers of the product were separated on a Daicel Chiralpak AD-H using *n*-hexane and ethanol in a gradient elution: ethanol 2% to 10% over 0 to 40 minutes, held at 10% ethanol for 5 minutes, and then decreased from 10% to 2% ethanol over 40 to 50 minutes.

Supplementary Figure 140 Chiral HPLC spectrum of P-60

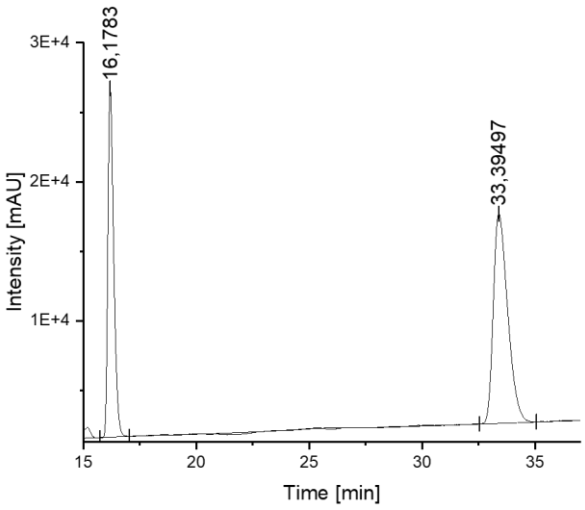

Peak	Time [min]	Area	Area %
1	16.178	7537.3	40.35
2	33.395	11142.6	59.65

The reactions used acetic acid, octanal and cyclohexyl isocyanide in equimolar ratios. The reactions were carried out in *n*-hexane at a concentration of 0.025 mol×L^{-1}. The crude product was analysed after 44 hours *via* chiral HPLC analysis. The enantiomers of the product were separated on a Daicel Chiralpak AD-H using *n*-hexane and ethanol in a gradient elution: ethanol 2% to 10% over 0 to 40 minutes, held at 10% ethanol for 5 minutes, and then decreased from 10% to 2% ethanol over 40 to 50 minutes.

Supplementary Figure 141 Chiral HPLC spectrum of P-61

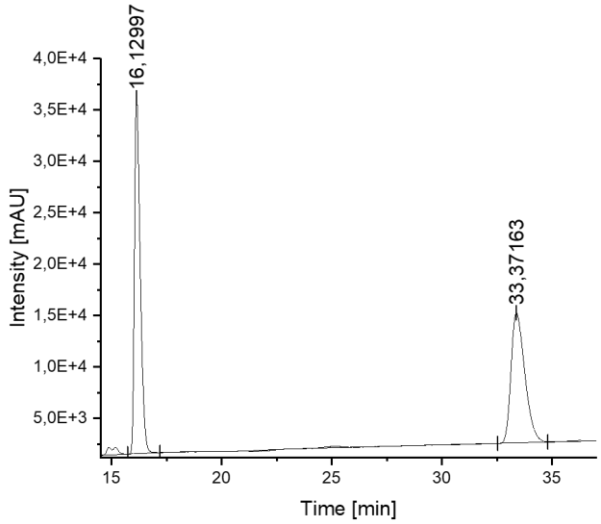

Peak	Time [min]	Area	Area %
1	16.130	10554.1	53.49
2	33.372	9176.3	46.51

The reactions used acetic acid, octanal and cyclohexyl isocyanide in equimolar ratios. The reactions were carried out in *n*-hexane at a concentration of 0.025 mol×L^{-1}. The crude product was analysed after 44 hours *via* chiral HPLC analysis. The enantiomers of the product were separated on a Daicel Chiralpak AD-H using *n*-hexane and ethanol in a gradient elution: ethanol 2% to 10% over 0 to 40 minutes, held at 10% ethanol for 5 minutes, and then decreased from 10% to 2% ethanol over 40 to 50 minutes.

Supplementary Figure 142 Chiral HPLC spectrum of P-62

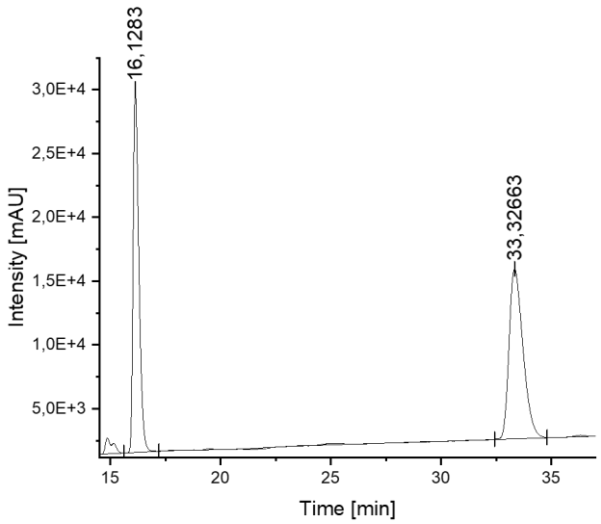

Peak	Time [min]	Area	Area %
1	16.128	8622.1	47.00
2	33.327	9722.5	53.00

The reactions used acetic acid, octanal and cyclohexyl isocyanide in equimolar ratios. The reactions were carried out in *n*-hexane at a concentration of 0.025 mol×L^{-1}. The crude product was analysed after 44 hours *via* chiral HPLC analysis. The enantiomers of the product were separated on a Daicel Chiralpak AD-H using *n*-hexane and ethanol in a gradient elution: ethanol 2% to 10% over 0 to 40 minutes, held at 10% ethanol for 5 minutes, and then decreased from 10% to 2% ethanol over 40 to 50 minutes.

Supplementary Figure 143 Chiral HPLC spectrum of racemic P-63

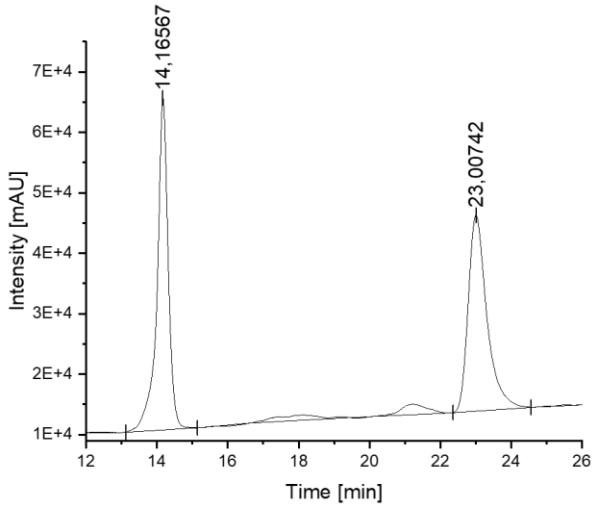

Peak	Time [min]	Area	Area %
1	14.166	20023.4	50.16
2	23.007	19894.9	49.84

The reactions used acetic acid, octanal and isocyano benzene in equimolar ratios. The reactions were carried out in *n*-hexane at a concentration of 0.025 mol×L^{-1}. The crude product was analysed after 44 hours *via* chiral HPLC analysis. The enantiomers of the product were separated on a Daicel Chiralpak AD-H using *n*-hexane and ethanol in a gradient elution: ethanol 2% to 10% over 0 to 40 minutes, held at 10% ethanol for 5 minutes, and then decreased from 10% to 2% ethanol over 40 to 50 minutes.

Supplementary Figure 144 Chiral HPLC spectrum of P-64

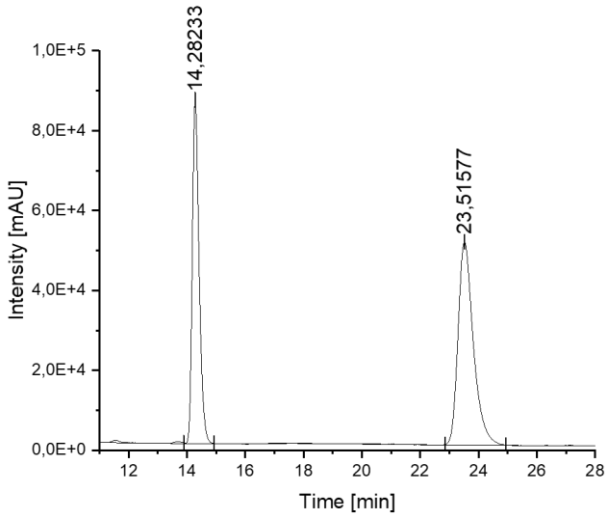

Peak	Time [min]	Area	Area %
1	14.282	23314.3	43.04
2	23.516	30849.7	56.96

The reactions used acetic acid, octanal and isocyano benzene in equimolar ratios. The reactions were carried out in *n*-hexane at a concentration of 0.025 mol×L^{-1}. The product was purified after 44 hours and a sample was taken for chiral HPLC analysis. The enantiomers of the product were separated on a Daicel Chiralpak AD-H using *n*-hexane and ethanol in a gradient elution: ethanol 2% to 10% over 0 to 40 minutes, held at 10% ethanol for 5 minutes, and then decreased from 10% to 2% ethanol over 40 to 50 minutes.

Supplementary Figure 145 Chiral HPLC spectrum of racemic P-65

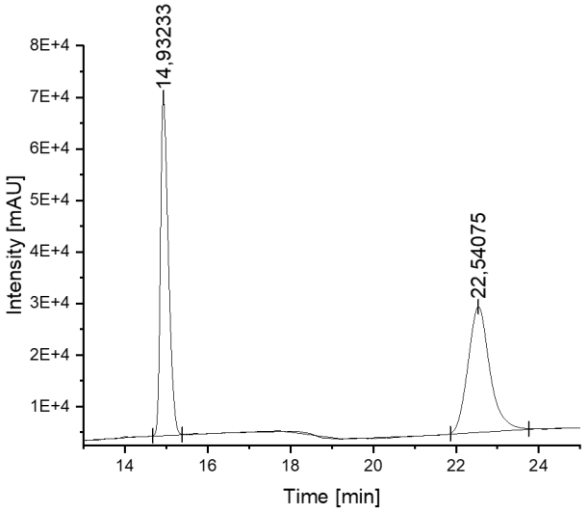

Peak	Time [min]	Area	Area %
1	14.932	14792.1	49.83
2	22.541	14891.1	50.17

The reactions used acetic acid, octanal and butyl isocyanide in equimolar ratios. The reactions were carried out in *n*-hexane at a concentration of 0.025 mol×L^{-1}. The product was purified after 44 hours and a sample was taken for chiral HPLC analysis. The enantiomers of the product were separated on a Daicel Chiralpak AD-H using *n*-hexane and ethanol in a gradient elution: ethanol 2% to 10% over 0 to 40 minutes, held at 10% ethanol for 5 minutes, and then decreased from 10% to 2% ethanol over 40 to 50 minutes.

Supplementary Figure 146 Chiral HPLC spectrum of P-66

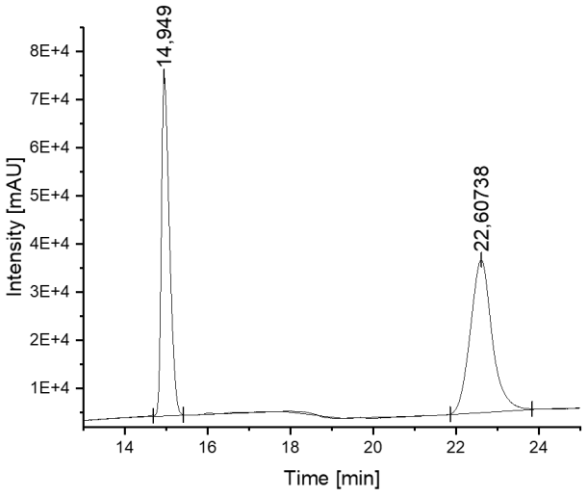

Peak	Time [min]	Area	Area %
1	14.949	15950.4	45.17
2	22.607	19359.8	54.83

The reactions used acetic acid, octanal and butyl isocyanide in equimolar ratios. The reactions were carried out in *n*-hexane at a concentration of 0.025 mol×L^{-1}. The product was purified after 44 hours and a sample was taken for chiral HPLC analysis. The enantiomers of the product were separated on a Daicel Chiralpak AD-H using *n*-hexane and ethanol in a gradient elution: ethanol 2% to 10% over 0 to 40 minutes, held at 10% ethanol for 5 minutes, and then decreased from 10% to 2% ethanol over 40 to 50 minutes.

Supplementary Figure 147 Chiral HPLC spectrum of racemic P-67

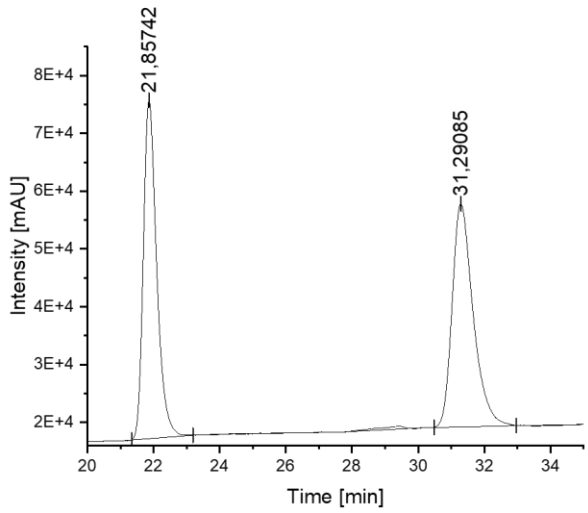

Peak	Time [min]	Area	Area %
1	21.857	27962.2	49.76
2	31.291	28231.1	50.24

The reactions used benzoic acid, octanal and benzyl isocyanide in equimolar ratios. The reactions were carried out in *n*-hexane at a concentration of 0.025 mol×L^{-1}. The product was purified after 44 hours and a sample was taken for chiral HPLC analysis. The enantiomers of the product were separated on a Daicel Chiralpak AD-H using *n*-hexane and ethanol in a gradient elution: ethanol 2% to 10% over 0 to 40 minutes, held at 10% ethanol for 5 minutes, and then decreased from 10% to 2% ethanol over 40 to 50 minutes.

Supplementary Figure 148 Chiral HPLC spectrum of P-68

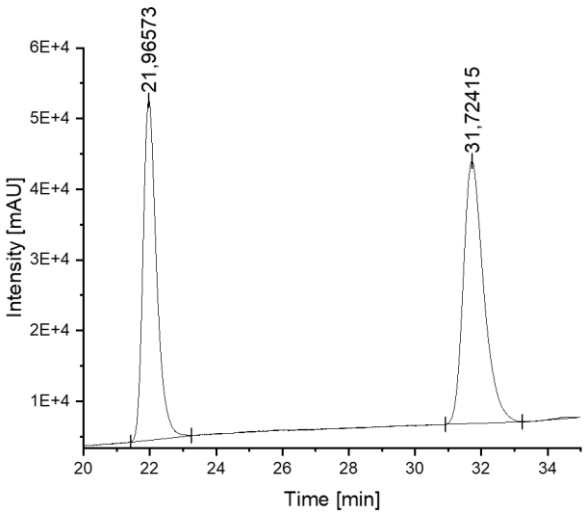

Peak	Time [min]	Area	Area %
1	21.966	22733.2	46.24
2	31.724	26429.2	53.76

The reactions used benzoic acid, octanal and benzyl isocyanide in equimolar ratios. The reactions were carried out in *n*-hexane at a concentration of 0.025 mol×L^{-1}. The product was purified after 44 hours and a sample was taken for chiral HPLC analysis. The enantiomers of the product were separated on a Daicel Chiralpak AD-H using *n*-hexane and ethanol in a gradient elution: ethanol 2% to 10% over 0 to 40 minutes, held at 10% ethanol for 5 minutes, and then decreased from 10% to 2% ethanol over 40 to 50 minutes.

Supplementary Figure 149 Chiral HPLC spectrum of racemic P-77

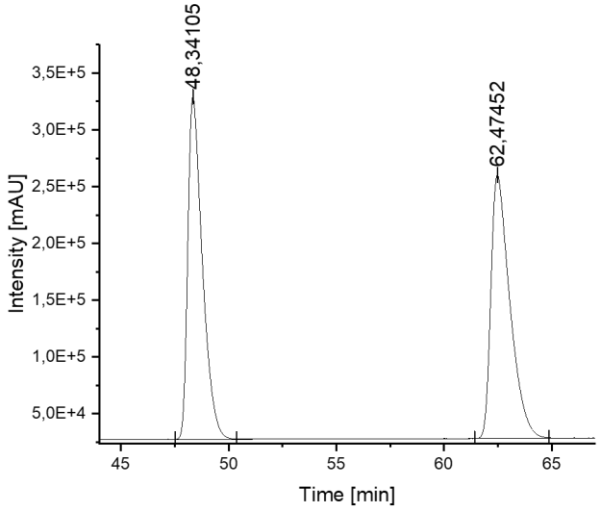

Peak	Time [min]	Area	Area %
1	48.341	235818.6	50.06
2	62.475	235291.8	49.94

The reactions used acetic acid, benzaldehyde and benzyl isocyanide in equimolar ratios. The reactions were carried out in *n*-hexane at a concentration of 0.025 mol×L^{-1}. The product was purified after 44 hours and a sample was taken for chiral HPLC analysis. The enantiomers of the product were separated on a Daicel Chiralpak AD-H using *n*-hexane and ethanol in a gradient elution: ethanol 2% to 10% over 0 to 80 minutes, held at 10% ethanol for 5 minutes, and then decreased from 10% to 2% ethanol over 85 to 90 minutes.

Supplementary Figure 150 Chiral HPLC spectrum of P-78

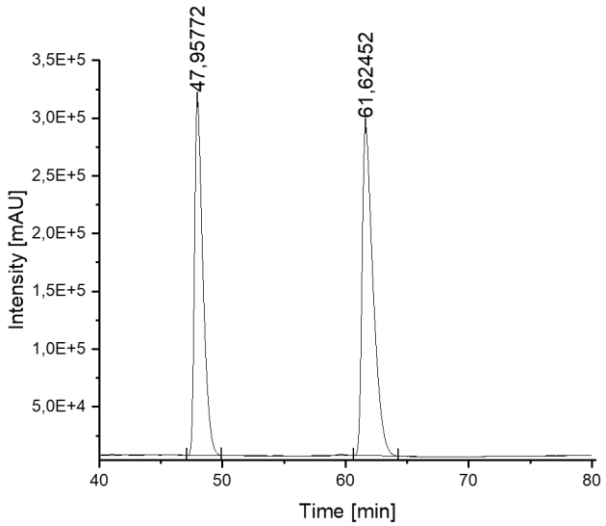

Peak	Time [min]	Area	Area %
1	47.958	243818.6	45.12
2	61.625	296613.8	54.88

The reactions used acetic acid, benzaldehyde and benzyl isocyanide in equimolar ratios. The reactions were carried out in *n*-hexane at a concentration of 0.025 mol×L^{-1}. The product was purified after 44 hours and a sample was taken for chiral HPLC analysis. The enantiomers of the product were separated on a Daicel Chiralpak AD-H using *n*-hexane and ethanol in a gradient elution: ethanol 2% to 10% over 0 to 80 minutes, held at 10% ethanol for 5 minutes, and then decreased from 10% to 2% ethanol over 85 to 90 minutes.

Supplementary Figure 151 Chiral HPLC spectrum of racemic P-79

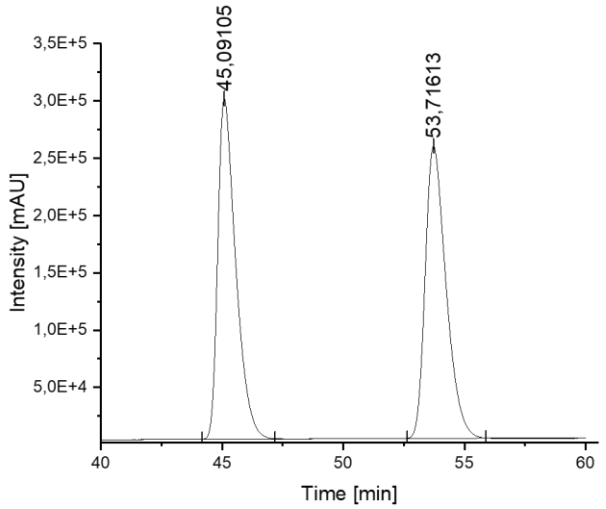

Peak	Time [min]	Area	Area %
1	45.091	254960.6	50.02
2	53.716	254758.6	49.98

The reactions used acetic acid, 2,3,5-trichlorobenzaldehyde and benzyl isocyanide in equimolar ratios. The reactions were carried out in *n*-hexane at a concentration of 0.025 mol×L^{-1}. The product was purified after 44 hours and a sample was taken for chiral HPLC analysis. The enantiomers of the product were separated on a Daicel Chiralpak AD-H using *n*-hexane and ethanol in a gradient elution: ethanol 2% to 10% over 0 to 80 minutes, held at 10% ethanol for 5 minutes, and then decreased from 10% to 2% ethanol over 85 to 90 minutes.

Supplementary Figure 152 Chiral HPLC spectrum of P-80

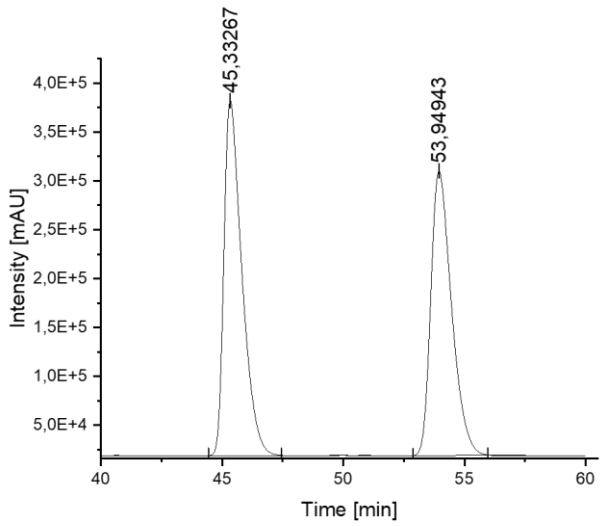

Peak	Time [min]	Area	Area %
1	45.333	312525.9	52.02
2	53.949	288293.8	47.98

The reactions used acetic acid, 2,3,5-trichlorobenzaldehyde and benzyl isocyanide in equimolar ratios. The reactions were carried out in *n*-hexane at a concentration of 0.025 mol×L^{-1}. The product was purified after 44 hours and a sample was taken for chiral HPLC analysis. The enantiomers of the product were separated on a Daicel Chiralpak AD-H using *n*-hexane and ethanol in a gradient elution: ethanol 2% to 10% over 0 to 80 minutes, held at 10% ethanol for 5 minutes, and then decreased from 10% to 2% ethanol over 85 to 90 minutes.

Supplementary Figure 153 Chiral HPLC spectrum of P-81

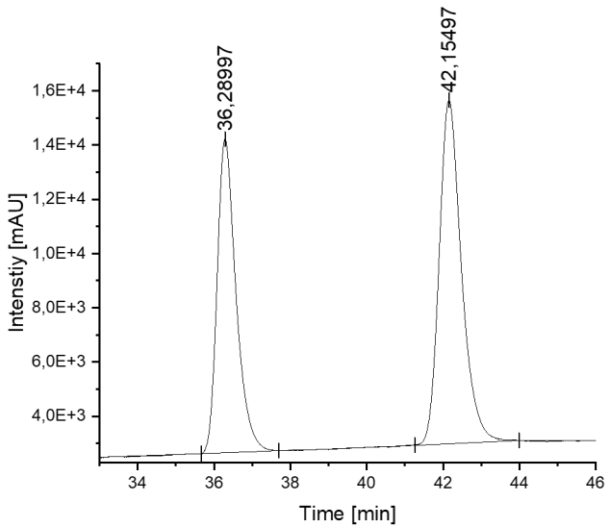

Peak	Time [min]	Area	Area %
1	36.290	6658.9	43.13
2	42.155	8780.2	56.87

The reactions used acetic acid, octanal and benzyl isocyanide. The reactions were carried out in *n*-hexane at a concentration of 0.025 mol×L^{-1}. The product was purified after 44 hours and a sample was taken for chiral HPLC analysis. The enantiomers of the product were separated on a Daicel Chiralpak AD-H using *n*-hexane and ethanol in a gradient elution: ethanol 2% to 10% over 0 to 40 minutes, held at 10% ethanol for 5 minutes, and then decreased from 10% to 2% ethanol over 45 to 50 minutes.

Supplementary Figure 154 Chiral HPLC spectrum of P-82

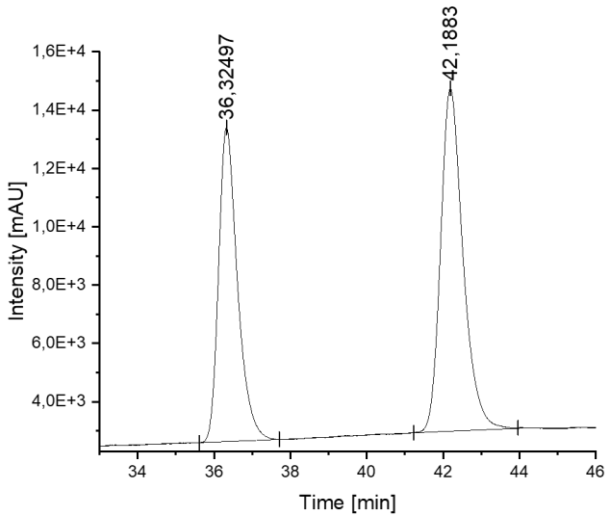

Peak	Time [min]	Area	Area %
1	36.325	6141.1	42.83
2	42.188	8197.1	57.17

The reactions used acetic acid, octanal and benzyl isocyanide. The reactions were carried out in *n*-hexane at a concentration of 0.025 mol×L^{-1}. The product was purified after 44 hours and a sample was taken for chiral HPLC analysis. The enantiomers of the product were separated on a Daicel Chiralpak AD-H using *n*-hexane and ethanol in a gradient elution: ethanol 2% to 10% over 0 to 40 minutes, held at 10% ethanol for 5 minutes, and then decreased from 10% to 2% ethanol over 45 to 50 minutes.

Supplementary Figure 155 Chiral HPLC spectrum of P-83

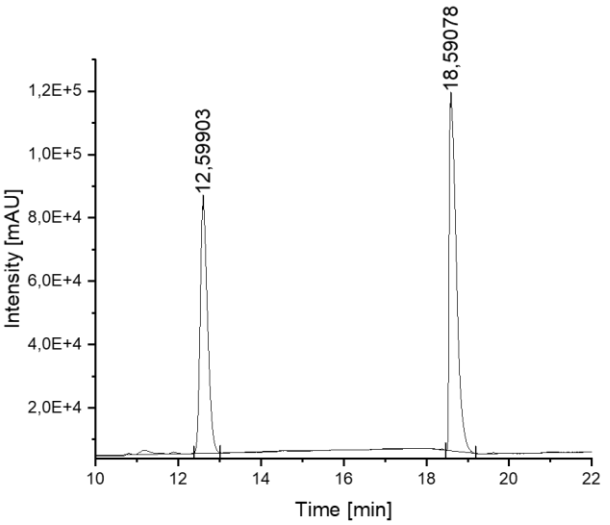

Peak	Time [min]	Area	Area %
1	12.599	16509.6	42.12
2	18.591	39200.8	57.88

The reactions used acetic acid, octanal and cyclohexyl isocyanide. The reactions were carried out in *n*-hexane at a concentration of 0.025 mol×L^{-1}. The product was purified after 44 hours and a sample was taken for chiral HPLC analysis. The enantiomers of the product were separated on a Daicel Chiralpak AD-H using *n*-hexane and ethanol in a gradient elution: ethanol 2% to 10% over 0 to 40 minutes, held at 10% ethanol for 5 minutes, and then decreased from 10% to 2% ethanol over 45 to 50 minutes.

Supplementary Figure 156 Chiral HPLC spectrum of racemic U-01

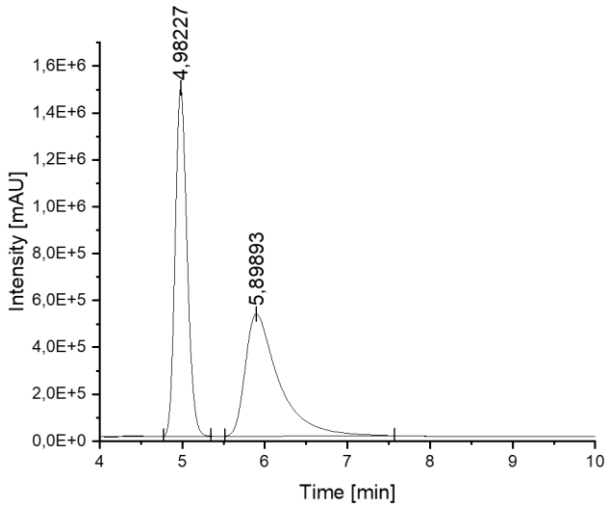

Peak	Time [min]	Area	Area %
1	4.983	248723.5	50.12
2	5.899	247513.6	49.88

The reactions used benzoic acid, *p*-toluidine, 4-methoxybenzaldehyde and *tert*-butyl isocyanide in equimolar ratios. The reactions were carried out in *n*-hexane at a concentration of 0.025 mol×L^{-1}. The product was purified after 44 hours and a sample was taken for chiral HPLC analysis. The enantiomers of the product were separated on a Daicel Chiralpak AD-H using *n*-hexane and ethanol in an isocratic mixture of: 90% *n*-hexane and 10% ethanol for 60 minutes.

Supplementary Figure 157 Chiral HPLC spectrum of U-02

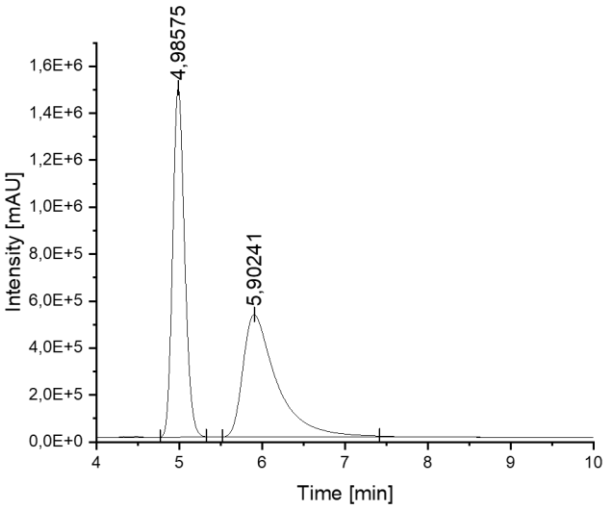

Peak	Time [min]	Area	Area %
1	4.986	249743.4	49.86
2	5.902	251113.6	50.14

The reactions used benzoic acid, *p*-toluidine, 4-methoxybenzaldehyde and *tert*-butyl isocyanide in equimolar ratios. The reactions were carried out in *n*-hexane at a concentration of 0.025 mol×L^{-1}. The product was purified after 44 hours and a sample was taken for chiral HPLC analysis. The enantiomers of the product were separated on a Daicel Chiralpak AD-H using *n*-hexane and ethanol in an isocratic mixture of: 90% *n*-hexane and 10% ethanol for 60 minutes.

Supplementary Figure 158 Chiral HPLC spectrum of U-07

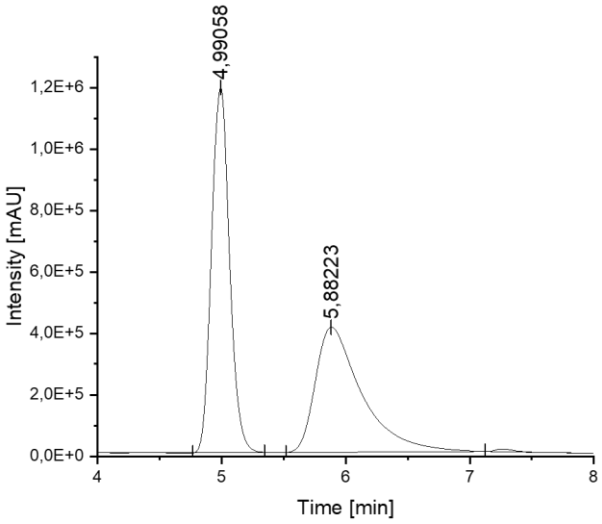

Peak	Time [min]	Area	Area %
1	4.991	200724.9	53.15
2	5.882	176915.9	46.85

The reactions used benzoic acid, *p*-toluidine, 4-methoxybenzaldehyde and *tert*-butyl isocyanide in equimolar ratios. The reactions were carried out in *n*-hexane at a concentration of 0.025 mol×L^{-1}. The product was purified after 44 hours and a sample was taken for chiral HPLC analysis. The enantiomers of the product were separated on a Daicel Chiralpak AD-H using *n*-hexane and ethanol in an isocratic mixture of: 90% *n*-hexane and 10% ethanol for 60 minutes.

Supplementary Figure 159 Chiral HPLC spectrum of U-08

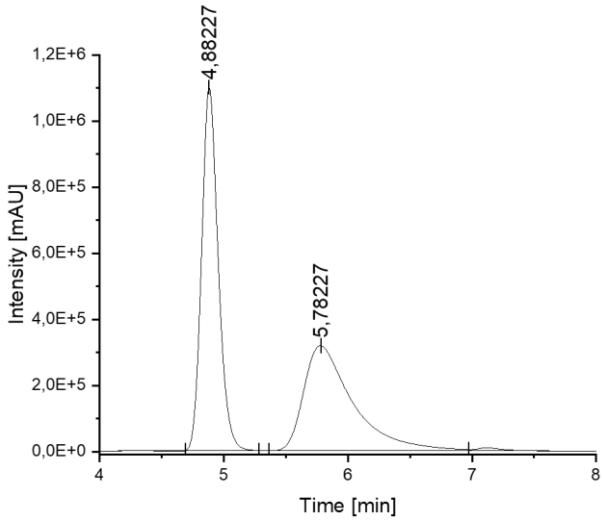

Peak	Time [min]	Area	Area %
1	4.883	170090.9	53.84
2	5.783	145846.3	46.16

The reactions used benzoic acid, *p*-toluidine, 4-methoxybenzaldehyde and *tert*-butyl isocyanide in equimolar ratios. The reactions were carried out in *n*-hexane at a concentration of 0.025 mol×L^{-1}. The product was purified after 44 hours and a sample was taken for chiral HPLC analysis. The enantiomers of the product were separated on a Daicel Chiralpak AD-H using *n*-hexane and ethanol in an isocratic mixture of: 90% *n*-hexane and 10% ethanol for 60 minutes.

Supplementary Figure 160 Chiral HPLC spectrum of U-09

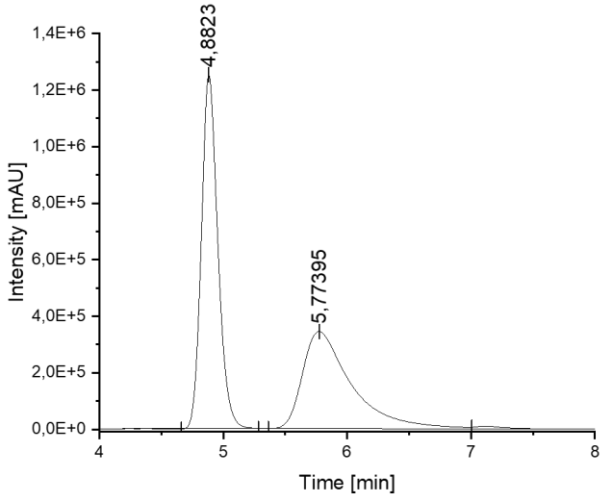

Peak	Time [min]	Area	Area %
1	4.882	192256.2	55.17
2	5.774	156257.3	44.83

The reactions used benzoic acid, *p*-toluidine, 4-methoxybenzaldehyde and *tert*-butyl isocyanide in equimolar ratios. The reactions were carried out in *n*-hexane at a concentration of 0.025 mol×L^{-1}. The product was purified after 44 hours and a sample was taken for chiral HPLC analysis. The enantiomers of the product were separated on a Daicel Chiralpak AD-H using *n*-hexane and ethanol in an isocratic mixture of: 90% *n*-hexane and 10% ethanol for 60 minutes.

Supplementary Figure 161 Chiral HPLC spectrum of U-10

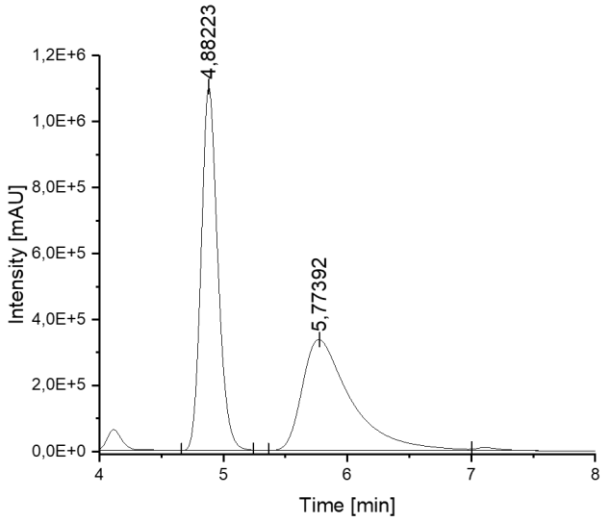

Peak	Time [min]	Area	Area %
1	4.882	171147.4	52.71
2	5.774	153533.7	47.29

The reactions used benzoic acid, *p*-toluidine, 4-methoxybenzaldehyde and *tert*-butyl isocyanide in equimolar ratios. The reactions were carried out in *n*-hexane at a concentration of 0.025 mol×L^{-1}. The product was purified after 44 hours and a sample was taken for chiral HPLC analysis. The enantiomers of the product were separated on a Daicel Chiralpak AD-H using *n*-hexane and ethanol in an isocratic mixture of: 90% *n*-hexane and 10% ethanol for 60 minutes.

Supplementary Figure 162 Chiral HPLC spectrum of U-11

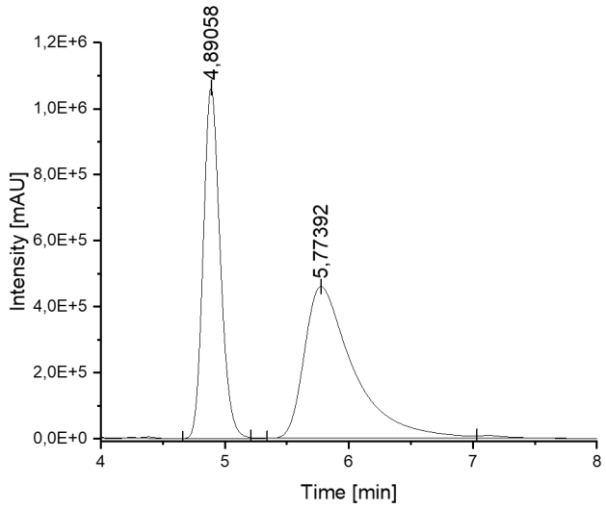

Peak	Time [min]	Area	Area %
1	4.891	168029.1	44.38
2	5.774	210622.1	55.62

The reactions used benzoic acid, *p*-toluidine, 4-methoxybenzaldehyde and *tert*-butyl isocyanide in equimolar ratios. The reactions were carried out in *n*-hexane at a concentration of 0.025 mol×L^{-1}. The product was purified after 44 hours and a sample was taken for chiral HPLC analysis. The enantiomers of the product were separated on a Daicel Chiralpak AD-H using *n*-hexane and ethanol in an isocratic mixture of: 90% *n*-hexane and 10% ethanol for 60 minutes.

Supplementary Figure 163 Chiral HPLC spectrum of U-12

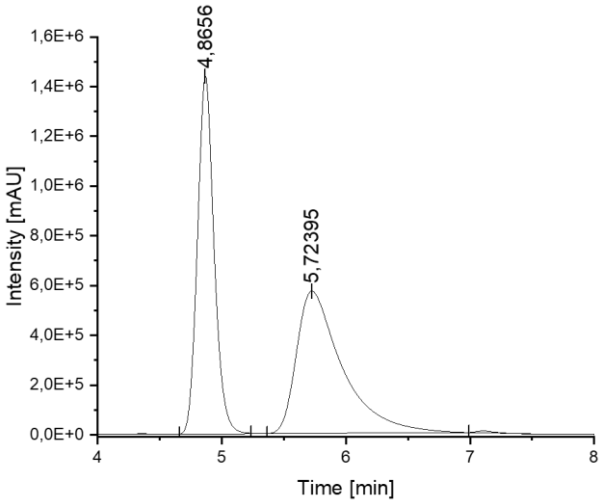

Peak	Time [min]	Area	Area %
1	4.866	159778.6	45.54
2	5.724	191100.8	54.46

The reactions used benzoic acid, *p*-toluidine, 4-methoxybenzaldehyde and *tert*-butyl isocyanide in equimolar ratios. The reactions were carried out in *n*-hexane at a concentration of 0.025 mol×L^{-1}. The product was purified after 44 hours and a sample was taken for chiral HPLC analysis. The enantiomers of the product were separated on a Daicel Chiralpak AD-H using *n*-hexane and ethanol in an isocratic mixture of: 90% *n*-hexane and 10% ethanol for 60 minutes.

Chapter 7 Bibliography

1 Kakaei, K., Esrafili, M. D. & Ehsani, A. in *Interface Science and Technology* Vol. 27 (eds Karim Kakaei, Mehdi D. Esrafili, & Ali Ehsani) 1-21 (Elsevier, 2019).

2 Schmidt, F. in *Basic Principles in Applied Catalysis* (ed Manfred Baerns) 3-16 (Springer Berlin Heidelberg, 2004).

3 Armor, J. N. A history of industrial catalysis. *Catalysis Today* **163**, 3-9 (2011).

4 Zhou, Q.-L. Transition-metal catalysis and organocatalysis: where can progress be expected? *Angewandte Chemie (International ed. in English)* **55**, 5352-5353 (2015).

5 Zecchina, A. & Califano, S. *The development of catalysis: a history of key processes and personas in catalytic science and technology*. (John Wiley & Sons, 2017).

6 Grand View Research - Catalyst Market Size, Share & Trends Analysis Report By Raw Material (Chemical Compounds), By Product by Application (Heterogeneous, Homogeneous), By Region, And Segment Forecasts, 2024 - 2030. (Grand review research, 2023).

7 Wisniak, J. The History of Catalysis. From the Beginning to Nobel Prizes. *Educación Química* **21**, 60-69, doi:https://doi.org/10.1016/S0187-893X(18)30074-0 (2010).

8 Abbass, K. *et al.* A review of the global climate change impacts, adaptation, and sustainable mitigation measures. *Environmental Science and Pollution Research* **29**, 42539-42559 (2022).

9 Adedeji, O. Global climate change. *Journal of Geoscience and Environment Protection* **2**, 114 (2014).

10 Seddon, N. *et al.* Understanding the value and limits of nature-based solutions to climate change and other global challenges. *Philosophical Transactions of the Royal Society B* **375**, 20190120 (2020).

11 Häder, D.-P. *et al.* Anthropogenic pollution of aquatic ecosystems: Emerging problems with global implications. *Science of the Total environment* **713**, 136586 (2020).

12 MacLeod, M., Arp, H. P. H., Tekman, M. B. & Jahnke, A. The global threat from plastic pollution. *Science* **373**, 61-65 (2021).

13 Moshood, T. D. *et al.* Sustainability of biodegradable plastics: New problem or solution to solve the global plastic pollution? *Current Research in Green and Sustainable Chemistry* **5**, 100273 (2022).

14 Rentschler, J. & Leonova, N. Global air pollution exposure and poverty. *Nature communications* **14**, 4432 (2023).

15 Gu, D., Andreev, K. & Dupre, M. E. Major trends in population growth around the world. *China CDC weekly* **3**, 604 (2021).

16 Dauvergne, P. *The shadows of consumption: Consequences for the global environment*. (MIT press, 2010).

17 Research, G. V. Catalyst Market Size, Share & Trends Report, Catalyst Market Size, Share & Trends Analysis Report By Raw Material (Chemical Compounds, Zeolites, Metals), By Product (Heterogeneous, Homogeneous), By Application, By Region, And Segment Forecasts, 2020 - 2027. (2020).

18 Sheldon, R. A. Atom efficiency and catalysis in organic synthesis. *Pure and Applied Chemistry* **72**, 1233-1246, doi:doi:10.1351/pac200072071233 (2000).

19 Anastas, P. & Eghbali, N. Green Chemistry: Principles and Practice. *Chemical Society Reviews* **39**, 301-312, doi:10.1039/B918763B (2010).

20 Rodríguez-Padrón, D., Puente-Santiago, A. R., Balu, A. M., Muñoz-Batista, M. J. & Luque, R. Environmental Catalysis: Present and Future. *ChemCatChem* **11**, 18-38, doi:https://doi.org/10.1002/cctc.201801248 (2019).

21 Krištofíková, D., Modrocká, V., Mečiarová, M. & Šebesta, R. Green Asymmetric Organocatalysis. *ChemSusChem* **13**, 2828-2858, doi:10.1002/cssc.202000137 (2020).

22 Dalko, P. I. & Moisan, L. Enantioselective Organocatalysis. *Angewandte Chemie International Edition* **40**, 3726-3748, doi:https://doi.org/10.1002/1521-3773(20011015)40:20<3726::AID-ANIE3726>3.0.CO;2-D (2001).

23 Hoffmann, R. *The same and not the same*. (Columbia University Press, 1995).

24 Brunner, H. *Rechts oder links*. (Wiley-Vch, 1999).

25 Noyori, R. Asymmetric Catalysis: Science and Opportunities (Nobel Lecture). *Angewandte Chemie International Edition* **41**, 2008-2022, doi:https://doi.org/10.1002/1521-3773(20020617)41:12<2008::AID-ANIE2008>3.0.CO;2-4 (2002).

26 Bonner, W. A. Chirality and life. *Origins of Life and Evolution of the Biosphere* **25**, 175-190 (1995).

27 Bentley, R. The nose as a stereochemist. Enantiomers and odor. *Chemical reviews* **106**, 4099-4112 (2006).

28 Burke, D. & Henderson, D. Chirality: a blueprint for the future. *British Journal of Anaesthesia* **88**, 563-576 (2002).

29 Tokunaga, E., Yamamoto, T., Ito, E. & Shibata, N. Understanding the Thalidomide Chirality in Biological Processes by the Self-disproportionation of Enantiomers. *Scientific Reports* **8**, 17131, doi:10.1038/s41598-018-35457-6 (2018).

30 Franks, M. E., Macpherson, G. R. & Figg, W. D. Thalidomide. *The Lancet* **363**, 1802-1811, doi:https://doi.org/10.1016/S0140-6736(04)16308-3 (2004).

31 Brown, J. M. & Davies, S. G. Chemical asymmetric synthesis. *Nature* **342**, 631-636, doi:10.1038/342631a0 (1989).

32 Borman, S. Chirality emerges as key issue in pharmaceutical research. *Chemical & Engineering News* **68**, 9-14 (1990).

33 Zhang, J. *et al.* Asymmetric phosphoric acid–catalyzed four-component Ugi reaction. *Science* **361**, eaas8707, doi:10.1126/science.aas8707 (2018).

34 Passerini, M. *Gazz. Chim. Ital.* **51, 126** (1921).

35 I. Ugi, U. F., C. Steinbrückner. *Angew. Chem.* **71, 386** (1959).

36 Zhang, J., Lin, S.-X., Cheng, D.-J., Liu, X.-Y. & Tan, B. Phosphoric Acid-Catalyzed Asymmetric Classic Passerini Reaction. *Journal of the American Chemical Society* **137**, 14039-14042, doi:10.1021/jacs.5b09117 (2015).

37 Yu, J., Shi, F. & Gong, L.-Z. Brønsted-Acid-Catalyzed Asymmetric Multicomponent Reactions for the Facile Synthesis of Highly Enantioenriched Structurally Diverse Nitrogenous Heterocycles. *Accounts of Chemical Research* **44**, 1156-1171, doi:10.1021/ar2000343 (2011).

38 Ramón, D. J. & Yus, M. Asymmetric multicomponent reactions (AMCRs): the new frontier. *Angew Chem Int Ed Engl* **44**, 1602-1634, doi:10.1002/anie.200460548 (2005).

39 Winters, K. R. & Montchamp, J.-L. Design, synthesis, and evaluation of chiral thiophosphorus acids as organocatalysts. *Beilstein Journal of Organic Chemistry* **18**, 1471-1478, doi:10.3762/bjoc.18.154 (2022).

40 Schreiner, P. R. Metal-free organocatalysis through explicit hydrogen bonding interactions. *Chemical Society Reviews* **32**, 289-296, doi:10.1039/B107298F (2003).

41 Nickisch, R., Gabrielsen, S. M. & Meier, M. A. R. Novel Access to Known and Unknown Thiourea Catalyst via a Multicomponent-Reaction Approach. *ChemistrySelect* **5**, 11915-11920, doi:https://doi.org/10.1002/slct.202003336 (2020).

42 Schreiner, P. R. & Wittkopp, A. H-Bonding Additives Act Like Lewis Acid Catalysts. *Organic Letters* **4**, 217-220, doi:10.1021/ol017117s (2002).

43 Wittkopp, A. & Schreiner, P. R. Metal-Free, Noncovalent Catalysis of Diels–Alder Reactions by Neutral Hydrogen Bond Donors in Organic Solvents and in Water.

Chemistry – A European Journal **9**, 407-414, doi:https://doi.org/10.1002/chem.200390042 (2003).

44 Fan, Y. & Kass, S. R. Electrostatically Enhanced Thioureas. *Organic Letters* **18**, 188-191, doi:10.1021/acs.orglett.5b03213 (2016).

45 Huang, H. & Jacobsen, E. N. Highly Enantioselective Direct Conjugate Addition of Ketones to Nitroalkenes Promoted by A Chiral Primary Amine−Thiourea Catalyst. *Journal of the American Chemical Society* **128**, 7170-7171, doi:10.1021/ja0620890 (2006).

46 Bhagat, U. K. & Peddinti, R. K. Asymmetric Organocatalytic Approach to 2,4-Disubstituted 1,2,3-Triazoles by N2-Selective Aza-Michael Addition. *The Journal of Organic Chemistry* **83**, 793-804, doi:10.1021/acs.joc.7b02793 (2018).

47 Vakulya, B., Varga, S., Csámpai, A. & Soós, T. Highly Enantioselective Conjugate Addition of Nitromethane to Chalcones Using Bifunctional Cinchona Organocatalysts. *Organic Letters* **7**, 1967-1969, doi:10.1021/ol050431s (2005).

48 Taylor, M. S. & Jacobsen, E. N. Asymmetric Catalysis by Chiral Hydrogen-Bond Donors. *Angewandte Chemie International Edition* **45**, 1520-1543, doi:https://doi.org/10.1002/anie.200503132 (2006).

49 Robak, M. T., Trincado, M. & Ellman, J. A. Enantioselective Aza-Henry Reaction with an N-Sulfinyl Urea Organocatalyst. *Journal of the American Chemical Society* **129**, 15110-15111, doi:10.1021/ja075653v (2007).

50 Sohtome, Y., Takemura, N., Iguchi, T., Hashimoto, Y. & Nagasawa, K. Diastereoselective Henry Reaction Catalyzed by Guanidine-Thiourea Bifunctional Organocatalyst. *Synlett* **2006**, 0144-0146 (2006).

51 Luan, Y., Zheng, N., Qi, Y., Tang, J. & Wang, G. Merging metal–organic framework catalysis with organocatalysis: A thiourea functionalized heterogeneous catalyst at the nanoscale. *Catalysis Science & Technology* **4**, 925, doi:10.1039/c3cy00864a (2014).

52 Kotke, M. & Schreiner, P. R. Acid-free, organocatalytic acetalization. *Tetrahedron* **62**, 434-439, doi:https://doi.org/10.1016/j.tet.2005.09.079 (2006).

53 Lee, Y., Klausen, R. S. & Jacobsen, E. N. Thiourea-Catalyzed Enantioselective Iso-Pictet–Spengler Reactions. *Organic Letters* **13**, 5564-5567, doi:10.1021/ol202300t (2011).

54 Klausen, R. S., Kennedy, C. R., Hyde, A. M. & Jacobsen, E. N. Chiral Thioureas Promote Enantioselective Pictet–Spengler Cyclization by Stabilizing Every Intermediate and Transition State in the Carboxylic Acid-Catalyzed Reaction. *Journal of the American Chemical Society* **139**, 12299-12309, doi:10.1021/jacs.7b06811 (2017).

55 Wenzel, A. G. & Jacobsen, E. N. Asymmetric Catalytic Mannich Reactions Catalyzed by Urea Derivatives: Enantioselective Synthesis of β-Aryl-β-Amino Acids. *Journal of the American Chemical Society* **124**, 12964-12965, doi:10.1021/ja028353g (2002).

56 Odagi, M. *et al.* Insights into the Structure and Function of a Chiral Conjugate-Base-Stabilized Brønsted Acid Catalyst. *European Journal of Organic Chemistry* **2019**, 486-492, doi:https://doi.org/10.1002/ejoc.201801024 (2019).

57 Neuvonen, A. J., Földes, T., Madarász, Á., Pápai, I. & Pihko, P. M. Organocatalysts Fold To Generate an Active Site Pocket for the Mannich Reaction. *ACS Catalysis* **7**, 3284-3294, doi:10.1021/acscatal.7b00336 (2017).

58 Lin, B. & Waymouth, R. M. Urea Anions: Simple, Fast, and Selective Catalysts for Ring-Opening Polymerizations. *Journal of the American Chemical Society* **139**, 1645-1652, doi:10.1021/jacs.6b11864 (2017).

59 Thomas, C. & Bibal, B. Hydrogen-bonding organocatalysts for ring-opening polymerization. *Green Chem.* **16**, 1687-1699, doi:10.1039/c3gc41806e (2014).

60 Stanbury, P. F., Whitaker, A. & Hall, S. J. *Principles of fermentation technology*. (Elsevier, 2013).

61 Paul Ross, R., Morgan, S. & Hill, C. Preservation and fermentation: past, present and future. *International Journal of Food Microbiology* **79**, 3-16, doi:https://doi.org/10.1016/S0168-1605(02)00174-5 (2002).

62 Cordus, V. *Le guidon des apotiquaires. C'est à dire, la vraye forme et maniere de composer les médicamens ... / Traduite de latin en françoys, et repurgée*. (Lyon: Cloquemin, 1575).

63 Parmentier, A. A. Expériences et Réflexions Relatives à l'Analyse du Blé et des Farines. (1781).

64 Kirchhoff, S. K. *Bull. Neusten. Wiss. Naturwiss.* **10**, 88-92 (1811).

65 Roberts, M. W. Birth of the catalytic concept (1800-1900). *Catalysis Letters* **67**, 1-4, doi:10.1023/A:1016622806065 (2000).

66 Davy, H. VIII. Some new experiments and observations on the combustion of gaseous mixtures, with an account of a method of preserving a continued light in mixtures of inflammable gases and air without flame. *Philosophical Transactions of the Royal Society of London* **107**, 77-85, doi:doi:10.1098/rstl.1817.0009 (1817).

67 Berzelius, J. J. Sur un Force Jusqu'ici Peu Remarquée qui est Probablement Active Dans la Formation des Composés Organiques, Section on Vegetable Chemistry,. *Jahres-Bericht* **14**, 237 (1835).

68 A. Zecchina, S. C. in *The Development of Catalysis* 155-204 (2017).

69 Ostwald, W. *Referate Zeit. Phys. Chem.* **15**, 705-706 (1894).

70 Roduner, E. Understanding catalysis. *Chemical Society Reviews* **43**, 8226-8239, doi:10.1039/C4CS00210E (2014).

71 Ostwald, W. Century of Nobel Prizes: 1909 Chemistry Laureate.

72 Ertl, G. & Freund, H. J. Catalysis and Surface Science. *Physics Today* **52**, 32-38, doi:10.1063/1.882569 (1999).

73 Laidler, K. J. A glossary of terms used in chemical kinetics, including reaction dynamics (IUPAC Recommendations 1996). *Pure and Applied Chemistry* **68**, 149-192, doi:doi:10.1351/pac199668010149 (1996).

74 Kozuch, S. & Martin, J. M. L. "Turning Over" Definitions in Catalytic Cycles. *ACS Catalysis* **2**, 2787-2794, doi:10.1021/cs3005264 (2012).

75 Kozuch, S. WIREs Comput. Mol. Sci. 2012, 2, 795− 815.(b) Kozuch, S.; Shaik, S. *Acc. Chem. Res* **44**, 101-110 (2011).

76 Kozuch, S. & Martin, J. M. What makes for a bad catalytic cycle? A theoretical study on the Suzuki− Miyaura reaction within the energetic span model. *ACS Catalysis* **1**, 246-253 (2011).

77 Ostrovskii, N. General equation for linear mechanisms of catalyst deactivation. *Chemical Engineering Journal* **120**, 73-82 (2006).

78 Laidler, K. J. The development of the Arrhenius equation. *Journal of Chemical Education* **61**, 494, doi:10.1021/ed061p494 (1984).

79 Goldberger, M. L. & Watson, K. M. *Collision theory*. (Courier Corporation, 2004).

80 Greco, F. A. On catalysis and equilibrium. *Journal of Chemical Education* **63**, 382, doi:10.1021/ed063p382 (1986).

81 Li, L., Chang, X., Lin, X., Zhao, Z.-J. & Gong, J. Theoretical insights into single-atom catalysts. *Chemical Society Reviews* **49**, 8156-8178, doi:10.1039/D0CS00795A (2020).

82 Mitchell, S. & Pérez-Ramírez, J. Single atom catalysis: a decade of stunning progress and the promise for a bright future. *Nature Communications* **11**, 4302, doi:10.1038/s41467-020-18182-5 (2020).

83 Wang, A., Li, J. & Zhang, T. Heterogeneous single-atom catalysis. *Nature Reviews Chemistry* **2**, 65-81, doi:10.1038/s41570-018-0010-1 (2018).

84 Hölderich, W., Hesse, M. & Näumann, F. Zeolites: Catalysts for Organic Syntheses. *Angewandte Chemie International Edition in English* **27**, 226-246, doi:https://doi.org/10.1002/anie.198802261 (1988).
85 Weitkamp, J. Zeolites and catalysis. *Solid State Ionics* **131**, 175-188, doi:https://doi.org/10.1016/S0167-2738(00)00632-9 (2000).
86 Whitesides, G. M. & Wong, C.-H. Enzymes as Catalysts in Synthetic Organic Chemistry [New Synthetic Methods (53)]. *Angewandte Chemie International Edition in English* **24**, 617-638, doi:https://doi.org/10.1002/anie.198506173 (1985).
87 Basso, A. & Serban, S. Industrial applications of immobilized enzymes—A review. *Molecular Catalysis* **479**, 110607, doi:https://doi.org/10.1016/j.mcat.2019.110607 (2019).
88 Zhou, Q.-L. Transition-Metal Catalysis and Organocatalysis: Where Can Progress Be Expected? *Angewandte Chemie International Edition* **55**, 5352-5353, doi:10.1002/anie.201509164 (2016).
89 Rothenberg, G. in *Catalysis* 77-125 (2008).
90 Van Leeuwen, P. W. *Homogeneous catalysis: understanding the art*. (Springer Science & Business Media, 2006).
91 Cole-Hamilton, D. J. Homogeneous catalysis--new approaches to catalyst separation, recovery, and recycling. *Science* **299**, 1702-1706 (2003).
92 Cornils, B. & Herrmann, W. A. Concepts in homogeneous catalysis: the industrial view. *Journal of Catalysis* **216**, 23-31, doi:https://doi.org/10.1016/S0021-9517(02)00128-8 (2003).
93 Bond, G. C. Heterogeneous catalysis. (1987).
94 Schlögl, R. Heterogeneous catalysis. *Angewandte Chemie International Edition* **54**, 3465-3520 (2015).
95 Bell, E. L. *et al.* Biocatalysis. *Nature Reviews Methods Primers* **1**, 1-21 (2021).
96 Schmid, A. *et al.* Industrial biocatalysis today and tomorrow. *nature* **409**, 258-268 (2001).
97 Herrmann, W. A. & Cornils, B. Organometallic homogeneous catalysis—Quo vadis? *Angewandte Chemie International Edition in English* **36**, 1048-1067 (1997).
98 Chiusoli, G. P. & Maitlis, P. M. *Metal-catalysis in industrial organic processes*. (Royal Society of Chemistry, 2019).
99 Parshall, G. W. Industrial applications of homogeneous catalysis. A review. *Journal of Molecular Catalysis* **4**, 243-270, doi:https://doi.org/10.1016/0304-5102(78)85023-8 (1978).
100 Roy, A. K. in *Advances in Organometallic Chemistry* Vol. 55 (eds Robert West, Anthony F. Hill, & Mark J. Fink) 1-59 (Academic Press, 2007).
101 Dondoni, A. & Massi, A. Asymmetric Organocatalysis: From Infancy to Adolescence. *Angewandte Chemie International Edition* **47**, 4638-4660, doi:https://doi.org/10.1002/anie.200704684 (2008).
102 Hajos, Z. G. & Parrish, D. R. Asymmetric synthesis of optically active polycyclic organic compounds. *German patent DE* **2102623** (1971).
103 Hajos, Z. & Parrish, D. in *Chem. Abstr.*
104 Deer, U. DE 2014757, 1971; b) U. Eder, G. Sauer, R. Wiechert. *Angew. Chem* **83**, 492-493 (1971).
105 Eder, U., Sauer, G. & Wiechert, R. Neuartige asymmetrische Cyclisierung zu optisch aktiven Steroid-CD-Teilstücken. *Angewandte Chemie* **83**, 492-493 (1971).
106 Zhang, Y. & Wang, W. Recent advances in organocatalytic asymmetric Michael reactions. *Catal. Sci. Technol.* **2**, 42-53, doi:10.1039/c1cy00334h (2012).
107 Gioia, C., Hauville, A., Bernardi, L., Fini, F. & Ricci, A. Organocatalytic Asymmetric Diels–Alder Reactions of 3-Vinylindoles. *Angewandte Chemie International Edition* **47**, 9236-9239, doi:https://doi.org/10.1002/anie.200804275 (2008).

108 Poulsen, P. H., Vergura, S., Monleón, A., Jørgensen, D. K. B. & Jørgensen, K. A. Controlling Asymmetric Remote and Cascade 1,3-Dipolar Cycloaddition Reactions by Organocatalysis. *Journal of the American Chemical Society* **138**, 6412-6415, doi:10.1021/jacs.6b03546 (2016).

109 Maher, D. J. & Connon, S. J. Acceleration of the DABCO-promoted Baylis–Hillman reaction using a recoverable H-bonding organocatalyst. *Tetrahedron letters* **45**, 1301-1305 (2004).

110 Okino, T., Hoashi, Y. & Takemoto, Y. Enantioselective Michael reaction of malonates to nitroolefins catalyzed by bifunctional organocatalysts. *Journal of the American Chemical Society* **125**, 12672-12673 (2003).

111 Sohtome, Y., Tanatani, A., Hashimoto, Y. & Nagasawa, K. Development of bis-thiourea-type organocatalyst for asymmetric Baylis–Hillman reaction. *Tetrahedron Letters* **45**, 5589-5592, doi:https://doi.org/10.1016/j.tetlet.2004.05.137 (2004).

112 Retini, M., Bartoccini, F., Zappia, G. & Piersanti, G. Novel, Chiral, and Enantiopure C2-Symmetric Thioureas Promote Asymmetric Protio-Pictet-Spengler Reactions by Anion-Binding Catalysis. *European Journal of Organic Chemistry* **2021**, 825-829 (2021).

113 Verkade, J. M. M., Hemert, L. J. C. V., Quaedflieg, P. J. L. M. & Rutjes, F. P. J. T. Organocatalysed asymmetric Mannich reactions. *Chem. Soc. Rev.* **37**, 29-41, doi:10.1039/b713885g (2008).

114 Wang, Y., Yang, H., Yu, J., Miao, Z. & Chen, R. Highly enantioselective Biginelli reaction promoted by chiral bifunctional primary amine-thiourea catalysts: asymmetric synthesis of dihydropyrimidines. *Advanced Synthesis & Catalysis* **351**, 3057-3062 (2009).

115 Su, J. T., Vachal, P. & Jacobsen, E. N. Practical synthesis of a soluble schiff base catalyst for the asymmetric strecker reaction. *Advanced Synthesis & Catalysis* **343**, 197-200 (2001).

116 Curran, D. P. & Kuo, L. H. Acceleration of a dipolar Claisen rearrangement by Hydrogen bonding to a soluble diaryl^ urea. *Tetrahedron letters* **36**, 6647-6650 (1995).

117 Pratt, R. C. *et al.* Exploration, optimization, and application of supramolecular thiourea− amine catalysts for the synthesis of lactide (co) polymers. *Macromolecules* **39**, 7863-7871 (2006).

118 Knowles, R. R., Lin, S. & Jacobsen, E. N. Enantioselective Thiourea-Catalyzed Cationic Polycyclizations. *Journal of the American Chemical Society* **132**, 5030-5032, doi:10.1021/ja101256v (2010).

119 Buckley, B. R., Kimber, M. C. & Slater, N. H. Organocatalysis. *Annual Reports Section "B" (Organic Chemistry)* **108**, 98, doi:10.1039/c2oc90018a (2012).

120 Volz, N. & Clayden, J. The Urea Renaissance. *Angewandte Chemie International Edition* **50**, 12148-12155, doi:https://doi.org/10.1002/anie.201104037 (2011).

121 Madarász, Á. *et al.* Thiourea Derivatives as Brønsted Acid Organocatalysts. *ACS Catalysis* **6**, 4379-4387, doi:10.1021/acscatal.6b00618 (2016).

122 Yu, X. & Wang, W. Hydrogen-Bond-Mediated Asymmetric Catalysis. *Chemistry – An Asian Journal* **3**, 516-532, doi:https://doi.org/10.1002/asia.200700415 (2008).

123 Maji, R., Mallojjala, S. C. & Wheeler, S. E. Chiral phosphoric acid catalysis: from numbers to insights. *Chemical Society Reviews* **47**, 1142-1158, doi:10.1039/C6CS00475J (2018).

124 Terada, M. Chiral phosphoric acids as versatile catalysts for enantioselective transformations. *Synthesis* **2010**, 1929-1982 (2010).

125 Seayad, J. & List, B. Asymmetric organocatalysis. *Organic & Biomolecular Chemistry* **3**, 719, doi:10.1039/b415217b (2005).

126 List, B. *Asymmetric organocatalysis*. Vol. 291 (Springer, 2009).

127 Antenucci, A., Dughera, S. & Renzi, P. Green Chemistry Meets Asymmetric Organocatalysis: A Critical Overview on Catalysts Synthesis. *ChemSusChem* **14**, 2785-2853, doi:https://doi.org/10.1002/cssc.202100573 (2021).
128 Dalko, P. I. & Moisan, L. In the golden age of organocatalysis. *Angewandte Chemie International Edition* **43**, 5138-5175 (2004).
129 Connon, S. J. Organocatalysis Mediated by (Thio)urea Derivatives. *Chemistry – A European Journal* **12**, 5418-5427, doi:https://doi.org/10.1002/chem.200501076 (2006).
130 Hans Wedepohl, K. The composition of the continental crust. *Geochimica et Cosmochimica Acta* **59**, 1217-1232, doi:https://doi.org/10.1016/0016-7037(95)00038-2 (1995).
131 Ludwig, J. R. & Schindler, C. S. Catalyst: Sustainable Catalysis. *Chem* **2**, 313-316, doi:10.1016/j.chempr.2017.02.014 (2017).
132 Mineral commodity summaries 2024. Report No. 2024, 212 (Reston, VA, 2024).
133 Moss, G. P. Basic terminology of stereochemistry (IUPAC Recommendations 1996). *Pure and Applied Chemistry* **68**, 2193-2222, doi:doi:10.1351/pac199668122193 (1996).
134 Jacques, J., Collet, A. & Wilen, S. H. *Enantiomers, racemates, and resolutions*. (Wiley, 1981).
135 Gnas, Y. & Glorius, F. Chiral auxiliaries-principles and recent applications. *Synthesis* **2006**, 1899-1930 (2006).
136 Diaz-Muñoz, G., Miranda, I. L., Sartori, S. K., de Rezende, D. C. & Alves Nogueira Diaz, M. Use of chiral auxiliaries in the asymmetric synthesis of biologically active compounds: A review. *Chirality* **31**, 776-812 (2019).
137 Blaser, H. U. The chiral pool as a source of enantioselective catalysts and auxiliaries. *Chemical Reviews* **92**, 935-952, doi:10.1021/cr00013a009 (1992).
138 Denmark, S. E. & Fu, J. Catalytic Enantioselective Addition of Allylic Organometallic Reagents to Aldehydes and Ketones. *Chemical Reviews* **103**, 2763-2794, doi:10.1021/cr020050h (2003).
139 Grabowski, S. J. Hydrogen bonding strength—measures based on geometric and topological parameters. *Journal of Physical Organic Chemistry* **17**, 18-31, doi:https://doi.org/10.1002/poc.685 (2004).
140 Jeffrey, G. A. & Jeffrey, G. A. *An introduction to hydrogen bonding*. Vol. 12 (Oxford university press New York, 1997).
141 (International Union of Pure and Applied Chemistry (IUPAC), 2019).
142 Gawley, R. E. Do the Terms "% ee" and "% de" Make Sense as Expressions of Stereoisomer Composition or Stereoselectivity? *The Journal of Organic Chemistry* **71**, 2411-2416, doi:10.1021/jo052554w (2006).
143 Schroeder, D. C. Thioureas. *Chemical Reviews* **55**, 181-228, doi:10.1021/cr50001a005 (1955).
144 Nickisch, R. *Activation of Elemental Sulfur via Multicomponent Reactions for more Sustainable Organocatalysts and Sulfur-containing Polymers*, (2023).
145 Kumamoto, K., Misawa, Y., Tokita, S., Kubo, Y. & Kotsuki, H. High-pressure-promoted condensation of isothiocyanates with aminopyridines: efficient synthesis of pyridine–thiourea conjugates as building blocks for hydrogen-bonding receptors. *Tetrahedron Letters* **43**, 1035-1038, doi:https://doi.org/10.1016/S0040-4039(01)02295-X (2002).
146 M. L. Moore and F. S. Crossley, J. W. S., New York. *Organic Syntheses* (1955).
147 Karagoz, Z., Genc, M., Yılmaz, E. & Keser, S. Synthesis and antitumor, antioxidant effects studies of N-ethylpiperazine substitute thiourea ligands and their copper (II) complexes. *Spectroscopy Letters* **46**, 182-190 (2013).
148 Singh, B. Synthesis of New Unsymmetrical 1, 3-Disubstituted-thioureas. *Agricultural and Biological Chemistry* **42**, 1285-1286 (1978).

149 Verlinden, B. K. *et al.* Discovery of novel alkylated (bis) urea and (bis) thiourea polyamine analogues with potent antimalarial activities. *Journal of medicinal chemistry* **54**, 6624-6633 (2011).
150 Viana, G. M. *et al.* Antileishmanial thioureas: synthesis, biological activity and in silico evaluations of new promising derivatives. *Chemical and Pharmaceutical Bulletin* **65**, 911-919 (2017).
151 Sudhamani, H., Thaslim Basha, S., Adam, S., Bhaskar, B. V. & Raju, C. N. Synthesis, characterization, and bio-activity evaluation of thiourea derivatives of epinephrine as antimicrobial and antioxidant agents: molecular docking studies. *Monatshefte für Chemie-Chemical Monthly* **148**, 1525-1537 (2017).
152 Elseginy, S. A. *et al.* Design, synthesis, and computational validation of novel compounds selectively targeting HER2-expressing breast cancer. *Bioorganic & Medicinal Chemistry Letters* **30**, 127658 (2020).
153 Eschliman, K. & Bossmann, S. H. Synthesis of Isothiocyanates: An Update. *Synthesis* **51**, 1746-1752 (2019).
154 Dains, F. B., Brewster, R. & Olander, C. Phenyl Isothiocyanate: Isothiocyanic acid, phenyl ester. *Organic Syntheses* **6**, 72-72 (2003).
155 Waibel, K. A., Nickisch, R., Möhl, N., Seim, R. & Meier, M. A. R. A more sustainable and highly practicable synthesis of aliphatic isocyanides. *Green Chemistry* **22**, 933-941, doi:10.1039/c9gc04070f (2020).
156 Maddani, M. R. & Prabhu, K. R. A Concise Synthesis of Substituted Thiourea Derivatives in Aqueous Medium. *The Journal of Organic Chemistry* **75**, 2327-2332, doi:10.1021/jo1001593 (2010).
157 Štrukil, V., Gracin, D., Magdysyuk, O. V., Dinnebier, R. E. & Friščić, T. Trapping Reactive Intermediates by Mechanochemistry: Elusive Aryl N-Thiocarbamoylbenzotriazoles as Bench-Stable Reagents. *Angewandte Chemie International Edition* **54**, 8440-8443, doi:https://doi.org/10.1002/anie.201502026 (2015).
158 Lin, Y. *et al.* A selenourea-thiourea Brønsted acid catalyst facilitates asymmetric conjugate additions of amines to α, β-unsaturated esters. *Journal of the American Chemical Society* **142**, 5627-5635 (2020).
159 Wu, J. *et al.* Synthesis and bioactivity of pyrazole acyl thiourea derivatives. *Molecules* **17**, 5139-5150 (2012).
160 Yonova, P. & Stoilkova, G. Synthesis and biological activity of urea and thiourea derivatives from 2-aminoheterocyclic compounds. *Journal of Plant Growth Regulation* **23**, 280-291 (2004).
161 Richter, C. P. The development and use of alpha-naphthyl thiourea (ANTU) as a rat poison. *Journal of the American Medical Association* **129**, 927-931 (1945).
162 Rosove, M. H. Agranulocytosis and antithyroid drugs. *Western Journal of Medicine* **126**, 339 (1977).
163 Masereel, B., Lambert, D., Dogné, J.-M., Poupaert, J. & Delarge, J. Anticonvulsant activity of pyrid-3-yl-sulfonyl ureas and thioureas. *Epilepsia* **38**, 334-337 (1997).
164 Loev, B. *et al.* Amidines. 3. Thioureas possessing antihypertensive activity. *Journal of medicinal chemistry* **15**, 1024-1027 (1972).
165 Quy Huong, D., Duong, T. & Nam, P. C. Effect of the structure and temperature on corrosion inhibition of thiourea derivatives in 1.0 M HCl solution. *ACS omega* **4**, 14478-14489 (2019).
166 Dawood, K. M. Bis-thiourea Derivatives and Their Utility in Synthesis of Mono-heterocyclic, Bis-heterocyclic, and Fused Heterocyclic Systems. *Journal of Heterocyclic Chemistry* **56**, 1701-1721 (2019).
167 Rajappa, S., Nair, M. D., Advani, B. G., Sreenivasan, R. & Desai, J. A. A general synthesis of thiazoles. Part 3. Comparative evaluation of different functionalised

thioureas as precursors. *Journal of the Chemical Society, Perkin Transactions 1*, 1762-1764 (1979).
168 Kaila, J. C. *et al.* A convenient synthesis of di-and trisubstituted 2-aminoimidazoles from 1-amidino-3-trityl-thioureas. *Tetrahedron Letters* **50**, 3955-3958 (2009).
169 Hargrave, K. D., Hess, F. K. & Oliver, J. T. N-(4-Substituted-thiazolyl) oxamic acid derivatives, new series of potent, orally active antiallergy agents. *Journal of medicinal chemistry* **26**, 1158-1163 (1983).
170 Heinelt, U. *et al.* A convenient method for the synthesis of 2-amino substituted aza-heterocycles from N, N′-disubstituted thioureas using TsCl/NaOH. *Tetrahedron* **60**, 9883-9888 (2004).
171 Biswas, K. & Greaney, M. F. Insertion of arynes into thioureas: A new amidine synthesis. *Organic Letters* **13**, 4946-4949 (2011).
172 Maryanoff, C. A., Stanzione, R. C., Plampin, J. N. & Mills, J. E. A convenient synthesis of guanidines from thioureas. *The Journal of Organic Chemistry* **51**, 1882-1884 (1986).
173 Linton, B. R., Carr, A. J., Orner, B. P. & Hamilton, A. D. A versatile one-pot synthesis of 1, 3-substituted guanidines from carbamoyl isothiocyanates. *Journal of Organic Chemistry* **65**, 1566-1568 (2000).
174 Saetan, T., Sukwattanasinitt, M. & Wacharasindhu, S. A mild photocatalytic synthesis of guanidine from thiourea under visible light. *Organic Letters* **22**, 7864-7869 (2020).
175 Khan, M. *et al.* Synthesis, characterization, crystal structure, in-vitro cytotoxicity, antibacterial, and antifungal activities of nickel (II) and cobalt (III) complexes with acylthioureas. *Journal of Coordination Chemistry* **73**, 1790-1805 (2020).
176 Chen, W. *et al.* (Wiley Online Library, 2006).
177 Schwade, V. D., Kirsten, L., Hagenbach, A., Lang, E. S. & Abram, U. Indium (III), lead (II), gold (I) and copper (II) complexes with isophthaloylbis (thiourea) ligands. *Polyhedron* **55**, 155-161 (2013).
178 Zhao, X. *et al.* Nano-diamond particles functionalized with single/double-arm amide–thiourea ligands for adsorption of metal ions. *Journal of colloid and interface science* **469**, 109-119 (2016).
179 Henderson, W., Nicholson, B. K. & Tiekink, E. R. Synthesis, characterisation, supramolecular aggregation and biological activity of phosphine gold (I) complexes with monoanionic thiourea ligands. *Inorganica chimica acta* **359**, 204-214 (2006).
180 Ulatowski, F. & Jurczak, J. Chiral recognition of carboxylates by a static library of thiourea receptors with amino acid arms. *The Journal of Organic Chemistry* **80**, 4235-4243 (2015).
181 Nishizawa, S., Bühlmann, P., Iwao, M. & Umezawa, Y. Anion recognition by urea and thiourea groups: Remarkably simple neutral receptors for dihydrogenphosphate. *Tetrahedron Letters* **36**, 6483-6486, doi:https://doi.org/10.1016/0040-4039(95)01296-T (1995).
182 Boas, U., Karlsson, A. J., De Waal, B. & Meijer, E. Synthesis and properties of new thiourea-functionalized poly (propylene imine) dendrimers and their role as hosts for urea functionalized guests. *The Journal of organic chemistry* **66**, 2136-2145 (2001).
183 Manna, U. & Das, G. Progressive cation triggered anion binding by electron-rich scaffold: Case study of a neutral tripodal naphthyl thiourea receptor. *Crystal Growth & Design* **18**, 3138-3150 (2018).
184 Mike Kotke, R. R. S. in *Hydrogen Bonding in Organic Synthesis* (ed P. M. Pihko) 204 (Wiley-VCH, 2009).
185 Grabowski, S. J. *Hydrogen bonding: new insights*. Vol. 3 (Springer, 2006).
186 Hine, J., Ahn, K., Gallucci, J. C. & Linden, S. M. 1,8-Biphenylenediol forms two strong hydrogen bonds to the same oxygen atom. *Journal of the American Chemical Society* **106**, 7980-7981, doi:10.1021/ja00337a060 (1984).

187 Kelly, T. R., Meghani, P. & Ekkundi, V. S. Diels-alder reactions: Rate acceleration promoted by a biphenylenediol. *Tetrahedron Letters* **31**, 3381-3384, doi:https://doi.org/10.1016/S0040-4039(00)97402-1 (1990).
188 Etter, M. C. Hydrogen bonds as design elements in organic chemistry. *The Journal of Physical Chemistry* **95**, 4601-4610, doi:10.1021/j100165a007 (1991).
189 Etter, M. C. Encoding and decoding hydrogen-bond patterns of organic compounds. *Accounts of Chemical Research* **23**, 120-126, doi:10.1021/ar00172a005 (1990).
190 Etter, M. C. & Panunto, T. W. 1, 3-Bis (m-nitrophenyl) urea: An exceptionally good complexing agent for proton acceptors. *Journal of the American Chemical Society* **110**, 5896-5897 (1988).
191 Wilcox, C. S. *et al.* Experimental and theoretical studies of substituent effects in hydrogen bond based molecular recognition of a zwitterion by substituted arylureas. *Tetrahedron* **51**, 621-634, doi:https://doi.org/10.1016/0040-4020(94)00921-G (1995).
192 Curran, D. P. & Kuo, L. H. Altering the Stereochemistry of Allylation Reactions of Cyclic .alpha.-Sulfinyl Radicals with Diarylureas. *The Journal of Organic Chemistry* **59**, 3259-3261, doi:10.1021/jo00091a007 (1994).
193 Sigman, M. S., Vachal, P. & Jacobsen, E. N. A general catalyst for the asymmetric Strecker reaction. *Angewandte Chemie* **112**, 1336-1338 (2000).
194 Takemoto, Y. Recognition and activation by ureas and thioureas: stereoselective reactions using ureas and thioureas as hydrogen-bonding donors. *Organic & biomolecular chemistry* **3**, 4299-4306 (2005).
195 Nziko, V. d. P. N. & Scheiner, S. Interactions between Thiourea and Imines. Prelude to Catalysis. *The Journal of Organic Chemistry* **80**, 10334-10341, doi:10.1021/acs.joc.5b01985 (2015).
196 Blain, M. *et al.* Urea- and Thiourea-Catalyzed Aminolysis of Carbonates. *ChemSusChem* **9**, 2269-2272, doi:https://doi.org/10.1002/cssc.201600778 (2016).
197 Limnios, D. & Kokotos, C. G. 196-255 (Royal Society of Chemistry, 2015).
198 Lippert, K. M. *et al.* Hydrogen-Bonding Thiourea Organocatalysts: The Privileged 3,5-Bis(trifluoromethyl)phenyl Group. *European Journal of Organic Chemistry* **2012**, 5919-5927, doi:https://doi.org/10.1002/ejoc.201200739 (2012).
199 Freund, M. *Synthese und Anwendung von neuen bifunktionellen Organokatalysatoren in asymmetrischen C-C-Verknüpfungsreaktionen: Henry-, Michael- und Aldol-Reaktionen* Dissertation thesis, Friedrich-Alexander-Universität Erlangen-Nürnberg (2011).
200 Dömling, A. & Ugi, I. Multicomponent Reactions with Isocyanides. *Angewandte Chemie International Edition* **39**, 3168-3210, doi:https://doi.org/10.1002/1521-3773(20000915)39:18<3168::AID-ANIE3168>3.0.CO;2-U (2000).
201 Dömling, A. Recent Developments in Isocyanide Based Multicomponent Reactions in Applied Chemistry. *Chemical Reviews* **106**, 17-89, doi:10.1021/cr0505728 (2006).
202 Cioc, R. C., Ruijter, E. & Orru, R. V. A. Multicomponent reactions: advanced tools for sustainable organic synthesis. *Green Chemistry* **16**, 2958-2975, doi:10.1039/C4GC00013G (2014).
203 Zhu, J., Wang, Q. & Wang, M. *Multicomponent reactions in organic synthesis*. (John Wiley & Sons, 2014).
204 Brauch, S., van Berkel, S. S. & Westermann, B. Higher-order multicomponent reactions: beyond four reactants. *Chemical Society Reviews* **42**, 4948-4962, doi:10.1039/C3CS35505E (2013).
205 Elders, N. *et al.* The Efficient One-Pot Reaction of up to Eight Components by the Union of Multicomponent Reactions. *Angewandte Chemie International Edition* **48**, 5856-5859, doi:https://doi.org/10.1002/anie.200902683 (2009).

206 Söyler, Z. *et al.* Sustainable succinylation of cellulose in a CO2-based switchable solvent and subsequent Passerini 3-CR and Ugi 4-CR modification. *Green Chemistry* **20**, 214-224, doi:10.1039/C7GC02577G (2018).
207 Onwukamike, K. N., Grelier, S., Grau, E., Cramail, H. & Meier, M. A. On the direct use of CO 2 in multicomponent reactions: introducing the Passerini four component reaction. *RSC advances* **8**, 31490-31495 (2018).
208 Esen, E. & Meier, M. (2020).
209 Ugi, I., Werner, B. & Dömling, A. The Chemistry of Isocyanides, their MultiComponent Reactions and their Libraries. *Molecules* **8**, 53-66 (2003).
210 Ugi, I., Werner, B. & Dömling, A. The Chemistry of Isocyanides, their MultiComponent Reactions and their Libraries. *Molecules* **8**, 53-66, doi:10.3390/80100053 (2003).
211 Rudick, J. G., Shaabani, S. & Dömling, A. Editorial: Isocyanide-Based Multicomponent Reactions. *Frontiers in Chemistry* **7**, doi:10.3389/fchem.2019.00918 (2020).
212 Ugi, I., Dömling, A. & Hörl, W. Multicomponent reactions in organic chemistry. *Endeavour* **18**, 115-122 (1994).
213 Akritopoulou-Zanze, I. Isocyanide-based multicomponent reactions in drug discovery. *Current Opinion in Chemical Biology* **12**, 324-331, doi:https://doi.org/10.1016/j.cbpa.2008.02.004 (2008).
214 Kreye, O., Tóth, T. & Meier, M. A. R. Introducing Multicomponent Reactions to Polymer Science: Passerini Reactions of Renewable Monomers. *Journal of the American Chemical Society* **133**, 1790-1792, doi:10.1021/ja1113003 (2011).
215 Kakuchi, R. The dawn of polymer chemistry based on multicomponent reactions. *Polymer Journal* **51**, 945-953, doi:10.1038/s41428-019-0209-0 (2019).
216 Slobbe, P., Ruijter, E. & Orru, R. V. Recent applications of multicomponent reactions in medicinal chemistry. *MedChemComm* **3**, 1189-1218 (2012).
217 Solleder, S. C., Wetzel, K. S. & Meier, M. A. R. Dual side chain control in the synthesis of novel sequence-defined oligomers through the Ugi four-component reaction. *Polymer Chemistry* **6**, 3201-3204, doi:10.1039/C5PY00424A (2015).
218 Wetzel, K. S. *et al.* Dual sequence definition increases the data storage capacity of sequence-defined macromolecules. *Communications Chemistry* **3**, 63, doi:10.1038/s42004-020-0308-z (2020).
219 Holloway, J. O., Wetzel, K. S., Martens, S., Du Prez, F. E. & Meier, M. A. Direct comparison of solution and solid phase synthesis of sequence-defined macromolecules. *Polymer Chemistry* **10**, 3859-3867 (2019).
220 Solleder, S. C., Zengel, D., Wetzel, K. S. & Meier, M. A. A scalable and high-yield strategy for the synthesis of sequence-defined macromolecules. *Angewandte Chemie International Edition* **55**, 1204-1207 (2016).
221 Strecker, A. *Liebigs Ann. der Chemie* **75, 27** (1850).
222 Hantzsch, A. Ueber die Synthese pyridinartiger Verbindungen aus Acetessigäther und Aldehydammoniak. *Justus Liebigs Annalen der Chemie* **215**, 1-82, doi:https://doi.org/10.1002/jlac.18822150102 (1882).
223 Hantzsch, A. Neue Bildungsweise von Pyrrolderivaten. *Berichte der deutschen chemischen Gesellschaft* **23**, 1474-1476, doi:https://doi.org/10.1002/cber.189002301243 (1890).
224 Biginelli, P. Ueber Aldehyduramide des Acetessigäthers. *Berichte der deutschen chemischen Gesellschaft* **24**, 1317-1319, doi:https://doi.org/10.1002/cber.189102401228 (1891).
225 Mannich, C. & Krösche, W. Ueber ein Kondensationsprodukt aus Formaldehyd, Ammoniak und Antipyrin. *Archiv der Pharmazie* **250**, 647-667, doi:https://doi.org/10.1002/ardp.19122500151 (1912).

226 Robinson, R. LXXV.—A theory of the mechanism of the phytochemical synthesis of certain alkaloids. *Journal of the Chemical Society, Transactions* **111**, 876-899 (1917).
227 Petasis, N. A. & Akritopoulou, I. The boronic acid mannich reaction: A new method for the synthesis of geometrically pure allylamines. *Tetrahedron Letters* **34**, 583-586 (1993).
228 Wu, P., Givskov, M. & Nielsen, T. E. Reactivity and synthetic applications of multicomponent Petasis reactions. *Chemical Reviews* **119**, 11245-11290 (2019).
229 Tang, B. Z. & Hu, R. *Polymer Synthesis Based on Triple-bond Building Blocks*. (Springer, 2018).
230 Nolte, R. J. M. & Drenth, W. in *New Methods for Polymer Synthesis* (ed W. J. Mijs) 273-310 (Springer US, 1992).
231 Nef, J. U. Ueber das zweiwerthige Kohlenstoffatom. *Justus Liebigs Annalen der Chemie* **270**, 267-335, doi:https://doi.org/10.1002/jlac.18922700302 (1892).
232 Giustiniano, M. *et al.* To each his own: isonitriles for all flavors. Functionalized isocyanides as valuable tools in organic synthesis. *Chemical Society Reviews* **46**, 1295-1357, doi:10.1039/C6CS00444J (2017).
233 Ramozzi, R., Chéron, N., Braïda, B., Hiberty, P. C. & Fleurat-Lessard, P. A valence bond view of isocyanides' electronic structure. *New Journal of Chemistry* **36**, 1137, doi:10.1039/c2nj40050b (2012).
234 Groebke, K., Weber, L. & Mehlin, F. Synthesis of imidazo [1, 2-a] annulated pyridines, pyrazines and pyrimidines by a novel three-component condensation. *Synlett* **1998**, 661-663 (1998).
235 Blackburn, C., Guan, B., Fleming, P., Shiosaki, K. & Tsai, S. Parallel synthesis of 3-aminoimidazo [1, 2-a] pyridines and pyrazines by a new three-component condensation. *Tetrahedron letters* **39**, 3635-3638 (1998).
236 Bienayme, H. & Bouzid, K. A new heterocyclic multicomponent reaction for the combinatorial synthesis of fused 3-aminoimidazoles. *Angewandte Chemie International Edition* **37**, 2234-2237 (1998).
237 Heck, S. & Doemling, A. A versatile multi-component one-pot thiazole synthesis. *Synlett* **2000**, 424-426 (2000).
238 Van Leusen, A. M., Wildeman, J. & Oldenziel, O. H. Chemistry of sulfonylmethyl isocyanides. 12. Base-induced cycloaddition of sulfonylmethyl isocyanides to carbon, nitrogen double bonds. Synthesis of 1, 5-disubstituted and 1, 4, 5-trisubstituted imidazoles from aldimines and imidoyl chlorides. *The Journal of Organic Chemistry* **42**, 1153-1159 (1977).
239 Sisko, J. *et al.* An investigation of imidazole and oxazole syntheses using aryl-substituted TosMIC reagents1. *The Journal of organic chemistry* **65**, 1516-1524 (2000).
240 Zheng, X., Ma, Z. & Zhang, D. Synthesis of imidazole-based medicinal molecules utilizing the van leusen imidazole synthesis. *Pharmaceuticals* **13**, 37 (2020).
241 Gracias, V., Gasiecki, A. F. & Djuric, S. W. Synthesis of fused bicyclic imidazoles by sequential van Leusen/ring-closing metathesis reactions. *Organic Letters* **7**, 3183-3186 (2005).
242 Lipp, M., Dallacker, F. & Köcker, I. M. z. Über die Addition von Schwefel und Selen an Isonitrile. *Monatshefte für Chemie und verwandte Teile anderer Wissenschaften* **90**, 41-48, doi:10.1007/BF00901130 (1959).
243 Liu, H., Fang, Y., Wang, S.-Y. & Ji, S.-J. TEMPO-Catalyzed Aerobic Oxidative Selenium Insertion Reaction: Synthesis of 3-Selenylindole Derivatives by Multicomponent Reaction of Isocyanides, Selenium Powder, Amines, and Indoles under Transition-Metal-Free Conditions. *Organic letters* **20**, 930-933 (2018).
244 Nguyen, T. B., Ermolenko, L. & Al-Mourabit, A. Three-Component Reaction between Isocyanides, Aliphatic Amines and Elemental Sulfur: Preparation of

Thioureas under Mild Conditions with Complete- Atom Economy. *Synthesis* **46**, 3172-3179 (2014).

245 Bode, M. L., Gravestock, D. & Rousseau, A. L. Synthesis, Reactions and Uses of Isocyanides in Organic Synthesis. An Update. *Organic Preparations and Procedures International* **48**, 89-221, doi:10.1080/00304948.2016.1138072 (2016).

246 Lieke, W. Ueber das Cyanallyl. *Justus Liebigs Annalen der Chemie* **112**, 316-321, doi:https://doi.org/10.1002/jlac.18591120307 (1859).

247 Gautier, A. *Justus Liebigs Annalen der Chemie* **146**, doi:https://doi.org/10.1002/jlac.18691520211 (1869).

248 Hoffmann, A. W. *Ber. Dtsch. Chem. Ges.* **144, 114** (1867).

249 Patil, P., Ahmadian-Moghaddam, M. & Dömling, A. Isocyanide 2.0. *Green Chemistry* **22**, 6902-6911, doi:10.1039/d0gc02722g (2020).

250 Creedon, S., áKevin Crowley, H. & McCarthy, D. Dehydration of formamides using the Burgess Reagent: a new route to isocyanides. *Journal of the Chemical Society, Perkin Transactions 1*, 1015-1018 (1998).

251 Meyr, I. U. R. *Angew. Chem.* **70, 702** (1958).

252 Neochoritis, C. G. *et al.* Leuckart–Wallach route toward isocyanides and some applications. *ACS combinatorial science* **17**, 493-499 (2015).

253 Singleton, E. & Oosthuizen, H. E. in *Advances in Organometallic Chemistry* Vol. 22 (eds F. G. A. Stone & Robert West) 209-310 (Academic Press, 1983).

254 Mamoru, T. & Naoto, C. Renaissance of Organic Synthesis Using Isocyanides. *Chemistry Letters* **40**, 330-340, doi:10.1246/cl.2011.330 (2011).

255 Rothe, W. [The new antibiotic xanthocillin]. *Dtsch Med Wochenschr* **79**, 1080-1081, doi:10.1055/s-0028-1119307 (1954).

256 Edenborough, M. S. & Herbert, R. B. Naturally occurring isocyanides. *Natural Product Reports* **5**, 229-245, doi:10.1039/NP9880500229 (1988).

257 Scheuer, P. J. Isocyanides and cyanides as natural products. *Accounts of Chemical Research* **25**, 433-439, doi:10.1021/ar00022a001 (1992).

258 Garson, M. J. & Simpson, J. S. Marine isocyanides and related natural products – structure, biosynthesis and ecology. *Natural Product Reports* **21**, 164-179, doi:10.1039/B302359C (2004).

259 Zhang, X., Evanno, L. & Poupon, E. Biosynthetic Routes to Natural Isocyanides. *European Journal of Organic Chemistry* **2020**, 1919-1929, doi:https://doi.org/10.1002/ejoc.201901694 (2020).

260 Banfi, L. & Riva, R. in *Organic Reactions* 1-140.

261 Banfi, L., Basso, A., Lambruschini, C., Moni, L. & Riva, R. The 100 facets of the Passerini reaction. *Chemical Science* **12**, 15445-15472, doi:10.1039/D1SC03810A (2021).

262 Maeda, S., Komagawa, S., Uchiyama, M. & Morokuma, K. Finding Reaction Pathways for Multicomponent Reactions: The Passerini Reaction is a Four-Component Reaction. *Angewandte Chemie International Edition* **50**, 644-649, doi:https://doi.org/10.1002/anie.201005336 (2011).

263 Ramozzi, R. & Morokuma, K. Revisiting the Passerini Reaction Mechanism: Existence of the Nitrilium, Organocatalysis of Its Formation, and Solvent Effect. *The Journal of Organic Chemistry* **80**, 5652-5657, doi:10.1021/acs.joc.5b00594 (2015).

264 Wang, Q., Wang, D.-X., Wang, M.-X. & Zhu, J. Still Unconquered: Enantioselective Passerini and Ugi Multicomponent Reactions. *Accounts of Chemical Research* **51**, 1290-1300, doi:10.1021/acs.accounts.8b00105 (2018).

265 Kobayashi, S., Busujima, T. & Nagayama, S. A Novel Classification of Lewis Acids on the Basis of Activity and Selectivity. *Chemistry – A European Journal* **6**, 3491-3494, doi:https://doi.org/10.1002/1521-3765(20001002)6:19<3491::AID-CHEM3491>3.0.CO;2-P (2000).

266 Wang, S. X., Wang, M. X., Wang, D. X. & Zhu, J. Catalytic enantioselective Passerini three-component reaction. *Angew Chem Int Ed Engl* **47**, 388-391, doi:10.1002/anie.200704315 (2008).
267 Denmark, S. E. & Fan, Y. The First Catalytic, Asymmetric α-Additions of Isocyanides. Lewis-Base-Catalyzed, Enantioselective Passerini-Type Reactions. *Journal of the American Chemical Society* **125**, 7825-7827, doi:10.1021/ja035410c (2003).
268 Kusebauch, U., Beck, B., Messer, K., Herdtweck, E. & Dömling, A. Massive Parallel Catalyst Screening: Toward Asymmetric MCRs. *Organic Letters* **5**, 4021-4024, doi:10.1021/ol035010u (2003).
269 Andreana, P. R., Liu, C. C. & Schreiber, S. L. Stereochemical Control of the Passerini Reaction. *Organic Letters* **6**, 4231-4233, doi:10.1021/ol0482893 (2004).
270 Carvalho, M. H., Amarante, G. W. & Castro, P. P. d. Recent Synthetic Developments of Asymmetric Multicomponent Transformations: Strecker, Mannich, Passerini and Ugi Reactions. *Journal of the Brazilian Chemical Society* **34**, 1041-1070 (2023).
271 Marcaccini, S. & Torroba, T. The use of the Ugi four-component condensation. *Nature Protocols* **2**, 632-639, doi:10.1038/nprot.2007.71 (2007).
272 Rocha, R. O., Rodrigues, M. O. & Neto, B. A. D. Review on the Ugi Multicomponent Reaction Mechanism and the Use of Fluorescent Derivatives as Functional Chromophores. *ACS Omega* **5**, 972-979, doi:10.1021/acsomega.9b03684 (2020).
273 van Berkel, S. S., Bögels, B. G. M., Wijdeven, M. A., Westermann, B. & Rutjes, F. P. J. T. Recent Advances in Asymmetric Isocyanide-Based Multicomponent Reactions. *European Journal of Organic Chemistry* **2012**, 3543-3559, doi:https://doi.org/10.1002/ejoc.201200030 (2012).
274 Marcaccini, S., Pepino, R., Polo, C. & Pozo, M. C. Studies on Isocyanides and Related Compounds; A Facile Synthesis of 4-Phenyl-1-(2H)phthalazinone-2-alkanoic Acid Amides. *Synthesis* **2001**, 0085-0088 (2001).
275 Ugi, I. & Bodesheim, F. Isonitrile, XIV. Umsetzung von Isonitrilen mit Hydrazonen und Carbonsäuren. *Justus Liebigs Annalen der Chemie* **666**, 61-64 (1963).
276 Campian, E., Lou, B. & Saneii, H. Solid-phase synthesis of α-sulfonylamino amide derivatives based on Ugi-type condensation reaction using sulfonamides as amine input. *Tetrahedron letters* **43**, 8467-8470 (2002).
277 v. Zychlinski, A. & Ugi, I. MCR. Part 9. A New and Easy Way for the Preparation of Piperazine-2-keto-carboxamides. *ChemInform* **30**, no-no (1999).
278 Ugi, I. & Bodesheim, F. Isonitrile, VIII. umsetzung von isonitrilen mit hydrazonen und stickstoffwasserstoffsäure. *Chemische Berichte* **94**, 2797-2801 (1961).
279 Ugi, I. & Offermann, K. Isonitrile, XVIII. Hydantoin-imide-(4). *Chemische Berichte* **97**, 2276-2281 (1964).
280 El Kaïm, L., Grimaud, L. & Oble, J. Phenol Ugi–Smiles Systems: Strategies for the Multicomponent N-Arylation of Primary Amines with Isocyanides, Aldehydes, and Phenols. *Angewandte Chemie* **117**, 8175-8178 (2005).
281 Caputo, S. *et al.* Diastereoselective Ugi reaction of chiral 1,3-aminoalcohols derived from an organocatalytic Mannich reaction. *Beilstein Journal of Organic Chemistry* **12**, 139-143, doi:10.3762/bjoc.12.15 (2016).
282 Ugi, I. & Meyr, R. Isonitrile, V. Erweiterter Anwendungsbereich der Passerini-Reaktion. *Chemische Berichte* **94**, 2229-2233 (1961).
283 Bock, H. & Ugi, I. Multicomponent reactions. II. Stereoselective synthesis of 1(S)-camphor-2-cis-methylidene-isocyanide and its application in Passerini- and Ugi-reaction. *Journal für Praktische Chemie/Chemiker-Zeitung* **339**, 385-389, doi:https://doi.org/10.1002/prac.19973390167 (1997).
284 Chéron, N., Ramozzi, R., Kaïm, L. E., Grimaud, L. & Fleurat-Lessard, P. Challenging 50 Years of Established Views on Ugi Reaction: A Theoretical

Approach. *The Journal of Organic Chemistry* **77**, 1361-1366, doi:10.1021/jo2021554 (2012).

285 Iacobucci, C., Reale, S., Gal, J.-F. & De Angelis, F. Insight into the Mechanisms of the Multicomponent Ugi and Ugi–Smiles Reactions by ESI-MS(/MS). *European Journal of Organic Chemistry* **2014**, 7087-7090, doi:https://doi.org/10.1002/ejoc.201403179 (2014).

286 Faggi, C., García-Valverde, M., Marcaccini, S. & Menchi, G. Isolation of Ugi Four-Component Condensation Primary Adducts: A Straightforward Route to Isocoumarins. *Organic Letters* **12**, 788-791, doi:10.1021/ol9028622 (2010).

287 Ramos, L. M., Rodrigues, M. O. & Neto, B. A. D. Mechanistic knowledge and noncovalent interactions as the key features for enantioselective catalysed multicomponent reactions: a critical review. *Organic & Biomolecular Chemistry* **17**, 7260-7269, doi:10.1039/C9OB01088B (2019).

288 Cho, S., Kim, S.-H. & Shin, D. Recent applications of hydantoin and thiohydantoin in medicinal chemistry. *European Journal of Medicinal Chemistry* **164**, 517-545, doi:https://doi.org/10.1016/j.ejmech.2018.12.066 (2019).

289 Abd Elhady, H., El Desoky, S., Al-Shareef, H. F. & El-mekawy, R. Synthesis, reactions, and applications of hydantoin and 2-thiohydantoin derivatives. *Acta Poloniae Pharmaceutica-Drug Research* **76**, 971-986 (2019).

290 Fresneda, P. M., Castaneda, M., Sanz, M. A. & Molina, P. Trapping of a phosphazide intermediate in the Staudinger reaction of tertiary phosphines with azides and its application to the synthesis of analogs of the marine alkaloid midpacamide. *Tetrahedron letters* **45**, 1655-1657 (2004).

291 Khodair, A. I., Bakare, S. B., Awad, M. K., Al-Issa, S. A. & Nafie, M. S. Design, synthesis, and computational explorations of novel 2-thiohydantoin nucleosides with cytotoxic activities. *Journal of Heterocyclic Chemistry* **59**, 664-685, doi:10.1002/jhet.4405 (2022).

292 Chen, Y., Su, L., Yang, X., Pan, W. & Fang, H. Enantioselective synthesis of 3,5-disubstituted thiohydantoins and hydantoins. *Tetrahedron* **71**, 9234-9239, doi:https://doi.org/10.1016/j.tet.2015.10.041 (2015).

293 Fresneda, P. M., Castaneda, M., Sanz, M. A., Bautista, D. & Molina, P. An iminophosphorane-based approach for the synthesis of spiropyrrolidine–imidazole derivatives. *Tetrahedron* **63**, 1849-1856 (2007).

294 El-Sharief, A. M. S. & Moussa, Z. Synthesis, characterization and derivatization of some novel types of mono-and bis-imidazolidineiminothiones and imidazolidineiminodithiones with antitumor, antiviral, antibacterial and antifungal activities–part I. *European journal of medicinal chemistry* **44**, 4315-4334 (2009).

295 Abadi, A. H., Gary, B. D., Tinsley, H. N., Piazza, G. A. & Abdel-Halim, M. Synthesis, molecular modeling and biological evaluation of novel tadalafil analogues as phosphodiesterase 5 and colon tumor cell growth inhibitors, new stereochemical perspective. *European journal of medicinal chemistry* **45**, 1278-1286 (2010).

296 Moussa, Z., El-Sharief, M. A. S. & El-Sharief, A. M. S. Synthesis and characterization of new types of halogenated and alkylated imidazolidineiminothiones and a comparative study of their antitumor, antibacterial, and antifungal activities. *European journal of medicinal chemistry* **46**, 2280-2289 (2011).

297 Azizmohammadi, M. *et al.* 2H-chromene derivatives bearing thiazolidine-2, 4-dione, rhodanine or hydantoin moieties as potential anticancer agents. *European journal of medicinal chemistry* **59**, 15-22 (2013).

298 Küçükbay, H., Durmaz, R., Orhan, E. & Günal, S. Synthesis, antibacterial and antifungal activities of electron-rich olefins derived benzimidazole compounds. *Il Farmaco* **58**, 431-437 (2003).

299 Ali, O. M., El-Sayed, W. A., Eid, S. A., Abdelwahed, N. & Abdel-Rahman, A. Antimicrobial activity of new synthesized [(oxadiazolyl) methyl] phenytoin derivatives. *Acta poloniae pharmaceutica* **69**, 657-667 (2012).

300 Yildiz, I. & Bozdag-Dundar, O. Three-dimensional common-feature hypotheses for hypoglycemic flavonyl-2, 4-thiazolidinedione derivatives. *Medicinal chemistry research* **19**, 211-219 (2010).

301 Murasawa, S. *et al.* Small-molecular inhibitors of Ca2+-induced mitochondrial permeability transition (MPT) derived from muscle relaxant dantrolene. *Bioorganic & medicinal chemistry* **20**, 6384-6393 (2012).

302 Zhu, Q. *et al.* Synthesis and potential anticonvulsant activity of new N-3-substituted 5,5-cyclopropanespirohydantoins. *European Journal of Medicinal Chemistry* **44**, 296-302, doi:https://doi.org/10.1016/j.ejmech.2008.02.024 (2009).

303 Obniska, J. *et al.* Design, synthesis, and anticonvulsant activity of new N-Mannich bases derived from spirosuccinimides and spirohydantoins. *Bioorganic & Medicinal Chemistry* **18**, 6134-6142, doi:https://doi.org/10.1016/j.bmc.2010.06.064 (2010).

304 Sondhi, S. M., Singh, J., Kumar, A., Jamal, H. & Gupta, P. Synthesis of amidine and amide derivatives and their evaluation for anti-inflammatory and analgesic activities. *European journal of medicinal chemistry* **44**, 1010-1015 (2009).

305 da Silva Guerra, A. S. H. *et al.* Anti-inflammatory and antinociceptive activities of indole–imidazolidine derivatives. *International Immunopharmacology* **11**, 1816-1822 (2011).

306 Procopiou, P. A. *et al.* The discovery of long-acting saligenin β2 adrenergic receptor agonists incorporating a urea group. *Bioorganic & medicinal chemistry* **19**, 6026-6032 (2011).

307 Handzlik, J. *et al.* Pharmacophore models based studies on the affinity and selectivity toward 5-HT1A with reference to α1-adrenergic receptors among arylpiperazine derivatives of phenytoin. *Bioorganic & medicinal chemistry* **19**, 1349-1360 (2011).

308 Handzlik, J. *et al.* Synthesis, α1-adrenoceptor antagonist activity, and SAR study of novel arylpiperazine derivatives of phenytoin. *Bioorganic & medicinal chemistry* **16**, 5982-5998 (2008).

309 Stilz, H. U. *et al.* Discovery of an orally active non-peptide fibrinogen receptor antagonist based on the hydantoin scaffold. *Journal of medicinal chemistry* **44**, 1158-1176 (2001).

310 Flosi, W. J. *et al.* Discovery of imidazolidine-2, 4-dione-linked HIV protease inhibitors with activity against lopinavir-resistant mutant HIV. *Bioorganic & medicinal chemistry* **14**, 6695-6712 (2006).

311 Kim, D. *et al.* Discovery of human CCR5 antagonists containing hydantoins for the treatment of HIV-1 infection. *Bioorg Med Chem Lett* **11**, 3099-3102, doi:10.1016/s0960-894x(01)00654-0 (2001).

312 Kim, D. *et al.* Design, synthesis, and SAR of heterocycle-containing antagonists of the human CCR5 receptor for the treatment of HIV-1 infection. *Bioorg Med Chem Lett* **11**, 3103-3106, doi:10.1016/s0960-894x(01)00655-2 (2001).

313 Romine, J. L. *et al.* Inhibitors of HCV NS5A: from iminothiazolidinones to symmetrical stilbenes. *ACS Medicinal Chemistry Letters* **2**, 224-229 (2011).

314 Basappa, Ananda Kumar, C. S., Nanjunda Swamy, S., Sugahara, K. & Rangappa, K. S. Anti-tumor and anti-angiogenic activity of novel hydantoin derivatives: Inhibition of VEGF secretion in liver metastatic osteosarcoma cells. *Bioorganic & Medicinal Chemistry* **17**, 4928-4934, doi:https://doi.org/10.1016/j.bmc.2009.06.004 (2009).

315 Jung, M. E. *et al.* Structure-activity relationship for thiohydantoin androgen receptor antagonists for castration-resistant prostate cancer (CRPC). *J Med Chem* **53**, 2779-2796, doi:10.1021/jm901488g (2010).

316 Malancona, S. *et al.* Identification of MK-5710 ((8aS)-8a-methyl-1,3-dioxo-2-[(1S,2R)-2-phenylcyclopropyl]-N-(1-phenyl-1H-pyrazol-5-yl)hexahydroimid

azo[1,5-a]pyrazine-7(1H)-carboxamide), a potent smoothened antagonist for use in Hedgehog pathway dependent malignancies, part 1. *Bioorg Med Chem Lett* **21**, 4422-4428, doi:10.1016/j.bmcl.2011.06.024 (2011).

317 Takahashi, N. *et al.* Necrostatin-1 analogues: critical issues on the specificity, activity and in vivo use in experimental disease models. *Cell death & disease* **3**, e437-e437 (2012).

318 Sergent, D., Wang, Q., Sasaki, N. A. & Ouazzani, J. Synthesis of hydantoin analogues of (2S,3R,4S)-4-hydroxyisoleucine with insulinotropic properties. *Bioorg Med Chem Lett* **18**, 4332-4335, doi:10.1016/j.bmcl.2008.06.081 (2008).

319 Handzlik, J. *et al.* Amine-alkyl derivatives of hydantoin: new tool to combat resistant bacteria. *Eur J Med Chem* **46**, 5807-5816, doi:10.1016/j.ejmech.2011.09.032 (2011).

320 Fujisaki, F. *et al.* Antibacterial activity of 5-dialkylaminomethylhydantoins and related compounds. *Chem Pharm Bull (Tokyo)* **58**, 1123-1126, doi:10.1248/cpb.58.1123 (2010).

321 Vega-Peñaloza, A., Sánchez-Antonio, O., Ávila-Ortiz, C. G., Escudero-Casao, M. & Juaristi, E. An Alternative Synthesis of Chiral (S)-Proline Derivatives that Contain a Thiohydantoin Moiety and Their Application as Organocatalysts in the Asymmetric Michael Addition Reaction under Solvent-Free Conditions. *Asian Journal of Organic Chemistry* **3**, 487-496, doi:https://doi.org/10.1002/ajoc.201400018 (2014).

322 Smit, B. *et al.* Synthesis, characterization and cytotoxicity of a palladium (II) complex of 3-[(2-hydroxybenzylidene) amino]-2-thioxoimidazolidin-4-one. *Journal of the Serbian Chemical Society* **78**, 217-227 (2013).

323 Ha, Y. M. *et al.* Analogs of 5-(substituted benzylidene) hydantoin as inhibitors of tyrosinase and melanin formation. *Biochimica et Biophysica Acta (BBA)-General Subjects* **1810**, 612-619 (2011).

324 Lu, G.-J., Nie, J.-Q., Chen, Z.-X., Yang, G.-C. & Lu, C.-F. Synthesis and evaluation of a new non-cross-linked polystyrene supported hydantoin chiral auxiliary for asymmetric aldol reactions. *Tetrahedron: Asymmetry* **24**, 1331-1335, doi:https://doi.org/10.1016/j.tetasy.2013.08.017 (2013).

325 Metallinos, C., John, J., Zaifman, J. & Emberson, K. Diastereoselective Synthesis of N-Substituted Planar Chiral Ferrocenes Using a Proline Hydantoin-Derived Auxiliary. *Advanced Synthesis & Catalysis* **354**, 602-606, doi:https://doi.org/10.1002/adsc.201100862 (2012).

326 Kotha, S., Gupta, N. K. & Aswar, V. R. Multicomponent Approach to Hydantoins and Thiohydantoins Involving a Deep Eutectic Solvent. *Chemistry – An Asian Journal* **14**, 3188-3197, doi:https://doi.org/10.1002/asia.201900744 (2019).

327 Meusel, M. & Gütschow, M. RECENT DEVELOPMENTS IN HYDANTOIN CHEMISTRY. A REVIEW. *Organic Preparations and Procedures International* **36**, 391-443, doi:10.1080/00304940409356627 (2004).

328 Metwally, M. A. & Abdel-Latif, E. Thiohydantoins: synthetic strategies and chemical reactions. *Journal of Sulfur Chemistry* **33**, 229-257, doi:10.1080/17415993.2011.643550 (2012).

329 Ware, E. The chemistry of the hydantoins. *Chemical Reviews* **46**, 403-470 (1950).

330 Savjani, J. K. & Gajjar, A. K. Pharmaceutical Importance and Synthetic Strategies for Imidazolidine-2-thione and. *Pakistan Journal of Biological Sciences* **14**, 1076-1089 (2011).

331 Bucherer, H. T. & Lieb, V. Über die bildung substituierter hydantoine aus aldehyden und ketonen. *Synthese von Hydantoinen. J. Prakt. Chem* **141** (1934).

332 Read, W. T. Researches on hydantoins. Synthesis of the soporific, 4, 4-phenylethyl-hydantoin (nirvanol). *Journal of the American Chemical Society* **44**, 1746-1755 (1922).

333 Biltz, H. Über die Konstitution der Einwirkungsprodukte von substituierten Harnstoffen auf Benzil und über einige neue Methoden zur Darstellung der 5.5-

Diphenyl-hydantoine. *Berichte der deutschen chemischen Gesellschaft* **41**, 1379-1393 (1908).

334 Konnert, L., Lamaty, F., Martinez, J. & Colacino, E. Recent Advances in the Synthesis of Hydantoins: The State of the Art of a Valuable Scaffold. *Chemical Reviews* **117**, 13757-13809, doi:10.1021/acs.chemrev.7b00067 (2017).

335 Yoshino, H. *et al.* Design and synthesis of an androgen receptor pure antagonist (CH5137291) for the treatment of castration-resistant prostate cancer. *Bioorganic & medicinal chemistry* **18**, 8150-8157 (2010).

336 Van Dort, M. E. & Jung, Y.-W. Synthesis and structure–activity investigation of iodinated arylhydantoins and arylthiohydantoins for development as androgen receptor radioligands. *Bioorganic & medicinal chemistry letters* **14**, 5285-5288 (2004).

337 Vavsari, V. F. *et al.* New functionalized 8-hydroxyquinoline-5-sulfonic acid mesoporous silica (HQS-SBA-15) as an efficient catalyst for the synthesis of 2-thiohydantoin derivatives. *Tetrahedron* **72**, 5420-5426 (2016).

338 Merino-Montiel, P., López, Ó., Álvarez, E. & Fernández-Bolaños, J. G. Synthesis of conformationally-constrained thio (seleno) hydantoins and α-triazolyl lactones from d-arabinose as potential glycosidase inhibitors. *Tetrahedron* **68**, 4888-4898 (2012).

339 Lin, M.-J. & Sun, C.-M. Microwave-assisted traceless synthesis of thiohydantoin. *Tetrahedron Letters* **44**, 8739-8742, doi:https://doi.org/10.1016/j.tetlet.2003.09.156 (2003).

340 Schmeyers, J. & Kaupp, G. Heterocycles by cascade reactions of versatile thioureido-acetamides. *Tetrahedron* **58**, 7241-7250 (2002).

341 Singh, M. S. & Chowdhury, S. Recent developments in solvent-free multicomponent reactions: a perfect synergy for eco-compatible organic synthesis. *Rsc Advances* **2**, 4547-4592 (2012).

342 Zhao, B., Du, H. & Shi, Y. A Cu (I)-catalyzed C− H α-amination of esters. Direct synthesis of hydantoins. *Journal of the American Chemical Society* **130**, 7220-7221 (2008).

343 Beller, M., Eckert, M., Moradi, W. A. & Neumann, H. Palladium-Catalyzed Synthesis of Substituted Hydantoins—A New Carbonylation Reaction for the Synthesis of Amino Acid Derivatives. *Angewandte Chemie International Edition* **38**, 1454-1457 (1999).

344 Vukelić, S., Koksch, B., Seeberger, P. H. & Gilmore, K. A Sustainable, Semi-Continuous Flow Synthesis of Hydantoins. *Chemistry–A European Journal* **22**, 13451-13454 (2016).

345 Cabordery, A.-C. *et al.* Kinetics and mechanism of racemization of Tic-hydantoins, potent sigma-1 agonists. *Tetrahedron: Asymmetry* **22**, 125-133, doi:https://doi.org/10.1016/j.tetasy.2011.01.015 (2011).

346 Wahby, Y., Abdel-Hamid, H. & Ayoup, M. S. Two decades of recent advances of Passerini reactions: synthetic and potential pharmaceutical applications. *New Journal of Chemistry* **46**, 1445-1468, doi:10.1039/D1NJ03832J (2022).

347 Hasöksüz, M., Kilic, S. & Saraç, F. Coronaviruses and sars-cov-2. *Turkish journal of medical sciences* **50**, 549-556 (2020).

348 Wu, D., Wu, T., Liu, Q. & Yang, Z. The SARS-CoV-2 outbreak: What we know. *International Journal of Infectious Diseases* **94**, 44-48, doi:https://doi.org/10.1016/j.ijid.2020.03.004 (2020).

349 Ludwig, S. & Zarbock, A. Coronaviruses and SARS-CoV-2: A Brief Overview. *Anesthesia & Analgesia* **131**, 93-96, doi:10.1213/ane.0000000000004845 (2020).

350 Lu, R. *et al.* Genomic characterisation and epidemiology of 2019 novel coronavirus: implications for virus origins and receptor binding. *The Lancet* **395**, 565-574, doi:10.1016/S0140-6736(20)30251-8 (2020).

351 COVID-19 deaths dashboard. *World Health Organization* **WHO Data, https://data.who.int/dashboards/covid19/deaths** (Accessed 12.11.2024).

352 Drosten, C. *et al.* Identification of a novel coronavirus in patients with severe acute respiratory syndrome. *N Engl J Med* **348**, 1967-1976, doi:10.1056/NEJMoa030747 (2003).

353 Benvenuto, D. *et al.* The 2019-new coronavirus epidemic: evidence for virus evolution. *Journal of medical virology* **92**, 455-459 (2020).

354 The species Severe acute respiratory syndrome-related coronavirus: classifying 2019-nCoV and naming it SARS-CoV-2. *Nat Microbiol* **5**, 536-544, doi:10.1038/s41564-020-0695-z (2020).

355 Rabaan, A. A. *et al.* SARS-CoV-2, SARS-CoV, and MERS-COV: a comparative overview. *Infez Med* **28**, 174-184 (2020).

356 Zumla, A., Chan, J. F. W., Azhar, E. I., Hui, D. S. C. & Yuen, K.-Y. Coronaviruses — drug discovery and therapeutic options. *Nature Reviews Drug Discovery* **15**, 327-347, doi:10.1038/nrd.2015.37 (2016).

357 Dijkman, R. & van der Hoek, L. Human Coronaviruses 229E and NL63: Close Yet Still So Far. *Journal of the Formosan Medical Association* **108**, 270-279, doi:https://doi.org/10.1016/S0929-6646(09)60066-8 (2009).

358 Hamre, D. & Procknow, J. J. A new virus isolated from the human respiratory tract. *Proceedings of the society for experimental biology and medicine* **121**, 190-193 (1966).

359 McIntosh, K., Dees, J. H., Becker, W. B., Kapikian, A. Z. & Chanock, R. M. Recovery in tracheal organ cultures of novel viruses from patients with respiratory disease. *Proceedings of the national academy of sciences* **57**, 933-940 (1967).

360 Markov, P. V. *et al.* The evolution of SARS-CoV-2. *Nature Reviews Microbiology* **21**, 361-379, doi:10.1038/s41579-023-00878-2 (2023).

361 Rota, P. A. *et al.* Characterization of a novel coronavirus associated with severe acute respiratory syndrome. *science* **300**, 1394-1399 (2003).

362 Van Der Hoek, L. *et al.* Identification of a new human coronavirus. *Nature medicine* **10**, 368-373 (2004).

363 Woo, P. *et al.* Phylogenetic and recombination analysis of coronavirus HKU1, a novel coronavirus from patients with pneumonia. *Archives of virology* **150**, 2299-2311 (2005).

364 Zhang, H.-R. *et al.* Mechanism and origin of enantioselectivity for asymmetric Passerini reaction in the synthesis of α-acyloxyamide catalyzed by chiral phosphoric acid. *Molecular Catalysis* **558**, 114014, doi:https://doi.org/10.1016/j.mcat.2024.114014 (2024).

365 Matsumura, T. & Nakada, M. Preparation of imidazolinium salts by the Pd-catalyzed reduction of thioureas with triethylsilane and trialkylsilyl triflate. *Tetrahedron Letters* **55**, 1412-1415, doi:https://doi.org/10.1016/j.tetlet.2014.01.022 (2014).

366 Yin, B.-L., Liu, Z.-G., Zhang, J.-C. & Li, Z.-R. N,N′-Di-Boc-Substituted Thiourea as a Novel and Mild Thioacylating Agent Applicable for the Synthesis of Thiocarbonyl Compounds. *Synthesis* **2010**, 991-999 (2010).

367 Takemoto, Y. Development of Chiral Thiourea Catalysts and Its Application to Asymmetric Catalytic Reactions. *Chemical and Pharmaceutical Bulletin* **58**, 593-601, doi:10.1248/cpb.58.593 (2010).

368 Survey, U. S. G. Mineral commodity summaries 2021. 200 (Reston, VA, 2021).

369 Davis, R. E. & Nakshbendi, H. F. Sulfur in Amine Solvents. *Journal of the American Chemical Society* **84**, 2085-2090, doi:10.1021/ja00870a017 (1962).

370 Zhang, Z., Bao, Z. & Xing, H. N,N′-Bis[3,5-bis(trifluoromethyl)phenyl]thiourea: a privileged motif for catalyst development. *Organic & Biomolecular Chemistry* **12**, 3151-3162, doi:10.1039/C4OB00306C (2014).

371 Ehrhard, A. A., Jäger, S., Malm, C., Basaran, S. & Hunger, J. CF3-groups critically enhance the binding of thiourea catalysts to ketones – a NMR and FT-IR study. *Journal of Molecular Liquids* **296**, 111829, doi:https://doi.org/10.1016/j.molliq.2019.111829 (2019).

372 Steppeler, F., Iwan, D., Wojaczyńska, E. & Wojaczyński, J. Chiral Thioureas—Preparation and Significance in Asymmetric Synthesis and Medicinal Chemistry. *Molecules* **25**, 401 (2020).

373 Hosangadi, B. D. & Dave, R. H. An efficient general method for esterification of aromatic carboxylic acids. *Tetrahedron Letters* **37**, 6375-6378, doi:https://doi.org/10.1016/0040-4039(96)01351-2 (1996).

374 Dhake, K. P., Tambade, P. J., Singhal, R. S. & Bhanage, B. M. An efficient, catalyst- and solvent-free N-formylation of aromatic and aliphatic amines. *Green Chemistry Letters and Reviews* **4**, 151-157, doi:10.1080/17518253.2010.524168 (2011).

375 Blicke, F. F. & Lu, C.-J. Formylation of Amines with Chloral and Reduction of the N-Formyl Derivatives with Lithium Aluminum Hydride. *Journal of the American Chemical Society* **74**, 3933-3934, doi:10.1021/ja01135a503 (1952).

376 Chen, F. M. F. & Benoiton, N. L. A General Method for Formylating Sensitive Amino Acid Esters. *Synthesis* **1979**, 709-710 (1979).

377 De Luca, L., Giacomelli, G., Porcheddu, A. & Salaris, M. A New, Simple Procedure for the Synthesis of Formyl Amides. *Synlett* **2004**, 2570-2572 (2004).

378 Hosseini-Sarvari, M. & Sharghi, H. ZnO as a New Catalyst for N-Formylation of Amines under Solvent-Free Conditions. *The Journal of Organic Chemistry* **71**, 6652-6654, doi:10.1021/jo060847z (2006).

379 Ganapati Reddy, P., Kishore Kumar, G. D. & Baskaran, S. A convenient method for the N-formylation of secondary amines and anilines using ammonium formate. *Tetrahedron Letters* **41**, 9149-9151, doi:https://doi.org/10.1016/S0040-4039(00)01636-1 (2000).

380 Rahman, M., Kundu, D., Hajra, A. & Majee, A. Formylation without catalyst and solvent at 80°C. *Tetrahedron Letters* **51**, 2896-2899, doi:https://doi.org/10.1016/j.tetlet.2010.03.097 (2010).

381 Conen, P. & Meier, M. A. R. Reactivities and mechanisms in organic reactions involving activation of elemental sulfur under basic conditions. *Tetrahedron Chem* **11**, 100086, doi:https://doi.org/10.1016/j.tchem.2024.100086 (2024).

382 Satchell, D. P. N. & Satchell, R. S. The kinetics and mechanism of aminolysis of isothiocyanates. *Journal of the Chemical Society, Perkin Transactions 2*, 1415-1420, doi:10.1039/P29900001415 (1990).

383 Nickisch, R., Conen, P., Gabrielsen, S. M. & Meier, M. A. R. A more sustainable isothiocyanate synthesis by amine catalyzed sulfurization of isocyanides with elemental sulfur. *RSC Advances* **11**, 3134-3142, doi:10.1039/D0RA10436A (2021).

384 Ceban, V., Hands, K., Meazza, M., Light, M. E. & Rios, R. Three-component diastereoselective cascade synthesis of thiohydantoins. *Tetrahedron Letters* **54**, 7183-7187, doi:https://doi.org/10.1016/j.tetlet.2013.10.110 (2013).

385 Laursen, R. A. Solid-Phase Edman Degradation. *European Journal of Biochemistry* **20**, 89-102, doi:https://doi.org/10.1111/j.1432-1033.1971.tb01366.x (1971).

386 Pearson, R. G. & Songstad, J. Application of the principle of hard and soft acids and bases to organic chemistry. *Journal of the American Chemical Society* **89**, 1827-1836 (1967).

387 Bogolubsky, A. V. *et al.* An Old Story in the Parallel Synthesis World: An Approach to Hydantoin Libraries. *ACS Combinatorial Science* **20**, 35-43, doi:10.1021/acscombsci.7b00163 (2018).

388 Henderson, R. K. *et al.* Expanding GSK's solvent selection guide – embedding sustainability into solvent selection starting at medicinal chemistry. *Green Chemistry* **13**, 854-862, doi:10.1039/C0GC00918K (2011).

389 Henderson, R. K., Hill, A. P., Redman, A. M. & Sneddon, H. F. Development of GSK's acid and base selection guides. *Green Chemistry* **17**, 945-949, doi:10.1039/C4GC01481B (2015).

390 Alder, C. M. *et al.* Updating and further expanding GSK's solvent sustainability guide. *Green Chemistry* **18**, 3879-3890, doi:10.1039/C6GC00611F (2016).

391 Diemoz, K. M. & Franz, A. K. NMR Quantification of Hydrogen-Bond-Activating Effects for Organocatalysts including Boronic Acids. *The Journal of Organic Chemistry* **84**, 1126-1138, doi:10.1021/acs.joc.8b02389 (2019).

392 Nödling, A. R., Jakab, G., Schreiner, P. R. & Hilt, G. 31P NMR Spectroscopically Quantified Hydrogen-Bonding Strength of Thioureas and Their Catalytic Activity in Diels–Alder Reactions. *European Journal of Organic Chemistry* **2014**, 6394-6398, doi:https://doi.org/10.1002/ejoc.201402871 (2014).

393 Scheelje, F. C. M. & Meier, M. A. R. Non-isocyanate polyurethanes synthesized from terpenes using thiourea organocatalysis and thiol-ene-chemistry. *Communications Chemistry* **6**, 239, doi:10.1038/s42004-023-01041-x (2023).

394 Scheelje, F. C. M. *Organocatalytic activation of renewable resources for the synthesis of polyesters and non-isocyanate polyurethanes*, (2024).

395 Gawley, R. E. & Aubé, J. *Principles of asymmetric synthesis*. (Elsevier, 2012).

396 Doyle, A. G. & Jacobsen, E. N. Small-Molecule H-Bond Donors in Asymmetric Catalysis. *Chemical Reviews* **107**, 5713-5743, doi:10.1021/cr068373r (2007).

397 Marqués-López, E., Alcaine, A., Tejero, T. & Herrera, R. P. (Wiley Online Library, 2011).

398 Walsh, P. J. & Kozlowski, M. C. *Fundamentals of asymmetric catalysis*. (University Science Books, 2009).

399 Barwick, V. J. Strategies for solvent selection — a literature review. *TrAC Trends in Analytical Chemistry* **16**, 293-309, doi:https://doi.org/10.1016/S0165-9936(97)00039-3 (1997).

400 Brunelli, F., Russo, C., Giustiniano, M. & Tron, G. C. Exploiting the Different Nucleophilicity of the Isocyano Group: A Strategy for the Isocyanide Functionalization. *The Journal of Organic Chemistry* **89**, 5833-5840, doi:10.1021/acs.joc.3c02529 (2024).

401 Tumanov, V. V., Tishkov, A. A. & Mayr, H. Nucleophilicity Parameters for Alkyl and Aryl Isocyanides. *Angewandte Chemie International Edition* **46**, 3563-3566, doi:https://doi.org/10.1002/anie.200605205 (2007).

402 Nhean, S. *et al.* COVID-19: A Review of Potential Treatments (Corticosteroids, Remdesivir, Tocilizumab, Bamlanivimab/Etesevimab, and Casirivimab/Imdevimab) and Pharmacological Considerations. *Journal of Pharmacy Practice* **36**, 407-417, doi:10.1177/08971900211048139 (2023).

403 Ferner, R. E. & Aronson, J. K. Remdesivir in covid-19. *BMJ* **369**, m1610, doi:10.1136/bmj.m1610 (2020).

404 Beigel, J. H. *et al.* Remdesivir for the Treatment of Covid-19 — Final Report. *New England Journal of Medicine* **383**, 1813-1826, doi:doi:10.1056/NEJMoa2007764 (2020).

405 Layer, R. W. The Chemistry of Imines. *Chemical Reviews* **63**, 489-510, doi:10.1021/cr60225a003 (1963).

406 Belowich, M. E. & Stoddart, J. F. Dynamic imine chemistry. *Chemical Society Reviews* **41**, 2003-2024, doi:10.1039/C2CS15305J (2012).

407 Wenzel, A. G., Lalonde, M. P. & Jacobsen, E. N. Divergent Stereoinduction Mechanisms in Urea-Catalyzed Additions to Imines. *Synlett* **2003**, 1919-1922 (2003).

408 Carey, F. A. & Sundberg, R. J. *Advanced organic chemistry: part A: structure and mechanisms*. (Springer Science & Business Media, 2007).

Chapter 8 Appendix

8.1 List of Abbreviation

Abbreviation	Explanation
°C	Degree centigrade
ATP	Adenosine triphosphate
ATR	Attenuated total reflection
Aq.	Aqueous
B-3CR	Biginelli reaction
b (NMR)	Broad (NMR)
$CDCl_3$	Deuterated chloroform
COSY	Correlated spectroscopy
d	days
d (NMR)	Doublet (NMR)
DABCO	1,4-Diazabicyclo[2.2.2]octane
DBN	1,5-Diazabicyclo[4.3.0]non-5-ene
DBU	1,8-Diazabicyclo[5.4.0]und-7-ene
DCM	Dichloromethane
DIPA	Diisopropylamine
DIPEA	*N*,*N*-Diisopropylethylamine
DMAP	4-Dimethylaminopyridine
DMC	Dimethyl carbonate
DMF	Dimethyl formamide
DMSO	Dimethyl sulfoxide
DMSO-d_6	Deuterated dimethyl sulfoxide
e.g.	For example
E-Factor	Ecological factor
EA	Ethyl acetate
ee	Enantiomeric excess
EI	Electron ionization
Eq.	Equivalent

er	Enantiomeric ratio
et al.	Et alii, et aliae, et alia. Lat.: and others
EWG	Electron-withdrawing group
FAB	Fast atom bombardment
FG	Functional group
FID	Flame ionization detector
FTIR	Fourier transform infrared spectroscopy
g	grams
GBL	γ-Hydroxybutyric acid lactone
GC	Gas chromatography
h	hours
HB	Hydrogen bond(ing)
HOMO	Highest occupied molecule orbital
HSQC	Heteronuclear single quantum coherence
IMCR	Isocyanide-based multicomponent reaction
*i*Pr	Isopropyl
IR	Infrared spectroscopy
IS	Internal standard
J (NMR)	Coupling constant (NMR)
KIT	Karlsruhe Institute of Technology
LUMO	Lowest unoccupied molecular orbital
M	Molar
M-3CR	Mannich reaction
MCR	Multicomponent reaction
m (NMR)	Multiplet (NMR)
2-Me-THF	2-Methyl-tetrahydrofuran
MeOH	Methanol
mg	Milligram
MHz	Mega Hertz
Mio.	Million
min	Minutes
mL	Milliliter
mm	Millimeters
MEP	Molecular electrostatic potential
mol	Mole
mol%	Mole percent
MS	Mass spectrometry

NMR	Nuclear magnetic resonance
NMI	1-Methyl-1H-imidazole
P-3CR	Passerini-3 component reaction
ppm	Parts per million
q (NMR)	Quartet (NMR)
Q-TOF	Quadrupole – time of flight
quint. (NMR)	Quintet
r.t.	Room temperature
R_f	Retardation factor
S-3CR	Strecker synthesis
s (NMR)	Singlet (NMR)
t (NMR)	Triplett (NMR)
TBD	1,5,7-Triazabicyclo[4.4.0]dec-5-ene
TEA	Triethylamine
THF	Tetrahydrofuran
TLC	Thin layer chromatography
TMG	*N*,*N*,*N*′,*N*′-Tetramethylguanidine
TMS	Trimethylsilane
TOF	Time of flight
U-4CR	Ugi-4 component reaction
wt%	Weight percent
δ	Chemical shift
µmol	Micromol